Surface Orders, Cyclic Time and the Arithmetic Spectral Bridge

Dessins, resolutions, Auslander–Reiten theory, quantum models and verifiable research

Amelie Schreiber

Research development edition

November 6, 2026

Reader's guide and mathematical status

This book develops the surface-order and cyclic-time constructions of the supplied *Emergent cyclic time* manuscripts together with the subsequent projective-resolution, arithmetic and spectral work. The originals remain immutable. Their final unconditional GRH claims do not survive the identified arithmetic and operator-theoretic gaps. Here every construction has a specified category, coefficient field and determinant target. Established results, conditional implications, computed experiments and open comparisons play different roles.

The first two parts give the shared article constructions and their expanded proofs. The next part develops entire AR components, corrects the face-unfolding and Hom-control claims, and relates valid meshes to derived triangles and determinantal semi-invariants. The physics part retains the original topics while replacing invalid positivity, hardware and continuum inferences by proved finite statements or explicit research models. Computational chapters supply trained finite neural architectures, higher-genus dessins and a local interactive companion. The final comparison problem remains an independent arithmetic theorem, not a consequence of the pictures or learned parameters.

A reader may start with cellular dessins and the node, then projective resolutions, then the AR atlas. The more advanced arithmetic chapters use character sums and Fredholm determinants. The physics chapters can be read with finite-dimensional linear algebra and elementary quantum mechanics. Each computational claim has a script, seed and stated backend. The genus-two and genus-three sheet views are projections; the torus views are topological embeddings, not asserted uniformizing metrics.

The provenance manifest records the source hashes and chapter inventory. Its location is `book/source-provenance.json`. The review records state the audit coverage. The supplied 2053 file is byte-identical to the pinned source called COMPLETED in the source clone; the other supplied COMPLETED file is a shorter, different version. This naming discrepancy is retained in the provenance record. No filename certifies a theorem.

The companion is served on this machine at `http://127.0.0.1:8765`. It contains adjustable dessins, category-labelled AR diagrams, quantum carrier circuits, and saved training curves. The public repository and its project page provide the authoritative source and hosted companion. Selected lemmas are checked in Lean4; a full formalization of this entire book has not yet been completed.

Contents

I Constructions and statements **1**

1 Cellular dessins and their infinite orders **2**

2 Projective resolutions, dual dessins and determinants **4**
2.1 Auxiliary staircase resolutions over the order 5
2.2 A monotone quantum comparison with exact finite ranks 6
2.3 A correct DG model of the infinite node 7

3 Determinant semi-invariants and Schur constructions **8**
3.1 Young tableaux and a cyclic representation stratum 9

4 Lattice almost-split sequences and genuine diamond quotients **11**
4.1 Polynomial strings, completed lattices and the Fukaya category 12

5 Leavitt relations, the constrained Fock algebra and spectrum **14**
5.1 A graph presentation and an actual pullback 15
5.2 A separate diagonal-fiber C* completion retaining the pairing 16

6 Arithmetic attachment, descent and the remaining comparison **18**
6.1 A constructive arithmetic benchmark on the theta dessin 19
6.2 A genuine cellular carrier, and what still fails for the order 19
6.3 Arbitrary projective actions: an obstruction and a genuine determinant repair 20
6.4 Tame descent: a surviving order and a sharper obstruction 22
6.5 Whole components, derived endpoints and determinant relations 24

7 A genuine theta covering and its categorical limits **25**

8 Verification and research frontier **27**

II Proofs and calculations **29**

9 Expanded dessin, resolution and derived calculations **30**
9.1 The cycle order in coordinates 30
9.2 The two-arm complex and its calculations 30

10 Semi-invariants, tableaux and explicit intertwiners **32**
10.1 Derived information retained by a presentation 32
10.2 One Young operator and one LR decomposition in coordinates 32
10.3 Two precise functorial limitations 33

11 Full lattice and diamond diagrams **35**
11.1 The nodal exact diagram 35
11.2 Chebyshev geometry and the exact quotient 35
11.3 Nine actual strings and all maps 36

11.4 The pure-injective quotient and what its dimension means . . . 37

12 The operator extension in detail 38
12.1 A corrected cycle lift and the integer boundary map . . . 38
12.2 Spectral domain and arithmetic trace . . . 38

13 Abel determinant estimates and the arithmetic program 40
13.1 Precisely how classical and recent sources enter . . . 41
13.2 A concrete sequence of remaining constructions . . . 42

14 Graph pullbacks and completions with specified fibers 43
14.1 The complete Fock graph presentation . . . 43
14.2 A genuine application of the supplied pullback theorem . . . 43
14.3 Diagonal residue obstruction and the corrected pullback . . . 44
14.4 Generation, faithfulness and the exact failure of extension . . . 45
14.5 Invariant basis number and the Leavitt comparison . . . 46

15 String finiteness and the smooth quotient surface 47

16 Arithmetic character sums and the cellular determinant 49
16.1 The uniform calculation and its exceptional cases . . . 49
16.2 Deck descent and the actual cellular basis . . . 50
16.3 An explicit chain lift and determinant cancellation . . . 50
16.4 A decisive restriction at inert primes . . . 51
16.5 The remaining order and global spectral obligations . . . 52

17 The theta order interface beyond tensor insertion 53
17.1 Normal forms and the special fiber . . . 53
17.2 All projectives and all linear endomorphisms . . . 54
17.3 An actual integral determinant functor of multiplicity one . . . 55
17.4 The exact rotation obstruction and its allowed escape . . . 55

18 Explicit tame descent and the full-deck coefficient test 57
18.1 The action on genuine formal series . . . 57
18.2 A projective symmetry survives on the endomorphism order . . . 58
18.3 Determinants, Schur weights and the boundary correction . . . 58
18.4 Why the local Jacobi plane does not descend by this repair . . . 59
18.5 The full orbit is the normalization, and arbitrary kernels still fail . . . 59

19 Literal formal and computational coverage 62

20 Explicit covering calculations and derived transport 64

III AR components, derived categories and Hom-control 66

21 AR geometry and determinant relations 67
21.1 What an AR picture specifies . . . 67
21.2 The corrected elliptic-theta face example . . . 68
21.3 Hom control and coverings . . . 70
21.4 Homogeneous tubes . . . 71
21.5 Nodal lattice AR geometry . . . 72
21.6 An HLS component in a dessin quotient . . . 73
21.7 Derived AR triangles . . . 75
21.8 Ringel's wind-wheel tile . . . 76
21.9 Meshes and semi-invariants . . . 77
21.10Physical and arithmetic scope . . . 79

22 Coverings, equivariant AR theory and graded surfaces 80
22.1 Reading the three new sources together . . . 80
22.2 A cover that really preserves the relations . . . 80
22.3 Equivariant modules, not an unproved folding rule . . . 81
22.4 Derived and symplectic data needed for a determinant . . . 81
22.5 From a Hom decomposition to a semi-invariant calculation . . . 82

23 Linear relations, filtrations and actual branch modules 83
23.1 Linear relations and functorial branch filtrations . . . 83
23.2 Relation calculations, splitting functors and determinant limits . . . 84
23.3 A kernel-checked extension over the infinite dessin algebra . . . 87
23.4 Normal forms and the full module action . . . 88

24 DG foundations and actual clock lifts 93
24.1 Degrees, maps and a decisive contracting homotopy . . . 93
24.2 The genuine infinite node and its DG replacement . . . 94
24.3 Completion and the diagonal coefficient ring . . . 94
24.4 A clock that really lifts, and its semilinearity . . . 95
24.5 Theta self extensions require endpoints . . . 95
24.6 Higher products and a usable derived interface . . . 96
24.7 Derived traces and genuine filtered DG modules . . . 97
24.8 Executable windows and exact verification coverage . . . 98

IV Quantum models, trained renormalization and physical realizations 99

25 Positive evolution, clocks and holonomy 100
25.1 States and two different logarithms . . . 100
25.2 Total positivity, wiring and physical positivity . . . 101
25.3 Weyl clocks, Fourier phases and twisted successors . . . 101
25.4 Infinite clocks: rotations and odometers are distinct limits . . . 102
25.5 Holonomy, DG compatibility and persistence . . . 103

26 Entanglement, channels and RG requirements 104
26.1 An entangled pair and the finite first law . . . 104
26.2 Correlation geometry and the gravitational research question . . . 105
26.3 Pooling is a channel: an exact trainable example . . . 105
26.4 Trained QGCN and QGAT on ribbon graphs . . . 106
26.5 Associative memory with a correct measurement model . . . 107
26.6 Evidence categories for learned coarse-graining . . . 107

27 Noise, molecular spins and hyperbolic-code architectures 108
27.1 Ancillas, noise and measurement resources . . . 108
27.2 The peptide-spin evidence and its limits . . . 109
27.3 Control calculations: rotations and exchange . . . 109
27.4 A proposed molecular-design program . . . 110
27.5 Hyperbolic kagome geometry and the assembly problem . . . 111
27.6 CSS codes from boundary maps . . . 111
27.7 The arithmetic comparison is still an additional task . . . 112

28 Actual renormalization: effective actions and scale 114
28.1 Actual renormalization retains the effective action . . . 114
28.2 Controlled errors and a trained full-action RG approximation . . . 116

V Computational and learned constructions 119

29 Higher-genus dessins and reproducible finite carriers 120
29.1 A hyperelliptic family beyond the torus . . . 120
29.2 Larger genera and infinite hyperbolic windows . . . 121
29.3 What a three-dimensional view can claim . . . 122
29.4 Finite clocks and cross-backend agreement . . . 122

30 Quantum feature models and auxiliary compression 124
30.1 Exact teacher data from Ising decimation . . . 124
30.2 Shared quantum graph convolution . . . 125
30.3 QCNN compression with a genuine pooling channel . . . 125
30.4 A larger genus-four nine-qubit example . . . 126
30.5 Quantum-feature graph attention . . . 126
30.6 Photonic Gaussian pooling . . . 126
30.7 Reproduction and limits of the evidence . . . 127

31 Reading an architecture from its tensors 129
31.1 Three distinct kinds of evidence . . . 129
31.2 Shapes explain the operation . . . 129
31.3 Quantum and Gaussian inspection . . . 130
31.4 Spatial calculations and guided navigation . . . 130
31.5 A reproducible way to explore . . . 131
31.6 ConvexTok: certified path vocabularies . . . 131

32 Quantum TokenGT, concept navigation and error correction 135
32.1 Node and edge tokens with a quantum feature map . . . 135
32.2 Matched training on an actual effective action . . . 136
32.3 A defined mutual-information objective for concept directions . . . 136
32.4 Latent forests, analogy and persistent homology . . . 136
32.5 Continuous embedding-chart GFlowNets . . . 137
32.6 A genuine error-correction layer and a surface-code obstruction . . . 138
32.7 Tropical, categorical and physical applications . . . 139
32.8 Verification boundary . . . 139

33 Learned generative fields, width limits and quantum geometry 140
33.1 Learned fields, width limits and quantum geometry . . . 140
33.2 Physical generative models and their verification . . . 141
33.3 Covers, paths, pants and quantum games . . . 146
33.4 Learning objectives with explicit analytic guarantees . . . 150
33.5 A certifiable analytic learning lane . . . 150
33.6 Learning nonlocal strategies and checking their certificates . . . 155
33.7 Exact game calculations and the embedding boundary . . . 155
33.8 Hubs, spokes and the topology retained by a dessin . . . 157

34 Complementary physical datasets, dynamics and geometric inspection 159
34.1 Complementary physical datasets and checked dynamics . . . 159
34.2 Construction, curation and interpretation . . . 160
34.3 Molecular structure, complex transport and learned chemistry . . . 165
34.4 Geometry, orbitals and generative time . . . 165
34.5 Coherent electron-density clouds in an explicit spatial basis . . . 169

35 ToricGT and mirror interfaces **170**
35.1 A toric chart inside an actual dessin representation stratum . . . 170
35.2 Tropical charts and exactly what their certificates prove . . . 171
35.3 The quantum phase block and its cocycle . . . 172
35.4 A quantum–classical ToricGT extension with auditable interfaces . . . 173
35.5 Mirror symmetry supplies category comparisons, not a spectral shortcut . . . 174
35.6 What would make the learned component relevant to GRH? . . . 175
35.7 An executed hybrid spectral experiment . . . 175

36 Persistence and explicit resolutions **177**
36.1 The polynomial ring encodes the two commuting directions . . . 177
36.2 A complete three-grade example . . . 178
36.3 A bifiltered CW realization and the syzygies it creates . . . 179
36.4 Schur modules organize the generators and the first syzygies . . . 180
36.5 Fitting data, exactness and specialization . . . 180
36.6 A correct finite space of complexes and its incidence model . . . 181
36.7 Coefficients in a genuine infinite dessin order . . . 182
36.8 Quantum data, monotonicity and the next usable interface . . . 182
36.9 The executable staircase and quantum laboratory . . . 183
36.10What the polynomial Lean resolution actually verifies . . . 184

37 The remaining arithmetic theorem and a verifiable research loop **185**
37.1 A precise positive spectral target . . . 185
37.2 A surviving short-row reduction . . . 185
37.3 Why an absolute coprime pair-square estimate cannot close the short rows . . . 186
37.4 A signed Möbius decomposition and its termwise obstruction . . . 188
37.5 Formal coverage and the next research step . . . 191
37.6 A full-mask Hecke expansion for the type-I piece . . . 191
37.7 Primitive conductors, deleted factors and the scalar contour . . . 193

VI Certified analytic targets and weighted arithmetic moments **196**

38 Validated Dirichlet targets and finite readout certificates **197**
38.1 A finite, validated approximation result . . . 197
38.2 What this does and does not certify . . . 198
38.3 Validated primitive operations . . . 199
38.4 Recomputing the compact growth constants . . . 199
38.5 The completed-function integral and its tails . . . 200
38.6 High-order integration with a certified remainder . . . 200
38.7 Reproduction and remaining interfaces . . . 201
38.8 Requested-error readouts from preserved certified labels . . . 201
38.9 Objective semantics, precision floors and replay . . . 202
38.10Requested-error theta samples for three fixed conductors . . . 203
38.11Adaptive sampling parameters and precision termination . . . 205
38.12An end-to-end adaptive analytic readout . . . 207
38.13Termination, compression and the boundary of the guarantee . . . 208
38.14Learning the actual signed arithmetic correlations . . . 209
38.15Finite phase features, gradients and exact verification . . . 210

39 The original-family Hecke moment and exact masked transfer **212**
39.1 An arithmetic-family moment with every original row retained . . . 212
39.2 Family identification, the approximate functional equation and masks . . . 214

40 Weighted cutoffs and original-family moments 221
40.1 Recombining the actual weighted cutoff . . . 221
40.2 Euler packaging, coprimality and the analytic boundary . . . 222
40.3 A cutoff-uniform envelope for the original masked remainder . . . 223
40.4 All-ideal reciprocity and the surviving block obstruction . . . 225
40.5 High cutoffs, actual bilinear factors and a signed covariance test . . . 227
40.6 Proof details for the high-window and two-cutoff tests . . . 229
40.7 A quantitative covariance budget without a new exponent . . . 231
40.8 Proof and arithmetic boundary of the covariance budget . . . 232
40.9 The fourth-moment conductor and its full raw zero set . . . 234
40.10Scope of the raw fourth-moment reduction . . . 235
40.11A quadratic pivot on the cube factor . . . 237
40.12Proof and scope of the quadratic pivot . . . 238
40.13Joint completion before conductor absolute values . . . 239
40.14The surviving joint identity and its missing estimate . . . 239
40.15A radical-conductor refinement of the raw envelope . . . 240
40.16Proof of the ordinary-conductor refinement . . . 241
40.17Why the common profile must stay fixed . . . 244
40.18Proof and joint-mean boundary of the moving-profile construction . . . 246
40.19A bound for the signed coprime slice and an exact character twist . . . 249
40.20Proof of the signed-slice budget and its surviving analytic burden . . . 251
40.21The signed divisor mean and a complete-column laboratory . . . 255
40.22Proofs and limits of the signed-divisor development . . . 258
40.23A target-sized budget for rough-prime masks . . . 262
40.24Proof of the rough-prime mask budget . . . 265
40.25The coherent signed main and its remaining inputs . . . 271
40.26Proofs for the coherent main reductions . . . 273
40.27A sieve comparison indexed by the physical radicand . . . 281
40.28Proof of the physical-row sieve application . . . 283
40.29Coherent dual bands, actual cutoffs and arithmetic localization . . . 286
40.30Proofs for the coherent-band comparisons . . . 291
40.31An arithmetic Gauss tail with the original finite cutoff . . . 303
40.32Proofs for the finite-cutoff Gauss tail . . . 309
40.33Ramified theta transforms and the original pure dual prefix . . . 317
40.34Proofs of the ramified transform and full-coefficient prefix bound . . . 320
40.35Paired cutoffs, exact divisor signs and proved regimes . . . 332
40.36Sharp insertion and ordered cutoff estimates . . . 334
40.37Wide cutoff corrections and full-frequency compensation . . . 343
40.38Derivations for the wide cutoff correction . . . 344
40.39Joint moments for the wide cutoff pairing . . . 346
40.40Proofs of the joint cutoff estimates . . . 348

Part I

Constructions and statements

Chapter 1

Cellular dessins and their infinite orders

We start with the surface-order constructions of Schreiber [1, 2], retaining the original sources unchanged. The generic-resolution source [3] is background, not a substitute for exactness of a particular complex. All primary algebra examples below come from explicit clean Belyi maps. Finite-dimensional objects occur as modules or specified quotient strata of those infinite algebras, not as replacements for them. The initial arithmetic target is a primitive nonprincipal Dirichlet L-function. Finite-order Hecke characters, Dedekind zeta functions and general Artin representations require separate comparison theorems; Artin holomorphy is not assumed.

A clean dessin on a compact oriented surface is specified by a nonempty finite dart set H, a fixed-point-free involution α, and a permutation σ such that $\langle \alpha, \sigma \rangle$ is transitive. Contract the white vertices of degree two. The resulting cellular graph has vertices the σ-orbits, edges the α-orbits, and faces the ϕ-orbits, where

$$\tau = \sigma^{-1}, \qquad \phi = \alpha\sigma^{-1}, \qquad 2 - 2g = \#\operatorname{cyc}(\sigma) - |H|/2 + \#\operatorname{cyc}(\phi).$$

Write $[h] = \{h, \alpha h\}$. Our quiver has vertices these edges and arrows $a_h : [h] \to [\tau h]$. Paths are composed in travel order: ab traverses a first. Set

$$A = kQ/(a_h a_{\phi h} : h \in H), \quad J = A_{>0}, \quad \Lambda = \varprojlim A/J^m.$$

Each vertex has two incoming and two outgoing arrows. Each arrow has precisely one permitted successor $a_{\tau h}$ and one forbidden successor $a_{\phi h}$; these are distinct because α has no fixed points. The same holds for predecessors. This is the *locally gentle* condition. Every permitted cycle repeats indefinitely, so A is infinite dimensional. We reserve "gentle" without qualification for the convention additionally imposing finite dimension.

Proposition 1.1 (The actual split order)**.** *For a permitted cycle c of length ℓ, let B_c be the hereditary cycle order in $M_\ell(k[[u_c]])$: diagonal and forward matrix entries are in $k[[u_c]]$, and entries crossing the chosen cycle cut are in $u_c k[[u_c]]$. Then Λ is the suborder of $B = \prod_c B_c$ whose two diagonal constant terms labelled $h, \alpha h$ agree. With $R = k[[u]]$ acting by $u \mapsto (u_c I)_c$, it is finite free of rank $\sum_c \ell(c)^2$; the conductor contains uB.*

Proof. In a cycle order a path of length less than ℓ is the corresponding matrix unit, multiplied by u_c exactly when it crosses the cut; another full turn multiplies it by u_c. Thus completed paths in each permitted branch give all entries of B_c. An arrow belongs to only that branch,

whereas $e_{[h]}$ has diagonal entries at both occurrences $h, \alpha h$. Hence the only condition on branchwise formal coefficients is the displayed equality of diagonal constants. This proves both injectivity and surjectivity of the path-normal-form identification. Multiplication respects it: switching branches across a paired edge is precisely a forbidden pair. The quotient B/Λ is killed by u, so the submodule has the same generic rank as B. It is torsion free and finite over the DVR R, hence free of that rank. The path and u-adic topologies agree: $uA \subset J$, and if L is the longest permitted cycle, any path of length at least $L+1$ is u times a shorter nonempty path. Thus $J^{L+1} \subset uA$. This also justifies the completion used in the identification. □

The path-degree variable q below is not u: one full turn has path degree $\ell(c)$ but u-degree one. Formal, Laurent and operator-norm completions will likewise remain distinct.

Here are five explicit global inputs. Permutations list darts starting at zero; $E = |H|/2$.

Surface and Belyi map β	σ	α	$(g, \operatorname{rank}_R \Lambda)$
$\mathbb{P}^1$, $4z(1-z)$	(0)(1)	(01)	$(0, 2)$
$\mathbb{P}^1$, $(z+1)^2/(4z)$	(01)	(01)	$(0, 4)$
$y^2 = x^3 - 1$, x^3	(012)(345)	(03)(14)(25)	$(1, 18)$
$\mathbb{P}^1$, $4z^3/(1+z^3)^2$	(012)(345)	(03)(15)(24)	$(0, 18)$
$y^2 = x^3 - x$, x^2	(0123)	(02)(13)	$(1, 16)$

The first is the nodal interval: $A = k[x, y]/(xy)$ and $\Lambda = k[[x, y]]/(xy)$. The second has $A = k\langle x, y\rangle/(x^2, y^2)$, still infinite dimensional. The two theta dessins have the same two permitted three-cycles but different face cycles, respectively (051324) and (04)(13)(25). The elliptic square has one permitted and one forbidden four-cycle. For example x has pole order two on the cubic $y^2 = x^3 - 1$; x^3 has ramification $(3, 3)$ above zero, $(2, 2, 2)$ above one since $x^3 - 1 = y^2$, and (6) above infinity. The rational theta map has passport $(3, 3), (2, 2, 2), (2, 2, 2)$. These ramification computations, and the analogous direct zeros/poles in the other rows, verify cellular Belyi inputs rather than merely abstract quivers.

Chapter 2

Projective resolutions, dual dessins and determinants

Use right modules $P_i = e_i A$, $S_i = P_i/P_i J$. Internal shift $M\langle n\rangle$ places its old generator in degree n. Let $\mathcal{R}_n(i)$ be the *indexing words* of length n from i with every adjacent pair forbidden, including e_i for $n = 0$. Such a word is usually zero in A; it still labels a summand.

Theorem 2.1 (Exact resolutions)**.** *There is a minimal graded projective resolution, with $P_0(i) = e_i A$ and for $n \geq 1$,*

$$P_n(i) = \bigoplus_{p=a_1\cdots a_n \in \mathcal{R}_n(i)} e_{t(a_n)} A\langle n\rangle, \qquad d_n(x)_p = a_n x \text{ in the summand } a_1 \cdots a_{n-1}.$$

The augmentation $P_0(i) \to S_i$ is the quotient. For the completed order the identical finite-rank projective terms and formal-series maps resolve the residue simple. Ext and Tor against residue simples count forbidden words with the prescribed endpoints. In the graded case Ext has matching internal shift n.

Proof. The maps are right linear and degree zero. Adjacent differentials multiply by a forbidden pair. The augmentation kernel is the direct sum of aA over initial arrows. For any arrow a, multiplication $e_{t(a)}A \to e_{s(a)}A$ kills exactly the permitted paths beginning with its forbidden successor $f(a)$. All other basis paths survive to distinct basis paths. Thus its kernel is $f(a)A$. For a fixed prefix, different last arrows have disjoint surviving supports; there is no cancellation between summands. This proves exactness inductively. For formal series the same assertion holds coefficient by coefficient and identifies the entire closed kernel, not just its dense polynomial subspace. Terms are idempotent projectives and all entries are arrows. Consequently applying Hom or tensor with a residue simple kills every differential, proving minimality and the Ext/Tor count. In A minimality is graded; it does not require that J be its ordinary Jacobson radical. □

The two arms never terminate in this closed class. Their labelled patterns follow ϕ-cycles. An ungraded positive syzygy tail can have a shorter period by permutation of summands: the nodal interval has labelled period two but unordered tail period one; the elliptic theta has labelled period six and unordered tail period three. A simple need not be isomorphic to a positive syzygy; for the node it is R-torsion, whereas the positive syzygies are lattices.

Let $C_{ij}(q) = \sum_{d\geq 0} \dim_k(e_i A_d e_j) q^d$ and $E_{ij}(q) = \sum_{n\geq 0} (-1)^n \dim_k \operatorname{Ext}^n_A(S_i, S_j) q^n$. Degreewise Euler characteristic of the resolution gives $EC = I$: every coefficient is finite, because a summand in homological degree n starts in internal degree n. Constant terms are I, so the inverse is two-sided. Already signed $E(q)$ must not be evaluated at $-q$ again.

Proposition 2.2 (Dual dessin and cycle determinant)**.** *The complementary-relation algebra is another closed dessin algebra, with $\alpha^{\#} = \alpha$, $\sigma^{\#} = \phi^{-1}$, permitted successor ϕ, and forbidden successor τ. It exchanges graph vertices and faces and preserves genus. Its Cartan matrix satisfies $E(q) = C_{A^{\#}}(-q)$, with the opposite convention if required for Yoneda composition. For independent commuting arrow weights w_a,*

$$\det C_A(\mathbf{w}) = \frac{\prod_{f\in \mathrm{cyc}(\phi)}(1-(-1)^{|f|}w(f))}{\prod_{c\in \mathrm{cyc}(\sigma)}(1-w(c))}.$$

Proof. $\alpha(\sigma^{\#})^{-1} = \alpha\phi = \tau$, so the claimed relations and face data follow directly; the connectedness group is unchanged. To prove the determinant, put $S_{v,a} = w_a$ when $s(a) = v$, and $T_{a,v} = 1$ when $t(a) = v$, zero otherwise. On arrow states let $U_{a,b} = w_b$ for permitted adjacency and $V_{a,b} = w_b$ for forbidden adjacency. Then $TS = U + V$ and the path sum is $C = I + S(I - U)^{-1}T$. Sylvester's identity gives $\det C = \det(I + V)/\det(I - U)$. Each transition is a weighted permutation, whose cycle determinant is respectively $1 - (-1)^{\ell}w(c)$ and $1 - w(c)$. Everything holds in formal power series, hence as rational functions. This supplies a direct proof of the Bessenrodt–Holm formula in the closed dessin class [4]. □

The five univariate determinants are, in the order above,

$$\frac{1+q}{1-q},\quad \frac{1+q}{1-q},\quad \frac{1-q^6}{(1-q^3)^2},\quad \frac{(1-q^2)^3}{(1-q^3)^2},\quad 1.$$

The last cancellation does not imply finite global dimension: its forbidden resolution is infinite. These rational functions have cycle poles/zeros, not arithmetic prime Euler factors.

For clarity, a complex is a sequence with $d^2 = 0$, its homotopy category identifies maps differing by $dh + hd$, and $D(A)$ inverts maps inducing cohomology isomorphisms. A perfect complex is represented by a bounded complex of finite projectives. Our infinite simple resolutions compute derived Hom and tensor but are generally not perfect. The two-term presentation $[P_1 \to P_0]$ is perfect even if its kernel is nonzero. Quadratic linearity is a Koszul statement; it is not by itself an equivalence between all completed derived categories. Likewise a finite-dimensional gentle graded-curve theorem [6] cannot simply be transferred to these closed infinite orders. Here the surface walks explicitly compute the resolution endpoints: τ turns round a graph vertex and ϕ follows a face. For longer string objects all maps can be computed from the occurrence matrices; a universal geodesic-intersection classification for this completed category remains a separate theorem.

2.1 Auxiliary staircase resolutions over the order

The two filtration parameters below are not dessin arrows. Let $R = k[x, y]$ for a field k, and let $I = (g_0, \dots, g_{m-1})$, $m \geq 2$, where $g_i = x^{a_i}y^{b_i}$,

$$a_0 > \cdots > a_{m-1} = 0, \qquad 0 = b_0 < \cdots < b_{m-1}.$$

The positive outer exponents make R/I finite length. Write $R(-a, -b)$ for a free generator born in bidegree (a, b).

Proposition 2.3 (Adjacent syzygies)**.** *A minimal bigraded free resolution of $M = R/I$ is*

$$0 \longrightarrow \bigoplus_{i=0}^{m-2} R(-a_i, -b_{i+1}) \xrightarrow{d_2} \bigoplus_{i=0}^{m-1} R(-a_i, -b_i) \xrightarrow{d_1} R \longrightarrow M \longrightarrow 0,$$

where $d_1(e_i) = g_i$ *and* $d_2(f_i) = -y^{b_{i+1}-b_i}e_i + x^{a_i-a_{i+1}}e_{i+1}$. *Deleting row* i *from* d_2 *gives determinant* $(-1)^i g_i$. *The Hilbert series numerator is* $1 - \sum_i s^{a_i}t^{b_i} + \sum_{i=0}^{m-2} s^{a_i}t^{b_{i+1}}$.

Proof. Each column maps to zero. In a relation $\sum h_i g_i = 0$, all terms except the last contain $x^{a_{m-2}}$. Coprimality with $y^{b_{m-1}}$ implies $h_{m-1} = x^{a_{m-2}}q$. Subtract $qd_2(f_{m-2})$ from the coefficient vector; its last component vanishes. Factor $x^{a_{m-2}}$ from the remaining generators. They form a smaller staircase with the same strict inequalities, ending in a pure y-power. Induction expresses the remaining relation in the preceding adjacent columns. The base of one generator has no relations, since R is a domain. Hence $\ker d_1 = \operatorname{im} d_2$. If $d_2(q) = 0$, its first row gives $-y^{b_1}q_0 = 0$; successive rows then force all $q_i = 0$. This proves injectivity. Every differential entry has positive degree, so reduction modulo (x, y) kills the differentials and the resolution is minimal. In the row-deleted matrix the unique nonzero permutation term uses the negative y entries before row i and the positive x entries after it. Their exponents telescope to b_i, a_i, respectively, and the sign is $(-1)^i$. Finally take the degreewise Euler characteristic; the free summands have Hilbert denominator $(1 - s)(1 - t)$. □

For $I = (x^2, xy, y^2)$ the underlying sequence is also kernel checked in Lean 4 over the actual ring MvPolynomial(Fin 2, k). The verification proves the kernel/image equalities, the stated ideal image, surjective quotient augmentation, projective free terms, and vanishing of both induced Hom differentials to the constant-coefficient residue field. It uses regular multiplication on the free modules, distinct from the residue action on k. General staircases, graded minimality and the surface-order coefficient cone remain separately scoped prose arguments.

At grade $\nu \in \mathbb{N}^2$, M_ν has dimension one exactly when no generator degree is componentwise at most ν. Its comparable-grade map has rank one exactly when both endpoint grades satisfy this condition. A CW realization takes one loop and attaches a disk once along it at each generator degree. The active indices form an interval: the x inequality selects a final interval, the y inequality an initial interval. With c active disks, the cellular map $k^c \to k$ has every entry one. Thus $\dim H_1 = \mathbf{1}_{c=0}$ and $\dim H_2 = \max(c - 1, 0)$, the latter counting active adjacent syzygies. This auxiliary CW complex is not the dessin surface.

For the actual nodal order $\Lambda = k[[\xi, \eta]]/(\xi\eta)$ put $u = \xi + \eta$ and $E = \Lambda/u^2\Lambda$. The basis $(1, \xi, u, u\xi)$ of E satisfies $\xi^2 = u\xi$, $u^2 = 0$, $\eta = u - \xi$. Tensoring the resolution above with $0 \to \Lambda \xrightarrow{u^2} \Lambda \to E \to 0$ gives, over $\mathcal{B} = \Lambda[x, y]$, free ranks $(1, m + 1, 2m - 1, m - 1)$. Indeed the scalar resolution stays exact after tensoring over the field; its degree-zero module is free over Λ on the standard monomials. Multiplication by u^2 is injective there and on all free terms, so the long exact homology sequence of its mapping cone gives positive-degree homology zero and degree-zero module $E \otimes_k M$. In contrast, as an R-module this object has ranks $4(1, m, m - 1)$ in its minimal resolution. Neither finite-length E nor these parameter rings replace the infinite parent dessin algebra or its lattice category.

2.2 A monotone quantum comparison with exact finite ranks

Proposition 2.4 (One common channel)**.** *Let* T *be a positive trace-preserving linear map between finite complex matrix algebras. For density matrices* ρ, σ, *their trace distance* $d(\rho, \sigma) = \frac{1}{2}\|\rho - \sigma\|_1$ *satisfies* $d(T\rho, T\sigma) \le d(\rho, \sigma)$. *For finitely many labelled states, keep fixed vertex birth grades* e_i. *At* (r, e) *include vertices with* $e_i \le e$ *and edges with distance at most* r, *and take the flag complex. Then* T *gives an identity-on-labels inclusion from the input to the output bifiltration, natural in* (r, e).

Proof. Write the Hermitian difference as $A = A_+ - A_-$ with $A_\pm \ge 0$. Positivity, the trace norm triangle inequality and trace preservation give $\|TA\|_1 \le \|TA_+\|_1 + \|TA_-\|_1 = \operatorname{tr} A_+ + \operatorname{tr} A_- = \|A\|_1$. Thus every input edge is an output edge; the fixed births preserve vertices, and all cliques are

preserved. Increasing either parameter preserves the simplices, and every map is the same label inclusion, so the squares commute. Complete positivity is sufficient but is not needed for this norm argument. □

For a finite inclusion $K \subset L$, work over a field and embed a basis Z_K of source one-cycles into the target edge space. If B_L is the matrix of target two-boundaries, the induced H_1 rank is

$$\rho_1(K, L) = \operatorname{rank}[B_L \; Z_K] - \operatorname{rank} B_L.$$

Its image is $(Z_K + \operatorname{im} B_L)/\operatorname{im} B_L$; source boundaries already map into target boundaries. This proves the formula, including empty complexes. Computing a flag two-skeleton suffices for H_0, H_1, but does not compute the full flag complex's H_2. Integer ceilings of scaled exact distances preserve the inclusion. For numerical distances, frozen integer labels define an exact combinatorial diagram only after their inequality is checked; this is not an interval certificate of the underlying quantum distances. None of these finite ranks identifies a completed arithmetic determinant or proves GRH.

2.3 A correct DG model of the infinite node

Use cohomological degrees and an uncurved differential of degree $+1$. An odd element ε with $d\varepsilon = 1$ contracts the underlying k-complex of every unital left DG module: $h(m) = \varepsilon m$ satisfies $dh + hd = 1$ by the graded Leibniz rule. Thus this example has zero cohomology, contrary to the original ground-field-resolution claim. An isomorphism on H^0 alone is also insufficient for a DG quasi-isomorphism; all degrees must be checked.

Proposition 2.5 (Nodal Koszul model)**.** *Let k be a field, $R = k[\xi, \eta]$ and $f = \xi\eta$ and $K = R \oplus R\varepsilon$, with $|\varepsilon| = -1$, $\varepsilon^2 = 0$, $dR = 0$ and $d\varepsilon = f$. The augmentation $K \to A = R/(\xi\eta)$, $a + b\varepsilon \mapsto [a]$, is a DG-algebra quasi-isomorphism onto the actual infinite nodal dessin algebra. Branch rescaling $\xi \mapsto q\xi$, $\eta \mapsto q^{-1}\eta$, $\varepsilon \mapsto \varepsilon$ for $q \in k^\times$ lifts to a DG automorphism.*

Proof. Multiplication is $(a + b\varepsilon)(c + e\varepsilon) = ac + (ae + bc)\varepsilon$. The differential kills degree zero and sends $b\varepsilon$ to fb. Its square is zero. For two odd inputs the Leibniz right side is $fbc\varepsilon - bfc\varepsilon = 0$; the other homogeneous cases follow by R-linearity. Multiplication by f is injective in the polynomial domain. Hence $H^{-1}(K) = 0$, $H^0(K) = R/(f)$, and all other groups vanish. The augmentation preserves products and kills boundaries. Rescaling fixes f, so its coefficientwise extension commutes with d and has inverse obtained by replacing q with q^{-1}. This is a one-relation Koszul construction [78, 79]. □

Replacing R by $k[[\xi, \eta]]$ gives the completed order: setting each variable separately to zero maps onto the branch pullback, and the kernel consists precisely of mixed monomials, hence equals $(\xi\eta)$. Rescaling is generally semilinear over the coefficient ring, rather than linear over the fixed diagonal DVR $k[[u]]$, $u = \xi + \eta$. It preserves that DVR as a subring exactly when $q^2 = 1$, and fixes it pointwise exactly when $q = 1$. No Hilbert norm or arithmetic spectrum follows.

The corresponding Lean file checks the actual exterior-line algebra, differential, sign-Leibniz, homotopy and polynomial ambient-resolution identities. Full graded/category/completion objects remain separately scoped. The two theta dessins likewise require endpoint-sensitive Ext: self Ext^1 is zero in both; for the elliptic theta self Ext^3 has dimension two, while for the spherical theta positive even self Ext has dimension two. Outdegree alone does not count self extensions. Minimal A_∞ models use additional graded data [77, §3.3]; m_3 is not automatically a physical curvature.

Chapter 3

Determinant semi-invariants and Schur constructions

Assume k algebraically closed of characteristic zero for invariant-ring statements. A finite-dimensional representation of the *infinite* A has spaces N_i, arrow matrices $N(a)$ satisfying the monomial relations, and base-change group $G = \prod_i \mathrm{GL}(N_i)$. With column vectors, $N(a) \mapsto g_{t(a)} N(a) g_{s(a)}^{-1}$. Let $P_0 = \bigoplus P_i^{a_i}$, $P_1 = \bigoplus P_i^{b_i}$, and $f : P_1 \to P_0$ be a finite path-matrix map. When $\sum a_i \dim N_i = \sum b_i \dim N_i$, define

$$c_f(N) = \det D_f(N), \qquad D_f(N) = \mathrm{Hom}_A(f, N).$$

It is intrinsically a determinant-line section; chosen bases give this scalar.

Proposition 3.1 (Weights and exact homological scope)**.** $c_f(gN) = \prod_i \det(g_i)^{b_i - a_i} c_f(N)$. *Restricted determinants of this form span all semi-invariants on a closed G-stable relation or nilpotence locus. Set $M = \operatorname{coker} f$. On the square locus,*

$$c_f(N) \neq 0 \quad \Longleftrightarrow \quad \mathrm{Hom}(M, N) = 0 \quad \Longleftrightarrow \quad \mathrm{Hom}(M, N) = \mathrm{Ext}^1(M, N) = 0.$$

If f is injective, $\operatorname{coker} D_f = \mathrm{Ext}^1(M, N)$ *and higher Ext vanish. Without injectivity neither that cokernel equality nor higher vanishing follows.*

Proof. Naturality gives $D_f(gN) = G_1 D_f(N) G_0^{-1}$, where G_j repeats the relevant g_i. Take determinants. The contragredient coordinate-ring action has the inverse character. Schofield–van den Bergh's spanning theorem allows oriented cycles [36, Theorem2.3]. Exactness of invariants for reductive G in characteristic zero lifts a fixed-weight function from any closed stable locus to the ambient representation space; restrict the spanning determinants. Injectivity of the path map need not survive that restriction. Finally $\ker D_f = \mathrm{Hom}(M, N)$. Writing $K = \operatorname{im} f$, the exact sequence with projective P_0 expresses $\mathrm{Ext}^1(M, N)$ as $\mathrm{Hom}(K, N)/\operatorname{im} \mathrm{Hom}(P_0, N)$; the epimorphism $P_1 \to K$ embeds this quotient in $\operatorname{coker} D_f$. A square finite matrix with zero kernel has zero cokernel. If f is injective it is the actual length-one resolution, giving the stronger assertion. □

For the node, $f = \times x$, $M = \Lambda/(x)$, $N = \Lambda/(x, y^2)$ give $\dim \operatorname{coker} D_f = 2$ but $\dim \mathrm{Ext}^1(M, N) = 1$. For the elliptic square name arrows so that $a, b : 0 \to 1$, $c, d : 1 \to 0$, permitted cycle *acbd* and forbidden cycle *adbc*. With $f = a$ and $N(a) = 1$, $N(b) = N(c) = N(d) = 0$, its Hom matrix is [1], yet the subsequent forbidden resolution gives $\mathrm{Ext}^{2,3}(M, N) = k$. Thus nonvanishing is not all-degree derived orthogonality.

Proposition 3.2 (What completion does to invariants)**.** *A continuous d-dimensional representation of Λ kills J^d. On the reduced nilpotent representation variety of fixed dimension vector every invariant regular function is constant. Nonzero-weight semi-invariants need not be constant.*

Proof. Continuity with discrete finite-dimensional target kills some J^m; its Loewy filtration has at most d nonzero strict steps. Choose vertexwise complements to this filtration. An arrow sends a layer p into layers $q \geq p+1$. Scaling layer p by z^p conjugates each component by z^{q-p}. At $z = 0$ the representation tends to the zero-arrow representation. Every invariant therefore has the same value at all points; reducedness and the Nullstellensatz give the ring assertion. In the square example the scalar $N(a)$ varies on a nilpotent locus and has weight g_1/g_0, so semi-invariants survive. Formal entries in a projective map are evaluated on this locus by truncating modulo J^d, a legitimate finite polynomial operation. □

On the node, $u = x+y$ is regular and A is free of rank two over $k[u]$. The polynomial presentation $\times(u-\lambda)$ for $\lambda \neq 0$ is injective and its determinant on N is $\det(u_N - \lambda I)$, the characteristic polynomial of u_N up to the sign $(-1)^d$. But $u-\lambda$ is a unit in Λ, with its geometric-series inverse, so those modules do not extend continuously to the completion. An R-free lattice and its u-nilpotent quotients are different categories. On a lattice a separately specified endomorphism F has a meaningful relative characteristic polynomial over R; the scalar base action uI alone does not create Frobenius.

3.1 Young tableaux and a cyclic representation stratum

For a nonempty partition $\lambda \vdash m$, choose a numbering T of its boxes. On $V^{\otimes m}$ let $Y_T = R_T C_T$, the unnormalized row sum followed by the signed column sum. The classical identity $Y_T^2 = h_\lambda Y_T$, where h_λ is the hook product, makes Y_T/h_λ an idempotent in characteristic zero. Its image is $S_\lambda(V)$, one Schur copy, rather than the whole symmetric-group isotypic component [31, 32]. Its character is s_λ, computed by semistandard tableaux (weak rows, strict columns), and

$$\dim S_\lambda(k^d) = \prod_{(i,j)\in\lambda} \frac{d+j-i}{h_{ij}}.$$

Since $f^{\otimes m}$ commutes with the place permutations, it induces $S_\lambda(f)$ and respects composition and zero maps. Applying this at every vertex and arrow therefore gives a genuine representation of the monomial dessin algebra: $S_\lambda(N(b))S_\lambda(N(a)) = S_\lambda(0) = 0$ for a forbidden pair. The empty partition does not have this property: it sends zero arrow maps to the identity of k.

The Littlewood–Richardson rule gives natural intertwiners

$$S_\lambda(V) \otimes S_\mu(V) \cong \bigoplus_\nu S_\nu(V)^{\oplus c^\nu_{\lambda\mu}}.$$

Here $c^\nu_{\lambda\mu}$ counts semistandard tableaux of skew shape ν/λ and content μ whose row-reading word is Yamanouchi. Naturality makes the same decompositions intertwine all the arrows. The tensor operation is vertexwise with synchronous arrow maps, not $\otimes_A$ and not a Hopf-algebra tensor structure. There is no automatic tensor unit preserving these zero relations. These functors are not additive or exact; they cannot simply be applied degreewise to a projective resolution. They also need not preserve the fixed R-action on lattices.

In the elliptic theta set one of the two permitted three-cycle branches to zero. The other has arbitrary maps $X_1 : V_0 \to V_2$, $X_2 : V_2 \to V_1$, $X_3 : V_1 \to V_0$, with all spaces of dimension d. This is a closed representation stratum of our infinite dessin algebra. Put $M = X_3X_2X_1$.

Theorem 3.3 (Cyclic invariants and a local positive kernel)**.** *The invariant ring on this stratum is $k[c_1(M), \dots, c_d(M)]$, where c_j are characteristic coefficients. Its total-arrow-degree Hilbert series is $\prod_{j=1}^{d}(1-t^{3j})^{-1}$. Common multidegree (m,m,m) has basis $\chi_\lambda(M) = \operatorname{tr} S_\lambda(M)$, $\lambda \vdash m$, $\ell(\lambda) \le d$; other multidegrees have no invariants. Products obey the Littlewood–Richardson rule. Over $\mathbb{C}$, if $\|M_i\| \le R_0$ and $0 \le r$ and $rR_0^2 < 1$, the kernel*

$$K_r(M_i, M_j) = \det(I - rM_i \otimes \overline{M_j})^{-1} = \sum_\lambda r^{|\lambda|} \chi_\lambda(M_i)\overline{\chi_\lambda(M_j)}$$

is absolutely convergent and positive semidefinite.

Proof. Cycle-trace generation for quivers, including relation quotients, is the Le Bruyn–Procesi theorem [29, 30]. Every cycle here is a power of the full three-cycle, up to cyclic rotation. In characteristic zero Newton identities give the generators c_j. They are algebraically independent: take $X_1 = X_2 = I$ and arbitrary X_3. Scalar changes at the three vertices force equal arrow multidegrees. Restriction to that same section identifies degree (m,m,m) with degree-m symmetric polynomials in eigenvalues, whose Schur basis and product rule give the assertion. For the kernel use the ordinary Cauchy identity, first as a formal identity in eigenvalues. On Schur modules the operator norm of $S_\lambda(M)$ is at most $R_0^{|\lambda|}$, so its trace is bounded by $\dim S_\lambda(\mathbb{C}^d) R_0^{|\lambda|}$. The dimension Cauchy identity bounds the absolute series by $(1 - rR_0^2)^{-d^2}$. Each summand is a rank-one Gram kernel, proving positivity by absolute summation. □

The term for the empty partition is a constant scalar feature, not an allowed module-valued tensor unit. In dimension two,

$$(\operatorname{tr} M)^2 = \operatorname{tr} \operatorname{Sym}^2 M + \det M, \qquad \operatorname{tr} \operatorname{Sym}^2 M = \tfrac{1}{2}((\operatorname{tr} M)^2 + \operatorname{tr} M^2).$$

More generally $\det(I - zM) = \sum_j (-z)^j \operatorname{tr} \bigwedge^j M$ and its reciprocal is $\sum_m z^m \operatorname{tr} \operatorname{Sym}^m M$. These are actual determinant/Schur connections, not identifications with an arithmetic L-function. On continuous finite-length Λ-modules the monodromy is nilpotent and all positive-degree characters vanish. The displayed Cauchy positivity is local representation-theoretic positivity, not the global Weil form.

Chapter 4

Lattice almost-split sequences and genuine diamond quotients

For the interval dessin let $X = (x)$, $Y = (y)$ in $\Lambda = k[[x, y]]/(xy)$, $R = k[[u]]$, $u = x + y$. A lattice is a finitely generated Λ-module free over R.

Theorem 4.1 (The nodal lattice calculation)**.** *Every lattice is $\Lambda^r \oplus X^a \oplus Y^b$. The almost-split sequences in this lattice category are*

$$0 \to Y \hookrightarrow \Lambda \xrightarrow{\times x} X \to 0, \qquad 0 \to X \hookrightarrow \Lambda \xrightarrow{\times y} Y \to 0.$$

In particular $\tau X = Y$, $\tau Y = X$. Multiplication by u between two copies of either row, followed by reduction modulo u, gives an actual nonzero exact three-by-three diagram.

Proof. Normalize M *inside its total quotient module*: $\overline{M} = BM$, $B = k[[x]] \times k[[y]]$. The conductor gives $u\overline{M} \subset M \subset \overline{M}$. Both branch projections of $W = M/u\overline{M} \subset k^p \oplus k^q$ are onto. Intersect W with the two factors; its remaining quotient identifies their two residual quotients. Separate bases for these pure factors and the common quotient put W into pure first lines, pure second lines and diagonal pairs. Lift branch bases over the DVRs. These are respectively the summands X, Y, Λ. Their endomorphism rings are local.

Exactness of the first sequence is $\operatorname{ann} x = Y$. It does not split: a map $X \to \Lambda$ lands in $\operatorname{ann} y = X$, and its composite with $\times x$ is a nonunit in $\operatorname{End} X = k[[x]]$. Every map $\Lambda \to X$ factors through this epimorphism, $\operatorname{Hom}(Y, X) = 0$, and every nonunit endomorphism of X is divisible by x and factors through $X \hookrightarrow \Lambda \to X$. Classification handles all finite sums; a unit X component would be a retraction. This is right almost splitness. The dual argument for nonsections out of Y proves left almost splitness. Endomorphisms fixing either structure map have constant term one, hence are units, proving minimality. Swap x, y for the other sequence. Finally all three terms are R-free. Multiplication by u is injective and reduction preserves exactness, proving the diagram assertion. □

The lattice AR quiver has arrows $Y \to \Lambda \to X$ and $X \to \Lambda \to Y$; the mesh composites are zero. Its projective vertex Λ is not the endpoint of another nonsplit AR sequence. AR meshes do not mean that all rows and columns of any drawn grid are short exact.

For a second, explicit family fix $n \geq 3$ and the rational Belyi map

$$\beta_n(z) = \frac{1}{1 - T_n(z)^2} = \frac{1}{(1 - z^2)U_{n-1}(z)^2},$$

where T_n, U_{n-1} are Chebyshev polynomials. It has passport $(2n), (2^n), (2^{n-1}, 1, 1)$. Its contracted dual graph is a path, identifying its genus-zero dessin. The associated infinite algebra has vertices

$1, \dots, n$, endpoint loops l, r, opposite arrows $a_i : i \to i+1$, $b_i : i+1 \to i$, and precisely the relations $l^2, r^2, a_i b_i, b_i a_i$. Its single permitted cycle is $l a_1 \cdots a_{n-1} r b_{n-1} \cdots b_1$; the order rank is $(2n)^2$.

Retain one arrow at each edge in an orientation Ω, and kill its opposite. The quotient is exactly the string algebra $H_n(\Omega)$ of Huang–Lin–Su [46]; the killed-arrow ideal contains J^{n+2}, so it is also an actual quotient of Λ_n. Inflation identifies its module category with the full abelian quotient-annihilator subcategory $\mathcal{C}_\Omega$ of Λ_n-modules. This is generally not extension closed in the whole order category. The imported AR property is intrinsic to $\mathcal{C}_\Omega$, not automatically an ambient lattice or finite-length AR property. The extended edition gives nine explicit string modules, all twelve maps and the four exact meshes from the supplied diamond resource, now situated in this actual dessin quotient.

The other supplied resources also have a precise home. For the interval order the subcategory annihilated by J^2 is $\operatorname{Mod} B_0$, $B_0 = \Lambda/J^2$. This is a domestic string quotient, not itself a gentle algebra. Inflation is full and preserves purity, and $\operatorname{Zg} B_0$ is a closed subspace of $\operatorname{Zg} \Lambda$. Ringel's infinite-word/pure-injective program and its proof by Puninski–Prest apply there [43, 44]; the isolated band xy^{-1} gives Krull–Gabriel and relative Cantor–Bendixson dimension two by [45, Theorem10.19]. This is not an ambient rank calculation for all Λ-modules. The parameter in $x = J_2, y = \lambda J_2$ survives even though all cycle traces vanish; the pp condition $\exists v\ (z = xv \ \wedge \ (y - \lambda x)v = 0)$ detects it. These modules are u-torsion and are not nonzero order lattices. Infinite-string and locally finite AR theorems must retain their distinct finiteness hypotheses; a surviving permitted cycle has infinitely many paths at a vertex.

4.1 Polynomial strings, completed lattices and the Fukaya category

Crawley–Boevey's theorem [38, Theorems1.1–1.4] applies directly to the infinite polynomial dessin algebra: its finitely controlled modules decompose into strings and finite-dimensional bands; its pointwise artinian modules additionally allow primitive injective bands. For our finite quiver, these conditions mean finitely generated and artinian respectively. The words may be infinite, but their modules have algebraic direct-sum bases. This is not a classification of every module or of arbitrary formal completions.

In fact no nonzero completed-order lattice, restricted to A, meets either finiteness condition. The polynomial A is finite over $k[u]$: remove full turns from sufficiently long paths as in Proposition 1.1. If an R-free lattice were finitely generated over A, it would be finite torsion free, hence free, over the PID $k[u]$. Multiplication by $1 - u$ would then fail to be onto, whereas it is a unit over $R = k[[u]]$. Also $M \supsetneq uM \supsetneq u^2M \supsetneq \cdots$ excludes artinianity. For a concrete indecomposable outside the ordinary string/band list take $k[[x]]$ with $y = 0$: its endomorphisms are multiplication by formal series, so its endomorphism ring is local. Its x is injective and nonsurjective, while $1 - x$ is invertible; these properties exclude every pure-x ordinary string or band. The extended edition gives the full word argument.

The Fukaya connection requires equally precise categories. Lekili–Polishchuk explicitly allow infinite-dimensional locally gentle algebras, but their equivalence is for *perfect dg modules* of a homologically smooth algebra, with specified grading, line field and stops [66, Definition3.1.1, Lemma3.1.3, Theorem3.2.2]. Every nonempty closed dessin here has both permitted and forbidden cycles, so its polynomial algebra is neither proper nor smooth by their criterion. This does not exclude appropriate singular or completed variants; it prevents a direct use of that particular theorem. Infinite word, graded curve and geodesic are not interchangeable without a surface realization and boundary/grading data.

There is a genuine positive example inside our setting: the polynomial interval quotient $A/(y) =$

$k[x]$ is still infinite dimensional, is smooth, and has no forbidden cycle. Its perfect category has the partially wrapped annulus model with one stop total. In degree zero $\mathrm{Perf}(k[x]) = D^b(\mathrm{mod}_{\mathrm{fg}}\, k[x])$. Inflation of this quotient is fully faithful on ordinary modules, but not on derived categories: $\mathrm{Ext}^2_A(k[x], k[x]) = k$, whereas $\mathrm{Ext}^2_{k[x]}(k[x], k[x]) = 0$. The former follows from the alternating y, x resolution. Thus this quotient bridge does not identify the whole closed dessin's perfect category with the annulus category.

Finally, Leavitt path algebras *can* fail invariant basis number, but need not. The permitted-state Laurent algebras here have finite-dimensional matrix quotients, and therefore invariant basis number. The polynomial and completed dessin algebras have their vertex-simple quotients, giving the same conclusion. The complex Leavitt algebra of G_α below is a dense *-subalgebra of its graph C*-algebra, on that specified graph; it is not the original gentle algebra with ordinary CK1 imposed.

Chapter 5

Leavitt relations, the constrained Fock algebra and spectrum

Work now over $\mathbb{C}$. Ordinary Leavitt and graph C* constructions [47, 48] cannot simply impose our original forbidden products: if $ab = 0$ and CK1 says $a^*a = p_{t(a)}$, then $0 = a^*ab = b$. Every arrow is a forbidden successor, hence every arrow and then every vertex is zero. CK2 is not needed. The ordinary graph-Toeplitz CK1 setting has the same collapse.

The valid permitted-arrow-state graph instead consists of the disjoint directed σ-cycles. Its Leavitt algebra is $\bigoplus_c M_{|c|}(k[z, z^{-1}])$, and its graph C* algebra is $\bigoplus_c M_{|c|}(C(\mathbb{T}))$. These forget the α-gluing; both theta dessins give the same answer. They are not the completed original order. Nor is the ordinary Toeplitz algebra of a cycle of length $\ell > 1$ equal to $M_\ell(\mathcal{T})$: their K_0 ranks are ℓ and one respectively [50].

Let $\mathcal{H} = \ell^2(\mathcal{P})$ for all permitted finite paths, including vacua e_v. Define $L_a\delta_p = \delta_{ap}$ when the prefix is permitted and composable, and zero otherwise. Let P_v project onto paths starting at v, $Q_a = L_aL_a^*$ and v_v onto the vacuum. Then

$$L_aL_{\phi(a)} = 0, \quad L_a^*L_a = P_{t(a)} - Q_{\phi(a)} = v_{t(a)} + Q_{\tau(a)}, \quad P_v - \sum_{s(a)=v} Q_a = v_v.$$

These follow on basis vectors. The different initial projection avoids CK1 collapse. Write $\mathcal{T}_A = C^*(P_v, L_a)$, a constrained-path Fock C* algebra in the monomial/subproduct setting [51, 52]. The polynomial A acts faithfully: applying a finite path sum to the sum of vacua recovers its coefficients. This representation need not extend to all formal Λ series: $\sum_{m\geq 0} c^m$ along a cycle would send its vacuum to a nonsquare-summable sum.

Theorem 5.1 (Compact extension and incidence index)**.** *Let $\mathcal{H}_v$ be the terminal-path sector. There is an exact sequence*

$$0 \longrightarrow \bigoplus_{v\in Q_0} \mathcal{K}(\mathcal{H}_v) \longrightarrow \mathcal{T}_A \longrightarrow \bigoplus_{c\in \mathrm{cyc}(\sigma)} M_{|c|}(C(\mathbb{T})) \longrightarrow 0.$$

With $\delta[u] = [1 - W^*W] - [1 - WW^*]$, its boundary map is $\delta(c) = -\sum_{h\in c} e_{[h]}$, minus the unsigned incidence map B_Γ of the cellular graph. Thus, for its E edges,

	$K_0(\mathcal{T}_A)$	$K_1(\mathcal{T}_A)$
Γ *bipartite*	$\mathbb{Z}^{E+1}$	$\mathbb{Z}$
Γ *nonbipartite*	$\mathbb{Z}^E \oplus \mathbb{Z}/2$	0.

Proof. All prefixes preserve the terminal sectors. For paths p, q ending at v, $L_p v_v L_q^* = |\delta_p\rangle\langle\delta_q|$. Therefore the vacuum ideal is exactly the displayed sum of compacts: it contains these matrix units and that sum is itself an ideal. In the quotient, L_a has initial projection $Q_{\tau(a)}$ and range Q_a, a graph CK family for the permitted-state cycles. The Q_a have infinite rank and nonzero quotient images; the length gauge action descends. Gauge-invariant uniqueness [48, Theorem2.1] identifies the quotient as claimed.

For a cycle c based at arrow a, lift its corner unitary by $W = L_c Q_a + (1 - Q_a)$. Then $W^*W = 1$ and $1 - WW^* = Q_a - L_c Q_a L_c^*$ projects onto the first $|c|$ paths starting with a. Their terminal vertices count exactly its incident darts, including twice for a loop. This proves the index formula. The six-term exact sequence gives $K_1 = \ker B_\Gamma$ and $0 \to \operatorname{coker} B_\Gamma \to K_0 \to \mathbb{Z}^{\#\,\mathrm{cyc}\,\sigma} \to 0$. The free last term splits abstractly. Spanning-tree integer elimination gives Smith entries 1 repeated $V - 1$ times and one zero in the bipartite case; an odd cycle instead adds the entry two. This proves the groups. □

The nodal interval has $K_0 = \mathbb{Z}^2$, $K_1 = \mathbb{Z}$; the single-loop sphere has $\mathbb{Z} \oplus \mathbb{Z}/2$, zero. Both theta dessins have $\mathbb{Z}^4$, $\mathbb{Z}$. Coarse K-theory does not recover genus or the arithmetic factors.

5.1 A graph presentation and an actual pullback

The Fock algebra itself has a graph presentation, on a different graph from the original gentle quiver. Let G_α have vertices q_h for $h \in H$ and sinks b_e for $e \in Q_0$, and edges

$$s_h : q_h \to q_{\tau h}, \qquad t_h : q_h \to b_{[\tau h]}.$$

Proposition 5.2. *$C^*(G_\alpha) \cong \mathcal{T}_A$, by $q_h \mapsto Q_{a_h}$, $b_e \mapsto v_e$, $s_h \mapsto L_{a_h} Q_{a_{\tau h}}$ and $t_h \mapsto L_{a_h} v_{[\tau h]}$. The integer graph relation at h is $q_h - q_{\tau h} - b_{[\tau h]}$. Eliminating these relations recovers $K_1 = \ker B_\Gamma$ and $K_0 \cong \operatorname{coker} B_\Gamma \oplus \mathbb{Z}^{\#\,\mathrm{cyc}\,\sigma}$.*

Proof. The two edges at q_h have orthogonal initial pieces and orthogonal ranges summing to Q_{a_h}, by the Fock initial-projection identity. All vertex projections are nonzero. The length gauge acts with degree one on both edge families, so gauge-invariant uniqueness applies. They generate since $L_{a_h} = s_h + t_h$ and $P_e = v_e + \sum_{[h]=e} Q_{a_h}$. In the integer matrix a kernel coefficient is constant around each permitted cycle; its sink equations are exactly $B_\Gamma c = 0$. In the cokernel, eliminate all but one state per cycle; its remaining relation is the sum of its incident sink generators. The remaining cycle generators are free, proving the stated groups. □

For the nodal interval, G_α has two loop vertices, each with an exit to the common vacuum sink. Chirvasitu–Hajac–Tobolski's actual pullback theorem [65, Theorem3.4] gives

$$\{T \in \mathcal{T}_A : \pi(T) \in \mathbb{C}^2\} \cong C^*(E_1), \qquad \mathbb{C}^2 \hookrightarrow C(\mathbb{T})^2 \text{ by constants},$$

where E_1 has the same three vertices and countably many arrows from each loop vertex to the sink, with no loops. The arrow numbered $n \geq 0$ maps to loop^n followed by exit. This algebra is AF, with $K_0 = \mathbb{Z}^3$, $K_1 = 0$. The extended edition verifies every hypothesis. The theorem does not turn arbitrary cycle-vertex identifications into pullbacks: its first graph is acyclic and its path functor must cover all pointed paths. Its sink-extension Theorem4.3 has further injection and path-coverage requirements.

5.2 A separate diagonal-fiber C* completion retaining the pairing

The formal order's residue gluing cannot be copied by taking diagonals of arbitrary full matrices: $\operatorname{diag}(E_{12}E_{21}) \neq \operatorname{diag}(E_{12})\operatorname{diag}(E_{21})$. For $\ell > 1$ there is no nonzero *-homomorphism from $M_\ell(C(\mathbb{T}))$ to a commutative C*-algebra, as restriction to its constant matrix units shows. Restrict the distinguished fiber first. Define

$$D_\ell = \{f \in C(\mathbb{T}, M_\ell(\mathbb{C})) : f(1) \text{ is diagonal}\}, \qquad \mathcal{D}_H = \Big(\prod_c D_{|c|}\Big) \underset{\mathbb{C}^H}{\times} \mathbb{C}^{Q_0},$$

where the first map evaluates diagonal entries at one and the second repeats λ_e at the two darts paired by α.

Theorem 5.3 (A faithful polynomial pullback model)**.** *There is a split exact sequence*

$$0 \to \bigoplus_c C_0(\mathbb{T} \setminus \{1\}, M_{|c|}) \to \mathcal{D}_H \to \mathbb{C}^{Q_0} \to 0,$$

so $K_0(\mathcal{D}_H) = \mathbb{Z}^{|Q_0|}$ and $K_1(\mathcal{D}_H) = \mathbb{Z}^{\#\operatorname{cyc}\sigma}$. The polynomial dessin algebra embeds faithfully and generates this C-algebra with its adjoints. This embedding does not extend to a unital algebra map from all of Λ.*

Proof. The section consists of the constant paired diagonal projections. The kernel is the displayed vanishing fiber, a sum of matrix suspensions, giving the groups by split exactness and suspension. For an explicit embedding set $g(z) = |1 - z|^2/4$, choose one cut arrow per permitted cycle, and send a_h to $g(z)z^{\epsilon_h}E_{h,\tau h}$ in its branch, where $\epsilon_h = 1$ at the cut and zero otherwise. Send e_e to the constant paired diagonal projection. Every forbidden product is zero. A full cycle at h maps to $w_c(z)E_{hh}$, $w_c = g^{|c|}z$. This scalar function is injective on the circle: away from its unique zero at one its argument recovers z. Continuous functional calculus therefore supplies every $f(z)E_{hh}$ with $f(1) = 0$. Multiplying by path images and approximating division away from one supplies every vanishing off-diagonal entry. Together with the constant paired diagonals these generate $\mathcal{D}_H$. Path normal forms in a fixed entry are a nonzero prefactor times a polynomial in w_c; its infinite range proves independence. Evaluation at one first separates the zero-length coefficients. Finally for $z_0 \neq 1$, $1 - w_c(z_0)^{-1}c_h$ is a unit in the formal order, but its proposed image is singular at z_0. A unital map preserves units, proving nonextension. □

This is the C* algebra generated by a faithful polynomial representation and its adjoints, distinct from the completed order and from $\mathcal{T}_A$. The norm closure of the polynomial image alone need not contain those adjoints. Their K groups already differ. The pairing belongs to the labelled presentation; an unmarked isomorphism class need not recover the ribbon ordering. No arithmetic descent, Frobenius action or completed-L positive determinant is inferred from this additional valid gluing model.

Proposition 5.4 (The degree spectral triple)**.** *Define $N\delta_p = |p|\delta_p$ on $\{\xi : \sum_p |p|^2|\xi_p|^2 < \infty\}$. With the polynomial creation/annihilation *-algebra this is an ungraded spectral triple, p-summable exactly for $p > 1$. With N_+^{-s} zero on the kernel,*

$$\operatorname{Tr} e^{-tN} = E + \frac{2E}{e^t - 1}, \quad \operatorname{Tr} N_+^{-s} = 2E\zeta(s), \quad \operatorname{Tr}\big(\chi(N)N_+^{-s}\big) = 2EL(s,\chi)$$

for $t > 0$ and $\operatorname{Re} s > 1$ in the last two formulas, where χ is an externally chosen Dirichlet character.

Proof. There are E vacua and $2E$ paths of every positive length: each starting arrow has a unique continuation. The real diagonal operator is self-adjoint on the stated maximal domain; finite supports are a core and its resolvent is compact. Prefixes preserve the domain and $[N, L_a] = L_a$, $[N, L_a^*] = -L_a^*$, so polynomial commutators are bounded. The trace formulas and summability reduce to the corresponding scalar series. The character multiplier is bounded; membership in $\mathcal{T}_A$ is not asserted. □

Length parity anticommutes with the creators but commutes with N, so it is not an even-spectral-triple grading. The ordinary odd Fredholm class of this positive N is trivial: $N(1 + N^2)^{-1/2} - I$ is compact. The spectrum depends only on E; zeros of the scalar zeta trace are not eigenvalues of N.

Chapter 6

Arithmetic attachment, descent and the remaining comparison

The compact ideal gives a precise home for an arithmetic determinant, with no claim that the arithmetic is derived from the dessin. Fix one terminal sector. Its two paths of each length $n \geq 1$ give orthonormal vectors $\xi_n = (\delta_{p_{n,1}} + \delta_{p_{n,2}})/\sqrt{2}$ and an isometry $U : \ell^2(\mathbb{N}_{\geq 1}) \to \mathcal{H}_v$.

For a nonprincipal character χ put $A_n = \sum_{j \leq n} \chi(j)$, $B_0 = \sup |A_n| \leq q_\chi$, and, on $2^k \leq n < 2^{k+1}$, set

$$w_n = \sqrt{n}(k+1), \quad u_n = A_n/w_n, \quad v_n(s) = w_n(n^{-s} - (n+1)^{-s}), \quad \varphi_s(z) = \sum_n v_n(s) z_n - z_1.$$

Here $u_1 = 1$. For $\operatorname{Re} s > 0$, $u, v(s) \in \ell^2$ and the pairing is complex linear, with no conjugation of s. Define

$$\widetilde{K_s} = U(u \otimes \varphi_s)U^*, \qquad \det_F(I + \widetilde{K_s}) = L(s, \chi).$$

Indeed dyadic blocks give $\|u\|^2 \leq 2B_0^2$, and on a compact set $\operatorname{Re} s \geq \sigma_0 > 0$, $|s| \leq M$, the squared v tail is bounded by $M^2 \sum_{k \geq J} (k+1)^2 2^{-2\sigma_0 k}$. Thus the rank-one family is trace-norm holomorphic. Its determinant is $1 + \varphi_s(u)$, equal by Abel summation to L. Replacing v by $P_N v$ and adding $A_N(N+1)^{-s} e_1^*$ to the functional gives exactly every raw partial sum S_N, with compact-uniform trace-norm convergence; $\|UXU^*\|_1 = \|X\|_1$. For primitive χ, completion replaces the functional by $g(s) \sum v_n(s) z_n - z_1$, with the standard nonzero gamma factor g, rather than multiplying the whole old functional. The extended edition supplies the quantitative estimates.

This inserts a scalar encoding into one actual dessin compact ideal; it is not known to be A-linear, a derived chain map or Frobenius compatible. A common fixed positive metric cannot make this same fixed-range family symmetric for all critical heights: symmetry forces its functionals to be proportional, whereas the coefficient ratio at heights $0, t \neq 0$ is asymptotic to $(\sigma + it)n^{-it}/\sigma$, with two opposite subsequential limits. Different positive realizations remain possible.

Proposition 6.1 (Complex dessin data do not determine arithmetic descent)**.** *The rational Belyi pairs $E_d : y^2 = x^3 - d$, $\beta_d = x^3/d$, for $d = 1, 2$, are isomorphic over $\mathbb{C}$ but have distinct Frobenius polynomials at the good prime seven: $1 - 4T + 7T^2$ and $1 - T + 7T^2$.*

Proof. Choose $a^3 = d$, $b^2 = d$. The projective isomorphism $(x, y) \mapsto (ax, by)$ from E_1 to E_d preserves the Belyi map. The degree-six clean passports are the elliptic theta passport already computed. Directly counting y for $x = 0, \ldots, 6$ gives respectively $(0, 1, 1, 0, 1, 0, 0)$ and $(0, 0, 0, 2, 0, 2, 2)$. Including infinity yields four and seven points, hence $a_7 = 8 - \#E_d(\mathbb{F}_7) = 4, 1$. Both discriminants $-432d^2$ are nonzero modulo seven. □

Any invariant of the complex dessin or its undecorated order/Fock algebra alone is the same for these two inputs, so cannot recover both factors without descent data. This does not obstruct a theory including a specified rational model and compatible Galois action. Elliptic H^1 has weight one and unshifted center $s = 1$, unlike Dirichlet center $1/2$; the example is not a counterexample to GRH.

6.1 A constructive arithmetic benchmark on the theta dessin

The preceding twists can be distinguished constructively once their finite-field descent data are retained. This closes the elementary local-factor computation, not the global positive-determinant problem. Let $\kappa = \mathbb{F}_q$, $\operatorname{char}\kappa \neq 2, 3$ and $d \in \kappa^*$. Put $E_d : y^2 = x^3 - d$ and $a_q(d) = q + 1 - \#E_d(\kappa)$. For $q \equiv 1 \pmod 3$, fix a nontrivial cubic character ρ and the quadratic character η, both extended by zero at zero. Define

$$J = \sum_{u \in \kappa} \rho(u)\eta(1-u), \qquad j = -\eta(-1)J, \qquad \lambda_d = \eta(d)\rho(d), \quad \pi_d = \lambda_d j.$$

Theorem 6.2 (Uniform local factor)**.** *For every such prime power and nonzero d,*

$$a_q(d) = \pi_d + \overline{\pi_d}, \quad |\pi_d|^2 = q, \quad P_d(T) := 1 - a_q(d)T + qT^2 = (1 - \pi_d T)(1 - \overline{\pi_d}T).$$

If $q \equiv 2 \pmod 3$, instead $a_q(d) = 0$. The split-case values lie in $\mathbb{Z}[\omega]$, $\omega^2 + \omega + 1 = 0$.

Proof. Cube fibers have size $1 + \rho(t) + \overline{\rho(t)}$, including at zero; the first term is the literal constant one, not the zero-extended trivial character. Counting square fibers gives $a_q(d) = -\sum_x \eta(x^3 - d)$. Grouping by $t = x^3$ removes the constant term since $\sum_t \eta(t - d) = 0$. Substitution $t = du$ gives $\sum_t \rho(t)\eta(t - d) = \rho(d)\eta(-d)J$; the other term is its conjugate. This proves the signed trace formula.

For a nontrivial additive character ψ, write $G(\chi) = \sum_x \chi(x)\psi(x)$. Character orthogonality gives $|G(\chi)|^2 = q$ for nontrivial χ: substitute $x = uy$ in its squared norm; the inner sum over $y \neq 0$ is $q - 1$ at $u = 1$ and -1 otherwise. Grouping $G(\rho)G(\eta)$ by $x + y$ gives $JG(\rho\eta)$, the zero-sum fiber vanishing since $\rho\eta$ is nontrivial. The three Gauss norms yield $|J|^2 = q$. Neither purity nor RH was assumed. The remaining signs and character values have modulus one. For $q \equiv 2 \pmod 3$ cubing is bijective, so the quadratic-character sum is zero. Finally all split-case summands are signs times cube roots of unity. These are the classical Gauss–Jacobi methods [68, pp.499–502], with our normalization proved explicitly. □

At $q = 7$, choose $\rho(3) = \omega$. Then $j = 3 + 2\omega$, $\lambda_2 = \omega^2$, and $\pi_2 = -1 - 3\omega$, giving the two factors already counted. At $q = 13$, $\rho(2) = \omega$ gives $J = 1 + 4\omega$ but $j = -1 - 4\omega$; this detects the essential sign hidden by the first example.

6.2 A genuine cellular carrier, and what still fails for the order

Assume $q \equiv 1 \pmod 3$ in this cellular construction. The elliptic theta dessin has cellular chains $C_2 = \mathbb{Q}$, $C_1 = \mathbb{Q}^3$, $C_0 = \mathbb{Q}^2$. Orient the three edges from v_+ to v_-; then $\partial_1(e_i) = v_- - v_+$ and $\partial_2 = 0$. Thus H_1 is the sum-zero plane, with basis $e_0 - e_1, e_1 - e_2$. Rotation σ acts there by

$$C = \begin{pmatrix} 0 & -1 \\ 1 & -1 \end{pmatrix}, \qquad G = \begin{pmatrix} 2 & -1 \\ -1 & 2 \end{pmatrix}.$$

G is the actual Euclidean edge Gram matrix in this basis. The deck involution α acts as $-I$. Consequently the six-element deck group $\langle \sigma, \alpha \rangle$ acts on this homology and permutes the original quiver and its entire projective resolution.

Write $\pi_d = A_d + B_d\omega$. Its multiplication action on this *actual cellular* plane is

$$M_d = A_d I + B_d C = \begin{pmatrix} A_d & -B_d \\ B_d & A_d - B_d \end{pmatrix}, \qquad \det(I - TM_d) = P_d(T), \qquad M_d^t G M_d = qG.$$

This constructs the local matrix from finite-field character sums and the dessin's deck action, rather than fitting its trace. Positivity follows from $2x^2 - 2xy + 2y^2 = (x-y)^2 + x^2 + y^2$. The normalized matrix is G-unitary, not asserted self-adjoint. The extended edition supplies a rational cellular chain lift, its exact determinant cancellation, and Kummer descent compatibility on homology. Its odd-over-even determinant ratio is the classical finite-field curve zeta function

$$Z(E_d/\kappa, T) = \frac{P_d(T)}{(1-T)(1-qT)}.$$

Identification with the geometric ℓ-adic Frobenius polynomial uses the standard elliptic trace and determinant theorem; a canonical integral comparison or an order-derived Frobenius functor has not been constructed here.

There is also a precise obstruction to extending this same real two-dimensional carrier to $q \equiv 2 \pmod 3$. Frobenius then conjugates the cubic deck action. The relation $MC = C^2 M$ forces $M = \left(\begin{smallmatrix} a & b \\ a+b & -a \end{smallmatrix}\right)$, whose determinant is $-a^2 - ab - b^2 \le 0$, contradicting the required positive determinant q. This excludes that real carrier with its fixed deck action, not complex or enlarged Hilbert–Pólya constructions. The extended edition gives a compatible complex local replacement.

For the following insertion test use the characteristic-zero theta order $\Lambda_{\mathbb{Q}}$ over $R_{\mathbb{Q}} = \mathbb{Q}[[u]]$, with residue simple $S_e = \mathbb{Q}$. The limitation is concrete. The deck action has finite order and cannot alone supply the norm-$\sqrt{q}$ Jacobi coefficient. Inserting M_d into $S_e \otimes \mathbb{Q}^2$ gives an actual residue-module endomorphism with determinant P_d, but that simple is not perfect over the order and choosing it breaks full deck symmetry. Inserting the same matrix $\Lambda_{\mathbb{Q}}$-linearly into the regular projective instead gives the $R_{\mathbb{Q}}$-determinant P_d^{18}, or P_d^6 on $e\Lambda_{\mathbb{Q}} \otimes \mathbb{Q}^2$. Taking a root is not an established determinant-line comparison; a deck-semilinear lift is a different map. These surviving multiplicity/equivariance obligations prevent promoting the local computation to the required arithmetic order functor.

For the global comparison fix a nonzero rational d and use its good reductions. The finite-field curve zeta has center $1/2$ after $T = q^{-s}$. The *global elliptic* L-function over $\mathbb{Q}$ has unshifted center one, whereas Dirichlet L-functions have center $1/2$. Local weight-one purity does not determine either global zero set. The elementary local bound proves absolute convergence of the elliptic Euler product on $\operatorname{Re} s > 3/2$; the new local identities give no determinant-preserving continuation with the desired global positive spectrum.

6.3 Arbitrary projective actions: an obstruction and a genuine determinant repair

The preceding tensor test has a stronger replacement. Keep the characteristic-zero completed elliptic theta order Λ over $R = \mathbb{Q}[[u]]$, and write $K = \mathbb{Q}((u))$. All determinants in the next theorem are *ordinary underlying-R determinants*; they are not reduced norms.

Theorem 6.3 (Projective determinant multiplicity)**.** *Let P be any finitely generated projective right Λ-module and $f \in \mathrm{End}_\Lambda(P)$. Then $P \simeq \bigoplus_{i=0}^{2} (e_i\Lambda)^{n_i}$. Let $A_i \in M_{n_i}(\mathbb{Q})$ be the induced maps on its three top multiplicity spaces. Then*

$$\det_R(1 - Tf)\Big|_{u=0} = \left(\prod_{i=0}^{2} \det(1 - TA_i)\right)^6.$$

For any bounded complex of these projectives and any Λ-linear chain endomorphism, its alternating determinant ratio specializes to a sixth power in $\mathbb{Q}(T)$. Generically, the ordinary ratio is a cube in $K(T)$.

Proof. The arrow ideal is the Jacobson radical: its elements admit geometric-series inverses after subtracting from one, and the quotient is $\mathbb{Q}^3$. A projective's top lifts to a map from the displayed sum; Nakayama gives surjectivity, projectivity splits it, and another application of Nakayama kills the kernel.

Put $B = \Lambda/u\Lambda$. Each e_iB has path layers of dimensions $1, 2, 2, 1$: the identity, two length-one paths, two length-two paths, and one length-three path. The two full cycles based at i add to ue_i, so become negatives; all length-four paths vanish. A positive-length entry of a projective homomorphism strictly raises path length. Consequently the associated graded map has six copies of $A = \mathrm{diag}(A_0, A_1, A_2)$, giving the formula by triangular block determinants. Base change of determinants justifies specialization. Multiplicativity along filtrations is ordinary linear algebra, consistent with [69, Tags0FJ9,0GSX]; no purity assumption enters.

Each term's determinant has constant term one in T, so every denominator has nonzero specialization. Taking the finite alternating product therefore preserves the sixth power, even after cancellation. Finally $\Lambda_K = M_3(K) \times M_3(K)$; a projective's branch modules are sums of three-dimensional simples. A commuting endomorphism acts on each multiplicity space, repeating every factor three times. This proves the generic assertion. □

Thus no such ordinary perfect-complex ratio can equal the constant-in-u quadratic $P_d(T)$, or the full local curve zeta $P_d(T)/((1-T)(1-qT))$. For P_d, the valuation at infinity is -2, not a multiple of six. For the zeta ratio, $P_d(1) = q + 1 - a_q > 0$ by the local bound $|a_q| \le 2\sqrt{q} < q + 1$, so its pole at $T = 1$ is simple. This also covers square prime powers where the numerator may have a double root. It is an obstruction for the specified ordinary determinant and linear category, not all spectral or determinant theories.

There is nevertheless a *genuine integral functor* removing this multiplicity. Choose a permitted branch and its cycle cut. Its projection $\Lambda \to B_+ \subset M_3(R)$ makes the column lattice $W_+ = R^3$ a left Λ-module. Define

$$\Phi_+ : \mathrm{Perf}(\Lambda) \longrightarrow \mathrm{Perf}(R), \qquad P^\bullet \longmapsto P^\bullet \otimes_\Lambda W_+.$$

Bounded projectives compute this derived tensor functor; flatness of W_+ on all modules is unnecessary. Since $e_iW_+ \simeq R$, its determinant on $e_i\Lambda \otimes_{\mathbb{Q}} V$ with external action $1 \otimes M_d$ is exactly P_d, whereas on the regular module it is P_d^3. This is a defined change of determinant functor, not an arbitrary polynomial root. It does not construct the arithmetic action independently: the already computed M_d is still the input.

The price of this repair is precise. Branch swap α exchanges W_+ and W_-; pairing them yields P_d^2 on that basic-projective input. The chosen branch determinant cannot intertwine α on all endomorphisms: the corner unit $e_i + c_i^+$ acting on $e_i\Lambda$, with c_i^+ a plus full cycle, acts on its determinant by $1 + u$, whereas its α-image acts by one. Also no rank-one-per-vertex column lattice supported on one branch admits an R-linear lift of the rotation σ fixing u. Its three nonzero arrow

scalars have nonnegative u-valuations summing to one; an invertible cyclic lift would make all three equal. This contradiction concerns that lattice, not every determinant-level rotation comparison. Ramification $u = v^3$ *and a new lattice* with all three arrow scalars v admits such a rotation, changing the stipulated base/lattice data. A descent-compatible arithmetic determinant retaining the required symmetry and a global positive realization remains open.

6.4 Tame descent: a surviving order and a sharper obstruction

We now test the proposed ramified repair rather than assume that its rotation descends. Extend coefficients explicitly to $k = \mathbb{Q}(\omega)$, $\omega^2 + \omega + 1 = 0$. Put $R = k[[u]]$, $S = k[[v]]$, $u = v^3$, and let $g(v) = \omega v$, fixing k. On the balanced plus column $W = S^3$, let $C\epsilon_i = \epsilon_{i+1}$ and

$$\Theta = Dg, \qquad D = \operatorname{diag}(1, \omega^2, \omega).$$

The plus arrows act by $vE_{i,i-1}$, and minus arrows by zero. Direct calculation gives $\Theta^3 = 1$, compatibility of Θ with this Λ_R-action, and

$$\Theta C = \omega^2 C\Theta, \qquad L = W^\Theta = R\epsilon_0 \oplus Rv\epsilon_1 \oplus Rv^2\epsilon_2.$$

Thus invariants restore precisely the original cut lattice. The extension $R \to S$ is finite *free* of rank three and faithfully flat; the group quotient is not a torsor at $v = 0$. The comparison $S \otimes_R L \to W$ has matrix $\operatorname{diag}(1, v, v^2)$, determinant u and cokernel $S/(v) \oplus S/(v^2)$. Hence this semilinear group action alone is not effective descent of the column to R. This is the explicit local root-stack situation, consistent with the trivial-stabilizer criterion for vector-bundle descent [70, Theorem10.3]; no stack theorem is needed for the displayed calculation.

Two positive constructions survive. The determinant line $\bigwedge_S^3 W$ has trivial D and C actions and does descend, but the natural map

$$\det_R(L) \longrightarrow (\det_S W)^\Theta$$

has image uR inside R, not an isomorphism. Determinant and coarse invariants cannot be interchanged while dropping this nonunit comparison. Also the *carrier* endomorphism algebra $\operatorname{End}_S(W)^\Theta$, conjugated to the invariant basis, is exactly the hereditary order with entries R on and below the diagonal and uR above. Its rotation descends as $\operatorname{Ad}(A)$, where

$$A = \begin{pmatrix} 0 & 0 & u \\ 1 & 0 & 0 \\ 0 & 1 & 0 \end{pmatrix}, \qquad A^3 = uI.$$

The algebra automorphism has order three although A is not an integral unit. This is not $\operatorname{End}_\Lambda(W)$ or a descended arithmetic cohomology group.

The natural arithmetic attempt fails: $aI + bC$ does not commute with Θ when $b \neq 0$, as in both prime-seven Jacobi examples. The original cellular sum-zero plane is not Θ-stable either. Replacing C by vC does give the descended operator A on L, but

$$\det(1 - T(aI + bA)) = (1 - aT)^3 - ub^3T^3,$$

whose special fiber is $(1 - aT)^3$, not the required local quadratic. These carrier maps are not automatically Λ-linear arithmetic endomorphisms.

There is a stronger category-level conclusion.

Theorem 6.4 (Full-deck coefficient kernels)**.** *Let W_0 be a finite R-free left Λ_R-module on which the central u acts by the given scalar. Suppose it has invertible R-linear intertwiners lifting the order automorphisms σ and α. Then, for some $m \geq 0$, every $e_i W_0$ has rank $6m$. For any finite projective P and Λ_R-linear $f : P \to P$, let A_i be its top blocks. The genuine coefficient functor $\Phi_{W_0} = - \otimes^{\mathbf{L}}_{\Lambda} W_0$ satisfies*

$$\det_R(1 - T\Phi_{W_0}(f))\Big|_{u=0} = \left(\prod_i \det_k(1 - TA_i)\right)^{6m}.$$

Bounded perfect ratios retain this exponent. Thus this whole class of full-deck, fixed-center finite free coefficient kernels cannot supply either the single local quadratic or the full local curve zeta.

Proof. In the generic fiber intersect W_0 with its two central branch summands to obtain finite free integral lattices $W_\pm$; an integral direct-sum decomposition is not assumed. Rotation preserves them and branch swap exchanges them. On a branch let the common vertex rank be r. The three arrow matrices have cyclic product uI_r. Their determinant valuations are nonnegative, sum to r, and rotation intertwiners make them equal. Therefore $3 \mid r$. Branch swap makes the two ranks equal, so the full vertex rank is $6m$.

For the determinant formula, filter W_0/uW_0 by the arrow radical, whose fourth power vanishes. A positive-length entry of f raises the filtration; a top block A_i repeats across its i-th graded pieces a total of $\dim_k e_i(W_0/uW_0) = 6m$ times. Triangular determinants give the assertion. Finite alternating products preserve it. Quadratic degree and the uncancelled simple pole of the full local zeta exclude the targets as before. □

This theorem is sharp: $W_0 = \Lambda_R$ has vertex rank six. It requires neither left projectivity nor left flatness of a general kernel. It excludes this coefficient category, not arbitrary semilinear correspondences, twisted determinant lines or infinite spectral constructions. The extended edition identifies the full character-orbit repair with the hereditary normalization and explains why Schur commutator cancellation is insufficient. All determinant multiplicities here are relative to the stated k-valued base; restricting a rational quadratic factor to the former $\mathbb{Q}$-base squares it. No arithmetic descent or global positive determinant has been recovered by this ramification.

The recent NCG literature supplies concrete comparison targets, with strong hypotheses. Connes–Consani construct finite abelian covers of the adelic Riemann sector with prime-orbit length $\log p$ and arithmetic Frobenius monodromy [53, Theorem3.12]. The prolate/local-factor and moment constructions [54, 55] give particular finite-prime analytic models, not a uniform positive comparison for all completed L-functions. The zeta-spectral-triple determinant theorem [56, Theorem5.10] assumes a specified restricted Weil form, simple even bottom eigenfunction and boundary normalization. Its infinite comparison is still an additional step. The distributional real-zero theorem [57, Theorem6.1] concerns a particular interval quadratic form, essential self-adjointness on its trigonometric core and an even simple ground state; a Fock vacuum alone verifies none of those arithmetic identifications. Deninger's periodic-packet construction and real-cohomology obstruction [60, 62] further specify, rather than remove, these issues. Full theorem-level reading coverage and exact versions are recorded alongside this draft.

A complete approach must construct arithmetic descent and prime actions on actual order/derived or analytic objects, prove determinant-line and local-factor compatibility, control regularization and conductor/gamma normalization, and establish a positive realization for that *same* function. Finite-field cohomological trace formulas and Deligne purity supply the classical model [20, 21]; alternating duality alone is not positivity or purity. In a number-field construction these are obligations, not imported conclusions.

For a sharply testable final analytic target, put $F_\chi(z) = \Lambda(1/2 + iz, \chi)$. Suppose entire functions $h_m(z)\det(zI - H_m)$, with H_m finite self-adjoint and h_m entire nowhere zero, converge locally uniformly on $\mathbb{C}$ to this nonzero completed function. Hurwitz on every disk disjoint from $\mathbb{R}$ then proves all its zeros real, hence the Dirichlet critical-line assertion. Establishing this convergence with independently constructed H_m is exactly the missing load-bearing claim; a rank-one encoding or a reformulation does not establish it. Hecke, Dedekind and Artin extensions must state their analytic scope anew.

6.5 Whole components, derived endpoints and determinant relations

The full node lattice category has precisely the three indecomposables X, Λ, Y and arrows $X \to \Lambda \to Y$, $Y \to \Lambda \to X$. Its stable category has only X, Y, no irreducible arrows, and suspension exchanging them; its AR triangles have zero middle term. For the polynomial node at a smooth support $x = \lambda + t$, $y = 0$, $\lambda \neq 0$, the modules $T_r = k[t]/t^r$ form an ambient homogeneous tube:

$$0 \longrightarrow T_r \xrightarrow{(\pi,t)} T_{r-1} \oplus T_{r+1} \xrightarrow{(t,-\pi)} T_r \longrightarrow 0, \quad T_0 = 0, \quad \tau T_r = T_r.$$

The shift changes the derived placement, not the quasi-length. These nonzero-central-support objects do not extend to continuous finite-length modules of the arrow-adic completion. At its singular point even the candidate pure-branch tube fails ambient almost-splitness: $T_2^y \to k$ cannot factor through $T_2^x \to k$, since every intervening map lands in the x-socle, killed by the last map.

The nine HLS strings above sit in an entire intrinsic quotient component $T_{p,q}$, $(p, q) \in \mathbb{Z}^2$, with arrows increasing one coordinate and $\tau T_{p,q} = T_{p-1,q-1}$ [46]. Its central object $E = M(ab)$ has infinite projective dimension: restriction to the first corner gives the dual-number simple with its infinite loop resolution, while restricted projectives are free or zero. Its module AR sequence therefore yields a distinguished derived triangle but not a derived AR triangle ending at E. Ringel's four-quarter wind-wheel tile [43], with infinite-word diagonals and mixed center, is a different category's quilt; it is not silently identified with that HLS component or the Belyi surface.

There is no general equation "AR mesh equals polynomial semi-invariant syzygy." The intrinsic $k(1 \to 2)$ quotient of the infinite Chebyshev algebra has AR row $0 \to S_2 \to E \to S_1 \to 0$ and a free presentation determinant z on dimension $(1, 1)$, so its semi-invariant ring $k[z]$ has no generator relation. A genuine framed elliptic-square stratum has $Z = [x_1, x_2, y_1, y_2] \in \mathrm{Mat}_{2\times 4}$ with six minors and relation

$$p_{12}p_{34} - p_{13}p_{24} + p_{14}p_{23} = 0.$$

These minors have the same determinant character for the target GL_2 with framed source; they are not all semi-invariants for the full unframed vertex group. In contrast, the nodal lattice AR row gives a genuine relative determinant identity over R: multiplication by $a + bx$ on the basis $(y, 1)$ has matrix $\left(\begin{smallmatrix} a & -b \\ 0 & a+ub \end{smallmatrix}\right)$ and characteristic factor $(1 - Ta)(1 - T(a + ub))$. The endpoints have infinite order-projective dimension but are R-perfect.

Finally, the three-vertex theta algebra has no unital surjection onto a six-vertex radical-square-zero circular algebra: its semisimple image has at most three primitive idempotent images. Duplicating face vertex spaces instead gives an exact faithful unfolding which is not full; it does not inherit quotient or AR-transfer claims. Zwara Hom-control means that the Hom-dimension defect is bilinear on K_0, not merely a covering direct-sum formula [72, 73]. The book supplies explicit fixed-dimension counterexamples, corrected circular-complex incidence resolutions, complete drawn component windows and all category hypotheses. These additions do not supply the arithmetic determinant comparison.

Chapter 7

A genuine theta covering and its categorical limits

Use column matrices, hence covariant quiver representations (left modules); opposite categories translate the right-module convention in [74]. Let A be the infinite elliptic theta dessin algebra: vertices $i \in \mathbb{Z}/3$, arrows $a_i, b_i : i \to i+1$, and all mixed length-two paths zero. For the arrow ideal J and $L \geq 2$ put $B_L = A/J^L$. This is a finite string quotient of our actual infinite gentle algebra; for $L > 2$ its length-L relations prevent treating it as quadratic gentle.

Proposition 7.1 (A locally bounded integer cover)**.** *The category $\widetilde{B}_L$ with vertices $r \in \mathbb{Z}$, two arrows $a_r, b_r : r \to r+1$, and the same mixed and length-L zero relations, has orbit B_L under $r \mapsto r+3$. For finite-support representations, push-down F is exact and*

$$\operatorname{Hom}_{B_L}(FM, FN) \simeq \bigoplus_{g \in \mathbb{Z}} \operatorname{Hom}_{\widetilde{B}_L}(M, T_g N), \qquad (T_g N)_r = N_{r-3g}.$$

Only finitely many summands are nonzero. In general F is neither full, dense, nor Hom-controlled in Zwara's sense.

Proof. A nonzero path is constant-branch with length less than L. Thus the incoming and outgoing total Hom dimensions at a cover vertex are $2L-1$, and $\dim B_L = 3(2L-1)$. Paths and relations lift uniquely; the deck action is free and has the stated orbit. Push-down sums spaces of equal residue. A morphism decomposes uniquely into blocks with target lift index minus source index equal to $-3g$. The arrow commutation equations preserve that difference, proving the formula; finite supports bound the possible differences. Direct sums of vector spaces preserve exact sequences. The following explicit witnesses prove the three failures. □

For $L = 5$, let P be the cover interval on $0, 1, 2, 3, 4$ with all its a-maps one and b-maps zero, and let S be the sum of the five simples at the same vertices. They have the same K_0 class, but

	$\dim \operatorname{End}_{\widetilde{B}_5}$	$\dim \operatorname{End}_{B_5}(F(-))$	defect
S	5	9	4
P	1	2	1

Indeed the pushed-down simple multiplicities are $(2, 2, 1)$, whereas $\operatorname{End}_{B_5}(FP) = kI \oplus kX^3$ for its single nilpotent five-step chain X. The extra endomorphism X^3 proves non-fullness; the unequal defects at the same class exclude a bilinear K_0 defect. To use Zwara's finite-algebra definition literally, restrict the source to the finite convex interval $[0, 4]$, then extend by zero before push-down. This exact functor has the same endomorphism spaces and K_0 comparison.

Proposition 7.2 (An indecomposable module outside this cover image)**.** *Over a characteristic-zero field, B_3 has a nine-dimensional indecomposable representation which is not the push-down of any finite-support $\widetilde{B}_3$ representation.*

Proof. Label its basis by $0, \dots, 8$ with vertex residues $(0, 1, 0, 1, 2, 1, 2, 0, 2)$, and use matrix units E_{ij} acting on columns. Set

$$X = E_{10} + E_{32} + E_{43} + E_{65} + E_{76} + E_{08},$$
$$Y = E_{12} + E_{45} + E_{78}.$$

Their restrictions between adjacent vertex spaces give the a_i, b_i maps. They satisfy $XY = YX = X^3 = Y^3 = 0$, hence every length-three path is zero. The endomorphism ring preserving vertex spaces is $kI \oplus \mathfrak{r}$, where

$$\mathfrak{r} = \langle E_{02} + E_{13}, E_{15}, E_{35} + E_{46}, E_{48}, E_{68} + E_{70}, E_{72} \rangle, \qquad \mathfrak{r}^3 = 0.$$

Solving the arrow commutation equations gives exactly these seven basis elements. The ring is local: an element $cI + n$ is invertible exactly when $c \neq 0$, by the finite geometric series. It has no nontrivial idempotents, so the representation is indecomposable.

A finite-support lift would define an Euler operator D acting by r on the summand at lift vertex r. Then $[D, X] = X$ and $[D, Y] = Y$. Every displayed nonzero arrow is the unique nonzero entry in its row and column in its own matrix. Its commutator entry is therefore $D_{ii} - D_{jj}$. Add the six X equations and subtract the three Y equations. Each diagonal term cancels, leaving $0 = 6 - 3 = 3$, a contradiction. This argument allows arbitrary D, not just a diagonal matrix in the displayed basis. □

Corollary 7.3 (Higher-genus and derived non-density)**.** *For the clean dessin with rotations $\sigma = (0 \cdots m-1)(m \cdots 2m-1)$ and $\alpha = \prod_{i=0}^{m-1}(i\, i+m)$, odd $m \geq 3$, and genus $(m-1)/2$, the analogous A_m/J^3 has a $3m$-dimensional representation outside its integer-cover image in characteristic zero. Its bounded-derived push-down is not dense either.*

Proof. Use basis $v_0, \dots, v_{3m-1}$, assign vertices $i, i+1, i$ to $v_{3i}, v_{3i+1}, v_{3i+2}$ modulo m, and set

$$Xv_{3i} = v_{3i+1}, \quad Xv_{3i+2} = v_{3i+3}, \quad Yv_{3i+2} = v_{3i+1},$$

with indices modulo $3m$ and all other values zero. Again mixed products and cubes vanish. An Euler operator would yield $2m - m = m = 0$ by the same telescoping calculation, impossible in characteristic zero. If a bounded finite-support complex pushed to this module in degree zero, exactness would make its zeroth cohomology a module lift, a contradiction. □

The source's derived result is a *precovering* in the stated bounded categories [74, Theorem 4.28]; density remains an additional condition. Neither this result nor the GLS equivariant classification [75] identifies our completed order with a GLS algebra. Graded surface/Fukaya models [76] likewise require their own dg category, stops and grading. These categorical tools do not construct the independent positive arithmetic determinant.

Chapter 8

Verification and research frontier

The two nodal/invariant Lean files construct the node as an actual subring of $k[[X]] \times k[[X]]$ with equal constants, prove its annihilators, regular common parameter, augmentation, alternating projective resolution and a bijective pair of power-series coordinates. A second file proves CK1 collapse under the stated permutation/coverage hypotheses, determinant base change, actual 2×2 symmetric-square functoriality and relation preservation, a Schur character identity and the fixed-parameter lattice failure. These thirty printed theorem types have only standard Lean foundations. They do not formalize general dessins, abstract Ext/AR/Schur–Weyl, C* exactness, Fredholm determinants, arithmetic descent or GRH. Earlier formal layers remain preserved with their literal scopes.

Exact-rational diagnostics independently check the displayed dessins, path identities, Schur and Young examples and the nine-object grid. These finite checks supplement the proofs, rather than prove infinite spectral or arithmetic assertions. The next arithmetic target is an exact descent/Frobenius-compatible construction on the labelled order/Fock data, with a determinant-preserving positive comparison. The local Schur kernel and the simple degree spectrum alone do not supply it. All source clones and earlier research are retained; the earlier general focused PDFs are archived at the preceding commit.

Ten further declarations in `DessinPullbackComponents.lean` check actual matrix-unit identities, nonmultiplicativity of raw diagonal extraction, impossibility of a unital two-state matrix residue into a nonzero commutative ring, multiplicativity on diagonal fibers, and genuine equal-image pullback subring/projection components. The analytic suite then contained187printed declarations at unchanged pins. The circle-function C* model, functional calculus, generation, graph uniqueness and K-theory remain prose/external-theorem arguments, not hidden assumptions of these component checks.

Sixteen additional declarations in `ThetaJacobi.lean` check genuine finite-field MulChar Jacobi conjugation, norm and rescaling with explicit nontriviality hypotheses; cubic–quadratic noncancellation; the cyclotomic multiplication determinant and positive Gram identity; and actual theta cellular boundary, homology-inclusion, restriction and rational chain-map matrices. The full analytic suite now contains203declarations. The point-count proof, deck/Kummer comparison, cohomological trace interpretation and global arithmetic comparison are not thereby fully formalized.

The final three `ThetaJacobi.lean` declarations verify the actual conjugation matrix identities and the real two-dimensional inert-prime determinant obstruction. They do not assume any unknown zero location or exclude complex/enlarged spectral realizations.

`ThetaProjectiveMultiplicity.lean` adds five declarations. Arbitrary upper-block matrices with six identical diagonal blocks have the sixth-power determinant and characteristic-factor

formulas. A literal power-series constant-coefficient map specializes matrix determinants, for each scalar parameter; the coefficientwise polynomial/order interface remains prose. A nonzero quadratic cannot be a rational-function sixth power, proved by polynomial degrees. Three genuine power series with product X cannot have the cyclically equivalent residue-vanishing conditions forced by invertible rank-one arrow intertwiners. The derivation of the path blocks from the full theta order, projective decomposition, derived branch functor and deck intertwiners is not fully formalized. The complete analytic suite now has208printed declarations; no hidden arithmetic positivity assumption occurs.

`ThetaTameDescent.lean` adds twelve printed component declarations (and one auxiliary polynomial lemma). They use genuine formal-power-series rescaling and its coefficient operator, proving the coefficient action, invariant-coefficient vanishing and the tame operator's cube. Actual three-state matrices satisfy the clock/rotation commutator, comparison determinant and closed-fiber equations, weighted-cycle cube and full characteristic polynomial, noncommutation of a nonconstant rotation polynomial, trivial whole-column determinant actions, and the same-operator comparison for vC. The classification of all fixed series by residues, full order action and hereditary invariant algebra, stack interpretation, valuation/rank theorem, general coefficient-functor filtration and GRH are not thereby fully formalized. No unknown positivity premise is assumed.

Part II

Proofs and calculations

Chapter 9

Expanded dessin, resolution and derived calculations

9.1 The cycle order in coordinates

Number a permitted cycle in travel order $0, \dots, \ell-1$. Map an arrow $i \to i+1$ to $E_{i,i+1}$ for $i < \ell-1$, and the final arrow to $u_c E_{\ell-1,0}$. A path from i to j then gives $u_c^r E_{ij}$, where r counts cut crossings. These are linearly independent path normal forms, and every positive-length permitted path has exactly one such expression on exactly one branch. The full-cycle sum in a branch is $u_c I$. At a paired edge its two diagonal occurrences come from a single original idempotent; no positive-length coefficients are identified. This proves the order description including self-pairings within one cycle. Although the suborder is generically a product of full matrix algebras, it is not their unglued product at the special fiber.

For the interval this becomes the literal fiber product

$$\Lambda = \{(f,g) \in k[[X]]^2 : f(0) = g(0)\}, \qquad x = (X,0),\ y = (0,X),\ u = (X,X).$$

Every element has a unique expression $a(u) + b(u)x$: take $a = g$ and $b = (f-g)/X$. Thus it is R-free on $1, x$ with $x^2 = ux$ and $y = u - x$. The annihilator of x consists of pairs $(0,g)$ with $g(0) = 0$, exactly $y\Lambda$; the other branch is symmetric. Multiplication by u is injective, coefficientwise. These are actual formal power-series statements, not conclusions from finite truncations.

9.2 The two-arm complex and its calculations

For an arrow a write $f(a)$ for its unique forbidden successor. The summand in $P_n(i)$ indexed by the initial arrow a has endpoint $t(f^{n-1}(a))$. Its map multiplies by that last arrow. Thus the resolution can be computed by iterating a finite permutation, while the projectives themselves remain infinite-dimensional. The Hom complex against a module N is the direct sum of the endpoint spaces with differentials given by the same arrow matrices. Tensor against a left module instead uses the same path entries acting on the left. No rank or exactness claim for an arbitrary N is inferred by counting endpoints alone.

For the nodal residue field the maps are particularly explicit:

$$\cdots \xrightarrow{\mathrm{diag}(x,y)} \Lambda^2 \xrightarrow{\mathrm{diag}(y,x)} \Lambda^2 \xrightarrow{(x \quad y)} \Lambda \longrightarrow k \longrightarrow 0.$$

If $xz_1 + yz_2 = 0$, its first branch says the first branch of z_1 is zero, and its second branch says the second branch of z_2 is zero. Hence $z_1 = yw_1$, $z_2 = xw_2$. The same annihilator calculation proves

the alternating kernels in all degrees. Projectivity is genuine: the terms are regular modules or their finite direct sums. It is not a finite free resolution, despite the period of its positive tail.

For the elliptic theta the quiver vertices are $v_0 = \{0, 3\}$, $v_1 = \{1, 4\}$, $v_2 = \{2, 5\}$. The arrows a_0, a_3 go $v_0 \to v_2$, a_2, a_5 go $v_2 \to v_1$, and a_1, a_4 go $v_1 \to v_0$. The two forbidden arms from v_0 are

$$a_0, a_5, a_1, a_3, a_2, a_4, \ldots, \qquad a_3, a_2, a_4, a_0, a_5, a_1, \ldots.$$

Their top pairs are $(v_2, v_2), (v_1, v_1), (v_0, v_0)$, repeated. The three steps exchange the arms. Their distinct top pairs exclude shorter unordered positive periods. The spherical theta instead has forbidden two-cycles and successive top pairs $(v_2, v_1), (v_0, v_0)$, giving period two. Thus even identical hereditary overorders need not give identical resolutions.

Quadratic Koszul duality here has a directly checkable local meaning: relations complement the two possible successors. The dual dessin replaces the graph rotation by ϕ^{-1}. In the Ext algebra against A/J, concatenating the forbidden-word basis gives the product when the join is forbidden; a permitted join gives zero. One can see this by lifting a length-r basis class to the resolution: discard the prescribed initial r letters and identify the remaining summand with its suffix resolution, taking zero on other prefixes. These prefix-discard comparison maps commute with the suffix differentials, with the standard shift signs when viewed as shifted complexes. The concatenated indexing word exists exactly when its join is forbidden; evaluation of the two basis classes on that word gives one. If the join is permitted there is no such indexing word and the product is zero. Composition therefore concatenates indexing words, with the chosen right-module/Yoneda opposite convention. This is a graded algebra statement; it neither makes the unbounded resolution perfect nor constructs an equivalence of all formal-completion derived categories.

For an arbitrary bounded projective complex $P^\bullet$, its determinant line over a commutative coefficient ring is $\bigotimes_n (\det P^n)^{(-1)^n}$, with determinant duals for negative exponents. A chain automorphism acts on this line; a quasi-isomorphism gives the corresponding determinant-functor isomorphism. For a general endomorphism F, the expression for $1 - zF$ uses the locus where it is invertible and gives a rational determinant-line action/trivialization, not an everywhere invertible line map at singular parameters. Additivity is compatible with exact triangles under the usual determinant-functor conventions [17, 18]. In our order context an R-linear determinant uses the finite free underlying R-modules; it must specify a separate endomorphism. Determinants of a differential presentation, alternating determinants of a chain action, regularized analytic determinants and the Cartan path matrix are four distinct constructions. Their equality requires a proof, not their shared name.

The geometric model literature [6, 8, 9] is useful for identifying which crossings and gradings would have to be represented by a functor. To apply it here one must specify the category of polynomial strings, completed lattices or finite-length quotients; construct its surface/curve objects; and prove that degree-r intersections compute the Hom group into shift r, with local systems and boundary exceptions included. We have supplied explicit walks and maps in the examples, not claimed this general completed-order theorem. On a finite word, a map can already be computed rigorously without such a theorem: assign a coefficient matrix between equal-vertex occurrences and solve $F_{t(a)} N(a) = N'(a) F_{s(a)}$ for every arrow. The diamond calculations below implement exactly this system.

Chapter 10

Semi-invariants, tableaux and explicit intertwiners

10.1 Derived information retained by a presentation

Let $K = \operatorname{im} f$. The injection $\operatorname{Hom}(K, N) \to \operatorname{Hom}(P_1, N)$ descends to the Ext injection used in Theorem 3.1; its kernel modulo $\operatorname{im}\operatorname{Hom}(P_0, N)$ is zero because the map $P_1 \to K$ is onto. The missing part of the cokernel detects maps on P_1 not descending through K. This explains exactly why an injective resolution map is needed for its full Euler interpretation.

In the node example the resolution of $M = \Lambda/(x)$ has maps $x, y, x, y, \ldots$. On $N = k[y]/(y^2)$ the Hom cochain maps are $0, y, 0, y, \ldots$. Thus $\operatorname{Hom}(M, N) = N$ and $\operatorname{Ext}^1(M, N) = \ker y$ have dimensions two and one; the cokernel of the first zero map is two-dimensional. In the elliptic-square example the first four Hom maps are $1, 0, 0, 0$, periodically. Hence degrees zero and one vanish, degrees two and three are k, and degree four vanishes. This also makes clear why a nonzero scalar semi-invariant does not give a derived orthogonality theorem.

With coordinate action $(gF)(N) = F(g^{-1}N)$ the Schofield weight is $a - b$, the negative of the point-evaluation weight. For a single arrow it is the same elementary distinction as the action on $\operatorname{Hom}(V, W)$ versus on its coordinate functions $V \otimes W^*$. The Cauchy decomposition for coordinate functions is

$$\operatorname{Sym}^m(V \otimes W^*) \cong \bigoplus_{\lambda \vdash m} S_\lambda(V) \otimes S_\lambda(W)^*.$$

A relation quotient can kill these components; its ambient multiplicities do not descend unchanged. Acyclic-quiver semi-invariant/LR results such as [35] retain their acyclicity assumptions. The explicit two-arrow slice below is acyclic, whereas the whole theta quiver is not.

10.2 One Young operator and one LR decomposition in coordinates

For $\lambda = (2, 1)$ number the first row $1, 2$ and second row 3. Then

$$Y = (I + P_{12})(I - P_{13}), \quad Y^2 = 3Y, \quad \dim \operatorname{im}(Y \mid (k^2)^{\otimes 3}) = 2.$$

The hook product is three; its Specht dimension is $3!/3 = 2$, also two here for a different reason. The normalized projector extracts one $S_{(2,1)}$ copy. The trace $\operatorname{tr}((Y/3)M^{\otimes 3})$ is therefore the Schur character, not twice that character. This fixes the common row/column normalization ambiguity.

Write $t = \operatorname{tr} M$, $\Delta = \det M$ for a two-dimensional endomorphism. Its complete characters obey $h_0 = 1$, $h_1 = t$, $h_m = th_{m-1} - \Delta h_{m-2}$, and

$$\chi_{(a,b)}(M) = \Delta^b h_{a-b}(M), \quad a \geq b \geq 0.$$

In particular $h_2 = t^2 - \Delta$, $h_3 = t^3 - 2t\Delta$, and $\chi_{(2,1)} = t\Delta$. Thus $th_2 = h_3 + \chi_{(2,1)}$ is the LR identity $V \otimes \operatorname{Sym}^2 V \cong \operatorname{Sym}^3 V \oplus S_{(2,1)}V$, with $S_{(2,1)}V \cong \det V \otimes V$.

An explicit natural splitting avoids relying just on characters. In characteristic zero multiplication $m : V \otimes \operatorname{Sym}^2 V \to \operatorname{Sym}^3 V$ has natural section

$$s(v_1v_2v_3) = \tfrac{1}{3}\sum_{i=1}^{3} v_i \otimes \prod_{j\neq i} v_j.$$

The map $j : \bigwedge^2 V \otimes V \to V \otimes \operatorname{Sym}^2 V$ sends $(v \wedge w) \otimes z$ to $v \otimes wz - w \otimes vz$. In dimension two it is injective: for a basis e_1, e_2 its images at $z = e_1, e_2$ have distinct independent coordinates. They lie in $\ker m$, whose dimension is $6 - 4 = 2$. Hence (s, j) is the required isomorphism. Tensorial definitions make both maps commute with every linear endomorphism, including singular arrow maps. This is a genuine LR intertwiner on our dessin representation stratum.

For a concrete theta representation take

$$X_1 = \begin{pmatrix} 1 & 1 \\ 0 & 1 \end{pmatrix}, \quad X_2 = \begin{pmatrix} 2 & 0 \\ 0 & 1 \end{pmatrix}, \quad X_3 = \begin{pmatrix} 1 & 0 \\ 1 & 1 \end{pmatrix}.$$

Then $M = X_3X_2X_1 = \left(\begin{smallmatrix} 2 & 2 \\ 2 & 3 \end{smallmatrix}\right)$, $t = 5$, $\Delta = 2$, $h_2 = 23$, $h_3 = 105$ and $\chi_{(2,1)} = 10$. The identity is $115 = 105 + 10$. Since the other permitted branch is zero, every forbidden product is zero; this is an actual representation of the infinite elliptic dessin algebra.

In the invertible-arrow open stratum one can gauge X_1, X_2 to the identity, leaving conjugation of M. The invariant-ring proof in the core works also at singular arrows by cycle-trace generation, not by assuming that this gauge choice extends there. The degree-one monodromy coefficients have total arrow degree three; this is why the Hilbert-series denominator uses $3j$, not j.

For the Cauchy kernel choose the Schur subspace inside the tensor power with its inherited Hilbert norm. $M^{\otimes m}$ preserves it and has norm at most $\|M\|^m$. This proves the trace bound for nonnormal matrices as well as diagonal ones. Formal Cauchy identities extend by polynomial continuity in matrix entries; the stated absolute bound then justifies analytic summation. Gram positivity does not assert entrywise positivity or positivity of an unrelated arithmetic form. For three exact test matrices M, $\left(\begin{smallmatrix} 1 & 1 \\ 0 & 2 \end{smallmatrix}\right)$, $\left(\begin{smallmatrix} 0 & 1 \\ -1 & 1 \end{smallmatrix}\right)$, the choice $r = 1/100$ satisfies $rR_0^2 \leq 21/100 < 1$ using Frobenius norms, and all seven principal minors of the rational kernel matrix are nonnegative.

10.3 Two precise functorial limitations

At any actual vertex simple S of A, the split exact sequence $0 \to S \to S \oplus S \to S \to 0$ uses first inclusion and second projection. Termwise Sym^2 has dimensions $1, 3, 1$ at that vertex; its middle kernel contains the mixed monomial as well as the first square, but its first image contains only the first square. Middle homology is S. Thus even split exactness is not preserved. Genuine derived Schur constructions instead use mixed tensor degrees, signed total differentials and suitable flat/projective replacements [32, 33]; their membership in a particular order category must still be checked.

The R-lattice $M = Re_x \oplus Re_y$ with $x = \operatorname{diag}(u, 0)$, $y = \operatorname{diag}(0, u)$ has $x + y = uI$. On $\operatorname{Sym}^2_R M$ the images are $\operatorname{diag}(u^2, 0, 0)$ and $\operatorname{diag}(0, 0, u^2)$. Their sum kills the mixed vector, hence equals

neither uI nor u^2I. This is a specific failure to retain the original central action, not a failure of the polynomial monomial representation functor. Even a common ramified base substitution does not repair this mixed vector.

Semi-invariants retain useful moduli on nilpotent modules. In the theta quiver keep only $a_0, a_3 : v_0 \to v_2$, put their scalar values $(x, y) = (1, \lambda)$ and all other arrows zero. The v_1 simple splits off. Every length-two path acts by zero, so these are continuous completed modules. The two scalars have the same weight g_{v_2}/g_{v_0}, and y/x is a rational invariant on $x \neq 0$, giving the projective pencil $[x : y]$. It is not a regular invariant on the whole affine locus, whose orbit closures meet zero.

For the interval quotient take $x = J_2$, $y = \lambda J_2$. With its top and socle specified, the separated Kronecker coordinates are again $(1, \lambda)$; the relation to the same-weight ratio is exact. The pp formula in the core is stronger than merely noticing a ratio: on M_λ its solution set is $\operatorname{im} x$, whereas on M_μ, $\mu \neq \lambda$, the equation $(\mu - \lambda)xv = 0$ forces $z = xv = 0$. Different parameters are therefore distinguishable by actual positive-primitive conditions even though every cycle trace is zero.

Chapter 11

Full lattice and diamond diagrams

11.1 The nodal exact diagram

The normalization proof of Theorem 4.1 uses BM inside the generic module. Replacing it without justification by $B \otimes_\Lambda M$ could introduce torsion and would not prove the same statement. Once the subdirect residue subspace is decomposed, the branch basis changes lift over complete DVRs; taking inverse images modulo the conductor gives the direct decomposition, not just a decomposition of residues.

Here is the promised diagram, with the terminal short exact column for every position:
The canonical diagram appears in Chapter 21; the proof and calculation below are retained.

Each vertical column is completed by zero above and below. In the bottom row identify $Y/uY = k$ via generator y, $X/uX = k$ via x, and $\Lambda/u\Lambda = k[\epsilon]/(\epsilon^2)$ with $x = \epsilon$, $y = -\epsilon$. Its first map is $1 \mapsto -\epsilon$, its second the augmentation. It is nonsplit as a dual-number sequence. This explicit order reduction, not an unrelated finite algebra, explains its appearance.

For a further Ext calculation, resolve $X \cong \Lambda/(y)$ with successive maps $y, x, \ldots$. On Y the first is multiplication by y and the second zero, so $\mathrm{Ext}^1(X, Y) = Y/yY = k$; on X the first is zero and the second injective, so $\mathrm{Ext}^1(X, X) = 0$. Interchanging branches gives the other two cases. The two nonsplit lattice rows realize the nonzero cross classes. Their Hom spaces are finite over R, generally infinite over k.

11.2 Chebyshev geometry and the exact quotient

The identity $1 - T_n(z)^2 = (1 - z^2)U_{n-1}(z)^2$ follows from $z = \cos\theta$ and the sine/cosine multiple-angle formulas, hence as a polynomial identity. $T_n' = nU_{n-1}$. Therefore β_n has its only zero at infinity, of order $2n$; its n points over one are double since $\beta_n - 1 = T_n^2/(1 - T_n^2)$; and its poles are simple at ± 1 and double at the $n - 1$ interior roots of U_{n-1}. The derivative has no additional critical values. The total ramification is $(2n - 1) + n + (n - 1) = 4n - 2$, as required for a degree-$2n$ rational Belyi map. The dual graph has $n + 1$ vertices of degrees $1, 1, 2, \ldots, 2$, and n edges; it is a connected path. Its planar ribbon embedding is unique, so this identifies the particular nested-loop dessin, not only its passport.

In the quotient retaining orientation Ω, any surviving path traverses each chain edge at most once and either endpoint loop at most once. Its length is at most $n + 1$; thus the killed-arrow ideal contains J^{n+2}. The quotient of A_n and of its completion is the same $H_n(\Omega)$. For $n = 3$ with forward chain arrows, its path counts in lengths zero through four are $3, 4, 3, 2, 1$, total thirteen. These

counts describe a quotient representation category of the infinite order, not a change of primary object.

Inflation is full because the two algebras have exactly the same actions on these annihilated objects. It preserves internal exact sequences. It does not preserve arbitrary ambient extension closure: the two adjacent simples are annihilated by the killed reverse arrow, but the two-dimensional extension having only that arrow nonzero is not. Likewise endpoint-local freeness over $k[l]/l^2$ or $k[r]/r^2$ in [46] is not R-freeness. To transfer an almost-split property to a larger category one must prove the requisite approximation/factorization statements; locally finite quiver criteria [40, 41, 42] do not apply just because each vertex has two arrows. The permitted cycles violate interval/Hom finiteness.

11.3 Nine actual strings and all maps

Take $n = 3$ with $1 \xrightarrow{a} 2 \xrightarrow{b} 3$, loops l, r and $l^2 = r^2 = 0$ in the quotient. Here b denotes the retained forward a_2, not a reverse arrow of the original doubled chain. The following words are in travel order. A superscript $-$ means a formal inverse in a word, not an inverse algebra element.

Object	word	start	dimension vector
A	$l^-abrb^-a^-l^-$	1	$(4,2,2)$
B	l^-ab	1	$(2,1,1)$
C	l^-abr^-	1	$(2,1,2)$
D	$abrb^-a^-l^-$	1	$(3,2,2)$
E	ab	1	$(1,1,1)$
F	abr^-	1	$(1,1,2)$
G	$r^-b^-a^-labrb^-a^-l^-$	3	$(4,3,4)$
H	$r^-b^-a^-lab$	3	$(2,2,3)$
I	$r^-b^-a^-labr^-$	3	$(2,2,4)$

A basis vector is assigned to each visited position $0, \dots, \ell(w)$ at its vertex. A direct letter sends its preceding vector to its following vector; an inverse letter sends the following vector to the preceding vector. Sum these elementary maps for each arrow and put all unmentioned entries zero. This defines every matrix, including repeated loops, and verifies the relations. Set the killed reverse arrows to zero to obtain actual Λ_3-modules.

Their signed grid is

The canonical diagram appears in Chapter 21; the proof and calculation below are retained.

Horizontal projections keep the initial word positions and kill the remaining positions. Horizontal inclusions append the final r^-, keeping old positions. Upper vertical projections delete the initial l^-: old position $j \geq 1$ maps to position $j-1$, and old position zero maps to zero. Lower vertical inclusions prepend $r^-b^-a^-l$: position j maps to $j+4$. Multiply these maps by the indicated signs. For every arrow these formulas commute with the string action, including the two positions adjacent to a cut or join; those are exactly where the loop inverse and chosen orientation matter.

Every small square has two length-two composites whose sum is zero. The exact sequences are

$$0 \to A \to B \oplus D \to E \to 0, \qquad 0 \to B \to C \oplus E \to F \to 0,$$
$$0 \to D \to E \oplus G \to H \to 0, \qquad 0 \to E \to F \oplus H \to I \to 0.$$

For example the maps out of A retain its initial positions $0,1,2,3$ in B and delete its first position in D, so their joint kernel is zero. The maps to E are onto, and the dimension vectors give $\dim A + \dim E = \dim B + \dim D$ vertexwise. The zero composite plus this equality proves exactness.

The other three use precisely the same keep/delete or append/prepend rules; their vertexwise dimension equalities and jointly injective/surjective maps prove exactness. The shipped exact checker constructs all matrices and verifies these assertions independently over $\mathbb{Q}$.

The stronger almost-split property is imported by identifying $E = w = ab$ as the minimal string of type $(2, 2)$ and these exact hook/cohook words with [46, Proposition3.12], using that paper's Propositions2.6/2.9 and Lemma3.10. Opposite-module conventions are reconciled by reversing travel/composition conventions; the closed doubled quiver is isomorphic to its opposite by exchanging the two arrows at each chain edge. Thus intrinsically $\tau E = A$, $\tau F = B$, $\tau H = D$, $\tau I = E$. The rows and columns of this grid are *not* generally short exact, unlike the nodal diagram. Two small cautions in that source are not needed here: a tube-rank label in Example3.9(3) is inconsistent with its listed mouth, and a general homogeneous-tube statement must not be read as a converse classifying every such object as a band. Neither is used to import these four meshes.

11.4 The pure-injective quotient and what its dimension means

For $B_0 = \Lambda/J^2 = k\langle x, y\rangle/(x, y)^2$, words alternate direct and inverse letters because every direct/direct and inverse/inverse adjacent pair is forbidden. Up to rotation and inverse its only primitive band is xy^{-1}; the bridge quiver has two oriented band vertices with no connecting nontrivial bridge. The longest path has length zero. The domestic string results [44, 45] therefore give relative dimension $0 + 2 = 2$, not an automatic dimension three for every one-domestic algebra. Finite-dimensional points have relative CB rank zero; the appropriate Prüfer/adic and one-sided periodic string points have rank one; the unique generic point has rank two. These statements concern the quotient category with its inherited pp structure.

Indeed a pp formula is a finite system of linear equations with existentially quantified unknowns. On a module annihilated by J^2 every coefficient reduces to B_0, so purity and pure-injectivity are preserved in both directions under inflation. The condition $MJ^2 = 0$ is a definable closed condition, giving the closed Ziegler subspace. Its relative ranks need not be ranks in the entire Λ spectrum. This subcategory is not extension closed: $\Lambda/(x^3, y)$ gives an extension of objects killed by J^2 that is not itself killed by J^2. Since u^2 annihilates every object of the subcategory, it contains no nonzero R-free lattice. Ringel's representation-theoretic node construction is also not a Morita equivalence identifying the geometric nodal order with the Kronecker algebra. Infinite-dimensional polynomial string classifications [38] retain finitely-controlled or pointwise-artinian assumptions; an arbitrary complete lattice does not automatically satisfy them as an algebraic A-module.

Chapter 12

The operator extension in detail

12.1 A corrected cycle lift and the integer boundary map

In the permitted-state graph each length-ℓ cycle has a full matrix-corner Laurent/circle coordinate. Its chosen K_1 generator is the full cycle at one state plus the complementary identity. In Fock space $L_c^* L_c = Q_a + v_{s(a)}$. Thus the tempting lift $L_c + (1 - Q_a)$ has overlapping initial pieces and is not an isometry. The corrected lift in Theorem 5.1 first restricts to Q_a:

$$W = L_c Q_a + (1 - Q_a), \quad W^* W = I, \quad I - W W^* = Q_a - L_c Q_a L_c^*.$$

A path starting with a and length greater than ℓ has uniquely the full prefix c followed by another path starting with a. The missing range consists exactly of lengths $1, \ldots, \ell$. Its terminal multiset is the original graph's incident-edge multiset at that cycle vertex. These finite defect vectors all lie in terminal compact ideals; their classes give the claimed unsigned incidence entries. The sign convention affects only the overall sign of the boundary map.

Here is the Smith calculation without spectral assumptions. Choose a spanning tree of the connected underlying graph and one root. By changing signs on one bipartition of the tree, its $E \times V$ incidence submatrix becomes the ordinary oriented tree incidence, with $V - 1$ unit pivots. After eliminating these pivots, a remaining column represents the common root coordinate, and each nontree edge evaluates on it as zero when its fundamental cycle is even, or ± 2 when odd. A loop is the latter case. If all are even the graph is bipartite and this column is zero; otherwise its entries have gcd two, giving the final pivot two. Remaining rows are free. Consequently the kernel/cokernel, then the six-term sequence, give the K groups stated in the core. No theorem reconstructing a cyclic embedding from those groups is asserted.

The compact ideal is block diagonal, not $\mathcal{K}(\mathcal{H})$: prefixes never move terminal vertices, so cross-terminal rank-one maps do not belong to the displayed ideal. This is why the arithmetic insertion must choose one terminal sector. A graph/Cuntz boundary quotient kills the vacua and hence this ideal, so that insertion need not survive passage to the quotient.

12.2 Spectral domain and arithmetic trace

A vector belongs to the adjoint domain of the diagonal N precisely when its coefficientwise product by the real sequence $|p|$ is square summable; this proves self-adjointness on the given domain. The truncations by length prove finite supports are a core. Resolvent coefficients $(|p| - i)^{-1}$ tend to zero and each length space is finite dimensional, giving compactness. Prefix and deletion shift the length

by at most one, so preserve the domain and prove the commutator formulas there. Leibniz then handles the dense polynomial *-algebra.

Every terminal sector has one vacuum and two paths at each length $n \geq 1$, even when some graph endpoints coincide: distinct formal paths remain distinct basis vectors. Thus restriction to a sector still has a simple vacuum, but it need not be a faithful representation of the whole concrete algebra. The trace of e^{-tN^2} is $E + 2E\sum_{n\geq 1} e^{-tn^2}$, distinct from the semigroup trace of N in the core. The trace identity with $\chi(N)$ is only on $\operatorname{Re} s > 1$, where the product is trace class. Analytic continuation of the scalar L-function does not make that same operator product trace class on $\operatorname{Re} s > 0$.

Chapter 13

Abel determinant estimates and the arithmetic program

For completeness the inserted family has a full elementary convergence proof. Since complete nonprincipal character periods sum to zero, $|A_n| \le B_0 \le q_\chi$. On $2^k \le n < 2^{k+1}$,

$$\sum |u_n|^2 \le \frac{B_0^2}{(k+1)^2}, \qquad \sum |v_n(s)|^2 \le M^2 (k+1)^2 r^k, \quad r = 2^{-2\sigma_0} < 1.$$

The second follows from $n^{-s} - (n+1)^{-s} = s \int_n^{n+1} x^{-s-1}\, dx$. Define

$$Q_J(r) = r^J \left(\frac{(J+1)^2}{1-r} + \frac{2(J+1)r}{(1-r)^2} + \frac{r(1+r)}{(1-r)^3} \right).$$

Expanding $(J+j+1)^2$ in the three geometric moment sums proves $Q_J = \sum_{k \ge J} (k+1)^2 r^k \to 0$. Locally uniform ℓ^2 convergence of the holomorphic finite-coordinate vectors proves Banach holomorphy. The linear functional $z \mapsto \sum v_n z_n$ has norm $\|v\|$; this is the complex-linear coefficient pairing, not a conjugate-linear dependence on s.

Write $\mathcal{I}(v)(z) = \sum_n v_n z_n$ for the coefficient functional, distinct from the arrow ideal J. For $N_J = 2^J - 1$, $J \ge 1$, let $K_N = u \otimes (\mathcal{I}(P_N v) - e_1^*)$. Then

$$\|K - K_{N_J}\|_1 \le \sqrt{2} B_0 M \sqrt{Q_J(r)}.$$

Finite summation by parts gives

$$T_N = \det_F(I + K_N) = \sum_{n \le N} A_n (n^{-s} - (n+1)^{-s}) = S_N - A_N (N+1)^{-s}.$$

Adding the last endpoint times e_1^* to the functional recovers S_N exactly because $u_1 = 1$. Its trace-norm error is at most

$$\sqrt{2} B_0 (M \sqrt{Q_J(r)} + B_0 (N_J + 1)^{-\sigma_0}).$$

For arbitrary cutoffs use the last whole dyadic block for an enclosing tail. Galerkin compressions also converge: $\|u - P_{N_J} u\| \le B_0 / \sqrt{J}$. With $C_K = 1 + M\sqrt{(1+r)/(1-r)^3}$,

$$\|K - P_{N_J} K P_{N_J}\|_1 \le \frac{B_0 C_K}{\sqrt{J}} + \sqrt{2} B_0 M \sqrt{Q_J(r)}.$$

The raw endpoint adds the same endpoint bound as before. Isometric insertion by U preserves nonzero singular values, every norm estimate, and the Fredholm determinant. Everything is in one compact ideal of the actual infinite dessin Fock algebra.

For primitive parity a use $g(s) = (q_\chi/\pi)^{(s+a)/2}\Gamma((s+a)/2)$, holomorphic nonzero on $\operatorname{Re} s > 0$. The completed functional is $g(s)\mathcal{I}(v) - e_1^*$, and the completed raw functional is $g(s)(\mathcal{I}(P_N v) + A_N(N+1)^{-s}e_1^*) - e_1^*$. Their determinants are exactly gL and gS_N. Scaling the entire old perturbation would instead give $1 + g(L-1)$, the wrong normalization. Trace-class background is standard [26], while these special rank-one identities follow directly from $\det_F(I + u \otimes \varphi) = 1 + \varphi(u)$.

The metric obstruction is likewise elementary. With inner product conjugate-linear in its first variable, symmetry of $T = u \otimes \varphi$ implies

$$\varphi(z)\langle u, u\rangle = \overline{\varphi(u)}\langle u, z\rangle.$$

A nonzero φ cannot have $\varphi(u) = 0$; thus all symmetric maps with that range have proportional functionals. For $n \geq 2$ the coefficient ratios at $\sigma + it$ and σ satisfy

$$\frac{v_n(\sigma + it)}{v_n(\sigma)} = \frac{\sigma + it}{\sigma}\, n^{-it}(1 + O_{\sigma,t}(1/n)).$$

Integers nearest $\exp(2\pi k/|t|)$ and $\exp((2\pi k + \pi)/|t|)$ give opposite nonzero subsequential limits. Hence no common positive metric symmetrizes this family for all critical heights. Restricting any proposed metric on the inserted family to $U\ell^2$ gives the same contradiction. An independently constructed positive comparison is still a possible different route.

13.1 Precisely how classical and recent sources enter

Over a finite field the Grothendieck trace-formula architecture writes a zeta function as alternating determinants on finite-dimensional cohomology; Deligne's purity supplies the weights of eigenvalues [22, 20, 21]. If a weight-w Frobenius is $q^{w/2}$ times a positive-metric unitary, each eigenvalue has modulus $q^{w/2}$. The norm conclusion is immediate; constructing that form or proving purity is the deep step. Symplectic/alternating duality $F^t J F = q^w J$ alone only pairs reciprocal eigenvalues and does not give their individual moduli. An order resolution or Schur-positive character expansion alone cannot replace this step in number-field cohomology.

The recent primary comparisons used here are specific:

- [53, Theorem3.12, pp.15–17] gives finite abelian covers with local orbit length $\log p$ and genuine arithmetic monodromy. It suggests what a descent-equipped order functor should match; it does not identify our u or a face cycle with a prime without such a functor.

- [54, Propositions4.1–4.3, Theorem4.6] builds finite-prime local models with archimedean Fourier factors. Its Hilbertian isomorphisms are not an asserted uniformly controlled common isometry for our arithmetic approximants. [55, Proposition3.1] gives determinacy of a particular local moment problem; positive finite Hankel matrices are not the missing global Weil inequality.

- [56, Theorem3.6] gives discreteness/lower boundedness for the stated restricted Weil form. Theorem5.10, pp.23–24, additionally assumes a finite truncation, $\lambda > 1$, a simple even bottom eigenfunction ξ and $\delta_N \xi = 1$. Its quotient metric is positive and its regularized determinant is $-i\lambda^{-iz}\widehat{\xi}(z)$. Passing to the infinite arithmetic comparison, including the ground-state and convergence conditions in its §8, is not automatic.

- [57, Theorem6.1, p.13] assumes a specified real distribution on an interval, the corresponding trigonometric-core form, essential self-adjointness, and an isolated simple lowest eigenvalue with reflection-even eigenfunction. Its Fourier transform then has only real zeros. Our degree operator's vacuum and length parity are not those data.
- [60, Theorem6.1] gives prime-indexed periodic packets in its dynamical construction, not one proved orbit per prime with the full desired cohomological trace formula. [62] isolates an obstruction to a particular real-coefficient cohomology with full functorial Artin multiplicities; it is not a theorem excluding every Hilbert–Pólya operator. The current survey [58] distinguishes remaining steps. The recent Picard-monoid construction [59] is not already a polarized abelian variety with a number-field purity theorem. [63] uses RH as an input in the cited spectral identification, so cannot be used circularly as its proof.

These are targeted theorem/proof readings, not claims that every page of every cited work has been audited. The preserved review records specify actual page coverage and hashes, including inaccessible original PDFs where the modern primary proof was used instead.

13.2 A concrete sequence of remaining constructions

First choose a number-field model of a Belyi pair, its finite covers and conductor/ramification data. Construct actions or exact correspondences on the labelled order/module or analytic categories that recover the local prime Frobenius polynomials. The elliptic twists show why omitting this datum loses information. Test at more than one arithmetic model of the same complex dessin, not just its topological passport.

Second specify a finite projective or otherwise determinant-admissible complex and its *independent* arithmetic endomorphism. Prove exact-sequence/determinant-line compatibility. Use semi-invariants to encode presentation degeneracies, and Schur/exterior characters to calculate local factors, retaining every central-action and nilpotence distinction above. General derived Schur replacements require their own construction; termwise Schur on the resolution fails the exhibited split sequence test.

Third prove the same local factors, gamma terms and conductor give a globally convergent or correctly regularized determinant. Trace-norm convergence must be established for the chosen analytic perturbations; strong convergence is insufficient in general. The inserted Abel family supplies this topology for an elementary scalar encoding, but has neither the independent arithmetic spectrum nor the positive metric needed for zero location.

Finally produce an independently proved positive form or self-adjoint determinant-preserving realization. One acceptance criterion is the Hurwitz target in the core; another is equality with the precise arithmetic quadratic form in the recent spectral theorems, with all their domain, ground-state, normalization and limit hypotheses verified. The local Cauchy kernel, K-group computation and graph spectral dimension alone meet none of these final comparison hypotheses. No remaining condition is silently asserted true here. Dirichlet, Hecke, Dedekind and Artin scopes must remain individually recorded.

Chapter 14

Graph pullbacks and completions with specified fibers

14.1 The complete Fock graph presentation

For graph C* conventions the edge operator has initial projection at its range vertex and final projection under its source vertex. Put

$$S_h = L_{a_h} Q_{a_{\tau h}}, \qquad T_h = L_{a_h} v_{[\tau h]}.$$

The two right-hand projections are orthogonal subprojections of $L_{a_h}^* L_{a_h} = Q_{a_{\tau h}} + v_{[\tau h]}$. Thus $S_h^* S_h = Q_{a_{\tau h}}$, $T_h^* T_h = v_{[\tau h]}$, and $S_h^* T_h = 0$. For distinct h the prefix ranges are orthogonal, so every other cross-edge CK1 product is zero. Their final projections sum to Q_{a_h}. The vacua have no outgoing edges. The resulting graph has $|H| + |Q_0|$ vertices and $2|H|$ edges, with cycles only among its state vertices and exits to the paired sinks. Gauge covariance and nonzero vertices prove faithfulness as well as surjectivity. This explains precisely how a graph C* algebra is obtained without imposing the incompatible original-quiver CK1 relations.

The graph integer map has one column for each regular vertex h and no sink columns:

$$d : \mathbb{Z}^H \longrightarrow \mathbb{Z}^H \oplus \mathbb{Z}^{Q_0}, \qquad d(e_h) = e_h - e_{\tau h} - b_{[\tau h]}.$$

The state part of $d(x) = 0$ says $x_h = x_{\tau^{-1} h}$; the sink part then says the constant cycle coefficients are in $\ker B_\Gamma$. For the cokernel choose a base state on each cycle and successively use $q_h = q_{\tau h} + b_{[\tau h]}$ to eliminate all other states. Closing the cycle leaves $\sum_{h \in c} b_{[h]} = 0$, while its base state remains free. Hence

$$\operatorname{coker} d \cong \mathbb{Z}^{\#\,\mathrm{cyc}\,\sigma} \oplus \operatorname{coker} B_\Gamma.$$

This gives an independent integral check of the previous compact-extension computation. The full labelled graph, diagonal projections and edge families carry more information than those coarse groups.

14.2 A genuine application of the supplied pullback theorem

For the interval dessin let $E_2 = G_\alpha$ have loop vertices q_x, q_y, common sink b, loops s_x, s_y and exits t_x, t_y. Remove b to obtain F_2, two disjoint loop graphs. Its quotient is exactly $C(\mathbb{T})^2$. Let E_1 have the same three vertices and edges $e_{x,n} : q_x \to b$, $e_{y,n} : q_y \to b$, $n \geq 0$, and no other edges. Remove b to obtain the edgeless F_1, whose algebra is $\mathbb{C}^2$.

The inclusions $F_i \subset E_i$ are admissible in the precise sense of [65, Definition3.1]: the removed sink set is hereditary/saturated; all edges ending at retained vertices are retained; no vertex emits infinitely many edges into the removed set and a positive finite number outside it. For E_1 the latter outside count is zero, which is allowed. Define a path functor identity on objects by

$$e_{x,n} \longmapsto s_x^n t_x, \qquad e_{y,n} \longmapsto s_y^n t_y.$$

Images of distinct positive edges are prefix incomparable: at the first different length one has an exit and the other a loop. Source vertices and identities cause no exception. The image consists of all positive pointed paths in E_2, whose last edge is not a short loop; vertices are included separately. The first graph is acyclic and the removed sink has no short loop in the second. All hypotheses of Theorem3.4 are now verified, giving

$$C^*(E_1) \cong \mathcal{T}_A \underset{C(\mathbb{T})^2}{\times} \mathbb{C}^2.$$

The quotient of $C^*(E_1)$ by its sink ideal is $\mathbb{C}^2$, and its sink ideal is compact operators on the paths ending at b. The graph is acyclic, hence its algebra is AF. There are no regular vertices in E_1: the two sources are infinite emitters and b is a sink. The graph K matrix has no columns and three rows, yielding $K_0 = \mathbb{Z}^3$ and $K_1 = 0$.

This is a positive instance of the new source inside our infinite dessin framework. It is a constants-symbol subalgebra of the Fock model, not the entire Fock algebra or the formal order. For a permitted cycle of length greater than one, its full closed path is itself pointed in this paper's convention, so an object-preserving acyclic path functor cannot cover all such paths. That simple obstruction prevents copying this example to every cycle by analogy. The sink-extension Theorem4.3 also requires a specified original pullback, injective gluing maps, annihilation of glued vertex projections and coverage of all paths ending at the gluing sinks. A two-to-one identification of sink occurrences within one branch does not satisfy these assumptions without another construction.

14.3 Diagonal residue obstruction and the corrected pullback

Suppose one tries to glue full matrix-circle blocks by their diagonal values. In M_2, $E_{12}E_{21} = E_{11}$, although both factors have zero diagonal. Thus the proposed boundary map is not a homomorphism. For $\ell > 1$, more generally any *-homomorphism from the full matrix-circle algebra to a commutative C*-algebra has equal images of $E_{ii} = E_{ij}E_{ji}$ and $E_{jj} = E_{ji}E_{ij}$. These images are both orthogonal and equal, hence zero; summing the diagonal units kills the image of one and then the whole homomorphism. This works for nonunital *-maps as well: a nonzero image of one would give a nonzero unital corner map. The failure concerns full matrix-circle blocks, not the already-restricted fiber algebra D_ℓ.

Evaluation $D_\ell \to \mathbb{C}^\ell$ is a genuine surjective *-homomorphism since at one both factors are diagonal. Its kernel is $C_0(\mathbb{T} \setminus \{1\}, M_\ell)$. Pulling it back along the repeated-coordinate embedding $\Delta_\alpha : \mathbb{C}^{Q_0} \to \mathbb{C}^H$ gives exactly the fiber conditions of $\mathcal{D}_H$. The paired constant diagonal matrices give a unital *-section. Hence this is a split C*-extension, not a claim deduced from a merely commutative diagram of nonmultiplicative maps. Since $\mathbb{T} \setminus \{1\} \cong \mathbb{R}$, each kernel block is a matrix suspension of $\mathbb{C}$, with $K_0 = 0$, $K_1 = \mathbb{Z}$. Split exactness now proves Theorem 5.3.

The pairing is retained in this specified presentation, not recovered from the unmarked isomorphism class. In particular arbitrary constant permutation matrices can relabel a branch's diagonal positions, so the spherical and elliptic theta examples have isomorphic unmarked $\mathcal{D}_H$ despite different ribbon orderings. Keep the labelled arrows, cycle cuts and distinguished fiber as

additional data when using it as a dessin model. Also the central branch unitary zI_ℓ represents ℓ times the primitive corner generator in K_1, not a new independent generator per matrix entry.

14.4 Generation, faithfulness and the exact failure of extension

Let ρ denote the polynomial representation in Theorem 5.3. Its vertex images are orthogonal projections summing to one. Every arrow image lies under the correct source and range vertex projections. A forbidden product vanishes because the intermediate state indices are τh and $\alpha\tau h$, which are distinct. Thus ρ is an actual algebra map, not a fitted characteristic polynomial.

For a full turn starting at h, $\rho(c_h) = w_c E_{hh}$ with $w_c(z) = g(z)^{|c|}z$. It is a normal element of $\mathcal{D}_H$. The function w_c vanishes exactly at one; away from that point $w_c/|w_c| = z$. Therefore it is injective on all of $\mathbb{T}$, and a homeomorphism to its image. Nonunital continuous functional calculus at $\rho(c_h)$, using functions zero at zero, gives every fE_{hh} with $f \in C(\mathbb{T})$, $f(1) = 0$. The zero condition makes the result vanish in all other matrix entries and branches.

To obtain an off-diagonal entry choose the unique shortest permitted path from state h to j within its cycle, of length $r > 0$ and cut-crossing count $\kappa \in \{0, 1\}$. Its image is $g^r z^\kappa E_{hj}$. Given $f(1) = 0$, multiply it on the left by the already available diagonal element

$$\frac{f(z)z^{-\kappa}}{g(z)^r + \varepsilon} E_{hh}, \qquad \varepsilon > 0.$$

The product is $fg^r/(g^r + \varepsilon)E_{hj}$ and converges uniformly to fE_{hj}. Indeed near one $|f|$ is small, and on the complement of that neighborhood g^r has a positive minimum. These two bounds prove uniform convergence without assuming division by a function vanishing at the fiber. Thus the generated algebra contains the whole kernel ideal. Its quotient contains the entire paired diagonal algebra, so it is $\mathcal{D}_H$.

For injectivity let a finite linear combination of path images vanish. At one, all positive paths vanish, forcing the coefficients of the original vertex idempotents to vanish. Fix a state-matrix entry in a branch. Its remaining paths have lengths $r + m\ell$ and images

$$g^r z^\kappa \sum_m a_m (g^\ell z)^m E_{hj},$$

with a possible initial zero coefficient if $r = 0$. On $\mathbb{T} \setminus \{1\}$ the prefactor is nonzero, and w_c has infinite range, so the polynomial has infinitely many distinct zeros. All coefficients are zero. Repeating by entries proves faithfulness.

No boundedness improvement repairs full formal extension. Pick any $z_0 \neq 1$, let $\lambda = w_c(z_0)^{-1}$, and consider $1 - \lambda c_h$. Its inverse $\sum_{m \geq 0} \lambda^m c_h^m$ exists in the arrow-adic order. The matrix image at z_0 has a zero eigenvalue on state h, so cannot be invertible. A unital algebra homomorphism would preserve the inverse identity, an immediate contradiction. This proves nonextension without any continuity assumption. It does not rely on the false claim that a norm greater than one alone forces a geometric-series denominator to be singular. Scaling g to have norm at most one still does not allow arbitrary formal series.

The two valid operator completions are structurally different. In the bipartite case $K_0(\mathcal{T}_A) = \mathbb{Z}^{E+1}$ differs from $K_0(\mathcal{D}_H) = \mathbb{Z}^E$; in the nonbipartite case the former has the extra $\mathbb{Z}/2$ torsion. Neither is automatically the norm completion of the arrow-adic topology. No invariant constructed solely from these complex objects distinguishes the rational twists already exhibited; arithmetic descent remains a separate input.

14.5 Invariant basis number and the Leavitt comparison

If a unital k-algebra R_1 has a unital representation on a nonzero finite-dimensional vector space V, an isomorphism $R_1^m \cong R_1^n$ induces an isomorphism $V^m \cong V^n$ by tensoring. Comparing dimensions gives $m = n$. This proves invariant basis number without requiring the representation to be faithful. Every original dessin algebra and completed order has a vertex-simple representation, and each permitted-state Laurent algebra has evaluation onto a nonzero matrix block. The Leavitt algebra of G_α has the same finite-dimensional representation after killing the vacuum sinks and evaluating one boundary cycle. Thus all of these examples have invariant basis number. Leavitt's free-rank phenomena are important elsewhere but cannot be assumed in this class simply from the name LPA.

For the specified finite graph G_α, the usual complex Leavitt path algebra embeds in $C^*(G_\alpha)$ with norm-dense image, using its canonical generators and involution [67, Theorem7.3]. Those generators are the split S_h, T_h, not the unsplit original gentle arrows equipped with ordinary CK1. This is the exact algebraic/analytic twin relationship applicable here.

Chapter 15

String finiteness and the smooth quotient surface

For a finite quiver, finitely controlled implies finitely generated: choose one finitely generated submodule containing each vertex space and sum the finitely many choices. Conversely the module itself works. Stabilization at each of finitely many vertices likewise gives ordinary artinianity. Crawley–Boevey's polynomial theorem therefore applies directly to our finitely generated and artinian polynomial modules, with its primitive injective bands in the latter case. It does not assert a classification of every possible algebraic module.

The formal branch $M = k[[x]]$, $y = 0$, gives a precise counterexample to that stronger assertion. An A-endomorphism F preserves each $x^n M$. For the polynomial truncation f_n of f, one has $F(f) - f_n F(1) \in x^n M$. Separatedness and all n imply $F(f) = fF(1)$. Hence $\mathrm{End}_A(M) = k[[x]]$ is local, so M is indecomposable. If an ordinary word module has $y = 0$, its word cannot contain y or y^{-1}, since such a letter would create a nonzero basis map. A reduced word using only $x^{\pm 1}$ cannot change direction. Its nonperiodic choices are finite strings, the free ray $k[x]$, and the opposite locally nilpotent ray. The first and last fail injectivity of x, and the free ray fails invertibility of $1 - x$. A two-sided pure-x word is periodic, and in every associated band x acts invertibly. On M, x is injective but not onto. None of these possibilities equals M. This includes arbitrary nonzero indecomposable Laurent coefficient modules, not just finite bands.

For a general nonzero completed lattice, finite generation over A would imply finite generation over $k[u]$. Every nonzero polynomial in u is a power of u times a unit of $k[[u]]$, so it acts injectively. The lattice would be a nonzero finite free $k[u]$-module. Multiplication by $1 - u$ on such a free module has a nonzero cokernel, but the same map is invertible over $k[[u]]$. This proves the contradiction in the core. The strictly descending u-adic chain separately excludes artinianity. These are actual failed hypotheses, not merely unverified applicability.

Lekili–Polishchuk's precise convention takes $D(A)$ to mean perfect dg modules. Their locally gentle definition allows infinite dimension, and their smoothness criterion says no forbidden cycle; properness says no permitted cycle. Both fail for every nonempty closed dessin here. Their Theorem3.2.2 therefore does not apply to the full polynomial dessin algebra, even though it applies to suitable infinite-dimensional quotients. The OPS finite-dimensional geometric-intersection theorem has its own grading, local-system, boundary and exceptional coincident-curve conditions. An unrestricted statement that every gentle/string derived object is an ungraded geodesic crossing is not justified by either source.

For the interval quotient $B = A/(y) = k[x]$, global dimension one follows from its PID structure: every submodule of a finite free module is free, giving finite projective resolutions of all finitely

generated modules. Thus $\mathrm{Perf}(B) = D^b(\mathrm{mod}_{\mathrm{fg}}\, B)$ in grading zero. Its permitted loop gives one unmarked boundary component and its length-one forbidden thread x gives one stop on the other boundary, the annulus of the smooth partially wrapped model. This construction uses the infinite polynomial quotient, not the completed $k[[x]]$ category.

Finally the quotient does not give a derived fully faithful embedding by ordinary inflation. Resolve B over A by the alternating maps $y, x, y, x, \ldots$. Hom into B gives $0, x, 0, x, \ldots$, so $\mathrm{Ext}^{2r}_A(B, B) = B/xB = k$ for every $r \geq 1$, whereas all positive self-Ext over B vanish. Consequently its inflation is not derived fully faithful, and the perfect B-module B becomes an infinite-projective-dimension A-module. A surface functor transferring these categories must account for that difference explicitly.

Chapter 16

Arithmetic character sums and the cellular determinant

16.1 The uniform calculation and its exceptional cases

In the finite-field calculation write $k = \mathbb{F}_q$; the final order-insertion paragraphs specify a separate characteristic-zero coefficient field. The curve is nonsingular because its discriminant is $-432d^2 \neq 0$, and has one point at infinity. Thus counting $1 + \eta(x^3 - d)$ in each affine fiber proves the trace formula in Theorem 6.2 directly. The multiplicative group of k is cyclic. When $3 \mid q - 1$, a nonzero cube has three roots and a noncube none, detected by $1 + \rho(t) + \bar{\rho}(t)$. At zero this expression is one, using the *constant* one. This convention differs from mathlib's zero-extended trivial multiplicative character, whose value there is zero. The proof and formal components never replace the constant by that character.

The substitution is valid including $u = 0, 1$ because the characters are zero extended:

$$\sum_t \rho(t)\eta(t - d) = \sum_u \rho(du)\eta(du - d) = \rho(d)\eta(-d) \sum_u \rho(u)\eta(1 - u).$$

Multiplying by the initial minus sign gives exactly $\pi_d + \bar{\pi}_d$. Changing ρ to ρ^{-1} conjugates both j and λ_d, so does not change the unordered roots or the integer trace. Characteristics two and three and $d = 0$ are excluded throughout. For a residue characteristic $p \equiv 2 \pmod 3$, odd extension degrees have trace zero by cube bijectivity, whereas even degrees lie in the split case; no claim of zero trace for all extensions of that characteristic is made.

For completeness, choose a nonzero $\mathbb{F}_p$-linear functional on k and compose it with $t \mapsto e^{2\pi i t/p}$ to obtain ψ. For a nontrivial multiplicative character χ,

$$\begin{aligned} |G(\chi)|^2 &= \sum_{u \neq 0} \chi(u) \sum_{y \neq 0} \psi((u - 1)y) \\ &= (q - 1) - \sum_{u \neq 0,1} \chi(u) = q. \end{aligned}$$

Both orthogonality identities follow by translating a finite character sum by an element on which its character is not one. The $z = 0$ terms in $G(\chi)G(\theta)$ sum to $\theta(-1) \sum_x (\chi\theta)(x)$, zero if the product is nontrivial. For $z \neq 0$ set $x = zu$, $y = z(1 - u)$ to obtain $J(\chi, \theta)G(\chi\theta)$. Coprime orders three and two ensure our product character is nontrivial. Taking norms proves $|J|^2 = q$, rather than presuming a desired positivity. This is the classical calculation reviewed directly in [68]; no claim of novelty is made.

At seven the five nonzero summands are $-\omega^2, -\omega, \omega, -\omega^2, 1$, so $J = 3 + 2\omega$. Multiplication by $\lambda_2 = \omega^2$ gives $-1 - 3\omega$. Their matrices are

$$\begin{pmatrix} 3 & -2 \\ 2 & 1 \end{pmatrix}, \qquad \begin{pmatrix} -1 & 3 \\ -3 & 2 \end{pmatrix}.$$

Both have determinant seven and the same positive Gram form; their traces are four and one. The arithmetic distinction between the rational models now comes from explicit finite-field characters, while their complex dessin is unchanged. Exact prime-field diagnostics test every nonzero twist for the listed nineteen primes; the theorem itself is uniform in prime powers and rests on the proof, not that finite list.

16.2 Deck descent and the actual cellular basis

The CM cellular construction in this and the next subsection assumes $q \equiv 1 \pmod 3$. The cover $\beta = x^3/d$ has deck transformations $(x, y) \mapsto (\zeta_3 x, y)$ and $(x, y) \mapsto (x, -y)$, generating $C_3 \times C_2 = C_6$. Label their actions on darts by $\sigma = (012)(345)$ and $\alpha = (03)(14)(25)$; they commute. Their product is $(0\,4\,2\,3\,1\,5)$. They preserve the edge pairing and both successor permutations. Consequently they define algebra automorphisms, preserve J and its completion and fix the common u. The projective-resolution maps are compatible since $\theta_g(a_h x) = a_{gh}\theta_g(x)$. Twisting module actions gives an exact functor and the corresponding relabelled resolution, without an assumption of arithmetic Frobenius.

Over an algebraic closure choose $a^3 = d$, $b^2 = d$ and $\varphi(x, y) = (ax, by)$ from E_1 to E_d. For the q-power Frobenius morphisms,

$$\varphi^{-1} \circ F_d \circ \varphi = h_d \circ F_1, \qquad h_d(x, y) = (a^{q-1}x, b^{q-1}y).$$

When $q \equiv 1 \pmod 6$, the first coordinate is the cubic residue $d^{(q-1)/3}$ and the second $\eta(d)$. Choose the embedding of cube roots defining ρ consistently. On the deck eigenspace labelled by dx/y, the *deck* character is their ratio, $\rho(d)/\eta(d) = \lambda_d$. This labels the twist, not a nonzero Frobenius action on differentials in characteristic p: that pullback is zero. An inverse convention for arithmetic Galois Frobenius changes the action convention; our displayed formula uses the geometric curve morphism explicitly. The character-sum polynomial fixes its trace without an unstated convention.

Orient the three geometric edges as in the core. Each occurs twice with opposite orientation in the single face, so $\partial_2 = 0$; ∂_1 has columns $(-1, 1)^t$. The homology basis $b_0 = e_0 - e_1$, $b_1 = e_1 - e_2$ has Gram matrix G inherited from the orthonormal cellular edges. Rotation sends $b_0 \mapsto b_1$, $b_1 \mapsto -b_0 - b_1$, exactly C. The involution swaps vertices and reverses each edge, hence acts as $-I$ on this plane. Thus multiplication by $A + B\omega$ is literally $AI + BC$, not merely an abstract matrix with the correct trace. Expanding its determinant gives the norm $A^2 - AB + B^2$, and multiplication of this norm proves $M^t G M = qG$. The displayed positive quadratic decomposition proves the metric independently of unknown zeros.

16.3 An explicit chain lift and determinant cancellation

Let P be the three-cycle permutation on C_1. Write $\pi_d = A + B\omega$ and $\gamma = A + B$. Define

$$F_1 = AI + BP, \qquad F_0 = \frac{1}{2}\begin{pmatrix} 1+\gamma & 1-\gamma \\ 1-\gamma & 1+\gamma \end{pmatrix}, \qquad F_2 = q.$$

These are rational cellular maps. The sum-zero plane of F_1 has restriction M_d, while the edge-sum line has eigenvalue γ. On C_0 the vertex-sum line has eigenvalue one and the boundary line eigenvalue γ. It follows directly that $F_0\partial_1 = \partial_1 F_1$; the other chain condition is zero. The induced maps on H_0, H_1, H_2 have characteristic factors $1-T$, $P_d(T)$, $1-qT$. In particular

$$\det(I - TF_0) = (1-T)(1-\gamma T), \qquad \det(I - TF_1) = (1-\gamma T)P_d(T).$$

The contractible boundary factor cancels, giving

$$\frac{\det(I - TF_1)}{\det(I - TF_0)\det(I - TF_2)} = \frac{P_d(T)}{(1-T)(1-qT)}.$$

This equality holds as a formal rational identity and by cancellation at apparent intermediate singularities. The alternating determinant with exponent $(-1)^i$ is its inverse; signs are not changed silently. The standard elliptic trace and determinant theorem identifies the right side with the finite-field curve zeta function [22, 20]. The elementary proof above supplies its actual trace and norm here; it does not independently reprove the general cohomological trace formalism.

This lift also has the required descent character on H_1. Write the base Jacobi value as $j = A_1 + B_1\omega$. Then h_d acts there by $\eta(d)C^r$ when $\rho(d) = \omega^r$, so twisting $A_1 I + B_1 C$ multiplies its eigenvalue j by λ_d, giving $M_d = A_d I + B_d C$. Reduction modulo $C^2 + C + I = 0$ gives the coefficients of π_d. If the corresponding full three-edge polynomials differ by $c(I + P + P^2)$, the coefficients are $c = 0, \eta(d)B_1, \eta(d)A_1$ for $r = 0, 1, 2$ respectively; they have the same homology action and differ only on the contractible boundary pair. An explicit homotopy sends $v_- - v_+$ to $c(e_0 + e_1 + e_2)$ and the vertex sum to zero. Its $\partial H + H\partial$ is the edge difference and the boundary scalar difference $3c$. Thus this normalization is compatible up to rational chain homotopy. It is not asserted to arise from a continuous Frobenius map of the complex Riemann surface, or to give a canonical integral Tate-lattice comparison.

16.4 A decisive restriction at inert primes

For $q \equiv 2 \pmod 3$, Frobenius sends ζ_3 to ζ_3^{-1}. Thus its cohomological relation with the cubic deck action requires $MC = C^2 M$ (the pullback convention yields the equivalent reversed relation). On a real two-dimensional carrier with our fixed C, comparing entries forces

$$M = \begin{pmatrix} a & b \\ a+b & -a \end{pmatrix}, \qquad \det M = -a^2 - ab - b^2 = -\tfrac{1}{2}(a^2 + b^2 + (a+b)^2) \le 0.$$

The genuine elliptic Frobenius determinant is $q > 0$, so such a real carrier is impossible. This is an elementary instance of the real-coefficient cohomology issue discussed by Deninger [62]. It does not rule out a complex realization, a larger real space, a different coefficient theory or an infinite-dimensional height operator. In particular it is not a refutation of an unrestricted Hilbert–Pólya approach.

There is a local complex replacement, with its limitations explicit. The conjugation matrix

$$K = \begin{pmatrix} 1 & -1 \\ 0 & -1 \end{pmatrix} \quad \text{satisfies} \quad K^2 = I,\ KC = C^2 K,\ K^t G K = G.$$

Set $F = i\sqrt{q}\,K$ on the complexification. Then $\operatorname{tr} F = 0$, $\det F = q$, $F^2 = -qI$ and $F^* G F = qG$, giving the correct trace-zero local factor. This is a two-dimensional complex, hence four-dimensional

real, local model. This is a one-q model; independently choosing $i\sqrt{q}K$ for each extension field does not give Frobenius-power compatibility. Such a family would need to start from one F_p and prove the comparison for its powers. The inserted $i\sqrt{q}$ is not a canonical rational or integral Tate comparison or a construction of a global positive determinant. The fixed real two-dimensional model has genuinely failed; its surviving split-prime construction and this complex alternative must not be conflated.

16.5 The remaining order and global spectral obligations

The deck automorphism has finite order, so over characteristic zero its eigenvalues are roots of unity. Its permutation action alone cannot supply a weight-one norm $\sqrt{q} > 1$. The independently computed Jacobi coefficient is essential. The above construction closes the specified local cellular benchmark, not a reconstruction of arithmetic from bare complex dessin data.

For these order-insertion tests take $\Lambda = \Lambda_{\mathbb{Q}}$ over $R = \mathbb{Q}[[u]]$, with rational residue simples and $V_d = \mathbb{Q}^2$. This is distinct from reducing the matrix in characteristic p, where its determinant p becomes zero. There are two concrete failures of a naive order lift. First, a residue simple S_e is annihilated by all arrows; $S_e \otimes V_d$ with independent endomorphism $I \otimes M_d$ has the desired underlying finite-$\mathbb{Q}$ determinant. But its projective dimension is infinite by the nonterminating forbidden resolution, and σ permutes all three vertex labels, so choosing S_e does not preserve full deck symmetry. This is not a perfect-order determinant realization.

Second, $\Lambda \otimes V_d$ is free of rank two over Λ, but the underlying R-rank of Λ is eighteen. In an R-basis, the Λ-*linear* $I \otimes M_d$ is eighteen copies of M_d, hence its determinant is P_d^{18}. On $e\Lambda$ the rank is six: each of its two hereditary branches contributes a row of length three, with finite conductor gluing changing no rank. This gives P_d^6. Restoring all three residue vertices similarly gives P_d^3 for this untwisted tensor action. A genuine deck-semilinear map permutes factors as well and need not have these powers; it requires its own comparison. No justified determinant-line root or multiplicity-removing functor is supplied here.

Finally fix a nonzero rational d when forming its global Euler product from good reductions. Local purity cannot be multiplied into a global zero-location proof. Since each reciprocal root has modulus $\sqrt{p}$, the product of good elliptic factors is absolutely convergent on $\operatorname{Re} s > 3/2$. The local zeros at $\operatorname{Re} s = 1/2$ are outside that initial product argument. The finite-field curve zeta's center is $1/2$; the global elliptic L-function's unshifted center is one, or $1/2$ only after a half-unit shift. Neither is an identification with the primitive Dirichlet function targeted earlier. Ramified factors, archimedean normalization, adelic descent and the global determinant-preserving positive spectral limit remain separate obligations.

Chapter 17

The theta order interface beyond tensor insertion

We prove the multiplicity theorem and construct its actual functorial escape, retaining the completed infinite order as the primary algebra. The finite algebra used below is its specified special fiber, not a replacement primary example.

17.1 Normal forms and the special fiber

Index the three quiver vertices by $i \in \mathbb{Z}/3$. Let $a_i^{\pm} : i \to i-1$ be the two permitted branches. Only paths of constant sign survive. Write $p_{i,r}^{\pm}$ for their length-r paths and $c_i^{\pm} = p_{i,3}^{\pm}$. The split order model gives

$$ue_i = c_i^{+} + c_i^{-}, \qquad p_{i,r+3}^{\pm} = up_{i,r}^{\pm} \quad (r \geq 1).$$

The second identity follows because multiplying by the opposite full cycle switches branch and vanishes. An R-basis of $e_i\Lambda$ is

$$e_i,\ a_i^{+}, a_i^{-},\ p_{i,2}^{+}, p_{i,2}^{-},\ c_i^{+}.$$

These span by the two identities and completion. They are independent in the two hereditary branch orders: off-diagonal entries distinguish the four shorter paths; the remaining combination $xe_i + yc_i^{+}$ has paired diagonal entries $(x + uy, x)$, forcing $x = y = 0$. This is an actual power-series basis, not just a generic rank calculation.

In $B = \Lambda/u\Lambda$, the same eighteen basis vectors remain. A product of nonempty paths is zero if branches switch or the total length exceeds three; the length-three minus path is the negative of the plus path. A length-four path is u times a length-one path, hence zero. The radical $\mathfrak{r}$ is the positive-length ideal, with $\mathfrak{r}^4 = 0$ and $B/\mathfrak{r} = \mathbb{Q}^3$. Each e_iB has radical-layer dimensions $(1, 2, 2, 1)$ and has two composition factors at each vertex, so the Cartan matrix is

$$C_B = \begin{pmatrix} 2 & 2 & 2 \\ 2 & 2 & 2 \\ 2 & 2 & 2 \end{pmatrix}.$$

The Cartan matrix alone does not establish the endomorphism formula; the path filtration supplies that step.

17.2 All projectives and all linear endomorphisms

Let J be the completed arrow ideal. Every $1-x$, $x \in J$, has its convergent formal inverse; the same applies to $1-yx$ for arbitrary $y \in \Lambda$. Thus J is contained in the Jacobson radical, and $\Lambda/J = \mathbb{Q}^3$ implies equality. If P is finitely generated projective, choose a basis of each multiplicity space in P/PJ and lift its vectors into Pe_i. This gives

$$Q = \bigoplus_i (e_i\Lambda)^{n_i} \longrightarrow P$$

inducing an isomorphism on tops. Nakayama makes this surjective. Its split kernel N is finitely generated and satisfies $N/NJ = 0$, hence vanishes by Nakayama. This proves the decomposition for every such projective without an unproved freeness assumption over Λ.

An entry $e_i\Lambda \to e_j\Lambda$ is left multiplication by an element of $e_j\Lambda e_i$. Its degree-zero part is possible only when $i = j$ and is a scalar multiple of e_i. For f on P, write its top blocks A_i and set $A = \operatorname{diag}_i A_i$. The remainder has positive path length. On P/uP it strictly raises the path filtration. At each of the two length-one and two length-two slots, and the length-zero and length-three slots, the degree-preserving map is exactly A. In an increasing-degree basis the matrix is lower block triangular. For the formal upper-block convention order the six slots instead as

$$3+,\ 2+,\ 2-,\ 1+,\ 1-,\ 0.$$

There are six diagonal copies of A, allowing arbitrary positive-length off-diagonal entries. Hence

$$\det_{\mathbb{Q}}(1 - T\overline{f}) = \det_{\mathbb{Q}}(1 - TA)^6.$$

Specializing the finite R-matrix determinant coefficientwise gives Theorem 6.3. No simultaneous diagonalizability, tensor form of f, arithmetic purity or deck equivariance is required.

For a bounded complex $P^\bullet$ with a linear chain map $f^\bullet$, fix either parity convention and write

$$D_R(P^\bullet, f^\bullet; T) = \prod_j \det_R(1 - Tf^j)^{(-1)^j}.$$

The inverse convention gives the reciprocal and the same obstruction. Each factor has constant coefficient one, so its reduction is nonzero. Specialization of this displayed rational expression is defined and equals

$$\left[\prod_{j,i} \det_{\mathbb{Q}}(1 - TA_i^j)^{(-1)^j}\right]^6.$$

Cancellations cannot change the divisibility of divisor multiplicities. In particular adding contractible projective pairs cannot repair it. Here a perfect endomorphism means a bounded-projective chain representative; no statement about an arbitrary infinite resolution or nonperfect lattice is inferred.

Generically put $N = \sum_i n_i$. As a right module over $M_3(K) \times M_3(K)$, P_K is the sum of N copies of each branch's three-dimensional row simple. Any commuting map has matrices $F_+, F_- \in M_N(K)$ on their multiplicity spaces, so

$$\det_K(1 - Tf_K) = \left(\det(1 - TF_+)\det(1 - TF_-)\right)^3.$$

For example, left multiplication by c_i^+ on $e_i\Lambda$ has ordinary characteristic determinant $(1-uT)^3$, so a sixth power is forced only at the special fiber. This also shows why generic reduced determinants

and ordinary determinants must not be conflated. We do not need an integral choice of either generic matrix to derive the cube obstruction.

For the local numerator, suppose a sixth power $A(T)^6/B(T)^6$ equals a nonzero quadratic $P(T)$ with $B \neq 0$. Polynomial degrees would give $6 \deg A = 2 + 6 \deg B$, impossible. This includes repeated roots. For the complete curve zeta, $q > 1$ and $|a_q| \leq 2\sqrt{q}$ imply $P(1) > 0$ and $P(1/q) = P(1)/q > 0$. Its two denominator roots are distinct uncancelled simple poles, again impossible for a sixth power. These arguments do not assume global RH or Artin holomorphy.

17.3 An actual integral determinant functor of multiplicity one

Project to one hereditary cycle order $B_+ \subset M_3(R)$. Its standard column $W_+ = R^3$ is a left Λ-module with $e_i W_+ = R\epsilon_i$. More explicitly a_i^+ acts by $u^{w_i} E_{i,i-1}$, with $(w_0, w_1, w_2) = (1, 0, 0)$ for one cut, while every a_i^- acts by zero. These matrices respect travel-order multiplication as written: $E_{ij}E_{jk} = E_{ik}$. Each plus full cycle is uE_{ii}, so the common central u acts by uI. Nonempty paths tend to zero u-adically, giving the action of the *full completed order*, not just its polynomial subalgebra.

This (Λ, R)-bimodule defines $- \otimes^{\mathbf{L}}_{\Lambda} W_+$. On a bounded complex of finite projectives it is computed termwise, and its terms are finite free over R. An acyclic bounded projective complex is split contractible, and tensor preserves that contraction. Thus it descends to a genuine triangulated functor $\Phi_+ : \mathrm{Perf}(\Lambda) \to \mathrm{Perf}(R)$. No assertion of exactness on all un-derived modules or flatness of W_+ is needed. In fact W_+ has infinite projective dimension as a left Λ-module: Λ is noetherian, being finite over the central noetherian ring R, and W_+ is finitely generated. A finite projective resolution could thus be chosen with finite terms. Every left projective term has R-rank divisible by six by the same top argument, whereas W_+ has rank three, contradicting the alternating rank identity. This does not prevent tensoring bounded right-projective complexes.

The isomorphism $e_i\Lambda \otimes_\Lambda W_+ \to e_i W_+$ sends $e_i\lambda \otimes w \mapsto e_i\lambda w$. Its inverse is $e_i w \mapsto e_i \otimes e_i w$, proving rank one directly. Consequently $e_i\Lambda \otimes_{\mathbb{Q}} V$, with action $1 \otimes M$, maps to $R \otimes_{\mathbb{Q}} V$ with action M. Its characteristic determinant is $\det(1 - TM)$ *once*. On the regular input, the three vertex lines survive and the factor appears three times. A full symmetric vertex orbit therefore is not silently replaced by a chosen vertex.

Different cycle cuts give different integral column lattices. Their generic modules are isomorphic, and branch endomorphism characteristic determinants agree by generic conjugation; equality over K implies equality over R. Nevertheless an equivariant lattice is stronger data. Branch selection also changes the functor: for the unit $f = e_i + c_i^+$ on $e_i\Lambda$, the plus determinant is $1 + u$ and its characteristic factor is $1 - (1 + u)T$. Under α, c_i^+ becomes c_i^-, whose plus action is zero; the determinant becomes one and the characteristic factor $1 - T$. Since these scalar automorphisms differ, no natural isomorphism of determinant lines can make this chosen branch functor α-invariant for all endomorphisms. Pairing both branch functors makes this branch-swap data available but doubles the local factor on the basic-projective tensor input.

17.4 The exact rotation obstruction and its allowed escape

Consider any left Λ-lattice supported on the plus branch, free of rank one at every e_i, and with central u acting as multiplication by u. Write its plus arrow scalars as $a_0, a_1, a_2 \in R$. Their product is u, so they are nonzero and their nonnegative valuations sum to one. A strict R-linear lift of σ that intertwines the order rotation permutes the three vertex lines by units. Its arrow-intertwining

identities make the three arrow valuations equal. Thus $3m = 1$ for an integer $m \geq 0$, impossible. The argument already excludes an invertible intertwiner; imposing that its cube be one cannot help.

There is an elementary coefficient proof of the same obstruction. Intertwining by units makes vanishing of the three arrow constant coefficients equivalent. Their product has constant coefficient zero, so all three vanish. Factoring u from two of them would make $a_0a_1a_2$ divisible by u^2, contradicting that it equals u. This is the literal power-series component checked in Lean.

After the explicit ramified change $R' = \mathbb{Q}[[v]]$, $u = v^3$, *choose a new column lattice* with all three plus arrow maps $vE_{i,i-1}$. Cyclic permutation of the basis is an order-three intertwiner fixing v. The full-cycle relation is now $v^3 = u$ as required. Merely base-changing the old cut lattice gives arrow valuations $(3, 0, 0)$ and does not produce that linearization. This construction changes the base and lattice and does not establish an unramified descent comparison. It also still needs both branches to address α.

The rotation obstruction is about actual central-fixed rank-one branch lattices, not every possible determinant-level natural transformation. The branch characteristic determinants may be rotation-invariant through their generic reduced interpretation even without a lattice lift. Neither this theorem nor the ordinary-determinant obstruction excludes semilinear correspondences, other determinant categories or infinite analytic models.

The next arithmetic task is therefore narrower and more concrete: choose a branch functor, a ramified lattice or a different equivariant replacement only after proving the required descent comparison, and construct its prime action from arithmetic data rather than feed in the already known M_d. Bad primes, integral/Tate comparison, local-to-global conductor and gamma factors, and a positive spectral limit for the same completed function remain unresolved.

Chapter 18

Explicit tame descent and the full-deck coefficient test

The preceding ramified column is a precisely specified object of the original infinite theta-order framework. We compute its descent instead of treating a semilinear group action as automatically effective integral descent. All constructions below are over the new *mathematical* coefficient field $k = \mathbb{Q}(\omega)$; they do not replace the original rational model or its source history.

18.1 The action on genuine formal series

Write $R = k[[u]]$, $S = k[[v]]$ with $u = v^3$. Every $f(v) \in S$ has a unique expansion $f_0(u) + vf_1(u) + v^2 f_2(u)$. Hence S is finite free of rank three over R. Let $g(f)(v) = f(\omega v)$. On $W = S^3$ with basis $\epsilon_0, \epsilon_1, \epsilon_2$, put

$$\Theta(f_i\epsilon_i) = \omega^{-i} f_i(\omega v)\epsilon_i, \qquad C\epsilon_i = \epsilon_{i+1} \quad (i \bmod 3).$$

The plus arrow a_i^+ acts by $vE_{i,i-1}$, the minus arrow by zero. The cyclic product is uE_{ii} and arbitrarily long permitted paths tend to zero v-adically, so this is a module over the full completed order. For $i = 0$, the coefficient in the target under Θa_i^+ is ωv and in the source under $a_i^+\Theta$ it is $v\omega^{-2}$; these agree. The same calculation for $i = 1, 2$ proves compatibility with every arrow and therefore the completed algebra. Also $\Theta^3 = 1$.

For all coefficients, not just a truncated diagnostic,

$$[v^n](\Theta w)_i = \omega^{n-i}[v^n]w_i.$$

Thus invariance is equivalent to support in $n \equiv i \pmod 3$, and

$$L = W^\Theta = \bigoplus_{i=0}^{2} Rb_i, \qquad b_i = v^i\epsilon_i.$$

The arrows on this basis have scalar valuations $(1, 0, 0)$, since $a_0^+ b_2 = ub_0$, $a_1^+ b_0 = b_1$ and $a_2^+ b_1 = b_2$. Tame invariants return the old cut column rather than a new strict unramified rotation carrier.

The extension $R \subset S$ is faithfully flat. Its group quotient has a fixed point at $v = 0$, however, and is not a μ_3-torsor there: $S \otimes_R S$ is not the product of the three group graphs at that point. Semilinear μ_3 data are therefore not by themselves the full effective fpqc descent data for a vector bundle on $\operatorname{Spec} R$. The adjunction comparison is explicitly

$$S \otimes_R L \longrightarrow W, \qquad \operatorname{diag}(1, v, v^2),$$

with determinant $v^3 = u$, cokernel $S/(v) \oplus S/(v^2)$ and closed-fiber rank one. This proves its failure to be an isomorphism directly. The quotient stack $[\operatorname{Spec} S/\mu_3]$ retains the stabilizer at zero; its coarse space is $\operatorname{Spec} R$. This local root construction is described in [71]. Alper's vector-bundle criterion [70, Theorem10.3, pp.2386–2387] distinguishes precisely this nontrivial closed-fiber action from effective coarse descent. We use these sources for interpretation; all displayed module comparisons have already been calculated explicitly.

18.2 A projective symmetry survives on the endomorphism order

Directly on the three basis vectors,

$$\Theta C = \omega^{-1} C\Theta = \omega^2 C\Theta.$$

Thus the rotation does not preserve L. The corrected vC does preserve it, since the factor ω from $g(v)$ cancels the commutator. In the invariant basis it has matrix A from the core, with $A^3 = uI$ and $\det A = u$. This is generically invertible and gives an order-three projective rotation after passing to the fraction field; it is not an invertible integral lattice intertwiner.

There is nevertheless a true algebra-level escape. Let $F = (f_{ij})$ be an arbitrary S-linear endomorphism of the *carrier* W, not assumed Λ-linear. Its tame conjugate has entries $\omega^{j-i} g(f_{ij})$. Invariance therefore means

$$f_{ij} \in v^{[i-j]_3} R,$$

where $[r]_3 \in \{0, 1, 2\}$ is the least residue. After replacing ϵ_i by $b_i = v^i \epsilon_i$, the entry becomes

$$v^{[i-j]_3 + j - i} R = \begin{cases} R & i \geq j, \\ uR & i < j. \end{cases}$$

Consequently $\operatorname{End}_S(W)^\Theta$ is exactly the hereditary three-cycle order B_+ in the previously fixed cut convention. Multiplication is preserved by conjugation in the generic matrix algebra; no entrywise projection is being misused as a ring map.

The scalar commutator cancels under conjugation. Hence $\operatorname{Ad}(C)$ commutes with tame conjugation, descends to B_+, and is represented there by $\operatorname{Ad}(A)$ because v is central. Since $A^3 = uI$, this algebra automorphism has order three and preserves the hereditary order despite A^{-1} not lying in its unit group. This explains the surviving rotation of the branch order; it does not construct a rotated integral column or a Frobenius endomorphism. The other branch is identical and the paired-diagonal residue gluing still defines the original Λ_R inside $B_+ \times B_-$. Its label automorphisms remain the already constructed dessin symmetries.

18.3 Determinants, Schur weights and the boundary correction

On $\det_S W = \bigwedge_S^3 W$, both $\det D = 1$ and $\det C = 1$. Thus this line has the scalar action g and genuinely descends to the trivial R-line with trivial rotation. This is a real positive determinant-level result. On the other hand,

$$b_0 \wedge b_1 \wedge b_2 = v^3(\epsilon_0 \wedge \epsilon_1 \wedge \epsilon_2),$$

so the natural comparison

$$\det_R(W^\Theta) \longrightarrow (\det_S W)^\Theta$$

is multiplication by u, with cokernel $R/(u)$. Both lines are abstractly free of rank one, but their given comparison is not an isomorphism. It records the divisor of the ramified lattice change and

cannot be discarded when claiming a determinant-preserving integral comparison. For the *same* operator vC, the scalar on both determinant lines is u; naturality is respected. Comparing $\det C = 1$ with $\det A = u$ without the extra factor v would instead compare different operators.

For an induced nonzero homogeneous tensor/Schur carrier of degree d, the same functorial calculation gives commutator ω^{-d}. The two induced invertible operators commute exactly when $3 \mid d$. This is a group-action statement, not sufficient for coarse vector-bundle descent: $\mathrm{Sym}^3(S^3)$ has closed-fiber inertia multiplicities $(4, 3, 3)$ for the three characters, so its inertia is still nontrivial even though the commutator vanishes. A mixed tensor $W^{\otimes a} \otimes (W^*)^{\otimes b}$ has net exponent $a - b$; $\mathrm{End}_S(W)$ is the concrete net-zero escape computed above.

These carrier functors are not automatically functors on unital Λ-modules. Applying global $\bigwedge^3$ to the rank-one vertex idempotents kills all three, although their sum is the identity before applying this nonadditive functor. Vertexwise $\bigwedge^3$ of the rank-one column is zero. Vertexwise Sym^d for $d > 0$ does retain the monomial zero relations but changes the full-cycle scalar from u to u^d. It leaves the fixed central-action problem unless that change of base is included. None of the Schur cancellations supplies the missing two-dimensional arithmetic carrier.

18.4 Why the local Jacobi plane does not descend by this repair

On constant vectors Θ acts by D. It sends the sum-zero cycle $\epsilon_0 - \epsilon_1$ to $\epsilon_0 - \omega^2\epsilon_1$, whose coordinate sum is nonzero. It also does not preserve the edge-sum line. Thus this order column is not already a tame descent of the earlier cellular chain complex or its H_1.

For the split local coefficient $\pi = a + b\omega$, the natural rotation polynomial on the balanced carrier is $F = aI + bC$. Since g fixes $a, b \in k$, its commutator is

$$\Theta F - F\Theta = b(\omega^2 - 1)C\Theta.$$

It is nonzero when $b \neq 0$. In particular both prime-seven twists $(a, b) = (3, 2), (-1, -3)$ fail this test. Prime powers with $b = 0$ are not excluded by this particular calculation; that exceptional commutation does not prove a global comparison.

Replacing C by vC gives an invariant carrier map, whose matrix on L is $aI + bA$. Direct determinant expansion gives

$$\det(1 - T(aI + bA)) = (1 - aT)^3 - ub^3T^3.$$

At $u = 0$ this is $(1 - aT)^3$, not $P_d(T)$, which has degree two. The weighted replacement therefore does not recover the established local factor. Neither C nor vC is generally Λ-linear: they intertwine its rotation. Their sums with the identity have not thereby become endomorphisms in the ordinary order-module category. They are legitimate carrier tests, with exactly the failures just exhibited.

18.5 The full orbit is the normalization, and arbitrary kernels still fail

Twist the tame action by the three characters: $\Theta_r = \omega^r\Theta$, $r \in \mathbb{Z}/3$. Its fixed lattice is

$$L_r = \bigoplus_i Rv^{[i-r]_3}\epsilon_i,$$

with the cut at arrow r. Rotation gives an actual R-linear isomorphism $C : L_r \to L_{r+1}$, taking each displayed basis vector to the corresponding next one. Thus the direct sum of all three cuts has

a strict rotation, at the cost of vertex rank three. Before invariants the orbit is S-rank nine and underlying R-rank twenty-seven; its invariant lattice is R-rank nine. The original orbit S-lattice still has nontrivial inertia at zero and need not be the base change of these invariants.

There is an explicit integral identification of the invariant orbit. In the standard hereditary order B_+, the j-th column has entries $u^{t_{ij}}R$ with $t_{ij} = 1$ for $i < j$ and zero otherwise. In its natural column basis the arrow coefficient has exponent

$$\delta_{i0} + t_{i-1,j} - t_{ij} = \delta_{ij}.$$

Its cut is therefore exactly j, identifying B_+e_j with L_j. Consequently $\bigoplus_r L_r \simeq B_+$ as left Λ_R-modules. Adding the exchanged minus-branch orbit gives the hereditary normalization $\widetilde{\Lambda} = B_+ \times B_-$, with full deck action and vertex rank six. On a basic projective with external arithmetic matrix this yields P_d^6.

In fact this normalization replacement restores the *ordinary determinant for every linear endomorphism*. For a finite projective P, the inclusion $P \to P \otimes_\Lambda \widetilde{\Lambda}$ becomes an isomorphism over $K = k((u))$, since $\widetilde{\Lambda}_K = \Lambda_K$. Its extended endomorphism and the original f therefore have the same generic characteristic determinant. Both polynomials have coefficients in R, which injects into K, so they agree already over R. The bounded-complex ratios also agree. This symmetry repair returns the previously refuted ordinary determinant, not merely its external tensor exponent.

For completeness we now prove Theorem 6.4 for arbitrary finite free kernels, without assuming they split integrally into branches or are projective over the order. Let

$$p_\pm = u^{-1} \sum_i c_i^\pm \in \Lambda_K.$$

These are central generic branch idempotents. Put $W_\pm = W_0 \cap p_\pm(W_0 \otimes_R K)$. They are finite free R-lattices spanning those generic summands, stable under Λ_R. Rotation fixes them, branch swap exchanges them. Their vertex ranks are constant on each branch: the arrow maps become invertible over K because a full cycle acts by u. Write these ranks r_+, r_-. No equality $W_0 = W_+ \oplus W_-$ over R has been assumed.

On the plus branch choose integral vertex bases. The three square arrow matrices X_0, X_1, X_2 have product uI_{r_+} around every cycle. Thus

$$\sum_i \operatorname{val}_u(\det X_i) = r_+.$$

The rotation lift is an invertible matrix between each pair of vertex lattices, hence its determinant is an R-unit. Its intertwining identities make all three arrow determinant valuations equal. Therefore $r_+ = 3m_+$; similarly $r_- = 3m_-$. The branch-swap lift gives $r_+ = r_-$, so generic rank additivity gives $\operatorname{rank}_R e_i W_0 = 6m$. Only invertible intertwiners were used; imposing the full deck group relations is stronger than necessary.

For the general determinant statement reduce modulo u and filter each vertex by $e_i J^a(W_0/uW_0)$. Since $J^4 \subset u\Lambda$, this is a finite filtration. In $\Phi_{W_0}(P) = \bigoplus_i (e_i W_0)^{n_i}$, positive-length entries of f raise the filtration, while the degree-zero matrix A_i repeats on its i-th graded pieces. Their total dimension is $6m$. Multiplying the graded characteristic determinants proves the asserted power for *every* f. Flatness of the kernel as a left Λ-module was not used; bounded right projectives compute the derived functor and give finite free R-outputs. Denominator constant terms one permit specialization of every bounded alternating ratio. The regular left kernel Λ_R attains $m = 1$, making the rank bound sharp.

The remaining arithmetic problem therefore requires a different hypothesis: a genuinely twisted determinant target, a specified non-linear/semilinear correspondence with its own comparison, or an infinite analytic realization. One cannot continue searching inside this closed finite-free, fixed-center, full-deck kernel class for a missing small estimate. The local purity and descent computations supply no global positive spectral limit. Moreover $k/\mathbb{Q}$ has degree two: ordinary restriction of scalars sends a rational local factor P_d to P_d^2. A relative k-determinant must not silently be identified with the former rational determinant. Finite-field curve zeta, global elliptic L-functions and Dirichlet GRH keep their distinct scopes and centers.

Chapter 19

Literal formal and computational coverage

`DessinNodeOrder.lean` defines the fiber-product subring of two genuine power-series rings. Its twenty printed declarations establish diagonal injectivity, nonzero branches, branch zero products, factorizations and annihilator identities, regular u, augmentation surjectivity and exactness, bijective power-series coordinates, square-zero alternating maps, three kernel-equals-range statements and projectivity of the actual regular/product terms. The coordinate statement is a bijection; the file does not yet package it as an R-linear equivalence or declare the general order freeness theorem.

`DessinInvariantComponents.lean` has ten printed declarations: three CK1-collapse components, determinant change of bases with an actual inverse, symmetric-square zero, identity, composition and relation preservation, the degree-two Schur character identity, and the nodal central-parameter obstruction. Its symmetric-square matrix is

$$\operatorname{Sym}^2\begin{pmatrix} a & b \\ c & d \end{pmatrix} = \begin{pmatrix} a^2 & ab & b^2 \\ 2ac & ad+bc & 2bd \\ c^2 & cd & d^2 \end{pmatrix}.$$

This is the ordinary monomial basis convention; composition is proved universally over any commutative ring. The full project suite prints types and foundational dependencies; no theorem about general LR decompositions, abstract derived equivalences, C* K-theory or GRH is inferred from these component proofs.

The exact Python checks use fixed rational matrices and exhaustive finite sets, with no random seeds. They construct the displayed permutations and paths, evaluate rational Cartan identities, check formal Euler products through a stated degree, verify unrestricted-output Fock basis identities on bounded input sets, compute incidence Smith data, construct all nine string representations and signed maps, and test Young/LR/Cauchy examples and the seven-element-field counts. Those diagnostics are reproducible finite corroboration. The universal infinite claims rest on the proofs or explicitly cited theorems, and the arithmetic comparison remains open.

The ten additional `DessinPullbackComponents.lean` statements use literal two-state matrix units and a subring of a product of arbitrary rings, with equal images under two ring homomorphisms. The section hypothesis of its projection-surjectivity theorem is explicit. It does not construct a topological C*-pullback or assert that a commutative diagram is automatically a pullback. The no-residue theorem is universal algebra, with a nontrivial commutative target; it is not an assumed arithmetic positivity premise.

`ThetaJacobi.lean` adds sixteen declarations, with actual finite fields and MulChar rather than

a hypothetical arithmetic kernel. Its norm theorem invokes mathlib's proved Jacobi inverse-product identity and derives characteristic inequality from finiteness; all three character nontrivialities are explicit. Other declarations verify the rescaling substitution, CM multiplication/polynomial/Gram positivity components, exact prime-seven matrix polynomials, and actual 2-by-3 boundary/3-by-2 cellular inclusion, homology restriction, three-edge determinant and rational vertex chain-map equations. It does not formalize elliptic point counting or an order-to-Frobenius functor.

The final three `ThetaJacobi.lean` declarations verify the actual conjugation matrix identities and the real two-dimensional inert-prime determinant obstruction. They do not assume any unknown zero location or exclude complex/enlarged spectral realizations.

`ThetaProjectiveMultiplicity.lean` adds five declarations. Arbitrary upper-block matrices with six identical diagonal blocks have the sixth-power determinant and characteristic-factor formulas. A literal power-series constant-coefficient map specializes matrix determinants, for each scalar parameter; the coefficientwise polynomial/order interface remains prose. A nonzero quadratic cannot be a rational-function sixth power, proved by polynomial degrees. Three genuine power series with product X cannot have the cyclically equivalent residue-vanishing conditions forced by invertible rank-one arrow intertwiners. The derivation of the path blocks from the full theta order, projective decomposition, derived branch functor and deck intertwiners is not fully formalized. The complete analytic suite now has208printed declarations; no hidden arithmetic positivity assumption occurs.

`ThetaTameDescent.lean` adds twelve printed component declarations (and one auxiliary polynomial lemma). They use genuine formal-power-series rescaling and its coefficient operator, proving the coefficient action, invariant-coefficient vanishing and the tame operator's cube. Actual three-state matrices satisfy the clock/rotation commutator, comparison determinant and closed-fiber equations, weighted-cycle cube and full characteristic polynomial, noncommutation of a nonconstant rotation polynomial, trivial whole-column determinant actions, and the same-operator comparison for vC. The classification of all fixed series by residues, full order action and hereditary invariant algebra, stack interpretation, valuation/rank theorem, general coefficient-functor filtration and GRH are not thereby fully formalized. No unknown positivity premise is assumed.

Chapter 20

Explicit covering calculations and derived transport

Here are the linear details behind Proposition 7.2. Write $x_i = F_{ii}$ for diagonal entries of an endomorphism F preserving the three vertex spaces. Solving $FX = XF$, $FY = YF$ leaves a common diagonal c and six free entries. More explicitly its only off-diagonal entries are

$$F_{02} = F_{13} = t_0, \quad F_{15} = t_1, \quad F_{35} = F_{46} = t_2, \quad F_{48} = t_3, \quad F_{68} = F_{70} = t_4, \quad F_{72} = t_5.$$

All others vanish. This can be checked column by column using the displayed partial permutation matrices X, Y: their nonzero columns specify all constraints, and the zero columns force the remaining entries to zero. If $r_0, \dots, r_5$ are the six radical generators in the displayed order, the only nonzero products are

$$r_0 r_2 = r_1, \qquad r_2 r_4 = r_3, \qquad r_4 r_0 = r_5.$$

Every product of three radical generators vanishes. Thus the listed space is a local algebra, not merely a seven-dimensional vector-space count.

For clarity, the Euler equations used in the obstruction are

$$\begin{aligned} &d_1 - d_0 = 1, && d_3 - d_2 = 1, && d_4 - d_3 = 1, \\ &d_6 - d_5 = 1, && d_7 - d_6 = 1, && d_0 - d_8 = 1, \\ &d_1 - d_2 = 1, && d_4 - d_5 = 1, && d_7 - d_8 = 1, \end{aligned}$$

where $d_i = D_{ii}$. Subtract the last row from the first two rows after summing: the left side is zero and the right side is three. This is an identity in every characteristic-zero coefficient field. In characteristic three this particular obstruction disappears; no conclusion there is asserted. The closed walk

$$a_0 b_0^{-1} a_0 \, a_1 b_1^{-1} a_1 \, a_2 b_2^{-1} a_2$$

explains the computation: six forward steps and three backward steps have net lift displacement three. Arbitrary changes of basis cannot remove the Euler contradiction. This is an algebraic lift obstruction, not an assertion about the topological fundamental group of the compact torus.

The Hom formula also has a constructive perfect-complex version. Each cover representable is finite support and pushes to its corresponding vertex projective. For a bounded complex $P^\bullet$ of finite sums of such representables and a bounded finite-support complex $N^\bullet$, decompose the entire Hom complex by deck displacement. The differential preserves that displacement, and only finitely

many displacements occur across the finitely many degrees. Taking cohomology gives

$$\mathrm{Hom}_{D(B_L)}(FP^\bullet, FN^\bullet[q]) \simeq \bigoplus_g \mathrm{Hom}_{D(\widetilde{B}_L)}(P^\bullet, T_g N^\bullet[q]).$$

Bounded projective complexes compute these derived Hom spaces, which justifies the equality rather than assuming every module perfect. This elementary proof does not assert an equivalence of entire bounded derived categories or cover objects of infinite projective dimension. The broader precovering statement has its exact hypotheses in [74, Theorem 4.28].

Finally the branch involution $\sigma(a_i) = b_i$, $\sigma(b_i) = a_i$ preserves B_L. In characteristic different from two one can study $B_L \# k[\mathbb{Z}/2]$ through equivariant representations. For the nine-dimensional module above, $\operatorname{rank} X = 6$ and $\operatorname{rank} Y = 3$, so $M \not\simeq \sigma M$. The sum $M \oplus \sigma M$ has canonical swap equivariance. This is an explicit orbit construction; it neither chooses a nonexistent fixed-object linearization nor identifies this skew group algebra with the particular GLS algebras in [75].

`CoveringBand.lean` verifies the actual matrices' mixed products, cubic nilpotence and absence of an arbitrary Euler matrix. The general covering, module endomorphism classification, derived functors and the surface/Fukaya equivalence are not fully formalized by these three matrix statements. Exact rational code additionally checks thirty-six Hom pairs, the full radical multiplication and the two Hom-control defects.

Part III

AR components, derived categories and Hom-control

Chapter 21

Almost-split geometry, Hom control and determinant relations

The infinite locally gentle algebra and its completed order are the primary objects in this chapter. Finite algebras enter through specified quotients or special fibers, with their categories named. This distinction makes the pictures more useful: a mesh is an exact sequence in an actual category, a tube is an entire component, and a diagram of limiting words records additional objects rather than suggesting an unproved equivalence.

We work over an algebraically closed field k of characteristic zero unless stated otherwise. Paths are written in travel order, so ab traverses a first. We use right projectives e_iA with this convention. Column representations may instead be read over the opposite algebra; all displayed arrow-intertwining identities use the usual column convention. This change of handedness does not identify different categories or change any of the explicit Hom dimensions.

21.1 What an AR picture specifies

For an infinite polynomial dessin algebra $A = kQ/I$, write $\operatorname{mod}_{\mathrm{fd}} A$ for finite-dimensional modules. Its arrow-adic completion is $\Lambda = \varprojlim A/J^n$. A continuous finite-dimensional Λ-module kills some J^n. A lattice over an order finite over $R = k[[u]]$ is instead a finitely generated module free over R. A nonzero lattice has infinite dimension over k and is not a continuous finite-length module. These distinctions persist even when the same quiver describes the arrow actions.

The polynomial string classification has its own finiteness boundary. For a finite quiver, finitely controlled modules are precisely finitely generated modules: sum the finitely many finitely generated submodules containing their vertex spaces. Pointwise artinian is likewise equivalent to artinian, by taking a common stabilization index over the finitely many vertices. Thus [122, Theorems 1.2–1.4] genuinely applies to finitely generated and artinian modules over our infinite polynomial string algebras, with its specified strings, finite-dimensional bands and primitive injective bands. It does not say that every module, or every infinite word, satisfies these finiteness conditions.

A nonzero completed node lattice is outside both classes after restriction to $A = k[x, y]/xy$. Indeed A is finite over $k[u]$, $u = x + y$. If the lattice were finitely generated over A, it would be finite torsion free over the PID $k[u]$, hence finite free of positive rank. Multiplication by $1 - u$ would then have a nonzero cokernel. On a $k[[u]]$-lattice it is a unit, a contradiction. The strictly decreasing chain $M \supset uM \supset u^2M \supset \cdots$ also excludes artinianness. The lattice classification below is proved independently.

An almost-split sequence in an exact category is a nonsplit conflation

$$0 \longrightarrow L \xrightarrow{i} E \xrightarrow{p} M \longrightarrow 0$$

whose first map factors every nonsection out of L and whose second map factors every nonretraction into M. Minimality removes redundant summands. The Auslander–Reiten translate is $\tau M = L$. Irreducible maps give the arrows of the AR quiver; projective vertices do not have nonsplit almost-split sequences ending there. The mesh relation says that the two component composites, with the appropriate signs, sum to zero. It is an identity between module maps. It is not, without a further construction, a polynomial relation between functions on a representation variety.

A quotient $A \twoheadrightarrow B$ gives a fully faithful exact inflation $\operatorname{mod} B \to \operatorname{mod} A$. Its image is the full subcategory annihilated by the kernel. That image need not be extension closed. Even when it is closed under the relevant exact operations, an almost-split factorization in the smaller category need not factor every map from the larger category. Throughout, the word *intrinsic* records this boundary.

21.2 The corrected elliptic-theta face example

21.2.1 Permutations, genus and the actual algebra

The six-dart data

$$\sigma = (1\,2\,3)(4\,5\,6), \qquad \alpha = (1\,4)(2\,5)(3\,6)$$

are transitive and commute. With composition acting rightmost first,

$$\sigma\alpha = (1\,5\,3\,4\,2\,6), \qquad \phi = (\sigma\alpha)^{-1} = (1\,6\,2\,4\,3\,5).$$

The uncontracted dessin has two black vertices, three white vertices, six edges and one face. Thus $2 - 2g = 2 + 3 - 6 + 1 = 0$, and $g = 1$. After contracting the clean white vertices the counts are two vertices, three edges and one face. A global Belyi realization is $y^2 = x^3 - 1$, $\beta = x^3$.

Its algebra has vertices x_1, x_2, x_3 and arrows

$$a_1 : x_1 \to x_2, \quad a_2 : x_2 \to x_3, \quad a_3 : x_3 \to x_1,$$
$$b_3 : x_1 \to x_2, \quad b_1 : x_2 \to x_3, \quad b_2 : x_3 \to x_1.$$

The forbidden travel pairs are

$$a_1b_1,\ b_1a_3,\ a_3b_3,\ b_3a_2,\ a_2b_2,\ b_2a_1.$$

This is the same presentation as the corresponding right-to-left list after reversing each product. For an explicit dart identification use

$$1 \mapsto a_1, \quad 2 \mapsto a_3, \quad 3 \mapsto a_2, \quad 4 \mapsto b_3, \quad 5 \mapsto b_2, \quad 6 \mapsto b_1.$$

Then the face is the forbidden indexing cycle $a_1b_1a_3b_3a_2b_2$. It repeats vertices; it does not create six distinct primitive idempotents. The algebra is infinite dimensional because its two permitted three-cycles can be traversed indefinitely. Its completed order has R-rank 18.

Proposition 21.1 (A face unfolds to a complex, not a six-vertex quotient)**.** *Put $B_6 = k\widetilde{A}_5/J^2$, with the cyclic orientation. Every representation of the theta algebra gives a B_6-representation by unfolding the face:*

$$(V_1, V_2, V_3, V_1, V_2, V_3), \qquad (D_1, \ldots, D_6) = (a_1, b_1, a_3, b_3, a_2, b_2).$$

The resulting functor is additive, exact and faithful, but is not full. There is no unital surjection from this theta algebra to B_6.

Proof. Every consecutive product $D_{i+1}D_i$ is zero by the displayed relation list. A theta morphism repeats its three vertex maps at the two corresponding face positions, so it gives a complex morphism and is recovered from those repeated maps. Kernels and cokernels are computed vertexwise, proving exactness and faithfulness. On the vertex simple at x_1 its image is the sum of the two B_6-simples at positions $1, 4$. The original endomorphism space has dimension one and the image endomorphism space dimension two. Thus fullness fails.

If a unital surjection to B_6 existed, compose it with $B_6 \twoheadrightarrow k^6$. Every theta arrow joins distinct idempotents. Its image in this commutative algebra is therefore zero, since those two idempotent images are orthogonal. The image is generated by the three vertex idempotents and has dimension at most three, whereas a surjection to k^6 would have image dimension six. This is impossible. □

For a fixed theta dimension vector (d_1, d_2, d_3), the arrays of six matrices satisfying the equations are indeed the same affine variety as the circular complex variety of dimensions $(d_1, d_2, d_3, d_1, d_2, d_3)$, after identifying the repeated vector spaces and bases. The acting groups differ:

$$G_A = \prod_{i=1}^{3} \mathrm{GL}_{d_i}, \qquad G_{B_6} = \prod_{i=1}^{6} \mathrm{GL}_{d_i}, \qquad d_{i+3} = d_i.$$

The first embeds diagonally in the second. Its orbits, Hom spaces and orbit closures cannot be read by forgetting that diagonal restriction. For example $a_1 = 1, b_3 = \lambda$, all other arrows zero, gives pairwise nonisomorphic theta representations when $\lambda \in k^\times$ varies. Their unfolded complexes are all isomorphic: the two disjoint nonzero edge maps may be rescaled independently by G_{B_6}.

21.2.2 Correct rank strata and the incidence resolution

The standalone circular-complex model remains valuable. Let $V_i = k^{d_i}$, with indices modulo six, and set

$$\mathcal{X}(\mathbf{d}) = \{(D_i) : D_i : V_i \to V_{i+1}, \quad D_{i+1}D_i = 0\}.$$

A feasible rank vector satisfies

$$0 \le r_i, \qquad r_{i-1} + r_i \le d_i.$$

At each vertex choose a decomposition into the incoming image, a homology space and an outgoing complement. Each outgoing complement maps isomorphically onto the next incoming image. This proves that ranks classify orbits for the *six-factor* group. It also decomposes a complex into simple vertex modules and length-two arrow modules. Thus B_6 is representation finite, with six simples and six indecomposable length-two projectives; it is not the category of the HLS diamond or of band tubes.

Theorem 21.2 (Kernel incidence resolution)**.** *For a feasible* $\mathbf{r}$*, use subspaces of dimension* $d_i - r_i$ *and define*

$$Z(\mathbf{r}) = \{(D, R) : \dim R_i = d_i - r_i, \quad \operatorname{im} D_{i-1} \subset R_i \subset \ker D_i\}.$$

This is smooth, and its projection is proper and birational onto the closure of the rank-$\mathbf{r}$ *stratum. The maximal feasible vectors, in componentwise order, give the irreducible components of* $\mathcal{X}(\mathbf{d})$*.*

Proof. Over $\prod_i \mathbf{Gr}(d_i - r_i, V_i)$ the allowed maps are precisely

$$D_i \in \operatorname{Hom}(V_i/R_i, R_{i+1}).$$

They form a vector bundle, so its total space is smooth and irreducible. The incidence conditions are closed, and projection from the Grassmannian product is proper. Its image is the locus of

complexes with ranks at most $\mathbf{r}$. To see surjectivity onto that locus, extend the incoming image to a $(d_i - r_i)$-dimensional subspace inside the kernel; feasibility gives both inequalities needed for that extension. Full ranks r_i occur in the bundle, since $r_i \le d_{i+1} - r_{i+1}$. On this open locus $R_i = \ker D_i$ is forced and varies regularly, giving an inverse there. The image is consequently the closure of this stratum. Every complex has a feasible rank vector and these closures are ordered by componentwise rank, proving the last assertion. □

The index in $d_i - r_i$ matters. With all $d_i = 1$ and the maximal vector $(1, 0, 1, 0, 1, 0)$, the alternative $d_i - r_{i-1}$ asks for a one-dimensional R_1 inside the zero kernel of D_1. It has no fiber on the intended dense stratum. This elementary counterexample rules out that incorrect resolution. The theorem above describes the circular variety and its own group, not a nonexistent quotient map of Proposition 21.1.

21.3 Zwara's Hom control and covering Hom decompositions

For finite-dimensional algebras B, A, an exact k-linear functor $F : \operatorname{mod} B \to \operatorname{mod} A$ is *Hom-controlled* in the sense used by Zwara if there is a bilinear form $\beta : K_0(B) \times K_0(B) \to \mathbb{Z}$ with

$$\dim_k \operatorname{Hom}_A(FU, FV) - \dim_k \operatorname{Hom}_B(U, V) = \beta([U], [V]) \tag{21.1}$$

for all U, V. This is the explicit definition in [119, Section 6, p.71], following [118]. A fully faithful exact functor satisfies it with $\beta = 0$, when these finite-dimensional hypotheses apply. The definition does not consist of a sum indexed by deck translates.

The face unfolding fails even this weaker numerical test on a finite radical-square-zero quotient. Take dimension $(1, 1, 0)$, let M_0 have $a_1 = 1, b_3 = 0$, and M_1 have $a_1 = b_3 = 1$, all other maps zero. Their original endomorphism dimensions are both one. After unfolding, M_0 has one edge summand and two isolated simples, so its endomorphism dimension is three; M_1 has two disjoint edge summands, so its endomorphism dimension is two. The defects are two and one at the same K_0 class. No bilinear form in (21.1) can describe them.

Under suitable covering and support hypotheses a Galois push-down has the separate identity

$$\operatorname{Hom}(F_\lambda M, F_\lambda N) \cong \bigoplus_{g \in G} \operatorname{Hom}(M, {}^g N).$$

The support hypotheses ensure the asserted direct sum is the appropriate space; an arbitrary infinite-support category may require other finiteness conditions. Even when this formula holds, the nonidentity summands can depend on the module structures rather than only on their K_0 classes.

Proposition 21.3 (A finite covering counterexample)**.** *A Galois push-down need not be Hom-controlled in Zwara's sense, even for a finite group and finite-dimensional algebras.*

Proof. Let B be the two-cycle $1 \rightleftarrows 2$ with all length-two paths zero, and let $A = k[t]/t^2$. The deck involution exchanges vertices and arrows; the quotient sends either arrow to t. Its push-down adds the vertex spaces. Put $M = S_1 \oplus S_2$ and $N = P_1$. Both have dimension vector $(1, 1)$. The first pushes to k^2 with $t = 0$, the second to a single nilpotent Jordan block of size two. Thus

	$\dim \operatorname{End}_B$	$\dim \operatorname{End}_A(F(-))$	defect
M	2	4	2
N	1	2	1

while $[M] = [N]$ in $K_0(B)$. This contradicts any proposed bilinear defect. The example satisfies the ordinary finite covering Hom decomposition; it is the inference from that decomposition to (21.1) which fails. □

The geometric conclusion must also be stated accurately. The module-scheme result of [118] gives the specified smooth-then-immersion factorization on connected components. The smoothness results for orbit closures and rank schemes in [119, Theorems 6.1–6.2] have their own source, image and singularity-type hypotheses. They do not say that every induced map into the entire module variety is smooth. For example the quotient $k[t]/t^2 \twoheadrightarrow k$ has fully faithful inflation, but the point with $t = 0$ is not a smooth immersion into the positive-dimensional square-zero matrix variety in dimension two.

21.4 Homogeneous tubes in a polynomial dessin algebra

Let $A = k[x, y]/xy$ be the actual polynomial interval dessin algebra. At the smooth support $(x-\lambda, y)$, with $\lambda \neq 0$, put

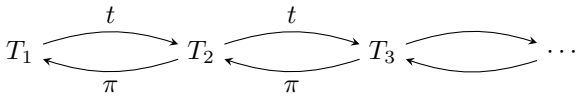
$$T_r = k[t]/t^r, \qquad x = \lambda + t, \quad y = 0, \qquad r \geq 1.$$

All finite-dimensional modules at that support decompose into these modules. This is the elementary divisor theorem for the nilpotent operator t. Modules at different maximal supports have no nonzero maps between them.

Proposition 21.4 (A full tube with explicit meshes)**.** *In* $\mathrm{mod}_{\mathrm{fd}}\, A$ *the* T_r *form a homogeneous tube,* $\tau T_r = T_r$*. With* $T_0 = 0$ *its sequences are*

$$0 \to T_r \xrightarrow{(\pi,t)} T_{r-1} \oplus T_{r+1} \xrightarrow{(t,-\pi)} T_r \to 0.$$

Proof. The two composites cancel. The first map is injective, including when $r = 1$, and the second is surjective; their dimensions then prove exactness. A nonsurjective map into T_r lands in tT_r and factors through the first summand of the right map. A surjective nonretraction from an indecomposable T_s has $s > r$ and factors through T_{r+1}. Decomposing a general source proves right almost splitness; finite-dimensional duality proves the left property. The sequence is nonsplit and its endpoints have local endomorphism rings. Maps from other support blocks are zero, so this is an ambient finite-dimensional-module assertion, not merely an intrinsic quotient claim. □



$$\tau T_r = T_r$$

Figure 21.1: The entire rank-one tube, continued to every quasi-length. The translation fixes quasi-length; the irreducible arrows change it.

The same construction is available on each branch of the polynomial theta algebra at a nonzero central value. After inverting u, its algebra is the product of two matrix algebras over $k[u, u^{-1}]$. Morita equivalence at a fixed nonzero λ gives one such tube on each branch, with dimension vector (r, r, r). Two arrows may be identities and the third $J_r(\lambda)$. These are two *families* indexed by λ, not two tubes in total. They do not extend to continuous finite-dimensional completed-order modules: there the central u must be nilpotent.

There are also mixed inverse bands. Already $a_1 b_3^{-1}$ is a primitive cyclic string. More generally

$$(a_1 a_2 a_3)^j a_1 b_3^{-1}, \qquad j \geq 0,$$

has no forbidden subword in any power and is primitive because its cyclic period contains exactly one inverse letter. Their different lengths give infinitely many band classes. This disproves a classification by just the two pure permitted triangles. Existence of these modules does not by itself identify their entire ambient completed-order AR components.

At the singular central support, a pure-branch tube has only an intrinsic meaning. The augmentation of the y-Jordan block T_2^y onto k cannot factor through $T_2^x \to k$: any map $T_2^y \to T_2^x$ lands in $\operatorname{ann}(x) = \operatorname{soc}(T_2^x)$, which that projection kills. Thus even the first right almost-split factorization would fail in the larger node finite-length category.

21.5 The whole nodal lattice AR category and its stable triangles

Let $\Lambda = k[[x,y]]/xy$, $u = x + y$, $X = (x)$ and $Y = (y)$. Normalize inside a lattice's total quotient module using $B = k[[x]] \times k[[y]]$. If $\overline{M} = BM$, the conductor gives $u\overline{M} \subset M \subset \overline{M}$. The subspace $M/u\overline{M}$ projects onto both branch residue spaces. Separate its pure branch intersections and its common quotient; bases put it into pure lines and diagonal pairs. Lifting those bases over the two DVRs gives

$$M \cong \Lambda^r \oplus X^a \oplus Y^b. \tag{21.2}$$

This is a classification of the finite R-free lattice category. It is not a claim that ordinary polynomial strings classify every completed lattice.

Theorem 21.5 (The full nodal lattice meshes)**.** *The two almost-split sequences in this category are*

$$0 \to Y \hookrightarrow \Lambda \xrightarrow{x} X \to 0, \qquad 0 \to X \hookrightarrow \Lambda \xrightarrow{y} Y \to 0.$$

Its indecomposable lattice vertices are Λ, X, Y, with $\tau X = Y$, $\tau Y = X$.

Proof. The first kernel is $\operatorname{ann} x = Y$. It does not split: a map $X \to \Lambda$ lands in X, and its composite with multiplication by x is a nonunit of $\operatorname{End} X = k[[x]]$. Every map $\Lambda \to X$ factors through the displayed epimorphism, $\operatorname{Hom}(Y, X) = 0$, and each nonunit of $\operatorname{End} X$ is divisible by x, so factors through $X \hookrightarrow \Lambda \to X$. Classification (21.2) now proves right almost splitness for every finite sum: a unit component from X would already be a retraction. For the left property, maps $Y \to X$ are zero, maps $Y \to \Lambda$ extend to multiplication on Λ, and each nonunit endomorphism of Y factors through $Y \hookrightarrow \Lambda \xrightarrow{y} Y$. A unit component into a Y summand would be a section. This proves the factorization for every target in the classification. Endomorphisms of Λ fixing a structure map have constant term one, hence are units; this proves minimality. Interchange x, y for the other sequence. There are no other nonprojective indecomposables in this category. □

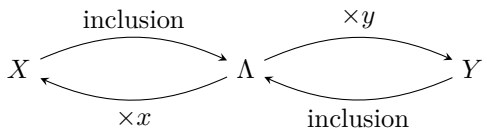


Figure 21.2: The full lattice AR quiver. Its two opposite-branch mesh composites are zero. The central vertex is projective.

Reduction by the regular parameter gives a genuine exact diagram:

$$\begin{array}{ccccccccc}
0 & \longrightarrow & Y & \hookrightarrow & \Lambda & \xrightarrow{x} & X & \longrightarrow & 0 \\
 & & \downarrow{\scriptstyle u} & & \downarrow{\scriptstyle u} & & \downarrow{\scriptstyle u} & & \\
0 & \longrightarrow & Y & \hookrightarrow & \Lambda & \xrightarrow{x} & X & \longrightarrow & 0 \\
 & & \downarrow & & \downarrow & & \downarrow & & \\
0 & \longrightarrow & k & \xrightarrow{-\epsilon} & k[\epsilon]/\epsilon^2 & \longrightarrow & k & \longrightarrow & 0.
\end{array}$$

All three terms are R-free, so the columns are exact and the free quotient X prevents a Tor term in the bottom row. With generators y, x on the two ends, $y = -\epsilon$ explains the sign. This diagram is stronger than a drawing of four mesh diamonds with arbitrary rows and columns.

The lattice category is Frobenius. Alternating annihilator resolutions give

$$\operatorname{Ext}^1(X, \Lambda) = \operatorname{Ext}^1(Y, \Lambda) = 0.$$

The embeddings above give enough injectives, and Λ gives enough projectives. The projective-injectives are its finite free sums. Modulo them,

$$\underline{\operatorname{End}}(X) = \underline{\operatorname{End}}(Y) = k, \qquad \underline{\operatorname{Hom}}(X, Y) = \underline{\operatorname{Hom}}(Y, X) = 0.$$

For example maps through Λ give precisely $xk[[x]]$ inside $\operatorname{End} X = k[[x]]$. The two rows identify $\Sigma X = Y$ and $\Sigma Y = X$. Hence its stable AR triangles are

$$Y \to 0 \to X \xrightarrow{\sim} \Sigma Y, \qquad X \to 0 \to Y \xrightarrow{\sim} \Sigma X.$$

The four ordinary arrows through Λ disappear in the stable category. A tube or a stable three-vertex

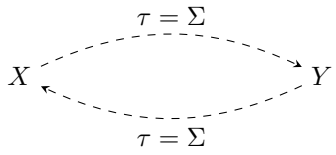


Figure 21.3: Stable node data: two isolated ordinary-quiver vertices. The dashed arrows indicate translation and suspension, not irreducible morphisms.

grid would describe a different category.

21.6 A complete HLS component inside a genuine dessin quotient

For $n \geq 3$ take the infinite closed algebra with chain vertices $1, \ldots, n$, endpoint loops l, r, opposite chain arrows a_i, b_i, and relations

$$l^2 = r^2 = a_i b_i = b_i a_i = 0.$$

Its single permitted cycle goes along the chain and back, with the endpoint loops. It is an actual sphere dessin: the Chebyshev map

$$\beta_n(z) = \frac{1}{1 - T_n(z)^2}$$

has passport $(2n), (2^n), (2^{n-1}, 1, 1)$; the dual contracted graph is a path. Its completed order has rank $(2n)^2$. Kill one arrow at every chain edge, retaining an orientation Ω. The quotient is exactly $H_n(\Omega)$ of [116]. A surviving path has length at most $n+1$, so the killed-arrow ideal contains J^{n+2}. The polynomial algebra and its completion have the same finite quotient. Denote its intrinsic module category by $\mathcal{C}_\Omega$.

For H_3 retain $1 \xrightarrow{a} 2 \xrightarrow{b} 3$. The following table fixes all nine modules, not merely nine unlabelled points. A superscript $-$ denotes a formal inverse, not an inverse in the algebra. Each word is read in travel order; its basis consists of its successive visited positions.

Label	word	start	dimension vector
A	$l^-abrb^-a^-l^-$	1	$(4,2,2)$
B	l^-ab	1	$(2,1,1)$
C	l^-abr^-	1	$(2,1,2)$
D	$abrb^-a^-l^-$	1	$(3,2,2)$
E	ab	1	$(1,1,1)$
F	abr^-	1	$(1,1,2)$
G	$r^-b^-a^-labrb^-a^-l^-$	3	$(4,3,4)$
H	$r^-b^-a^-lab$	3	$(2,2,3)$
I	$r^-b^-a^-labr^-$	3	$(2,2,4)$

A direct letter sends the preceding position vector to the following one; an inverse letter sends the following vector to the preceding one. These rules satisfy $l^2 = r^2 = 0$ and specify every arrow matrix.

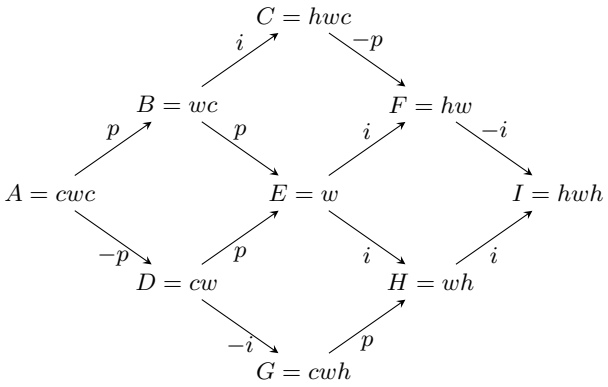


Figure 21.4: The actual signed HLS nine-object window, rotated to show four meshes. Hook/cohook labels are operation labels from the source convention; the preceding table fixes their travel words.

The maps p are projections and i embeddings. In the rectangular version, horizontal projections retain initial positions and horizontal embeddings append the final r^- position. Upper vertical projections delete the initial l^-, and lower vertical embeddings prepend $r^-b^-a^-l$. The signs in Figure 21.4 give

$$0 \to A \to B \oplus D \to E \to 0, \qquad 0 \to B \to C \oplus E \to F \to 0,$$
$$0 \to D \to E \oplus G \to H \to 0, \qquad 0 \to E \to F \oplus H \to I \to 0.$$

Their module intertwinings and exactness follow by these basis rules; for example the two maps out of A have joint kernel zero, the maps to E are onto, and the displayed dimension vectors give the kernel dimension at each vertex. The almost-split property is the additional content of the source's hook/cohook theorem, after identifying $w = ab$ as minimal of type $(2,2)$.

21.6.1 Extending the window to the whole component

Let X_p mean p left hooks when $p \geq 0$ and $-p$ left cohooks when $p < 0$; let Y_q mean q right hooks when $q \geq 0$ and $-q$ right cohooks when $q < 0$. These are operations on strings, not paths. Lemma 3.10 and the four-region induction in [116, Proposition 3.12] give every vertex of this component as

$$M(p,q) = M(X_p w Y_q), \qquad (p,q) \in \mathbb{Z}^2.$$

There are arrows increasing one coordinate at a time and

$$\tau M(p,q) = M(p-1, q-1).$$

The meshes are

$$0 \to M(p-1,q-1) \to M(p,q-1) \oplus M(p-1,q) \to M(p,q) \to 0.$$

The nine labels are $A = M(-1,-1), E = M(0,0), I = M(1,1)$ and the six intermediate positions. This is the whole $\mathbb{Z}A_\infty^\infty$ component, continued in all four directions. Its two outgoing axis rays are monomorphisms and its two incoming axis corays epimorphisms. It is not an exact array of rows and columns.

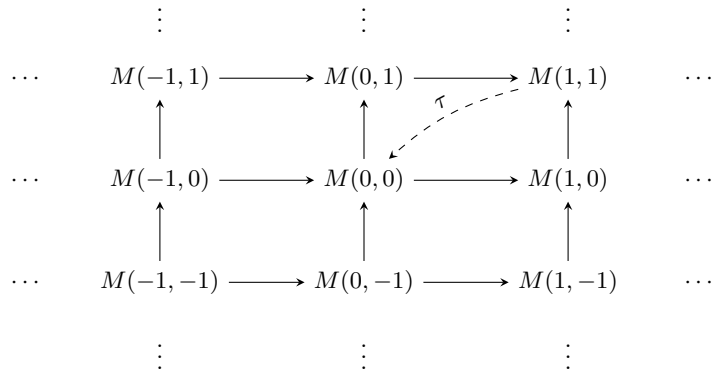


Figure 21.5: The coordinate model of the entire HLS component: continue this lattice for all $(p,q) \in \mathbb{Z}^2$. Ordinary arrows increase one coordinate; translation decreases both. Only mesh diagonals give the exact sequences above. The dashed arrow is translation, not an additional irreducible map.

The complete H_n module AR inventory is also known [116, Theorem 3.14]: one component containing the projective and injective modules; one exceptional tube of rank $n-1$; homogeneous band tubes; and the components above indexed by minimal type $(2,2)$ strings. In H_3 the exceptional tube has rank two. The source's Figures 3–4 show the projective-injective component, not another view of this stable grid. None of these classifications is silently asserted for every module of the completed infinite order.

21.7 Derived AR triangles and an explicit infinite-pd endpoint

A short exact sequence gives a triangle in a bounded derived category, but almost splitness is tested against all objects there, including shifts. For a finite-dimensional algebra an indecomposable endpoint admits a derived AR triangle precisely when it is perfect; its translate is the derived

Nakayama functor followed by $[-1]$. In the finite-dimensional gentle setting, [120, Section 5.1] applies this criterion to finite homotopy strings and bands, and describes the graded endpoint rotations. The finite-dimensional, grading, boundary and local-system hypotheses remain part of that theorem.

For our $E = M(ab)$ the failure of perfectness can be seen directly. In the travel/right convention the cover $P_1 \to E$ has the eight-element basis

$$e_1, l, a, la, ab, lab, abr, labr,$$

and retains e_1, a, ab. Its kernel is $lP_1 \oplus abrP_3$. Multiplication by $l : P_1 \to P_1$ has kernel lP_1, since exactly the paths already starting with l are killed. The terminal simple repeats through $r : P_3 \to P_3$ in the same way. Thus its minimal projective resolution has nonzero terms in arbitrarily high degrees. In particular the module AR sequence ending in E in Figure 21.4 does not become an AR triangle ending in E in $D^b(\operatorname{mod} H_3)$.

By contrast, the smooth-support block of Proposition 21.4 is hereditary. The operator $(x - \lambda)^r$ is a nonzerodivisor of the polynomial node algebra and its cokernel is T_r, so it gives a length-one free resolution. The indecomposables in that block's bounded derived category are $T_r[n]$; each fixed shift has the same homogeneous tube and the AR triangles are induced by its exact sequences. The nodal stable lattice triangles above give another actual triangulated model. These two positive descriptions do not identify all of D^b, Perf and the stable lattice category.

21.8 Ringel's wind-wheel tile: limits are part of the object

Ringel's $\mathcal{T}(45)$ is the tile of the five-bar wind wheel specified in [117, Section 12.5, p.30], drawn in Section 13.3, pp.38–40. It is part of an AR *quilt*, not just a finite-module mesh. Four finite-word quarters surround a nonperiodic two-sided word. The diagonals consist of one-sided limiting words; contracting ones use ordinary strings, expanding ones need completion, and the central mixed word needs partial completion. The five-tile example glues to a torus with five holes. Deleting the infinite-word points recovers its finite string components. This is a category construction, not an assertion that its quilt genus equals the genus of our original Belyi pair.

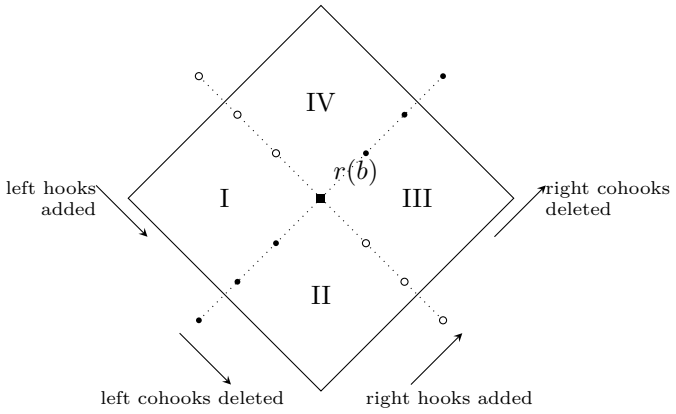


Figure 21.6: A scoped schematic of Ringel's tile, with the directions and limit symbols of the primary picture: circles are contracting one-sided words, bullets expanding ones, and the black square the two-sided limit. The border and neighboring-tile identifications are additional data.

This picture is a finite-dimensional special-biserial wind-wheel category. It is not already our completed node or the H_n quotient. No map identifying its algebra with a present dessin quotient

has been supplied here. Such an import would have to specify that map and the category in which almost-split or pure-injective statements are retained. In particular deleting diagonals from one tile leaves four quarters, not one HLS grid. Ringel also lists indecomposable algebraically compact modules omitted from the quilt; it is not itself a classification of all ordinary modules or all pure-injectives.

21.9 What meshes can and cannot say about semi-invariants

21.9.1 Presentation determinants and their exact scope

Let $P_0 = \bigoplus_i (e_i A)^{a_i}$, $P_1 = \bigoplus_i (e_i A)^{b_i}$ and $f : P_1 \to P_0$. When the evaluated Hom map is square, chosen bases give

$$c_f(N) = \det \mathrm{Hom}_A(f, N), \qquad c_f(gN) = \prod_i \det(g_i)^{b_i - a_i} c_f(N).$$

The action on coordinate functions has inverse weight. Put $M = \operatorname{coker} f$. The kernel is $\mathrm{Hom}(M, N)$. If f is the injective first map of a short projective resolution, its cokernel after Hom is Ext^1 and higher Ext vanish. A general presentation keeps its other cohomology. These distinctions are part of the semi-invariant construction, not consequences of an AR drawing [121].

Proposition 21.6 (A mesh whose determinant is a free generator)**.** *An actual dessin quotient has an almost-split mesh whose presentation semi-invariant generates a polynomial algebra with no relation.*

Proof. In the Chebyshev order above kill vertex3, both loops and the reverse arrow, retaining only $a : 1 \to 2$. This is the genuine continuous quotient $B = k(1 \to 2)$. Its three indecomposables are S_1, S_2 and $E = (k \xrightarrow{1} k)$, by rank decomposition of a linear map. Its sequence

$$0 \to S_2 \xrightarrow{i} E \xrightarrow{p} S_1 \to 0$$

is almost split: a nonretraction to S_1 from these indecomposables factors through p, and dually for i. At dimension $(1, 1, 0)$ the single arrow coordinate z transforms by g_2/g_1. The short projective resolution $P_2 \to P_1 \to S_1$ gives the determinant z. Its semi-invariant algebra is $k[z]$, with no algebraic relation among this one generator, although $pi = 0$ is a mesh relation. □

This quotient AR sequence is not ambient. A module supported at vertex1 with $l = J_2$ has a nonsplit epimorphism to S_1. Every map from it to E has zero vertex1 component, because $E(a) = 1$ while its own arrow a is zero. That epimorphism cannot factor through $E \to S_1$ in the larger category.

Proposition 21.7 (The product theorem with its hypotheses)**.** *Suppose $0 \to M' \to M \to M'' \to 0$ is exact and M', M'' have resolutions of length one by finite projectives. At a dimension vector where both end presentation Hom matrices are individually square, compatible bases give $c_M = c_{M'} c_{M''}$, up to the fixed basis sign.*

Proof. Lift the projective cover of M'' through M. Its horseshoe kernel sits in a split sequence of the two projective kernels, so the middle resolution has differential $\left(\begin{smallmatrix} d' & \xi \\ 0 & d'' \end{smallmatrix}\right)$. Applying contravariant Hom gives a triangular square matrix, with diagonal the two prescribed Hom maps. Its determinant is their product. □

Total squareness alone does not give the two factors. In the A_2 mesh at $(1,1)$, S_1 has balanced Euler value, but P_1 and P_2 do not. The three individual Schofield factors are therefore not all defined there. Nor is the infinite-pd H_3 object $E = ab$ eligible for the short-resolution hypothesis just because it sits in a diamond.

21.9.2 Relative nodal determinants really are multiplicative

The lattice AR sequence of Theorem 21.5 is split after forgetting to R. It therefore has the canonical line comparison

$$\det_R \Lambda \cong \det_R Y \otimes_R \det_R X.$$

For any compatible endomorphisms it gives

$$\det_R(1 - TF_\Lambda) = \det_R(1 - TF_Y) \det_R(1 - TF_X). \tag{21.3}$$

Indeed an R-splitting gives a triangular matrix. For every Λ-linear endomorphism of Λ, multiplication by $f = a(u) + b(u)x$, the basis $(y, 1)$ makes that matrix and its two scalar actions explicit:

$$F_\Lambda = \begin{pmatrix} a & -b \\ 0 & a + ub \end{pmatrix}, \qquad F_Y = a, \quad F_X = a + ub.$$

Both sides of (21.3) are $(1 - Ta)(1 - T(a + ub))$. This is a determinant-functor statement after the specified passage to R-perfect modules, not a nonexistent finite Λ-projective resolution of X, Y. On applying $\mathrm{Hom}_\Lambda(-, Y)$ the map between the first two R-lines is multiplication by u; its cokernel is $\mathrm{Ext}^1(X, Y) = k$. Thus underived Hom is not exact on this AR row.

On the reduced continuous finite-length representation variety of the one-vertex node, the ordinary semi-invariant ring is in fact just k. Scalar matrices act trivially by conjugation, forcing a nonzero character $\det^m$ to have $m = 0$. The nilpotent filtration gives a one-parameter conjugation degeneration to zero arrows, so all invariant regular functions are constant. This coexists with the nontrivial lattice AR sequences and the relative determinant identity; the target data differ.

21.9.3 An inherited relation and a framed Plücker relation

A genuine unframed relation is obtained by retaining both arrows $a : 1 \to 2$, $b : 2 \to 1$ in a Chebyshev quotient and killing all other vertices and arrows. At dimension $(1, 1, 0)$ its coordinate ring is $k[a, b]/(ab)$. The two coordinates have opposite torus weights and are semi-invariants. Their relation $ab = 0$ comes from the inherited zero relation; it was not deduced merely from a mesh picture.

For a richer example use the actual elliptic-square order. Its dessin has $\sigma = (1\,2\,3\,4)$ and $\alpha = (1\,3)(2\,4)$; there is one face, so $1 + 2 - 4 + 1 = 0$ gives genus one. The two quiver vertices are the two clean edges. The four arrows form one permitted alternating four-cycle, with two arrows in each direction; every mixed consecutive choice is forbidden. Put $V_0 = k^2, V_1 = k^2$, set both reverse arrows to zero, and let the two forward arrows have arbitrary matrices X, Y. These modules kill J^2 and therefore extend continuously to the completed order. *Frame the source* V_0: the acting group in the next statement is only $\mathrm{GL}(V_1)$. Write $Z = [x_1, x_2, y_1, y_2]$ and $p_{ij} = \det(z_i, z_j)$.

Theorem 21.8 (A genuine framed generator relation)**.** *All six p_{ij} have target character* det*, and their subalgebra is*

$$k[p_{12}, p_{13}, p_{14}, p_{23}, p_{24}, p_{34}]/(p_{12}p_{34} - p_{13}p_{24} + p_{14}p_{23}).$$

The stated quadratic is the full ideal of relations of these six functions.

Proof. On the dense open $p_{12} \neq 0$, express the other columns in the basis x_1, x_2 and expand determinants. This gives the quadratic; polynomial continuation proves it everywhere. Conversely any nonzero six-tuple satisfying it is realized by four columns. After choosing a nonzero p_{12} by permutation, one may take

$$z_1 = (1,0)^t, \qquad z_2 = (0, p_{12})^t,$$
$$z_3 = (-p_{23}/p_{12}, p_{13})^t, \quad z_4 = (-p_{24}/p_{12}, p_{14})^t.$$

Their last minor has the required value by the equation. The zero tuple is also realized. The quadratic is irreducible: its nondegenerate quadratic form has rank six, whereas a product of linear forms has rank at most two. Its ideal is prime, so this image description proves it is the kernel of the polynomial map on coordinate rings. □

The exact diagram behind decomposability is $0 \to \ker Z \to k^4 \xrightarrow{Z} k^2 \to 0$ on the rank-two locus. Its exterior comparison relates complementary kernel minors. The relation extends to the lower-rank boundary; the diagram is not an almost-split sequence.

The framing is indispensable. With $X = I$ and $Y = \left(\begin{smallmatrix} 0 & 0 \\ 1 & 0 \end{smallmatrix}\right)$, $p_{13} = 1$, but swapping the source basis makes it zero. Thus p_{13} is not a semi-invariant for the full original source-and-target group. The coefficients of

$$\det(X + tY) = p_{12} + t(p_{14} - p_{23}) + t^2 p_{34}$$

are full-group semi-invariants. The framed six-generator relation must not be misidentified as their unframed presentation.

21.10 What this supplies to the physical and arithmetic program

The chapter supplies exact categories, explicit maps, parameter spaces and some genuine determinant identities. These can organize an effective model's states and couplings, but τ is a categorical translation, not by itself a unitary time evolution or a self-adjoint Hamiltonian. A physical realization must supply its Hilbert space, domain, positive metric and dynamics independently. Likewise an arbitrary tube parameter is not a prime norm or a Frobenius eigenvalue.

A valid route from a mesh to polynomial functions requires a universal family, the correct group action, determinant-admissible complexes and rank hypotheses. A route from those functions to an arithmetic L-function additionally requires descent, local factors, conductor and archimedean data, convergence or regularization, and a determinant-preserving positive comparison. The relative nodal identity and framed Plücker model give usable intermediate constructions. They do not discharge those arithmetic or analytic obligations, and no full GRH conclusion is asserted.

Chapter 22

Coverings, equivariant AR theory and graded surfaces

The new covering calculation in Section 7 is useful for computations, precisely because its limitations are explicit. The parent algebra is our infinite elliptic theta algebra, its truncation is a finite quotient, and its cover has vertices indexed by integers. They are three different categories. The nine-dimensional module in Proposition 7.2 and the higher-genus family in Corollary 7.3 show that even this genuine covering does not reach every module or bounded derived object.

22.1 Reading the three new sources together

The lecture [74] supplies the covering language: locally bounded categories, exact push-down/pull-up and graded adjunctions. Its Theorems 4.23 and 4.28 give precoverings on the specified module and bounded derived categories. The AR-quiver covering theorem 4.18 assumes an actual Galois covering between Hom-finite Krull–Schmidt categories; density cannot be dropped. A universal bound-quiver cover also depends on its relations and presentation. It is not automatically a covering of the compact surface.

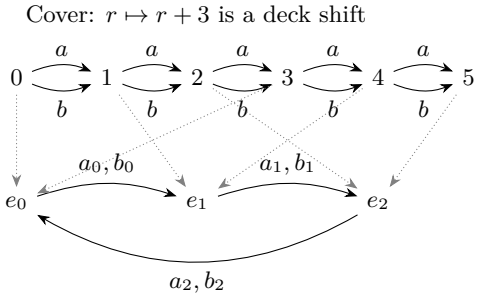
The GLS paper [75] works over an algebraically closed characteristic-zero field. Its finite-dimensional GLS algebras are not automatically our surface orders. Equivariantization transports string/band information to certain non-string algebras. Theorem B includes $\mathbb{Z}D_\infty$, $\mathbb{Z}A_\infty^\infty$ and tube components, with its stated indexing. Theorem C corrects a naive root-only prediction by the additional rank vectors $\beta_i + (2r+1)\delta$ in the named tame affine family. Here vertexwise local freeness and its rank vector concern the GLS vertex algebras; they are not freeness over the central DVR of a surface order.

Schroll's survey [76], particularly Sections 4–5, organizes graded gentle categories through curves, local systems, crossings and twisted complexes, with grading encoded by a line field. Its framework distinguishes perfect objects from finite-total-cohomology objects, and properness from homological smoothness. These distinctions matter for our infinite algebras and for any completed or operator-algebra version.

22.2 A cover that really preserves the relations

At finite L the cover is locally bounded: only lengths below L survive. Without the cutoff, each vertex has infinitely many nonzero outgoing Hom spaces, so the locally bounded hypothesis used above fails. Locally finite dimensional Hom spaces alone do not repair that failure. Conversely the

truncated algebra has extra length relations and is not entitled to all quadratic-gentle surface-model theorems.



Mixed paths and all paths of length L vanish on both rows.

The dotted lines are the residue map, not irreducible module maps. The top row is a finite window of the quiver of the cover, not an AR component. The proof of the Hom decomposition, the unequal Hom-control defects and the full nine-dimensional calculation appear in Sections 7 and 20; they are not inferred from the drawing. The genus-four instance has dimension 27, and the genus-nine instance dimension 57, with the same exact lift obstruction.

22.3 Equivariant modules, not an unproved folding rule

The branch swap preserves J^L. Thus it acts on B_L and defines the skew-group algebra $B_L \# k[\mathbb{Z}/2]$. An equivariant object needs an isomorphism $c : M \to \sigma M$ satisfying the cocycle equation $\sigma(c)c = 1$. A fixed isomorphism class alone does not choose c. For the nine-dimensional witness, the unequal branch ranks rule out even $M \simeq \sigma M$; the induced pair $M \oplus \sigma M$ instead has a canonical swapping action. This is a concrete use of equivariant machinery without asserting a GLS identification or drawing a folded AR component whose almost-split property has not been checked.

22.4 Derived and symplectic data needed for a determinant

Let $\mathrm{Perf}(A)$ be the compact objects of $D(A)$ and write $D_{\mathrm{fd}}(A)$ for finite-dimensional total cohomology. For our infinite zero-graded A, its regular projective is perfect but has infinite k-dimension; hence it does not belong to $D_{\mathrm{fd}}(A)$. This is already a counterexample to silently embedding the former category in the latter. In proper smooth finite-dimensional situations the familiar equivalences have stronger conclusions; these hypotheses cannot be omitted here.

A curve model must retain the dissection, stops or punctures, line field, intersection grading, local systems and dg or A_∞ enhancement. For perfect complexes, the finite deck decomposition of the Hom complex is proved in Section 20. For a matrix of paths representing a differential one must still check $d^2 = 0$; intersections without degrees and composition data do not prove this identity. A marked surface used for the Fukaya model is not automatically the original compact Riemann surface with its analytic metric and all boundary data forgotten.

Completion to Λ requires continuous modules and the chosen topology. The finite quotient modules extend continuously because a power of J annihilates them. They are not central-DVR-free lattices: in the nine-dimensional example the central length-three parameter already acts by zero. The cutoffs A/J^L must not be renamed Λ/u^L.

For a useful arithmetic determinant, these categorical constructions still need a prime correspondence, a perfect or analytically controlled target, a determinant-line comparison, conductor and

archimedean normalization, and positivity for that same arithmetic function. A derived equivalence or an AR translation does not supply a Hilbert-space adjoint, self-adjoint domain or trace-class convergence. These remain the spectral program's independent load-bearing obligations.

The executable calculation is `examples/coverings/theta_cover.py`. The exact matrix obstruction is checked in `lean-analytic/CoveringBand.lean`. The latter verifies selected actual matrices, not every category or equivalence discussed here.

22.5 From a Hom decomposition to a semi-invariant calculation

For a finite-dimensional quotient, a specified projective presentation $P_1 \xrightarrow{d} P_0$ can define a determinant semi-invariant by applying $\mathrm{Hom}(-, V)$, provided the resulting vector spaces have equal dimension and bases or determinant lines have been fixed. The covering Hom decomposition makes this matrix computable by deck components; it does not make it block diagonal. Cross-degree terms matter. Already

$$\det \begin{pmatrix} 1 & a \\ b & 1 \end{pmatrix} = 1 - ab$$

differs from the product of its two diagonal entries. A product over deck blocks is justified only after proving that the relevant differential or endomorphism preserves those blocks. AR mesh relations concern morphism compositions; a presentation of a ring of semi-invariants requires additional generation and relation proofs, as in the earlier determinant chapters. Neither the GLS root lattice nor a surface intersection form provides the missing positive Hilbert inner product or arithmetic factor identity by itself.

Chapter 23

Linear relations, filtrations and actual branch modules

This chapter develops original 2053 lines 1097–1307 on the genuine infinite dessin algebra, correcting the graph and category conventions before using them in a determinant calculation. The finite module category is specified inside the infinite algebra; a finite diagram is not substituted for that algebra. The companion exposes every kernel/image dimension, the branch monodromy and its polynomial-versus-completed-order status.

23.1 Linear relations and functorial branch filtrations

The original linear-relations chapter mixes graphs, partial relations and stable kernels. We keep these different objects separate. For a field k, a linear relation is a subspace $C \subseteq V \oplus V$; its inverse swaps coordinates and $DC = \{(x,z) : \exists y, (x,y) \in C, (y,z) \in D\}$. The full graph $\Gamma_T = \{(x, Tx) : x \in V\}$ always has dimension $\dim V$, including pairs with zero output. In particular $\Gamma_T^n(0) = 0$, whereas $(\Gamma_T^{-1})^n(0) = \ker T^n$. Thus the source's $\kappa(\Gamma_T) = \bigcup_n \Gamma_T^n(0)$ is zero, not the ordinary stable kernel.

For odd $m \geq 3$, use the actual clean dessin of $y^2 = x^m - 1$, $\beta = x^m$, on the compact smooth curve, in characteristic zero. Its genus is $(m-1)/2$; its infinite locally gentle algebra A_m has vertices $i \in \mathbb{Z}/m$, arrows $a_i, b_i : i \to i-1$, and mixed consecutive branch products zero. Below paths act in their direction of travel on left representations over any coefficient field k. Let $\mathcal{E}_m$ be the full category of finite-dimensional representations with every $b_i = 0$ and a_i invertible for $i \neq 0$.

Theorem 23.1 (A concrete relation category on an infinite dessin algebra)**.** *The category $\mathcal{E}_m$ is equivalent to finite-dimensional pairs (V,T) with intertwining maps. A normal form $N_m(T)$ puts V at each vertex, $a_0 = T$, and all other $a_i = 1$. For $n = \dim V$,*

$$V = K(T) \oplus I(T), \qquad K(T) = \ker T^n, \quad I(T) = \operatorname{im} T^n.$$

These summands and their kernel/image filtrations are functorial. The first restriction is nilpotent and the second invertible. The central full-turn parameter u acts as T. A finite $N_m(T)$ extends continuously to the u-adically completed order precisely when T is nilpotent. Such modules are torsion, not nonzero order lattices.

Proof. Transport all vertex spaces to vertex zero along the invertible arrows; the remaining map is the full-turn monodromy T. Arrow-compatible maps become exactly $hT = T'h$. Finite kernel/image chains stabilize by step n. If $v = T^n w$ and $T^n v = 0$, then $w \in \ker T^{2n} = \ker T^n$, hence $v = 0$;

rank-nullity proves the direct sum. Stability gives the two restrictions, and $hT^r = T'^r h$ proves functoriality. Continuity on a finite-dimensional discrete space means some u^r kills it. Conversely nilpotence makes every formal series act by a finite sum. This proves the completion assertion. □

Over an algebraically closed k, the indecomposable branch pairs are $J_r(\lambda)$. The value $\lambda = 1$ is permitted for a polynomial band; it is not a forbidden deformation parameter. The nilpotent blocks are strings, but are not all rigid: $N_m(J_2(0))$ is a nonsplit self-extension of $N_m(J_1(0))$. The Hom dimension between two such Jordan pairs is $\min(r, s)$ for equal eigenvalues and zero otherwise. These assertions concern this specified full subcategory, not all infinite modules.

If L transports once along the a-arrows on $\bigoplus_i V$, then

$$\det(1 - zL) = \det(1 - z^m T). \tag{23.1}$$

Eliminating the identity arrow blocks leaves the final monodromy block; the eliminated identity blocks have determinant one. For $J_r(\lambda)$ the answer is $(1 - \lambda z^m)^r$. Nilpotent strings therefore contribute one, and arbitrary bands have no forced unit-circle zero location. This determinant is an actual cyclic-quiver invariant; it is not the missing arithmetic positive determinant comparison.

23.2 Relation calculations, splitting functors and determinant limits

23.2.1 Correct graphs and stable spaces

In the original basis let $fe_1 = e_2$, $fe_2 = e_3$, $fe_3 = 0$ and $ge_1 = 0$, $ge_2 = e_1$, $ge_3 = e_2$. Then

$$\begin{aligned}\Gamma_f &= \langle (e_1, e_2), (e_2, e_3), (e_3, 0)\rangle,\\ \Gamma_{f^2} &= \langle (e_1, e_3), (e_2, 0), (e_3, 0)\rangle,\\ \Gamma_{gf^2} &= \langle (e_1, e_2), (e_2, 0), (e_3, 0)\rangle.\end{aligned}$$

Each graph has dimension three. Omitting zero-output generators changes the relation into a partial graph and changes its powers and domain. The following are subspaces of V, not lists of pairs in $V \oplus V$:

T	$\bigcup_r \ker T^r$	$\bigcap_r \operatorname{im} T^r$
f, g	V	0
$gf = \operatorname{diag}(1, 1, 0)$	ke_3	$ke_1 \oplus ke_2$
$fg = \operatorname{diag}(0, 1, 1)$	ke_1	$ke_2 \oplus ke_3$

For all four full graphs $\bigcup_r \Gamma_T^r(0) = 0$. This corrects both the source's graph convention and its interchanged gf, fg kernel entries. For an arbitrary multivalued relation there need not even be a linear map on its domain; its regular-part theorem requires the appropriate relation subquotients and finiteness conditions. We do not replace those hypotheses by the graph calculation. For comparison, in [38, Section 4, Lemmas 4.2,4.5–4.6] write $C' = \bigcup_n C^n(0)$ and let C'' consist of vectors with a compatible infinite backward chain. In finite dimension $C'' = \bigcap_n C^n V$; this equality is not automatic for arbitrary infinite-dimensional spaces. The regular quotient is $C^\sharp/C^\flat$, where

$$C^\sharp = C'' \cap (C^{-1})'', \qquad C^\flat = (C'' \cap (C^{-1})') + (C' \cap (C^{-1})'').$$

The automorphism statement uses this quotient for an arbitrary relation. The splitting statement additionally requires its finite-dimensionality, rather than the source's unqualified ι/κ expression.

23.2.2 Proof of the dessin-category equivalence

Write $a_i : V_i \to V_{i-1}$ for $i = 1, \dots, m-1$ and $p_i = a_1 \cdots a_i : V_i \to V_0$, with $p_0 = 1$; the rightmost map acts first. Every p_i is an isomorphism. Conjugating the arrow maps by these identifications makes $a_i = 1$ for $i \neq 0$, and makes $T = p_{m-1}a_0$ at the remaining arrow. All b-relations vanish. An intertwiner is transported to maps h_i with $h_i = h_{i-1}$ for $i \neq 0$ and $h_{m-1}T = T'h_0$. Hence every $h_i = h$ and $hT = T'h$. This proves full faithfulness and essential surjectivity, with inverse given by $(V, T) \mapsto N_m(T)$. It is also an exact equivalence: kernels and cokernels of intertwiners are the usual invariant kernels/cokernels; the identity arrow maps remain identities. Finite dimension is a condition on modules, while A_m itself is infinite dimensional through its arbitrarily long permitted branch paths.

The sum of the full permitted turns on both branches is central in this closed dessin algebra. On the chosen modules the b-turns vanish and each a-turn equals T, so u acts as T at every vertex. If $T^n = 0$, the action factors through $A_m/(u^n)$ and extends to the completion. If T has a nonzero invertible Fitting summand, no power of u kills that summand, precluding continuity. For $T = J_r(\lambda)$ with $\lambda \neq 0$, the obstruction is stronger: $u - \lambda$ is a unit of $k[[u]]$ but its rth power annihilates the proposed module, impossible for a nonzero unital module. This rules out even an unqualified algebraic extension of that band, not just a chosen topology.

23.2.3 Functoriality and the actual filtration

Kernel dimensions are nondecreasing and at most n. Once two successive kernels agree, applying T^{-1} shows that all later kernels agree. Thus they stabilize by n; rank-nullity gives image stabilization as well. On $K(T)$, $T^n = 0$. On $I(T)$, $T(I(T)) = I(T)$; finite dimension makes this a bijection. If $hT = T'h$, induction gives $hT^r = T'^r h$, hence

$$h(\ker T^r) \subseteq \ker T'^r, \qquad h(\operatorname{im} T^r) \subseteq \operatorname{im} T'^r.$$

This proves functoriality even when $\dim V \neq \dim V'$: choose a common stabilization exponent for the two finite objects. The decomposition projection onto $K(T)$ along $I(T)$ is canonical and commutes with all intertwiners; the existence of a Jordan basis is not needed. Finite dimension is essential. On $V = k[t]$, multiplication by t has stable kernel zero and stable image $\bigcap_r t^r k[t] = 0$, although $V \neq 0$. The same construction $N_m(V, t)$ is an actual infinite-dimensional module of A_m. Thus the finite Fitting split cannot be extended to every module of our infinite algebra merely by repeating its notation.

Let $k_r = \dim \ker T^r$, with $k_0 = 0$, and form $G_r = \ker T^r / \ker T^{r-1}$. For a nilpotent Jordan block of size s, $k_r = \min(r, s)$, so $\dim G_r$ counts the blocks of size at least r, and $2k_r - k_{r-1} - k_{r+1}$ counts blocks of size exactly r. For $J_3(0) \oplus J_1(0) \oplus J_2(1)$ the stable dimensions are 4 and 2; the kernel dimensions begin $0, 2, 3, 4, 4$. The G_r are functorial subquotients. Their dimensions do not specify a natural choice of basis or split each filtration step.

Proposition 23.2 (What the source's splitting-functor assumptions imply)**.** *Let $\mathcal{A}, \mathcal{B}_i$ be additive categories with finite biproducts. Suppose additive functors $S_i : \mathcal{B}_i \to \mathcal{A}$ and $F_i : \mathcal{A} \to \mathcal{B}_i$ satisfy $F_iS_i \cong 1$, $F_iS_j \cong 0$ for $i \neq j$; only finitely many F_iM are nonzero for each M; the F_i jointly reflect isomorphisms; and maps $\gamma_{i,M} : S_iF_iM \to M$ have invertible F_i-images. Then $M \cong \bigoplus_i S_iF_iM$. Every nonzero indecomposable is S_iB for a unique index and an indecomposable B up to isomorphism.*

Proof. Sum the finitely many nonzero $\gamma_{i,M}$ to a map γ_M. After applying F_j, all off-diagonal summands vanish, leaving the assumed isomorphism $F_j\gamma_{j,M}$, or $0 \to 0$. Joint reflection therefore makes γ_M invertible. For an indecomposable M, exactly one of the nonzero summands can occur.

Conversely, if $S_iB = X \oplus Y$ and B is indecomposable, applying F_i makes one summand vanish, say $F_iX = 0$; every other F_jX also vanishes. Joint reflection applied to $0 \to X$ gives $X = 0$ up to isomorphism. Finally apply F_i to an isomorphism $S_iB \cong S_jB'$ to recover both index and object. □

The direction of γ matters: it is into M, contrary to one source diagram. Local finiteness is objectwise in i, not a finiteness assertion over all objects of a category. Abelian categories require kernels, cokernels and the usual exactness axioms; addition is on Hom groups, not on an alleged group of quiver vertices. The abstract assumptions above do not assert that the family F_i is faithful on arbitrary morphisms. Our Fitting example is concrete: $\mathcal{B}_0$ consists of nilpotent pairs, $\mathcal{B}_\times$ of invertible pairs, S are inclusions and $F_0, F_\times$ the two stable summands.

23.2.4 Strings, bands, Hom and one non-rigid string

In this branch category, Jordan normal form classifies indecomposables over an algebraically closed field. Over a general field replace Jordan eigenvalues by powers of monic irreducible polynomials. A Jordan block $J_r(0)$ is one directed string with mr basis visits and $mr - 1$ nonzero successor arrows; $J_r(\lambda)$ for $\lambda \neq 0$ is a permitted cycle band. Formal inverse letters are reverse traversals, not inverse elements of A_m. Strings and their reverses describe the same string module under the usual isomorphism convention. Arbitrary infinite modules are not all classified by this finite calculation; the actual finiteness hypotheses in [38] remain essential.

Identify a Jordan pair with $k[t]/(t - \lambda)^r$. An intertwiner from size r to size s is determined by the image of 1, annihilated by $(t - \lambda)^r$. For equal eigenvalues this subspace has dimension $\min(r, s)$. For different eigenvalues, Bezout's identity makes $t - \lambda$ invertible on the target, so only zero remains. Full faithfulness above transfers this Hom computation to A_m. The sequence $0 \to J_1(0) \to J_2(0) \to J_1(0) \to 0$ is not split: with $J_2(0)e_1 = e_2$, a lift of the quotient generator has nonzero first coordinate and is not killed by $J_2(0)$. Its image under N_m is a nonsplit ambient-A_m self-extension. Thus even the string $N_m(J_1(0))$ is not rigid. No assertion that this exact full subcategory is derived fully faithful is needed for the nonsplitting argument.

For this particular closed A_m, every oriented or inverse letter has exactly two admissible successors: continue on its branch in the same orientation, or switch branch and reverse orientation. Cancellation and forbidden pairs, including inverse forbidden pairs, remove the other choices. A fixed ordering of these choices identifies each first-letter cylinder with $\{0, 1\}^{\mathbb{N}}$. The whole infinite-word space is a finite disjoint union of Cantor spaces, hence itself Cantor. There are no terminating words inside that space to remove. Arbitrary gentle quivers can have isolated or eventually forced paths, so this conclusion is not universal. Algebraic covers retain the lifted zero-relations and deck equivariance data; arbitrary periodic cover representations are not automatically bands or a unitary time evolution.

23.2.5 A determinant comparison with its exact limits

On $\bigoplus_i V_i$, $L^m = \mathrm{diag}(T, \ldots, T)$. For a direct determinant proof of (23.1), successively eliminate the blocks 1 at vertices $1, \ldots, m - 1$ in $1 - zL$. Block row additions preserve determinant and leave $1 - z^mT$ at vertex zero. This works over $k[z]$ without inverting z or T; the zero-size case gives one on both sides. The Fitting splitting separates a nilpotent factor 1 and the determinant on the invertible summand. For instance $m = 5$, $T = J_2(2)$ gives $(1 - 2z^5)^2$, whose complex roots have modulus $2^{-1/5}$, despite being a genuine genus-two dessin module.

Under conjugation of T this is an invariant polynomial. With independent source/target bases a presentation determinant is instead a semi-invariant with its determinant-character weight; those actions must not be conflated. The polynomial equality does not construct a positive Hermitian

metric, an arithmetic Euler factor, a regularized determinant or a zero-preserving map to completed L-functions. Functorial kernel filtrations similarly do not construct an equivalence of derived/Fukaya categories. A fixed graded surface category and a determinant-compatible arithmetic realization remain separate obligations.

The exact rational checker evaluates actual genus-two/four quivers, Hom equations, full-turn matrices, both filtration directions and the nonsplit extension. `lean-analytic/LinearRelations.lean` proves full graph identities, semiconjugacy and filtration preservation, actual finite-space Fitting splitting/stabilization and unit-power annihilation. It does not package the entire dessin category, Jordan classification, general splitting-functor proposition or determinant proof in Lean.

23.3 A kernel-checked extension over the infinite dessin algebra

The preceding branch example can be realized on every element of the infinite algebra, rather than verified only on sampled arrow matrices. Use the complex genus-two clean dessin $y^2 = x^5 - 1$, $\beta = x^5$, and any coefficient field k. Put $H \subseteq M_5(k[t])$ equal to the matrices whose reduction modulo t is upper triangular. Let

$$B = H \times_{k^5} H,$$

where each map to k^5 takes the constant diagonal. Equivalently, B is generated inside $M_5(k[t])^2$ by

$$e_i = (E_{ii}, E_{ii}), \quad a_i = (w_i E_{i-1,i}, 0), \quad b_i = (0, w_i E_{i-1,i}), \qquad w_0 = t, \quad w_i = 1 \ (i \neq 0).$$

Indices are modulo five. Matrix multiplication acts on left column modules. The path-normal-form proof below identifies B with A_5; this is a polynomial algebra, not an arrow-truncated finite quotient.

Theorem 23.3 (An ambient module extension)**.** *Let $D = k[\epsilon]/(\epsilon^2)$, $M_1 = k^5$ and $M_2 = D^5$. For $(C(t), D'(t)) \in B$, act on M_1 by $C(0)$ and on M_2 by $C(\epsilon)$. These are unital B-modules, and*

$$0 \longrightarrow M_1 \xrightarrow{i} M_2 \xrightarrow{p} M_1 \longrightarrow 0, \qquad i(x) = \epsilon x, \quad p(x + \epsilon y) = x,$$

is exact and nonsplit. Moreover B is infinite dimensional over k. The assertions hold in every characteristic, including two.

Proof. Evaluation of polynomials gives both actions. Multiplying $C(\epsilon) = C_0 + \epsilon C_1$ proves B-linearity of i, p; their kernel and image follow coordinatewise. If s were a B-linear section, the constant coefficient of $(se_0)_0$ would be one. But a_0 kills M_1, while $(a_0 s e_0)_4 = \epsilon (se_0)_0$ has nonzero ϵ coefficient, a contradiction. Finally the permitted turn $c = a_1 a_2 a_3 a_4 a_0$ has first component tE_{00}. The unital algebra map $k[t] \to B$, $f \mapsto f(c)$, is injective: its $(0,0)$ first-component entry is $f(t)$. Thus B cannot be finite dimensional. □

In the preceding notation these modules are $N_5(J_1(0))$ and $N_5(J_2(0))$. They are finite torsion modules over an infinite algebra; they are not nonzero lattices over its completed surface order. The nonsplit sequence defines a nonzero Yoneda extension class in the ambient module category. No assertion that it is almost split in that entire category is needed or inferred. In particular it does not supply an arithmetic spectral determinant or a zero-location theorem.

Theorem 23.4 (Unbounded normal-image faithfulness)**.** *In $M_5(k[t])^2$, index the stationary images by i and the positive images by (b, i, j, q), where $b \in \{a, b\}$, $0 \leq i, j < 5$, $q \geq 0$ and $i < j$ or $q > 0$. The positive image is $t^q E_{ij}$ in factor b, with zero in the other factor. Its path length is $5q + j - i > 0$. All these images, including the shared stationary images, are linearly independent over every field. Every finite normal expansion has uniquely recoverable coefficients, without a bound on degree or path length.*

Proof. Read a stationary coefficient from the first factor's constant diagonal; read a positive coefficient from the indicated factor, entry and degree. The index restriction ensures that no positive image contributes to a constant diagonal. These linear selectors are biorthogonal to the images, so applying each selector to a finite expansion recovers its coefficient. □

This theorem is now kernel checked for actual polynomial matrix pairs. The membership and spanning steps are supplied by the next theorem. Comparison with a separately constructed path quotient remains a distinct algebraic formalization task.

Theorem 23.5 (Normal coordinates in the generated algebra)**.** *Let $A \subseteq M_5(k[t])^2$ be the algebra generated by the displayed vertices and arrows, and let $\mathcal{K}$ be the normal index set of Theorem 23.4. Every normal image belongs to A. The actual A-valued finite expansion*

$$E : k^{(\mathcal{K})} \longrightarrow A, \qquad c \longmapsto \sum_{x \in \mathcal{K}} c_x v_x$$

is a linear isomorphism, whose inverse is $(E^{-1}a)_x = \lambda_x(a)$. Thus the normal images form a basis of the infinite generated algebra, not merely an independent family in its ambient matrix space.

Proof. Write $P_b(i, j)$ for the shortest positive branch walk from j to i, using a full turn when $i = j$. Its image is $t^d E_{ij}$ in branch b, where $d = 0$ if $i < j$ and $d = 1$ otherwise. The actual arrow product $P_b(i, i)^n P_b(i, j)$ has image $t^{n+d} E_{ij}$ for every $n \geq 0$. Admissibility gives $q \geq d$, so $n = q - d$ proves membership.

The normal span contains the generators and $1 = \sum e_i$ and is multiplicatively closed: stationary factors select endpoints; positive factors either multiply to zero or to $t^{q+r} E_{il}$ in the same branch. When $q + r = 0$, the two strict upper inequalities imply $i < l$, so this output slot is still permitted. Adjoin induction gives spanning of A. The previous coefficient selectors prove uniqueness and the inverse formula. □

All membership, spanning and finite-expansion assertions in this theorem are now Lean checked over arbitrary fields. The formal linear equivalence is not asserted to be an algebra map from an independently defined path quotient, nor a statement about completed orders, derived categories or GRH.

23.4 Normal forms and the full module action

23.4.1 Why the polynomial matrix algebra is the path algebra

With our convention a path from j to i acts as E_{ij}; the rightmost arrow acts first. Every nonzero positive path uses only the a-branch or only the b-branch, because mixed consecutive arrows are the defining quadratic zero relations. Along either branch the path of length ℓ starting at j is unique. Write

$$\ell = j - i + 5q, \qquad 0 \leq i, j < 5.$$

Its image is $t^q E_{ij}$ in the chosen factor and zero in the other. For $i < j$, $q \geq 0$; for $i > j$, $q \geq 1$; for $i = j$ and positive length, $q \geq 1$. The stationary path is the shared (E_{ii}, E_{ii}).

These images are linearly independent: off-diagonal matrix units, positive diagonal monomials, branch factors and degrees are independent; the shared constant diagonal units are independent of all positive paths. They span $H \times_{k^5} H$, since upper entries permit all polynomials, lower entries are divisible by t, and only the constant diagonals of the two factors must agree. Products of paths agree with matrix products. Thus the arrow assignment induces a bijective algebra map from

$kQ/(a_ib_{i+1}, b_ia_{i+1})$ to B. This argument includes arbitrarily long paths; it imposes no nilpotence relation on a full turn.

The central parameter u, the sum of all full turns on both branches, has image (tI_5, tI_5). Completing in this parameter is a separate operation. The polynomial algebra and its completion are not identified by the normal-form calculation. The finite modules below are annihilated by u^2, so their continuous completed actions require only a finite Taylor polynomial.

23.4.2 Coefficient selectors without a truncation

Here is an explicit proof of Theorem 23.4 and the coordinate convention used by the implementation. Let

$$\mathcal{S} = \{(i,j,q) : 0 \le i,j < 5,\ q \in \mathbb{N},\ i < j \text{ or } q > 0\}, \qquad \mathcal{K} = \{0,\dots,4\} \sqcup (\{a,b\} \times \mathcal{S}).$$

For a stationary index set $v_i = (E_{ii}, E_{ii})$; for a positive index set $v_{a,i,j,q} = (t^q E_{ij}, 0)$ and $v_{b,i,j,q} = (0, t^q E_{ij})$. These are elements of the ambient polynomial matrix-pair space, with no degree cutoff. For $M = (M_a, M_b)$ define

$$\lambda_i(M) = [t^0](M_a)_{ii}, \qquad \lambda_{b,i,j,q}(M) = [t^q](M_b)_{ij}.$$

Here the subscript b in the second formula denotes either branch. Every λ_x is k-linear, since extraction of a fixed matrix entry and polynomial coefficient is linear.

We verify $\lambda_x(v_y) = \delta_{xy}$, including the cases at degree zero. For two stationary indices this is the ordinary diagonal matrix-unit identity. A stationary selector vanishes on a positive image in the other factor. In its own factor it could see a constant diagonal only if $i = j$ and $q = 0$, which the definition of $\mathcal{S}$ excludes. Conversely, a positive selector applied to a stationary image could be nonzero only at precisely the same forbidden slot. For two positive indices, different branches have disjoint supports. In one branch the matrix entry forces both endpoints to agree and the monomial coefficient forces the degrees to agree. These conditions give equality of the full indices. The witness of the condition defining $\mathcal{S}$ carries no extra algebraic data. This proves biorthogonality in every characteristic, using no division.

For any finitely supported $c : \mathcal{K} \to k$, linearity now gives

$$\lambda_x\left(\sum_{y \in \mathcal{K}} c_y v_y\right) = c_x.$$

If the sum vanishes, every c_x vanishes; if two sums agree, their coefficients agree. This proves linear independence and injectivity of normal expansion on the actual k-module of finitely supported functions. It does not replace finite support by a convergent or formal infinite sum.

The length formula also contains useful information beyond independence. If $i < j$ then $5q + j > i$ even at $q = 0$; otherwise $q > 0$ and $i \le 4$ give the same strict inequality. Hence $\ell = 5q + j - i$ is a positive integer, and $\ell + i = 5q + j$. For fixed starting vertex j and length ℓ, two such equations imply $i - i' = 5(q - q')$. Since $i, i' \in \{0,\dots,4\}$, this forces $i = i'$ and then $q = q'$. In Lean the subtraction is natural subtraction; positivity is proved before using the rearranged equation.

For example the a-path of length 12 from vertex 4 ends at vertex 2 and has image $(t^2E_{24}, 0)$. The length-4 a-path from 3 to 4 has image $(tE_{43}, 0)$. Their product, with the rightmost path first, is $(t^3E_{23}, 0)$, of length 16. Replacing the second path by its b-branch version makes the product zero. Degree-zero upper entries such as $(E_{24}, 0)$ are permitted, but $(E_{22}, 0)$ is not a stationary image: the stationary element is the shared pair (E_{22}, E_{22}). This last distinction prevents a spurious extra idempotent in the proposed basis.

The selector theorem alone gives the faithfulness part of the intended quotient comparison. The next construction proves membership and spanning inside the generated algebra without assuming that comparison. A separately defined path algebra, mixed-zero quotient and its universal algebra map still require formal packaging. Completion, module-category and almost-split universal properties require their own subsequent constructions. None of these finite-support identities supplies an arithmetic self-adjoint determinant or controls zeta zeros.

23.4.3 Constructing every normal image from actual arrows

We now prove Theorem 23.5. This closes the membership and spanning gap left by ambient coefficient recovery. Let $p(j) = j - 1$ modulo five and, inside the actual generated algebra, define

$$W_b(0, j) = e_j, \qquad W_b(n + 1, j) = W_b(n, p(j))\, b_j.$$

In this formula b_j denotes the arrow in the chosen branch; it may be an a-arrow. The rightmost arrow acts first. This recursive definition is an element of A for every n, because it uses only its generators and multiplication. Set

$$d_{ij} = \begin{cases} 0 & i < j, \\ 1 & i \geq j, \end{cases} \quad L_{ij} = j - i + 5d_{ij}, \quad P_b(i, j) = W_b(L_{ij}, j), \quad C_b(i) = P_b(i, i).$$

The integer L_{ij} lies between one and five. In particular $P_b(i, i)$ is a positive full turn, whereas $W_b(0, i)$ is the shared stationary idempotent. These two elements are not interchangeable.

Directly following the arrows, the path $P_b(i, j)$ crosses the weighted arrow b_0 exactly d_{ij} times. Its image is therefore $t^{d_{ij}} E_{ij}$ in factor b, with zero in the other factor. The Lean proof checks all five-by-five endpoint pairs for each of the two branches; this is a finite verification of a finite combinatorial case split, not a bound on permitted path lengths. For all $n \in \mathbb{N}$, induction gives

$$\mathrm{view}\big(C_b(i)^n P_b(i, j)\big) = t^{n+d_{ij}} E_{ij} \quad \text{in factor } b.$$

For $n = 0$ the power is the unit of the whole two-factor algebra, so multiplication by $P_b(i, j)$ still selects the correct branch. The induction step uses $C_b(i)$ with image tE_{ii} and $E_{ii}E_{ij} = E_{ij}$. No assertion that a branch-only degree-zero diagonal belongs to the algebra is needed. Since a permitted slot satisfies $q \geq d_{ij}$, the choice $n = q - d_{ij}$ constructs its preimage in A. This proves membership at every polynomial degree.

For clarity, if $i = 2$, $j = 4$, $q = 2$, then $P_a(2, 4) = a_3 a_4$ and $C_a(2)^2 P_a(2, 4)$ realizes $(t^2 E_{24}, 0)$ by a length-12 arrow word. For $i = 4$, $j = 0$, $q = 1$, we have $P_a(4, 0) = a_0$ and the exponent $q - d_{40}$ is zero. The corresponding exponent must never be replaced by a negative power or by an inverse arrow. The construction works over $\mathbb{F}_2$ as well as characteristic zero.

23.4.4 Spanning, multiplication and the inverse coordinate map

Let S be the k-linear span of all normal images in the ambient space. Membership just proved gives $S \subseteq A$. We prove the reverse inclusion by showing that S is closed under the operations used to generate A. The product rules are

$$e_i e_j = \delta_{ij} e_i, \qquad e_r v_{b,i,j,q} = \delta_{ri} v_{b,i,j,q}, \qquad v_{b,i,j,q} e_r = \delta_{jr} v_{b,i,j,q},$$

and for two positive images

$$v_{b,i,j,q} v_{c,r,l,s} = \begin{cases} v_{b,i,l,q+s} & b = c \text{ and } j = r, \\ 0 & \text{otherwise.} \end{cases}$$

The displayed nonzero output is always an admissible positive image. If $q + s > 0$ this follows from its degree. If $q + s = 0$, nonnegativity gives $q = s = 0$, so the input conditions imply $i < j = r < l$. Thus $i < l$ and the output is admissible even at degree zero. This explains why closure cannot be justified merely by ignoring the lower-triangular constraints.

By bilinearity the product of two finite linear combinations lies in S. Every vertex is one of its normal images, and each arrow is a permitted image with degree zero except the wrap arrow, which has degree one. The sum of the shared vertices is the unit. Scalar multiples of this unit belong to S. Induction on the algebra generated by the arrows and vertices therefore gives $A \subseteq S$. In Lean this is actual `Algebra.adjoin_induction`, not a predicate that assumes the desired normal form for every element. Consequently $A = S$ as submodules of the polynomial matrix-pair space.

Now lift each v_x to an element $\widetilde{v}_x \in A$ using its proved membership. Their images under the injective inclusion are the already independent ambient images, so the lifts are independent. The equality $A = S$ gives surjectivity of finite expansion; independence gives injectivity. This constructs the linear equivalence E on the genuine generated algebra. For any $a \in A$, apply the ambient coefficient recovery identity to $E^{-1}a$ to obtain

$$(E^{-1}a)_x = \lambda_x(\mathrm{view}(a)).$$

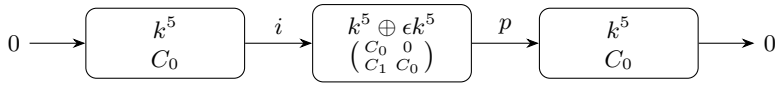
The formula holds for every element of A, not only on a sampled list of paths or generators. Its finite support follows from the equivalence with finitely supported functions. No convergence of an infinite expansion is asserted. Although the product table has been used to prove span closure, we have not yet supplied the formal universal map from a separately constructed bound-quiver path quotient. The distinction between a linear coordinate equivalence and that algebraic quotient interface is retained.

23.4.5 Exactness for arbitrary algebra elements

In coordinates $M_2 = k^5 \oplus \epsilon k^5$ let $C(t) = \sum_{r \geq 0} C_r t^r$ be the first component of an arbitrary B-element. Its action is

$$(x, y) \longmapsto (C_0 x, C_1 x + C_0 y), \qquad \rho_2(C) = \begin{pmatrix} C_0 & 0 \\ C_1 & C_0 \end{pmatrix}.$$

Evaluation is multiplicative: the constant coefficient of a product is $C_0 C_0'$ and the linear coefficient is $C_0 C_1' + C_1 C_0'$. Consequently the formula is a representation of the entire algebra. The second branch acts by zero but has not been removed from the algebra. Both maps in the sequence commute with this general block action, not merely with a finite test list of generators.



Every vector in $\ker p$ is $(0, y) = i(y)$, i is injective, and p is surjective by $x = p(x, 0)$. The section obstruction uses only a_0: it is zero on M_1, while on M_2 it sends the coordinate-zero constant coefficient to the coordinate-four infinitesimal part. A section commuting with this arrow would force $1 = 0$. No algebraic closure, eigenvalue classification, division by two or positivity premise occurs.

23.4.6 Formal and computational coverage

The file `lean-analytic/BranchExtension.lean` defines B as the actual generated subalgebra of polynomial matrix pairs, proves its infinite dimensionality through injective polynomial evaluation,

and constructs i, p as B-linear maps. The original 21 printed theorem types and axiom reports cover the generators, infinite embedding, actions, exactness and absence of a module section. Eight additional reports in `NormalPath` cover slot extensionality, positive length, the length equation, recovery from start and length, biorthogonality, coefficient recovery, linear independence and injective normal expansion. Ten further printed reports now establish actual generated-algebra membership, equality with the normal span, lifted independence, bijective finite expansion and its explicit inverse coefficients. The normal-form isomorphism with the separately constructed path quotient above is proved in prose; it is not packaged as a Lean categorical equivalence. Nor is a Yoneda-Ext object or the universal factorization property of an almost-split sequence formalized by these maps alone.

The exact checker `examples/relations/check_extension.py` independently uses unbounded normal paths and polynomial matrix pairs. It checks 405 distinct paths through length 40, 7,225 products, 30 distinct loop powers and 80 whole-polynomial module actions. The full generator system for a hypothetical section has coefficient rank 49 and augmented rank 50 over $\mathbb{Q}, \mathbb{F}_2, \mathbb{F}_3, \mathbb{F}_5$. These finite diagnostics complement the symbolic proof; their finite cutoffs do not establish infinite dimensionality by themselves.

The separate exact checker `examples/relations/check_normal_paths.py` checks 475 normal images at degrees up to 1,000,003 (length 5,000,019), all 225,625 selector pairs, 1,030 direct arrow steps, 15,625 composable-or-zero product comparisons and 200 finite expansions over $\mathbb{Q}, \mathbb{F}_2, \mathbb{F}_3, \mathbb{F}_5$. Invalid constant slots are rejected. These are finite diagnostics of the code and conventions; the unbounded assertion is established by the Lean theorem, not by the size of the tests.

A further deterministic checker, `examples/relations/check_normal_algebra.py`, constructs all 50 shortest arrow words and 375 actual preimages, including degree 1,000,003, using sparse binary powers of the full turns. It checks 5,625 product round trips and 200 exact expansions over the four stated fields. Three ambient matrices with forbidden constant shapes fail reconstruction, as required. These diagnostics test the implementation independently of finite degree bounds; the general membership/span/equivalence result is the Lean theorem, not an extrapolation from these samples.

Chapter 24

DG foundations, clock lifts and endpoint-sensitive extensions

A derived construction begins with a differential and its cohomology, not with a proposed physical clock. This chapter develops the DG material of the original 2053 manuscript, lines1308–1478. Throughout this chapter k is a field. We use the actual infinite nodal and theta dessin algebras. The source is preserved unchanged. Its unit-boundary example and self-extension count require corrections; its higher-product and physical interpretations require explicit additional data.

24.1 Degrees, maps and a decisive contracting homotopy

We use cohomological grading. A unital DG algebra is a graded algebra $B = \bigoplus_{n\in\mathbb{Z}} B^n$ with $d : B^n \to B^{n+1}$, $d^2 = 0$ and $d(ab) = d(a)b + (-1)^{|a|}a\,d(b)$ on homogeneous elements. A DG map preserves multiplication, the unit, degrees and the differential. It is a quasi-isomorphism when it induces isomorphisms on every cohomology group. A left DG module has the corresponding Leibniz rule for its action. The exterior generator's degree must be declared; the notation $\Lambda^\bullet(V)$ alone does not specify negative degrees.

Proposition 24.1 (A unit boundary is contractible)**.** *If $\varepsilon \in B^{-1}$ satisfies $d\varepsilon = 1$, the underlying k-complex of every unital left DG B-module is contractible. In particular $H^*(B) = 0$; it is not a DG resolution of a nonzero field with zero differential.*

Proof. Define $h : M^n \to M^{n-1}$ by $h(m) = \varepsilon m$. Then $d_M h(m) = m - \varepsilon d_M m$, so $d_M h + h d_M = 1$. Every cocycle m is therefore $d_M h(m)$. For a right module the correct formula is $h(m) = (-1)^n m\varepsilon$: its two compositions have opposite $d_M m\varepsilon$ terms and again sum to m. Taking the regular module proves the algebra assertion. The displayed homotopy is k-linear; graded B-linearity would require an additional compatibility, such as graded centrality of ε. A unital chain map to a nonzero field would send $d\varepsilon$ both to zero and to one, which is impossible. □

The qualifier is essential for a general noncommutative DG algebra. Over our actual nodal algebra A, let $C = (A \xrightarrow{1} A)$ in degrees $-1, 0$ and $B = \mathrm{End}_A(C)$ with commutator differential. The inverse-arrow homotopy ε satisfies $d_B\varepsilon = 1$. But a degree--1 graded B-linear endomorphism of C must commute with the even projection onto C^0; its only possible component $C^0 \to C^{-1}$ is then zero. Thus C is acyclic and its underlying complex contracts, without being contractible by a B-linear homotopy. Derived and homotopy categories must not be conflated.

For the source's two-piece example $k \oplus k\varepsilon$, the differential is the identity $k\varepsilon \to k$. Both cohomology groups vanish. The auxiliary identity $dh + hd = f$ for a Koszul relation f is useful instead of assuming nonzero cohomology [78].

24.2 The genuine infinite node and its DG replacement

The clean interval dessin on the sphere gives $A = k[\xi, \eta]/(\xi\eta)$, with basis $1, \xi, \xi^2, \ldots, \eta, \eta^2, \ldots$. It remains infinite dimensional. The variables ξ, η here are actual dessin loops; they are distinct from the auxiliary persistence parameters x, y used later in the book. Set $R = k[\xi, \eta]$ and consider

$$K^0 = R, \qquad K^{-1} = R\varepsilon, \qquad K^n = 0 \quad (n \neq 0, -1), \qquad d(b\varepsilon) = \xi\eta b.$$

The product is ordinary coefficient multiplication, with $\varepsilon^2 = 0$ and ε commuting with degree-zero coefficients. The odd square relation is imposed also in characteristic two. Proposition 2.5 proves all Leibniz cases and the cohomology. Explicitly, writing $p = a + b\varepsilon$ and $q = c + e\varepsilon$ gives

$$d(pq) = d(p)q + \varsigma(p)d(q), \quad \varsigma(a + b\varepsilon) = a - b\varepsilon, \quad h(a + b\varepsilon) = a\varepsilon, \quad dh + hd = (\xi\eta)\, 1_K.$$

This sign formula extends the homogeneous rule linearly; d is not an ordinary ungraded derivation of this commutative square-zero algebra.

$$\begin{array}{ccccccccc} 0 & \longrightarrow & R\varepsilon & \xrightarrow{\xi\eta} & R & \longrightarrow & 0 \\ & & \downarrow{\scriptstyle 0} & & \downarrow{\scriptstyle \pi} & & \\ 0 & \longrightarrow & 0 & \longrightarrow & A & \longrightarrow & 0 \end{array}$$

The diagram compares cochain degrees $-1, 0$. The map π is quotient augmentation, not an inclusion of A into R. Its kernel is $(\xi\eta)$, and multiplication by $\xi\eta$ is injective since R is a domain. Thus the cohomology comparison is an isomorphism in every degree. The two ambient terms are free over R. They are not asserted to be free A-modules: the nonzero element $\xi\eta$ acts on them, so their action does not even factor through A. This DG replacement does not shorten the infinite projective resolution of a nodal residue simple over A.

For an explicit calculation, $\xi^3\eta^2 = d(\xi^2\eta\varepsilon)$, whereas ξ^3 and η^2 survive in H^0. A polynomial has a unique normal form $a(\xi) + b(\eta) - c$, where $a(0) = b(0) = c$; remove every monomial divisible by $\xi\eta$. Their linear independence follows by setting each variable to zero. This identifies the quotient with the polynomial branch pullback.

24.3 Completion and the diagonal coefficient ring

Write $S = k[[\xi, \eta]]$. The same two-term construction over S maps to

$$\Lambda = S/(\xi\eta) \cong \{(a(\xi), b(\eta)) : a(0) = b(0)\}.$$

Here is a coefficientwise proof, avoiding an unjustified interchange of completion and arbitrary cohomology. The branch-evaluation map sends F to $(F(\xi, 0), F(0, \eta))$. Every equal-constant pair is the image of $a(\xi) + b(\eta) - a(0)$. Its kernel consists of series whose coefficients on both coordinate axes are zero. Such a series is uniquely $\xi\eta G$ by shifting both exponents down one. The same shift proves multiplication by $\xi\eta$ injective. Consequently the completed Koszul model has $H^{-1} = 0$, $H^0 = \Lambda$ and no other cohomology. All these maps are continuous for the maximal-ideal topologies: evaluation

preserves powers, and the product relation raises order by two. This is the actual completed surface order already used in the node chapter.

An isomorphism $H^0(B) \cong \Lambda$ by itself is not this result. For example $B = \Lambda \oplus \Lambda\delta$, $|\delta| = -1$, $d = 0$, $\delta^2 = 0$, has the same H^0 and nonzero $H^{-1} = \Lambda$. Projection to Λ is not a quasi-isomorphism. A DG enhancement must specify the DG map or a justified zigzag and prove the required cohomology comparisons. Equivalences of derived DG-module categories use an external change-of-algebra theorem with its hypotheses; they do not follow from a single ordinary algebra isomorphism on H^0.

24.4 A clock that really lifts, and its semilinearity

For $q \in k^\times$, define $\sigma_q(\xi) = q\xi$, $\sigma_q(\eta) = q^{-1}\eta$. Substitution is a polynomial algebra automorphism, inverse to $\sigma_{q^{-1}}$, and fixes $\xi\eta$. It acts coefficientwise on K, fixing ε, so

$$\sigma_q d(b\varepsilon) = \sigma_q(\xi\eta b) = \xi\eta\sigma_q(b) = d\sigma_q(b\varepsilon).$$

Multiplicativity follows from the two-piece product formula. The completed substitution preserves each maximal-ideal power, so extends continuously, with continuous inverse, to the formal DG model and branch pullback. It is a semilinear chain automorphism over the ambient coefficient ring: $\sigma_q(rp) = \sigma_q(r)\sigma_q(p)$, not generally an R-linear map.

The diagonal DVR $k[[u]]$, $u = \xi + \eta$, has branches $(F(\xi), F(\eta))$. The clock sends u to the pair $(q\xi, q^{-1}\eta)$. If this is a diagonal series $G(u)$, its two linear coefficients must agree; hence $q = q^{-1}$. Conversely, if $q^2 = 1$, substitution sends $F(u)$ to $F(qu)$ and preserves the diagonal subring. It fixes that subring pointwise exactly when $q = 1$, as the image of u shows. In characteristic two these alternatives may coincide. Thus preserving the relation and order topology does not by itself preserve a chosen fixed coefficient action.

For $k = \mathbb{C}$ and $q = e^{i\theta}$, the coefficient of $\xi^i\eta^j$ acquires phase q^{i-j}. A selected finite monomial space with its declared orthonormal basis then has a unitary diagonal action. Choosing that finite norm does not construct a canonical Hilbert completion of the order, a self-adjoint arithmetic generator or an L-function comparison. The positive-transfer and unitary-logarithm distinctions in the physics chapters still apply. Gluing DG clocks further requires actual compatible maps and coherences; no gluing theorem is inferred here.

24.5 Theta self extensions require endpoints

The source calls its double-three-cycle example spherical. Keep that rational theta distinct from the elliptic theta. Both have $\sigma = (012)(345)$, but their dart involutions are respectively $\alpha = (03)(15)(24)$ and $(03)(14)(25)$. Write vertices as the sorted α-pairs $0, 1, 2$; for the elliptic case these are $\{0,3\}, \{1,4\}, \{2,5\}$. The simples S_i are the residue simples of the actual infinite dessin algebra. The exact forbidden-word resolution of Theorem 2.1 has two positive-degree arms. After Hom to a residue simple, every arrow differential vanishes, so Ext dimension counts the terminal vertices of these arms, not just arrows leaving the initial vertex.

Proposition 24.2 (Two different Ext tables)**.** *For $n = 0$ the dimension matrix is the identity. For $n > 0$, using right-module and path-travel conventions of the resolution chapter, the elliptic theta has*

$$\dim_k \operatorname{Ext}^n(S_i, S_j) = 2\,\mathbf{1}_{j=i-n \bmod 3}.$$

For the spherical theta, positive even n give 2 on the diagonal and zero elsewhere; odd n give zero on the diagonal and 1 at each other vertex.

Proof. For the elliptic involution, both initial arrows lower the vertex label by one modulo three; every next forbidden arrow does the same. Hence both length-n indexing words end at $i-n$. For the spherical involution the forbidden dart permutation has cycles $(04),(13),(25)$. Each two-step arm returns to its initial vertex, while its first step reaches one of the two other vertices, one arm each. This proves all positive degrees; degree zero is Hom between pairwise distinct residue simples. Minimality of the exact resolution supplies the Hom differential vanishing already used above. □

Thus neither example has two-dimensional self Ext^1. The two self-extension tables are

n	0	1	2	3	4	5	6
elliptic	1	0	0	2	0	0	2
spherical	1	0	2	0	2	0	2

These are module Ext groups, not stable AR arrows, finite-cutoff quotient Ext groups or an asserted surface-intersection classification. The completed residue-simple calculation follows the earlier formal-series resolution; other continuous-module and derived equivalences need their own arguments.

24.6 Higher products and a usable derived interface

For an uncurved cohomological A_∞ algebra, m_n has degree $2-n$. With the graded tensor sign convention its identities are

$$\sum_{r+s+t=n} (-1)^{r+st} m_{r+1+t}(1^{\otimes r} \otimes m_s \otimes 1^{\otimes t}) = 0, \qquad s \geq 1.$$

When $m_1 = 0$, the $n = 3$ identity makes m_2 associative. The operation m_3 is therefore not its ordinary associator. Minimal-model existence over a field and the appropriate derived comparison are external results of Keller [77, §§3.1,3.3,6.2]; they are not formalized here. For an ordinary algebra concentrated in degree zero, taking m_2 to be its product and all other operations zero already gives a minimal model. For our nodal DG resolution the cohomology is likewise concentrated in zero, so every higher m_n, $n \geq 3$, has zero target by degree. This model therefore supplies no compulsory nonzero higher operation or physical curvature.

The Ext algebra of a sum of simples is a different graded object. To build its derived composition data, choose an appropriate projective resolution P and use the DG endomorphisms with $\partial f = d_P f - (-1)^{|f|} f d_P$. Expanding twice cancels the mixed terms and leaves $d_P^2 f - f d_P^2 = 0$. Bounded-above projective resolutions in the ordinary module category give the familiar derived-Hom model; completed and topological versions must specify their Hom spaces and admissible maps.

There is also a useful grading test. Suppose an Ext minimal model is diagonal in cohomological/internal degree and its operations preserve internal weight. On inputs of cohomological degrees $a_1, \ldots, a_n$, m_n has output degree $\sum a_i + 2 - n$ but internal weight $\sum a_i$. Diagonality forces $n = 2$ unless the output vanishes. The polynomial quadratic-monomial theta resolutions are linear, so their Ext has this diagonal grading. A transfer using contractions chosen separately in each internal weight over a field retains it. Thus an internally compatible model can have every higher m_n zero. This statement concerns that graded polynomial interface; it is not an identification of all ungraded or completed enhancements, nor an assertion that an arbitrary numerically fitted operation is a minimal model. No physical curvature or arithmetic positivity follows from the symbol m_3.

24.7 Derived traces and genuine filtered DG modules

The graded enveloping algebra is $B^e = B \otimes_k B^{\mathrm{op}}$ with Koszul signs; Hochschild objects are the derived tensor $B \otimes^{\mathbf{L}}_{B^e} B$ and derived Hom $\mathbf{R}\,\mathrm{Hom}_{B^e}(B, B)$, with their homological or cohomological conventions declared. Derived base tensor or flatness is needed beyond the field setting. Completed continuous Hochschild theory also requires its completed tensor and continuity conventions. These objects are not interchangeable with an arbitrary ordinary matrix trace.

For the ordinary commutative nodal algebra, one concrete calculation is $HH_0(A) = A/[A, A] = A$: the degree-one Hochschild boundary sends $a \otimes b$ to $ab - ba = 0$. This quotient of the infinite-dimensional algebra carries universal trace classes but chooses neither a functional nor a positive state. Over $\mathbb{C}$ declare ξ, η self-adjoint and conjugate coefficients under $*$. The origin evaluation $\varphi(a) = a(0, 0)$ is a clock-invariant positive state, since $\varphi(a^*a) = |a(0, 0)|^2$. Its negative is still an invariant trace but is not positive, as its value at one shows. Even the positive choice has GNS null space (ξ, η), so its GNS Hilbert space is just $\mathbb{C}$. This follows directly from the displayed seminorm, and shows that trace classes, positivity and a useful spectral representation are three separate choices. No arithmetic determinant is obtained here.

A strict filtered DG module is a functor from a poset: its maps preserve degrees, actions and differentials, identities are identities, and every comparable triple has exactly the same composite map. A homotopy-coherent replacement must supply the higher coherences too; pairwise homotopies alone do not define it. For an actual example over our nodal DG model,

$$F_{a,b} = \xi^a \eta^b K, \qquad (a, b) \in (\mathbb{N}^2)^{\mathrm{op}},$$

forms a family of DG K-submodules, with inclusion maps when $a \geq c$ and $b \geq d$. Indeed multiplying by the central degree-zero monomial commutes with d, and these ideals are closed under the K-action. Inclusions compose literally; the clock preserves each ideal up to its scalar q^{a-b}. Componentwise divisibility also gives $F_{a,b} \cap F_{c,d} = F_{\max(a,c),\max(b,d)}$. This is a decreasing module filtration indexed with the declared reversed order.

The declared involution also matters. For self-adjoint ξ, η, a nonreal phase q makes σ_q an algebra automorphism which is not a $*$-automorphism. If a unitary implements it in a $*$-representation and $X = \pi(\xi)$ is self-adjoint, then $UXU^* = qX$ is self-adjoint, so $(q - \overline{q})X = 0$ and hence $X = 0$; the same holds for $\pi(\eta)$. Thus this particular nonreal clock cannot act faithfully by unitary conjugation with those self-adjoint branch conventions. This does not exclude other involutions or graph-operator constructions with different adjoint generators; it forbids silently identifying their adjoints with these declared ones.

The finite monomial windows below instead form increasing subcomplexes of k-vector spaces. They are not R-submodules or DG K-submodules, because multiplying by a variable leaves the box. Inverting both variables to manufacture increasing fractional modules would make $f = \xi\eta$ a unit: then $d(\varepsilon/f) = 1$ and the localized DG algebra contracts. Such localization loses the node rather than improving its derived resolution.

The remaining source interfaces need their own constructions: bar/cobar, Ginzburg and Fukaya enhancements are not selected by merely matching H^0; gluing up to homotopy requires coherent maps. Nor does a symbol m_3 identify a Hochschild deformation or a measured curvature. The existing unitary-logarithm discussion is retained in the physics chapter. Its nonunitary counterpart needs care: a singular finite matrix cannot be an exponential, since every matrix exponential is invertible. An invertible unipotent matrix has a finite nilpotent logarithm in characteristic zero, which is not a self-adjoint generator unless the matrix is the identity. These observations delimit the operator interface without assuming a physical realization of the algebraic clock.

24.8 Executable windows and exact verification coverage

The canonical laboratory shows a finite subcomplex, not a finite parent algebra. For $d\varepsilon = \xi\eta$ it retains source monomials $0 \le i, j \le N-1$ and target monomials $0 \le i, j \le N$. Every source maps injectively to the distinct target $(i+1, j+1)$. The finite rank is N^2, negative cohomology vanishes, and the surviving $2N+1$ target monomials lie on the two axes. These windows exhaust the polynomial resolution. For $d\varepsilon = 1$ both layers instead use the same box and contract; for $d = 0$ both layers survive. The window is not an R-submodule and is not closed under multiplication, so it must not be advertised as a finite DG subalgebra. The phase weight $i - j$ is equal at the two ends of every arrow. The second view displays the exact endpoint-sensitive theta Ext matrices.

`NodalDG.lean` uses the actual square-zero exterior-line coefficient algebra, with even/odd embeddings, differential and parity sign. It checks the Leibniz, homotopy, augmentation and semilinear-clock identities, as well as the exact ambient polynomial sequence for the nodal relation. These are actual algebra/module components. A categorical $\mathbb{Z}$-graded DG object, completed topology, A-infinity transfer and derived equivalence are not thereby kernel checked. Exact Python diagnostics check symbolic identities, normal forms and the two actual dart systems. Browser figures provide finite windows and phase illustrations; they are not numerical proofs of the infinite statements or of GRH.

Part IV

Quantum models, trained renormalization and physical realizations

Chapter 25

Positive evolution, clocks and holonomy

A surface order specifies algebraic paths, relations and gluing. A quantum model additionally specifies a complex Hilbert space, an adjoint, a state, a Hamiltonian and a measurement rule. Calling a path a clock does not make those choices. Keeping them explicit turns the physical interpretation into a sequence of calculable questions.

This part retains finite clocks, infinite observable algebras, quantum field theory, learned graph networks and molecular hardware. We distinguish a finite identity, a theorem with hypotheses, a reported experiment and a proposed design. A conditional arithmetic spectral criterion belongs to the second category: its missing determinant comparison cannot be supplied by a hardware analogy.

25.1 States and two different logarithms

A finite system has Hilbert space $\mathcal{H} = \mathbb{C}^d$, inner product v^*w, and density matrix $\rho = \rho^* \succeq 0$, $\operatorname{Tr}\rho = 1$. An observable is Hermitian and has expectation $\operatorname{Tr}(\rho O)$. A pure state is vv^* for a unit vector v; its global phase is invisible. A self-adjoint energy operator gives two different evolutions:

$$U(t) = e^{-itH/\hbar}, \qquad T(a) = e^{-aH/\hbar}, \qquad H = H^*. \tag{25.1}$$

Here t and a have time units. The first is unitary, the second positive. The formal substitution $t = -ia$ is Wick rotation. A continuum field theory needs additional reconstruction and convergence hypotheses.

Proposition 25.1 (Unitary and positive logarithms)**.** *For any unitary U and $\Delta t > 0$ there is a bounded self-adjoint H with $U = e^{-iH\Delta t/\hbar}$. For a positive-definite finite matrix T, the matrix $H = -(\hbar/a)\log T$ is Hermitian. These are distinct operations.*

Proof. Choose a bounded real Borel argument ϑ on the circle. Functional calculus gives $H = -(\hbar/\Delta t)\vartheta(U)$. For the second assertion, unitary diagonalization of T gives positive eigenvalues λ_j and $\log T = V \operatorname{diag}(\log\lambda_j)V^*$. □

The Borel argument need not be continuous or lie in the original C^*-algebra. The coordinate z on S^1 has no continuous logarithm because of its winding. A singular nilpotent matrix has no matrix logarithm: every exponential is invertible. One must model such a truncation by a contraction or channel instead. For a unitary clock, different phase branches change energies by integer multiples of $2\pi\hbar/\Delta t$; identical ticks can thus conceal different dynamics between ticks.

For positive T, top-eigenvalue normalization has the precise sign

$$\widetilde{T} = T/\lambda_{\max}, \qquad \widetilde{H} = H + (\hbar/a)\log\lambda_{\max} I \succeq 0.$$

In contrast, $i\log T$ is skew-Hermitian, not this Hamiltonian. If $\rho > 0$ is a density matrix, $K = -\log\rho$ is a dimensionless, nonnegative modular Hamiltonian. Its interpretation as physical energy requires a chosen scale and a state-dynamics comparison.

25.2 Total positivity, wiring and physical positivity

A real matrix is totally nonnegative when all minors are nonnegative, and totally positive when all are positive. These are ordered-basis conditions. Hilbert-space positivity means Hermitian positive semidefiniteness. The matrix $\left(\begin{smallmatrix}1 & 2\\ 3 & 7\end{smallmatrix}\right)$ is totally positive but not Hermitian. Its positive real eigenvalues do not make its logarithm self-adjoint in the given inner product.

The oscillation theorem and planar-network parametrizations remain valuable [123]. In an acyclic directed planar network, the Lindström–Gessel–Viennot cancellation expresses a minor of its path matrix as a sum over disjoint path families. With compatible boundary orderings the surviving signs are positive. Missing families can give zero minors, so positive edge weights do not guarantee strict positivity. Concatenation preserves total nonnegativity, but not symmetry. Positive Grassmannians organize these minors; they do not alone identify a physical scattering amplitude or reconstruct a quantum field theory.

Proposition 25.2 (A finite positive-energy certificate)**.** *A real symmetric positive-definite transfer matrix has a self-adjoint logarithmic Hamiltonian. Normalization by its largest eigenvalue makes the energy nonnegative. Symmetric total positivity is sufficient, not necessary.*

Proof. Use Proposition 25.1 and the normalization formula. Only positivity of the eigenvalues is needed. □

An exactly soluble transfer. For $T = \left(\begin{smallmatrix}2 & 1\\ 1 & 2\end{smallmatrix}\right)$, let $|\pm\rangle = (1, \pm 1)^T/\sqrt{2}$. Its eigenvalues are $3, 1$, hence

$$T/3 = |+\rangle\langle+| + \tfrac{1}{3}|-\rangle\langle-|, \qquad \widetilde{H} = (\hbar\log 3/a)|-\rangle\langle-|.$$

The normalized state $T/4$ instead has eigenvalues $3/4, 1/4$, with modular energies $\log(4/3), \log 4$. Transfer normalization, Gibbs normalization and energy extraction answer different questions.

For a row-stochastic P, detailed balance $\pi_i P_{ij} = \pi_j P_{ji}$ makes $S = D^{1/2} P D^{-1/2}$ symmetric, where $D = \operatorname{diag}\pi$. Its positivity is extra: $P = \left(\begin{smallmatrix}1/4 & 3/4\\ 3/4 & 1/4\end{smallmatrix}\right)$ is reversible but has eigenvalues $1, -1/2$. The lazy transition $(I + P)/2$ has eigenvalues $1, 1/4$ and a positive logarithmic interpretation. Laziness changes the process; it is not a proof of positivity for the original process.

In Euclidean QFT, reflection positivity is a condition on reflected correlations. Together with the other reconstruction axioms it produces a Hilbert space and positive-energy translations [124]. Entrywise nonnegative Boltzmann weights are not that condition. A family of finite positive matrices does not alone prove locality, covariance or a continuum limit.

25.3 Weyl clocks, Fourier phases and twisted successors

On $\mathbb{C}^d$ with $\omega = e^{2\pi i/d}$ set

$$X_d|j\rangle = |j + 1 \bmod d\rangle, \qquad Z_d|j\rangle = \omega^j|j\rangle.$$

Acting on basis vectors proves $Z_dX_d = \omega X_dZ_d$ and $X_d^d = Z_d^d = I$. The unitary Fourier matrix $(F_d)_{jk} = d^{-1/2}\omega^{jk}$ satisfies $F_dX_dF_d^* = Z_d$. For a qutrit the explicit matrices are

$$X_3 = \begin{pmatrix} 0 & 0 & 1 \\ 1 & 0 & 0 \\ 0 & 1 & 0 \end{pmatrix}, \qquad Z_3 = \operatorname{diag}(1, \omega, \omega^2).$$

Their commutator $Z_3X_3Z_3^*X_3^* = \omega I$ gives an interference calibration. The differently ordered product $Z_3X_3X_3^*Z_3^* = I$ contains no Weyl phase. Discrete X_d, Z_d generate a finite Pauli group, not all of $\mathrm{SU}(d)$. Universality needs suitable continuous controls and entangling gates.

A successor with wrap-around entry $r \in \mathbb{C}$ obeys

$$S_d(r)^d = rI, \qquad S_d(r)^*S_d(r) = \operatorname{diag}(1, \ldots, 1, |r|^2).$$

It is unitary precisely when $|r| = 1$. For a phase $r = e^{i\phi}$ this is an explicit twisted clock. A formal uniformizer in a surface order is not already a complex phase. A representation, specialization and norm must be supplied before interpreting it physically. A weight with $|r| \leq 1$ is a contraction, for which ancilla implementation is available below.

25.4 Infinite clocks: rotations and odometers are distinct limits

On $\ell^2(\mathbb{Z})$ let $U|n\rangle = |n+1\rangle$ and $V|n\rangle = e^{2\pi i\theta n}|n\rangle$. Then $VU = e^{2\pi i\theta}UV$. Under Fourier transformation, U becomes multiplication by e^{it} and V becomes angle translation. They are not two names for the same multiplication operator. The universal algebra on this relation is the rotation algebra A_θ.

Proposition 25.3 (Finite dimension detects a rational phase)**.** *If q-dimensional unitaries satisfy this relation, then $q\theta \in \mathbb{Z}$. For $\theta = p/q$, the pair X_q, Z_q^p gives a finite representation, but not a faithful representation of the entire universal $A_{p/q}$.*

Proof. Take determinants and cancel the nonzero determinants of U, V. At a rational phase U^q, V^q are central; the finite model fixes them to I, whereas other central circle values are possible. □

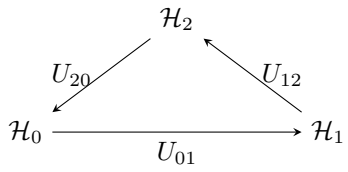
The irrational algebra has a canonical trace selecting the coefficient of U^0V^0 in a Fourier polynomial. This is not the ordinary trace of the identity on an infinite Hilbert space. Abstract algebraic states, normal states in a representation and trace-class densities are distinct notions.

Continued fractions provide rational approximations $|\theta - p_j/q_j| < q_j^{-2}$, but the denominators need not divide one another: successive Fibonacci numbers already refute that assertion. Exact isometries intertwining both Weyl generators at different phases would imply $(e^{2\pi i\theta_j} - e^{2\pi i\theta_{j+1}})J = 0$, which is impossible for a nonzero J. A limiting construction must specify approximate embeddings or a continuous field. Elliott–Evans approximations use matrix algebras over the circle, not a naive AF limit of finite matrix algebras [125].

A separate infinite clock chooses $n_j \mid n_{j+1}$ and forms $X = \varprojlim \mathbb{Z}/n_j\mathbb{Z}$. Addition by one is an odometer with Haar invariant measure. Compatible local extensions $\mathbb{C}((u^{1/n_j}))/\mathbb{C}((u))$ have these finite cyclic groups. Their inverse Galois limit and the direct union of fields point in opposite directions. The full set of denominators gives $\widehat{\mathbb{Z}}$; a selected tower gives the corresponding procyclic quotient. This preserves the ramification interpretation without identifying it with one irrational rotation algebra.

25.5 Holonomy, DG compatibility and persistence

Assign Hilbert fibers to graph vertices and unitary transports to oriented edges, with inverse on reversed edges. Their based loop product is holonomy; changing vertex bases conjugates it. For a triangular loop of complex lines with phases $e^{i\phi_j}$ it is $e^{i(\phi_1+\phi_2+\phi_3)}$. This is a gauge-invariant phase defect, not yet a gravitational redshift.



Operators on different tensor-product registers instead define many-body observables. Their product is not automatically transport on one fiber. The distinction must be fixed before designing a holonomy measurement.

Chapter 24 gives a corrected DG model of the actual infinite node, its clock lift and the endpoint-sensitive theta Ext calculation. A DG enhancement has $d^2 = 0$ and a graded Leibniz rule. A clock must commute with d to act on cohomology. On $\mathbb{C} \xrightarrow{0} \mathbb{C}$, phases on the two terms can be chosen independently. On $\mathbb{C} \xrightarrow{1} \mathbb{C}$, compatible scalar actions agree but cohomology vanishes. Thus the differential alone creates no physical time. Higher A_∞ operations have their own degrees and signs; periodic syzygies are not themselves a Hamiltonian or a time period.

A state-derived bifiltration can use increasing spatial radius and a decreasing correlation threshold. The order must give actual inclusions. For example, four edges around a square give an H_1 class; adding two triangles fills it. Multiparameter rank invariants, Betti tables and jump loci are meaningful diagnostics, but there is generally no canonical complete two-parameter barcode. Stability needs bounds on the actual filtration functions, including the statistical error of a nonlinear correlation-to-distance conversion. It does not identify a spectral or arithmetic determinant.

Chapter 26

Entanglement, channels and RG requirements

A renormalization channel needs an objective: which observables, states or phase labels should its coarse variables retain? Training selects parameters from data. This chapter supplies a solvable optimization task and a graph extension, while distinguishing an analytic optimum from an executed training run.

26.1 An entangled pair and the finite first law

Entropy is $S(\rho) = -\operatorname{Tr}(\rho \log \rho)$, with $0 \log 0 = 0$. Reduced states use partial trace; mutual information is $I(A:B) = S(\rho_A) + S(\rho_B) - S(\rho_{AB})$. We use natural logarithms. For

$$|\psi_p\rangle = \sqrt{p}|00\rangle + \sqrt{1-p}|11\rangle, \quad 0 < p < 1,$$

the reductions are $\operatorname{diag}(p, 1-p)$, so $S(\rho_A) = h(p) = -p \log p - (1-p)\log(1-p)$ and $I(A:B) = 2h(p)$. The modular Hamiltonian is $K_A = \operatorname{diag}(-\log p, -\log(1-p))$. At $p = 1/2$ its flow is trivial although the pair is maximally entangled. Entanglement amount therefore does not determine a nontrivial local modular clock rate.

Proposition 26.1 (Finite first law)**.** *If $\sigma > 0$ is a density matrix and $\rho(\epsilon)$ is differentiable, $\rho(0) = \sigma$, then*

$$\frac{d}{d\epsilon} S(\rho(\epsilon))\Big|_0 = \operatorname{Tr}(\rho'(0)(-\log \sigma)).$$

Proof. In a diagonal basis, the derivative under the trace is $d \operatorname{Tr}(X \log X)[Y] = \operatorname{Tr}(Y(\log X + I))$; off-diagonal divided-difference terms have zero trace. Use $\operatorname{Tr} \rho'(0) = 0$. □

For the pair above, $h'(p) = \log((1-p)/p)$ is exactly $\operatorname{Tr}(\operatorname{diag}(1,-1)K_A)$. The reference modular Hamiltonian stays fixed in this variation. A rank-deficient reference needs support control or a declared regularization such as $(1-\eta)\rho + \eta I/d$.

Relative entropy $D(\rho\|\sigma) = \operatorname{Tr} \rho(\log \rho - \log \sigma)$ is nonnegative, with equality only at equal states; incompatible supports give infinity. This is a strict matrix-convexity result, not the assertion that equality in a limit forces equality in an intermediate Hölder inequality. For the Gibbs state $\sigma = e^{-\beta H}/Z$ one obtains $K = \beta H + \log Z$. A general reduced state has no automatically identified physical energy or physical time parameter.

26.2 Correlation geometry and the gravitational research question

On a finite graph assign symmetric regularized lengths

$$\ell_e = \ell_* \max\{\varepsilon, -\log(\max\{I_e, \delta\}/I_*)\}, \qquad \ell_*, \varepsilon, \delta, I_* > 0.$$

They define a shortest-path metric. Zero lengths would yield a pseudometric; infinite lengths could disconnect the graph. If two length assignments differ by at most η on a graph with N vertices, shortest simple paths have at most $N-1$ edges, hence their distances differ by at most $(N-1)\eta$. A patchwise bound can be smaller. The logarithm is ill conditioned near zero correlation, which makes the regularization and its error propagation part of the model.

A regular tree and $\mathbb{H}^2$ are both hyperbolic metric spaces but have different boundaries, Cantor and circle, and are not quasi-isometric. Negative curvature does not alone give logarithmic diameter for every finite quotient. Expansion or a controlled family is needed. Arbitrary edge lengths need not form valid triangles for angle-defect curvature; metric-only curvature surrogates also require their neighborhood measures.

One can postulate a rate ratio $r_v/r_* = e^{-\alpha\varepsilon_v}$ for an entanglement proxy. This is a falsifiable ansatz. A bounded cyclic number expectation cannot increase forever, so an operational rate should use an unwrapped phase, counted transitions or calibrated oscillations. Matched noise-only controls must distinguish frequency changes from lost contrast. The entanglement-equilibrium route to Einstein equations has extra geometric, area, energy and continuum assumptions [126]. The finite first law does not supply them. Persistence can test stability across thresholds; it cannot convert this ansatz into Einstein dynamics.

26.3 Pooling is a channel: an exact trainable example

A channel has Kraus form $\mathcal{E}(\rho) = \sum_m K_m \rho K_m^*$, $\sum_m K_m^* K_m = I$. For unitary evolution followed by discarding one qudit,

$$\mathcal{P}_\theta(\rho) = \mathrm{Tr}_2(U_\theta \rho U_\theta^*), \qquad K_m = (I \otimes \langle m|) U_\theta.$$

The completeness identity follows by summing the environment projectors. An isometry $\mathbb{C}^{d^2} \to \mathbb{C}^d$ would be injective and is impossible for $d > 1$. Stinespring instead adds an environment [127]. Outcome-dependent unitaries replace K_m by $V_m K_m$. Ignoring the outcome remains linear; normalization of a selected branch by its success probability is nonlinear. Partial trace alone is not a nonlinear activation.

A solvable training objective. Encode inputs as $R_y(x)|0\rangle \otimes R_y(y)|0\rangle$, where $R_y(t) = e^{-itY/2}$, and choose

$$U_\theta = e^{-i\theta X \otimes X/2}, \qquad f_\theta(x,y) = \mathrm{Tr}((Z \otimes I) U_\theta \rho_{x,y} U_\theta^*).$$

This encoding varies with its input; $Z^j|0\rangle$ and $e^{ix\hat{n}}|0\rangle$ do not. Anticommutation gives

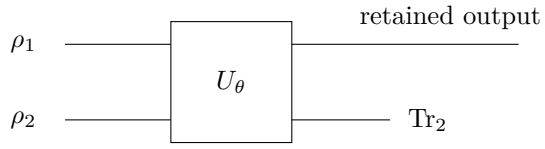
$$U_\theta^*(Z \otimes I)U_\theta = \cos\theta (Z \otimes I) + \sin\theta (Y \otimes X), \qquad f_\theta(x,y) = \cos\theta \cos x.$$

The second term averages to zero for these real product states. Before training, this proves a limitation: that readout cannot retain y. Richer objectives need a changed ansatz or another observable.

For targets $t_j = c\cos x_j$, $-1 < c < 1$, put $A = M^{-1}\sum_j \cos^2 x_j > 0$. The exact squared loss and gradient are

$$L(\theta) = A(\cos\theta - c)^2, \qquad L'(\theta) = -2A\sin\theta(\cos\theta - c).$$

The minima satisfy $\cos\theta = c$ and have zero loss. The stationary points $0, \pi$ must not be mistaken for a trained solution. A numerical optimizer can be tested against this answer; no run is asserted here. For comparison, CNOT followed by target-Z readout gives $f(x, y) = \cos x \cos y$, a true two-input feature.



26.4 Trained QGCN and QGAT on ribbon graphs

Give the graph its cyclic half-edge ordering and a proper edge-coloring. Shared two-site gates can run in parallel on each color class. A simple bounded-degree graph requires at most $\Delta + 1$ colors, not universally Δ. Matching-based pooling specifies disjoint retained/discarded subsystems and a ribbon contraction. Independently applying channels to overlapping marginals does not automatically produce a consistent global coarse state.

Quantum convolutional and graph-network proposals offer concrete ansatz families [128, 129, 130]. A trained RG task may target phase classification, selected correlators, a reconstructed state, or an effective Hamiltonian. Success on one does not prove success on the others. A possible loss combines observable errors and symmetry penalties:

$$\frac{1}{M}\sum_{j,a} w_a (f_{\theta,a}(\rho_j) - t_{j,a})^2 + \lambda \sum_e |\theta_e - \theta_{\mathrm{rot}(e)}|^2.$$

The penalty encourages cyclic weight sharing; exact equivariance requires intertwining by the architecture. Geodesic CNN coordinates and ribbon orderings are related design inputs, not identical constructions. Random quanvolutional circuits provide a useful untrained baseline. They must be compared with trained circuits and a classical model on the same data rather than credited with an automatic quantum advantage.

For a gate $e^{-i\theta P/2}$ with $P^2 = I$, parameter-shift differentiation gives

$$\partial_\theta f = \tfrac{1}{2}(f(\theta + \pi/2) - f(\theta - \pi/2)).$$

Indeed the surrounding expectation has only constant, cosine and sine terms in this parameter. Other generators require a different rule. Finite-shot gradients and exact-state-vector gradients have different noise and optimization costs. Clifford layers can create entangled graph and GHZ states; non-Clifford gates are needed for universality, not for entanglement itself.

QGAT scores can be obtained from edge-register query/key circuits followed by classical softmax. For $d > 2$, Z_d is not Hermitian, so choose real quadratures

$$C_m = (Z_d^m + Z_d^{-m})/2, \qquad S_m = (Z_d^m - Z_d^{-m})/(2i).$$

For example, $s_{vu} = -(\langle C_m\rangle_{q_v} - \langle C_m\rangle_{k_u})^2$ gives real weights $\alpha_{vu} = e^{\beta s_{vu}} / \sum_w e^{\beta s_{vw}}$. The normalization is classical. The mixture $\sum_u \alpha_{vu}\rho_u$ is a state; a coherent sum of arbitrary unknown value states needs a separate physical protocol.

Generic amplitude loading of a D-component classical vector can cost order D input operations; $\log D$ qubits do not remove that cost. Several commuting heads can reuse one measurement basis, but their expectations still require repeated preparation. Quantum circuits are linear in ρ; nonlinear input encoding and classical processing are where these feature maps can become nonlinear in classical data.

26.5 Associative memory with a correct measurement model

A normalized readout uses positive effects E_a summing to I, with $p_a = \mathrm{Tr}(E_a U \rho U^*)$. An incomplete readout has sum at most I and a failure effect. For orthogonal rank-one projectors and pure input,

$$E_a = |\xi_a\rangle\langle\xi_a|, \qquad p_a = |\langle U^*\xi_a, \psi\rangle|^2.$$

This is exact. A common unitary preserves the templates' inner products; it does not independently prescribe arbitrary nonorthogonal templates. Arbitrary projectors are not a POVM: two identical $|0\rangle\langle 0|$ projectors give probability sum two at $|0\rangle$. A general Hermitian observable also need not be positive and cannot be interpreted as one rank-one pattern effect through a generalized square root.

For a two-pattern test, measure the computational basis on $R_y(x)|0\rangle$. Then $p_0 = \cos^2(x/2)$ and $p_1 = \sin^2(x/2)$. A larger-probability rule retrieves zero for $|x| < \pi/2$ modulo 2π. Sampling makes queries near the boundary difficult. This is a concrete retrieval task, not an exponential-capacity theorem.

Classical modern Hopfield networks have capacity and retrieval guarantees under specified separation, normalization and temperature assumptions [131]. Substituting d^{n_q} for their associative dimension does not prove a QGAT memory theorem. A neighborhood with δ keys contains δ explicit candidates per head. Capacity requires a precision criterion, a dataset and a resource model. A D-dimensional system perfectly distinguishes at most D orthogonal states in one use; nonorthogonal packing, classical parameter storage and repeated queries are different resources.

Holographic reduced representations bind classical vectors by circular convolution. For the unnormalized discrete transform, $\widehat{a * b} = \widehat{a}\,\widehat{b}$. Correlation is an exact inverse only under additional nonvanishing/normalization conditions. A qudit's $\langle Z_d^m\rangle = \sum_j \rho_{jj}\omega^{mj}$ determines diagonal populations when all modes are known, but no off-diagonal phases. Additional bases distinguish $|+\rangle$ and $|-\rangle$, which have equal populations.

A channel hierarchy can be drawn as a tensor network with coarse bulk variables and fine boundary variables. Holographic-code models use a specified isometric encoding and reconstruction property [132]. Arbitrary discarding does not have it: a channel sending both $|0\rangle$ and $|1\rangle$ to one state destroys the label. A pooling tree alone proves neither boundary-area scaling of an actual state, error-correcting reconstruction nor AdS/CFT. These remain separate questions that a trained graph model can investigate.

26.6 Evidence categories for learned coarse-graining

An executable example must record graph, encoding, task, ansatz, loss, train/validation split, seed, optimizer and stopping rule. It should save parameters, predictions and loss history, compare classical and untrained baselines, and distinguish exact, finite-shot and hardware expectations. A noise study must name the channel and where it is applied. A successful finite toy task does not certify a thermodynamic RG limit, quantum speedup, Einstein dynamics or an arithmetic determinant.

The solvable pooling objective supplies a precise acceptance test for the separate executable examples. A training result is reported only when its checkpoint and verification outputs exist. The mathematical model and its analytic optimum remain meaningful independently of such a run.

Chapter 27

Noise, molecular spins and hyperbolic-code architectures

An architecture needs controls, interactions, preparation, measurement and a noise model. A coupling graph supplies none of these calibrations by itself. Exact small operations provide useful acceptance tests before considering larger processors or molecular assemblies.

27.1 Ancillas, noise and measurement resources

For a contraction A, the map

$$v \longmapsto Av \otimes |0\rangle + (I - A^*A)^{1/2} v \otimes |1\rangle$$

is an isometry: its squared norm is $\|v\|^2$. It extends to a unitary with an environment. Postselecting zero realizes A with probability $\mathrm{Tr}(A\rho A^*)$. Tracing out the ancilla includes both branches and does not produce just $A\rho A^*$ as a trace-preserving map. An operator of norm above one must first be scaled, with its success probability and amplitude normalization accounted for.

Amplitude damping has Kraus matrices

$$K_0 = \begin{pmatrix} 1 & 0 \\ 0 & \sqrt{1-\gamma} \end{pmatrix}, \qquad K_1 = \begin{pmatrix} 0 & \sqrt{\gamma} \\ 0 & 0 \end{pmatrix}, \quad 0 \le \gamma \le 1.$$

Direct multiplication gives $K_0^*K_0 + K_1^*K_1 = I$ and multiplies the excited population by $1-\gamma$. Pure dephasing instead can preserve populations while reducing coherences. Under a Markovian qubit model, $1/T_2 = 1/(2T_1) + 1/T_\phi$; these relaxation times alone do not determine pulse calibration, leakage or gate fidelity.

A Hadamard test estimates $\mathrm{Re}\,\mathrm{Tr}(\rho U)$; a changed ancilla basis estimates the imaginary part. Repeated preparations are required. Local randomized measurements and classical shadows can reuse settings for many observables, with locality-dependent costs [133]. Entropy is nonlinear, so a linear-observable sample bound does not automatically estimate mutual information. Reconstructing small marginals or using dedicated purity/entropy estimators is necessary.

At $N = 10^4$ sites and maximum degree Δ, at most $\Delta N/2$ edge marginals are needed. This defines a proposed workload, not an available processor specification. Routing, state preparation, correlated readout errors and reset must enter a resource estimate. Likewise 10^5 qudits of dimension eight require at least 3×10^5 binary qubits, before ancillas and coding. A generic encoded qudit entangler does not cost merely $\log_2 d$ two-qubit gates. Its actual compilation and unused basis states

must be checked. An infinite rotor needs a cutoff and a bound on leakage/aliasing; a cyclic quotient and a hard truncation have different boundary behavior.

27.2 The peptide-spin evidence and its limits

Lanthanide-binding peptides offer chemically programmable spin organization. Rosaleny and collaborators reported ensemble pulsed X-band EPR in frozen solutions at 4 K, with representative relaxation values [134]:

Complex	T_1	T_2
GdLBT	approximately $10\,\mu$s	approximately $2\,\mu$s
NdLBT	approximately $3\,\mu$s	approximately $1\,\mu$s

Driven nutations motivate a molecular-spin platform, but are not randomized-benchmark gate fidelities or individual single-shot register readout. Proposed multispin organization and transport interfaces must be distinguished from a demonstrated controlled multi-qubit processor. Binding-affinity improvements are not measurements of increased coherence.

PDB 1TJB is a 2.00 Å Tb-bound structure [135]. Its motif has seventeen amino acids, YIDTNNDGWYEGDELLA, with a terminal amide entry in the deposited entity. Eight nearby oxygen donors come from Asp3, Asn5, Asp7, the Trp9 backbone carbonyl, and bidentate Glu11 and Glu14. Deposited residue identifiers and sequence indices need reconciliation in atomic constraints. Replacing the metal or scaffold requires new coordination and magnetic validation; a Tb structural model is not already a calibrated Gd or Nd control model.

An effective spin Hamiltonian is

$$H_{\mathrm{spin}} = H_{\mathrm{CF}} + \mu_B \mathbf{B}\cdot\mathbf{g}\mathbf{J} + \mathbf{I}\cdot\mathbf{A}\mathbf{J} + H_{\mathrm{drive}}.$$

Selecting a qubit requires a named transition, selection rules and leakage bounds. In a positive-field spin-7/2 Zeeman model, the lowest states have $m = -7/2, -5/2$; the central $-1/2 \leftrightarrow 1/2$ transition is not the lowest doublet. Spectroscopic selection can still use it, but must not be justified by a false energy ordering.

For an ideal two-level splitting hf, the thermal polarization is

$$p_0 - p_1 = \tanh\!\left(\frac{hf}{2k_BT}\right).$$

At $f = 9.3$ GHz, $hf/k_B \simeq 0.446$ K; at 4 K the polarization is only about 0.056. Initialization near a pure state needs a separate protocol. A peptide's melting temperature and a spin's operational temperature therefore answer different questions.

27.3 Control calculations: rotations and exchange

Choose the laboratory drive convention

$$H(t) = \frac{\hbar\omega_0}{2}Z + \hbar\Omega\cos(\omega_0 t + \phi)X.$$

The resonant rotating-wave approximation gives $H_{\mathrm{rot}} = \hbar\Omega(\cos\phi X + \sin\phi Y)/2$ with the stated rotating-frame convention. For $\phi = 0$, a pulse of length π/Ω gives $R_x(\pi)$, equal to X up to phase.

A virtual Z changes the microwave reference phase; avoiding a separate physical pulse does not mean infinite fidelity of all subsequent gates. Spectral separation and drive strength control the approximation and leakage.

For dimensionless $\mathbf{S} = \boldsymbol{\sigma}/2$, isotropic exchange is $H_{12} = J\mathbf{S}_1 \cdot \mathbf{S}_2$, with J in energy units. If P swaps qubits, then $P = (I + XX + YY + ZZ)/2$, so

$$e^{-itH_{12}/\hbar} = e^{iJt/(4\hbar)} \left[\cos\left(\frac{Jt}{2\hbar}\right) I - i \sin\left(\frac{Jt}{2\hbar}\right) P\right]. \tag{27.1}$$

Thus $Jt/\hbar = \pi$ gives SWAP up to phase and $\pi/2$ gives $\sqrt{\text{SWAP}}$. The latter sends $|01\rangle$ to a Bell-type superposition proportional to $|01\rangle - i|10\rangle$. It is not iSWAP: an XY Hamiltonian omits the ZZ term and has different evolution. Whether a peptide pair realizes any of these models needs measurement; dipolar anisotropy and g-tensor orientation can be essential.

Echo decay, nutations, addressability, gate fidelity and single-shot measurement are distinct experimental tasks. EPR generally measures an ensemble signal. CISS and spin-dependent transport are possible future interfaces, requiring a calibrated relation to a qubit observable. A discussed SOMO–lanthanide exchange energy is not a measured Ln–Ln exchange across two nanometres. A fitted law $J_0 e^{-\kappa r}$ also needs consistent units: with $J_0 = 25$ cm^{-1}, $\kappa = 1$ Å^{-1} and $r = 20$ Å, it predicts about 5.2×10^{-8} cm^{-1}, not an order-one coupling. Geometry and chemistry must determine an actual model.

27.4 A proposed molecular-design program

RFdiffusion3 supports atomically conditioned protein design and structural benchmarks [136]. Proteína-style backbone generation and BoltzDesign-style inverse-predictor optimization are complementary candidate methods. None guarantees a target spin coherence time, interaction graph or gate. A reproducible calculation pins a release, checkpoint, input schema, atomic identifiers and constraints; generated structures become preserved inputs for later evaluation. Current RFD3 documentation uses structured input specifications and its model-specific design interface, not an assumed legacy RFdiffusion invocation.

A conservative motif workflow fixes a resolved coordination cage, specifies metal/donor atoms and the intended state, generates surrounding scaffolds, assigns sequences with fixed motif positions, and tests structure and metal-aware energetics before synthesis. Hydrogen-bond conditioning is not a lanthanide coordination validator. RMSD and prediction confidence are filters, not physical yields or gate measurements. A small-motif benchmark does not guarantee a pass rate for a seven-motif, 1000-residue assembly.

ThermoGFN-IF can be formulated as a proposed multi-fidelity optimization [137]. SPURS supplies mutation stability predictions, BioEmu-v1 protein backbone ensembles, and UMA learned atomistic energies and forces in evaluated domains [138, 139, 140]. Model domains matter: BioEmu-v1 does not explicitly represent metal ions and their donor-oxygen geometry, so it cannot directly certify an intact Ln cage. All-atom reconstruction and a separately validated metal-aware calculation would be extra stages. Atom-count throughput is not a certificate of spin-vibronic accuracy.

For declared dimensionless scores define $R(x) = \exp(\sum_j w_j s_j(x))$. If positive $\Delta\Delta G$ denotes destabilization, its stability reward contribution should have a negative sign. A GFlowNet aims to sample terminal candidates proportionally to this specified reward. Trajectory balance compares full forward/backward path probabilities to the terminal reward; subtrajectory balance additionally uses weighted subpath constraints. A unique construction path restricts the legal backward policy. These definitions can be implemented and tested without claiming a synthesized or operating processor.

Increasing melting temperature need not monotonically raise a Debye scale, suppress a particular spin-phonon channel or improve T_2. At a fixed transition frequency, Bose occupation depends on that frequency and the temperature, not directly on bulk rigidity. A dephasing power law needs its spectral density, coupling operator and mechanism, including direct or Raman processes when relevant. One nanosecond of dynamics does not alone estimate a converged folded/unfolded partition-function ratio. Proposed tables mapping ΔT_m to numerical coherence, gate fidelity and fault tolerance are therefore hypotheses, not measured outcomes.

27.5 Hyperbolic kagome geometry and the assembly problem

A regular $\{p, q\}$ tiling has p sides per face and q faces at a vertex. At curvature -1, a face has angle $2\pi/q$ and area $\pi(p - 2 - 2p/q)$. In a closed genus-g quotient, $pF = 2E$, $qV = 2E$ and $V - E + F = 2 - 2g$. For $\{7, 3\}$,

$$E = 42(g - 1), \quad V = 28(g - 1), \quad F = 12(g - 1), \quad A_f = \pi/3. \tag{27.2}$$

Then $FA_f = 4\pi(g - 1)$ as Gauss–Bonnet requires. The orientation-preserving $(2, 3, 7)$ triangle group has coarea $\pi/21$; a torsion-free subgroup has index $84(g - 1)$. Its reflection triangle has half this area. The Klein quartic, with usual model $x^3y + y^3z + z^3x = 0$, has genus three and $(V, E, F) = (56, 84, 24)$. It is not a construction of every proposed quotient.

For a simple cubic tiling graph, its line graph places a qubit at each edge and joins pairs that share a vertex. Each qubit has four neighbors; the line graph has E vertices and $2E$ edges. Quotient degeneracies such as loops or repeated incidences need separate counting. Equal hyperbolic edge lengths do not automatically become equal Euclidean separations or physical couplings in an assembly.

A finite graph can be embedded and routed in three-dimensional space, but this does not create a complete smooth isometric $\mathbb{H}^2$ in $\mathbb{R}^3$. A gyroid has varying intrinsic curvature. Schwarz–Pick concerns holomorphic metric contraction, not an SE(3) protein-placement algorithm. A finite assembly needs target Euclidean coordinates, distortion and steric bounds, mechanical constraints and explicit chemical ownership of shared sites. Kabsch alignment is a least-squares rigid fit; it does not remove inconsistent global distances. Two independently generated chunks cannot both contain one supposedly shared physical peptide without an actual chemical construction realizing that sharing.

27.6 CSS codes from boundary maps

Let a finite connected closed orientable cellulation have

$$C_2(\Sigma; \mathbb{F}_2) \xrightarrow{\partial_2} C_1(\Sigma; \mathbb{F}_2) \xrightarrow{\partial_1} C_0(\Sigma; \mathbb{F}_2), \qquad \partial_1\partial_2 = 0.$$

This is a chain complex, not a short exact sequence. Its first homology is precisely the code's logical information. Put qubits on edges and set $H_X = \partial_1$, $H_Z = \partial_2^T$. A binary row x defines an X product and a row z a Z product. Their commutation sign is $(-1)^{x\cdot z}$, so the boundary identity proves commutation. The code is the common $+1$ eigenspace in $(\mathbb{C}^2)^{\otimes E}$, not a binary kernel intersection regarded as that Hilbert space.

Proposition 27.1 (Surface-code dimension and distance)**.** *For this genus-g cellulation,*

$$k = E - \operatorname{rank} H_X - \operatorname{rank} H_Z = 2g.$$

Distance is the smaller weight of a nontrivial primal homology class and a nontrivial dual homology class.

Proof. Connectedness gives $\operatorname{rank}\partial_1 = V - 1$, and the one-dimensional top homology gives $\operatorname{rank}\partial_2 = F - 1$. Thus $k = E - V - F + 2 = 2g$. A commuting Z error is a cycle; multiplication by Z stabilizers changes it by a boundary. A nontrivial logical Z is therefore a nonzero homology class. The dual argument treats X errors. □

A noncontractible separating curve can be null homologous. Searching one geometric systole therefore does not certify a code's distance. In a $\{7, 3\}$ code, vertex X checks have weight three and face Z checks weight seven; a global swap of X, Z conventions also swaps the logical descriptions.

At genus thirteen, (27.2) gives 504 data qubits and 26 logical qubits. If $E = 1008$, the genus is 25 and $k = 50$. The asymptotic rate is $1/21$. A $\{5, 4\}$ cellulation gives $E = 20(g - 1)$ and rate $1/10$. Syndrome ancillas add physical resources. Suitable hyperbolic quotient families have logarithmic distance at constant rate [141, 142]; topology alone gives no such lower bound for every quotient, or distance eight for an unspecified finite surface. A finite certificate needs its incidence matrices and primal/dual logical-operator search. Logical qubit count grows linearly, not exponentially, with the number of physical qubits.

A finite acceptance test. An $L \times L$ periodic square cellulation, $L \geq 3$, has $V = F = L^2$, $E = 2L^2$. Thus $k = 2$ and $d = L$: a straight winding row or column gives an L-edge logical cycle in either lattice, and a lifted winding cycle must traverse at least L edges. This yields $[[2L^2, 2, L]]$ with weight-four checks. The ranks $L^2 - 1, L^2 - 1$ verify k directly. This is a useful exact decoder test before claiming a larger unprovided hyperbolic instance.

A storage code is not yet a fault-tolerant computer. Generic exchange and Zeeman terms do not commute with every stabilizer. An XX interaction meeting a Z check on exactly one site anticommutes with it, giving a commutator of order the coupling. Syndrome extraction needs ancillas, controlled operations, reset and measured error models; three exchange pulses alone do not prove nondemolition parity measurement. A threshold is conditional on code family, decoder and noise model. Code-capacity noise with ideal checks and circuit-level noisy checks are different. A gate estimate from another model cannot be compared to one threshold and declared fault tolerance.

27.7 The arithmetic comparison is still an additional task

A physical graph, a complex Belyi dessin and a rational arithmetic model are different data. A passport need not determine a Galois orbit, and one finite dessin cannot support a faithful action of the entire absolute Galois group on its finite sheet set. Frobenius requires descent and good reduction. Measured couplings do not automatically recover an Euler factor. The earlier finite-field theta benchmark is a concrete comparison test with its already specified scope, not a global GRH proof.

There is a useful circuit sanity check. XY exchange annihilates $|00\rangle$, so its exponential fixes it. A network of these gates, on an all-zero register preceded only by diagonal Z rotations, has a vacuum overlap that is just a phase. It cannot generate L-function zeros. Also e^{-izG} for Hermitian G is not generally unitary at complex z. Finite products $\prod_p (1 - \chi(p)p^{-s})$ are exponential polynomials in s, not degree-N polynomials; their unramified factor zeros have $\operatorname{Re} s = 0$, not the critical line.

A Hilbert–Pólya proposal still has to identify its determinant with the same completed arithmetic function, including gamma and conductor factors. The transformation $\rho \mapsto 1 - \overline{\rho}$ fixes a zero on the critical line; it does not reverse the ordinate. Conjugate twists matter for complex characters. Chiral

symmetry is extra structure. An unbounded $\pm$-paired self-adjoint spectrum has no Gibbs trace $e^{-\beta H}$; $e^{-\beta H^2}$ or $e^{-\beta|H|}$ is a different diagnostic. Similarly $\sqrt{\Delta - 1/4}$ needs a spectral restriction away from negative shifted modes and a treatment of continuous spectrum.

These chapters give finite calculations, trainable channels and concrete experiments. They preserve the physical research program while leaving its arithmetic determinant, purity, convergence and positive-realization obligations explicit. They establish no complete proof of GRH.

Chapter 28

Actual renormalization: effective actions and scale

Renormalization changes the description while preserving a specified set of physical predictions. To make that claim testable, we carry the effective action, its constant, observables and scale convention. Neural state compression and principal-axis alignment can be useful auxiliary techniques, but their training losses do not replace these objects.

28.1 Actual renormalization retains the effective action

A compression score does not specify an RG transformation. Following the real-space formulation of Wilson and Kogut [81], we specify the eliminated variables, effective action, normalization and scale map. Our exact finite decimation is distinct from an approximate tensor-network truncation such as Levin–Nave TRG [82].

Definition 28.1 (Finite classical RG step)**.** Let the fine configuration be $(s,t) \in S \times E$, with finite nonempty sets S, E, and dimensionless log Boltzmann weight $V(s,t) = -\beta H(s,t)$. Define

$$(\mathcal{R}V)(s) = \log \sum_{t \in E} e^{V(s,t)}, \qquad Z(V) = \sum_{s,t} e^{V(s,t)}.$$

The full action includes its additive constant. A truncation or a learned approximation is a further operation with its own error, not this identity.

Proposition 28.2 (Partition, observables and composition)**.** *One has $Z(\mathcal{R}V) = Z(V)$, and the normalized expectation of every observable depending only on s agrees in the two descriptions. Eliminating E_1 and then E_2 equals eliminating $E_1 \times E_2$ at once, with the same tensor labels and inverse temperature.*

Proof. Exponentiating the definition gives $e^{\mathcal{R}V(s)} = \sum_t e^{V(s,t)}$. Sum over s, optionally multiplying by an observable $O(s)$, and divide both sides by the same strictly positive Z. Reordering finite sums proves the composition statement. No projection onto pair interactions is used. □

For an even homogeneous periodic Ising chain, write the transfer matrix as $T_{ab} = \exp(C + Kab + h(a+b)/2)$, $a, b \in \{-1, 1\}$. Its partition function is $\operatorname{tr} T^N$. Summing alternate spins replaces T by T^2 and N by $N/2$; the physical spacing doubles. Writing $P = T^2$, its positive entries determine

$$K' = \tfrac{1}{4} \log \frac{P_{++}P_{--}}{P_{+-}^2}, \quad h' = \tfrac{1}{2} \log \frac{P_{++}}{P_{--}}, \quad C' = \tfrac{1}{4} \log(P_{++}P_{--}P_{+-}^2).$$

These three parameters reproduce every entry of P, so no normalization is lost. At $h = 0$, $\tanh K' = \tanh^2 K$ and the eigenvalue-ratio correlation length of the homogeneous extension in blocked units halves. Its product with the spacing stays fixed. The fixed points in $t = \tanh K$ are $t = 0, 1$; the latter is zero temperature, not a positive-temperature transition. Odd dessin examples below use the full-action definition, not this even-chain shortcut.

28.1.1 Genuine dessin incidence models

For odd m, the clean dessin $y^2 = x^m - 1$, $\beta = x^m$ has two black vertices, m white vertices and one face; its genus is $(m-1)/2$. Its incidence graph is $K_{2,m}$ with $2m$ clean edges. Its infinite locally gentle order quiver instead has m vertices and completed DVR-rank $2m^2$. We place physical spins $B_+, B_-, s_0, \ldots, s_{m-1}$ on the incidence vertices; this is a specified finite spin model, not a faithful representation of that infinite algebra or order. The abstract incidence graph alone does not recover the ribbon embedding or genus.

With $\eta_j = (-1)^j$ and fixed nonuniform fields h_j, choose

$$V = J_+ B_+ \sum_j s_j + J_- B_- \sum_j \eta_j s_j + b B_+ - \tfrac{3}{5} b B_- + \sum_j h_j s_j.$$

Summing the two black spins gives the *entire* effective action

$$V'(s) = \sum_j h_j s_j + \log\left[2\cosh\left(b + J_+ \sum_j s_j\right)\right] + \log\left[2\cosh\left(-\tfrac{3}{5} b + J_- \sum_j \eta_j s_j\right)\right].$$

Every one of the $2m$ physical edges is present, although its couplings belong to a tied three-parameter family. The Walsh expansion $V'(s) = \sum_{A \subseteq \{0,\ldots,m-1\}} c_A \prod_{j \in A} s_j$, with $c_A = 2^{-m} \sum_s V'(s) \prod_{j \in A} s_j$, is unique by Boolean orthogonality. It retains the constant $c_\varnothing$ and genuinely generated higher-body interactions. Our genus-two and genus-four examples use $m = 5, 9$ and continue by exact nested marginalization. Dropping all terms of degree greater than two is displayed as a measured approximation.

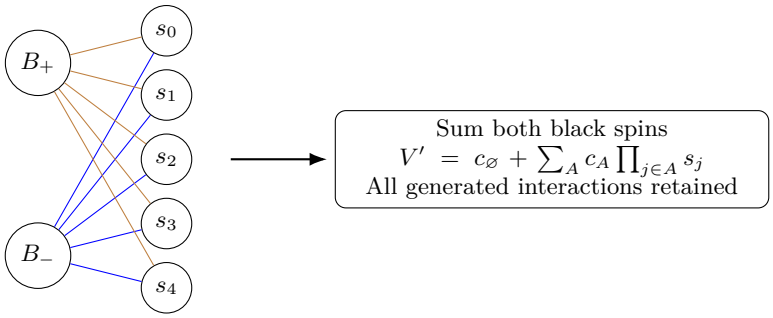
28.1.2 Quantum thermal effective Hamiltonians

For a finite Hermitian Hamiltonian H on nonzero finite-dimensional $\mathcal{H}_S \otimes \mathcal{H}_E$ and $\beta > 0$, define

$$W' = \operatorname{Tr}_E e^{-\beta H}, \qquad H_{\text{eff}}(\beta) = -\beta^{-1} \log W'.$$

The matrix W' is strictly positive: for $v \neq 0$, sum the strictly positive quadratic forms of $v \otimes e_j$ over an orthonormal basis of $\mathcal{H}_E$. Its Hermitian spectral logarithm is therefore defined. The identity $e^{-\beta H_{\text{eff}}} = W'$ proves partition and retained *equal-time* observable preservation by the partial-trace property. Repeated traces compose. The full Pauli expansion, including its identity coefficient, is retained. It is generally nonlocal and depends on β; this statement does not preserve all fine real-time dynamics or supply a local zero-temperature/thermodynamic RG fixed point.

`FiniteRG.lean` checks nine actual finite scalar marginal, exponential-action, partition, observable, composition, error-sandwich and transfer-trace statements. The quantum spectral-log and complete thermodynamic/field-theory interfaces are not formalized by these lemmas. These physics constructions give no arithmetic determinant comparison or new GRH conclusion.



This incidence schematic displays the physical elimination, not a planar uniformization of the genus-two surface. The explicit σ, α and face cycle determine the ribbon embedding; the interactive laboratory shows actual radial lifts and labels its four-real-coordinate projection.

28.2 Controlled errors and a trained full-action RG approximation

Proposition 28.3 (Classical action-error propagation)**.** *If* $|\widehat{V}(s,t) - V(s,t)| \le \varepsilon$ *at every finite configuration, then* $|\mathcal{R}\widehat{V}(s) - \mathcal{R}V(s)| \le \varepsilon$*. The partition ratio lies in* $[e^{-\varepsilon}, e^{\varepsilon}]$*. Every further* exact *marginalization preserves the same action bound.*

Proof. The pointwise inequalities $e^{-\varepsilon}e^{V} \le e^{\widehat{V}} \le e^{\varepsilon}e^{V}$ survive finite summation. Taking logarithms proves the first assertion; summing also over the retained variables proves the second. Iterate the same argument. For normalized measures the likelihood ratio lies between $e^{-2\varepsilon}$ and $e^{2\varepsilon}$, so a bounded observable error is at most $\|O\|_\infty \min(2, e^{2\varepsilon} - 1)$. Per-step learned errors would add; a single initial error does not grow under subsequent exact elimination. This scalar proof is not an assertion that the matrix exponential is operator-monotone. □

28.2.1 Executed finite calculations

The implementation checks full enumeration against the closed black-spin formula, Walsh reconstruction, raw partition equality, retained-spin magnetizations and two-stage versus direct elimination. At the quantum $\Gamma = 0$, $\beta = 1$ limit, every Pauli coefficient agrees with the classical effective action, with the required minus sign between energy and logweight. At nonzero transverse field the model is

$$H = -J_+ Z_+ \sum_j Z_j - J_- Z_- \sum_j \eta_j Z_j - bZ_+ + \tfrac{3}{5} bZ_- - \sum_j h_j Z_j - \Gamma \sum_i X_i.$$

At general β, the classical zero-transverse-field limit uses βV, including the fixed white fields, rather than scaling only the three varied controls. For $m = 5$, its full dimension is 128 and the first retained dimension is 32. Every one of the 1024 five-spin Pauli coefficients is computed; later retained dimensions are 8,4,2. Spectral-log/exponential and full Pauli reconstruction residuals, exact-trace composition and retained-observable comparisons are recorded separately. Floating-point residuals are numerical checks of the proved finite identities, not interval certificates.

The local laboratory exposes every scale, coupling/field controls for the classical model, selected generated interaction supports on actual dessin radial lifts, the even-chain K, h, C trajectory and physical correlation length, and three fixed quantum matrix calculations. Live quantum parameter sliders are not offered for uncomputed Hamiltonians. Pair truncation carries the identity term and reports both partition and probability/density errors. A late-scale floating-point loss of the small eigenvalue is avoided by transporting the exact log-eigenratio coordinate $\log r \mapsto 2 \log r$; this is explicitly the transfer RG identity, not a newly diagonalized value.

28.2.2 A quantum-feature model trained on actual RG

The learner targets all 32 unnormalized logweights of the $7 \to 5$ spin $m = 5$ decimation. Its three inputs are (J_+, J_-, b), with ranges $[0.15, 1.1]^2 \times [-0.6, 0.6]$. Fixed fields are $h_j = 0.045\cos(1.7j) + 0.02j/5$. Seed 20261103 fixes 160 input samples, a 120/40 train/test split, and 40 OOD samples with $J_\pm \in [1.15, 1.5]$, $b \in [-0.8, 0.8]$. The three feature qubits encode the couplings by $R_y(1.5J_+) \otimes R_y(1.5J_-) \otimes R_y(2b)|000\rangle$. Two local R_y, R_z layers, with a CZ triangle after each, contain 12 nominal optimizer angles. The final three R_z phases commute with the measured Z products and are structurally inactive for this loss; they still change the displayed state phases. We count them as nominal parameters, not additional effective expressive directions. Seven nonempty Pauli-Z products feed an affine 8×32 readout. There are 268 parameters. Feature registers are not the seven physical spin sites or five quiver vertices.

The training objective is full-action MSE, including the constant; KL alone would ignore that constant. A training-only ridge fit initializes the head, then 120 Adam updates optimize both circuit and head. Actual PennyLane analytic expectation calls implement the feature circuit. Parameter-shift derivatives of each feature are combined with the classical head gradient; full-loss finite differences agree to 6.46×10^{-11}. All data, parameters, intermediate checkpoints and complete loss curves are preserved.

The held-out full-action MSE is approximately 0.00985, mean $D_{\mathrm{KL}}(p_{\mathrm{exact}} \| p_{\mathrm{learned}}) = 0.00300$, mean TV 0.0290, and mean absolute log-partition error 0.0610. A classical quadratic-feature baseline with the same 256 readout parameters obtains 0.00613,0.00240,0.0233 and 0.0138, respectively. OOD action MSE increases to 0.267 for the quantum hybrid, versus 0.0555 for the baseline. The quantum-feature constant MAE is 0.0444 and higher-body coefficient RMSE is 0.00900, versus 0.0124 and 0.0130 for the classical baseline; different metrics favor different aspects. The aggregate results show no quantum advantage. They expose genuine full-action approximation errors rather than substituting state-compression success for RG.

Each saved example computes its maximum error over all 32 coarse states; the proposition then applies to its subsequent exact marginalizations. These per-example finite bounds are not uniform over the input parameter box. The synchronized architecture inspector shows literal gate outputs, Pauli features, head, logweights, generated interactions and partition value, linked to the exact genus-two dessin/order context. No full order representation, continuum universality, material-specific accuracy or arithmetic zero-location bridge is inferred.

28.2.3 Quantum TokenGT and the geometric error-correction boundary

A further executed node/edge-token hybrid uses the same exact RG teacher, with frozen three-qubit features, trained Q/K/V and a full-action head. Softmax, componentwise max-plus and hybrid variants are compared with a matched classical feature model; the latter has lower held-out action error. An explicit intervention-code/change variational MI objective learns concept directions; a 61-candidate latent forest and a held-out analogy transfer are scored on exact physical observables. Rips H_1 is actually reduced over $\mathbf{F}_2$, and a continuous Gaussian GFlowNet trains a trajectory-balance objective with specified root/Lebesgue measures. Empirical residuals do not prove exact terminal sampling, semantic reasoning or categorical equivalence.

The physical bit-flip repetition channel is separately executed and has $p_L = 3p^2 - 2p^3$ under ideal recovery. A genuine cellular CSS calculation on the genus-two one-face dessin gives $[[10, 4, 1]]$: vertex-incidence rank 6, zero face boundary, X-distance 1 and Z-distance 4. Thus this cellulation provides no useful protection merely from its genus. These finite layers, full formulas, proofs, parameters and scope are developed in the research book and interactive laboratories; the physical

models are not faithful representations of the infinite completed order and supply no GRH bridge.

28.2.4 An actual finite gentle cut for the categorical interface

On the genuine $m = 5$ dessin quiver write $a_i, b_i : i \to i - 1$ with indices modulo 5; cross-branch consecutive pairs are forbidden. Remove both arrows with source 0. The surviving algebra B has vertices 0 through 4, arrows a_i, b_i for $i = 1, \ldots, 4$, and relations $a_i b_{i-1} = b_i a_{i-1} = 0$ for $i = 2, \ldots, 4$. It is an explicit finite gentle quotient, not the completed order itself.

Every surviving positive path stays on one branch and has length at most 4. For length $\ell = 1, \ldots, 4$ there are $2(5 - \ell)$ paths, while length 0 contributes five idempotents. Therefore $\dim_k B = 5 + 2(4 + 3 + 2 + 1) = 25$. The forbidden-chain resolution already proved for monomial gentle algebras has two alternating chains of length n from vertex i to $i - n$ when $1 \le n \le i$, and none for $n > i$. Applying Hom to simples kills its arrow differentials. Hence $\mathrm{pd}_B S_i = i$ and $\mathrm{Ext}^4_B(S_4, S_0) \cong k^2$. The split finite-dimensional simple-module criterion gives $\mathrm{gldim}\, B = 4$.

Every full branch cycle crosses a removed arrow, so the common completed order parameter u maps to zero. Thus B is a finite u-torsion quotient, not a DVR-free surface order. The difference is visible in derived Hom: S_0 is projective over B, whereas in the original completed order the two forbidden arms of length 5 return to vertex 0 and give $\mathrm{Ext}^5_\Lambda(S_0, S_0) \cong k^2$. The exact restriction along $\Lambda \twoheadrightarrow B$ is consequently not derived fully faithful. This supplies a concrete cut on which to investigate graded gentle/Fukaya models, while proving why its equivalence cannot simply be transported to the original completed order. Boundary/stops/line-field data and an actual module-valued neural decoder would still have to be supplied. Exact path and endpoint enumeration accompanies the prose proof; this cut/category comparison is not claimed wholly Lean formalized.

Part V

Computational and learned constructions

Chapter 29

Higher-genus dessins and reproducible finite carriers

The companion separates three objects: an exact combinatorial dessin, a chosen visualization of its surface, and a finite operator model. Agreement of their dimensions is not an equivalence of categories. We give constructions for which these distinctions can be checked directly.

29.1 A hyperelliptic family beyond the torus

For odd $m \geq 3$, let C_m be the smooth compactification of

$$y^2 = x^m - 1, \qquad \beta = x^m : C_m \longrightarrow \mathbb{P}^1.$$

The affine curve is smooth: simultaneous vanishing of $2y$ and mx^{m-1} would force $x = y = 0$, which does not lie on the curve in characteristic zero. Its double cover of the x-line branches over the m roots of unity and infinity. Riemann–Hurwitz gives $g = (m-1)/2$.

Proposition 29.1 (Clean passports and infinite orders)**.** *The degree-$2m$ Belyi map β has passport*

$$(m, m), \quad (2, \ldots, 2)\ (m \text{ entries}), \quad (2m).$$

Its contracted dessin has two vertices, m edges and one face. With darts $0, \ldots, 2m-1$, one may take

$$\sigma = (0\ 1\ \cdots\ m-1)(m\ m+1\ \cdots\ 2m-1), \quad \alpha = \prod_{j=0}^{m-1} (j\ j+m).$$

The associated completed order has $k[[u]]$-rank $2m^2$, and the polynomial locally gentle algebra is infinite dimensional.

Proof. Over zero, x is a local coordinate at the two points $y = \pm i$, and x^m has index m. At a root ξ of unity, y is a local coordinate and $\beta - 1 = y^2$, giving index two. At the unique point at infinity, x has pole order two, so β has pole order $2m$. Away from these points, differentiating x^m introduces no further branching. This proves the passport and the Belyi property. The two cycles describe the two lifts of the radial segments in the x-plane. The involution exchanges their lifts at the clean branch points. For odd m, $\phi = \alpha\sigma^{-1}$ is a single $2m$-cycle: its square advances two steps in each m-cycle, and two is invertible modulo m. Hence $2 - 2g = 2 - m + 1$. Each permitted m-cycle repeats without meeting a forbidden pair. This proves infinite dimension; the earlier split-order theorem gives rank $m^2 + m^2$. □

For $m = 5$ this gives genus two and order rank fifty; for $m = 7$ genus three and rank ninety-eight. These are actual cellular dessins, not finite-dimensional stand-ins. The all-degree resolutions are obtained by iterating their forbidden successor permutation, as in the general resolution theorem. The number of vertices of the algebra is m, while its coefficient-order rank is $2m^2$; they should not be interchanged in a quantum register count.

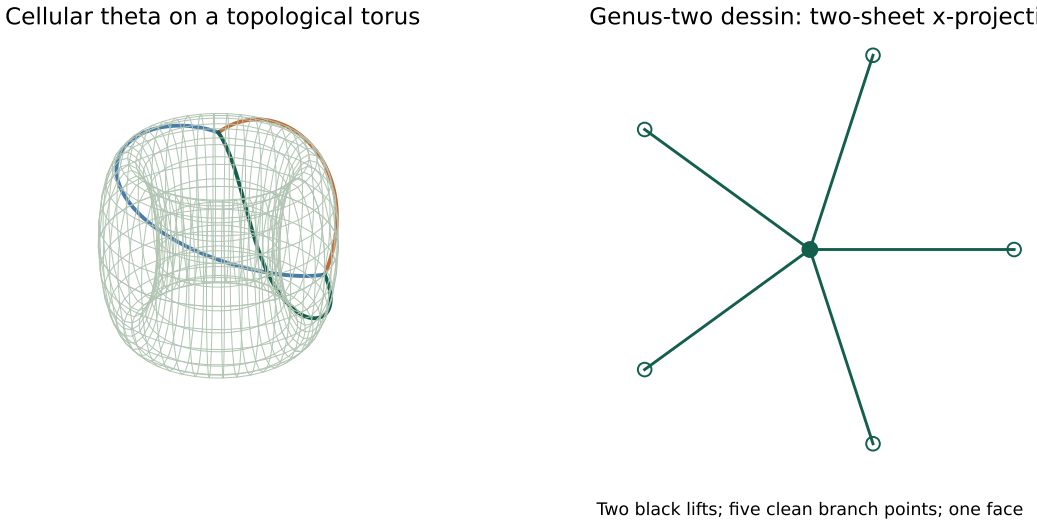


Figure 29.1: Two distinct kinds of faithful data display. Left: a topological torus embedding with the three periodic lifts of the theta graph. Right: the genus-two dessin's x-projection; every radial segment has two lifts. The right-hand disk is not the genus-two surface itself.

29.2 Larger genera and infinite hyperbolic windows

The same exact family gives genus five ($m = 11$, rank242), genus nine ($m = 19$, rank722) and genus sixteen ($m = 33$, rank2178). These ranks refer to the infinite completed orders over $k[[u]]$, not finite vector-space dimensions. The browser includes these examples and a four-dimensional rotation control: write $(x, y) \in \mathbb{C}^2$ in real coordinates (x_1, x_2, y_1, y_2), rotate the (x_1, y_1) plane, then project to three coordinates. The omitted coordinate and projected intersections are explicitly identified. This is a view of the affine double-cover sheets, not a claimed injective embedding of a compact higher-genus surface.

A separate example is the infinite regular hyperbolic $\{7, 3\}$ tiling. Its heptagons have angles $2\pi/3$, so the defect formula gives area $5\pi - 7(2\pi/3) = \pi/3$ at curvature -1. For a regular $\{p, q\}$ tiling, its central polygon's Poincaré circumradius is

$$r = \sqrt{\frac{\cos(\pi/p + \pi/q)}{\cos(\pi/p - \pi/q)}}.$$

To derive this, bisect the polygon into right triangles with acute angles π/p and π/q. The hyperbolic right-triangle identity is $\cosh R = \cot(\pi/p)\cot(\pi/q)$, while the disk radius is $r = \tanh(R/2)$. Substituting and applying elementary sum-to-product identities gives the formula. The condition $1/p + 1/q < 1/2$ ensures positive real radius.

A side is an arc of a circle with center c and squared radius $|c|^2 - 1$, orthogonal to the unit disk. Its endpoints a, b determine $\mathrm{Re}(a\bar{c}) = (|a|^2 + 1)/2$ and the analogous equation for b. Circle inversion gives its hyperbolic reflection

$$z \longmapsto c + \frac{|c|^2 - 1}{\bar{z} - \bar{c}}.$$

If a side is a diameter, the circle formula is replaced by reflection in the line through the origin; the implementation handles that case separately. Reflecting adjacent polygons constructs finite windows of the infinite tiling. The implementation caps both depth and tile count and reports those bounds. It never calls a truncated window the whole infinite lattice. An optional Lorentz-hyperboloid view maps z to $(2\,\mathrm{Re}\, z, 2\,\mathrm{Im}\, z, 1 + |z|^2)/(1 - |z|^2)$, satisfying $T^2 - X^2 - Y^2 = 1$. Its metric is Lorentzian ambient data, not the Euclidean metric of the rendered mesh. A finite compact surface quotient, its side pairings and an arithmetic correspondence would require separate certificates. The current lattice patch supplies none of them.

29.3 What a three-dimensional view can claim

The genus-one examples use a standard torus parameterization

$$((R + r\cos v)\cos u, (R + r\cos v)\sin u, r\sin v), \quad R > r > 0.$$

The theta paths lift from $(0,0)$ to $(1/3, 1/3)$ with translation vectors $(0,0), (-1,0), (0,-1)$ in the universal covering plane. Their interiors are disjoint on the quotient, and their complement is a disk; the induced rotations at the two black vertices give the one-face theta dessin. The elliptic square uses the two fundamental loops. These are topological realizations; the induced Euclidean torus metric is not asserted to be the constant-curvature or uniformizing metric of the algebraic curve.

For $m \geq 5$, the companion instead plots a three-real-coordinate projection of the two sheets of $y^2 = x^m - 1$. Branch cuts, changes of sheet and the compact point at infinity remain part of the mathematical construction. Projected sheets can meet. No injective embedding or numerical uniformization follows from a screen image. The Sage source gives exact passports, quivers, forbidden pairs and determinant calculations. The installed `sage` launcher on this machine points to a missing application, so those Sage scripts are supplied but have not been executed in Sage in this milestone. Exact stdlib Python checks independently verify the displayed permutations, genus and ramification counts.

29.4 Finite clocks and cross-backend agreement

For $d \geq 2$, let $Ue_j = \zeta^j e_j$, $Ve_j = e_{j+1}$, with $\zeta = e^{2\pi i/d}$. Then

$$UV = \zeta VU, \quad U^d = V^d = I.$$

Applying the two sides to e_j proves the first identity, including the wraparound because $\zeta^d = 1$. The discrete Fourier matrix prepares the uniform superposition. The executable comparison applies F, then U, then V, on a four-level carrier; its relative phases are nonconstant. Cirq, Qiskit and PennyLane statevectors are compared to the reference vector. Strawberry Fields realizes the same $U(4)$ matrices on the single-photon subspace of four optical modes and compares the entire density block, including its off-diagonal phases. Preparing a Fock state need not leave the simulator's internal representation marked pure, so reading only a ket would be incorrect.

The photonic cutoff two is exact for this passive, single-photon computation: photon number is preserved and no mode ever contains more than one photon. This justification does not extend to arbitrary squeezing or multiphoton simulations. Separate NVIDIA cuQuantum and CUDA-Q adapters and pinned upstream forks are provided. GPU execution is not performed on this Mac; source availability is distinct from a successful accelerator run.

Chapter 30

Quantum feature models and auxiliary compression

These preserved experiments have distinct objectives. Local Ising regressors approximate selected coarse couplings but omit normalization and a full iterated action. QCNN compression, photonic principal-axis alignment and the Harper surrogate are auxiliary benchmarks. Actual partition-preserving RG and a trained full-action approximation are developed in Chapter 28. Here the exact targets, held-out samples, recorded seeds, classical optimizer and feature readouts are retained without calling these different objectives a complete RG flow.

30.1 Exact teacher data from Ising decimation

For spins $s_1, s_2, s_3 \in \{-1, 1\}$, summing the middle spin gives

$$\sum_{s_2} e^{K_1 s_1 s_2 + K_2 s_2 s_3} = 2\cosh(K_1 s_1 + K_2 s_3) = A e^{K' s_1 s_3},$$

where

$$K' = \tfrac{1}{2}\log\frac{\cosh(K_1+K_2)}{\cosh(K_1-K_2)} = \operatorname{arctanh}(\tanh K_1 \tanh K_2), \quad A = 2\sqrt{\cosh(K_1+K_2)\cosh(K_1-K_2)}.$$

Checking $s_1 s_3 = \pm 1$ proves the identities. Thus the normalization and coupling have separate roles. The network below learns K', not the full partition-function normalization A.

For a three-valent star, let $s = (s_1, s_2, s_3)$ be boundary spins and sum its center. The exact boundary logarithmic weight is

$$f_K(s) = \log(2\cosh(K_1 s_1 + K_2 s_2 + K_3 s_3)).$$

Fourier expansion on the Boolean cube is orthogonal for $2^{-3}\sum_s$. The symmetry $f_K(-s) = f_K(s)$ removes every odd monomial. Consequently

$$f_K(s) = c(K) + \sum_{i<j} J_{ij}(K) s_i s_j, \quad J_{ij} = 2^{-3}\sum_s f_K(s) s_i s_j.$$

This proves the zero-field star-to-triangle reduction and supplies exact labels. Such trivalent patches occur at the black vertices of the theta dessin. The associated Ising Hamiltonian is a finite model on that graph, not a faithful representation of its completed surface order.

30.2 Shared quantum graph convolution

The input patch (K_1, K_2) is encoded by $R_y(K_1) \otimes R_y(K_2)|00\rangle$. Two layers of local R_y, R_z rotations, a CZ entangler after each layer, and a final CNOT define an eight-parameter circuit Q_θ. The three features are

$$z_\theta(K) = \big(\langle Z_0\rangle, \langle Z_1\rangle, \langle Z_0 Z_1\rangle\big).$$

A shared affine head predicts $\widehat{K'} = w \cdot z_\theta + b$. Twelve trainable parameters include the four readout coefficients. Independent samples are drawn uniformly from $[0.05, 1.7]^2$: ninety are used for training and thirty are held out. The loss is the mean-square error against exact decimation. The independent constant predictor is fitted only on training targets.

For a gate $e^{-itP/2}$, $P^2 = I$, and a fixed state and observable, the expectation has the form $a + b\cos t + c\sin t$. Hence

$$\partial_t z = \tfrac{1}{2}\big(z(t + \pi/2) - z(t - \pi/2)\big).$$

Each gate parameter occurs once. The code differentiates the expectation features with this formula and then applies the classical chain rule to the squared loss and affine head. Applying parameter shift to the squared loss itself would generally give a wrong gradient. A central finite-difference check of the implemented full loss gradient is recorded.

30.3 QCNN compression with a genuine pooling channel

The four-site periodic transverse-field Ising Hamiltonian is

$$H(h) = -\sum_{(i,j)\in C_4} Z_i Z_j - h\sum_{i=0}^{3} X_i.$$

We diagonalize its 16×16 Hermitian matrix at thirty-six fields in $[0.15, 2.4]$, using the normalized lowest eigenvectors as input states. Every fourth field, starting at index zero, is held out. The circuit has two shared-layout local rotation layers with CZ edges on C_4, followed by CNOTs $(0, 2)$ and $(1, 3)$. Its sixteen parameters are optimized to minimize

$$\mathcal{L}(\theta) = 1 - \frac{1}{N_{\text{train}}}\sum_j \langle\psi_j|Q_\theta^*(I_{01} \otimes |00\rangle\langle 00|_{23})Q_\theta|\psi_j\rangle.$$

The output on retained qubits is

$$\mathcal{E}_\theta(\rho) = \mathrm{Tr}_{23}(Q_\theta \rho Q_\theta^*).$$

Its Kraus maps are $K_b = (I \otimes \langle b|)Q_\theta$, so $\sum_b K_b^* K_b = I$. Thus it is completely positive and trace preserving. For $\rho \geq 0$ and any v, each summand $v^* K_b \rho K_b^* v$ is nonnegative; cyclicity of the finite trace proves trace preservation. The Lean interface verifies the finite-matrix positivity and trace statements with explicit completeness hypotheses. It does not formalize the optimizer or claim convergence of an infinite renormalization flow.

The compression loss is the weight discarded by the chosen vacuum projection. Its successful decrease measures improved concentration for this finite input family. It does not imply exact recovery of arbitrary four-qubit states, an isometry from dimension sixteen to four, or a critical fixed-point construction. The held-out loss remains appreciable, and is reported without calling the model lossless.

30.4 A larger genus-four nine-qubit example

The $m = 9$ hyperelliptic dessin has genus four and completed-order rank162. Its nine edge labels index a permitted quiver cycle. A separate finite transverse-field Ising model is placed on this nine-cycle, with Hilbert-space dimension512. This uses the dessin's combinatorics, without claiming a faithful representation of its infinite order.

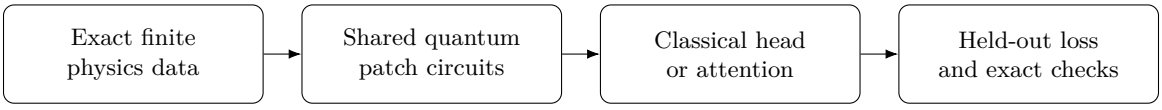
The larger experiment uses twelve ground states over fields $h \in [0.2, 1.9]$, with nine training and three held-out states. These are numerical lowest-eigenstate approximations. The residual alone is not a rigorous lowest-energy certificate. A sparse Hermitian eigensolver has maximum recorded eigenpair residual 1.32×10^{-13}. The circuit has two layers of local R_y, R_z gates and nearest-neighbor CZ around the cycle, with thirty-six parameters. Four CNOTs connect retained to discarded qubits, and tracing out four leaves a five-qubit output. Actual PennyLane gate simulation and parameter-shift gradients train for fifty updates. Final training and held-out discard losses are approximately 0.548 and 0.409. These substantial residuals are reported: this architecture is not an accurate lossless coarse graining. It is a reproducible larger testbed, with saved parameters, held-out examples and numerical ground-state residuals. The local page permits comparison with the smaller four-qubit model, while retaining their different data families and capacities.

30.5 Quantum-feature graph attention

Three two-qubit patch encoders use the same eight circuit parameters on the three pairs of the Ising star. Let their features be $z_e \in \mathbb{R}^3$. A learned query q defines

$$\alpha_e = \frac{e^{q \cdot z_e}}{\sum_f e^{q \cdot z_f}}, \quad c = \sum_e \alpha_e z_e, \qquad \widehat{J}_e = w_{\text{local}} \cdot z_e + w_{\text{context}} \cdot c + b.$$

There are eighteen trainable parameters. One hundred star couplings are sampled from $[0.1, 1.5]^3$, with seventy-five training and twenty-five held-out examples. The objective compares the three predictions with the exact Boolean-Fourier couplings above. The nonlinear attention head is differentiated by central differences of the complete training objective. This experiment is quantum-feature attention with a classical softmax head; it is not a fully coherent attention algorithm. The scalar labels do not assert permutation equivariance under conventions the implementation has not checked.



30.6 Photonic Gaussian pooling

The Strawberry Fields experiment prepares two modes with opposite real squeezing r and $-r$, then applies a fixed unknown-to-the-optimizer beam splitter angle $\alpha = 0.47$. A learned shared beam splitter θ is optimized on twelve of sixteen squeezing values in $[0.1, 0.9]$, holding out every fourth value. With $\hbar = 2$, the covariance convention is (x_0, x_1, p_0, p_1). The objective is

$$\operatorname{Var}(x_0) + \operatorname{Var}(p_1) = 2\left[e^{-2r}\cos^2(\alpha + \theta) + e^{2r}\sin^2(\alpha + \theta)\right].$$

This follows by applying the real beam-splitter rotation to the diagonal covariance of the two squeezed modes. Since $r > 0$, its minimum occurs at $\theta = -\alpha$ modulo π, with value $2e^{-2r}$. The code

trains the angle with central-difference gradients and compares its result with this known optimum. Pooling subsequently discards a mode; the experiment itself optimizes principal axes before that discard. It is a Gaussian finite-mode surrogate, not a demonstration of an interacting field-theory RG flow.

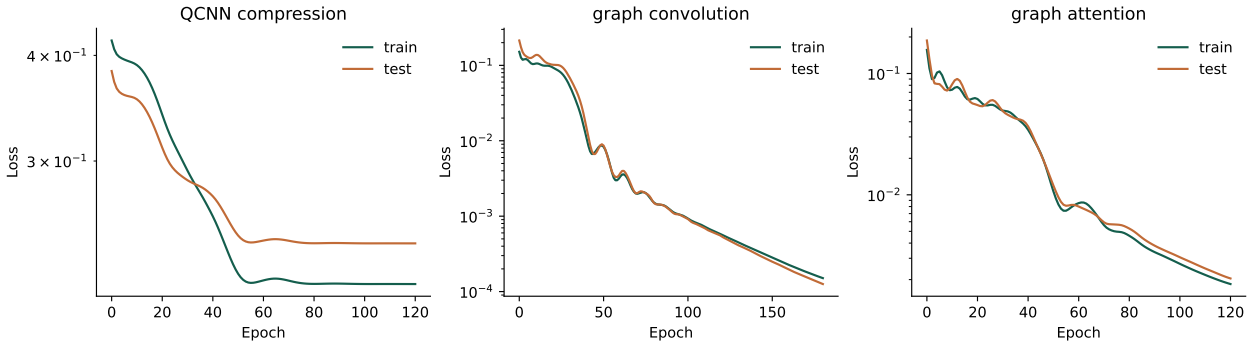


Figure 30.1: Actual PennyLane CPU training runs, seed 20261103. Green is training loss; orange is held-out loss. Architectures have different objectives, so their vertical scales are not cross-model performance rankings.

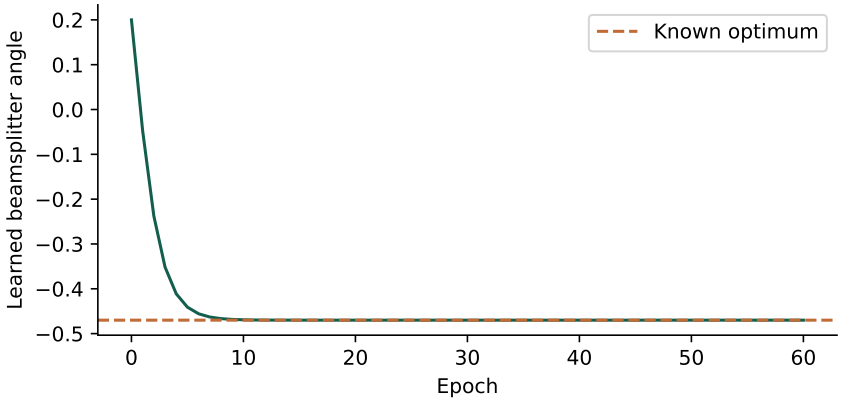


Figure 30.2: Actual Strawberry Fields Gaussian simulation: the learned principal-axis angle approaches its independently known optimum.

Model	Initial held-out loss	Final held-out loss
Four-qubit QCNN compression	0.38332	0.239725
Shared quantum graph convolution	0.213652	0.000125897
Quantum-feature graph attention	0.187065	0.00204477

30.7 Reproduction and limits of the evidence

The scripts in `examples/quantum` specify each circuit, data generator, random seed and optimizer. The approved isolated environment is recorded in `requirements-cpu.lock`; existing environments and all pinned Lean toolchains remain unchanged. NumPy reference and actual PennyLane runs are saved separately. Cross-framework tests exercise a nontrivial Fourier/clock/shift state, not just

a vacuum on which every diagonal clock is invisible. The Strawberry Fields run uses its Gaussian backend for training and its Fock backend for the separate one-photon comparison.

The companion's checkpoint slider selects a saved loss checkpoint. Its held-out examples use final weights; no intermediate predictions are implied. There are no hardware shots, cloud jobs or accelerator benchmarks. The training/test splits are deterministic interpolation tests on small synthetic families, not out-of-distribution or broad physical-validity tests. A model can help rank a proposed construction; it cannot discharge arithmetic holomorphy, determinant convergence, positivity or zero-location obligations merely by achieving low loss.

Chapter 31

Reading an architecture from its tensors

The trained models of Chapter 29 and the ToricGT references have a common computational interface: a finite directed acyclic graph whose vertices contain actual tensors and whose edges record the inputs to each operation. The local inspector at `http://127.0.0.1:8765/architecture.html` makes this graph navigable. Its scene is a computation graph, not a hardware layout or a physical embedding of the infinite surface order. The source code and numerical records are part of the project.

31.1 Three distinct kinds of evidence

The twenty-two saved cases cover six trained CPU model families and six fixed-weight reference variants. The QCNN4 and QCNN9 weights, shared two-qubit convolution, quantum-feature attention, Gaussian photonic pooling and finite Harper hybrid are replayed without further optimizer steps. The classical TokenGT-style, tropical, block-ring, attention-hybrid and two expert-routing variants use explicit seeded weights. They are executable miniatures, not upstream trained language-model checkpoints. The adjustable forward clock is a separately computed finite carrier. GPU and hardware execution remain unavailable, and optional upstream heads remain proposals unless their own numerical evidence is supplied.

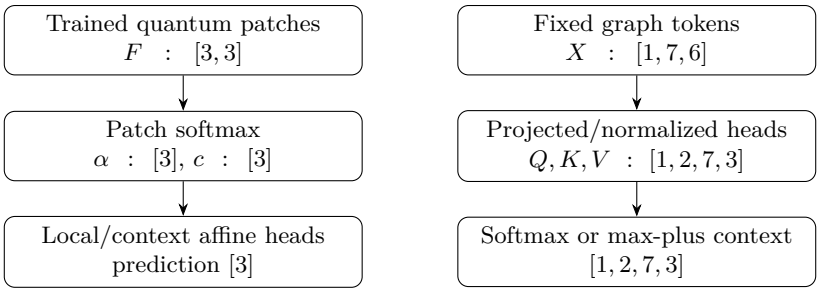
The record contains the source/checkpoint hashes, seed, conventions, formulas, shapes, axes, parameter values and checked errors. Each saved record is immutable and content addressed; its SHA-256 is verified before the interface accepts it. The inspector never changes the trained weights. Selecting a forward-operation step is not selecting a training epoch.

31.2 Shapes explain the operation

Two different attention mechanisms illustrate why the axes matter. The trained quantum-feature model produces three feature vectors,

$$F \in \mathbb{R}^{3\times 3}, \quad \ell = Fq \in \mathbb{R}^3, \quad \alpha = \operatorname{softmax}(\ell), \quad c = \alpha^{\mathsf{T}} F \in \mathbb{R}^3.$$

Softmax here runs over three patches. The classical reference has seven token positions, including one padded node, model width six and two heads. After projection and splitting, its Q, K, V have shape $[1, 2, 7, 3]$. These heads are different from the three observables of the quantum circuit. Its Q, K also undergo the source's maximum shift and Euclidean normalization before dot scores.



The shape labels are literal exported dimensions. The two columns are different finite models; no equivalence of their learned functions is asserted.

For tropical aggregation, a scalar output is

$$C_{bhic} = \max_{j \text{ legal}} (S_{bhij} + V_{bhjc}), \qquad S = QK^{\mathsf{T}}/\sqrt{d_{\text{head}}}.$$

The inspector shows every maximizing key and the gap between the largest two legal values. A tie means equality of computed floating-point values, not a symbolic equality certificate. A query with no legal key has zero context by an explicit guard. Invalid block entries are stored as zero *with a validity mask*; including these zeros in a maximum would be incorrect. Softmax weights displayed in tropical records are comparison diagnostics rather than the tropical aggregation rule.

Soft-MoE dispatch normalizes across valid tokens for each expert-slot; combination normalizes across expert-slots for each valid token. These are different axes. Strict-prefix slots exclude the current and later token indices, while equal-rank attention can permit different tokens with the same reveal rank. The two rules must not be conflated into a stronger causality assertion. Likewise padding can acquire projection bias in a residual, so its mask must remain in later routing and pooling.

31.3 Quantum and Gaussian inspection

The stored StatePrep input precedes the displayed circuit. The variational gates have their exact wire order and angle metadata. Qubit zero is most significant. For QCNN9, the final CNOT targets start at wire five; the retained density matrix has shape $[32, 32]$, not a five-qubit pure state obtained by discarding amplitudes. The partial trace follows the unitary gates and is distinct from their dimension-preserving action.

The photonic model uses covariance order (x_0, x_1, p_0, p_1) and $\hbar = 2$. Its ellipse is a one-standard-deviation contour of a selected two-coordinate Gaussian marginal, with the marginal covariance taken from the actual intermediate record. It is not a plot of a trained interacting field theory. The Harper page separately displays the learned proposal and the fifteen exact rational principal-minor certificates. Rejected proposals are labelled as repaired. The carrier uses backward V, so $VU = iUV$; the live forward-clock example instead has $UV = \omega VU$.

31.4 Spatial calculations and guided navigation

The interaction reference is Brendan Bycroft's *LLM Visualization*, reviewed at the pinned source revision recorded in `planning/reference-inspector/source-manifest.json`. Its model overview and self-attention walkthrough place the narrative beside dimensioned tensor planes, parallel query/key/value projections, attention heads and residual paths. The source's picking code maps a

selected output cell to input rows or columns and dot-product terms; its camera code interpolates toward walkthrough targets. These specific mechanisms motivate the local redesign. Reference hover inspection was limited by a renderer crash; source inspection is distinguished from successful live observation.

The local implementation uses original browser code and the project's own immutable records. Its spatial scene follows dependency ranks and semantic lanes, rather than putting every operation in an identical card. A tensor's dimensions determine its grid; head planes, selected literal coordinates and level-of-detail windows remain labelled. Overview retains the whole recorded computation, while a focused step moves toward its neighbourhood. The narrative gives the actual operation and evidence type. Supported cell expansions show numerical input terms and their computed result; other operations retain graph dependencies without inventing a scalar derivation. Surface and circuit views explain a separate geometric or physical interpretation of the finite carrier.

The rendering is a lightweight axonometric projection rather than a copy of the reference's WebGL engine. Neither perspective effects nor a quantum-state array make an attention model a coherent quantum transformer. Checkpoint replay, fixed-weight reference calculations and separately proposed extensions keep their different status throughout the interface.

31.5 A reproducible way to explore

Choose an evidence category and example, then a step. Clicking an input follows its recorded dependency. Head/token/coordinate controls select literal array slices; paging exposes large states without pretending that a small viewport is the entire tensor. Color is a display convention and the selected coordinate gives its numerical real and imaginary parts. A zero amplitude has undefined phase and is labelled accordingly. Playback visits the forward pass, and stops when cases change or the tab becomes hidden. Orbit and zoom change the view, not the state or physical model.

The shared numerical records have independent quantum-backend and scalar reference checks. Browser checks exercise all saved cases, coordinate selection, masks, playback, view controls, circuits, covariance and certificate panels. These computational checks do not imply complete Lean formalization, generalization beyond the samples, quantum advantage or the arithmetic positive-determinant comparison. The general path/category and arithmetic interfaces remain the research obligations described in the final chapters.

31.6 ConvexTok: certified path vocabularies

The words "token" and "graph" have two different roles here. A TokenGT position represents a node or edge with features and incidence metadata. A tokenisation position instead represents a boundary in a word; an edge jumps across a contiguous substring. ConvexTok, introduced by Tempus, Whittington, Schmidt, Komm and Pimentel, *Tokenisation via Convex Relaxations*, arXiv:2605.22821v1, optimises the second representation. We derive its small finite formulation, reproduce its six-word example, and give new certified examples for finite arrow-word corpora of our infinite surface algebras. This supplies an auditable compression layer; it does not identify the two kinds of token or change a trained graph model.

31.6.1 A vocabulary controls many occurrences

Let $\mathcal{D} = (w_1, \ldots, w_N)$ be a finite multiset of nonempty words over a mandatory alphabet Σ. For each word introduce boundary vertices $0, \ldots, |w_n|$. Include an edge (i, j) for each allowed contiguous

token $w_n[i:j]$. All single-symbol edges are free in the vocabulary budget, but cost one each in the segmentation objective. Longer candidates form a finite set C. Equal strings have the same colour even when they occur in different words or positions. Candidates never cross word boundaries.

Write x_e for occurrence flow and c_t for selection of token type t. Use incidence entries -1 at an edge's source and $+1$ at its target. For each word let d be -1 at its initial boundary and $+1$ at its final boundary. Separate unit-flow equations are equivalent to joining adjacent word terminals as in the paper: each word boundary must carry one unit, and there are no edges across words. The finite programme is

$$\begin{aligned} L_K = \min \quad & \sum_e x_e \\ \text{subject to} \quad & Bx = d, \qquad 0 \le x_e, c_t \le 1, \\ & x_e \le c_t \quad (e \text{ an occurrence of } t \in C), \qquad \sum_{t \in C} c_t \le K. \end{aligned} \tag{31.1}$$

Requiring $x_e, c_t \in \{0,1\}$ gives the integer problem. On the acyclic position graph its flow is one path per word, hence one segmentation. Conversely any segmentation with at most K extra token types gives such an integer point. Consequently the LP optimum is a lower bound for the integer optimum I_K. The constraint is per occurrence: selecting `ab` once permits both occurrences in `abab`, whose cost is two. Replacing these constraints by $\sum_{e:\, t(e)=t} x_e \le c_t$ would incorrectly prohibit that reuse.

For a fixed discrete vocabulary $V \supseteq \Sigma$, the exact segmenter is the backward recurrence

$$D(n) = 0, \qquad D(i) = 1 + \min_{t \in V:\, w[i:i+|t|]=t} D(i+|t|).$$

It returns a shortest path and a decoding by concatenation. Longest-first greedy need not do so: for $w =$ `abcd` and extra vocabulary $\{$`ab`, `bcd`$\}$ it returns `ab`|`c`|`d`, whereas the optimum is `a`|`bcd`. This segmentation issue is separate from BPE's greedy construction of the vocabulary itself.

31.6.2 An exact lower bound needs a feasible certificate

A floating solver's proposed objective alone is insufficient for an exact lower-bound claim. Our original CPU checker writes the LP in the form

$$\min q^{\mathsf{T}} v, \qquad Av = b, \quad Gv \le h, \quad v \ge 0,$$

where $v = (x, c)$ and G includes every upper-bound row $v_i \le 1$. It uses SciPy/HiGHS from the already approved environment to propose primal and dual solutions, reconstructs rational entries, and then checks *every* condition with exact rational arithmetic:

$$Av = b, \quad Gv \le h, \quad v \ge 0, \qquad z \le 0, \quad A^{\mathsf{T}} y + G^{\mathsf{T}} z \le q, \qquad q^{\mathsf{T}} v = b^{\mathsf{T}} y + h^{\mathsf{T}} z.$$

These are executable rational witnesses, not a claim that floating-point optimisation itself is a proof assistant.

Proposition 31.1 (Finite rational certificate)**.** *Every feasible primal v' obeys $q^{\mathsf{T}} v' \ge b^{\mathsf{T}} y + h^{\mathsf{T}} z$ for any dual pair satisfying the displayed inequalities. Equality with one feasible v certifies the exact LP optimum.*

Proof. Since $v' \geq 0$, the componentwise dual inequality gives

$$q^{\mathsf{T}} v' \geq y^{\mathsf{T}} A v' + z^{\mathsf{T}} G v' \geq y^{\mathsf{T}} b + z^{\mathsf{T}} h.$$

The second inequality uses $z \leq 0$ and $Gv' \leq h$. Equality therefore matches a lower and an upper bound. □

Independently, our checker exhausts every size-K subset of C and runs the shortest-path segmenter on each. This covers the at-most-K problem, because adding candidate tokens cannot increase a shortest-path cost. For $K > |C|$, all candidates suffice. Every stored witness is checked; deliberately perturbed primal and dual witnesses are rejected.

31.6.3 Three rounding rules and worked numerical gaps

The paper's Det rule chooses the K largest c_t; Bias chooses the K largest $c_t/|t|$; Int retains only values essentially equal to one. Our certificates are rational, so Int uses exact equality to one and Det/Bias use lexicographic tie-breaking. After choosing tokens we recompute a discrete shortest path; a fractional flow is not itself a tokenisation. An integral colour in one LP solution need not be present in every optimum. For example, with word `abc` and candidates `ab`, `bc`, either single-token choice is optimal.

The paper's example is

$$\mathcal{D}_0 = (\texttt{abc}, \texttt{abd}, \texttt{abe}, \texttt{bc}, \texttt{bd}, \texttt{be}), \qquad K = 3.$$

The mandatory-symbol count is fifteen. BPE first creates `ab`, saving three positions, then two merges save only one each: its cost is ten. Choosing `bc`, `bd`, `be` instead gives nine. Our exact primal/dual pair has value nine, and all $\binom{7}{3} = 35$ candidate vocabularies confirm $L_3 = I_3 = 9$. All three rounding rules give nine on the saved LP solution.

Our first new example is

$$\mathcal{D}_1 = (\texttt{cbcbc}, \texttt{cbca}, \texttt{cbabac}, \texttt{caaab}), \qquad K = 2.$$

One optimal fractional vocabulary has

$$c_{\texttt{cbc}} = \tfrac{1}{2}, \qquad c_{\texttt{caaab}} = \tfrac{1}{2}, \qquad c_{\texttt{cbabac}} = 1,$$

with all other values zero. Its per-word costs are $3, 3, 1, 3$, totalling ten; the rational dual certifies optimality. The integer optimum is eleven, witnessed by vocabulary $\{\texttt{caaab}, \texttt{cbabac}\}$ with costs $5, 4, 1, 1$ and confirmed by all $\binom{30}{2} = 435$ vocabularies. Det and Bias also yield eleven, while Int yields fifteen. The LP is therefore genuinely fractional even though its objective is an integer.

A second original corpus,

$$(\texttt{aaaab}, \texttt{baaccb}, \texttt{aac}, \texttt{babaab}, \texttt{cbbbca}), \qquad K = 2,$$

has $L_2 = 31/2 < I_2 = 16$. Its nonzero colour weights are $c_{\texttt{aa}} = c_{\texttt{babaab}} = 1/2$ and $c_{\texttt{cbbbca}} = 1$. The per-word fractional costs are $7/2, 11/2, 5/2, 3, 1$. Exhausting $\binom{42}{2} = 861$ vocabularies certifies the integer value. These examples demonstrate a relaxation gap; they do not supply a universal approximation ratio for rounding.

31.6.4 Application to permitted paths on actual higher-genus dessins

Set $m = 2g + 1$ for $g = 2, 4$, and retain the existing clean dessin of $y^2 = x^m - 1$, $\beta = x^m$. On $H = \{0, \dots, 2m - 1\}$ put

$$\sigma = (0\ \cdots\ m-1)(m\ \cdots\ 2m-1), \qquad \alpha(h) = h + m \pmod{2m}, \qquad \tau = \sigma^{-1}, \quad \phi = \alpha\tau.$$

There are two vertex cycles, m edges and one face, so $2 - 2g = 2 - m + 1$. Its polynomial algebra is the infinite locally gentle algebra

$$A_g = kQ/(a_h a_{\phi h} : h \in H), \qquad a_h : [h] \longrightarrow [\tau h].$$

Here products are written in travel order: ab traverses a first and then b. A left-operator matrix convention reverses these products. Define the nonzero permitted word $P(h, r) = a_h a_{\tau h} \cdots a_{\tau^{r-1} h}$. Our finite multiset is

$$\big(P(0, m+2), P(0, m+2), P(m-1, 4), P(m, m+2), P(2m-1, 4)\big).$$

Each arrow label is one alphabet symbol, even when its printed label has several characters. The duplicate first word retains its multiplicity. We allow every occurring subpath of length two or three as an extra candidate. The LP bound consequently concerns this explicitly restricted candidate set, not arbitrary-length vocabularies.

g	m	$\lvert C\rvert$	symbol count	$L_2 = I_2$	subsets checked
2	5	20	29	19	190
4	9	36	41	31	630

The exact witnesses attain these values, and Det/Bias/Int all attain them on the saved LP solutions. A token names a finite permitted subpath; concatenation recovers every original arrow, hence its quiver endpoints and original path length. This is finite corpus compression, not a finite-dimensional quotient of A_g. Arbitrary token concatenations may fail composability and need their own endpoint checks. Neither an algebra homomorphism on a freely generated token algebra nor a representation of arbitrary completed formal sums is asserted. The completed order still has rank $2m^2$ over $k[[u]]$; its rank, coefficients, multiplication, relations and modules are not reduced by counting tokens.

The companion laboratory at `http://127.0.0.1:8765/convextok.html` exposes the position DAG, literal fractional flows, vocabularies and discrete segmentations. Its five corpora and sixteen budget cases have sixteen exact primal/dual certificates and 2,312 exhausted integer vocabularies in total. The browser independently recomputes segmentation costs from local arrays; it does not solve a new LP when a user changes a vocabulary. The primary paper's NLP training and large GPU experiments are not reproduced. Compression of a finite path corpus proves no module or Fukaya equivalence, arithmetic determinant comparison, or GRH statement.

Chapter 32

Quantum TokenGT, concept navigation and error correction

This chapter connects executed finite methods through the same physical RG teacher. The completed order, ribbon dessin, physical Hamiltonian, token sequence and auxiliary quantum circuit retain their different dimensions. The surface is not reconstructed from a neural embedding, and the network is not silently declared a module over its completed order.

32.1 Node and edge tokens with a quantum feature map

The genus-two clean dessin of Chapter 28 has five quiver vertices and DVR-rank 50. Its physical $K_{2,5}$ incidence model has seven spin nodes and ten incidence edges. Our TokenGT-style input has these 17 valid node/edge tokens and one masked padding position. Each token carries its type and endpoint metadata through an explicit three-angle encoding. The normalized auxiliary state uses R_y data gates, fixed R_z rotations, CNOT $_{01}$, CNOT $_{12}$ and fixed R_x rotations. The measured features are

$$(\langle Z_0\rangle, \langle Z_1\rangle, \langle Z_2\rangle, \langle Z_0Z_1\rangle, \langle Z_1Z_2\rangle, \langle Z_0Z_2\rangle).$$

These are three feature qubits per token, not the seven physical spin sites or a faithful representation of the infinite order. The quantum feature map is frozen; the Q/K/V matrices and nonlinear readout are trained. A separate literal replay of the pinned elliptic-theta fixture is retained with its own input hash and category boundary. The physical RG training input is the genus-two incidence graph, not that different theta fixture.

With $Q = XW_Q$, $K = XW_K$, $V = XW_V$ and $S = QK^{\mathsf{T}}/\sqrt{6}$, define, on valid query/key indices,

$$C^{\mathrm{soft}} = \mathrm{softmax}(S)V, \qquad C^{\mathrm{trop}}_{ir} = \max_j (S_{ij} + V_{jr}), \qquad C^{\mathrm{hybrid}} = \tfrac{1}{2}(C^{\mathrm{soft}} + C^{\mathrm{trop}}).$$

Padding is masked in both softmax and max-plus operations and in pooling. The tropical output is a componentwise max-plus aggregation, with actual maximizing-key witnesses. It is not merely an argmax-key copy. A tanh context/residual pool and classical head predict all 32 coarse logweights, including the constant. These are quantum–classical transformers on measured features, not a coherent softmax unitary. TokenGT [83] motivates the node/edge organization; no general upstream expressivity or benchmark theorem is asserted for this compressed feature map. Numerical token-row permutation transport is checked, separately from arbitrary graph-relabel invariance and information lost by the encoding.

32.2 Matched training on an actual effective action

Four models use the same 120/40 split,40 OOD cases, seed 20261103, shared initialization/batches,900 Adam updates and 1,076 trained parameters each. The fourth uses six classical trigonometric features and the same hybrid head. The teacher is exactly $\mathcal{R}V$ from the seven-spin physical model, so partition, constant and retained-observable errors have physical meanings. The controlled input has three tied parameters, not 31 freely varied output couplings.

Features/context	action RMSE	log Z RMSE	magnetization RMSE	mean TV
Quantum/softmax	.10261	.09247	.01773	.03420
Quantum/tropical	.06530	.05923	.01846	.02167
Quantum/hybrid	.10125	.09653	.02709	.03212
Classical/hybrid	.04878	.04712	.01565	.01663

The classical baseline has lower held-out full-action error. Quantum OOD RMSE ranges from.555 to.763, versus.591 for the classical hybrid. One seeded experiment establishes neither quantum advantage nor general OOD robustness. The raw cases, every optimizer step and saved parameters are preserved. The tensor inspector replays actual token states, gates, Q/K/V, masks, scores, contexts and readout, and separately exposes the trained concept critic and continuous-GFlowNet MLP/density computations, with synchronized physical and algebraic support labels.

32.3 A defined mutual-information objective for concept directions

Let $z \in \mathbb{R}^6$ be a pooled embedding. We learn three normalized directions B_1, B_2, B_3 and a critic; their span need not be the whole embedding space. Choose C uniformly among the six direction/sign codes and define

$$\Delta = \tanh(0.3z + 0.7\,\mathrm{sign}(C)B_{\mathrm{dir}(C)}) - \tanh(0.3z).$$

A fixed vector is not a random variable: the random objects here are the intervention code and its induced embedding change. The GraphCG-inspired [84] objective is cross entropy for predicting C from Δ, plus $0.08\|BB^{\mathsf{T}} - I\|_F^2$. For any normalized critic q,

$$I(C;\Delta) \geq \log 6 - \mathbb{E}[-\log q(C \mid \Delta)].$$

Indeed the conditional cross entropy is conditional entropy plus an average nonnegative KL divergence. The held-out empirical functional is approximately 1.78844 nats. Its sampling estimate is not a certified lower confidence bound on an unknown population MI, nor proof of semantic identification: deliberately injected codes can already be distinguishable. The orthogonality penalty concerns the learned directions; it does not replace this probability model by ill-defined "MI between basis vectors." A training-only ridge decoder maps steered embeddings back to physical couplings, whose effects are evaluated with the exact RG teacher.

32.4 Latent forests, analogy and persistent homology

The latent forest branches along both signs of each learned direction, keeps a width-three beam and searches depthfour. All 61 candidates are scored by exact coarse log Z and the five retained magnetizations. Its best saved reward changes from -1.60383 to -0.70865; the residual is substantial. This is finite branching optimization in embedding space, without a claim of human or general language-model reasoning.

A distinct analogy test estimates a mean displacement from transformed training pairs for $(J_+, J_-, b) \mapsto (J_+ + 0.07, J_- - 0.04, b + 0.06)$, clipped to the training domain, and transfers it to 40 held-out embeddings. Decoded couplings go back through the exact physical teacher. Log Z RMSE is.09578 versus.15417 without transfer; magnetization RMSE is.02332 versus.04012. These are measured transformation-transfer results, not unrestricted "emergent analogical reasoning."

For an explicit finite point cloud with chosen metric, the Rips filtration contains each simplex at the maximum distance between its vertices. The implementation reduces the full boundary matrices of vertices, edges and triangles over $\mathbf{F}_2$, with faces ordered before cofaces at ties. A zero reduced edge column creates a one-cycle; a later triangle pivot kills its class. Triangles suffice to compute H_1. The 12-point learned embedding cloud has one positive-length interval approximately $[2.50049, 2.97133)$. The target and transferred physical-observable clouds, scaled as $(\log Z/3, m_0/.25, \ldots, m_4/.25)$, both have empty positive-length H_1 barcodes and pair-distance RMSE.29095. Empty matching barcodes alone are not faithful analogy. The 67-radius independent checks test this finite calculation, not a physical topological-order invariant or a mirror theorem.

32.5 Continuous embedding-chart GFlowNets

The executed GFlowNet [85] has root measure δ_0, three time steps, Lebesgue measure on each later $\mathbb{R}^2$ chart and deterministic termination at step 3. The forward MLP gives normalized Gaussian means and learned diagonal variances. At $t = 2, 3$ the backward kernel is

$$p_B(x_{t-1} \mid x_t) = \mathcal{N}\Big(\frac{t-1}{t} x_t, \frac{t-1}{3t} I\Big);$$

the final backward transition to the singleton root has unit probability. The positive terminal reward is

$$R(x) = \exp\left[-\frac{\|x\|^2}{2} + .35\{\log Z_{K_{2,5}}(.62 + .35\tanh x_0, .58 + .34\tanh x_1, .12) - 7\}\right].$$

The physical controls lie in a compact box, so the log-partition factor is bounded and the Gaussian confinement makes R integrable.

For a path, the trajectory-balance residual is

$$\delta = \log Z_\theta + \sum_{t=1}^{3} \log p_F(x_t \mid x_{t-1}) - \sum_{t=1}^{3} \log p_B(x_{t-1} \mid x_t) - \log R(x_3).$$

If this identity vanished almost everywhere for every path, exponentiating and integrating the normalized backward kernels would give $Z_\theta p_F^{\text{terminal}}(x) = R(x)$. This proves the desired terminal law under the exact density identity. A small empirical squared residual is not that identity and supplies no automatic global sampling guarantee.

Training uses 10,000 fixed continuous off-policy trajectories and 1,800 updates. Fresh held-out TB MSE is.002579 and on-policy MSE.002782. Learned log-normalization 1.70832 compares with finite-box quadrature 1.70734. Ten thousand new terminal samples give approximate histogram TV.04859 against a 20-by 20 midpoint histogram comparator on $[-5, 5]^2$, with cell width.5. The separate log-normalizer quadrature uses a 201-by 201 grid with spacing.05. Both grids are verification, not the state space or policy. Tail/quadrature/sampling errors are not interval certified. The two-dimensional physical latent chart is not a full-support flow on all six pooled embedding coordinates.

32.6 A genuine error-correction layer and a surface-code obstruction

For a logical qubit, use the repetition isometry $|0\rangle \mapsto |000\rangle$, $|1\rangle \mapsto |111\rangle$. Measure Z_0Z_1 and Z_1Z_2, and apply the X correction specified by the two syndrome bits. Under independent X noise of probability p on each physical qubit and ideal encoding/recovery, the weight-zero/one errors recover the state. Weight-two/three errors leave a logical X. Hence

$$p_L = 3p^2(1-p) + p^3 = 3p^2 - 2p^3, \qquad \mathcal{N}_L(\rho) = (1-p_L)\rho + p_L X\rho X.$$

The same channel identity holds with an entangled reference. The executed four-qubit Bell-reference density calculation compares actual BitFlip noise, syndrome projection and corrections with an independent eight-pattern sum. At $p = .1$ its entanglement fidelity is.972, versus.9 without coding. It corrects one X error under the stated ideal assumptions, with no phase protection or universal fault-tolerance claim.

Applied independently to each auxiliary token-feature qubit, this is an explicit physical feature-memory layer. For a measured Z product of weight r, the unencoded X channel multiplies its expectation by $(1-2p)^r$; the recovered channel replaces p by p_L. This follows by conjugating Z by X and tensoring the single-qubit channel identity, even for entangled feature states. It distinguishes actual syndrome recovery from embedding regularization or persistence diagnostics. The resulting attention/readout is evaluated on all 40 held-out physical RG actions. At $p = .1$, hybrid full-action RMSE is.89766 without coding,.31589 after one ideal recovery level and.10608 after two, compared with clean.10125. Tropical RMSE changes from.32676 to.11810 and.06733, compared with clean.06530. Seventy-five explicit logical-X density-mixture comparisons on actual entangled token states agree with the attenuation rule within 4.45×10^{-16}. The separately checksummed evaluation preserves every trained checkpoint. The three auxiliary feature qubits require 3,9 and 27 total physical qubits at zero, one and two recovery levels. The reported evaluations use the proved logical-channel identity, not a full noisy 9/27-qubit gate simulation; encoding and recovery gates are ideal throughout. Concatenating ideal blocks gives the noise recursion $p \mapsto 3p^2 - 2p^3$, improving $p < 1/2$; it is not an RG theorem about the physical Hamiltonian.

Proposition 32.1 (The one-face dessin is not a useful quantum memory)**.** *The CSS construction with qubits on the 10 clean edges of the genus-two $K_{2,5}$ dessin, vertex X checks and its single face Z check has parameters $[[10, 4, 1]]$, with X-distance 1 and Z-distance 4.*

Proof. The connected graph incidence matrix over $\mathbf{F}_2$ has rank $7 - 1 = 6$. Every edge occurs twice in its single face boundary, so the face boundary is zero. The chain relation holds. For independent commuting Pauli checks that do not generate $-I$, the projector is $\prod_j (I + S_j)/2$. Only its identity term has nonzero trace, so its rank is $2^{n-r_X-r_Z}$. Thus the CSS logical dimension is $10 - 6 - 0 = 4 = 2g$. All single-edge X operators commute with the zero face check. No singleton edge set is a cut/coboundary, since each edge lies on a four-cycle; thus it is not an X stabilizer, and the X-distance is 1. A Z logical operator is a nonzero cycle because the face-boundary subspace is zero. The simple bipartite graph has girth 4, proving Z-distance 4. Exact enumeration independently checks the ranks, commuting checks and shortest logical witnesses. □

Genus and logical dimension therefore do not imply noise protection. Useful surface-code families require controlled cellulations, local checks, growing primal and dual systoles, a stated noise model and verified decoders.

32.7 Tropical, categorical and physical applications

For real numbers a_j and $\tau > 0$,

$$\max_j a_j \le \tau \log \sum_j e^{a_j/\tau} \le \max_j a_j + \tau \log N.$$

Factor out the maximum; the remaining sum lies between 1 and N. This is a precise zero-temperature max-plus limit. Replacing the finite-temperature RG sum by a maximum discards entropy, including its normalization. An attention semiring alone supplies neither the physical energy calibration nor the valuations and curve/disk counts needed for tropical geometry and mirror symmetry [86].

For a categorical connection, Section 28.2.4 gives an actual 25-dimensional finite gentle cut with global dimension 4, kills u, and proves that restriction to the original completed order is not derived fully faithful. It is a constructive starting point, with a proved obstruction to transporting comparisons indiscriminately. Choose its grading and verify the relevant homological smoothness before invoking a geometric model. The partially wrapped Fukaya comparison for smooth graded gentle algebras requires boundary, stops and a line field [66]; it is not a blanket statement for the complete order on the original closed surface. One could then compute specified Hom/Ext or arc-intersection data and use them in a categorical learning objective. No such equivalence or learned categorical functor is produced by the three-qubit feature circuit. Physical RG marginalization is not automatically a derived equivalence either.

For materials models, one must supply a physical Hamiltonian/data family, symmetries, locality constraints and validated observables. The executed finite spin problem is a reproducible statistical-mechanics testbed, not a materials-discovery result. An executed five-qubit generative example uses a saved learned coarse action to compute $p(s) = e^{\widehat{V}(s)}/Z$ and prepares $|\psi\rangle = \sum_s \sqrt{p(s)}|s\rangle$. Born probabilities reproduce p to 2.78×10^{-17}. This coherent pure state is not the mixed Gibbs state. Applying the explicit local projector-Kraus dephasing channel gives $\mathrm{diag}(p)$ with the same residual. From 4096 seeded quantum Born samples, the maximum five-magnetization sampling error is.04377; the simultaneous 95% Hoeffding radius is.05086. The union bound uses $10\exp(-N\epsilon^2/2)$ for five observables in $[-1, 1]$. This bound controls shot error relative to the learned distribution, separately from its physical teacher bias. All 32 amplitudes are computed classically, with no efficient many-body preparation or quantum advantage claim. Sampling latent coupling controls, predicting a full action and generating physical configurations is therefore a concrete finite hybrid route, with its costs and errors exposed. Quantum-information uses of the physical feature-memory code require the stated noise/recovery model. None of these numerical, categorical or physical interfaces establishes the missing arithmetic Frobenius/determinant comparison for GRH.

32.8 Verification boundary

All optimizer histories, source hashes, parameters, held-out/OOD data, barcodes, candidate rewards and density checks are preserved. The six-panel laboratory and four trained architecture passes display literal arrays and gate states; the original 22 architecture records remain unchanged. Exact finite CSS enumeration and the bit-flip channel proof are distinguished from floating-point learned diagnostics. The finite classical RG identities are kernel checked in `FiniteRG.lean`; general neural optimization, continuous GFlowNet sampling, quantum recovery and categorical interfaces are not thereby wholly Lean formalized.

Chapter 33

Learned generative fields, width limits and quantum geometry

This chapter connects explicit learned functions to physical RG targets, categorical path calculations and checked quantum circuits. Each width, coefficient field and category is specified before comparisons are made.

33.1 Learned fields, width limits and quantum geometry

Learned functions enter this program as candidate generators, physical surrogates and control laws. A network may suggest an arithmetic metric, operator or gluing datum; a successful fit does not establish its positivity, analytic domain or identification with a completed L-function. Those are independent mathematical obligations. This section gives explicit interfaces and executed examples rather than treating "quantum", "tropical" or "infinite width" as a substitute for that comparison.

Proposition 33.1 (A specified quantum-feature width limit)**.** *Let $x \in \mathbb{R}^d$, $w \sim N(0, I_d)$ and $b \sim \mathrm{Unif}[0, 2\pi]$ be independent, and set $\phi_{w,b}(x) = \sqrt{2}\langle Z\rangle_{R_Y(w\cdot x+b)|0\rangle} = \sqrt{2}\cos(w \cdot x + b)$. For independent features,*

$$K_m(x, y) = m^{-1} \sum_{r=1}^{m} \phi_r(x)\phi_r(y) \longrightarrow K(x, y) = e^{-\|x-y\|^2/2}$$

almost surely on every specified finite set of pairs. Every K_m is a positive semidefinite Gram kernel. For a readout $f_a(x) = m^{-1/2} \sum_r a_r\phi_r(x)$ with only a trained, its tangent kernel is exactly K_m. These statements do not assert the same limit for a jointly trained finite quantum transformer.

Proof. Uniform-phase integration gives $\mathbb{E}_b[2\cos(u + b)\cos(v + b)] = \cos(u - v)$. The Gaussian characteristic function then gives K. Products are bounded by two, so the strong law applies to each pair and hence any finite union. For any finite coefficient vector c, the Gram quadratic form is $m^{-1} \sum_r |\sum_i c_i\phi_r(x_i)|^2 \geq 0$. Differentiating with respect to a_r gives the final assertion. □

The frozen-kernel squared-loss flow has residual $r(t) = \exp(-K_m t)r(0)$ when the loss normalization is absorbed into time. Null directions do not decay. A complex feature space instead uses the Hermitian kernel $\mathbb{E}[\phi(x)\overline{\phi(y)}]$. A finite coefficient field has neither this Gaussian law nor an ordered positive Hilbert metric; changing algebraic coefficients is a separate operation.

Proposition 33.2 (Tropical limit and a cancellation boundary)**.** *For real $s_1, \dots, s_n$ and $\tau > 0$,*

$$0 \le \tau \log \sum_j e^{s_j/\tau} - \max_j s_j \le \tau \log n.$$

An attention maximum therefore has a controlled log-sum-exp approximation. It does not by itself define a tropicalization of a variety or an HMS functor. In a valued coefficient field, valuation of a sum can increase by cancellation.

Proof. After subtracting $M = \max s_j$, the exponential sum lies between one and n. For the second statement, both $1+T$ and $-1+T$ have valuation zero in $\mathbb{Q}((T))$, whereas their sum $2T$ has valuation one. In characteristic two that sum is zero. Thus replacing every addition by its tropical minimum without tracking leading coefficients loses information. □

Kontsevich–Soibelman constructions require valued analytic and integral-affine gluing data; appropriate gentle/Fukaya comparisons require specified categories, gradings, stops and smoothness hypotheses [92, 91, 93]. Learned coefficients can propose such data, but the compatibility equations and arithmetic comparison still need proofs.

Executed physical examples. On the actual clean genus-two dessin, put seven quantum spins on its $K_{2,5}$ incidence graph and compute a normalized Gibbs state. Exact white-spin partial trace gives a two-spin quantum RG marginal. Twelve RTX4090 runs train four-qubit-feature diffusion and flow-matching models for its smoothed Z-measurement law: two objectives, entangled/product circuit controls, and three seeds. They have 5,810 nominal parameters and 2,000 steps each. A separate four-qubit variational purification flow learns the full known density interpolation, with 48 controls. Its minimum fidelity on a 33-point grid is 0.999903; this is not a uniform theorem or universal noise inverse. The matched controls show no consistent entanglement advantage.

Actual cuStateVec/cuTensorNet execution also covers 7-, 11- and 23-qubit finite circuits on genus-two, genus-four and genus-ten dessin incidence graphs. The 23-qubit case has 8,388,608 amplitudes and 447 gates. These larger circuits are untrained; the small cases have independent NumPy comparisons, while the largest has normalization and inverse-circuit checks. The exact environment and all failed/preliminary records are preserved.

Geometric and hardware interfaces. For the contracted m-edge dessin, the graph fundamental group is F_{m-1}, and its universal graph cover is the m-regular tree. The theta case $m = 3$ has a three-regular cover, distinct from the four-regular Cayley graph of F_2. Neither is the coefficient field $\mathbb{F}_2$ or the universal cover of the filled compact surface. Explicit path modules over the infinite genus-two algebra give Hom, Ext and Tor computations; Frobenius pants tensors give exact TQFT gluing, with a heralded physical implementation. CHSH gives a finite game benchmark, distinct from the unrestricted correlation separation in MIP*=RE [99]. Three executable tropical hardware references and a source-pinned chip-design survey complement the circuits. They are arithmetic/control designs, not synthesized chips, validated CFT/string dualities or a proof of GRH.

33.2 Physical generative models and their verification

33.2.1 From a dessin to an actual quantum RG target

Take $y^2 = x^5 - 1$, $\beta = x^5$. Its clean incidence graph has two black vertices and five white vertices, hence seven physical spin sites and ten incidence edges. These differ from the five quiver vertices

and the infinite-dimensional polynomial algebra. The physical Hilbert space below is finite; no faithful action of that whole algebra on it is assumed.

Let X_q, Z_q be Pauli matrices on physical site q, with the black sites numbered zero and one and the white sites $2 + j$. Our executed Hamiltonian is

$$\begin{aligned} H = & -.50 \sum_{j=0}^{4} Z_0 Z_{2+j} - .35 \sum_{j=0}^{4} (-1)^j Z_1 Z_{2+j} \\ & - .55 \sum_{q=0}^{6} X_q - .12 Z_0 + .072 Z_1 - \sum_{j=0}^{4} h_j Z_{2+j}. \end{aligned}$$

Here $h_j = .045 \cos(1.7j) + .02j/5$. All coefficients are dimensionless and inverse temperature is one. Diagonalizing the actual 128×128 Hermitian matrix gives $\rho = e^{-H}/\operatorname{tr}(e^{-H})$. We retain the two black spins:

$$\rho_R = \operatorname{Tr}_{\text{white}} \rho, \qquad (\rho_R)_{ab} = \sum_{j=0}^{31} \rho_{aj,bj}.$$

This is an actual coarse quantum state, with trace one and positive spectrum. An independent Pauli–Kronecker NumPy reconstruction agrees with the saved matrix to $2.04 \cdot 10^{-10}$. Its minimum eigenvalue is approximately 0.0806414, and its off-diagonal Frobenius norm is 0.300551. There is therefore quantum coherence that a probability histogram alone cannot describe. No chemical or experimental material dataset is involved: this is an exactly specified finite quantum-matter benchmark.

Let $p_s = (\rho_R)_{ss}$ for $s \in \{\pm 1\}^2$. The hybrid samplers learn

$$p_\sigma(x) = \sum_s p_s \mathcal{N}(x; s, \sigma^2 I_2), \qquad \sigma = .2.$$

This is a continuous dequantization of the measured spin law. A sign measurement of these samples differs from p by at most $2\Phi(-1/\sigma)$ in total variation, by a coordinatewise sign-flip coupling and the union bound. This is below $6 \cdot 10^{-7}$ here. It is small compared with finite-sampling error, but it is not zero. The samplers do not recover phases or the entire ρ_R. For example, ρ_R and $(Z \otimes I)\rho_R(Z \otimes I)$ have the same diagonal but different density matrices.

33.2.2 Diffusion and exact versus approximate reverse controls

For $T = 64$ use the cosine cumulative noise schedule, with endpoint offset .008, clipped step variances between .0001 and .999. Write $\alpha_k = 1 - \beta_k$ and $\bar{\alpha}_k = \prod_{j \le k} \alpha_j$. The forward noising law is

$$x_k = \sqrt{\bar{\alpha}_k}\, x_0 + \sqrt{1 - \bar{\alpha}_k}\, \epsilon, \qquad \epsilon \sim N(0, I_2).$$

A network $\epsilon_\theta(x_k, k/T)$ minimizes the ordinary mean squared noise-prediction error. It is a classical stochastic sampler containing quantum-circuit features, not an implemented coherent quantum channel. The executed reverse update uses

$$\mu_\theta = \frac{x_k - \beta_k \epsilon_\theta / \sqrt{1 - \bar{\alpha}_k}}{\sqrt{\alpha_k}}, \qquad \widetilde{\beta}_k = \beta_k \frac{1 - \bar{\alpha}_{k-1}}{1 - \bar{\alpha}_k}, \qquad x_{k-1} = \mu_\theta + \sqrt{\widetilde{\beta}_k}\, z.$$

The last step is deterministic. Even an exact conditional noise predictor does not make this Gaussian reverse kernel the exact reverse mixture at finite T: posterior uncertainty of the mixture component

remains. The oracle-noise control therefore retains a reverse-kernel approximation, finite schedule and Monte Carlo error, not just a numerical integration error.

There is also an exact, known-teacher reverse-mixture control. Conditional on center s, put $v_k = \bar{\alpha}_k\sigma^2 + 1 - \bar{\alpha}_k$ and $m_{k,s} = \sqrt{\bar{\alpha}_k}s$. At a supplied x_k, draw the center with posterior weights proportional to $p_s \exp(-\|x_k - m_{k,s}\|^2/(2v_k))$. Then draw

$$x_{k-1} \mid x_k, s \sim N\left(m_{k-1,s} + \frac{\sqrt{\alpha_k}v_{k-1}}{v_k}(x_k - \sqrt{\alpha_k}m_{k-1,s}), \frac{v_{k-1}\beta_k}{v_k}I_2\right).$$

These formulas follow by conditioning a jointly Gaussian pair with covariance $\sqrt{\alpha_k}v_{k-1}I_2$. Starting from the exact forward terminal mixture and composing these reverse conditionals recovers p_σ exactly in distribution, up to numerical and sampling error. It uses the full teacher, so it is a diagnostic rather than a learned solution.

33.2.3 Flow matching with a measurable target velocity

Independently sample $z \sim N(0, I_2)$ and $x_1 \sim p_\sigma$, set $x_t = (1-t)z + tx_1$, and train $v_\theta(x_t, t)$ toward $x_1 - z$. This is the conditional flow-matching regression objective. Conditional on center s, its time-t mean and variance are

$$ts, \qquad v_t = (1-t)^2 + t^2\sigma^2.$$

Let $\pi_s(x,t)$ be the corresponding mixture posterior. The exact conditional velocity is

$$v_*(x,t) = \sum_s \pi_s(x,t)\left[s + \frac{t\sigma^2 - (1-t)}{v_t}(x - ts)\right].$$

Indeed $\mathrm{Cov}(x_1 - z, x_t \mid s) = (t\sigma^2 - (1-t))I_2$; Gaussian conditioning gives the displayed formula. The positive variance v_t includes both endpoints. The code verifies this formula and the diffusion-score formula by independent finite differences of a separately written mixture log density. Learned sampling uses 128 Heun steps. Oracle-velocity sampling isolates finite integration and sampling error for this known smooth density; it is not an upstream QFM reproduction [94].

33.2.4 Architecture, matched controls and actual GPU results

The neural input is $[x_0, x_1, t, \sin 2\pi t, \cos 2\pi t, \sin 4\pi t, \cos 4\pi t]$. An affine encoder maps its seven channels to four angles through $\pi\tanh$. A two-layer four-qubit circuit uses angle-reuploading R_Y, R_Z gates and, for the entangled architecture, a CNOT ring. Fifteen commuting Z-string expectations are concatenated with the seven input channels. A $22 \to 64 \to 64 \to 2$ SiLU head predicts noise or velocity. The product control uses the same nominal parameters and removes the entanglers. Final diagonal phase rotations are invisible to the all-Z readout; equality of nominal parameter counts does not establish equality of effective Fisher capacity.

Every run has 5,810 nominal parameters, batch size 512 and 2,000 Adam steps. There are 16,384 training draws and 4,096 disjoint held-out draws, with seeds 20261104, 20261105 and 20261106. The four architectures/objectives were rerun at every seed. The following figures are mean and sample standard deviation across those three runs, not confidence intervals or asymptotic theorems.

Objective	circuit	sign-law TV	sliced W_1
Diffusion	product	$.0380 \pm .0113$	$.0768 \pm .0306$
Diffusion	entangled	$.0451 \pm .0133$	$.0939 \pm .0183$
Flow	product	$.0217 \pm .0079$	$.0460 \pm .0077$
Flow	entangled	$.0293 \pm .0130$	$.0522 \pm .0159$

The second metric uses sixteen fixed projection directions and an independent teacher draw. The experiment demonstrates learning but no consistent quantum or entanglement advantage; the product control has lower mean error on both reported metrics. No physical quantum processor, shot noise, industrial chemical prediction, OOD material transfer or complexity speedup was tested. All checkpoints, seeds, histories, runtimes and teacher controls are retained.

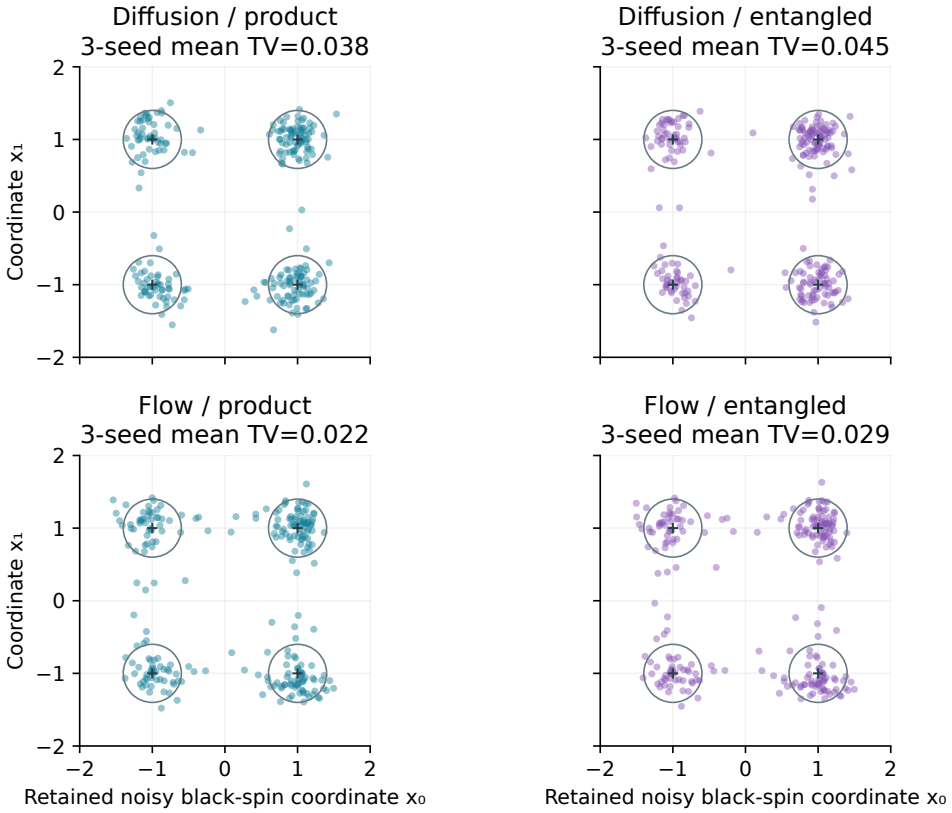


Figure 33.1: Actual final samples from seed20261104, with exact mixture centers and two-standard-deviation circles. Titles report mean sign-law TV over three seeds. The product control is competitive; no entanglement advantage is inferred.

33.2.5 A coherent learned purification flow

We separately implement quantum evolution, without identifying it with the classical samplers. Exact depolarizing diffusion is

$$D_t(\rho_R) = e^{-t}\rho_R + (1 - e^{-t})I_4/4.$$

It preserves trace and positivity and satisfies $D_s D_t = D_{s+t}$ by direct substitution. Its linear inverse on all matrices is not positive: $D_t^{-1}(P) = e^t P - (e^t - 1)I_4/4$ has a negative eigenvalue on the orthogonal complement of any rank-one projection P when $t > 0$. Thus a learned inverse cannot be a universal deterministic physical channel.

For a constructive state-preparation benchmark, take the family $R_t = (1 - t)I_4/4 + t\rho_R$, $0 \le t \le 1$, and its canonical purification $|\Psi_t\rangle = \mathrm{vec}\sqrt{R_t}$ in $\mathbb{C}^4 \otimes \mathbb{C}^4$. It is normalized because $\|\sqrt{R_t}\|_F^2 = \mathrm{tr}\, R_t = 1$. The initial purification is two Bell pairs. We train a six-block four-qubit

circuit: each block conjugates local R_Y rotations by a fixed CNOT network and its inverse; angles are $t\theta + t^2\omega$. All blocks are identity at the control time zero. The 48 learned controls are trained against full known purification states, using the fidelity loss. This ideal supervision is stronger than access to measured samples and is accounted for explicitly.

An RTX4090 run of 2,000 steps, batch 64, gives minimum fidelity 0.999903 on a 33-point grid and maximum reduced-density Frobenius error 0.009642. The reduced state is obtained by an actual ancilla partial trace and passes trace/positivity checks. These are grid diagnostics, not a uniform or out-of-family guarantee. The construction is a learned coherent control path for known targets, not a universally learned inverse to depolarization. Its full 76-gate replay and intermediate complex states are exported to the same numerical architecture inspector as the other models.

33.2.6 Width, fields, RG and arithmetic obligations

Proposition 33.1 fixes which width is being increased: the number of independent one-qubit features, with only their readout trained. At initialization let $a_r \sim N(0,1)$ be independent standard centered readout coefficients, independent of the frozen features. Conditional finite-dimensional outputs are then exactly centered Gaussian with covariance K_m. The almost-sure kernel convergence implies convergence of these finite-dimensional characteristic functions to the Gaussian law with covariance K. This proves the specified finite-dimensional GP limit. It does not prove tightness in a function-space norm, parameter-feature learning, a many-qubit limit or a continuum QFT. For frozen K_m, squared-loss gradient flow gives $\dot{r} = -K_m r$, whose eigencomponents decay at their kernel eigenvalues. A zero eigenvalue leaves a nonzero residual unchanged.

The executable width experiment fits the existing exact 32-configuration *classical* black-spin-decimated action on genus two, including its constant. This is a second true RG teacher, distinct from the quantum white-spin partial trace above. With 96 parameter triples for training, 32 for testing, eight feature seeds and ridge 10^{-5}, widths 16 and 4,096 give mean relative kernel errors 0.2990 and 0.01726 and mean full-action test MSE 0.02005 and 0.000743. The limiting RBF readout is also evaluated. Finite numerical convergence supports the implementation; the proposition supplies the limit proof. Quantum NTK literature requires its own parameterization, ensemble and lazy/large-width hypotheses [91, 90].

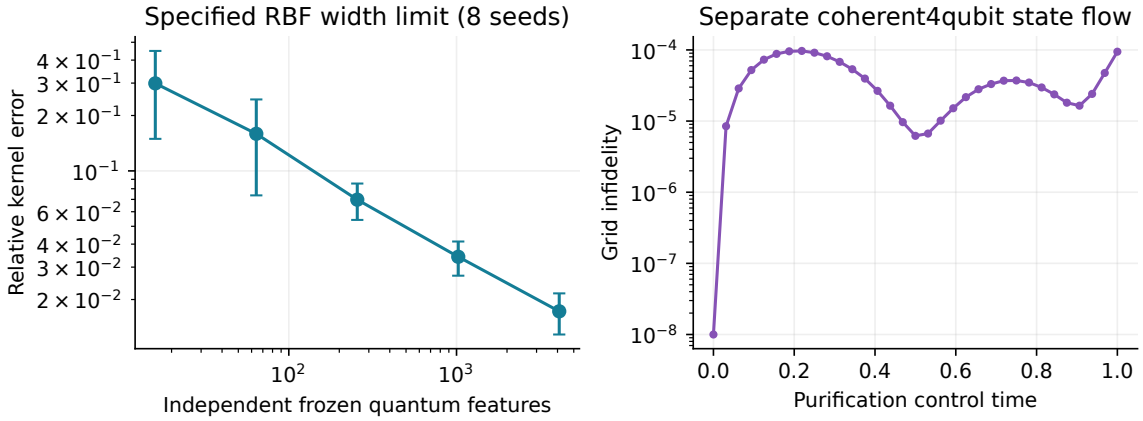


Figure 33.2: Left: eight-seed frozen-feature kernel errors, with sample standard deviations. Right: the separate learned coherent purification flow, evaluated on33time points. These are distinct width and quantum-control experiments.

For complex embeddings the Hermitian Gram form, realification $A + iB \mapsto \left(\begin{smallmatrix} A & -B \\ B & A \end{smallmatrix}\right)$, and conjugation must be respected. An arbitrary real network on twice as many channels need not be complex linear. In characteristic two, $1+1 = 0$; an embedding into real vectors cannot be a unital field homomorphism preserving that addition. Finite-field path algebras and cellular/CSS computations are still meaningful, but Gaussian integration, ordered Gibbs weights and real backpropagation do not transfer by renaming the field. An explicit discrete learner over $\mathbb{F}_p$, $p = 2, 3, 5$, uses features $1, x, y, xy$ and coefficients searched in the finite field to learn $f(x, y) = xy$. All p^2 inputs are verified; an affine-only learner has nonzero minimum error. The trained map compiles to the permutation unitary $U_f|x, y, z\rangle = |x, y, z + f(x, y) \bmod p\rangle$ on a complex Hilbert space of dimension p^3. Retaining x, y makes its inverse subtraction explicit. This is reversible encoding of a field-valued polynomial learner, not a field embedding into complex amplitudes or backpropagation in $\mathbb{F}_p$. Its training is exact finite coefficient search. A tropical semiring is not a field; coefficient cancellation, valuation signs and the underlying valued algebra must be specified.

For GRH, each architecture offers an experimentally testable role: quantum features can parameterize candidate metrics or probe observables; graph tokens can encode actual local incidence, masks and monodromy; tropical attention can search extremal valuations or active constraints; flow/diffusion can propose continuous operator/control parameters; RG can organize a genuine hierarchy of coarse actions. None of these roles proves that its Gram matrix is the arithmetic positive metric. One must still construct the arithmetic object with correct conductor, gamma factors, zero divisor and domain, prove compact-uniform control and zero location, and keep Dirichlet, Hecke, Dedekind and Artin hypotheses separate. A learned candidate is accepted only after its exact defining equations and analytic estimates are supplied.

33.3 Covers, paths, pants and quantum games

33.3.1 Which free group and which universal cover?

Write $F_2 = \langle x, y\rangle$, $\mathbb{F}_2$ and $\widehat{F}_2$ for the free group, coefficient field and profinite completion, respectively. For a theta graph with vertices A, B and edges a, b, c, an explicit cover has vertices $(g, A), (g, B)$, $g \in F_2$, and edges

$$a : (g, A) - (g, B), \qquad b : (g, A) - (gx, B), \qquad c : (g, A) - (gy, B).$$

Left multiplication is the deck action. Contracting all a-edges produces the usual four-regular Cayley tree of F_2; before contraction the graph is three-regular. Equivalently, vertices are reduced nonbacktracking edge paths from A, with an immediately reversed edge cancelled. This gives a tree and unique path lifting in every length. Its radius-r patch has $1 + 3\sum_{k=0}^{r-1} 2^k$ vertices, hence 766 at radius eight. With a planar ribbon structure the abstract graph is a spine of a topological pair of pants. The actual $m = 3$ dessin instead has the ribbon structure of a once-punctured torus. Forgetting the cyclic orders identifies the abstract graphs, not these thickenings. Graph distance is not automatically hyperbolic geodesic length.

For the contracted clean m-edge dessin there are two vertices and m parallel edges, so π_1 is F_{m-1} and the analogous universal tree is m-regular. The new examples include $m = 5, 9$, of genus two and four. Reinserting clean white bivalent vertices subdivides its edges. Attaching the face to recover the compact surface introduces a relation; the closed genus-two surface has its surface group and a disk universal cover, not one of these graph trees. Separately, $\mathbb{P}^1 \setminus \{0, 1, \infty\}$ has fundamental group F_2. The unbranched cover induced by a clean dessin removes all preimages of those three values. For our degree-$2m$ map there are $m + 3$ punctures; its Euler characteristic is $-2m$, not that

of the dessin's one-skeleton. Thus the occurrences of F_2 in monodromy, graph covers and arithmetic profinite theory must not be silently identified.

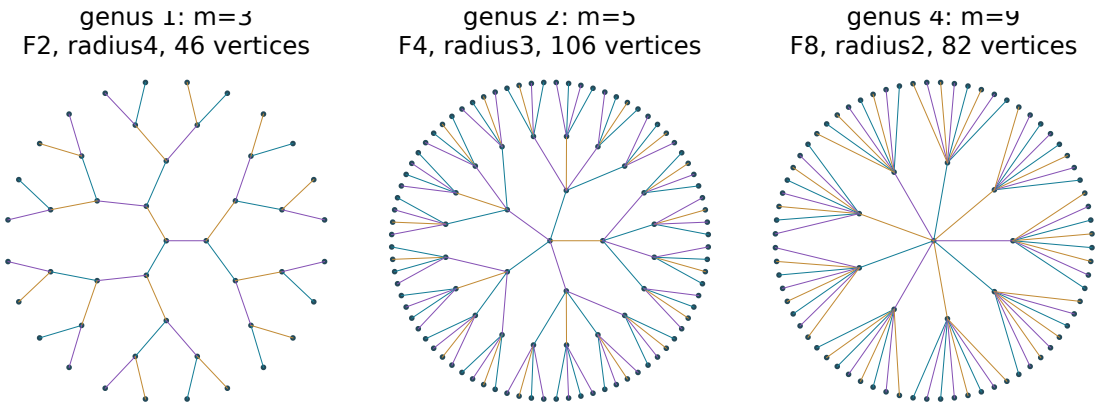


Figure 33.3: Finite windows of universal covers of contracted actual clean dessins. These are schematic graph trees, not uniformizing embeddings of the compact surfaces. Clean white bivalent vertices are suppressed.

For finite-supported representations of a suitably graded bound quiver, pushdown maps split into deck-homogeneous blocks. The arrow equations preserve the degree, and monomial zero relations are homogeneous. The resulting Hom direct sum controls all deck pieces, not just degree one. For an explicit graph-only diagnostic two lifted edge intervals have upstairs endomorphism dimension two, but downstairs endomorphism dimension four: the deck pieces have dimensions $2+1+1$. This graph-quiver calculation is *not* substituted for a dessin-algebra module example. The actual infinite polynomial module examples below supply that part. A Hom-controlled functor needs its specified exceptional/source/target subcategory and control statement; exactness, a deck-sum formula or equal dimensions alone is not an equivalence or an AR universality theorem. A derived comparison must control all $\mathrm{Hom}(X, Y[n])$ and composition, together with an actual derived/enhanced functor.

33.3.2 Actual infinite-algebra path modules and unbounded resolutions

To fix conventions, let A_{col} be the earlier rightmost-arrow-first polynomial matrix algebra acting on left columns. Here we use travel-order path multiplication and write $A_{\mathrm{trav}} = A_{\mathrm{col}}^{\mathrm{op}}$ for the prose-identified bound-quiver algebra. Right A_{trav} representations therefore encode the earlier covariant left-column representations. There are vertices $i \in \mathbb{Z}/5$ and arrows $a_i, b_i : i \to i-1$, with

$$a_i b_{i-1} = b_i a_{i-1} = 0.$$

Both pure branch paths survive at every length. No arrow-truncated finite algebra is being used. We work with ordinary polynomial modules, not with all completed lattices or all infinite strings.

Put $P_i = e_i A_{\mathrm{trav}}$ and let S_i be its residue simple. The augmentation kernel is $a_i A \oplus b_i A$. Multiplication by an arrow kills exactly the opposite-branch positive paths at its target, while each surviving path has a distinct normal image. Its kernel is therefore the right ideal generated by its unique forbidden successor, without cancellation. Iteration yields a projective resolution with

$$P_0 = P_i, \qquad P_n = P_{i-n} \oplus P_{i-n} \quad (n \geq 1).$$

The two arms are indexed by alternating-branch relation words. The *differential entry is the last arrow*, not the product of the zero relation word. This kernel description proves exactness in every

degree. Applying Hom to a simple kills every arrow entry, hence

$$\dim \mathrm{Hom}(S_i, S_j) = \mathbf{1}_{i=j}, \qquad \dim \mathrm{Ext}^n(S_i, S_j) = 2\mathbf{1}_{j=i-n} \quad (n \geq 1).$$

Tensoring with the left residue simple gives the same Tor dimensions. A graded version needs its internal degree shifts. In particular the residue simples have infinite projective dimension in this ambient algebra.

Let B be the one-arrow string supported at vertices zero and four, with $a_0 = 1$ and every other arrow zero. Its presentation is

$$P_4 \oplus P_3 \xrightarrow{(b_0,\ a_0 a_4)} P_0 \longrightarrow B \longrightarrow 0.$$

The two images have disjoint normal-path support and span the kernel, because B retains exactly e_0, a_0. The next entries are a_4 on the first arm and b_3 on the second; continue by their unique forbidden successors. This gives an unbounded exact resolution by the same normal-path argument. Full arrow-commuting equations give

$$\dim \mathrm{Hom}(B, B) = 1, \quad \dim \mathrm{Hom}(S_0, B) = 0, \quad \dim \mathrm{Hom}(B, S_0) = 1, \quad \dim \mathrm{Hom}(S_4, B) = 1.$$

In the Hom complex for $\mathrm{Ext}^1(B, B)$ both adjacent differentials vanish, so $\mathrm{Ext}^1(B, B) \simeq \mathbb{Q}$. A concrete nonsplit self-extension has $\mathbb{Q}^2$ at zero and four, $a_0 = I_2$, $b_0 = \left(\begin{smallmatrix} 0 & 1 \\ 0 & 0 \end{smallmatrix}\right)$, all other arrows zero. The first-coordinate submodule and quotient are B. A section at vertex zero would lift the quotient basis to a vector with second coordinate one; b_0 sends it to a nonzero first-coordinate vector, contradicting commutation with the zero b_0 action on B. Thus B is not rigid in this actual ambient category. No almost-split universality is inferred from this nonsplitting.

For finite-dimensional N let $DN = \mathrm{Hom}_{\mathbb{Q}}(N, \mathbb{Q})$. On each finite idempotent projective the evaluation pairing identifies $P \otimes_A DN$ with $D\,\mathrm{Hom}_A(P, N)$. Dualization is exact on these finite-dimensional terms, so the resulting complexes give $\mathrm{Tor}_n^A(M, DN) \simeq D\,\mathrm{Ext}_A^n(M, N)$ for the stated finitely generated resolutions. In particular $\mathrm{Tor}_1^A(B, DB) \simeq \mathbb{Q}$. The exact program checks six source/target pairs through degree twelve, all five simple-target formulas and 250 normal-kernel samples. The unbounded resolution assertions rest on the normal-form proof, not on the finite cutoff. These new homological proofs are prose/exact calculations; full corresponding resolution objects are not yet Lean packaged.

A geometric path may label a string after specifying the ribbon structure, relations and category. Turning it into a geodesic needs a metric and appropriate boundary/stop data. Intersections compute morphisms only under the hypotheses of an actual graded/Fukaya comparison. The homologically smooth graded-gentle perfect-category theorems do not identify our entire ordinary or completed module category with the Fukaya category by inspection [93]. In particular the residue resolutions warn against silently imposing smoothness or finite projective dimension.

33.3.3 Pants tensors, physical dilation and sewing boundaries

For $C = \mathbb{Q}[\epsilon]/\epsilon^2$, take $\varepsilon(1) = 0$, $\varepsilon(\epsilon) = 1$. In the ordered bases $(1, \epsilon)$ and $(1 \otimes 1, 1 \otimes \epsilon, \epsilon \otimes 1, \epsilon \otimes \epsilon)$, multiplication and comultiplication are

$$\mu = \begin{pmatrix} 1 & 0 & 0 & 0 \\ 0 & 1 & 1 & 0 \end{pmatrix}, \qquad \Delta = \begin{pmatrix} 0 & 0 \\ 1 & 0 \\ 1 & 0 \\ 0 & 1 \end{pmatrix}.$$

The pairing is $\left(\begin{smallmatrix}0&1\\1&0\end{smallmatrix}\right)$, with determinant -1. Associativity follows from $\epsilon^2 = 0$; coassociativity sends one to the three placements of a single one among two ϵ's and sends ϵ to $\epsilon^{\otimes 3}$. On the four tensor basis vectors, all three maps in

$$\Delta\mu = (\mu \otimes I)(I \otimes \Delta) = (I \otimes \mu)(\Delta \otimes I)$$

give, respectively, $1 \otimes \epsilon + \epsilon \otimes 1$, $\epsilon \otimes \epsilon$, $\epsilon \otimes \epsilon$, and zero. This proves the Frobenius identity. The unit and counit identities follow directly on the same basis. These are exact oriented 2D TQFT gluing data [95], not a presumed positive Hilbert structure.

The handle map $H = \mu\Delta$ sends $1 \mapsto 2\epsilon$ and $\epsilon \mapsto 0$. Closed genus-g contractions $\varepsilon H^g \eta$ are $0, 2, 0, 0, \ldots$. The genus-two value really vanishes in this example. In characteristic two the torus value also vanishes, illustrating a meaningful coefficient change rather than an embedding-space relabelling. After extending to $\mathbb{C}$ with the Euclidean metric, $\Delta^*\Delta = \mathrm{diag}(2, 1)$ and $\Delta \neq \mu^*$; $\mu : \mathbb{C}^4 \to \mathbb{C}^2$ is not an isometry. The exact code constructs $K = \mu/\sqrt{2}$ and a 4×4 failure block L with $K^*K + L^*L = I_4$. Stacking them gives an isometry into $\mathbb{C}^2 \oplus \mathbb{C}^4$, extendable to a unitary with ancillas. Its success probabilities on the four basis states are $1/2, 1/2, 1/2, 0$. Postselection implements K with state-dependent success; normalizing the selected outcome is not the original linear map μ.

For a closed genus-$g \geq 2$ surface a pants decomposition has $2g - 2$ pieces and $3g - 3$ sewn curves. Conformal sewing adds moduli-dependent propagators and analytic consistency [96]; string amplitudes need worldsheet, ghost and integration data beyond this finite tensor. A pants network or a hyperbolic graph is likewise not an AdS/CFT duality or a Ryu–Takayanagi derivation [97]. Such interpretations remain specified research targets until their extra structure is constructed. Arithmetic/anabelian reconstruction additionally requires arithmetic profinite fundamental-group data and its Galois structure under the proper field/curve hypotheses. Neither a discrete F_2 graph nor a coefficient $\mathbb{F}_2$ module supplies that arithmetic extension [98].

33.3.4 Quantum games and the Connes-embedding distinction

For uniform input bits x, y, CHSH accepts outputs u, v when $u \oplus v = xy$. With ± 1 observables its success probability is $1/2 + \langle T \rangle/8$, where

$$T = A_0 \otimes (B_0 + B_1) + A_1 \otimes (B_0 - B_1).$$

For a deterministic classical assignment one bracket vanishes and the other is ± 2, giving success at most $3/4$; all sixteen assignments are checked. On $|\Phi^+\rangle$, take $A_0 = Z, A_1 = X$, $B_0 = (Z + X)/\sqrt{2}, B_1 = (Z - X)/\sqrt{2}$. Then $T = \sqrt{2}(Z \otimes Z + X \otimes X)$ gives success $(2 + \sqrt{2})/4$. For arbitrary self-adjoint involutions, $T^2 = 4I - [A_0, A_1] \otimes [B_0, B_1]$ and each commutator has norm at most two. Hence $\|T\| \leq 2\sqrt{2}$, proving optimality. The exact matrix checker verifies the entire spectrum $\{-2\sqrt{2}, 0, 0, 2\sqrt{2}\}$, not just a numerical sample.

MIP*=RE, in its pinned v4, gives an external unrestricted correlation separation and a negative answer to Connes embedding [99]. We do not rerun its external formalization or claim a new proof of it. CHSH has its optimum on two qubits and the same commuting optimum by the preceding bound; it does not exhibit the general separation. A learned game strategy is useful for finite witness search and checked bounds, but unrestricted computability and dimension quantifiers cannot be settled by a finite game simulation.

33.3.5 Tropical accelerator reference designs and reproducibility

The chip-design campaign pins twenty public repositories, twenty-four focused document ranges and thirteen primary papers. It covers AlphaChip/Circuit Training, independent macro-placement

benchmarks, OpenROAD-family flows, quantum layout and low-level control. The source ledger records what was actually read, not a full audit or reproduction of every model. An exact public identity for the phrase “bare-metal Qiskit” was not established; no repository was invented.

Three original executable references implement a masked signed max-plus tile, an ordered mixed MAC/max-plus scheduler and a fail-closed synthetic IQ steering controller. Wide addition precedes winner selection and final saturation; earliest-index tie handling is explicit. Empty masks remain invalid, not an extra candidate of value zero. The controller requires a current calibration epoch, enough samples and a valid margin/deadline before allowlisting a steering action. Checks include all 65,536 signed eight-bit additions, 262,144 masked two-lane cases, reordered completions and twelve negative controls. These are digital reference models, not synthesized RTL, routed chips, measured RF feedback, power/area estimates or universal hardware speedups. A tropical context block can avoid multiplications inside that primitive while its projections, scores and other layers still require their own arithmetic.

The Linux snapshot preserves the Mac project, source clones, histories, checkpoints and environment archives. Linux GPU execution uses the existing Torch CUDA environment and a separately approved isolated cuQuantum prefix; macOS binaries are not treated as a Linux installation. The conda lock, setup instructions, gate/head replay records and all failures are retained. The on-page book contains one canonical laboratory for this chapter and links all five new checkpoint architectures into the existing tensor inspector. New physics, width and homological results have their explicit prose/numerical/external status; selected earlier Lean components do not constitute a full formalization of this extension or a proof of GRH.

33.4 Learning objectives with explicit analytic guarantees

A useful learned contribution must distinguish approximation of known L-functions from proof of their zero locations. We propose holomorphic coefficient/readout learning, certified contour losses, arithmetic trace and functional-equation residuals, Schatten-controlled operator refinement, certificate search for the original signed moment, and exact-algebra representation constraints. Each has a different acceptance test.

For an analytic target on $|s-c| \le r$, let $|F| \le M_r$ there and choose $R < \rho < r$. A degree-N holomorphic readout trained on $m > N$ equally spaced points of the radius-ρ circle has the explicit uniform error budget

$$\|p_k - F\|_{|s-c|\le R} \le E_{\mathrm{opt}}(k) + E_{\mathrm{oracle}} + E_{\mathrm{alias}} + E_{\mathrm{Taylor}}.$$

The following proofs give all four terms, a primitive-Dirichlet arithmetic bound for M_r, and an infinite-feature kernel limit with its actual rates. Thus known analytic families can be approximated to arbitrary requested accuracy with independently certified evaluation error. This does not prove GRH. Uniform approximation by an already-real-zero determinant class is a different, potentially GRH-equivalent requirement; it must not be assumed through an alleged universal-approximation theorem.

33.5 A certifiable analytic learning lane

33.5.1 Targets, fields and arithmetic scope

The output is a complex holomorphic function, not an unconstrained real MLP on $\mathbb{R}^2$. Fix a center c and a finite family of targets F_χ analytic on a neighborhood of the closed radius-r disk. Certified

values of $M_{r,\chi} \geq \sup |F_\chi|$ and of an evaluation error η are inputs to the quantitative theorem. They must be obtained without GRH or the desired arithmetic positivity. A finite conductor family uses the maximum of its independently bounded constants; this is not a uniform theorem over all conductors. Arithmetic character data are exact discrete inputs, not rounded embedding labels.

For primitive nonprincipal Dirichlet characters, the completed function is entire and a direct bound is given below. Pole-cleared zeta/Dedekind targets and known holomorphic Hecke or elliptic targets require their own explicit normalization and growth bounds. General Artin holomorphy is not assumed. Approximating on a compact domain avoiding possible poles does not prove that those poles are absent. Real/complex analytic norms, finite-field algebra and tropical semirings must likewise retain their distinct meanings.

33.5.2 A finite holomorphic readout theorem

Write $F(c+z) = \sum_{n\geq 0} a_n z^n$ and choose $0 < R < \rho < r$, integers $m > N \geq 0$ and sample angles $\theta_j = 2\pi j/m$. Let $|y_j - F(c+\rho e^{i\theta_j})| \leq \eta$, including all quadrature and rounding errors. The model and empirical objective are

$$p_b(c+z) = \sum_{n=0}^{N} b_n (z/\rho)^n, \qquad \mathcal{L}(b) = \frac{1}{2m} \sum_{j=0}^{m-1} \left| \sum_{n=0}^{N} b_n e^{in\theta_j} - y_j \right|^2 .$$

This is a fixed holomorphic feature layer and a learned complex linear readout. It is a genuine convex learning problem; no nonlinear feature-learning claim is attached to its guarantee.

Proposition 33.3 (Four-part uniform error bound)**.** *Put $u = R/\rho$, $v = R/r$ and $w = (\rho/r)^m$. Let $b_n^* = m^{-1} \sum_j y_j e^{-in\theta_j}$, and take gradient descent with $0 < \gamma < 2$. After k steps from b^0, on $|s - c| \leq R$,*

$$|p_{b^k}(s) - F(s)| \leq \frac{|1-\gamma|^k \|b^0 - b^*\|_2}{\sqrt{1-u^2}} + \eta \frac{1-u^{N+1}}{1-u} + M_r \frac{w}{1-w} \frac{1-v^{N+1}}{1-v} + M_r \frac{v^{N+1}}{1-v}.$$

The terms are optimization, certified sample error, Cauchy aliasing and analytic truncation, respectively.

Proof. Discrete Fourier orthogonality gives $A^*A/m = I$ for $A_{jn} = e^{in\theta_j}$, since $m > N$. In real and imaginary coordinates the gradient is $b - b^*$; hence $b^k - b^* = (1-\gamma)^k (b^0 - b^*)$. Cauchy–Schwarz bounds its evaluation by $\|b^k - b^*\|_2 (\sum_{n=0}^{N} u^{2n})^{1/2}$, giving the first term. The displayed iteration is in exact arithmetic. A numerical FFT/GD implementation must also bound coefficient-rounding error; a coefficient error of norm d_k adds at most $d_k/\sqrt{1-u^2}$ to the evaluation budget. This is convergence to the projected least-squares optimum; the empirical residual need not vanish when the labels have components outside the model.

For exact samples, the Fourier coefficient divided by ρ^n is $a_n + \sum_{\ell \geq 1} a_{n+\ell m} \rho^{\ell m}$. Uniform convergence on the sampling circle permits interchanging sums. Cauchy's estimate $|a_j| \leq M_r r^{-j}$ bounds the alias by $M_r r^{-n} w/(1-w)$. Sample errors contribute at most $\eta \rho^{-n}$. Multiply by R^n, sum the two finite geometric series and add $\sum_{n>N} M_r (R/r)^n$. These are exactly the last three terms. □

Choose N, then $m > N$, then η and the optimization tolerance so that each displayed term is at most $\varepsilon/4$. All four can tend to zero; thus any fixed compact subdisk and finite independently bounded target family have arbitrary-accuracy approximation. This claim needs a certified oracle bound, not an empirical test-set MSE. The present high-precision demonstrator is explicitly numerical and does not relabel its floating evaluations as interval certificates.

33.5.3 The infinite-width limit and its actual rate

Choose $R < \rho < r_0 < r$ and use features $\phi_n(z) = (z/r_0)^n$. Their kernel has the compact-uniform limit

$$K_N(z,w) = \sum_{n=0}^{N} \phi_n(z)\overline{\phi_n(w)} \longrightarrow K(z,w) = \frac{1}{1 - z\bar{w}/r_0^2}.$$

The geometric tail proves this limit directly; positivity follows because each quadratic form is a sum of squared feature combinations. The readout space is the sequence space ℓ^2 with bounded evaluation on $|z| < r_0$. On the radius-ρ circle its population coefficient Gram operator is diagonal with eigenvalues $\lambda_n = (\rho/r_0)^{2n}$.

Proposition 33.4 (Infinite-feature readout convergence)**.** *Suppose the initial coefficient error $e(0)$ is in ℓ^2, as for zero initialization and the analytic target above. Population gradient flow has $e_n(t) = e^{-\lambda_n t}e_n(0)$ and converges in ℓ^2, hence uniformly on every $|z| \le R < r_0$. If $\beta > 0$ and $\sum_n \lambda_n^{-2\beta}|e_n(0)|^2 \le B_\beta^2$, then*

$$\|p_t - F\|_{|z|\le R} \le \frac{B_\beta}{\sqrt{1-(R/r_0)^2}} \left(\frac{\beta}{et}\right)^{\beta}, \qquad t > 0.$$

For zero initialization this source condition holds whenever $(r_0/r)(r_0/\rho)^{2\beta} < 1$, with $B_\beta \le M_r[1 - ((r_0/r)(r_0/\rho)^{2\beta})^2]^{-1/2}$.

Proof. The diagonal loss gives the scalar ODE in each coordinate. Dominated convergence, with majorant $|e_n(0)|^2$, proves norm convergence. Evaluation is bounded by the geometric-series factor. Under the source condition, $\|e(t)\|_2 \le B_\beta \sup_{\lambda>0} \lambda^\beta e^{-t\lambda}$; the maximum occurs at $\lambda = \beta/t$. Cauchy's coefficient estimate gives $|a_n r_0^n| \le M_r(r_0/r)^n$, and summing the resulting geometric series proves the explicit source bound. □

There is no width-uniform exponential rate: $\lambda_n \to 0$. At finite degree the slowest mode has rate $(\rho/r_0)^{2N}$. Fourier whitening recovers the identity Gram matrix in Proposition 33.3, but its unbounded infinite-dimensional preconditioner must not be called a free uniform rate. Ridge adds a positive rate floor and a calculable bias; its coefficient bias factor is $\alpha/(\lambda_n + \alpha)$, and α must tend to zero for unbiased convergence. A standard Gaussian-process initialization need not lie in the kernel's RKHS; the stated ℓ^2 hypothesis cannot be silently applied to it. These exact fixed-feature statements are distinct from the nonlinear NTK limits of deep networks [110] and from the trained few-qubit feature-learning circuits.

33.5.4 An unconditional primitive-Dirichlet size oracle

For a primitive nonprincipal character of conductor q, parity $a \in \{0,1\}$ and root number $|\epsilon_\chi| = 1$, put $d = \pi/q$ and $\theta_\chi(t) = \sum_{n\ge1} \chi(n)n^a e^{-dn^2t}$. The standard primitive theta transformation and Mellin identity give

$$\Lambda(s,\chi) = \int_1^\infty \theta_\chi(t)t^{(s+a)/2-1}\,dt + \epsilon_\chi \int_1^\infty \theta_{\bar\chi}(t)t^{(1-s+a)/2-1}\,dt.$$

The character conjugation and root number are retained. These standard functional/analytic inputs are unconditional in the stated Dirichlet scope [111]; this text does not claim a new Lean proof of Poisson summation. Exponential decay makes both integrals entire in s.

For $|s-c| \le r$, choose an integer $k \ge \max(0, (1+|\operatorname{Re} c|+r+a)/2-1)$ and define

$$Q_k(x) = \sum_{j=0}^{k} \frac{k!}{(k-j)!x^{j+1}}.$$

Integration by parts gives $\int_1^\infty t^k e^{-xt}\,dt = e^{-x}Q_k(x)$. Consequently $M_r = 2\sum_{n\ge1} n^a e^{-dn^2} Q_k(dn^2)$ is a valid finite upper bound. For a computable finite version, choose $n_0 \ge 1$ and sum through $n_0 - 1$; the remaining one-integral sum is at most

$$C_a Q_k(dn_0^2)\frac{e^{-dn_0^2/2}}{1-e^{-dn_0}}, \qquad C_0 = 1, \quad C_1 = (de)^{-1/2}.$$

Indeed $n^a e^{-dn^2/2} \le C_a$, Q_k decreases, and $(n_0+j)^2 \ge n_0^2 + 2n_0 j$. Twice this tail covers both Mellin terms. The same bound controls theta truncation, with no assumption about zeros.

After truncating the n sum and the t integral, elementary interval exponential, logarithm, sine and cosine evaluation on a compact interval, with a bounded-derivative quadrature remainder, gives an arbitrary requested certified η. The explicit exponential tails control both truncations. This proves computability of the oracle; it does not assert that an ordinary high-precision special-function call is already a validated implementation. For a finite conductor cutoff, take the maximum of the computed bounds.

33.5.5 Additional objectives and what they can certify

Contour-aware approximation and active learning.

Augment the coefficient objective with independent interval enclosures of $|p-F|$ on contours, derivative-weighted losses and adaptive samples near small $|p|$. If $\sup_C |p-F| < \inf_C |p|$ on a Jordan contour, Rouché's theorem transfers the exact interior zero count of p to F. An interval root count and a strict margin are acceptance conditions. Sampling finitely many heights alone proves no exhaustion of the off-critical domain.

Arithmetic and functional-equation residuals.

Use exact character masks, conductor dependence, primitive Euler factors, gamma normalization and the conjugate functional equation as structural features or independently verified residuals. On $\operatorname{Re} s \ge 1+\delta$, with $\delta > 0$, for $N \ge 3$ the logarithmic-derivative Dirichlet tail has the elementary bound $N^{-\delta}(\log N/\delta + 1/\delta^2)$, from $\Lambda(n) \le \log n$ and integral comparison. This is a useful certified training region; it does not extend absolute convergence into the critical strip. A functional equation alone also does not locate zeros.

Operator and determinant refinement.

Learn compatible finite compressions, graph-norm/domain residuals, self-adjoint boundary conditions and uniform Schatten-tail bounds from the actual infinite dessin/order construction. Trace-norm convergence transfers ordinary Fredholm determinants, with the standard bound

$$|\det(I+A) - \det(I+B)| \le \|A-B\|_1 e^{1+\|A\|_1+\|B\|_1}$$

[112]. Strong resolvent convergence alone does not supply this bound. A reciprocal critical-spectrum model typically needs a genus-one regularized determinant and Hilbert–Schmidt control; it must not silently be treated as trace class. The arithmetic determinant identification remains an independent obligation even when the learned operators are Hermitian.

Certificate-guided moment and algebra learning.

For the actual original-family low-gcd moment, use adversarial legal masks, conductors, short rows and retained II–I covariance to search for a sharp envelope or counterexample. Rational/interval or exact symbolic checking must certify a proposed inequality uniformly. A sum-of-squares or dual certificate can prove its stated parameter box; extrapolating it to all conductors needs a separate analytic argument. Preserve exact locally gentle relations, surface-order completions, determinant semi-invariant weights and module category labels in the representation architecture. Small relation loss is not an exact functor or an arithmetic comparison.

Quantum kernels, width and proof search.

Quantum feature Gram positivity is not Weil/arithmetic positivity. A proved finite Gram lower bound gives a readout rate, while growing width requires the actual limiting kernel and initialization hypotheses. Proof-guided co-training can learn proposed identities or compression maps, then export rational/algebraic candidates for independent Lean/interval validation. Validation, rather than a confidence score, decides which claims survive.

33.5.6 A decisive obstruction to a false universal guarantee

Proposition 33.5. *No sequence of real-rooted polynomials converges locally uniformly on* $\mathbb{C}$ *to* $1+z^2$*. Every such polynomial has error at least* $7/16$ *somewhere on* $|z-i|=1/4$*.*

Proof. On that circle, $|1+z^2| = |z-i||z+i| \geq (1/4)(2-1/4) = 7/16$. A smaller uniform error would, by Rouché, force a zero of the polynomial inside the disk, whereas all of its zeros are real and the disk misses the real axis. The same argument excludes local-uniform convergence. □

Thus a claim that an everywhere-real-zero/self-adjoint determinant family universally approximates the completed arithmetic target may already contain the missing GRH bridge. Hurwitz transfers zero-freeness only after independent local-uniform convergence and a nonzero limit have been proved. The analytic learner above deliberately proves approximation without asserting that spectral restriction. Its learned functions are evidence-bearing candidates, not a completed GRH proof. All new analytic/probabilistic statements here are prose proofs and scoped computations; no complete new Lean layer is claimed.

33.5.7 Exact rational constants without transcendental rounding

The next implementation step certifies growth and analytic-tail constants, while leaving sample evaluation and coefficient rounding separate. Put $\delta = 3/q < \pi/q$ and, for an integer $L \geq 1$, define

$$U_L(x) = (1+x/L)^{-L}, \qquad x > 0.$$

The binomial coefficients give $(1+x/L)^L \leq \sum_{j\geq 0} x^j/j! = e^x$, so $e^{-x} \leq U_L(x) < 1$. Every evaluation of U_L at a positive rational argument is exact rational. With the same Q_k as above, choose $n_0 \geq 1$ and let

$$\widehat{M} = 2\left[\sum_{n=1}^{n_0-1} n^a U_L(\delta n^2) Q_k(\delta n^2) + C_a Q_k(\delta n_0^2) \frac{U_L(\delta n_0^2/2)}{1-U_L(\delta n_0)}\right], \quad C_0 = 1, \quad C_1 = \frac{1+\delta^{-1}}{2}.$$

This rational number bounds $|\Lambda(s,\chi)|$ on the specified disk. Indeed decreasing d to δ increases the positive integral majorant. For $a=1$, the maximum of $xe^{-\delta x^2/2}$ is $(\delta e)^{-1/2} \leq \delta^{-1/2} \leq (1+\delta^{-1})/2$.

Split the Gaussian exponent into two halves, use $(n_0 + j)^2 \geq n_0^2 + 2n_0 j$, and sum the resulting geometric tail. Replacing its numerator and ratio by U_L increases the bound, since its denominator stays strictly positive. This proves the formula.

For the actual conductors $3, 4, 5$, center $1/2$, radius $12/5$, $n_0 = 8$ and $L = 16$, exact fraction arithmetic gives respectively $\widehat{M} < 4$, $\widehat{M} < 10$, $\widehat{M} < 6$. Using $\widehat{M}$ (or these integer upper bounds) and the rational radii $R = 7/10$, $\rho = 6/5$ makes the Cauchy-alias and Taylor terms exact rational certificates as well. Full numerator/denominator records and the executable `certify_learning_constants.py` are supplied. This certifies constants, not the complex sample oracle, floating optimizer or GRH.

33.6 Learning nonlocal strategies and checking their certificates

A two-player nonlocal game samples questions x, y and scores outputs a, b. The players may share a state, but communicate neither questions nor outcomes during play. Our finite tensor strategies have $p(a, b|x, y) = \mathrm{Tr}[\rho(P_a^x \otimes Q_b^y)]$. Offline joint optimization is allowed and is distinct from communication during the game. We train local measurement frames and a Schmidt angle using the exact Born objective, and replay actual checkpoints, probabilities, correlations, word moments and simulated shots in the interactive laboratory.

For $0 \leq \alpha \leq 2$ use the tilted score

$$S_\alpha = \alpha\langle A_0\rangle + \langle A_0B_0 + A_0B_1 + A_1B_0 - A_1B_1\rangle.$$

Its classical maximum is $2 + \alpha$; its quantum maximum is $\sqrt{8 + 2\alpha^2}$ [113]. At $\alpha = 0$ the uniform CHSH winning probability is $1/2 + S_0/8$. This conversion does not apply unchanged to the tilted objective. The three seeds for each of $\alpha = 0, 1, 3/2$ give nine trained runs. One $\alpha = 3/2$ run remains at the classical value 3.5; the other runs reach the stated quantum maxima numerically. This retained failure rules out a claim of universal convergence of the optimizer.

The magic-square task uses two Bell pairs, local four-dimensional joint measurements, row parity $+1$ and column parities $(+1, +1, -1)$. Its classical value is $8/9$ and its quantum value is 1, as proved below. Three further trained local-frame runs reach values within $3 \cdot 10^{-13}$ of one. All twelve runs are small CPU simulations with saved seeds and parameters, not hardware Bell experiments or evidence for quantum training advantage.

These examples belong to both the closure of finite tensor correlations C_{qa} and the commuting-operator set C_{qc}. The external theorem $\mathrm{MIP}^* = \mathrm{RE}$ separates these sets and implies the negative answer to Connes embedding [115]. We do not reproduce that theorem. Finite learned strategies, positive state Gram matrices and finite NPA constraints do not witness its separation.

33.7 Exact game calculations and the embedding boundary

33.7.1 CHSH bounds and a constructive tilted strategy

For deterministic signs, either $B_0 = B_1$ or $B_0 = -B_1$, so the CHSH term is at most 2; choosing $A_0 = 1$ gives the tilted classical maximum $2 + \alpha$. Convex mixtures cannot improve a linear objective. For self-adjoint involutions, with operators of different parties commuting, write $\mathcal{B} = A_0(B_0 + B_1) + A_1(B_0 - B_1)$. The exact identity

$$2\sqrt{2}I - \mathcal{B} = \frac{1}{\sqrt{2}}\left[\left(A_0 - \frac{B_0 + B_1}{\sqrt{2}}\right)^2 + \left(A_1 - \frac{B_0 - B_1}{\sqrt{2}}\right)^2\right]$$

proves the CHSH quantum bound by positivity. Expanding the squares uses only the involution and cross-party commutation relations.

For the tilted case take $|\psi_\theta\rangle = \cos\theta|00\rangle + \sin\theta|11\rangle$, $A_0 = Z$, $A_1 = X$ and $B_{0,1} = \cos\mu Z \pm \sin\mu X$. Then $S_\alpha = \alpha\cos 2\theta + 2\cos\mu + 2\sin\mu\sin 2\theta$. Choosing

$$\sin 2\theta = \sqrt{\frac{4-\alpha^2}{4+\alpha^2}}, \qquad \tan\mu = \sin 2\theta$$

with $0 \le \theta \le \pi/4$ and $0 \le \mu \le \pi/4$, gives $\sqrt{8+2\alpha^2}$ by direct substitution (including the endpoints). This verifies attainment; the universal tilted upper bound uses the sum-of-squares theorem in [113] for $\alpha < 2$; the endpoint follows by continuity since $\|\mathcal{B}_2 - \mathcal{B}_\alpha\| \le 2 - \alpha$. This is not an unproved inference from our restricted two-qubit parametrization.

33.7.2 A full magic-square strategy

On two local qubits arrange the observables

$$\begin{pmatrix} Z\otimes I & I\otimes Z & Z\otimes Z \\ I\otimes X & X\otimes I & X\otimes X \\ Z\otimes X & X\otimes Z & Y\otimes Y \end{pmatrix} = (O_{ij}).$$

Entries commute within each row and column. Pauli multiplication gives row products $+I$ and column products $+I, +I, -I$. Alice measures a row, Bob the transpose of a column, and they share $|\Phi_4\rangle = \frac{1}{2}\sum_{k=0}^{3}|k,k\rangle$. The identity $\langle\Phi_4|A\otimes B|\Phi_4\rangle = \mathrm{Tr}(A^TB)/4$ gives correlation one at every intersection. The product identities force the required parities. Thus they win every question pair and the quantum value is one.

A classical perfect table would have total product $+1$ by multiplying the rows and -1 by multiplying the columns, a contradiction. At least one of the nine question pairs fails for any deterministic assignment. Conversely, Alice can output all $+1$; Bob outputs all $+1$ in the first two columns and $(-1,+1,+1)$ in the last, failing only one cell. The uniform classical value is exactly $8/9$; shared randomness cannot improve it. Our learner conjugates Alice's observables by one local unitary U_A and Bob's transposed observables by U_B, preserving each party's parity and commutation constraints at every optimization step. The exact score is $1/2 + \sum_{ij}\mathrm{Tr}(A_{ij}^TB_{ij})/72$.

33.7.3 Which learning objectives carry proofs?

Finite strategies and noisy experimental laws. Unitary parametrization preserves valid projective measurements, so negative Born loss searches inside the chosen finite strategy class. Mixing the state with I/d with visibility $v \in [0,1]$ preserves positivity, normalization and no-signalling. For K joint outcomes, N ideal independent samples and $\delta \in (0,1)$, Hoeffding plus a union bound gives maximum frequency error at most $\sqrt{\log(2K/\delta)/(2N)}$ with probability at least $1-\delta$. Browser sampling is an illustration of this conditional IID statement. With dimension fixed, compactness and explicit matrix-product Lipschitz bounds permit exhaustive finite nets for arbitrary-accuracy global value approximation. Local gradient descent alone has no such guarantee.

Moment and dual-certificate learning. For words u, v in measurement generators, define $\Gamma_{u,v} = \langle\psi|u^*v|\psi\rangle$ (or its mixed-state trace). For every c, $c^*\Gamma c = \|\sum_v c_v v\psi\|^2 \ge 0$; the mixed case follows by convexity. We compute these actual finite word Gram matrices, not an optimized outer relaxation. NPA learning may propose PSD moment matrices obeying word relations, while an

independently checked identity $\beta I - \mathcal{B} = \sum_j P_j^* P_j$ proves an upper bound. A small residual is not an exact certificate. Successive NPA levels converge to the commuting-operator value under the hierarchy's hypotheses [114]. Each level defines an outer relaxation; a validated optimized value or a dual-feasible certificate yields an upper bound. One feasible primal moment matrix alone does not bound the optimum and is not a realization theorem.

Tracial moments and Connes embedding. General vector-state moments need not be cyclic. A microstate learner for a tracial algebra must additionally preserve cyclic identities, positivity, norm bounds and compatibility across increasing word lengths, and compare with normalized matrix traces. Our displayed state moments do not fulfill that separate task merely because they are PSD. The external undecidability result [115] also precludes a single computable dimension/error schedule deciding all promised nonlocal games. It neither forbids certified solutions of specified finite games nor establishes any impossibility result for GRH. The valid connection to our program is certificate search with exact relation checks; neither Bell violation nor kernel positivity gives the missing arithmetic determinant/zero-location bridge. These new game proofs and computations are not claimed as complete Lean4 formalization.

33.8 Hubs, spokes and the topology retained by a dessin

The hubs-and-spokes construction in the HoTT book, Sections 6.6–6.8 [109], gives a useful language for attaching cells. For a loop $f : S^1 \to X$, form the homotopy pushout $X \cup_f CS^1$: add a fresh hub and paths from every $f(u)$ to that hub, continuously indexed by $u : S^1$. This attaches a disk, rather than merely a finite graph of radial edges. The book's Remark 6.7.1 explains why identifying the hub with an existing boundary point requires extra coherence; Remark 6.7.2 distinguishes propositional from judgmental computation.

For our dessins the useful distinction is geometric. A vertex star has a disk neighborhood with a specified cyclic ordering of its incident bands. Removing the disk center gives a punctured disk, which retains its peripheral loop. Removing only the vertex of a finite star instead leaves disconnected open rays. These operations cannot be interchanged. In a cellular dessin, filling a face imposes its attaching-word relation; leaving its center punctured retains a boundary component of the ribbon neighborhood.



disk
coherent circle of spokes

punctured disk
peripheral loop

The shaded regions are two-dimensional; the displayed finite spokes sample them. The annulus shown on the right is a deformation retract of the punctured disk, not a missing vertex in a one-dimensional graph.

Proposition 33.6 (Face filling changes the covering problem)**.** *Let a connected cellular dessin be a spine of an oriented genus-g ribbon surface with $n > 0$ boundary components. Its graph fundamental*

group is free of rank $2g + n - 1$*. Capping all boundary components gives the presentation*

$$\left\langle a_1, b_1, \ldots, a_g, b_g \;\middle|\; \prod_{i=1}^{g} [a_i, b_i] = 1 \right\rangle.$$

For the one-face clean dessins $K_{2,3}$ *and* $K_{2,5}$ *used here, these free ranks are respectively* 2 *and* 4*, before capping.*

Proof. A spanning-tree collapse of the connected spine leaves $E - V + 1$ circles. The ribbon surface retracts onto that spine and has Euler characteristic $2 - 2g - n = V - E$, proving the rank formula. Cutting a surface along a standard system of handle arcs gives the boundary word $\prod_i [a_i, b_i] \prod_j c_j$. Van Kampen therefore presents its group by these generators and this one relation. With a boundary present, eliminate c_n, leaving the stated free group. Capping attaches disks along the c_j, so van Kampen sets each $c_j = 1$, giving the closed-surface presentation. For our rotations on $K_{2,m}$, both black vertices have the same cyclic order on the m incident edges. Suppressing the bivalent white vertices gives dart rotations $(0 \cdots m-1)(m \cdots 2m-1)$ and involution $i \leftrightarrow i + m$. The face permutation is one $2m$-cycle for odd m. Thus $V = m + 2$, $E = 2m$, $F = 1$, and $g = (m-1)/2$, giving both examples. □

The once-punctured torus and closed torus both have $H_1 \cong \mathbb{Z}^2$, but their groups are F_2 and $\mathbb{Z}^2$; only the closed torus has $H_2 \cong \mathbb{Z}$. The analogous genus-two groups are F_4 and the four-generator surface group, with $H_1 \cong \mathbb{Z}^4$ in both cases. Indeed the standard closed-surface cellular complex has one vertex, $2g$ edges and one face. The face word is a product of commutators, so its abelianized boundary is zero. Removing the face leaves the wedge of circles. This computes the stated homology and also explains why H_1 alone misses the face relation. The torus group is abelian while F_2 is not; in higher genus the closed surface has nonzero H_2 while the graph does not.

Consequently the graph's universal cover is a tree, whereas the universal cover of the filled genus-two surface includes lifted faces and is a disk. Collapsing a spanning tree changes the combinatorial cover graph; the Cayley tree of a free basis is not literally the original biregular dessin cover. This distinction matters when lifting strings, periodic paths and boundary conditions in the infinite locally gentle algebra.

The gluing language organizes local patches and their compatibility maps. It does not reconstruct the ribbon cyclic order, complex structure, Belyi map, quadratic zero relations, coefficient ring or polynomial/formal/operator completion from the homotopy type alone. These data are retained explicitly in the existing dessin and order constructions. Descent of modules, derived categories, Hom-control, AR meshes or Fukaya categories needs a separately defined functor and hypotheses; a homotopy pushout of underlying spaces is not such a theorem. Nor does it imply an arithmetic determinant identity.

The accompanying tool computes the same one-face genus-one/two/four dart families and draws local disk/annulus patches and their surface polygon presentations, peripheral loops and face words. These are exact finite combinatorial checks plus the topological proof above. HoTT is referenced as a conceptual foundation; no univalence or higher inductive-type axiom is added to the pinned Lean4 development. Its complete cell-attachment and categorical formalization remains an explicit task.

Chapter 34

Complementary physical datasets, dynamics and geometric inspection

34.1 Complementary physical datasets and checked dynamics

The learned program now has two additional, separately constructed corpora: 16,384 effective-material response records and22,951 molecular conformer/force records in their default configurations. Time samples are not counted as independent systems. Source-linked and dynamical configurations are additional. The active HolonForge/Aster and Mora-3 repositories were read only; no data, vocabulary, checkpoint, source enrollment or training process was changed.

The material corpus covers SSH, Kitaev, QWZ, Rice–Mele, Harper and actual clean-dessin classical RG models. The molecular corpus includes designed amides and peptides, with explicit-H MMFF94 calculations, geometric persistence, and method-labelled conformations. Forty-eight existing Aster MP20 structures, 32 existing Mora PubChem identities and eight public PDB structures supply separately labelled anchors. Their new computed responses are not new experimental observations, DFT labels, binding affinities or CISS measurements.

All conformer, gauge, intervention and task descendants share a partition. Specified physical/chemical similarity edges are closed transitively before component-level stratification. Large components are kept intact even when 80/10/10 proportions or rare-class coverage become impossible. This gives a finite, threshold-relative separation statement; it cannot guarantee every kind of statistical independence or prevent overfitting. Source anchors are train only. Molecular anchors are also checked against every default heldout using the same chemical and applicable geometric thresholds; conflicting parent groups are excluded. Global exposure to the models' previous corpora is a separate evaluation gate.

For a number-conserving one-particle Hamiltonian H, write $P_{ij} = \langle c_j^\dagger c_i \rangle$ and $U(t) = e^{-itH}$. The data use $P(t) = U(t)P(0)U(t)^*$, occupations $n_i = P_{ii}$ and outgoing currents $J_{ij} = -2\,\mathrm{Im}(H_{ij}P_{ji})$. Then $\dot{n}_i = -\sum_j J_{ij}$, directly from $i\dot{P} = [H, P]$. Paired BdG evolution includes its independently computed condensate source; it is not falsely treated as electron-number-conserving normal transport. An exact interacting Hubbard dimer supplements Gaussian exchange correlations. Molecular nuclear dynamics uses MMFF94, with a separately labelled, uncalibrated effective π-orbital model for charge modulation.

Parquet configurations retain condition, target and evaluation roles, source versions/hashes, units, failures and audit evidence. The local dataset explorer shows actual structures, currents, time evolution, graph wavelets and checked circuit compilations. These computations support candidate discovery and model validation; the independent arithmetic determinant/zero-location

bridge remains open. No new whole-chapter Lean formalization is asserted.

34.2 Construction, curation and interpretation

34.2.1 A record is an evidence-bearing physical task

Each default Parquet row has a persistent record identity, parent/similarity group, partition, evidence class, lossless scientific payload and typed numeric columns. Forward inputs have the prefix `condition_`; supervision uses `target_`; `evaluation_` fields are excluded from inputs. The full payload, source hash, record identifier and audit text are not automatically fed into a model. Otherwise an apparent condition/target mask could still leak the target through metadata or a duplicated representation. An inverse task needs an explicit desired-condition contract and role change.

The origin fields distinguish a new simulation from a reused planned-source identity or geometry with new labels. The source-anchor configuration preserves existing train assignments. New public PDB coordinates retain their own source identity rather than being called members of PDBbind or newly acquired experimental quantum measurements. All anchors are train only: they do not establish blind performance on a model that may have encountered the parent.

The actual native interfaces are tested without changing either model. Aster accepts condition-only Hamiltonian records through its existing tokenizer. Changing a hidden target leaves those input tokens unchanged. Mora-3's scalar graphs preserve computed/predicted evidence. Its existing scalar/array supervision interfaces reject those targets under their observed-only policy. That rejection is recorded, not bypassed by changing the evidence label. Source construction is therefore distinct from the owning model's future admission, scaling, objective and evaluation decisions.

34.2.2 Effective material families and gap guards

The two-band QWZ model uses

$$H(k_x, k_y) = \sin k_x\, \sigma_x + \sin k_y\, \sigma_y + (m + \cos k_x + \cos k_y)\sigma_z.$$

Its continuum band gap is $2\min\{|m+2|, |m|, |m-2|\}$. To see this, put $u = \cos k_x$, $v = \cos k_y$. The squared positive energy is $2 + m^2 + 2m(u+v) + 2uv$, a bilinear function on $[-1,1]^2$; its minimum occurs at a corner. Thus an odd mesh that misses π cannot certify a gap near $m = 0$ or2. The corrected release uses this analytic guard, even32/64 meshes, random gauge checks and an unavailable label near closure. The occupied-band integer uses the oriented link-product convention of Fukui–Hatsugai–Suzuki [100]; the sign convention is retained in the row.

For the Rice–Mele pump, take $t_1 = 1 + \delta\cos\theta$, $t_2 = 1 - \delta\cos\theta$ and $\Delta = r\sin\theta$. With positive t_1, t_2, minimization over k first gives $(t_1 - t_2)^2 + \Delta^2$ at $k = \pi$; minimization over θ gives the exact gap $2\min(2\delta, r)$. Harper's direct gap has a conservative mesh/Lipschitz guard, explicitly distinguished from interval certification. The displayed bulk slice has $k_y = 0$; an open strip is evaluated separately at $k_y = .37$. A single strip is not a proof of its entire edge dispersion.

The SSH winding, Kitaev sign invariant and classical dessin RG retain their own hypotheses. Surface genus is not an electronic phase index. In the Kitaev row, a physical onsite defect changes particle and hole diagonals with opposite signs. Its gauge change has the form $\mathrm{diag}(G, \bar{G})$. These preserve the recorded particle–hole symmetry; arbitrary independent diagonal perturbations would not. A quarantined draft revealed this error before release. No failed draft replaces a verified artifact.

34.2.3 Molecular geometry and forces

The molecular set contains explicit chemical graphs, atom order, hydrogens, stereochemistry, method-labelled optimized references and bounded coordinate perturbations. MMFF94 supplies empirical molecular-mechanics energies, analytic forces and partial charges [101]. It supplies neither ab-initio electron density nor experimental affinity, ADMET, redox or biological efficacy. An optimization convergence code is not a theorem of a unique global minimum. Absolute MMFF energies are not cross-molecule atomization energies.

The checker reconstructs the stored bond graph in its *actual atom order*. A canonical SMILES string determines chemical identity but need not give the coordinate-array order. Geometry-assigned stereochemistry is checked against that identity; mirror controls fail. Energies and forces are recalculated on every accepted record. Central energy differences check force signs/units, and proper rotations/translations check the expected scalar/vector behavior. Missing or unsupported labels are not imputed.

For the heavy-atom point cloud, the complete finite Vietoris–Rips2-skeleton gives H_0, H_1 over $\mathbb{F}_2$. All edges and triangles, including ties, are ordered explicitly. Independent boundary-rank calculations verify selected Betti numbers against the barcodes. These are geometric distance-filtration features; a molecular loop or persistence bar is not an electronic topological phase. MMFF and the idealized π-orbital Hamiltonian retain separate labels.

34.2.4 What the split certificate proves

Let V be the finite parent set and connect two parents whenever a declared similarity test passes. Add edges for all shared source/variant lineages. Assign a partition to each connected component and inherit it for every row. If an accepted similarity edge joined two partitions, its endpoints would lie in one component with two assignments, a contradiction. This proves the exact finite no-crossing property for the declared relation.

For materials, normalized parameter and relative finite-spectrum thresholds are family/size-specific. SSH hopping swaps, Kitaev chemical-potential sign and the classical RG global-sign symmetry are folded conservatively. For molecules, stereo-agnostic constitution, nonempty Murcko scaffold and radius-two Morgan Tanimoto threshold .65 form chemical components. A second all-conformer pass adds edges for equal heavy-element multisets with sorted pair-distance RMS at most .10Å. This descriptor is rotation/permutation invariant but is not a complete congruence invariant or a certified RMSD optimizer; conservative false-positive grouping is possible.

Whole-component allocation balances row counts and declared family/topology or molecular-size/persistence strata. It never breaks a component to manufacture an80/10/10 result. The large peptide component makes the molecular training partition much larger than80%; rare/held-out peptide coverage can consequently be absent. Exact distributions and cross-partition nearest witnesses accompany the release. Protein TM-score, homology separation and global overlap with the models' complete historical corpora are not certified by small-molecule fingerprints. Threshold separation cannot itself guarantee freedom from all leakage or overfitting.

34.2.5 Motion, charge modulation and exchange

For normal free fermions, $P(t) = UP(0)U^*$ preserves Hermiticity, trace and the spectrum: $P^* = P$ follows by adjoints, trace follows by cyclicity, and $P(t) = UP(0)U^{-1}$ is a similarity. Thus $0 \le P \le I$ and projector occupancy remain valid. Computing the diagonal of $-i[H, P]$ gives

$$\dot{n}_i = 2\,\mathrm{Im}\sum_j H_{ij}P_{ji}, \qquad J_{ij} = -2\,\mathrm{Im}(H_{ij}P_{ji}) = -J_{ji}.$$

The currents therefore obey site continuity and conserve total particle number. Their arrows represent probability/particle flux, not measured trajectories of individual electrons. Charge modulation is $-[n_i(t) - n_i(0)]$ in the declared electron-charge convention.

For a paired model, put $\Psi = (c, c^\dagger)$ and $R = \langle \Psi\Psi^\dagger \rangle$. From an initial Slater projector use $R_0 = \mathrm{diag}(I - P_0, P_0^{\mathsf{T}})$. Evolve with the full BdG Hamiltonian and recover $P = I - R_{11}$, $F = R_{12}$. The independently computed pairing source is

$$S_i = -2\,\mathrm{Im}(\Delta F^*)_{ii}, \qquad \dot{n}_i = -\sum_j J_{ij} + S_i.$$

The commutator derivative and this separate source formula agree in the checks; the source is not defined as the residual of the desired equation. For a Gaussian state, Wick's rule gives, for $i \neq j$, $\mathrm{Cov}(n_i, n_j) = |F_{ij}|^2 - |P_{ij}|^2$; on the diagonal it is $n_i(1 - n_i)$. The negative term is an exchange hole, not a computed Coulomb exchange-energy functional. Explicit small Fock-space evolution independently checks the covariance, current and pairing conventions.

The interacting control is the two-site Hubbard model at two electrons:

$$H = -t \sum_\sigma (c_{0\sigma}^\dagger c_{1\sigma} + \mathrm{h.c.}) + U \sum_{a=0}^{1} n_{a\uparrow} n_{a\downarrow}.$$

In its singlet/doubly-occupied symmetric sector the matrix is $\left(\begin{smallmatrix} 0 & -2t \\ -2t & U \end{smallmatrix}\right)$; the triplet energy is zero. Diagonalizing gives the exact exchange gap $J = (\sqrt{U^2 + 16t^2} - U)/2$, approaching $4t^2/U$ for large positive U. The full six-state two-electron sector supplies density, spin-swap and current trajectories; a separate16-state Jordan–Wigner calculation checks them. This finite dimer is not a thermodynamic phase classification.

For nuclei, velocity Verlet uses actual MMFF forces and masses, with explicit time/energy units, finite energy drift and momentum checks. A Grad-only RDKit loop initially reused stale distance information. Refreshing energy at the same coordinates before the gradient restored the expected second-order step-size behavior in independent refinement tests. Failed trajectories are retained and excluded. The finite isolated trajectories are not equilibrium sampling. MMFF charges remain fixed. The separate uncalibrated π graph has its own dimensionless electronic time; it is not self-consistent TDDFT coupled to the nuclear femtosecond trajectory.

34.2.6 Source-backed peptides and genuine boundaries

Public wwPDB coordinates are supplied under CC0 [102]. The source packet includes Trp-cage1L2Y, villin1VII, historical Trp-zipper1HRW (superseded by 1LE0, with the actual file HEADER identity retained), pancreatic polypeptide1PPT, azurin1AZU, crambin1CRN, ubiquitin1UBQ and engrailed homeodomain1ENH. The full source file, checksum, DOI, first-model/chain selection and bounded residue-subsystem mapping remain explicit. An NMR ensemble's model order is not physical time. Azurin's electron-transport classification does not calibrate our coarse contact Hamiltonian or turn it into an electronic-structure result.

The CISS review and peptide-bridge charge-transfer preprint motivate future spin, environment and lead benchmarks [103, 104]; the source review is focused, not an independent reproduction of their experiments. A spinless contact graph cannot supply their spin polarization, electron-transfer rates or measured quantum-biological mechanism. Synthetic strain, vacancy, mirror, coupling and conformer variants have their own provenance and share the parent group. They are additional training candidates, not newly observed systems.

34.2.7 Circuits and geometric visualization

For a normal one-particle unitary U, adjacent row elimination gives Givens matrices G_k and diagonal phases D with $U = G_1^* \cdots G_m^* D$. For a, b in one column, the eliminating block is

$$G = \frac{1}{\sqrt{|a|^2 + |b|^2}} \begin{pmatrix} \bar{a} & \bar{b} \\ -b & a \end{pmatrix}.$$

Direct multiplication gives $G(a,b)^{\mathsf{T}} = (r, 0)^{\mathsf{T}}$ and $G^* G = I$. A two-mode second-quantized gate acts as 1 on the vacuum, as its one-particle block on the single-occupation sector and as the determinant on double occupation. The exported circuit verifies these matchgates and numerical recomposition. Browser replay applies the actual gates to the saved initial correlation matrix. BdG pairing needs a different Bogoliubov compiler; it is not passed by a number-conserving Givens circuit. The Hubbard example instead includes Jordan–Wigner parity and measured product-formula convergence.

Actual molecular structures use CPK colors and explicit atom/bond order, with SDF/XYZ views, ball-and-stick, sticks and space-filling representations. Effective material-site layouts are labelled schematic. Electron-colored Gaussian splats are declared kernels on discrete site values, not ab-initio volumetric density. For the symmetric graph Laplacian L, localized wavelets are $sLe^{-sL}\delta_i$; since $\mathbf{1}^{\mathsf{T}} L = 0$, they have zero sum. Their signed colors are not probabilities. Time as a fourth projection coordinate is a visualization operation, not a new spatial dimension.

The dataset page links the checked public releases and source code. The full new probabilistic/homological/physical interfaces are not yet packaged in Lean; the existing 360 printed reports retain their earlier scope. Neither a simulated transport law, dataset split certificate nor a compiled finite circuit closes the arithmetic comparison required for GRH.

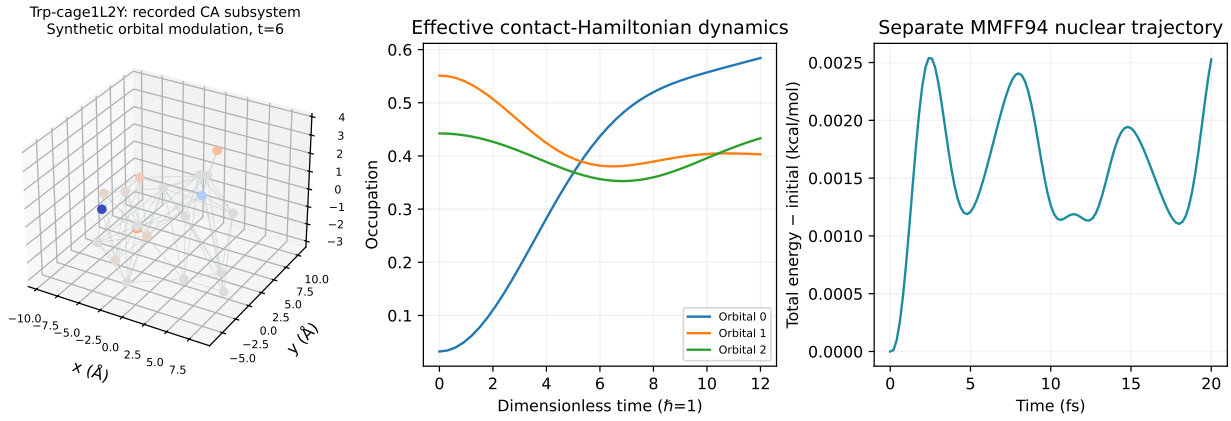


Figure 34.1: Actual source-backed and computed examples. Left: the recorded Trp-cage CA subsystem, colored by an uncalibrated contact-model orbital modulation. Middle: three of its finite orbital occupations. Right: total-energy drift of a separate explicit-H MMFF94 trajectory. Electronic time and nuclear femtoseconds are distinct; the contact model is neither an experimental transfer rate nor an ab-initio density. The interactive tool supplies the actual records and code.

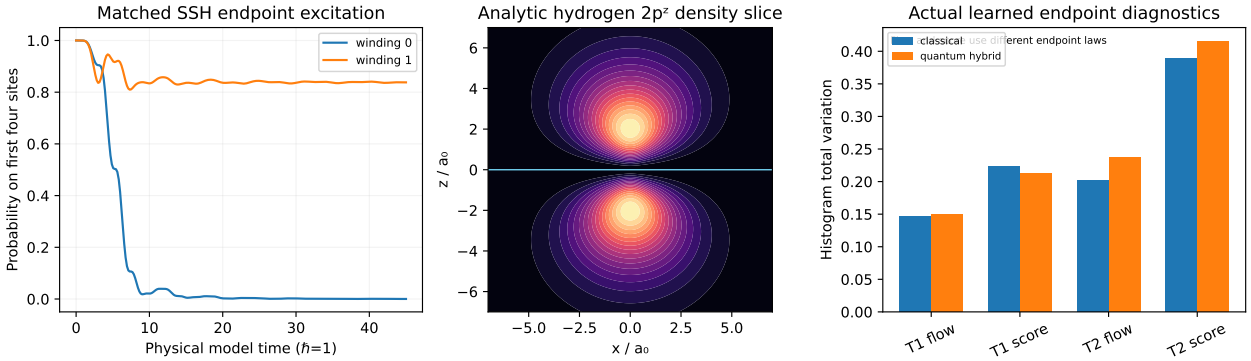


Figure 34.2: Computed matched SSH transport, an analytic hydrogen orbital slice and actual trained chemistry endpoint diagnostics. The diffusion endpoint retains positive heat time; its reference differs from the flow target. These finite results do not establish quantum advantage.

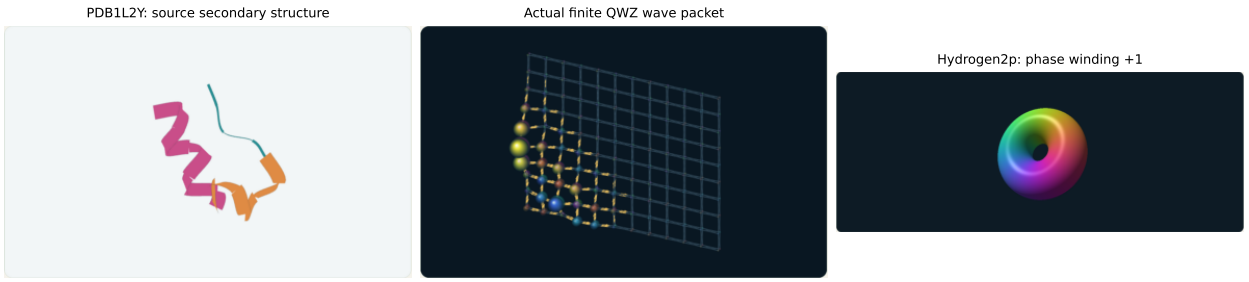


Figure 34.3: Native interactive renderings: deposited Trp-cage secondary structure, an actual finite QWZ wave packet and an analytic hydrogen phase vortex. Ribbon, probability-height and density-isosurface encodings have different source and physical meanings.

34.3 Molecular structure, complex transport and learned chemistry

The complementary-data laboratory now separates deposited protein structure, actual finite quantum transport and learned conformation generation. Covalent bonds use explicit molecular graphs or qualified PDB templates, with depth ordering and visible atom/bond scales. The ribbon view reads deposited `HELIX/SHEET` records; short synthetic peptide backbones remain unassigned rather than acquiring invented secondary structure.

Five additional finite propagation examples compare matched SSH/QWZ topological and trivial controls and an SSH domain wall. Complex phase, probability, current, coherence and selected eigenstates are distinct views. Analytic hydrogen volumes illustrate nodes, quantum beats and a phase vortex; they are not molecular electronic-structure calculations. Eight further CPU runs train classical and two-qubit hybrid score/flow models on periodic MMFF butane/pentane torsion spaces. All checkpoints, losses, controls and positive noise endpoints are explicit. These examples neither establish quantum advantage nor close the independent arithmetic bridge for GRH.

34.4 Geometry, orbitals and generative time

34.4.1 Chemical connectivity and source secondary structure

An atomic coordinate cloud does not determine chemical bonds merely by looking connected. SDF graphs retain their explicit bond indices. For the PDB source view we select the first model, blank/A alternate locations and positive occupancy; solvent is omitted from the display. Standard amino-acid templates, explicit `CONECT`, qualified ligand/hydrogen proximity and geometrically valid peptide C–N links have separate provenance. The complete original file remains available. Display connectivity is not a newly measured bond label.

The parser follows the wwPDB3.3 record definitions [105]. A class-one `HELIX` is an alpha helix; class five is a 3_{10} helix, not another alpha helix. `SHEET` retains strand identity, sheet membership and parallel/antiparallel sense. Ribbon patches follow the actual CA trace and carbonyl orientation, with strand arrows and narrower coils. A peptide bond must connect neighboring residues before a patch or spline-control neighbor is allowed: spatially nearby disconnected fragments and TER-separated chains must not acquire a phantom ribbon. Regression tests include these controls. Backbone recognition in a short synthetic SDF peptide supplies a trace, not a DSSP assignment or evidence of a stable secondary structure.

The full-source geometry is distinct from the capped effective contact graph. In the full-source view, only mapped modeled CA sites carry its electronic field. Nuclear display interpolation adds no new integration steps. An NMR model index, a ribbon parameter and a generative time are not physical time.

34.4.2 What the complex transport animation computes

For a finite Hermitian matrix $H = V\,\mathrm{diag}(E_k)V^*$ and a normalized initial vector ψ_0, the continuously evaluated browser state is

$$\psi_j(t) = \sum_k V_{jk} e^{-itE_k} (V^*\psi_0)_k.$$

Unitarity gives $\sum_j |\psi_j(t)|^2 = 1$. Differentiating gives $\dot{n}_i = 2\,\mathrm{Im}\sum_j H_{ij}\psi_j\bar{\psi}_i$ and hence $\dot{n}_i + \sum_j J_{ij} = 0$ for $J_{ij} = -2\,\mathrm{Im}(H_{ij}\psi_j\bar{\psi}_i)$. The actual complex one-particle coherence is $\rho_{ij} = \psi_i\bar{\psi}_j$. A common phase cancels from both current and coherence; node colors therefore use a stated phase reference.

The probability height is a display encoding, not another physical coordinate. Current arrows are fluxes, not classical electron paths.

Two48-site SSH controls use the same initial endpoint orbital and exchanged strong/weak hoppings. Their periodic bulk winding is respectively zero and one for $q(k) = t_1 + t_2 e^{ik}$, with gap $2|t_1 - t_2|$. A separate61-site domain-wall chain starts and ends with strong bonds and has two weak bonds adjacent to its central even site. Its sublattices have sizes31 and30. At zero energy, set the odd-site amplitudes to zero and solve the tridiagonal recurrence on even sites. The amplitudes decay away from the wall by the weak/strong ratio. The nonzero off-diagonal entries determine this vector up to scale, so the nullspace is one-dimensional. This proves a finite interface zero mode; it does not identify an arithmetic Hilbert–Pólya spectrum.

The QWZ examples have a 12×10 rectangle and two orbitals per site. They use the same unfiltered corner spinor for masses -1 and -3. Their bulk Chern numbers are -1 and0 in the existing link-product convention; 32/64 meshes and gauge controls agree. Finite boundary probability, spectral weights and coherence remain measurements of the particular finite state, not definitions or proofs of that bulk invariant. Independent matrix-exponential checks reproduce the five propagated states. The hydrogen phase winding below, chemical torsion torus, dessin genus and persistent-homology classes are also different invariants.

34.4.3 An analytic orbital benchmark with actual nodes

In atomic units, take $h = -\frac{1}{2}\Delta - r^{-1}$ on the usual hydrogen domain. The displayed normalized eigenfunctions are

$$\phi_{1s} = \pi^{-1/2} e^{-r}, \qquad \phi_{2s} = \frac{(2-r)e^{-r/2}}{4\sqrt{2\pi}}, \qquad \phi_{2p_j} = \frac{x_j e^{-r/2}}{4\sqrt{2\pi}}.$$

Their energies are $E_1 = -1/2$, $E_2 = -1/8$. The angular integrals and $\int_0^\infty r^n e^{-ar}\, dr = n! a^{-n-1}$ give their unit norms; opposite angular parity gives orthogonality of $1s$ and $2p_z$. Consequently

$$\psi(t) = \sqrt{1-a}\,\phi_{1s} + \sqrt{a}\, e^{-3it/8}\phi_{2p_z}, \qquad 0 \le a \le 1,$$

has unit norm after removing its unobservable common ground-state phase. Its density has the interference term $2\sqrt{a(1-a)}\phi_{1s}\phi_{2p_z}\cos(3t/8)$: this is the actual quantum beat shown in the volume. The $2s$ radial node is $r = 2$; the $2p_z$ nodal plane is $z = 0$.

The state $(\phi_{2p_x} + i\phi_{2p_y})/\sqrt{2}$ is proportional to $(x + iy)e^{-r/2}$. On a circle avoiding the nodal axis its phase winds once, and $L_z\psi = \psi$. Its current is $\mathrm{Im}(\bar{\psi}\nabla\psi)$ and has an azimuthal component. This stationary density with nonzero current need not show a moving classical particle. A finite-radius ray-marched volume and its opacity/exposure curve are rendering choices, distinct from the analytic density and normalization. These are nonrelativistic isolated-hydrogen benchmarks, not many-electron molecular orbitals or ab-initio peptide density.

34.4.4 A useful periodic chemical target

Butane has one selected torsion; pentane has two. All other internal coordinates are held at the recorded MMFF reference geometry. The finite grids have72 and 24^2 points, respectively. At300K define

$$p_k = Z^{-1}\exp[-(E_k - E_{\min})/(k_B T)], \qquad q_0(\theta) = \sum_k p_k\, K_{\sigma^2/2}(\theta - \theta_k), \quad \sigma = .05,$$

where the product wrapped heat kernel is used on $\mathbb{T}^d$ and $d = 1, 2$. Thus q_0 is an explicitly softened finite-grid Gibbs target. It is positive, smooth and normalized; it is not a full solvent or molecular-equilibrium distribution. No affinity, redox, efficacy or electronic-density label is inferred. The molecular animation rotates downstream atoms about each actual bond axis; its poses agree with independent RDKit dihedral assignments to numerical precision and preserve the bond graph and fixed bond lengths.

34.4.5 Score diffusion on the torus

For the unit circle,

$$K_\tau(x) = \sum_{m\in\mathbb{Z}} \frac{e^{-(x+2\pi m)^2/(4\tau)}}{\sqrt{4\pi\tau}}, \qquad \partial_\tau K_\tau = \partial_x^2 K_\tau.$$

The product kernel gives $q_\tau = q_0 * K_\tau$ and $\partial_\tau q_\tau = \Delta q_\tau$. A forward sample is $X_\tau = \mathrm{wrap}(X_0 + \sqrt{2\tau}\,\xi)$. Conditioning the wrapped Gaussian mixture shows

$$\nabla \log q_\tau(x) = \mathbb{E}[-\xi/\sqrt{2\tau} \mid X_\tau = x].$$

Indeed, differentiate each image term and divide by the mixture density; the Gaussian score is the stated latent-noise target. Conditional least squares therefore identifies the marginal score. The implemented weighted DSM loss uses weight 2τ, not an unlabelled Euclidean proxy on cut angles. The periodic-input network is trained over the full normalized time interval.

With reverse clock u, the ideal SDE is $dY_u = 2\nabla \log q_{T-u}(Y_u)\,du + \sqrt{2}\,dW_u$. Its Fokker–Planck equation at density q_{T-u} is $-2\Delta q + \Delta q = -\Delta q$, as required. This connection to score SDEs is the standard method [106]; the periodic mixture here supplies an explicit control. Initialization is sampled from the actual q_T, with $T = 2$, rather than silently assuming it is uniform. Sampling stops at $\tau = .03$, so the ideal endpoint is $q_{.03}$, whose Gaussian component variance is $\sigma^2 + .06$. It is not q_0. The initial run exposed this distinction; its source and outputs are preserved. The corrected run uses the proper endpoint reference and no excluded small-time training interval.

Exact wrapped-mixture scores, finite-difference checks, nested64/128-step Brownian controls and stored learned trajectories accompany the experiment. A finite Euler diagnostic is neither a convergence theorem nor a guarantee that a learned score recovers equilibrium. Remaining noise and learned-field error are shown separately from the MMFF target.

34.4.6 Wrapped-geodesic flow matching

Let X_0 be uniform on $\mathbb{T}^d$, independently let $X_1 \sim q_0$, put $D = \mathrm{wrap}(X_1 - X_0)$ and $X_t = \mathrm{wrap}(X_0 + tD)$. The cut locus has probability zero under these continuous laws. For every smooth periodic test function f,

$$\frac{d}{dt}\mathbb{E}f(X_t) = \mathbb{E}\langle \nabla f(X_t), D\rangle = \int \langle \nabla f(x), v_t(x)\rangle \rho_t(x)\,dx, \quad v_t(x) = \mathbb{E}[D \mid X_t = x].$$

This is the weak continuity equation with the correct uniform and q_0 endpoints. Writing $B = [-\pi, \pi]^d$, the conditional formulas are explicitly

$$\rho_t(x) = (2\pi)^{-d} \int_B q_0(x + (1-t)D)\,dD,$$
$$\rho_t(x)v_t(x) = (2\pi)^{-d} \int_B D\, q_0(x + (1-t)D)\,dD.$$

Because q_0 is smooth and strictly positive on the compact torus, these integrals are jointly smooth through both endpoints and $\rho_t \geq \min q_0 > 0$. Division gives a smooth bounded periodic v_t with a uniform spatial Lipschitz bound. In particular $v_1 = 0$ by symmetry. The usual unique flow of this globally Lipschitz time-dependent field transports the stated marginals. Conditional regression targets D and learns an approximation to v_t, following the flow-matching and manifold formulation [107, 108]. Neither the regression loss nor a visualization replaces endpoint-error measurement.

34.4.7 Physical state preparation, RG and phase-conditioned design

The earlier seven-spin dessin experiment supplies an actual quantum Gibbs state and its partial trace; its learned circuits approximate specified state/field targets. The exact coarse action in the RG chapter is produced by integrating out physical spins. Here the chemical learner transports a classical probability law on internal coordinates. A quantum channel, an RG partial trace and a score/noise schedule are three different constructions, with different states, clocks and acceptance tests.

A concrete materials-design constraint already appears in the QWZ controls. Any continuous mass path from $m = -3$ to $m = -1$ passes through $m = -2$. The explicit bulk gap formula then gives zero gap. Thus such a generator cannot both change between these two Chern sectors and preserve the gap throughout that path. Sector-conditioned sampling, explicit transition states and gap/invariant checks are meaningful design tasks. Merely drawing a continuous latent interpolation does not meet them. The finite transport controls and the earlier learned thermal-state experiments provide distinct physics benchmarks for these requirements, rather than unverified predictions of a synthesized topological material.

34.4.8 What the quantum hybrid actually contributes

Each hybrid has two re-uploading two-qubit layers: periodic R_z angle/time encoding, trainable R_y rotations and CZ, followed by eight actual Pauli expectations and a two-layer64-unit tanh classical readout. The angles and readout are trained together. Integer coordinate frequencies preserve 2π periodicity of the measured features, and composition preserves it in the vector field. These are classically simulated quantum-feature hybrids, not coherent quantum chemical evolution or quantum-assisted measurements. The matched classical controls use periodic first/second harmonics and the same readout width. Parameter counts and individual seeds remain explicit.

Eight2400-update CPU runs retain heldout objectives, checkpoint weights, periodicity errors, independent Kronecker/Pauli calculations, parameter finite differences, exact-score comparisons and actual endpoint histograms. The limited runs do not establish quantum advantage. Flow and diffusion have different positive-noise endpoint laws and must not be ranked as though their targets were identical. Generative interpolation time is not molecular time.

The chemical torus is a concrete internal-coordinate space. Drawing it next to a dessin, a noncommutative torus or a Fukaya construction does not construct a functor or prove homological mirror symmetry. Likewise none of these finite learners constructs the missing arithmetic self-adjoint determinant bridge. Adding heat/noise is also distinct from integrating out physical degrees of freedom in the earlier actual RG chapter; a noise schedule alone is not an RG construction. New source, operator-domain, arithmetic and Lean obligations remain explicit.

34.5 Coherent electron-density clouds in an explicit spatial basis

The density viewer now evolves spatial functions, including interference terms, instead of drawing independent spheres around occupied sites. Let $g_i(\mathbf{r})$ be normalized real Gaussian basis functions, let $S_{ij} = \int g_i g_j$ be their positive-definite overlap, and set $L = S^{-1/2}$. For a Hermitian orthonormal-basis Hamiltonian h and a matrix C_0 of p orthonormal occupied columns, put

$$C(t) = e^{-ith}C_0, \qquad \rho(\mathbf{r},t) = \sum_{a=1}^{p} \left| \sum_i g_i(\mathbf{r})(LC(t))_{ia} \right|^2 .$$

This density is nonnegative and has integral p: unitarity preserves $C(t)^*C(t) = I$, and integration yields $\mathrm{Tr}(C(t)^*L^*SLC(t)) = p$. The cross terms carry coherence. Replacing them by a sum of atomic densities generally changes the model. The displayed gain/loss field is $\rho(t) - \rho(0)$, whose full-space integral is zero; positive and negative colors indicate redistribution, not particles with negative probability. Time interpolation of saved density frames is a display operation and is not an extra time-integration step.

For fixed-nuclei H_2^+ at separation $2a_0$, six normalized s Gaussians (exponents $0.3, 1.2, 4.8$ at each nucleus) give an explicitly integrated one-electron Coulomb Galerkin model. We start in one normalized left-center Gaussian, then evolve with its time-independent Hamiltonian. The electronic ground energy is approximately -1.08675615 Hartree; adding nuclear repulsion gives -0.58675615 Hartree. This small basis is not a chemical-accuracy or basis-convergence result. Independent Coulomb quadrature, kinetic-integral and matrix-exponential checks pass.

The second example uses the deposited Trp-cage CA geometry, a specified twenty-orbital contact Hamiltonian and ten occupied model orbitals. Its spatial Gaussians have exponent $0.25\,\text{Å}^{-2}$. The resulting field is the exact density of this finite effective basis model, not a calibrated protein electron density, valence count or transfer-time prediction. The first example uses atomic units; the second retains its effective model time and length convention. These examples are separate from the fixed private dataset release and do not change its labels.

The viewer offers orbit/zoom, volume and isosurface rendering, time scrubbing, exposure and density/gain-loss palettes. The 64^3 grid and 41 saved frames are encoded as 8-bit square-root-density atlases. The maximum decoded integrated-charge errors are 0.00158 electron for H_2^+ and 0.00141 model particle for Trp-cage; analytical full-space charge conservation is exact. Rendering thresholds, finite boxes and quantization are explicit display limitations. The separate hydrogen viewer retains exact analytic hydrogen orbitals and their coherent time-dependent superpositions.

Chapter 35

ToricGT: quantum features, tropical certificates and mirror interfaces

ToricGT organizes graph tokens, trajectories and auxiliary algebraic data; its companion research program separates architecture, dynamics, memory, oracle labels and toric training objectives [143, 144]. This chapter extends that organization to the present surface-order problem. A quantum feature map can replace a specified finite feature block, and exact algebra can check a proposed relation or parameter. Neither operation supplies the arithmetic identification needed by Hilbert–Pólya.

The inspected ToricGT revision is `a5199bc989a6fb170e21220e5e87bf95bc2fc0b4`; the program revision is `f91ba1811b5a4f70d53c7120acf8ca2a0049f85b`. The files `toric_algebra.py`, `tropical_toric_certificates.py`, `cas_certificates.py` and the graph-token schemas are the concrete interfaces used here. Their mathematical objects are not inferred from repository names. In particular, we do not claim to have reproduced the upstream language-model training campaigns or their compression scores.

35.1 A toric chart inside an actual dessin representation stratum

Let A be the infinite polynomial elliptic-square dessin algebra of the preceding chapters. It has two quiver vertices, two arrows in each direction, and the specified locally gentle zero relations. Retain one arrow $X : V_0 \to V_1$, put the other arrows equal to zero, and frame $V_0 = V_1 = k^2$. Every path of length two now acts by zero, so these are genuine continuous finite-dimensional modules of the completed order as well. Impose the additional closed condition $\operatorname{rank} X \leq 1$. In the chosen frames write

$$X = \begin{pmatrix} z_{00} & z_{01} \\ z_{10} & z_{11} \end{pmatrix}, \qquad f = z_{00}z_{11} - z_{10}z_{01}.$$

The coordinate ring is $B = k[z_{00}, z_{01}, z_{10}, z_{11}]/(f)$. This is a representation *stratum with a rank condition*; it is not an assertion that the full order or its invariant ring is a toric variety.

Proposition 35.1 (The Segre semigroup and its full relation)**.** *The homomorphism*

$$\begin{aligned} \pi : k[z_{00}, z_{10}, z_{01}, z_{11}] &\longrightarrow k[s, x, y], \\ z_{ij} &\longmapsto s x^i y^j \end{aligned}$$

has kernel (f)*. Its image is the semigroup ring generated by* $(1,0,0),(1,1,0),(1,0,1),(1,1,1)$ *in* $\mathbb{Z}^3$*. With all* z *of degree one,*

$$H_B(t) = \frac{1-t^2}{(1-t)^4} = \frac{1+t}{(1-t)^3}, \qquad \dim_k B_n = (n+1)^2.$$

Proof. The displayed binomial maps to zero. Replace any factor $z_{00}z_{11}$ in a monomial by $z_{10}z_{01}$ until no such factor remains. The integer kernel of the exponent matrix is generated by $(1,-1,-1,1)$ in the order $(00,10,01,11)$. Two distinct reduced monomials cannot have the same image: their exponent difference would be a nonzero multiple of this vector, and the monomial at the positive end would contain both z_{00} and z_{11}. Distinct reduced monomials therefore have linearly independent images. Reducing a polynomial proves $\ker \pi = (f)$. Multiplication by f is injective in the polynomial domain $P = k[z]$, so the graded exact sequence $0 \to P(-2) \xrightarrow{f} P \to B \to 0$ gives the Hilbert series. In degree n, image monomials are exactly $s^n x^a y^b$ with $0 \le a, b \le n$: choose the overlap of the a x-positions and b y-positions between $\max(0, a+b-n)$ and $\min(a,b)$. This gives $(n+1)^2$ monomials. □

This supplies a small complete certificate rather than an unspecified "syzygy loss." A learned output $\widehat{z}$ can be penalized by $|f(\widehat{z})|^2$. After rationalization, checking $f(z) = 0$ exactly certifies the rank-one relation. It does not certify the learned point's interpretation as a module with other nonzero arrows, an arithmetic endomorphism, or a positive spectral family. The multiplicative parametrization $z_{ij} = a_i b_j$ enforces this one relation identically, including degenerate rank-zero points.

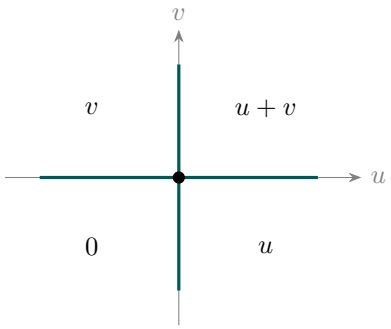
The projectivization of this cone is the Segre surface $\mathbb{P}^1 \times \mathbb{P}^1$. The full framed representation space, the rank-one cone, its projectivization and a quotient by the vertex group are different objects. Under the full left-right action on X, its individual entries are not all semi-invariants. The determinant has its usual determinant character, but is identically zero on this stratum. Framing is thus part of the example, not an invisible choice of gauge.

35.2 Tropical charts and exactly what their certificates prove

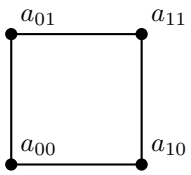
The same square of exponents defines the max-plus function

$$\psi(u,v) = \max\{0, u, v, u+v\} = \max\{0,u\} + \max\{0,v\}.$$

Its corner locus is the union of the coordinate axes. There are four one-dimensional rays of weight one, with primitive outgoing directions $(1,0),(-1,0),(0,1),(0,-1)$. Their sum is zero. This is an exact local balancing calculation. The Newton polygon is the unit square.



Four rays, weight one
local balance = 0



Dual Newton square
$a_{00} + a_{11} = a_{10} + a_{01}$

There are two associated tropical constructions, and they should not be conflated. The hypersurface of a four-term polynomial with this support lives in $\mathbb{R}^2$. The tropicalization of the two-term Segre ideal lives in $\mathbb{R}^4$ and satisfies

$$w_{00} + w_{11} = w_{10} + w_{01}.$$

The latter follows because the two terms of the binomial must have equal valuation. Over a valued field, tropicalization records valuations and initial degenerations; it is not a literal embedding of the tropical set as an ordinary algebraic subvariety of the complex toric variety. A fan specifies a toric compactification, while compatibility with that fan and the valued-field data specifies the relevant tropical geometry.

The inspected helper in `tropical_toric_certificates.py` uses integer supports, rational wall intersections and polygon edge normals. At this revision its input conversion applies `int` to floats. Consequently the exact claim here is restricted to inputs already verified to be integral; a nonintegral learned exponent cannot be silently rounded into an exact certificate. Pairwise ties also need their dimension checked. In the square example the pair $(00, 11)$ ties maximally only at the origin, as does $(10, 01)$. These zero-dimensional sets are not extra facets. A balancing sum for one dual polygon is not by itself a certified Chow class on an unspecified complete fan, nor an exact description of a higher-dimensional tropical variety. The stronger boolean names in the upstream record are not used as additional mathematical premises here.

A useful hybrid pipeline learns affine scores with real parameters, exports integer/rational candidates with an explicit approximation rule, and then recomputes active cells, dimensions, weights and balancing exactly. The approximation error belongs to the learned model; the certificate belongs to the exported data. Recording both prevents a small floating residual from becoming an alleged exact identity.

35.3 The quantum phase block and its cocycle

The ToricGT shift convention differs from the forward shift used in some other chapters. At $\theta = p/q$, with $\omega = e^{2\pi i\theta}$, its untwisted matrices act by

$$Ue_j = \omega^j e_j, \qquad Ve_j = e_{j-1 \bmod q}, \qquad VU = \omega UV.$$

If p, q are coprime they are a finite irreducible carrier of a central quotient. They do not faithfully represent the full rational rotation algebra. A boundary twist has to have modulus one if V is to be unitary. Rational approximants to an irrational θ produce a sequence of finite models, but not an automatically nested sequence of matrix-algebra inclusions.

Proposition 35.2 (Ordered and symmetric Weyl multipliers)**.** *For integer pairs $x = (a, b)$ and $y = (c, d)$ set $W(x) = U^a V^b$. Then*

$$W(x)W(y) = \omega^{bc} W(x + y).$$

Choose a real lift of θ and set $D(a, b) = e^{\pi i\theta ab} U^a V^b$. Then

$$D(x)D(y) = e^{\pi i\theta(bc-ad)} D(x + y), \qquad D(x)D(y) = e^{2\pi i\theta(bc-ad)} D(y)D(x).$$

These formulas are on $\mathbb{Z}^2$; descent to exponents modulo q requires retaining the resulting central phases.

Proof. Repeated use of $VU = \omega UV$, including inverses, gives $V^b U^c = \omega^{bc} U^c V^b$ and proves the first identity. The exponent introduced by the symmetric gauge is

$$\tfrac{1}{2}ab + \tfrac{1}{2}cd + bc - \tfrac{1}{2}(a+c)(b+d) = \tfrac{1}{2}(bc - ad).$$

Reversing x, y negates this last expression. Dividing the two multipliers proves the commutator formula. Associativity also follows directly from bilinearity: $bc + (b+d)e = de + b(c+e)$ for a third pair (e, f). □

The generic routine `projective_phase` instead evaluates $\exp(2\pi i x^T \Theta y)$. For skew Θ its commutator phase is $\exp(4\pi i x^T \Theta y)$. To match the preceding symmetric gauge, use the explicit matrix

$$\Theta = \begin{pmatrix} 0 & -\theta/2 \\ \theta/2 & 0 \end{pmatrix}.$$

This factor of two and the orientation sign matter for learned phase features, circuit comparisons and transport around a surface. A separate numerical skew matrix is not automatically the ordered multiplier ω^{bc}. For even q, writing $1/2$ modulo q would introduce another error; the real-lift formula avoids that operation.

For a density matrix ρ, one physically measurable feature is

$$f_x(\rho) = \operatorname{Tr}(\rho D(x)).$$

Its real and imaginary parts are expectations of the Hermitian operators $(D(x) + D(x)^*)/2$ and $(D(x) - D(x)^*)/(2i)$. They lie in $[-1, 1]$. Thus a classical graph-token block can receive measured finite-dimensional phase features; a variational circuit can learn the state preparation or bounded observables; and a classical head can combine these with exact combinatorial records. No claim of quantum speedup follows from replacing an already inexpensive matrix calculation by a circuit.

Proposition 35.3 (A genuine positive feature kernel)**.** *For any finite list x_i and any density matrix ρ, the matrix $K_{ij} = \operatorname{Tr}(\rho D(x_i)^* D(x_j))$ is positive semidefinite.*

Proof. For complex c_i put $B = \sum_i c_i D(x_i)$. Then $\sum_{ij} \overline{c}_i K_{ij} c_j = \operatorname{Tr}(\rho B^* B) = \operatorname{Tr}((B\sqrt{\rho})^* B\sqrt{\rho}) \geq 0$. □

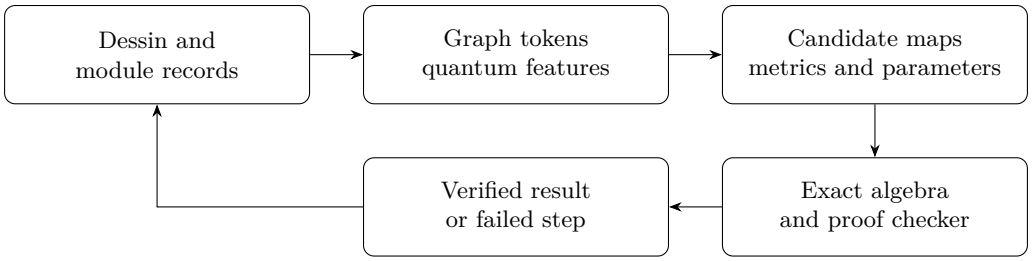
This proof applies to a physical Gram kernel. It does not identify that kernel with a Jensen metric, the arithmetic explicit-formula pairing, or the determinant family of a completed L-function. The latter comparison is an additional theorem, not a consequence of positivity of ρ.

35.4 A quantum–classical ToricGT extension with auditable interfaces

A typed record for a surface example should contain dart permutations, arrow endpoints, zero relations, central parameters, coefficient fields, module dimensions and category labels. Neural embeddings can be added to these records; they should not replace them. A candidate hybrid block is

$$h'_v = F_\eta\left(h_v, \sum_{w \sim v} \alpha_{vw} h_w, \{\Re f_x(\rho_v), \Im f_x(\rho_v)\}_x,\ c_v\right),$$

where α is a normalized classical attention rule, ρ_v is prepared by a specified finite circuit, and c_v is an exact certificate summary. Its architecture is meaningful even if the quantum features are first simulated classically, as in the finite training examples of the preceding computational chapter.



There are three distinct uses. First, supervised regression can learn a coarse-graining map against exact Ising or Gaussian targets, with a held-out parameter set. Second, a proposal model can search for a small module map or a polynomial identity, checked by exact substitution and stated presentation relations. Third, a proof-search policy can select candidate lemmas or tactics, whose accepted output must pass the proof assistant. Only the last two have the potential to yield new exact mathematical results, and only when the checker verifies the full exported statement. A classifier predicting that a proof is valid is not such a checker.

The ToricGT program's certificate distinction is particularly useful here: store exact CAS data, validated surrogates and unavailable backends as different provenance classes. When comparing a quantum feature head with a classical one, hold the data split, parameter budget and objective fixed; report sample or simulation cost as well as error. A network with extra features need not improve the objective. None of the finite experiments in this book is an upstream full-transformer language-model ablation.

An exact candidate metric G for a finite matrix M illustrates the proposal/check distinction. For rational real entries, symmetry and all principal-minor nonnegativity can certify $G \succeq 0$. Positive definiteness and $GM = M^*G$ then imply similarity to a Hermitian matrix: $G^{1/2}MG^{-1/2}$ is Hermitian. Checking a few sampled minors or a small floating residual does not prove these assertions, and applying the result to an arithmetic family still requires uniform positivity and the exact arithmetic determinant comparison.

35.5 Mirror symmetry supplies category comparisons, not a spectral shortcut

Kontsevich–Soibelman develop torus-fibration and homological-perturbation methods, including an A_∞ comparison for specified subcategories of abelian mirrors [145, Sections 6–8, Theorem 4]. A lattice of phase labels is useful computational data for such geometry, but a finite Weyl pair alone does not construct either Fukaya objects or an A_∞ functor. The latter must carry complexes of morphisms and all higher composition maps with their signs and convergence rules.

A concrete toric theorem provides a better model for the proposed link. For a smooth projective toric X, Abouzaid constructs a full A_∞ sub-pre-category of the relative Fukaya category of its Landau–Ginzburg mirror that is quasi-equivalent to the DG category of line bundles on X [146, Theorem 1.2 and Corollary 1.4]. The theorem gives an embedding after the indicated derived/split closure; it does not assert an unrestricted equivalence for every non-Fano toric variety or for our singular completed order.

For intuition, the customary toric mirror potential for the Segre surface is

$$W(z,w) = z + z^{-1} + w + w^{-1}, \qquad (z,w) \in (\mathbb{C}^*)^2.$$

Solving $z\partial_z W = w\partial_w W = 0$ gives $(z,w) = (\pm 1, \pm 1)$, with critical values $4, 0, 0, -4$. The logarithmic Hessian is diagonal with entries $z + z^{-1}$ and $w + w^{-1}$ and is nonsingular at those four points. This

is a direct calculation of a mirror *potential*. By contrast the two-level clock matrix $2Z + 2X$ has eigenvalues $\pm 2\sqrt{2}$, since $XZ + ZX = 0$. The critical values and matrix eigenvalues are plainly different data. A proposal to relate them must specify a functor or quantization and its normalization; visual resemblance of their torus coordinates is not that comparison.

For gentle surfaces, the precise positive input already used in this book is the equivalence for a homologically smooth graded locally gentle algebra with its prescribed stopped surface and line field [66, Theorem 3.2.2]. Our nonempty closed dessin algebras have forbidden cycles and fail that smoothness hypothesis. A stopped quotient or categorical resolution can be a meaningful intermediate object, but it requires its own functor. Ordinary exact quotient inflation does not automatically preserve derived Hom spaces, AR triangles or determinants. In particular, the polynomial node branch $k[x]$ has a valid stopped-annulus interpretation, whereas inflation into $k[x, y]/(xy)$ is not derived fully faithful, as proved earlier.

A finite training loss for $m_1^2 = 0$ or a chain-map residual checks only the displayed truncation. A genuine category construction additionally needs the remaining A_∞ equations, admissible geometric objects, grading, compactness or convergence, and the claimed generation result. Tropical gradient trees can guide computations of compositions under appropriate geometric hypotheses; they do not remove those obligations. This is a constructive research interface: learn a small candidate, calculate its maps exactly, and then prove the specified comparison.

35.6 What would make the learned component relevant to GRH?

For the present Hilbert–Pólya program the useful learned outputs are candidates for arithmetic correspondences, controlled positive metrics, coefficient kernels outside the classes already refuted, or estimates with an exact symbolic witness. Every candidate must be checked against local Frobenius factors, central and deck actions, determinant multiplicities, conductor and gamma normalizations, and compact-uniform convergence on the stated complex domain. A Dirichlet comparison is not a proof for Hecke or general Artin L-functions.

An exact finite witness can disprove a proposed universal construction, and that is valuable progress. A successful finite fit only proposes its next theorem. Neither a toric binomial certificate nor a positive quantum feature kernel proves that all arithmetic approximants have their zeros on the critical line. The small-gcd analytic estimate and the independent positive arithmetic determinant comparison therefore remain separate load-bearing research tasks. The role of the hybrid architecture is to make their search more explicit, testable and reproducible.

35.7 An executed hybrid spectral experiment

The executable example `examples/quantum/toricgt_hybrid.py` imports the pinned ToricGT rotation-algebra module. For $\theta = 1/4$ it obtains four-dimensional Weyl generators and forms the Hermitian Harper family

$$H_\lambda = U + U^* + \lambda(V + V^*), \qquad 0.1 \le \lambda \le 1.8.$$

A two-qubit PennyLane feature circuit and affine head, with twelve parameters, learn the smallest eigenvalue divided by six. Seed 20261104 specifies one hundred sampled couplings, with seventy-five training and twenty-five held-out samples. After 160 Adam updates the held-out mean-square loss is 4.01905×10^{-5}, compared with 0.220518 at initialization. These are finite simulated spectra, not L-function zeros.

For six rational test couplings, the program forms the exact rational matrix

$$H_\lambda = \operatorname{diag}(2, 0, -2, 0) + \lambda \operatorname{Adj}(C_4).$$

It rounds a learned proposal to a rational number E and checks all fifteen nonempty principal minors of $H_\lambda - EI$. A real symmetric matrix is positive semidefinite exactly when every principal minor is nonnegative, so an accepted proposal is an exact lower eigenvalue bound. A rejected proposal is repaired by rational bisection, starting from the independent Gershgorin lower bound $-2 - 2\lambda$ and the Rayleigh upper bound -2. The saved rational minors certify the resulting lower bounds. Thus learning proposes; an independent exact criterion accepts or repairs. The certificate does not depend on the neural prediction being accurate. No arithmetic operator or completed-order equivalence is claimed by this experiment.

This benchmark has an exact closed-form solution: $\det(tI - H_\lambda) = t^2(t^2 - 4(1 + \lambda^2))$, so $E_0 = -2\sqrt{1 + \lambda^2}$. For $\lambda > 0$, rows one and three of H_λ agree, and the difference of rows zero and two is $2/\lambda$ times row one. Thus its rank is at most two. Its trace is zero and $\operatorname{tr}(H_\lambda^2) = 8(1 + \lambda^2)$, giving the stated eigenvalues (and hence characteristic polynomial). The experiment deliberately has an exact oracle: it tests learning, certificate acceptance and repair on a known problem rather than presenting a numerical fit as a new spectral theorem.

Chapter 36

Two-parameter persistence, Schur syzygies and surface-order coefficients

A persistence diagram records how objects and maps change under an ordered family of inclusions. A projective resolution records the generators, relations and relations among relations of one module. These descriptions meet naturally over a polynomial parameter ring. They must still be distinguished from the infinite locally gentle algebra attached to the surface: the parameter ring describes the filtration, not a replacement surface algebra.

The three supplied papers motivate these interfaces [147, 148, 149]. We use their surface-order, lattice and finite-presentation ideas with the corrections already proved in this book. In particular, a matrix satisfying consecutive-product zero is a complex, not automatically a resolution; Fitting base change is not exact base change; and the existence of a generic resolution is not a finite terminating algorithm. The worked example below proves its own exactness and exhibits an actual topological realization.

36.1 The polynomial ring encodes the two commuting directions

Let k be a field and give $\mathbb{N}^2$ its coordinatewise order. A persistence module is a covariant functor $P : \mathbb{N}^2 \to \mathrm{Vect}_k$. Writing $P_{a,b} = P(a, b)$, put

$$R = k[x, y], \quad \deg x = (1, 0), \quad \deg y = (0, 1), \qquad \mathcal{P} = \bigoplus_{a,b \geq 0} P_{a,b}.$$

Multiplication by x and y is the map to the next coordinate in the corresponding direction. Functoriality makes their square commute. Conversely the graded pieces and multiplication maps of an $\mathbb{N}^2$-graded R-module define such a functor. General transition maps are multiplication by $x^{c-a}y^{d-b}$ when $(a, b) \leq (c, d)$. The exponents are nonnegative in this direction, a useful sign check.

This gives an equivalence for the stated discrete diagrams. Finite generation is an additional condition, not a consequence of having finite-dimensional pieces. A module can have infinitely many independent births. Finite cellular input with finitely many birth grades gives the finite presentations used here. A real-parameter filtration needs an appropriate discretization or a different coefficient algebra before being treated as a module over $k[x, y]$.

We write $R(-a, -b)$ for a free module whose generator has grade (a, b). Over a field, a finite graded module has a minimal graded free resolution of length at most two. Minimality means that every differential entry belongs to (x, y); tensoring with $k = R/(x, y)$ then kills the differentials. The numbers and grades of the surviving generators are the multigraded Betti numbers. The field

hypothesis matters: $\mathbb{Z}[x, y]$ has homological dimension three, and the regular sequence $(2, x, y)$ supplies a length-three example. The particular resolution below also works integrally, but that does not make every integral resolution length two.

36.2 A complete three-grade example

Set

$$M = R/(x^2, xy, y^2).$$

Its basis is $1, x, y$, in grades $(0,0), (1,0), (0,1)$. All other graded pieces vanish. The two nonzero proper transition maps send 1 to x and 1 to y. In particular, for comparable grades $\nu \leq \mu$,

$$\rho_M(\nu, \mu) = \operatorname{rank}(M_\nu \to M_\mu) = \begin{cases} 1 & \nu, \mu \in \{(0,0), (1,0), (0,1)\}, \\ 0 & \text{otherwise.} \end{cases}$$

This computes this module's rank invariant; rank invariants do not in general classify all two-parameter modules.

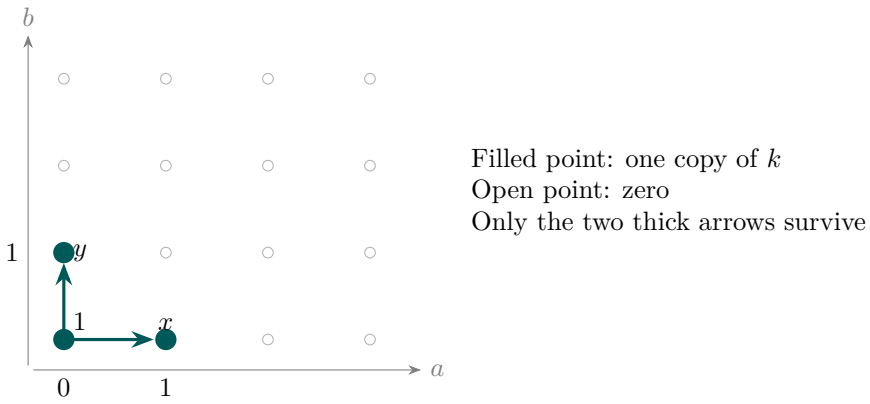


Figure 36.1: The actual rank diagram of $R/(x, y)^2$. Moving right or up outside its three-point support kills the class. Incomparable grades are not joined by a persistence map.

Theorem 36.1 (A minimal bigraded resolution)**.** *The following complex is a minimal graded free resolution of M:*

$$0 \longrightarrow F_2 \xrightarrow{d_2} F_1 \xrightarrow{d_1} R \longrightarrow M \longrightarrow 0,$$

where

$$F_1 = R(-2,0) \oplus R(-1,-1) \oplus R(0,-2),$$

$$F_2 = R(-2,-1) \oplus R(-1,-2), \qquad d_1 = \begin{pmatrix} x^2 & xy & y^2 \end{pmatrix}, \quad d_2 = \begin{pmatrix} -y & 0 \\ x & -y \\ 0 & x \end{pmatrix}.$$

Proof. Each column of d_2 has the indicated source grade, and multiplication gives $d_1 d_2 = 0$. If $d_2(a, b) = 0$, its first and last entries give $ya = xb = 0$. Since R is a domain, $a = b = 0$.

Suppose $x^2 f + xyg + y^2 h = 0$. Reducing modulo x shows $x \mid h$, say $h = xb$. Dividing the relation by x and reducing modulo y shows $y \mid f$, so write $f = -ya$. Substitution now gives

$y(-xa+g+yb)=0$, hence $g=xa-yb$. Thus $(f,g,h)=d_2(a,b)$. This proves exactness at F_1. The image of d_1 is its displayed ideal, giving exactness at R and the augmentation. Every entry of both matrices has positive grade, so the resolution is minimal. The divisibility argument also works in $\mathbb{Z}[x,y]$, where x,y remain prime and nonzerodivisors. □

The multigraded Betti numbers are consequently

$$\beta_{0,(0,0)}=1,\quad \beta_{1,(2,0)}=\beta_{1,(1,1)}=\beta_{1,(0,2)}=1,\quad \beta_{2,(2,1)}=\beta_{2,(1,2)}=1.$$

They are dimensions of the corresponding graded $\operatorname{Tor}_i^R(M,k)$. Taking degreewise Euler characteristics gives the same Hilbert series by two independent descriptions:

$$H_M(s,t)=1+s+t=\frac{1-s^2-st-t^2+s^2t+st^2}{(1-s)(1-t)}.$$

After forgetting the separate grading this becomes $(1-3z^2+2z^3)/(1-z)^2=1+2z$. The numerator records the alternating resolution shifts, not a characteristic polynomial whose zeros locate arithmetic L-zeros.

One can also see the dual calculation directly. Ignoring shifts only to write the matrices, the dual differential is

$$d_2^*=\begin{pmatrix}-y & x & 0\\ 0 & -y & x\end{pmatrix}.$$

The equations $-yA+xB=-yB+xC=0$ imply $(A,B,C)=(x^2q,xyq,y^2q)$, again using coprimality. Thus $\operatorname{Ext}^0_R(M,R)=\operatorname{Ext}^1_R(M,R)=0$. The second Ext is generated by e_1,e_2 with relations $ye_1=0$, $xe_1=ye_2$ and $xe_2=0$; its k-basis is e_1,e_2,xe_1. This keeps the syzygy calculation distinct from merely counting the support points of M.

36.3 A bifiltered CW realization and the syzygies it creates

Start with one vertex and an oriented loop e, both born at grade $(0,0)$. Attach three two-cells by degree-one maps to that loop, at grades

$$D_{20}:(2,0),\qquad D_{11}:(1,1),\qquad D_{02}:(0,2).$$

At grade (a,b) include precisely the cells whose birth grades are at most (a,b). Every boundary is already present, so these are actual subcomplex inclusions and their squares commute. The persistence cellular chain modules are

$$C_2=F_1,\qquad C_1=Re,\qquad C_0=R,\qquad \partial_2=(x^2\ \ xy\ \ y^2),\quad \partial_1=0.$$

Therefore $H_1=M$ exactly. No assertion that every abstract persistence module has this particular geometric form is needed.

The loop survives before any disk is present and dies when the first disk appears. Two disks attached along their common boundary form a sphere. The first two persistent H_2 generators are the compatible cell cycles

$$-yD_{20}+xD_{11}\quad\text{at }(2,1),\qquad -yD_{11}+xD_{02}\quad\text{at }(1,2).$$

Theorem 36.1 proves $H_2\cong R(-2,-1)\oplus R(-1,-2)$; there are no three-cells to kill them. At $(2,2)$ all three disks give two independent sphere classes. Thus the same matrix d_2 is a relation among the killing cells and a positive persistent homology class in the larger CW complex. This auxiliary CW space need not be a Riemann surface: three disks along one circle are not a manifold. It is a topological realization of the filtration module, not another claimed cellular dessin.

36.4 Schur modules organize the generators and the first syzygies

Assume now $\operatorname{char} k = 0$, put $V = kx \oplus ky$, and let $\mathrm{GL}(V)$ act on $R = \operatorname{Sym} V$ by linear substitution. The ideal $(x, y)^2$ is invariant. Its degree-two generators form $\operatorname{Sym}^2 V$, with basis x^2, xy, y^2. The linear syzygies form the kernel of multiplication

$$V \otimes \operatorname{Sym}^2 V \longrightarrow \operatorname{Sym}^3 V.$$

There is a natural equivariant map

$$\delta : \bigwedge^2 V \otimes V \longrightarrow V \otimes \operatorname{Sym}^2 V, \qquad (v \wedge w) \otimes z \longmapsto v \otimes wz - w \otimes vz.$$

Multiplication kills its image. On the two basis vectors its values are exactly the two columns of d_2:

$$(x \wedge y) \otimes x \mapsto x \otimes xy - y \otimes x^2, \qquad (x \wedge y) \otimes y \mapsto x \otimes y^2 - y \otimes xy.$$

They are independent, and the kernel has dimension $6 - 4 = 2$, so δ identifies it with $\det V \otimes V = S_{(2,1)}V$. The Littlewood–Richardson rule gives

$$V \otimes \operatorname{Sym}^2 V \cong \operatorname{Sym}^3 V \oplus S_{(2,1)}V.$$

Here the partition convention uses symmetric rows. The equivariant total- graded resolution has multiplicity spaces $k, \operatorname{Sym}^2 V, S_{(2,1)}V$ in generator degrees $0, 2, 3$. The diagonal torus recovers their bigraded weights $(2, 0), (1, 1), (0, 2)$ and $(2, 1), (1, 2)$.

The grading distinction is essential. General GL_2 substitutions mix x and y, so they preserve total degree, not the two original filtration coordinates. Only the diagonal torus preserves each bigrading. In positive characteristic the displayed maps and our exact resolution remain valid, but semisimple direct-sum representation theory must not be assumed. Nor does applying a Schur functor termwise to an arbitrary exact sequence preserve exactness, as the earlier counterexamples show.

36.5 Fitting data, exactness and specialization

For a finite presentation $R^p \xrightarrow{D} R^q \to N \to 0$ define

$$\operatorname{Fitt}_j(N) = I_{q-j}(D), \qquad I_0(D) = R,$$

where I_r is the ideal of r-minors, $I_r = R$ for $r \le 0$, and $I_r = 0$ for $r > \min(p, q)$. The ideal is independent of the chosen finite presentation. Its formation commutes with arbitrary base change because minors are polynomials in the presentation entries. For our cyclic module,

$$\operatorname{Fitt}_0(M) = (x, y)^2, \qquad \operatorname{Fitt}_j(M) = R \quad (j \ge 1).$$

The support is the origin, but its Fitting scheme retains a length-three thickening. This is not the same datum as the rank invariant of the ordered graded pieces.

The 2-minors of d_2 are $y^2, -xy, x^2$, so their ideal is also $(x, y)^2$. Expected ranks are $1, 2$ and this ideal has grade two; x^2, y^2 is a regular sequence. These facts agree with the finite-free acyclicity criterion of Buchsbaum–Eisenbud [150], independently of our direct proof. Over a general Noetherian ring, a height count cannot silently replace the criterion’s grade/regular-sequence hypotheses. The

criterion concerns a finite complex over a commutative ring; it does not certify every infinite path-algebra resolution.

Arbitrary specialization does not preserve that exactness. At $x = y = 0$ both matrices vanish, leaving positive homology k^3, k^2 in degrees one and two. More informatively, after setting only $y = 0$, the complex has

$$H_0 = k[x]/(x^2), \qquad H_1 = (k[x]/(x))^2, \qquad H_2 = 0.$$

These follow immediately from $d_1 = (x^2, 0, 0)$ and the two surviving entries x of d_2. They are the derived-base-change Tor groups. Flat base change, suitable Tor vanishing, or a new exactness proof is needed to obtain an ordinary specialized resolution. A generic parameter space and a small differential residual do not remove those conditions.

36.6 A correct finite space of complexes and its incidence model

For variety language in this section take k algebraically closed. Let V_i have dimensions n_i for $i = 0, 1, 2$. Fix feasible ranks a, b with

$$a \le \min(n_0, n_1), \qquad b \le \min(n_1, n_2), \qquad a + b \le n_1.$$

The reduced variety

$$\mathcal{C}_{a,b} = \{(A, B) : V_2 \xrightarrow{B} V_1 \xrightarrow{A} V_0,\ AB = 0,\ \operatorname{rank} A \le a,\ \operatorname{rank} B \le b\}$$

parametrizes based complexes with these upper bounds, not isomorphism classes of resolutions. Consider flags $L \subset K \subset V_1$ with $\dim L = b$, $\dim K = n_1 - a$, and impose

$$\operatorname{im} B \subset L \subset K \subset \ker A.$$

Over the flag variety the allowed maps form the vector bundle

$$\operatorname{Hom}(V_1/K, V_0) \oplus \operatorname{Hom}(V_2, L).$$

Its total space is smooth and irreducible. Projection is proper onto $\mathcal{C}_{a,b}$: for any complex with the rank bounds, first extend $\operatorname{im} B$ to a b-plane inside $\ker A$, then extend it to an $(n_1 - a)$-plane there. On the full-rank locus the choices are uniquely $L = \operatorname{im} B$, $K = \ker A$. Full ranks exist by feasibility, so this projection is birational. This proves the asserted incidence resolution of the reduced rank-bound variety.

For $(n_0, n_1, n_2) = (1, 3, 2)$ and $(a, b) = (1, 2)$, the two flag spaces coincide in a plane, and the base is $\mathbf{Gr}(2, k^3)$. The vector bundle has fiber dimension $1 + 4$ and base dimension two, giving total dimension seven. Full-rank points are exact in positive degrees because $\operatorname{im} B = \ker A$ and B is injective. The zero pair is also a point of the complex variety and is not exact. Our polynomial matrices map the punctured plane to the exact locus; the origin maps to that nonexact boundary. A specialization of the universal matrices therefore still needs its own homological check.

Bruns' generic-resolution construction uses a directed limit of rings which kills positive homology in the limit [151, Theorem 1, pp.35–36]. It does not assert that some finite stage always becomes exact, nor that every specialization of the resulting matrices preserves exactness. The finite example in this chapter makes its stronger local claims by explicit calculation rather than by invoking an unspecified generic object.

36.7 Coefficients in a genuine infinite dessin order

Return to the actual nodal interval dessin and distinguish its variables:

$$A = k[\xi,\eta]/(\xi\eta), \qquad \Lambda = k[[\xi,\eta]]/(\xi\eta), \qquad u = \xi + \eta.$$

Both A and Λ are infinite dimensional over k. The completed order is free of rank two over $k[[u]]$, on $1, \xi$, with $\xi^2 = u\xi$ and $\eta = u - \xi$. Multiplication by u is injective, as is clear in its two normalization branches. Set $E = \Lambda/u^2\Lambda$. It has basis $1, \xi, u, u\xi$ over k, nontrivial arrow actions, and

$$0 \longrightarrow \Lambda \xrightarrow{u^2} \Lambda \longrightarrow E \longrightarrow 0$$

is a genuine free resolution. The module E is finite length, not a $k[[u]]$-free lattice. Its finite dimension does not turn its parent order into a finite-dimensional substitute.

The family $E \otimes_k M$ is a persistence module valued in continuous Λ-modules: each nonzero piece is E, and its structure maps are the identity or zero as in Figure 36.1. The actions of x, y commute with the fixed action of u, ξ, η. There is no identification of either persistence direction with the order uniformizer.

More precisely put $\mathcal{B} = \Lambda \otimes_k k[x,y]$. Tensor the length-one Λ-resolution just displayed with Theorem 36.1 over k. Its finite total complex has free $\mathcal{B}$-ranks

$$(\operatorname{rank} F_0, \operatorname{rank} F_1, \operatorname{rank} F_2, \operatorname{rank} F_3) = (1, 4, 5, 2)$$

and resolves $E \otimes_k M$. If Q_i denotes the order resolution and P_j the persistence resolution, the total differential on $Q_i \otimes P_j$ is

$$D = \partial_Q \otimes 1 + (-1)^i 1 \otimes d_P.$$

Order the degree-n terms as $P_n \oplus (Q_1 \otimes P_{n-1})$. Suppressing only the tensor symbols, the three matrices are

$$D_1 = \begin{pmatrix} d_1 & u^2 \end{pmatrix}, \qquad D_2 = \begin{pmatrix} d_2 & u^2 I_3 \\ 0 & -d_1 \end{pmatrix}, \qquad D_3 = \begin{pmatrix} u^2 I_2 \\ -d_2 \end{pmatrix}.$$

The cross terms cancel, so consecutive products are zero. For exactness, write a positive-degree cycle as (a, b), with $da + u^2 b = 0$ and $db = 0$. Modulo u^2 the first component is a cycle in $E \otimes_k P_\bullet$. That complex is exact in positive degrees, since tensoring vector spaces over k is exact. Hence $\bar{a} = d\bar{c}$. Lift $\bar{c}$ to c in the free term and write $a - dc = u^2 e$. The original equation becomes $u^2(de + b) = 0$. Multiplication by u^2 is injective on every free term, so $b = -de$. Consequently $(a, b) = D(c, e)$, as required. The same argument includes the top degree by putting missing terms equal to zero. Degree-zero homology is $\mathcal{B}/(u^2, x^2, xy, y^2) = E \otimes_k M$. This proves exactness without assuming that an arbitrary tensor product of resolutions stays exact. The ranks follow from $(1 + z)(1 + 3z + 2z^2) = 1 + 4z + 5z^2 + 2z^3$.

This construction is compatible with the original center action. It does not shorten the infinite resolution of the nodal residue simple, make E a lattice, or construct Frobenius. Restriction to the commutative coefficient ring $k[[u]][x, y]$ doubles these free ranks. Determinant functors apply to the specified finite perfect complex, with virtual rank $1 - 4 + 5 - 2 = 0$, but determinant multiplicity and arithmetic comparison remain additional questions.

36.8 Quantum data, monotonicity and the next usable interface

An arbitrary time-varying interaction graph is not a bifiltration: an edge can disappear at a later time. One valid alternative fixes finite birth pairs (a_e, b_e) for edges and includes an edge exactly

when both coordinates are reached, then takes the flag complex. Another uses a cumulative union over times up to the first coordinate and decreasing interaction thresholds in the second. Both give inclusions; the second records cumulative history rather than individual snapshots. Vertices and higher cells must have compatible birth grades. Zigzag persistence is a different appropriate tool when deletions must be retained.

Quantum channels are linear on density matrices, but two unrelated channels need not commute. Assigning them to the two directions does not define a persistence functor unless the required squares commute. One may instead extract a declared classical correlation graph, choose a monotone filtration, and compute its homology with the conventions above. The data-to-distance rule and its statistical uncertainty still need justification.

For the research program this yields concrete trainable and checkable targets: propose birth grades, presentation entries or a low-degree syzygy; test inclusions, gradings, the matrix identities and actual exactness; record Betti and Fitting data before interpreting them. A loss penalizing D^2 checks only the complex equation. The exact module example, the flag-incidence model and the surface-order coefficient resolution show how to add the missing checks. None identifies those finite invariants with a completed arithmetic L-function, provides a positive arithmetic spectral limit, or proves GRH.

36.9 The executable staircase and quantum laboratory

The canonical on-page tool accompanies this chapter; other chapters link here. Proposition 2.3 generalizes the worked square-ideal resolution to every strict Artinian staircase. Four displayed ideals have lengths $3, 6, 13, 16$, with custom natural exponents also allowed. The tool shows generator and adjacent-syzygy degrees, standard monomials, exact comparable-grade maps and cellular incidence ranks. Coefficients in E multiply field dimensions by four; the displayed free ranks over $\Lambda[x, y]$ instead come from the u^2 cone. These are different rings.

Specializing the free resolution at a point over $\mathbb{F}_2$ computes its fiber-complex homology. At the origin its dimensions are $(1, m, m-1)$; at each of the three nonzero $\mathbb{F}_2$ points they vanish, since a pure-power generator becomes a unit. This is derived fiber data, not the CW homology at a filtration grade. The signed maximal minors and Hilbert numerator are checked independently with symbolic polynomials.

The quantum tab uses the single saved trained four-qubit QCNN unitary U and the channel $T(\rho) = \mathrm{Tr}_{2,3}(U\rho U^*)$. The designed inputs have their last three qubits in $|000\rangle$. Their first qubit runs over eight equatorial states $(|0\rangle + e^{2\pi ij/8}|1\rangle)/\sqrt{2}$ and both poles. This is an out-of-training-distribution illustrative family, not new training or a held-out performance claim. Birth labels are fixed from the input population $(I + Z_0)/2$: south 0, equator 500, north 1000. They are retained at the output; recomputing them from output energy would not justify the same identity inclusion.

Floating-point input/output trace distances are scaled by 1000 and rounded upward. Their frozen integer graph labels are saved with a SHA-256 checksum and checkpoint provenance. The inequality of output and input labels is verified directly, never imposed by taking their minimum. Proposition 2.4 explains the exact-channel contractivity; the numerical records are not interval certificates. For the recorded labels, all finite boundary matrices and induced ranks are computed exactly over $\mathbb{F}_2$. At grade $(400, 500)$ the input contains an equatorial 8-cycle and an isolated south pole, with $(\beta_0, \beta_1) = (2, 1)$. Its H_1 map to $(600, 500)$ has rank one, whereas its map to $(800, 1000)$ has rank zero. The plotted two-parameter rank table fixes the target and varies comparable source grades; it is not a complete multiparameter barcode. Rotating the drawing changes the input-qubit Bloch layout only. The same layout is used at output and does not embed its two-qubit state space.

Independent row elimination and the browser's bit-column implementation agree on both Betti numbers and inclusion ranks for the saved cases. These executable finite examples complement the proofs and the cited persistence theory. The worked square-ideal module now has a kernel-checked ungraded free resolution, described below. General staircase exactness, graded and categorical interfaces, the coefficient cone and channel norm contractivity remain separate formalization tasks. No learned component or finite homology calculation supplies the unresolved positive arithmetic determinant bridge.

36.10 What the polynomial Lean resolution actually verifies

The file `PersistenceResolution.lean` uses $R = \mathrm{MvPolynomial}(\mathrm{Fin}\,2, k)$ for an arbitrary field. Its free coordinate modules are $F_1 = R \times R \times R$ and $F_2 = R \times R$, with the matrices of Theorem 36.1. The augmentation is the actual R-linear quotient map to $R/(x^2, xy, y^2)$. The proof of `d1_kernel` quantifies over all polynomial coefficient vectors; it is not a sampled scalar-rank test.

The reusable lemma `relation_decomposition` starts with a commutative domain and a pair x, y such that $x \neq 0$ and $x \mid yz$ implies $x \mid z$. From $x^2a + xyb + y^2c = 0$ it constructs p, q with $(a, b, c) = (-yp, xp - yq, xq)$. For the actual polynomial variables, the regularity premise is discharged by viewing R as polynomials in x with coefficients in $k[y]$. A polynomial is divisible by x exactly when its constant coefficient vanishes; multiplication by the nonzero y cannot kill such a coefficient. Thus the final kernel theorem has no unproved regularity hypothesis. The first and last coordinates then prove `d2_injective`; `d1_range` identifies the image with the specified ideal. Augmentation exactness and surjectivity complete the sequence, and the free terms are proved projective.

The field k carries the residue action $r \cdot a = \mathrm{constantCoeff}(r)a$. The free modules retain ordinary polynomial multiplication. Both actions are explicit in the source, with action identities checked in the kernel. For every R-linear map from the appropriate free term to this residue field, precomposition with d_1 or d_2 is zero, since all displayed entries contain x or y. These are actual Hom statements with their module actions, not merely entrywise evaluations. Abstract Ext-group identifications and the graded minimal-resolution interface are not yet packaged as formal theorems.

All theorem types and axiom dependencies are printed. Only the standard Lean foundations occur; no project axioms or incomplete proofs are used. This establishes the entire underlying ungraded worked resolution and its residue Hom differential calculation. It does not formalize every staircase, the CW model, Schur equivariance, the E-coefficient tensor cone or any arithmetic determinant comparison. Those distinctions remain visible on the local verification page beside the executable laboratory.

Chapter 37

The remaining arithmetic theorem and a verifiable research loop

37.1 A precise positive spectral target

For a primitive nonprincipal Dirichlet character χ, choose the completed L-function with its parity, conductor and gamma factor fixed. A sufficient spectral program requires holomorphic functions F_N on a connected domain containing the critical strip, compact-uniform convergence $F_N \to \Lambda(s,\chi)$, and a proved zero-location property for every F_N. A self-adjoint determinant representation must include its domain, determinant regularization, nowhere-zero normalization and coefficient comparison. Self-adjointness of an unrelated finite matrix does not establish any of these identifications.

If every F_N is zero-free off the critical line, Hurwitz on each connected off-line component shows that the nonzero holomorphic limit is zero-free there. The limit cannot be identically zero on an open component if it is a nonzero holomorphic function on the connected containing domain. This last connected-domain hypothesis matters: componentwise convergence alone does not rule out an identically zero limit on a disconnected component. The conclusion is conditional until the arithmetic approximants and positive representation are constructed. General Artin functions also need their own holomorphy statement; Brauer quotients do not supply it. Hecke, Dedekind and elliptic-curve normalization and critical centers must remain distinct.

The original modular-geodesic argument fails at its prime identification. Integer hyperbolic traces and $e^{\ell/2}+e^{-\ell/2}=\sqrt{p}+1/\sqrt{p}$ cannot match all rational primes. An asymptotic similarity between prime and geodesic counts does not give a termwise equality of Euler factors. Nor does finite-field purity for a family of curves prove number-field GRH. The local Jacobi theta construction is a positive arithmetic benchmark with its own coefficient and symmetry obstructions, treated in the earlier chapters.

37.2 A surviving short-row reduction

Write $\mathcal{O}=\mathbb{Z}[\omega]$. For squarefree primary column ideals n of norm about D, good away from a fixed set containing 2 and 3, let χ_n be the original sextic residue character extended by zero at nonunits. At the unit ideal take $\chi_1(u)=1$, including $u=0$. For row-independent coefficients $|c_n|\le 1$, the normalized Gram expansion is

$$\mathcal{E}=D^{-1}\sum_{n,m} c_n\overline{c_m}K_H(n,m), \qquad K_H(n,m)=\sum_{0<Nu\le H}\chi_n(u)\overline{\chi_m(u)}.$$

For $n = ha, m = hb$ with h, a, b squarefree and pairwise coprime,

$$\chi_n(u)\overline{\chi_m(u)} = \mathbf{1}_{(u,h)=1}\psi_{a,b}(u), \qquad \psi_{a,b} = \chi_a\overline{\chi_b}.$$

The oscillatory primitive conductor is ab; its zero-preserving periodic modulus is hab. Cancelling h without its coprimality mask would change the row family. Möbius inversion gives

$$K_H(ha, hb) = \sum_{d|h} \mu(d)\psi_{a,b}(d) \sum_{0<Nv\le H/Nd} \psi_{a,b}(v).$$

A row weight has to be evaluated at dv in this identity.

For a fixed nonnegative radial Schwartz profile Φ, replace the sharp row cutoff by $\Phi(u/\sqrt{H})$. For an off-diagonal pair, $\psi_{a,b}$ is primitive nonprincipal. If $Q = N(ab)$, its complete Gauss transform and lattice Poisson summation give, for every $X > 0$,

$$\left|\sum_{v\in\mathcal{O}} \psi_{a,b}(v)\Phi(v/\sqrt{X})\right| \ll_\Phi \sqrt{Q}.$$

Indeed the nonzero dual frequencies have Gauss modulus at most $\sqrt{Q}$ and the zero frequency vanishes. After scaling, Fourier decay bounds their sum by $O_\Phi(Q/X)$: for $X \le Q$ use planar annuli; for $X > Q$ use a decaying power greater than two. The Poisson prefactor is $X/\sqrt{Q}$. The ideal generator rotates and scales the Eisenstein lattice, so radiality preserves the profile in the divisor sum. This includes scales $X < 1$.

For $Nh \asymp G$, the mask costs $\tau(h) \ll_\varepsilon D^\varepsilon$, each kernel is $O_\varepsilon(D^{1+\varepsilon}/G)$, and there are $O(D^2/G)$ pairs. Thus the off-diagonal normalized contribution satisfies

$$|\mathcal{E}_G^{\mathrm{off}}| \ll_{\Phi,\varepsilon} \frac{D^{2+\varepsilon}}{G^2}.$$

The diagonal is $O_\Phi(H)$ for $H \ge 1$. At $H = D^{3/4}$, the dyadic range $G \ge D^{5/8}$ is therefore controlled by $O_{\Phi,\varepsilon}(HD^\varepsilon)$. The small-gcd range, especially $h = 1$, remains open. This result is for one fixed smooth radial profile; it does not prove the source's stronger moving-profile or supremum uniformity. The derivation and surviving alternative routes are recorded in `research/short-row-high-gcd.md`.

37.3 Why an absolute coprime pair-square estimate cannot close the short rows

Keep the original sextic family

$$M_u(D) = D^{-1/2}\sum_n \mu(n)\nu(n)W(Nn/D)\chi_n(u), \qquad \chi_n(u) = (u/n)_6,$$

with squarefree primary column ideals outside the fixed excluded set, their full annular coefficients (fix W supported in $[1, 2]$), and all nonzero Eisenstein element rows $Nu \le H$. The cubic symbol is χ_n^2, not χ_n. The following classical frame inequality [80] gives a new obstruction to one proposed estimate in this arithmetic program.

Proposition 37.1 (Coprime pair-square obstruction)**.** *Let A be an R-by-N complex matrix with $|A_{ui}| = 1$, and put $K_{ij} = \sum_u A_{ui}\overline{A_{uj}}$. Then*

$$\sum_{i\ne j} |K_{ij}|^2 \ge NR(N - R).$$

For the original character kernels, let $B_1(H,D)$ be the sum of $|K_H(n,m)|^2$ over all distinct coprime squarefree column ideals in $[D,2D]$. At $H=D^{3/4}$,

$$B_1(H,D) \gg \frac{D^{11/4}}{(\log D)^2}.$$

In particular the proposed sufficient input $B_1(H,D) \ll H^2D^{\varepsilon}$ fails for each fixed $\varepsilon < 5/4$. This does not refute the signed Möbius mean square.

Proof. Set $F_{uv} = \sum_i A_{ui}\overline{A_{vi}}$. Reordering four finite sums proves $\sum_{i,j}|K_{ij}|^2 = \sum_{u,v}|F_{uv}|^2$. The row diagonal contributes RN^2; the column diagonal contributes NR^2. Removing the latter and retaining the former gives the inequality.

Restrict the column pairs in the nonnegative sum B_1 to distinct prime ideals p,q of norm in $[D,2D]$, outside the same fixed set. If $H < D$, no such prime divides a nonzero row element: divisibility would imply $Nu \geq Np$. Thus all original zero masks are exactly one on this ball, $|\chi_p(u)| = 1$, and the residual primitive finite character conductor is pq, of norm between D^2 and $4D^2$. All these pairs have common divisor1. The lattice count gives $R = (2\pi/\sqrt{3})H + O(\sqrt{H}+1)$. The classical unconditional fixed-field prime-ideal theorem gives $N \sim D/\log D$; this is an external analytic input, not a GRH hypothesis. At the stated endpoint $R = o(N)$, and the bound is therefore $(1-o(1))N^2R \gg D^{11/4}/(\log D)^2$. □

To see the exact failed step, write $c_n = \mu(n)\nu(n)W(Nn/D)$ and $C_D = \sum_n |c_n|^2 = O(D)$. Cauchy over coprime pairs bounds the absolute signed contribution by $D^{-1}C_DB_1^{1/2}$. The hoped-for pair-square upper bound would have closed this particular route, but is false. A large absolute pair-square mass is not a lower bound on the quadratic form with the fixed c_n. Nor is the prime part a positive summand of the full Möbius energy: prime–composite cross terms can cancel. The original low-gcd estimate and the positive arithmetic determinant bridge remain open.

37.3.1 Weighted profiles, exact arithmetic examples and the surviving task

The finite matrix proof also retains an arbitrary row profile. Suppose $|A_{ui}|^2 = w_u$ for every column, set $S = \sum_u w_u$ and $Q = \sum_u w_u^2$. The row diagonals are Nw_u and column diagonals are S, so the same identity proves

$$\sum_{i\neq j}|K_{ij}|^2 \geq N^2Q - NS^2.$$

This is a finite statement. Applying it to an infinite Schwartz tail would require its convergence and every newly encountered prime collision; these are not discarded. If a weighted pair-square attempt includes the annular W, one can instead choose a closed subannulus on which a nonzero $|W|$ is bounded below. Its prime count still has order $D/\log D$. The fixed ν has unit modulus outside its conductor. These facts do not replace the original coefficients in a signed estimate.

Here are exact sextic computations with all nonzero elements of the Eisenstein norm ball, and both prime ideals above each split rational prime in the column annulus. These kernel diagnostics use $\nu = 1$ and exclude only primes above2,3; they do not compute a signed Möbius energy. Values are integer norms in $\mathbb{Z}[\omega]$.

D	H	R	N	$\sum_{i\neq j}\lvert K_{ij}\rvert^2$	$NR(N-R)$
128	4	18	22	6840	1584
1024	9	36	138	651672	506736
4096	81	300	456	60080328	21340800
256	64	240	40	363672	−1920000

The final row has $H = D^{3/4}$ but $N < R$; its negative lower bound is correctly vacuous. The asymptotic theorem follows from the proof, not an extrapolation of these examples. For $p \equiv 1 \pmod 3$ and $w^2 + w + 1 = 0$ in $\mathbf{F}_p$, evaluate $a + b\omega$ as $a + bw$ and take its $(p-1)/6$ power, lifting the six roots via $\zeta_6 = 1 + \omega$. Every zero is tested before a unit value is assigned. For instance $1 + 3\omega$ has norm7 and vanishes at $\omega = 2$ modulo7, so the unimodularity hypothesis cannot be used beyond its stated domain.

`ShortRowPairBarrier.lean` verifies the finite frame identity, row-diagonal bound, weighted inequality and unimodular specialization, with actual complex sums and explicit hypotheses. It does not formalize the ideal-character comparison or prime-ideal theorem. The deterministic integer checker also verifies weighted profiles and256 scalar pair sums independently of its matrix computation. No numerical model or learned coefficient is used.

The next signed route must retain μ, ν, W before Cauchy. An exact starting identity in ideal Dirichlet convolution is

$$\mu = 2a - a * a * \mathbf{1} + b * b * \mathbf{1}, \qquad a = \mu\, \mathbf{1}_{Nn \le U}, \quad b = \mu - a.$$

Indeed $\mu * \mathbf{1} = \delta$ implies $(\mu - a) * (\mu - a) * \mathbf{1} = \mu - 2a + a * a * \mathbf{1}$. On squarefree n, each divisor factorization retains pairwise coprimality; the original row zeros still multiply along it. Estimating these type-I/type-II kernels with their true conductors is a new open arithmetic task. The identity alone supplies no cancellation or GRH proof.

37.4 A signed Möbius decomposition and its termwise obstruction

Keep the original squarefree good-ideal family, its fixed ν, its full $W(Nn/D)$ and every zero-extended sextic symbol. In ideal Dirichlet convolution, write $\zeta_0(n) = 1$ for every good ideal and let δ be the convolution unit. For $1 \le U < D$ put $a_U = \mu \mathbf{1}_{Nn \le U}$ and $b_U = \mu - a_U$. The classical Vaughan algebra gives

$$\mu = 2a_U - a_U * a_U * \zeta_0 + b_U * b_U * \zeta_0. \tag{37.1}$$

Indeed $\mu * \zeta_0 = \delta$, and expansion of the last product proves the identity without an analytic assumption. This is a classical decomposition, not a new cancellation theorem; compare [87, Lemma4.1].

On squarefree n all factors in $n = dc = abc$ are pairwise coprime. Define the actual, nonarbitrary coefficient functions

$$\beta_U(d) = \sum_{\substack{ab=d \\ Na, Nb \le U}} \mu(a)\mu(b), \qquad g_U(s) = \sum_{\substack{b \mid s \\ Nb > U}} \mu(b).$$

For squarefree d, $\beta_U(d)$ is $\mu(d)$ times the number of the displayed ordered factorizations. For $Ns > U$, $g_U(s) = -\sum_{b \mid s,\, Nb \le U} \mu(b)$. The two regrouped pieces are

$$I_u = D^{-1/2} \sum_{\substack{d,c \text{ squarefree} \\ (d,c)=1}} \beta_U(d)\nu(dc)\chi_d(u)\chi_c(u) W(NdNc/D),$$

$$II_u = D^{-1/2} \sum_{\substack{a,s \text{ squarefree} \\ Na, Ns > U,\, (a,s)=1}} \mu(a) g_U(s) \nu(as)\chi_a(u)\chi_s(u) W(NaNs/D).$$

Then $M_u = -I_u + II_u$. All ideals here remain outside the same fixed excluded set. The short $2a_U$ term vanishes because $U < D$ and W is supported in $[1, 2]$. No phase or coprimality mask was removed.

Proposition 37.2 (An all-cutoff separate-piece bound is false)**.** *Take the allowed principal ν, $U = 1$, and a fixed nonnegative smooth W supported in $[1, 2]$, bounded below by a positive constant on a closed subinterval of $(1, 2)$ of positive length. For each of the two pieces,*

$$\sum_{0<Nu\le H} |I_u|^2 \gg_W \frac{D}{\log^2 D}, \qquad \sum_{0<Nu\le H} |II_u|^2 \gg_W \frac{D}{\log^2 D} \quad (H \ge 1).$$

Consequently a proposed bound HD^ε for each piece at $H = D^{3/4}$ fails for $\varepsilon < 1/4$. In the exact original notation $H(HD)^\varepsilon$, it fails for $\varepsilon < 1/7$. This refutes an all-cutoff termwise strengthening, not the original signed mean square or a specified moving-cutoff argument.

Proof. At $U = 1$, $a_U = \delta$, so $a_U * a_U * \zeta_0 = \zeta_0$ and $b_U * b_U * \zeta_0 = \mu + \zeta_0 - 2\delta$. On the annulus the two coefficients are 1 and $1 + \mu(n)$, respectively. On squarefree ideals the latter is zero or two. At the actual unit row $u = 1$, every original character equals one. A fixed-field prime-ideal theorem gives $\gg D/\log D$ good prime columns in the subinterval, so $I_1 \gg_W \sqrt{D}/\log D$. Fix a good prime ideal q_0. Products $q_0 p$ with varying distinct good primes in the rescaled subinterval have $\mu(q_0 p) = 1$. Their nonnegative contributions give $II_1 \gg_W \sqrt{D}/\log D$. Keeping that one row in each nonnegative energy proves the result. The prime-ideal theorem is a classical unconditional external input, with the field and q_0 fixed. □

The factorization does not shorten the primitive row conductor: for squarefree coprime a, s it is as, not a or s separately. For two resulting columns n, n' with common factor h, the oscillatory conductor is nn'/h^2 and a zero-preserving period is nn'/h. The signed low-gcd estimate and the independent positive arithmetic determinant comparison therefore remain open.

37.4.1 Exact factorization, retained zeros and the failed Cauchy route

Proof of the regrouping with original coefficients

The monoid consists of nonzero integral ideals prime to the fixed excluded set S. Every divisor of a good ideal is good, so the identity $\mu * \zeta_0 = \delta$ holds on this same monoid. Expanding convolution in (37.1) gives finite divisor sums. Multiply the identity by $\mu(n)^2\nu(n)\chi_n(u)W(Nn/D)$ and sum. The extra squarefree indicator does not change $\mu(n)$, since $\mu(n)^3 = \mu(n)$. On its support $n = abc$ forces each factor to be squarefree and any two to be coprime. Sextic multiplicativity, including zeros, gives $\chi_n(u) = \chi_a(u)\chi_b(u)\chi_c(u)$; a collision with any factor makes both sides zero. The fixed character also satisfies $\nu(n) = \nu(a)\nu(b)\nu(c)$ on these good ideals.

In the small-factor piece group $d = ab$. The remaining variable c is squarefree and coprime to d; $Nd \le U^2$ is necessary, but not sufficient for a nonzero $\beta_U(d)$: its specified truncated factorizations must still exist. For each such factorization on squarefree d, $\mu(a)\mu(b) = \mu(d)$, proving the coefficient formula. In the large-factor piece group $s = bc$. The condition $Nb > U$ implies $Ns > U$, and summing that divisor gives exactly $g_U(s)$. Since $Ns > U \ge 1$, s is not the unit ideal; its complete Möbius divisor sum vanishes, proving the alternative formula for g_U. This regrouping never replaces the two-variable weight by $W(Ns/D)$, never deletes $(a, s) = 1$, and never replaces the resulting coefficients by a favorable arbitrary family.

One can instead keep the unrestricted convolution identity on nonsquarefree columns, but then both individual pieces and their local conductor description change. For $U = 1$ and a good prime p, the column p^2 contributes one to each of $a_U * a_U * \zeta_0$ and $b_U * b_U * \zeta_0$, even though $\mu(p^2) = 0$; these cancel only after the pieces are recombined. Its squared sextic symbol has a cubic local component. Thus dropping total squarefreeness is not a harmless piecewise simplification, although the full unrestricted algebraic identity still holds.

The two conductor scales are unchanged

For a squarefree $n = as$ with $(a, s) = 1$, every prime of n has one nontrivial sextic local component in the row variable. Hence its primitive finite conductor is the ideal as; $NaNs \asymp D$ on the column support. On multiplying a column by the conjugate of another, the local exponent is zero at common primes, 1 at a prime of n/h, and -1 at a prime of n'/h. The common prime still imposes its original zero on rows. Writing $n = hr$, $n' = ht$ therefore gives exactly

$$\chi_n(u)\overline{\chi_{n'}(u)} = \mathbf{1}_{(u,h)=1}\chi_r(u)\overline{\chi_t(u)}, \qquad q = rt, \quad \mathfrak{l} = hrt.$$

Here q is the primitive oscillatory conductor and $\mathfrak{l}$ a period of the full zero extension. These are ideals, not necessarily squarefree rational norms. In particular, conjugate primes over one split rational prime are distinct coprime ideal factors. Full defining moduli of ν and primary conventions remain fixed in S; this row-conductor calculation does not assert a new uniform reciprocity theorem in the column variable. In the coprime bulk $Nq \asymp D^2$ remains large.

Why a first generic Cauchy step does not supply the saving

On one type-II dyad let $Na \asymp A$, $Ns \asymp B$, $AB \asymp D$. Keep the full profile and coprimality restrictions in

$$X_a(u) = \nu(a)\chi_a(u) \sum_{\substack{s \text{ squarefree} \\ Ns \asymp B,\ (a,s)=1}} g_U(s)\nu(s)\chi_s(u)W(NaNs/D).$$

The exact elementary Cauchy inequality is

$$\sum_{0<Nu\le H} \left| D^{-1/2} \sum_{Na\asymp A} \mu(a)X_a(u) \right|^2 \le \frac{\sum_{Na\asymp A}|\mu(a)|^2}{D} \sum_{Na\asymp A} \sum_{0<Nu\le H} |X_a(u)|^2.$$

The a-mask has been kept inside X_a. Even if one granted an optimistic uniform slice bound $(H + B)\sum_{Ns\asymp B}|g_U(s)|^2 D^\varepsilon$, the ordinary divisor estimate $|g_U(s)| \le \tau(s)$ and the fixed-field ideal count would only yield the envelope

$$A(H + B)D^\varepsilon \asymp (AH + D)D^\varepsilon.$$

That hypothetical slice estimate is not established here. This is an insufficiency of the generic upper-bound calculation, not a lower bound on the signed energy. At balanced $A, B \asymp D^{1/2}$ and $H = D^{3/4}$, the AH term loses $D^{1/2}$ relative to the target; the D term also exceeds H. A sharper use of the actual g_U, cross-factor constraints or covariance between the original pieces is required. This calculation does not refute all bilinear, moving-cutoff or dispersion methods.

The fixed-$U = 1$ lower bounds in Proposition 37.2 are different: they are genuine energy lower bounds for the separate pieces. If $W \ge w_0 > 0$ on $[c_1, c_2] \subset (1, 2)$, count primes in $[c_1D, c_2D]$ for I_1 and in $[c_1D/Nq_0, c_2D/Nq_0]$ for II_1. Removing S and q_0 removes finitely many primes. The prime-ideal theorem gives positive constants times $D/\log D$ in both cases; the latter contribution has coefficient two. Because every coefficient of II_1 is nonnegative, keeping these products is valid. This is unlike isolating the prime part of the full signed Möbius energy, where uncontrolled cross terms remain. For the exact requested bound $H(HD)^\varepsilon$ at $H = D^{3/4}$, the competing power is $D^{3/4+7\varepsilon/4}$, giving the threshold $\varepsilon < 1/7$. Replacing $(HD)^\varepsilon$ by D^ε reparametrizes the loss and gives the equivalent $1/4$ formulation. The positivity argument is specific to $U = 1$. For a concrete control, the primary element $7 - 21\omega$ has norm $637 = 7\cdot 7\cdot 13$ and three distinct ideal prime factors. At $U = 7$ its type-I coefficient is -1, its type-II coefficient is -2, and its Möbius value is -1. Thus the separate pieces need not have nonnegative coefficients at another cutoff; no moving-cutoff obstruction follows from the preceding positivity proof.

Exact finite checks and formal boundaries

The deterministic checker represents every good ideal of norm at most 1024 once by its primary generator, including inert prime ideals and squarefree products of three distinct prime ideals. It checks 1535 coefficient/regrouping cases at five cutoffs, retains 19680 encountered original zeros in actual sextic sums, and verifies 900 pair-conductor exponent ledgers. It evaluates principal ν and the fixed Kummer character $\nu(n) = \chi_n(2)$ on the same good ideals. The finite diagnostic weight is the rational profile $((Nn - D)(2D - Nn))^2/D^4$ on $[D, 2D]$, zero elsewhere; it is not claimed to be the smooth analytic weight of the theorem. Every identity is algebraic for arbitrary finite weights; these samples do not prove seminorm or scale-supremum estimates.

For example, at $D = 128$, $H = 16$, principal ν and $U = 1$, the unit-row normalized sums have the following exact common scaling:

$$\begin{array}{r|r} D^{9/2}M_1 & -122721831 \\ D^{9/2}I_1 & 314726661 \\ D^{9/2}II_1 & 192004830 \end{array}$$

Their exact difference is $II_1 - I_1 = M_1$. The lower-bound theorem uses the prime-ideal proof, not extrapolation from these small numbers. An independent no-production-import oracle also checks convolution, squarefree regrouping and weighted sextic sums.

`MobiusSplit.lean` proves eight actual statements: the inverse-ring identity, natural-number arithmetic truncation/tail, the Möbius Dirichlet identity, the unit cutoff, its exact tail convolution and coefficient, and nonnegativity. The natural-number Dirichlet ring is an actual arithmetic object; it is not the ideal convolution ring. Ideal arithmetic, sextic/Hecke character construction, analytic prime counting and the unproved signed mean square remain prose or named classical inputs. No new zero-free region, full GRH proof or positive determinant bridge has been obtained.

37.5 Formal coverage and the next research step

The new Lean interface checks actual Plücker polynomials, nodal matrix relations and determinants, finite clock/shift identities and Kraus positivity/trace preservation. The short-row module checks finite-character masks, original finite Gram expansion, matched-row lower bounds and actual Eisenstein norm/evaluation identities. Full planar Poisson summation, ideal-character interfaces, the AR classifications, the derived functors and the complete physics program are not all formalized by these components. Their theorem types and axiom dependencies are printed in the verification logs.

The next load-bearing research task is an estimate for the remaining low-gcd original arithmetic kernel, or an independently constructed positive arithmetic determinant family escaping the precisely stated finite-kernel obstructions. A learned ToricGT-style component may propose a family, choose a search ordering or discover a candidate identity. Acceptance still requires exact algebra, analytic estimates, Lean interfaces where available and independent critical review. A fitted zero picture or a small training loss is an observation, not the desired proof.

37.6 A full-mask Hecke expansion for the type-I piece

We now continue the signed decomposition through its actual squarefree inner sum. Fix $K = \mathbb{Q}(\sqrt{-3})$, the finite-order Hecke character ν, and the same finite excluded prime set S, containing primes above 6 and the conductor of ν. For $u \in \mathcal{O}_K \setminus \{0\}$, let ψ_u be the primitive Hecke character induced

by $\nu(n)(u/n)_6$ away from $S \cup \mathrm{supp}(u)$. It is defined before, and independently of, the type-I divisor d. The abelian Kummer extension $K(u^{1/6})/K$ constructs the sextic factor; multiplying by ν gives the stated character. This uses classical abelian reciprocity, not general Artin holomorphy. Write $\psi_{u,2}$ for the primitive character inducing its square and $\mathfrak{f}_u, \mathfrak{f}_{u,2}$ for the two primitive conductors. For a squarefree good ideal d put

$$T = T(u,d) = S \cup \mathrm{supp}(u) \cup \mathrm{supp}(d), \qquad R_T = \prod_{p \in T} Np, \quad Q_u = |D_K| N\mathfrak{f}_u.$$

All primes in T are deleted even if absent from either primitive conductor.

Theorem 37.3 (Restoration and a uniform scalar contour bound)**.** *For $\Re s > 1$ the original type-I inner Dirichlet series is*

$$F_{u,d}(s) = \sum_{\substack{c \text{ squarefree} \\ (c,T)=1}} \frac{\psi_u(c)}{(Nc)^s} = \frac{L(s,\psi_u)}{L(2s,\psi_{u,2})}\, C_T(s), \tag{37.2}$$

$$C_T(s) = \frac{\displaystyle\prod_{p \in T,\ p \nmid \mathfrak{f}_u} (1 - \psi_u(p)(Np)^{-s})}{\displaystyle\prod_{p \in T,\ p \nmid \mathfrak{f}_{u,2}} (1 - \psi_{u,2}(p)(Np)^{-2s})}. \tag{37.3}$$

It continues meromorphically to $\Re s > 1/2$, with only a possible simple pole at $s = 1$ when $\psi_u = 1$. In that case its residue is

$$\rho_T = \frac{\mathrm{res}_{s=1}\, \zeta_K(s)}{\zeta_K(2)} \prod_{p \in T} (1 + (Np)^{-1})^{-1}.$$

Fix $0 < \delta < 1/2$, $\varepsilon > 0$ and $W \in C_c^\infty((0,\infty))$ supported in $[1,2]$. Set

$$\mathcal{M}_4(W) = \sum_{j=0}^{4} \sup_x |(x\partial_x)^j W(x)|.$$

Uniformly for $Y \geq 1$, u and d,

$$\sum_{\substack{c \text{ squarefree} \\ (c,T)=1}} \psi_u(c) W(Nc/Y) = \mathbf{1}_{\psi_u = 1} \rho_T Y \widehat{W}(1) + O_{\nu,S,\delta,\varepsilon}\Big(\mathcal{M}_4(W) Y^{1/2+\delta} Q_u^{1/4-\delta/2+\varepsilon} R_T^{\varepsilon} \Big). \tag{37.4}$$

Here $\widehat{W}(s) = \int_0^\infty W(x) x^{s-1}\, dx$. The continuation and functional equation of degree-one Hecke functions are classical external inputs; the contour argument is given below.

At a good prime with $v_p(u) = 3$, ψ_u is ramified while its square is unramified; the second product in (37.3) must restore a factor invisible to squaring the zero-extended primitive value. At $v_p(u) = 6$ both characters can forget the prime, but the original row still vanishes on columns divisible by it. In particular, for principal ν, $u = \pi^3$ and $u = \pi^6$ at $N\pi = 7$, the deleted local factors are

	primitive ratio at $s = 1$	restoration	full masked factor
$v_p(u) = 3$	48/49	49/48	1
$v_p(u) = 6$	8/7	7/8	1

These are exact local calculations, not numerical evidence about zeros.

For $1 \le U$, $U^2 \le D$, insert $Y = D/Nd$ into (37.4) and retain the actual $\beta_U(d)$ and outer $\nu(d)\chi_d(u)$. Classical tame Kummer conductors give $Q_u \ll_\nu Nu$. Thus the normalized I_u equals its displayed principal-residue sum plus an error E_u with

$$|E_u| \ll_{\nu,S,\delta,\varepsilon} \mathcal{M}_4(W) D^{\delta} U^{1-2\delta+\varepsilon} (Nu)^{1/4-\delta/2+\varepsilon}. \tag{37.5}$$

The resulting elementary energy envelope is only

$$\sum_{0<Nu\le H} |E_u|^2 \ll \mathcal{M}_4(W)^2 D^{2\delta} U^{2-4\delta+\varepsilon} H^{3/2-\delta+\varepsilon}. \tag{37.6}$$

It does not prove the short-row target of order H up to small losses. This is an insufficient upper bound, not a lower bound on the actual error or a counterexample to coefficient-sensitive averaging. The original signed mean square and positive determinant bridge stay open.

37.7 Primitive conductors, deleted factors and the scalar contour

37.7.1 Constructing the column character without losing its zeros

Let $\alpha^6 = u$. Since K contains μ_6, the extension $K(\alpha)/K$ is abelian, with character $g \mapsto g(\alpha)/\alpha$. At $p \nmid 6u$, arithmetic Frobenius gives the residue $u^{(Np-1)/6}$, exactly the source's sextic symbol. Abelian reciprocity makes it a finite-order Hecke character; multiply by ν and take its primitive inducing character. The classical reciprocity input is [89, Theorem 0.8 and Chapter I,§1]. The finite-order archimedean character is trivial, since $\mathbb{C}^\times$ is connected.

At $p \nmid 6$, write $u = \pi^e v$ with v a local unit. A sixth root of v lies in an unramified extension: its residue root is separable and lifts by Hensel's lemma. Inertia acts on a sixth root of π through μ_6, so on α the inertia character has order $6/\gcd(6,e)$. It is trivial exactly when $6 \mid e$; its square is trivial exactly when $3 \mid e$. A nontrivial tame one-dimensional character has conductor exponent one. Since ν is unramified outside S, it cannot cancel this inertia there. At primes above 6, the groups $K_p^\times/(K_p^\times)^6$ are finite; their finitely many characters have a uniform maximum conductor. Consequently

$$\mathfrak{f}_u \mid \mathfrak{c}_\nu \prod_{p\mid u,\ p\nmid 6} p, \qquad Q_u \ll_\nu Nu.$$

The fixed ideal $\mathfrak{c}_\nu$ includes the wild and fixed ν factors. No assertion identifies $\mathfrak{f}_u$ with the larger full zero modulus.

For $p \notin T$ put $z = \psi_u(p)(Np)^{-s}$. Its squarefree factor $1 + z = (1 - z^2)/(1 - z)$ proves the ratio using the *same* deleted set in numerator and denominator. Restoring the primitive Euler factors yields (37.3). At a prime where the primitive square becomes unramified its value cannot be obtained by squaring the sentinel zero $\psi_u(p) = 0$. For principal ν, $u = \pi^3$ has a quadratic Kummer character whose primitive square is globally principal. Its local value in that square is one, not zero. For $u = \pi^6$ both primitive characters are principal, although the full family still deletes p. These two cases prove the local table directly.

37.7.2 Why the half-plane above one half is available

For a character η write $L^T(s,\eta)$ for its Euler product with all primes of T removed. For $\sigma > 1/2$ the product $1/L^T(2s, \psi_{u,2})$ converges absolutely and is bounded by $\zeta_K(2\sigma)$, uniformly in the character, T and $t = \Im s$. Every deleted finite factor is nonzero there. Therefore

$$F_{u,d}(s) = L(s,\psi_u) \prod_{p\in T,\, p\nmid \mathfrak{f}_u} (1 - \psi_u(p)(Np)^{-s})/L^T(2s, \psi_{u,2})$$

has just the stated possible principal pole. This uses absolute convergence at $2\sigma > 1$, not a conjectural zero-free assertion on the critical line. For any fixed $\sigma > 0$ and $\eta > 0$,

$$\prod_{p \in T} (1 + (Np)^{-\sigma}) \ll_{\sigma,\eta} R_T^{\eta}.$$

Indeed $1 + q^{-\sigma} \le q^{\eta}$ for all sufficiently large q; the remaining finitely many prime ideals give a uniform fixed constant. This controls every moving deleted prime; the denominator has already been bounded by the full convergent zeta product.

We use the classical completed Hecke functional equation in the form

$$\Lambda(s, \psi_u) = Q_u^{s/2} (2\pi)^{-s} \Gamma(s) L(s, \psi_u), \qquad \Lambda(s, \psi_u) = w_u \Lambda(1 - s, \overline{\psi_u}), \quad |w_u| = 1.$$

This is a named external theorem, not a newly formalized analytic result; compare [88, Theorem 4.3, Corollary 4.4]. The cited notes sketch some of Tate's calculations; their incomplete displayed epsilon formulas are not used as independently checked constants here. At $\Re s = 1 + \eta$, absolute convergence bounds L by $\zeta_K(1 + \eta)$. The functional equation and Stirling's formula give on $\Re s = -\eta$ the bound $Q_u^{1/2+\eta}(1 + |t|)^{1+2\eta}$ up to a fixed constant. Phragmén–Lindelöf on this strip therefore gives, for fixed $0 < \sigma < 1$,

$$|L(\sigma + it, \psi_u)| \ll_{\sigma,\eta} Q_u^{(1-\sigma)/2+\eta} (1 + |t|)^{1-\sigma+2\eta}.$$

For the principal character apply the strip argument to $(s - 1)L(s, 1)/(s + 1)$, then divide back on the fixed line $\sigma < 1$. The constants need not be uniform as $\sigma \to 1$. Polynomial vertical strip growth and finite order, as supplied by classical Hecke theory, justify this application. No Lindelöf or subconvexity bound is inserted.

37.7.3 Mellin inversion, residues and profile uniformity

Initially, absolute convergence and compact smooth support give

$$S_{u,d}(Y) = \frac{1}{2\pi i} \int_{(1+\eta)} \widehat{W}(s) Y^s F_{u,d}(s)\, ds.$$

Four integrations by parts using $x\partial_x$ give $|\widehat{W}(\sigma + it)| \ll_{\sigma} \mathcal{M}_4(W)(1 + |t|)^{-4}$. Choose $0 < \eta < \min(\varepsilon/8, 1/8)$, decreasing it further when distributing the small losses, and shift to $\sigma = 1/2 + \delta$. The convergent reciprocal Euler product, the finite factor bound and convexity above control the complete integrand. Their polynomial t growth is integrable against this Mellin decay and makes the horizontal edges tend to zero. The only crossed pole is $s = 1$ when $\psi_u = 1$; evaluating its finite factors gives exactly ρ_T. Taking absolute values on the new vertical line proves (37.4), after renaming the small losses. This also proves uniformity over any family of profiles with bounded $\mathcal{M}_4$; it does not interchange a profile supremum with an arithmetic mean square.

In the original I_u, the inner profile is exactly $W(Nc/Y)$ with $Y = D/Nd$; no d-dependent derivative enlargement occurs. On the support of β_U, $Nd \le U^2 \le D$, hence $Y \ge 1$. Also $R_T \le C_S Nu\, Nd$. The principal term is explicitly

$$P_u = \mathbf{1}_{\psi_u = 1} \sqrt{D}\, \widehat{W}(1) \sum_{\substack{d \text{ squarefree} \\ (d,S)=1}} \frac{\beta_U(d) \nu(d) \chi_d(u)}{Nd} \rho_{T(u,d)}.$$

This sum retains all original phases and zeros; no positivity of it is assumed. For the error use the actual truncated factorizations, not a free coefficient bound:

$$\sum_{d \text{ squarefree}} \frac{|\beta_U(d)|}{(Nd)^{1/2+\delta-\eta}} \le \left(\sum_{Na \le U} (Na)^{-1/2-\delta+\eta} \right)^2 \ll_{\delta,\eta} U^{1-2\delta+2\eta}.$$

The fixed-field ideal count is $O_K(X)$; dyadic summation proves the last inequality for sufficiently small $\eta < \delta + 1/2$. Inserting this and the conductor/radical bounds proves (37.5). The elementary lattice count $\#\{u : 0 < Nu \le H\} = O_K(H)$ then gives (37.6). Rows are not divided by units.

At $H = D^{3/4}$ and $U = D^a$ with $0 \le a \le 1/2$, the power of the resulting error envelope *relative to* H is

$$\frac{3}{8} + \frac{5}{4}\delta + (2 - 4\delta)a$$

up to the arbitrarily small losses. It remains positive for every $0 < \delta < 1/2$. Thus this scalar convexity argument alone supplies no short-row saving. This is a limitation of the estimate just derived, not an obstruction to averaging the numerators over Kummer rows, retaining signed coefficients, or exploiting covariance with type II.

The seminorm uniformity is not a proof of the original scale supremum. For each independently chosen scale D' the displayed outer argument requires $U^2 \le D'$. If a fixed cutoff is retained while D' shrinks, then eventually even $D' \le U$: the short $2a_U$ term in the Vaughan identity can meet the support and must be restored. Neither that term nor the covariance with type II may be omitted in a supremum or reassembly.

37.7.4 Verification boundaries

`HeckeTypeI.lean` checks seven actual complex local/finite-product statements, including independent primitive coefficient arrays and their full deleted-factor restoration. It does not identify an ideal Hecke series with an abstract finite product or formalize a Mellin contour. The exact checker includes split and inert prime ideals, actual sextic phases, conductor drops, sixth-power rows and original mask zeros. The analytic theorem above uses classical abelian reciprocity, Hecke continuation/functional equation and standard complex-analytic tools as external inputs. Full ideal-character/formal analytic objects, the original signed low-gcd mean square and every GRH completion obligation remain open.

Part VI

Certified analytic targets and weighted arithmetic moments

Chapter 38

Validated Dirichlet targets and finite readout certificates

38.1 A finite, validated approximation result

Let $\chi_3 = (0, 1, -1)$, $\chi_4 = (0, 1, 0, -1)$ and $\chi_5 = (0, 1, -1, -1, 1)$, extended periodically, with parities $a = 1, 1, 0$. We approximate the completed functions

$$\Lambda_q(s) = (q/\pi)^{(s+a)/2}\Gamma((s + a)/2)L(s, \chi_q).$$

The primitive theta/Mellin identity is the explicit classical analytic input; no hypothesis about zeros is used. These three examples do not assert a uniform result for all conductors, general Hecke functions or Artin holomorphy.

Theorem 38.1 (Scope of the supplied finite certificate)**.** *For each $q = 3, 4, 5$, the supplied exact-rational calculation constructs a complex polynomial P_q of degree 28 satisfying*

$$\sup_{|s-1/2|\le 7/10} |P_q(s) - \Lambda_q(s)| < 5 \cdot 10^{-15}.$$

The computation includes enclosures of all 64 true Fourier-circle nodes, completed-function sample error, analytic truncation, Fourier aliasing, the exact closed-form 180-step gradient-descent iterate and coefficient midpoint rounding. The Python implementation and informal analytic proof have independent checks; this is not a kernel-checked Lean theorem.

Proof. Write $F(c+z) = \sum_{n\ge 0} a_n z^n$, with $c = 1/2$, $R = 7/10$, $\rho = 6/5$, $r = 12/5$. The independently recomputed rational theta majorants are strictly below $M_q = 4, 10, 6$, respectively, on $|z| \le r$. Use true roots $\zeta_j = e^{2\pi ij/64}$ and rational labels y_j with proved error $|y_j - F(c + \rho\zeta_j)| \le \eta$. Use the real Euclidean gradient on complex coefficient coordinates for

$$\mathcal{L}(b) = \frac{1}{128}\sum_{j=0}^{63}\left|\sum_{n=0}^{28} b_n\zeta_j^n - y_j\right|^2.$$

Discrete Fourier orthogonality gives the least-squares optimum $b_n^* = 64^{-1}\sum_j y_j\bar{\zeta}_j^n$, $0 \le n \le 28$, and gradient $\nabla\mathcal{L}(b) = b - b^*$. For step $1/4$ and zero initialization, the exact 180-step iterate is $b_n^{180} = (1 - (3/4)^{180})b_n^*$. The code evaluates this closed form; it does not claim an explicit180-update optimizer run.

Set $u = R/\rho = 7/12$, $v = R/r = 7/24$ and $w = (\rho/r)^{64} = 2^{-64}$. Let $\widehat{b}_n$ be an outward rectangle enclosing b_n^* and ϵ_n the sum of the coordinate halfwidths of the rectangle for b_n^{180}. Choose each actual polynomial coefficient as that rectangle's exact rational midpoint c_n. The normalized basis is explicit:

$$P_q(s) = \sum_{n=0}^{28} c_n \left(\frac{s - 1/2}{6/5}\right)^n.$$

Thus the exported coefficient with index n multiplies the normalized variable, rather than the raw power $(s - 1/2)^n$. Its error on the compact disk is bounded by

$$E_{\mathrm{opt}} = (3/4)^{180} \sum_{n=0}^{28} |\widehat{b}_n|_1 u^n, \qquad E_{\mathrm{arithmetic}} = \sum_{n=0}^{28} \epsilon_n u^n,$$

$$E_{\mathrm{oracle}} = \eta \frac{1 - u^{29}}{1 - u}, \qquad E_{\mathrm{alias}} = M_q \frac{w}{1 - w} \frac{1 - v^{29}}{1 - v},$$

$$E_{\mathrm{Taylor}} = M_q \frac{v^{29}}{1 - v}.$$

Here $|\widehat{b}_n|_1$ is the sum of the maximum absolute real and imaginary coordinates, a safe upper bound for every enclosed complex modulus. Cauchy's estimate $|a_n| \le M_q r^{-n}$ and the Fourier identity $b_n^* = a_n \rho^n + \sum_{\ell \ge 1} a_{n+64\ell} \rho^{n+64\ell}$ for exact labels prove the alias and Taylor bounds. Label perturbations contribute at most η per Fourier coefficient. The remaining two terms follow directly from the exact iterate and coefficient rectangles. Each term is rounded upward to a 180-bit dyadic rational; the reported total is the exact sum of those reported terms. The certified totals below are strictly below the asserted threshold. Detailed sample enclosures are proved in the extended edition and encoded with exact integer endpoints. □

Conductor	Maximum sample radius	Uniform polynomial bound
3	3.026×10^{-17}	1.786×10^{-15}
4	7.206×10^{-17}	4.455×10^{-15}
5	1.404×10^{-16}	2.906×10^{-15}

The displayed values are rounded upward; exact rational records establish the strict inequalities.

38.2 What this does and does not certify

The final JSON records exact rational centers, interval endpoints, source hashes and all five error terms. Float values are display summaries only. A high-precision comparison is an independent diagnostic, not the reason an interval contains its mathematical target. Arithmetic uses outward integer operations, and invalid float/order inputs are rejected, including through typed caches. Earlier pilots and failed validation probes are retained.

This is a fixed finite tolerance/configuration. Increasing accuracy needs new truncation and precision choices; the fixed $N = 11, T = 128$ interface is not an arbitrary-accuracy oracle. The broader approximation existence theorem is separate. The certificate says nothing about the location of zeros: P_q is not required to be real-rooted or a self-adjoint spectral determinant. The independent arithmetic determinant identity, positivity and original signed short-row/covariance estimates remain open. No GRH proof or complete new Lean4 formalization is claimed.

38.3 Validated primitive operations

Real intervals are closed dyadic intervals $[l2^{-224}, h2^{-224}]$ with integer endpoints; complex intervals are Cartesian products. Addition is exact at this scale. For multiplication take the minimum/maximum of all four integer endpoint products, divide by 2^{224} and round down/up. For a reciprocal whose interval omits zero, reverse the endpoint order and round $2^{448}/h$ down and $2^{448}/l$ up. Negative denominators and scalar division use the same endpoint rules. Each operation encloses all represented real values by monotonicity; induction proves inclusion for every expression built from them. Rectangular complex multiplication uses these real rules. The sum of coordinate halfwidths bounds the complex distance from its exact rational center. Binary floating arguments are never silently converted.

For $0 < x < 1$, the alternating arctangent sum and the endpoint obtained by adding the next signed term enclose $\arctan x$. Sixty terms at $1/5$ and $1/239$, together with Machin's identity $\pi = 16\arctan(1/5) - 4\arctan(1/239)$, give the interval for π. The negative coefficient reverses the second interval. The identity follows from tangent addition and the range of the two angles; no decimal value of π is a trusted input.

For rational $x > 0$, range-reduce $x = 2^k v$, $1 \le v < 2$. With $z = (v-1)/(v+1) \le 1/3$,

$$\log v = 2\sum_{j=0}^{J-1} \frac{z^{2j+1}}{2j+1} + \mathcal{R}, \qquad 0 \le \mathcal{R} \le \frac{2z^{2J+1}}{(2J+1)(1-z^2)}.$$

The geometric tail bounds each remaining denominator below by $2J+1$. Use $J = 92$, the analogous expression for $\log 2$, and sign-aware interval multiplication by k. This covers negative k as well.

For complex z, repeatedly halve until its interval ℓ^1 magnitude bound is $A \le 1/2$. The degree 60 Taylor polynomial for e^z then has remainder at most

$$\frac{A^{61}}{61!}\frac{1}{1-A/62}.$$

Successive absolute terms have ratio at most $A/62$, so geometric comparison proves this bound. Add its symmetric interval to each coordinate, then square outward the required number of times. The identity $e^{2z} = (e^z)^2$ and interval inclusion prove the final enclosure. Caches are type-sensitive: otherwise a cached exact argument can accidentally bypass rejection of an equal-valued float. No implementation change is allowed during the recorded run; the producer verifies source bytes again before emitting its certificate.

38.4 Recomputing the compact growth constants

For the larger growth disk, $c = 1/2$, $r = 12/5$, take $k = 2$ when $a = 1$ and $k = 1$ when $a = 0$. Both real Mellin exponents on that disk are at most k. Define

$$Q_k(x) = \sum_{j=0}^{k} \frac{k!}{(k-j)!x^{j+1}}, \qquad U_{16}(x) = (1 + x/16)^{-16}, \qquad \delta = 3/q.$$

Integration by parts gives $\int_1^\infty t^k e^{-xt}\,dt = e^{-x}Q_k(x)$. The same Gaussian split and geometric-tail comparison used below, now with cutoff $n_0 = 8$, imply the exact rational majorant

$$\widehat{M}_q = 2\left[\sum_{n=1}^{7} n^a U_{16}(\delta n^2)Q_k(\delta n^2) + C_a Q_k(64\delta)\frac{U_{16}(32\delta)}{1 - U_{16}(8\delta)}\right], \quad C_0 = 1, \quad C_1 = (1+\delta^{-1})/2.$$

Replacing the actual $d = \pi/q$ by the smaller positive δ increases the integral majorant. Exact fraction comparison gives $\widehat{M}_3 < 4$, $\widehat{M}_4 < 10$, $\widehat{M}_5 < 6$. The producer recomputes these fractions, asserts the strict comparisons and exports them; the constants in the readout proof are thus checked rather than supplied by a floating growth estimate.

38.5 The completed-function integral and its tails

Let $d = \pi/q$ and $\theta_q(t) = \sum_{n\ge1} \chi_q(n) n^a e^{-dn^2 t}$. The standard primitive theta transformation, followed by splitting the Mellin integral at1, gives

$$\Lambda_q(s) = \int_1^\infty \theta_q(t) t^{(s+a)/2-1}\, dt + \int_1^\infty \theta_q(t) t^{(1-s+a)/2-1}\, dt.$$

The second root-number coefficient is1 for these three characters: their finite Gauss sums are $i\sqrt{3}$, $2i$ and $\sqrt{5}$, respectively. For the last, $2\cos(2\pi/5) - 2\cos(4\pi/5) = \sqrt{5}$; the first two are direct conjugate-root differences. Division by $i^a\sqrt{q}$ gives the claimed normalization. Exponential decay makes the two integrals entire. This classical theta identity, not an assumption of Artin holomorphy or desired positivity, is the analytic input of the implementation.

The actual circle nodes are enclosed by computing $e^{2\pi ij/64}$ with the validated primitives. All input boxes fit $D = [-1,2] + i[-4/3, 4/3]$. Thus both exponents $p = (s+a)/2-1$ and $p' = (1-s+a)/2-1$ satisfy $|\Re p| \le 2$, $|\Im p| \le 2/3$. The domain guard precedes all term discards. Retain $1 \le n \le 11$ and integrate $1 \le t \le 128$.

Put $\delta = 3/q < d$, $U(x) = (1+x/128)^{-128}$ and $Q(x) = x^{-1} + 2x^{-2} + 2x^{-3}$. Since $(1+x/128)^{128} \le e^x$, $e^{-x} \le U(x) < 1$ for $x > 0$. Integration by parts gives $\int_1^\infty t^2 e^{-xt}\, dt = e^{-x}Q(x)$. With $C_0 = 1$, $C_1 = (1+\delta^{-1})/2$ the omitted-n tail of both integrals is

$$2C_a Q(\delta 12^2) \frac{U(\delta 12^2/2)}{1 - U(12\delta)}.$$

Indeed $n^a e^{-\delta n^2/2} \le C_a$, the function Q decreases, and $(12+j)^2 \ge 12^2 + 24j$. These inequalities yield a geometric bound after splitting the exponent in halves. The retained-n time tail is at most

$$\sum_{n=1}^{11} 2n^a 128^3 U(128\delta n^2) Q(128\delta n^2).$$

It follows by substituting $t = 128u$ and majorizing $t^{\Re p}$ by t^2. The two tails are disjoint: omitted n use the full integral, whereas retained n contribute only $t > 128$.

38.6 High-order integration with a certified remainder

Split each dyadic interval $[2^j, 2^{j+1}]$, $j = 0, \dots, 6$, into four equal panels. For its midpoint m and halfwidth h, $h/m \le 1/9$. For $f(z) = e^{-\lambda z} z^p$, $\lambda = \pi n^2/q$, the principal logarithm is analytic on $|z-m| \le \rho = m/2$. On that circle,

$$|f(z)| \le M_\rho = 3\max\{(3m/2)^2, (m/2)^{-2}, 1\} U(\delta n^2 m/2).$$

Here $\Re z \ge m/2$, $|\arg z| \le 1$ and $e^{|\Im p|} \le e^{2/3} \le 3$. The maximum handles both signs of $\Re p$. Cauchy's coefficient estimate and cancellation of odd powers on $[-h,h]$ therefore bound the error after degree $2K$ by

$$\frac{2hM_\rho (h/\rho)^{2K+2}}{(2K+3)(1-(h/\rho)^2)}.$$

Indeed integrate each remaining even term, replace its denominator by the first omitted denominator, then sum a geometric series. Here $K = 12$. Multiply by $2n^a$ for both Mellin terms and sum all 28 panels and retained n. Keeping this majorant even for later discarded terms only overcounts error.

To evaluate the polynomial stably, set $u = h/m$, $q_{-1} = 0$, $q_0 = 1$ and use

$$q_{j+1} = \frac{u(p - \lambda m - j)q_j - (\lambda m)u^2 q_{j-1}}{j+1}.$$

Multiplying $f' = (-\lambda + p/t)f$ by $t = m + x$ and matching coefficients proves this recurrence, with $q_j = f^{(j)}(m)h^j/(j!f(m))$. The integrated polynomial is $2he^{-\lambda m}m^p \sum_{j=0}^{K} q_{2j}/(2j+1)$; all its arithmetic is outward.

Fixed absolute exponential-rounding errors can be amplified by high-order coefficients in late panels. The code therefore first bounds a complete (n, panel) pair, including both powers, by

$$4hn^a(m+h)^2 U(\delta n^2(m-h)).$$

For real $t \geq 1$ its phase has modulus1 and $t^{\Re p} \leq (m+h)^2$, proving the bound. If it is below 2^{-90}, skip that pair entirely and add its bound to the final radius. This is controlled truncation, not numerical underflow. The final sample radius is the interval-sum halfwidth plus the omitted-n, time, Cauchy and discard bounds. All are recorded separately and checked as nonnegative. No high-precision special-function routine is trusted here.

38.7 Reproduction and remaining interfaces

Run the preserved source on the existing Linux Python environment with no new packages: `python3` on `examples/analytic_oracle/theta_oracle.py`, with argument `-output NEW`. It refuses to overwrite an existing experiment directory. The final-v5 experiment contains 192 samples, three rational degree 28 polynomials, copied source and SHA-256 hashes. Independent validation checks rational endpoint arithmetic, transcendental enclosures, 1160 exact coefficient identities, high- precision completed-function comparisons and the exported component sums.

The fixed-parameter oracle solves a concrete evaluation/certification gap. It does not identify a positive arithmetic operator, force real-rooted polynomials, prove the signed original-family short-row bound or supply complete Lean4 verification. Surface/order and neural architectures may use these certificates as independent targets, but a small learned loss is not a substitute for the remaining arithmetic and categorical theorems.

38.8 Requested-error readouts from preserved certified labels

The accepted final-v5 sample certificate is preserved unchanged. For each $q = 3, 4, 5$, it supplies $m = 64$ rational complex labels y_j, bounds $|y_j - \Lambda_q(c + \rho\zeta_j)| \leq \eta_j$, and outward rectangles enclosing the true roots $\zeta_j = e^{2\pi ij/m}$, where $c = 1/2$, $\rho = 6/5$. The classical primitive theta/Mellin identity and accepted growth bounds $M_q = 4, 10, 6$ on $|s - c| \leq r = 12/5$ remain the analytic inputs. This extension accepts an exact rational error request $\varepsilon > 0$ on the fixed compact $|s - c| \leq R = 7/10$. It changes the finite readout, while retaining the certified sample errors and the 64-node alias budget. It is not an arbitrary-accuracy theta-sampling interface.

Theorem 38.2 (Executed rational readout with explicit refusal)**.** *For each supported conductor and rational request, the finite-data selection below either returns a normalized rational polynomial*

P and an executed, exactly replayable gradient-descent trace with

$$\sup_{|s-c|\le R} |P(s) - \Lambda_q(s)| \le \varepsilon,$$

or refuses the request with the exact minimum base budget over all 64 *allowed degrees. Refusal concerns attainability by this particular fixed-data majorant; it is not an impossibility theorem for approximation.*

Proof. Let B_n be an outward rectangle enclosing $b_n^* = m^{-1}\sum_j y_j \bar{\zeta_j^n}$, $0 \le n < 64$, computed from the preserved root rectangles. Put $t_n = \mathrm{mid}(B_n)$ and let e_n be the sum of its coordinate halfwidths. These are exact rationals, and $|t_n - b_n^*| \le e_n$. For a selected $d < 64$ execute, using exact rational operations,

$$b_n^0 = 0, \qquad b_n^{k+1} = \tfrac{3}{4} b_n^k + \tfrac{1}{4} t_n, \qquad 0 \le n \le d.$$

This is genuine gradient descent with step $1/4$ for the explicitly specified real Euclidean objective $J(b) = \frac{1}{2}\sum_{n=0}^{d} |b_n - t_n|^2$, whose gradient is $b - t$. All iterates and exact objective values are retained. The output is literally

$$P_k(s) = \sum_{n=0}^{d} b_n^k \left(\frac{s-c}{\rho}\right)^n.$$

Set $u = R/\rho = 7/12$, $v = R/r = 7/24$, $w = (\rho/r)^{64} = 2^{-64}$, $S_d(x) = \sum_{n=0}^{d} x^n$ and $\eta = \max_j \eta_j$. The five budgets are

$$E_{\mathrm{opt}}(k) = \sum_{n=0}^{d} |b_n^k - t_n|_1 u^n, \qquad E_{\mathrm{oracle}} = \eta S_d(u),$$

$$E_{\mathrm{alias}} = M_q \frac{w}{1-w} S_d(v), \qquad E_{\mathrm{Taylor}} = M_q \frac{v^{d+1}}{1-v},$$

$$E_{\mathrm{arithmetic}} = \sum_{n=0}^{d} e_n u^n.$$

Here $|x + iy|_1 = |x| + |y|$. Cauchy's estimate and true-root Fourier orthogonality give the alias and Taylor terms; certified label errors give the oracle term. Triangle inequality applied to $b_n^k - b_n^* = (b_n^k - t_n) + (t_n - b_n^*)$ gives the other two. Thus their exact sum bounds the compact-uniform error.

Define $C_d = E_{\mathrm{oracle}} + E_{\mathrm{alias}} + E_{\mathrm{Taylor}} + E_{\mathrm{arithmetic}}$. Select the smallest $d < 64$ with $C_d < \varepsilon$; if none exists, report $\min_{d<64} C_d$ and refuse. For a selected degree, $E_{\mathrm{opt}}(k) = (3/4)^k \sum_n |t_n|_1 u^n \longrightarrow 0$. Therefore executing updates until $E_{\mathrm{opt}}(k) \le \varepsilon - C_d$ terminates after finitely many steps. The serialized coefficients, budgets, targets and trace use exact rational endpoints; displayed decimal approximations are not proof inputs. □

38.9 Objective semantics, precision floors and replay

The original true-circle sample-label least-squares objective is

$$\mathcal{L}_y(b) = \frac{1}{2m} \sum_{j=0}^{m-1} \left| \sum_{n=0}^{d} b_n \zeta_j^n - y_j \right|^2.$$

With $d < m$, Fourier orthogonality gives $A^*A = mI$ and the real Euclidean coordinate gradient $\nabla \mathcal{L}_y(b) = b - b^*$. The executed objective J instead has the exact rational midpoint target t. The

difference $\nabla\mathcal{L}_y - \nabla J = t - b^*$ is enclosed coefficientwise by e_n. Consequently this is an actual rational GD run for J and a certified perturbed-gradient implementation for $\mathcal{L}_y$. It is not the exact optimizer trajectory of the ideal-root objective, nor a replay of neural or quantum training. An interval enclosure of an ideal-root GD trajectory would be a different explicitly labelled object.

Each actual update contracts $b^k - t$ by $3/4$, so the exact stored losses satisfy $J(b^{k+1}) = (9/16)J(b^k)$. A replay recomputes every rational coordinate update, loss and weighted residual. The closed form $b^k = (1 - (3/4)^k)t$ is an independent check on the executed trace, not its producer. Exact rational loop coordinates introduce no further midpoint or floating export error. The arithmetic budget covers the difference between the certified Fourier rectangles and their midpoint targets, including the inherited root enclosure and outward interval operations. A subsequent float conversion requires its own exact conversion-error bound.

The normalized polynomial convention is essential: a stored coefficient with index n multiplies $((s - 1/2)/(6/5))^n$, not $(s - 1/2)^n$. The input certificate is pinned by SHA-256, including its source hashes, all 192 sample enclosures, root rectangles and analytic radius components. Producing source is captured at entry, checked unchanged before emission, and copied into a fresh output directory. An existing output is never overwritten. An independent replay should also check the fixed input hash, all dimensions, degree choice, the first stopping iterate, all five exact terms and their literal sum against the requested rational tolerance.

The attainable boundary of this majorant is

$$C_{\min,q} = \min_{0 \le d < 64} C_{q,d}.$$

Every request $\varepsilon > C_{\min,q}$ has strict budget slack for some degree and the proved finite stop rule. At or below that boundary this interface refuses. The degree minimizing C_d need not be 63: Taylor error decreases with degree while the oracle and arithmetic sums increase. In particular $C_d \ge \eta$ and $C_d \ge M_q 2^{-64}/(1 - 2^{-64})$. Increasing the number of optimization steps does not lower these fixed-data budgets. Approximate boundary values on the stated compact are $7.2929 \cdot 10^{-17}$, $1.7370 \cdot 10^{-16}$ and $3.3741 \cdot 10^{-16}$ for $q = 3, 4, 5$; only the exact exported rational minima are used for acceptance. These are certificate floors, not lower bounds on the actual errors.

A full adaptive theta oracle would separately need proof-preserving choices of omitted-n cutoff, time cutoff, quadrature order, whole-panel discard budget, primitive series lengths, interval precision and serialized-bound precision. The present $N = 11$, $T = 128$, 224-bit arithmetic, 60/92/60 primitive series lengths, 2^{-90} discard threshold and 180-bit rounded budgets cannot support every positive request. Increasing a nominal bit count alone leaves the fixed primitive remainders and analytic tails in place. The preserved labels are not recomputed here. The classical identity, finite arithmetic and informal proof are not new Lean declarations. No zero-location, all-conductor, positive arithmetic determinant, quantum-advantage or GRH conclusion follows.

The interactive replay is available at the certified readout laboratory. All decimal graphics are illustrative views of the linked exact records.

38.10 Requested-error theta samples for three fixed conductors

For the primitive characters $\chi_3 = (0, 1, -1)$, $\chi_4 = (0, 1, 0, -1)$, $\chi_5 = (0, 1, -1, -1, 1)$ with parities $a = 1, 1, 0$, retain the classical primitive theta/Mellin identity and root number one already stated above. Put $D = [-1, 2] + i[-4/3, 4/3]$ and $\delta = 3/q$. The following adaptive extension is implemented with independent interval and sample checks; it is an informal analytic theorem, not a Lean result.

Theorem 38.3 (Finite adaptive sample specification)**.** *For every supported conductor, exact rational $s \in D$, and rational $\eta > 0$, the choices below terminate and give a rational complex midpoint y and exact rational radius $R \le \eta$ with $|y - \Lambda_q(s)| \le R$. The same conclusion holds for a specified true circle node when its root and node enclosures are refined on every precision retry.*

Proof. For $x \ge 0$ define the exact rational bound $E(x) = 2^{-\lfloor x \rfloor}$. Since $e > 2$, $e^{-x} \le E(x)$; this bound is nonincreasing and tends to zero. Let $Q(x) = x^{-1} + 2x^{-2} + 2x^{-3}$ and $C_0 = 1$, $C_1 = (1 + \delta^{-1})/2$. For $N \ge 1$, $n_0 = N + 1$, $J \ge 1$, $T = 2^J$, use

$$B_n = 2C_a Q(\delta n_0^2) \frac{E(\delta n_0^2/2)}{1 - E(\delta n_0)},$$

$$B_t = \sum_{n=1}^{N} 2n^a T^3 E(\delta n^2 T) Q(\delta n^2 T).$$

Here $\delta n_0 \ge 6/5$ ensures a positive denominator; $E(x)$ equals one for $0 \le x < 1$, so this safeguard is essential. On the four panels of each $[2^j, 2^{j+1}]$, write midpoint m, halfwidth h, $\rho = m/2$, $v = h/\rho \le 2/9$, and $B(m) = \max\{(m + \rho)^2, (m - \rho)^{-2}, 1\}$. Use the Cauchy remainder

$$B_Q = \sum_{\text{panels}} \sum_{n=1}^{N} \frac{2n^a \, 2h \, 3B(m) E(\delta n^2 m/2) v^{2K+2}}{(2K + 3)(1 - v^2)}.$$

Choose in turn the first $N \ge 1$, first $J \ge 1$, and first $K \ge 0$ for which their respective budgets are at most $\eta/8$. Gaussian decay, then exponential time decay, then $v \le 2/9$ prove termination. These are the accepted tail and Cauchy arguments with each true exponential separately replaced by its upper bound E.

There are $P = 4JN$ potential pairs. A nonzero-character pair may be omitted only if its entire two-power contribution has bound

$$b = 4hn^a (m + h)^2 E(\delta n^2 (m - h)) \le \eta/(8P).$$

Add every omitted bound to B_{discard}, giving $B_{\text{discard}} \le \eta/8$. Evaluate all other integrated Taylor polynomials by the stated exact coefficient recurrence using outward rectangles. Refine both interval precision and all primitive series remainders until the final rectangle's sum of coordinate halfwidths satisfies $R_{\text{arith}} \le \eta/4$. For this fixed finite expression all input and primitive intervals shrink; continuity and outward arithmetic imply $R_{\text{arith}} \to 0$. Precision doubling therefore terminates, and the sum of the five raw components is at most $3\eta/4$. Choose an integer output scale B such that $5\,2^{-B} \le \eta/8$ and round each component upward by $\text{up}_B(x) = 2^{-B}\lceil 2^B x \rceil$. The reported radius is their literal exact sum. With $\mathbf{b} = (R_{\text{arith}}, B_n, B_t, B_Q, B_{\text{discard}})$, it obeys

$$|y - \Lambda_q(s)| \le \sum_{i=1}^{5} \text{up}_B(b_i) \le \frac{3\eta}{4} + 5\,2^{-B} \le \frac{7\eta}{8} < \eta.$$

The output retains exact rational midpoints, rounded components, B, raw interval radius, parameters, input metadata and source hashes. The raw analytic bounds are exactly reconstructible; they need not be serialized as potentially enormous fractions. The output precision varies with the request and introduces no fixed reporting floor. □

This fixed-conductor sample result uses no hypothesis on zeros. It does not remove a downstream fixed-node Fourier alias floor, supply an all-conductor theorem or a positive arithmetic determinant, or prove GRH.

38.11 Adaptive sampling parameters and precision termination

The primitive theta/Mellin identity with root number one yields

$$\Lambda_q(s) = \sum_{n\ge 1} \chi_q(n) n^a \int_1^\infty e^{-\pi n^2 t/q} \big(t^{(s+a)/2-1} + t^{(1-s+a)/2-1}\big)\, dt.$$

On $D = [-1,2] + i[-4/3, 4/3]$, both exponents p satisfy $|\Re p| \le 2$ and $|\Im p| \le 2/3$. For exact $x \ge 0$, put $E(x) = 2^{-\lfloor x \rfloor}$. The elementary inequality $e > 2$ gives $e^{-x} \le e^{-\lfloor x \rfloor} \le E(x)$ and $E(x) \le 2e^{-x\log 2}$. Use this solely as a pointwise nonincreasing upper bound; it is not multiplicative and has no asserted exponential integral identity.

Integration by parts gives $\int_1^\infty t^2 e^{-xt}\, dt = e^{-x} Q(x)$ for $Q(x) = x^{-1} + 2x^{-2} + 2x^{-3}$. For $a = 0$ the bound $n^a e^{-\delta n^2/2} \le C_0 = 1$ is immediate. For $a = 1$, $n \le (1+n^2)/2$ and $n^2 e^{-\delta n^2/2} \le 2/(e\delta) \le 1/\delta$ give $C_1 = (1 + 1/\delta)/2$. For $n = n_0 + j$, the inequality $n^2 \ge n_0^2 + 2n_0 j$ therefore bounds the omitted-n sum by

$$2C_a Q(\delta n_0^2) \frac{e^{-\delta n_0^2/2}}{1 - e^{-\delta n_0}} \le 2C_a Q(\delta n_0^2) \frac{E(\delta n_0^2/2)}{1 - E(\delta n_0)} = B_n.$$

Take $n_0 = N + 1 \ge 2$; then $\delta n_0 \ge 6/5$ and the latter denominator is positive. Substituting $t = Tu$ in each retained-n time tail gives

$$B_t = \sum_{n=1}^{N} 2n^a T^3 E(\delta n^2 T) Q(\delta n^2 T).$$

The two tails are disjoint because the omitted-n tail uses the whole integral and the time tail uses only retained n.

For $j = 0, \dots, J-1$ and $\ell = 0, \dots, 3$ take

$$m = 2^j \left(1 + \frac{2\ell + 1}{8}\right), \qquad h = \frac{2^j}{8}, \qquad T = 2^J.$$

These panels cover $[1, T]$ and have $h/m \le 1/9$. On $|z - m| = \rho = m/2$, principal log is analytic, $\Re z \ge m/2$, and $|\arg z| \le 1$. For $f(z) = e^{-\pi n^2 z/q} z^p$, the angular multiplier is at most $e^{2/3} \le 3$, whence

$$|f(z)| \le 3B(m) E(\delta n^2 m/2), \qquad B(m) = \max\{(3m/2)^2, (m/2)^{-2}, 1\}.$$

Cauchy's coefficient estimate, cancellation of odd terms, and geometric summation yield the B_Q in Theorem 38.3. Including zero-character or later discarded terms in that sum is harmless. Gaussian, time, and geometric decay prove termination of the sequential first-success searches with $B_n, B_t, B_Q \le \eta/8$. For fixed q and $L = \max\{1, \log(1/\eta)\}$ their asymptotic scales can be chosen as $N = O(\sqrt{L})$, $T = O(L)$, $J = O(\log L)$, and $K = O(L)$. Polynomial prefactors in N, T, J contribute only $O(\log L)$ to the logarithm of the error estimates; this is a truncation-size statement, not a rational-arithmetic bit-complexity bound.

For real $t \in [m-h, m+h]$, $t \ge 1$ and $t^{\Re p} \le (m+h)^2$. The bound for a whole pair, including both powers, is therefore $4hn^a(m+h)^2 E(\delta n^2 (m-h))$. There are $P = 4JN$ potential pairs; summing only bounds at most $\eta/(8P)$ gives $B_{\text{discard}} \le \eta/8$. No partial recurrence or isolated exponential is discarded. For active pairs retain the coefficient recurrence

$$r_{-1} = 0, \quad r_0 = 1, \quad r_{j+1} = \frac{(h/m)(p - \lambda m - j) r_j - \lambda m (h/m)^2 r_{j-1}}{j+1}, \qquad \lambda = \pi n^2/q.$$

Coefficient comparison in $tf' = (-\lambda t + p)f$ proves that the integrated Taylor polynomial is

$$2he^{p\log m - \lambda m} \sum_{j=0}^{K} \frac{r_{2j}}{2j+1}.$$

Outward arithmetic encloses its exact value, including the signed character weight and both powers.

Use an isolated p-bit dyadic context, with all primitive remainders refined as p increases. Put $\delta_p = 2^{-p-16}$. Each arctangent series separately stops when its next-term bound is at most δ_p, giving total weighted analytic tail width at most $20\delta_p$ in Machin's formula, before outward dyadic rounding. Each reduced logarithm series separately has tail at most δ_p; for $x = 2^k v$, the combined bound is $(1 + |k|)\delta_p$, before rounding. For the complex exponential, after reduction to $A \le 1/2$, choose the Taylor order so the bound

$$\frac{A^{H+1}}{(H+1)!} \frac{1}{1 - A/(H+2)}.$$

is at most δ_p. Choose H by finite exact search; its denominator is positive. Add a symmetric exponential error enclosure to each coordinate before outward squaring. The fixed guard16 is not itself an acceptance bound: the final complete rectangle radius must satisfy $R_{\text{arith}} \le \eta/4$. All interval caches must include p and preserve exact input-type guards. The successful p and retry precisions/radii are recorded. Individual series lengths are determined by these, the exact inputs and the pinned source and are reconstructible by replay; they are not explicitly stored.

For fixed N,J,K and exact target point, the expression has finitely many operations and only nonzero fixed integer denominators. Each primitive input is bounded for sufficiently large p; exponential halving counts are consequently bounded. Exact primitive tails and dyadic rounding widths tend to zero. Induction through the finite continuous expression, including finitely many outward squarings, gives $R_{\text{arith}} \to 0$. Doubling p after a failed comparison terminates. The argument also covers true roots and nodes regenerated at every p, since their widths tend to zero. A fixed nondegenerate s rectangle has no corresponding shrinking-input claim.

A growing-order primitive estimate. To justify convergence despite a growing exponential Taylor order, write $\epsilon_p = 2^{-p}$, $\delta_p = 2^{-p-16}$, and let $d(X)$ be the sum of a rectangle's coordinate widths and $m(X)$ its ℓ^1 magnitude bound. The rounded reduced input W satisfies $a = m(W) \le 1/2 + 2\epsilon_p < 3/5$ and $d(W) \le 2^{-k} d(Z) + 4\epsilon_p$; the remainder is at most 2^{-H}, so the first accepted order satisfies $H \le p + 18$. For the computed term boxes, outward multiplication and integer division give $m_j \le a m_{j-1} + 6\epsilon_p$ and $d_j \le a d_{j-1} + m_{j-1} d(W) + 12\epsilon_p$. Thus $m_j \le a^j + 15\epsilon_p$ and $\sum_{j=0}^{H} d_j \le (25/4) d(W) + 75H\epsilon_p$; adding the remainder increases width by at most $4(\delta_p + \epsilon_p)$. The pre-squaring width is therefore $O(d(Z) + p2^{-p})$ and its magnitude is bounded (indeed below 3 for $p \ge 32$). Each outward square has width at most $2m(X)d(X) + 8\epsilon_p$; the bounded number of squarings consequently preserves convergence to zero. Finally, exact rational partial sums and endpoint rounding give Machin width at most $20\delta_p + 40\epsilon_p$, and logarithm width at most $(1 + |k|)(\delta_p + 2\epsilon_p)$ for fixed $x = 2^k v$. These estimates justify the primitive-width step without assuming a fixed Taylor order or asserting a global arithmetic complexity bound.

For serialization, initialize

$$B = \max\{32, \operatorname{bitlen}(\operatorname{den}\eta) - \operatorname{bitlen}(\operatorname{num}\eta) + 8\}$$

and increase B until $5\,2^{-B} \le \eta/8$. Write $\widehat{x} = 2^{-B}\lceil 2^B x \rceil$ for each of the five raw components. Their exact reported sum is at most $3\eta/4 + 5\,2^{-B} \le 7\eta/8$, and every component remains an upper bound. The output records B, the raw interval radius and complete rectangle, N/J/K, discard threshold/pair

counts, exact target metadata and source hashes. These reconstruct all raw analytic bounds and pair sets without serializing huge exact tail denominators. For the practical requests below B is87 and114, respectively. Exact endpoints remain rational; the mathematical specification assumes an integer representation sufficient for the requested size. Dynamic rounding removes the old fixed reporting floor. For rational s, validate its exact coordinates in closed D before conversion: an outward dyadic enclosure of $\Im s = 4/3$ extends beyond D, but the analytic bounds concern the true point. Circle nodes satisfy the strict exact bounds $-7/10 \le \Re s \le 17/10$, $|\Im s| \le 6/5$.

The exact parameter-design checker gives

η	q	N	J	T	K	active pairs
10^{-24}	3	12	7	128	19	71
10^{-24}	4	14	8	256	20	65
10^{-24}	5	16	8	256	20	111
10^{-32}	3	14	7	128	25	84
10^{-32}	4	16	8	256	26	72
10^{-32}	5	18	8	256	26	129

with exact rational budgets and no special-function oracle. The arithmetic precision is selected from the actual interval radius, not inferred from this table. This extension retains the existing classical theta identity; it adds no zero-location, positive determinant, all-conductor, Lean or GRH claim. The following end-to-end adaptive readout supplies its own node-count, alias, degree, Fourier and optimization choices.

38.12 An end-to-end adaptive analytic readout

The new driver changes the sample truncations, interval precision, circle size and degree; it does not reuse the frozen labels to assert a smaller error. Its scope is still the three stated primitive quadratic characters and the fixed compact $|s - 1/2| \le 7/10$.

Theorem 38.4 (Requested-error construction in the stated finite family)**.** *Given a positive rational ε and $q \in \{3, 4, 5\}$, the specified exact-arithmetic algorithm terminates in the mathematical unbounded-resource model and returns a normalized rational polynomial P with*

$$\sup_{|s-1/2|\le 7/10} |P(s) - \Lambda_q(s)| \le \varepsilon.$$

Its sample enclosures, rational optimizer updates and all error budgets are explicit. This is an approximation theorem, with the stated classical theta identity as an input; it supplies no zero-location or positive determinant conclusion and is not a Lean theorem or a practical runtime bound.

Proof. Put $u = 7/12$, $v = 7/24$. Choose $d \ge 0$ so $10v^{d+1}/(1 - v) \le \varepsilon/8$, and choose $m > d$ so

$$10\frac{2^{-m}}{1 - 2^{-m}}\frac{1}{1 - v} \le \varepsilon/8.$$

The driver rounds m upward to a multiple of eight, which only decreases this bound. Set the requested sample error $\eta = \varepsilon(1 - u)/8$. The adaptive sampler gives all m true circle nodes and labels with error at most η. Form their outward Fourier rectangles through degree d, and refine the nodes and finite evaluation arithmetic if their weighted midpoint radii exceed $\varepsilon/8$. This refinement terminates: for these fixed finite d, m, node uncertainty and every finite-expression arithmetic width

tend to zero with precision. Merely lifting fixed boxes would not suffice, so the driver regenerates the nodes and samples on this retry.

Choose rational midpoint targets t_n and execute the previously specified quadratic-objective updates until $\sum_{n=0}^{d} |b_n^k - t_n|_1 u^n \le \varepsilon/4$. Their geometric contraction proves finite termination. The oracle, aliasing, Taylor and Fourier-midpoint terms are each at most $\varepsilon/8$, and the optimization term is at most $\varepsilon/4$. Hence the raw five-term sum is at most $3\varepsilon/4$. Choose a serialization precision B with $5\,2^{-B} \le \varepsilon/8$, round each term upward, then add the five reported rationals exactly. The printed bound is at most $7\varepsilon/8 \le \varepsilon$. The polynomial uses $((s-1/2)/(6/5))^n$, and the preceding Fourier/Cauchy proof gives its asserted compact-uniform bound. □

The trace is losslessly encoded by the fixed target vector and a rational scale extracted from each *executed* coefficient state, together with its objective, weighted residual and full-state hash. Every coefficient can be recovered exactly; a separate replay expands the states and checks every update. The producer does not generate its trace from a closed form. The saved objective remains the rational Fourier-midpoint quadratic, with its perturbation from ideal-root least squares explicitly budgeted.

38.13 Termination, compression and the boundary of the guarantee

The degree and circle-size choices use only rational comparisons. Since $0 < v < 1$, the Taylor test succeeds at finite d; since $2^{-m} \to 0$, the alias test succeeds at finite $m > d$. The common growth bound10 is safe for all three families; the certificate also recomputes the previously proved exact conductor-specific majorants below $4, 10, 6$.

At fixed d, m, η, the analytic truncation parameters are fixed while precision is doubled. The computed sample centers stay bounded: their underlying finite expression is fixed and the true completed-function values are bounded on the sample circle. Its arithmetic widths tend to zero, as do the regenerated true-root enclosures. Fourier computation is a finite composition of additions, products and division by the positive integer m. Its midpoint-radius sum therefore tends to zero. This proves the driver's additional precision retry, without pretending that changing a box's nominal precision shrinks its uncertainty.

The accepted sampler error may remain above its actual arithmetic width because its analytic tails and output bounds are fixed for this η. That causes no problem: the oracle allocation uses the total certified sample radius, whereas the Fourier-midpoint allocation uses only finite coefficient-rectangle width. No analytic sample error is silently moved into the latter term or removed by numerical convergence.

For the stored training trace, the exact loop gives $b^{k+1} = 3b^k/4 + t/4$ from $b^0 = 0$. Inductively every state is a rational scalar multiple of the same target vector. The producer first executes the actual vector updates, then extracts this scalar from a nonzero target coordinate, checks all coordinates, and records a canonical full-vector SHA-256 hash. If the entire target vector is zero, its zero state needs only scale0. The compressed record is thus an exact representation of the executed states, not a floating-point sketch. Hashes are integrity aids; exact vector reconstruction and the independently checked recurrence establish the mathematical claim.

Coefficient export uses exact rational numerators and denominators. A chunked decimal integer encoder/parser handles endpoints beyond Python's usual digit-conversion guard without changing global interpreter settings. No fixed 180-bit serialization floor remains. The decimal graphics are separate approximate projections, not polynomial coefficients to which the exact certificate may be applied without a conversion-error bound.

All producing source bytes are captured, copied into fresh output paths and checked unchanged. Historical fixed producers are pinned and untouched. For the new modules the run also checks the import-time source snapshots, so a stale imported module cannot be attributed to later source bytes. After output creation, a failed evaluation, final provenance check or serialization emits uncertified failure metadata. Invalid requests and stale import-time sources are refused before creating output artifacts. Old outputs are never overwritten. Extreme requests can be computationally impractical: the termination proof gives no machine-time or memory guarantee, and finite test runs establish only their reported cases.

Nothing requires the output polynomials to be real-rooted, to equal an arithmetic Fredholm determinant, or to have a self-adjoint realization. Consequently arbitrary compact approximation of these known functions does not imply GRH. Uniformity in changing conductor, general Hecke/Dedekind/elliptic/Artin scopes, the independent determinant comparison, and actual analytic/category Lean objects remain separate obligations.

38.14 Learning the actual signed arithmetic correlations

The unsigned refinement in Section 40.15 leaves a signed problem. Here is a separate, executed finite learning objective on the original correlations, with a certificate for every coordinate and observable. It is not a uniform estimate for an expanding family. For ordered distinct squarefree columns $m = hr, n = ht$, put $q = rt$ and

$$\Gamma_i = \sum_{u \in \mathcal{R}} \chi_r(u)\overline{\chi_t(u)}\mathbf{1}_{(u,h)=1}, \qquad i = (h, q, r).$$

The symbols vanish at every collision with q; the common-prime mask is retained separately. With principal ν, actual complementary divisor counts $r_U(m)$, and one common complex profile $W_m = W(Nm/D)$, define

$$d_i^{CC} = r_U(m)r_U(n)W_m\overline{W_n}, \qquad d_i^{C\mu} = r_U(m)W_m\overline{W_n}, \qquad \lambda_i = 1 + |d_i^{CC}|^2 + |d_i^{C\mu}|^2.$$

The exact diagonal Δ_X and these offdiagonal coordinates give

$$E_X = \Delta_X + D^{-1}\sum_i \mu(q_i)d_i^X\Gamma_i, \qquad X \in \{CC, C\mu\}. \tag{38.1}$$

Thus $E_{CC} = \sum_{u\in\mathcal{R}} |C_u|^2$ and $E_{C\mu} = \sum_{u\in\mathcal{R}} C_u\overline{M_u}$ for the actual normalized row sums. Neither the Möbius sign nor a complex conjugate is discarded.

Proposition 38.5 (A finite supervised certificate)**.** *Let g_i be complex readout coordinates and $L(g) = \sum_i \lambda_i|g_i - \Gamma_i|^2$. For $K_X = \sum_i |d_i^X|^2/\lambda_i$ and $\lambda_{\min} = \min_i \lambda_i$, the substituted readouts satisfy*

$$|\widehat{E}_X - E_X|^2 \le D^{-2}K_X L(g),$$
$$\max_i |g_i - \Gamma_i|^2 \le L(g)/\lambda_{\min}.$$

The executed metric-gradient update $g^{(t+1)} = (g^{(t)} + \Gamma)/2$ gives $L(g^{(t)}) = 4^{-t}L(g^{(0)})$. Therefore every positive rational requested tolerance on these three squared bounds is attained after finitely many updates on this fixed exact instance, with unrestricted resources.

The implementation's resource guard refuses requests beyond its update budget; termination in this proposition is not a practical runtime guarantee. The labels Γ_i are computed exactly before training, so no speedup over exact label evaluation or generalization to unseen conductors is claimed.

The supplied instance uses $D = 6000, U = 60, H = 625$, S above $2, 3$, principal ν, and all 15 good squarefree ideal columns at activated norms $7507, 7519, 8281, 10507$ (respectively $2, 4, 1, 8$ ideals). One explicitly specified common smooth four-bump profile is zero at every other integer norm. Both the 2262 literal rows and the separately labelled 2148 guaranteed nonprincipal subset are evaluated; the latter is not asserted to be the whole nonprincipal family. There are 95 offdiagonal (h, q) blocks, 65 with $h = 1$, and 210 ordered learned coordinates. Every row case retains 4530 raw column zeros. Real and complex profiles give four requested-10^{-12} certificates, using $53, 55, 53, 55$ metric updates respectively: 216 executed updates, with every full rational state saved. A separate 200 executed ordinary coordinate updates are budget-limited and carry no requested-error claim. The standalone replay is linked from the book and project page. No analytic saving, positive determinant, zero-location assertion, upstream quantum training, new Lean declaration or GRH conclusion follows.

38.15 Finite phase features, gradients and exact verification

For each block let $G_q = (\mathbb{Z}/6\mathbb{Z})^{\omega(q)}$. A literal admissible row determines local phases e_p at every prime of q; rows with a q-collision or a common-prime collision with h are deleted before forming the exact sparse histogram $n(e)$. Orientation r has

$$\theta_r(e) = \zeta_6^{\sum_{p|q} s_p e_p}, \qquad s_p = 1 \ (p \mid r), \quad s_p = -1 \ (p \mid t), \qquad \Gamma_r = \sum_e n(e)\theta_r(e).$$

Different active orientations have distinct exponent vectors modulo 6, so their characters are orthonormal for the uniform measure on G_q. The model and target projection are

$$F_g(e) = \sum_{r \in J_q} g_r \overline{\theta_r(e)}, \qquad F_\Gamma(e) = \sum_{r \in J_q} \Gamma_r \overline{\theta_r(e)}.$$

Indeed F_Γ is the orthogonal projection of $|G_q|n$ onto this character subspace, and $\mathbb{E}_{G_q} F_g \theta_r = g_r$. The positive spectral metric assigns weight λ_r to this orthonormal basis. Its squared error is exactly $\sum_r \lambda_r |g_r - \Gamma_r|^2$. Thus the run evaluates the full finite feature-projection loss by Parseval; it does not claim to have executed a sampled or stochastic training loss. This projection need not be a nonnegative density. A Hermitian readout matrix need not be positive semidefinite.

Gradient and contraction. Use ζ_6 coordinates $g = a + b\zeta_6$, so $|g|^2 = a^2 + ab + b^2$ and $M = \left(\begin{smallmatrix} 1 & 1/2 \\ 1/2 & 1 \end{smallmatrix}\right)$. For the objective $L/2$, the ordinary real-coordinate gradient in block i is $\lambda_i M(x_i - x_i^*)$. In the block metric $\lambda_i M$, the gradient is $x_i - x_i^*$. A metric step of size $1/2$ therefore halves every complex error and quarters L. Conjugate initial coordinates and this step preserve the Hermitian reverse orientations. The ordinary trajectory treats all ordered coordinates independently; asymmetric weights need not preserve that symmetry. For ordinary steps $\eta = 2/(3\lambda_{\max})$, the Hessian eigenvalues lie between $\lambda_{\min}/2$ and $3\lambda_{\max}/2$, whence

$$L_{t+1} \le \left(1 - \frac{\lambda_{\min}}{3\lambda_{\max}}\right)^2 L_t.$$

This last bound is conservative; the saved 50 ordinary steps per case are not asserted to attain the requested tolerance.

Proof of Proposition 38.5. Subtract (38.1) with the same exact diagonal. Weighted Cauchy–Schwarz, applied only to the error, gives

$$\left|\sum_i \mu(q_i) d_i^X (g_i - \Gamma_i)\right|^2 \le \left(\sum_i \frac{|d_i^X|^2}{\lambda_i}\right)\left(\sum_i \lambda_i |g_i - \Gamma_i|^2\right).$$

Here $|\mu(q_i)| = 1$ because q_i is squarefree; the predicted sum itself keeps its signs and phases. Each summand in the second factor is nonnegative, which proves the coordinate bound. The exact affine update gives $g^{(t)} - \Gamma = 2^{-t}(g^{(0)} - \Gamma)$, proving contraction. For finite rational positive λ_i, K_X, L_0 and $\tau > 0$, some integer t makes all three bounds at most τ^2. The zero-error case stops immediately. No varying-family constants enter this finite assertion. □

The activated original family. Let

$$\phi(t) = \begin{cases} \exp(1 - 1/(1-t^2)), & |t| < 1, \\ 0, & |t| \ge 1, \end{cases} \qquad W(y) = \sum_{N \in \{7507,7519,8281,10507\}} w_N \phi(4(6000y - N)).$$

These disjoint bumps are supported in $(1, 2)$ and $\phi(0) = 1$. For the real case $w_N = 1$; for the complex case $w_N = 1 + \zeta_6(4N - 30000)/6000$. At integer norms $W(n/6000) = w_n$ at the four activated norms and is zero elsewhere. Hence all active original squarefree columns are present, rather than an undeclared column submatrix. No exponential evaluation is needed at these exact nodes. The profile is a fixed finite demonstration and does not establish a profile-uniform analytic estimate. The counts r_U are $0, 2, 4, 2$ at the four norms. The guaranteed nonprincipal subset removes precisely those literal rows whose outside-S norm is 1; no classification of the omitted 114 rows as a whole is asserted. Every nonunit outside-S factor has a prime exponent from 1 to 3, since its prime norm is at least 7 and $7^4 > 625$; its nonzero residue modulo 6 gives a nontrivial local character. All six units and all original S-power rows belong to the separately saved full literal case.

The seed 20261105 selects deterministic rational conjugate initial coordinates by SHA256 of the ordered column identifiers. There is no random sampling. Exact $\mathbb{Q}(\zeta_6)$ arithmetic stores every metric and ordinary state. Training accepts only when both observable certificates and the uniform-coordinate certificate are at most τ^2, preventing a scalar cancellation from masquerading as accurate correlation learning. The real full-row targets are $E_{CC} = 2393/125$ and $E_{C\mu} = 431/50$; the guaranteed-subset targets are $4293/250$ and $771/100$. Complex-profile targets and the complete phase histograms are saved alongside. Each case has 64 nonzero negative-$\mu(q)$ C–C target orientations. Replacing all signs by plus is an explicit failing control, not an estimator.

Reproduction and scope. The complete run is reproducible.

The source is `examples/arithmetic_learning/learn.py`; its README states the exact smooth profile, CLI, resource guard and loss convention. The accepted immutable output is `outputs/experiments/2026-11-05-arithmetic-learning-v2/`. All source/helper hashes, exact input bytes and artifact hashes are bound before and after execution and checked on replay. Existing outputs, nonpositive or binary-float tolerances, and stale source/input/case bytes are refused. The preserved v1 logging failure is not the accepted run. The focused verifier independently reconstructs 31668 local symbols and 450 Gram targets, then checks the full saved metric trajectory. Independent mathematical review and exact code checks are recorded separately; finite arithmetic checks are not a proof of an asymptotic signed estimate. Full exact training labels are supervision, so this is a certified finite reference architecture, without an efficiency, generalization, PSD, zero-location or GRH claim. Analytic and categorical Lean remain unfinished.

Chapter 39

The original-family Hecke moment and exact masked transfer

39.1 An arithmetic-family moment with every original row retained

Let $K = \mathbb{Q}(\sqrt{-3})$, $\mathcal{O} = \mathbb{Z}[\omega]$, and write N for the ideal or element norm. Fix a finite-order Hecke character ν and a finite set S of prime ideals containing those above 6 and those dividing its conductor. For $0 \neq u \in \mathcal{O}$, let κ_u be the character of $K(u^{1/6})/K$ defined using arithmetic Frobenius, and put $\psi_u = \mathrm{prim}(\nu\kappa_u)$. Here prim means the underlying primitive Hecke character: it is formed before introducing any divisor variable or evaluating conductor-dependent zero extensions. The rows below are all actual Eisenstein elements, including units and prime powers supported in S.

The external inputs are abelian Kummer reciprocity and character uniqueness, the primitive Hecke functional equation and its usual vertical growth, Stirling's formula, scalar Dedekind-zeta convexity, and Blomer–Goldmakher–Louvel's large sieve for their specified sixth-order family. We use the pinned arXiv:1112.1650v1, Theorem 1.3, Lemma 2.1 and Appendix II; its Section 5 supplies the all-ideal decomposition whose fixed-twist proof is redone here. No statement about all primitive characters of comparable conductor, Artin holomorphy, Lindelöf bounds or zero locations is assumed.

Theorem 39.1 (The original-family numerator moment)**.** *For every $\varepsilon > 0$, uniformly for $H \geq 1$ and $t \in \mathbb{R}$,*

$$\sum_{0<Nu\leq H} |L(1/2+it,\psi_u)|^2 \ll_{\nu,S,\varepsilon} H^{1+\varepsilon}(1+|t|)^{1+\varepsilon}. \tag{39.1}$$

For every fixed $0 < \delta < 1/2$, the same estimate holds with $1/2+it$ replaced by $1/2+\delta+it$, with the constant also depending on δ. If the central bound has constant C_0 at an exponent $0 < \varepsilon_0 \leq 1/4$, an admissible off-central constant is

$$200C_0\left(\frac{3/2+\delta}{1/2-\delta}\right)^2. \tag{39.2}$$

Proof. For the canonical BGL character $\vartheta_{\mathfrak{a}}$, Appendix II gives a radicand $\alpha_{\mathfrak{a}}$ with $(\alpha_{\mathfrak{a}})_S = \mathfrak{a}\mathfrak{g}^{-6}$. Since $\mathcal{O}_S$ is principal, comparison with any literal u whose outside-S ideal is $\mathfrak{a}$ gives $\kappa_u = \eta\vartheta_{\mathfrak{a}}$ for one of finitely many fixed S-unit Kummer twists η. This is an equality of primitive characters, established outside a finite set and extended by uniqueness. For each outside-S ideal $\mathfrak{a}$ and S-supported integral ideal $\mathfrak{b}$, at most six elements generate $\mathfrak{a}\mathfrak{b}$. The resulting S-supported multiplicity sum converges at exponent $1+\varepsilon$.

For each fixed $\xi = \nu\eta$, split the canonical parameter as $\mathfrak{a} = \mathfrak{a}_0\mathfrak{a}_1\mathfrak{a}_2^6$, where $\mathfrak{a}_0$ is squarefree, $\mathfrak{a}_1$ is squarefull and sixth-power-free, and $(\mathfrak{a}_0, \mathfrak{a}_1) = 1$. The primitive conductor is at most a fixed multiple of $N(\mathfrak{a}_0\mathfrak{a}_1)$. The common-gamma approximate functional equation, with $X = H/(N\mathfrak{a}_2)^6$ and $T = 1 + |t|$, has common maximal length $B = X^{1/2}T(HT)^\eta$ for any sufficiently small fixed $\eta > 0$. Mellin inversion removes its row-dependent conductor weight. Split a column as $\mathfrak{b}_S\mathfrak{b}_1\mathfrak{b}_2$, with $\mathfrak{b}_S$ supported in S, $\mathfrak{b}_1$ squarefree and $\mathfrak{b}_2$ squarefull, the last two coprime and prime to S. The original primitive values at $\mathfrak{b}_S$ remain bounded row multipliers. The S-supported and squarefull column weights are summable at $1/2 + \eta$. Multiplying squarefree column coefficients by the fixed ξ preserves their squared norm, whatever its finite order. BGL's large sieve therefore bounds the energy for fixed $\mathfrak{a}_1, \mathfrak{a}_2$ by

$$(HT)^{O(\eta)}\{M + B + (MB)^{2/3}\}, \qquad M = X/N\mathfrak{a}_1.$$

Squarefull counting and summation give $X + B\sqrt{X} + (XB)^{2/3} \ll (HT)^{O(\eta)}XT$. The $\mathfrak{a}_2$ sum converges at exponent 6. Principal rows are separated before the pole-free functional equation and bounded by scalar zeta convexity. This proves (39.1).

For the off-central statement divide each $L(s, \psi)$ by $(s + 1)^{5/4}$ and, on principal rows, also multiply by $(s - 1)/(s + 1)$. These are bounded analytic functions on $\operatorname{Re} s > 1/2$, continuous on the boundary. Poisson representation and Jensen's inequality transfer the central squared moment. The convolution of $P_\delta(y) = \delta/[\pi(\delta^2 + y^2)]$ with $(1 + |t|)^{-3/2+\varepsilon_0}$ is at most eleven times that weight when $0 < \varepsilon_0 \le 1/4$. Restoring the denominator and the principal pole-removal factor gives (39.2). The extended edition gives the detailed derivation with all primitive local values. □

Separate fixed-unitary extension. The moment theorem also holds for any one fixed unitary Hecke character ν. For precision choose $\nu(\mathfrak{a}) = \nu_0(\mathfrak{a})(N\mathfrak{a})^{-i\tau}$, with angular parameter $m \in \mathbb{Z}$ and completed gamma factor

$$\gamma_\nu(s) = 2(2\pi)^{-(s+|m|/2+i\tau)}\Gamma(s + |m|/2 + i\tau).$$

All finite Kummer twists have this same infinity type. Use $T_\nu = 1 + |t + \tau| + |m|$, comparable to $1 + |t|$ with ν-dependent constants. Pure norm rows have $L(s, \psi) = \zeta_K(s + i\tau)$ and are separated before the pole-free functional equation; their pole at $1 - i\tau$ is removed by $(s - 1 + i\tau)/(s + 1 + i\tau)$. No uniformity in m, τ or the conductor of ν is asserted. This extension of the moment is separate from the following finite-order type-I residue formula.

39.1.1 The exact masked remainder and the remaining loss

Retain the original zero-extended symbol $\chi_d(u) = (u/d)_6$ on good squarefree ideals. Let μ be the ideal Möbius function and set

$$\beta_U(d) = \sum_{\substack{ab=d \\ Na, Nb \le U}} \mu(a)\mu(b), \quad T(u, d) = S \cup \operatorname{supp}(u) \cup \operatorname{supp}(d).$$

Let $\psi_{u,2} = \operatorname{prim}(\psi_u^2)$, formed independently of squaring any zero sentinel. With $\mathfrak{f}_u$ and $\mathfrak{f}_{u,2}$ the primitive conductors, the full-mask series is

$$F_{u,d}(s) = \frac{L(s, \psi_u)}{L(2s, \psi_{u,2})} C_{T(u,d)}(s), \tag{39.3}$$

$$C_T(s) = \frac{\prod_{p \in T,\ p \nmid \mathfrak{f}_u}(1 - \psi_u(p)(Np)^{-s})}{\prod_{p \in T,\ p \nmid \mathfrak{f}_{u,2}}(1 - \psi_{u,2}(p)(Np)^{-2s})}.$$

Initially it equals $\sum_{c \text{ squarefree},\ (c,T)=1} \psi_u(c)(Nc)^{-s}$ for $\operatorname{Re} s > 1$. Every prime of T remains deleted, including those forgotten by either primitive conductor.

For finite-order ν, $D \geq 1$, $U \geq 1$, $U^2 \leq D$, and $W \in C_c^\infty((0,\infty))$ supported in $[1,2]$, put

$$\widehat{W}(s) = \int_0^\infty W(x) x^{s-1}\, dx, \qquad \mathcal{M}_4(W) = \sum_{j=0}^{4} \sup_x |(x\partial_x)^j W(x)|.$$

On $\sigma = 1/2 + \delta$, the exact residue-subtracted type-I remainder is

$$E_u = \frac{D^\delta}{2\pi} \int_{\mathbb{R}} \widehat{W}(\sigma + it) D^{it} \sum_{\substack{d \text{ squarefree} \\ (d,S)=1}} \frac{\beta_U(d)\nu(d)\chi_d(u)}{(Nd)^{\sigma+it}} F_{u,d}(\sigma + it)\, dt. \tag{39.4}$$

This definition retains the actual β_U, all phases, d-masks, conductors and the independently primitive square.

Theorem 39.2 (An improved masked residual estimate)**.** *Under the preceding finite-order hypotheses, for every $\varepsilon > 0$,*

$$\sum_{0 < Nu \leq H} |E_u|^2 \ll_{\nu,S,\delta,\varepsilon} \mathcal{M}_4(W)^2 D^{2\delta} U^{2-4\delta} H (HD)^\varepsilon. \tag{39.5}$$

Proof. The same deleted set in both factors of (39.3) gives $|F_{u,d}(\sigma + it)| \ll (Nu\, Nd)^\eta |L(\sigma + it, \psi_u)|$: the reciprocal incomplete Euler product at $2\sigma > 1$ is bounded by $\zeta_K(2\sigma)$, and its remaining finite numerator is bounded by a small power of its radical. Apply Minkowski to (39.4) in the exact row space and use Theorem 39.1. The actual coefficient sum is at most

$$\sum_d \frac{|\beta_U(d)|}{(Nd)^{\sigma-\eta}} \leq \left(\sum_{Na \leq U} (Na)^{-\sigma+\eta} \right)^2 \ll U^{1-2\delta+2\eta}.$$

Four Mellin integrations by parts bound the remaining height integral by a constant times $\mathcal{M}_4(W)$. Square the result and absorb the small losses using $U^2 \leq D$. □

At $H = D^{3/4}$ and $U = D^a$ with fixed $0 < a \leq 1/2$, the upper bound's excess over H is $2\delta + (2 - 4\delta)a$, up to small losses; as $\delta \downarrow 0$ it still leaves $2a$. This is a limitation of the upper bound, not an energy lower bound. The extracted principal residue, the original short term at smaller scales and the signed type-II minus type-I covariance are not controlled by (39.5). The next arithmetic task is to estimate the complete d-weighted moment before its absolute coefficient sum, or establish sufficient signed covariance. No positive arithmetic determinant, zero-location theorem or GRH proof follows. The analytic argument uses the external classical inputs above; finite diagnostics and selected existing Lean local identities do not formalize the Hecke functions, approximate functional equation, Poisson transfer or these moment bounds.

39.2 Family identification, the approximate functional equation and masks

We prove the analytic statements of Section 39.1 from the explicit classical inputs stated there. Write $I(S)$ for the nonzero integral ideals prime to S, and $\mathcal{O}_S$ for the ring of S-integers. Constants may depend on the fixed field, S, ν and any declared positive small exponent. No such constant is asserted uniform in the conductor or infinity type of a varying ν.

39.2.1 A finite comparison with the literal Kummer rows

Use Appendix II of BGL, with $n = 6$. Its fixed local modulus and representatives may be chosen once, since S contains the primes above 6 and $\mathcal{O}_S$ has class number one. For each $\mathfrak{a} \in I(S)$ the construction writes

$$\mathfrak{a} = (x)E\mathfrak{g}^6, \qquad \alpha_{\mathfrak{a}} = xm_E, \qquad (m_E)_S = E,$$

so $(\alpha_{\mathfrak{a}})_S = \mathfrak{a}\mathfrak{g}^{-6}$. Choose $y \in K^\times$ generating $\mathfrak{g}$ as an $\mathcal{O}_S$-ideal. If $(u)_S = \mathfrak{a}$, then

$$e = \alpha_{\mathfrak{a}} y^6/u \in \mathcal{O}_S^\times, \qquad [\alpha_{\mathfrak{a}}] = [eu] \quad \text{in } K^\times/K^{\times 6}.$$

There is a precision here: Appendix II allows choosing $\mathfrak{g}$ relative to a tested denominator. Fix one admissible global decomposition first. Its radicand gives the canonical character $\vartheta_{\mathfrak{a}}$ on all primes outside the finite set $S \cup \operatorname{supp}(\mathfrak{a}\mathfrak{g})$ where that choice applies. Uniqueness of Hecke characters, equivalently Chebotarev in the finite abelian quotient, then identifies the underlying primitive characters everywhere. With matching arithmetic-Frobenius conventions,

$$\kappa_u = \kappa_{e^{-1}}\vartheta_{\mathfrak{a}}. \tag{39.6}$$

If the residue-symbol convention is conjugated, conjugate the canonical family and its coefficient sequence; the same large sieve follows.

The group $\mathcal{O}_S^\times/(\mathcal{O}_S^\times)^6$ is finite. Thus (39.6) uses one of a finite set of fixed Kummer twists η, all unramified outside S and of bounded S-conductor. This is a comparison of primitive characters, not a pointwise multiplication rule for independently zero-extended arrays at bad primes. In particular, a conductor drop must not be replaced by a product of artificial zeros.

Since $\mathcal{O}$ is principal with six units, for fixed $\mathfrak{a} \in I(S)$ and an S-supported integral ideal $\mathfrak{b}$ there are at most six u satisfying $(u) = \mathfrak{a}\mathfrak{b}$. For any nonnegative row quantity, the literal moment is consequently at most

$$6 \sum_{\substack{\mathfrak{b}\ S\text{-supported} \\ N\mathfrak{b} \le H}} \sum_{\eta} \sum_{\substack{\mathfrak{a} \in I(S) \\ N\mathfrak{a} \le H/N\mathfrak{b}}} \left|L(s, \operatorname{prim}(\nu\eta\vartheta_{\mathfrak{a}}))\right|^2. \tag{39.7}$$

An ideal bound $X^{1+\varepsilon}T^{1+\varepsilon}$ therefore transfers to all literal rows, since

$$\sum_{\mathfrak{b}\ S\text{-supported}} (N\mathfrak{b})^{-1-\varepsilon} = \prod_{p \in S} (1 - (Np)^{-1-\varepsilon})^{-1} < \infty.$$

No quotient of the original unit rows or deletion of S-prime powers has occurred.

39.2.2 Fixed twists, exact tame conductors and the squarefree sieve

Fix $\xi = \nu\eta$ and write $\rho_{\mathfrak{a}} = \operatorname{prim}(\xi\vartheta_{\mathfrak{a}})$. Its fixed conductor is supported in S before the Kummer twist. On columns prime to S, $|\xi(\mathfrak{b})| = 1$. BGL Theorem 1.3 thus gives, for any fixed $\mathfrak{a}_1$,

$$\begin{aligned}\sum_{\substack{\mathfrak{a}_0 \in I(S)\ \text{squarefree} \\ N\mathfrak{a}_0 \le M}} \left| \sum_{\substack{\mathfrak{b}_1 \in I(S)\ \text{squarefree} \\ N\mathfrak{b}_1 \le B}} \lambda_{\mathfrak{b}_1}\xi(\mathfrak{b}_1)\vartheta_{\mathfrak{a}_1}(\mathfrak{b}_1)\vartheta_{\mathfrak{a}_0}(\mathfrak{b}_1) \right|^2 \\ \ll (MB)^{\varepsilon}\{M + B + (MB)^{2/3}\} \sum_{\mathfrak{b}_1} |\lambda_{\mathfrak{b}_1}|^2.\end{aligned} \tag{39.8}$$

The first fixed multiplier preserves the coefficient norm; the second has modulus at most one. Restricting the positive outer row sum is harmless. A coprimality condition with another fixed ideal

belongs to λ. In particular, ν need not have order dividing six and is not asserted to belong to BGL's finite ray-class character set.

There is a unique valuation decomposition

$$\mathfrak{a} = \mathfrak{a}_0\mathfrak{a}_1\mathfrak{a}_2^6, \quad \mathfrak{a}_0 \text{ squarefree}, \quad \mathfrak{a}_1 \text{ squarefull and sixth-power-free}, \quad (\mathfrak{a}_0, \mathfrak{a}_1) = 1.$$

Indeed, for $v_p(\mathfrak{a}) = 6q + r$, $0 \le r \le 5$, put the residual prime in $\mathfrak{a}_0$ if $r = 1$, and its exponent r in $\mathfrak{a}_1$ if $2 \le r \le 5$. BGL Lemma 2.1 gives $\vartheta_{\mathfrak{a}\mathfrak{b}^6} = \vartheta_{\mathfrak{a}}$ and $\vartheta_{\mathfrak{a}_0\mathfrak{a}_1} = \vartheta_{\mathfrak{a}_0}\vartheta_{\mathfrak{a}_1}$ on ideals prime to S in this sixth-power-free case. Those are the identities needed here; no arbitrary multiplicativity assertion is substituted.

At a prime outside S, tame Kummer inertia at residual exponent r has order $6/\gcd(6, r)$. It is nontrivial for $r = 1, \dots, 5$ and has conductor exponent one. The fixed ξ is unramified there, so cannot cancel that inertia. At primes in S the local sixth-power classes are finite, hence only finitely many primitive conductor types occur after multiplication by the fixed ξ. Consequently

$$Q_{\rho_{\mathfrak{a}}} = |D_K| N\mathfrak{f}_{\rho_{\mathfrak{a}}} \le C_{\xi,S} N(\mathfrak{a}_0\mathfrak{a}_1), \tag{39.9}$$

independently of $\mathfrak{a}_2$. The equality of the conductor's outside-S part with $\mathrm{rad}(\mathfrak{a}_0\mathfrak{a}_1)$ does not identify that conductor with the original larger deleted set.

39.2.3 Removing the row-dependent functional-equation weights

First take finite-order ν. All characters then have trivial infinity type at the complex place. The primitive completion may be normalized as

$$\Lambda(s, \rho) = Q_\rho^{s/2}\gamma_K(s)L(s, \rho), \qquad \gamma_K(s) = 2(2\pi)^{-s}\Gamma(s), \qquad \Lambda(s, \rho) = \epsilon_\rho\Lambda(1 - s, \bar{\rho}), \quad |\epsilon_\rho| = 1.$$

For nonprincipal rows the completed function is entire. Apply this functional equation to the Mellin integral with even auxiliary factor $G(z) = e^{z^2}$ and denominator z, shifting across $z = 0$. At $s = 1/2 + it$ this gives two weighted Dirichlet series, truncated below to polynomials; the dual prefactor has modulus one. Principal rows are excluded from this pole-free step and treated separately below.

For fixed $\mathfrak{a}_2$, let $X = H/(N\mathfrak{a}_2)^6 \ge 1$ and $T = 1 + |t|$. An explicit normalized kernel is

$$V_t(x) = \frac{1}{2\pi i}\int_{(\eta)} e^{z^2}\frac{\Gamma(s + z)}{\Gamma(s)}T^{-z}x^{-z}\,\frac{dz}{z}, \qquad x = \frac{2\pi N\mathfrak{b}}{\sqrt{Q_\rho}T}, \tag{39.10}$$

with $\eta > 0$ small. Its factors combine to $(\sqrt{Q_\rho}/(2\pi N\mathfrak{b}))^z$ in the actual completed-L kernel; there is no extra factor of T. The denominator z supplies the residue at zero. On $z = \eta + iy$, Stirling and $|t + y| \le T(1 + |y|)$ give

$$\left|\frac{\Gamma(1/2 + \eta + i(t + y))}{\Gamma(1/2 + it)T^{\eta+iy}}\right| \ll_\eta (1 + |y|)^{C_\eta}e^{\pi|y|/2}.$$

The factor e^{-y^2} makes this an integrable majorant uniformly in t. The analogous bound holds on every fixed positive shifted line and for the dual gamma kernel. Moving far enough to the right gives arbitrary power decay beyond a common total-ideal cutoff

$$B' = X^{1/2}T(HT)^\eta, \tag{39.11}$$

up to fixed ξ, S, K constants. For any requested $A > 0$, a sufficiently large positive kernel shift, depending also on η, makes the truncation error $O((HT)^{-A})$ uniformly in all rows in this block.

Ideal counting $O_K(Y)$ bounds the absolute tails. Such errors are negligible after the finite row sums by taking A larger if needed.

Insert (39.10) on $\operatorname{Re} z = \eta$. The factor $(\sqrt{Q_\rho}T)^z$ is independent of the column and is a row multiplier of modulus at most $(CXT^2)^{\eta/2}$. Its imaginary part is a phase. The remaining column coefficient is $(N\mathfrak{b})^{-1/2-\eta-it-iy}$, apart from fixed constants. Minkowski or Cauchy with the integrable gamma majorant therefore removes the row-dependent weight at cost $(HT)^{O(\eta)}$ in the squared norm. No independence of the root numbers is assumed or needed.

For each column use the unique decomposition

$$\mathfrak{b} = \mathfrak{b}_S\mathfrak{b}_1\mathfrak{b}_2, \quad \mathfrak{b}_S \ S\text{-supported}, \quad \mathfrak{b}_1 \text{ squarefree}, \quad \mathfrak{b}_2 \text{ squarefull}, \quad (\mathfrak{b}_1, \mathfrak{b}_2) = 1,$$

where $\mathfrak{b}_1, \mathfrak{b}_2 \in I(S)$; a prime of outside-$S$ valuation one goes in $\mathfrak{b}_1$, and a prime of valuation at least two goes with its full exponent in $\mathfrak{b}_2$. For fixed $\mathfrak{b}_S, \mathfrak{b}_2$ retain $\rho_{\mathfrak{a}}(\mathfrak{b}_S)$ as the original primitive row value. On the good factors the exact canonical identity applies. The remaining factors involving $\mathfrak{b}_2$, including $\vartheta_{\mathfrak{a}_0}(\mathfrak{b}_2)$, are bounded row multipliers. Their moduli are at most one; only then are they discarded in an inequality. In particular the value at $\mathfrak{b}_S$ is not replaced by the product of zero-extended primitive arrays.

For the $\mathfrak{b}_1$ polynomial the coefficient sequence is independent of $\mathfrak{a}_0$; it includes the indicator $(\mathfrak{b}_1, \mathfrak{b}_2) = 1$ and the common cutoff $N\mathfrak{b}_1 \le B'/N(\mathfrak{b}_S\mathfrak{b}_2)$. Padding it by zeros up to B' is legitimate. Its squared norm is at most $\zeta_K(1 + 2\eta)$. Minkowski over $\mathfrak{b}_S, \mathfrak{b}_2$ is legitimate because

$$\sum_{\mathfrak{b}_S, \mathfrak{b}_2} N(\mathfrak{b}_S\mathfrak{b}_2)^{-1/2-\eta} < \infty.$$

The finite Euler product handles $\mathfrak{b}_S$; the squarefull series converges above $1/2$. Apply (39.8) to each such polynomial and to the conjugate dual family. For fixed $\mathfrak{a}_1, \mathfrak{a}_2$ the resulting energy is

$$(HT)^{O(\eta)}\{M + B' + (MB')^{2/3}\}, \qquad M = X/N\mathfrak{a}_1. \tag{39.12}$$

The additional condition $(\mathfrak{a}_0, \mathfrak{a}_1) = 1$ simply restricts the positive row sum. The large-sieve small exponent can be chosen sufficiently small along with η and absorbed in the indicated small loss.

39.2.4 All-ideal summation and principal rows

Every squarefull ideal $\mathfrak{c}$ has a unique expression $\mathfrak{d}^2\mathfrak{e}^3$ with $\mathfrak{e}$ squarefree. This follows primewise by using exponent zero or one in $\mathfrak{e}$ according to the parity of an exponent at least two. Therefore

$$\#\{\mathfrak{c} \text{ squarefull} : N\mathfrak{c} \le X\} \ll_K X^{1/2}, \qquad \sum_{\mathfrak{c} \text{ squarefull}} (N\mathfrak{c})^{-s} < \infty \quad (s > 1/2).$$

For the count, sum $O((X/(N\mathfrak{e})^3)^{1/2})$ and use $\zeta_K(3/2) < \infty$. Summing (39.12) over $\mathfrak{a}_1$ gives

$$(HT)^{O(\eta)}\{X + B'\sqrt{X} + (XB')^{2/3}\} \ll (HT)^{O(\eta)}XT,$$

since the squarefull series converges at 1 and $2/3$, $B' = \sqrt{X}\,T(HT)^\eta$, and $T^{2/3} \le T$ for $T \ge 1$. The $\mathfrak{a}_2$ sum is bounded by $H\sum_{\mathfrak{a}_2}(N\mathfrak{a}_2)^{-6} = H\zeta_K(6)$. Choosing all internal losses small for the requested final ε proves the fixed-twist all-ideal central moment.

There are $O_K(H)$ ideal rows in total. On any row where the primitive character is principal its L-function is ζ_K, and ordinary scalar convexity gives $|\zeta_K(1/2 + it)|^2 \ll_\varepsilon T^{1+\varepsilon}$. This treats those rows without a pole-free approximate functional equation. Finally (39.7) proves (39.1) for every actual nonzero Eisenstein element.

39.2.5 Poisson transfer with an explicit constant

For a nonprincipal row define

$$f_\psi(s) = \frac{L(s,\psi)}{(s+1)^{5/4}},$$

using the holomorphic logarithm on $\mathrm{Re}(s+1) > 0$. On a principal row additionally multiply by $(s-1)/(s+1)$. Analytic continuation and ordinary degree-two convexity, used separately at each fixed conductor, show that f_ψ is bounded analytic on the right half-plane $\mathrm{Re}\, s > 1/2$, with continuous boundary and decay at infinity. The principal pole is removed before applying Poisson representation to its real and imaginary parts. Jensen gives

$$|f_\psi(1/2+\delta+it)|^2 \le \int_{\mathbb{R}} P_\delta(t-v)|f_\psi(1/2+iv)|^2\,dv.$$

The exact row family is finite for fixed H, so its sum interchanges with the integral without a limiting-family issue. The boundary pole-removal factor has modulus at most one.

Take $0 < \varepsilon_0 \le 1/4$ and $\alpha = 3/2 - \varepsilon_0 \in [5/4, 3/2)$. Since $|3/2 + iv| \ge (1+|v|)/\sqrt{2}$, the central squared moment of the f_ψ is bounded by $3C_0H^{1+\varepsilon_0}w_\alpha(v)$, where $w_\alpha(v) = (1+|v|)^{-\alpha}$. For $|t| \ge 2$, split $|v-t| \le |t|/2$ from its complement. The near contribution to $P_\delta * w_\alpha$ is at most $2^\alpha w_\alpha(t) < 3w_\alpha(t)$. In the far region use $P_\delta(t-v) \le 4\delta/(\pi t^2)$ and $\int w_\alpha = 2/(\alpha-1)$, giving at most

$$\frac{2\delta 3^\alpha}{\pi(\alpha-1)} w_\alpha(t) \le 8w_\alpha(t).$$

Here $(1+|t|)^\alpha/t^2 \le 3^\alpha/4$ for $|t| \ge 2$. For $|t| \le 2$, the convolution is at most one and hence at most $3^\alpha w_\alpha(t) < 6w_\alpha(t)$. Thus $P_\delta * w_\alpha \le 11 w_\alpha$ uniformly for $0 < \delta < 1/2$. Restoring the denominator costs less than $6(1+|t|)^{5/2}$, and the inverse principal factor is bounded by $(3/2+\delta)/(1/2-\delta)$. The product $11 \cdot 3 \cdot 6 = 198 < 200$ proves (39.2). The constant is uniform as $\delta \downarrow 0$, but not as the contour approaches the principal pole line $\mathrm{Re}\, s = 1$. No zero-free hypothesis appears.

39.2.6 The separately scoped unitary infinity type

Let $\nu(\mathfrak{a}) = \nu_0(\mathfrak{a})(N\mathfrak{a})^{-i\tau}$ be fixed and unitary, with angular parameter m and gamma factor γ_ν stated in Section 39.1. The external primitive functional equation is explicitly

$$Q_\rho^{s/2}\gamma_\nu(s)L(s,\rho) = \epsilon_\rho Q_\rho^{(1-s)/2}\gamma_{\bar\nu}(1-s)L(1-s,\bar\rho), \qquad |\epsilon_\rho| = 1.$$

A constant norm-twist phase in another completion convention is absorbed in ϵ_ρ. All finite Kummer twists share this infinity type. Replace T in the kernel by $T_\nu = 1 + |t+\tau| + |m|$. The numerator gamma ratio now has real base $1/2 + |m|/2 > 0$ and vertical parameter $t+\tau$; its conjugate dual has parameter $-(t+\tau)$. Stirling gives the same integrable Gaussian-majorized kernel on each fixed shifted line. Constants can depend on m, τ; T_ν is comparable to T for this one fixed ν. The finite-prime conductor analysis, modulus-one coefficient twist, all-ideal decomposition and all original primitive row values remain unchanged.

A pure norm row has $L(s,\rho) = \zeta_K(s+i\tau)$; exclude it from the pole-free approximate functional equation and use scalar convexity at $t+\tau$. In the Poisson step cancel its actual pole by

$$h_\tau(s) = \frac{s-1+i\tau}{s+1+i\tau}.$$

This factor is analytic in the relevant right half-plane. On its boundary $|h_\tau| \le 1$, while inside $|h_\tau^{-1}| \le (3/2+\delta)/(1/2-\delta)$. Hence the same transfer factor 200 applies to the now ν-dependent

central constant. If the opposite norm convention is chosen, replace τ by $-\tau$ in the gamma factor and pole alike. This proves the separate fixed-unitary moment assertion; it does not claim uniformity in a family of infinity types or replace the finite-order principal-residue expression below.

39.2.7 Keeping the full type-I mask during transfer

For $\sigma = 1/2 + \delta$, define L^T by removing every prime of $T(u,d)$, not just conductor primes. The identity (39.3) is equivalently

$$F_{u,d}(s) = \frac{L(s,\psi_u)}{L^{T(u,d)}(2s,\psi_{u,2})} \prod_{p\in T(u,d),\ p\nmid \mathfrak{f}_u} (1-\psi_u(p)(Np)^{-s}).$$

Absolute convergence at $2\sigma > 1$ bounds the reciprocal incomplete product by $\zeta_K(2\sigma)$, without requiring any zero-free theorem in the critical strip. For every fixed $\eta > 0$,

$$\prod_{p\in T}(1+(Np)^{-\sigma}) \ll_{\sigma,\eta} (N\operatorname{rad} T)^{\eta}, \qquad N\operatorname{rad} T \le C_S Nu\, Nd.$$

Indeed $1 + q^{-\sigma} \le q^{\eta}$ beyond a fixed threshold, and only finitely many prime ideals lie below it. Therefore

$$|F_{u,d}(\sigma+it)| \ll_{\nu,S,\delta,\eta} (Nu\,Nd)^{\eta}|L(\sigma+it,\psi_u)|. \tag{39.13}$$

This is a bounded inequality after the exact mask identity, not an identity that removes original zeros. For example, with principal ν and $u = \pi^3$ or π^6 at $N\pi = 7$, the primitive local ratio, restoration and full masked factor at $s = 1$ are respectively

$v_\pi(u)$	primitive ratio	restoration	masked factor
3	48/49	49/48	1
6	8/7	7/8	1

The squared primitive character in the first row is unramified at π although the original primitive character is ramified there. Squaring a zero sentinel would give the wrong denominator.

For finite-order ν, the normalized type-I piece is the retained d sum of the smoothed squarefree series at $Y = D/Nd$, divided by $\sqrt{D}$. Its possible pole is only at $s = 1$, on principal rows. Contour shifting with the full mask gives $I_u = P_u + E_u$, with E_u exactly (39.4) and

$$P_u = \mathbf{1}_{\psi_u=1}\sqrt{D}\,\widehat{W}(1) \sum_{\substack{d \text{ squarefree}\\(d,S)=1}} \frac{\beta_U(d)\nu(d)\chi_d(u)}{Nd}\rho_{T(u,d)},$$

$$\rho_T = \frac{\operatorname{res}_{s=1}\zeta_K(s)}{\zeta_K(2)} \prod_{p\in T}(1+(Np)^{-1})^{-1}.$$

This does not impose positivity on P_u. Since β_U is supported on $Nd \le U^2 \le D$, every inner scale Y is at least one. Four integrations by parts give $|\widehat{W}(\sigma+it)| \ll_\sigma \mathcal{M}_4(W)(1+|t|)^{-4}$, which justifies the shifted integrals and their horizontal limits with the classical Hecke growth estimates.

Apply Minkowski to (39.4) in ℓ^2 of the actual u rows, then use (39.13) and the off-central moment. For sufficiently small internal losses this bounds $\|E\|_2$ by

$$CD^{\delta}H^{1/2+O(\eta)} \sum_d \frac{|\beta_U(d)|}{(Nd)^{\sigma-\eta}} \int_{\mathbb{R}} |\widehat{W}(\sigma+it)|(1+|t|)^{(1+O(\eta))/2}\,dt.$$

All original $\nu(d)\chi_d(u)$ have modulus at most one and remain inside the exact expression before this inequality. The actual truncated factorization gives, without replacing β_U by arbitrary coefficients,

$$\sum_d \frac{|\beta_U(d)|}{(Nd)^{\sigma-\eta}} \le \left(\sum_{Na\le U} (Na)^{-\sigma+\eta}\right)^2 \ll_{\delta,\eta} U^{1-2\delta+2\eta}.$$

Choose $\eta < \delta$ if necessary and use the fixed-field ideal count. The height integral is bounded by $C\mathcal{M}_4(W)$. Squaring and absorbing the small losses in $(HD)^{\varepsilon}$, using $U^2 \le D$, proves (39.5). Thus the formerly conditional numerator moment input in this residual transfer is discharged, while its positive-power cutoff loss is retained explicitly.

39.2.8 What remains open and what has been verified

The new remainder envelope improves the old scalar-convexity H power $3/2 - \delta + \varepsilon$ to $1 + \varepsilon$. At fixed U one may choose δ for a requested small-loss exponent; for $U = D^a$ with fixed $a > 0$, the remaining excess tends to $2a$ as $\delta \downarrow 0$. Neither statement controls P_u, the other signed piece, nor their covariance. In the original Vaughan identity the short $2a_U$ term must be restored at smaller scales where its support can meet the annulus. Uniform $\mathcal{M}_4$ bounds do not justify interchanging a profile supremum with the row moment or assuming $U^2 \le D'$ after a scale D' is reduced.

The independent prose audit is recorded in `planning/analytic-oracle/arithmetic-review/adversarial-afm-review-20261104.md`. The source-hashed finite checker tests valuation/support decompositions, squarefull coordinates, height exponents and rational Poisson envelopes. Its finite success does not prove reciprocity, analytic continuation, the large sieve, the approximate functional equation or the moments. No new Lean declarations accompany these analytic theorems. Existing Lean local Euler identities are a separately limited verification layer. The independent positive arithmetic determinant comparison, original signed low-gcd short-row estimate, all required contour uniformities and GRH remain open; Dirichlet, Hecke, Dedekind and general Artin scopes are not identified with one another.

Pinned primary sources and external inputs. The principal analytic family input is Blomer–Goldmakher–Louvel, arXiv:1112.1650v1, Theorem 1.3, Lemma 2.1, Appendix II and Section 5. Our fixed-ν proof changes column coefficients and redoes the functional-equation reduction; it does not claim the published corollary directly states every fixed twist. For comparison, Gao–Zhao, arXiv:2201.01885v2, Lemma 2.9 and Section 3.2, uses the sextic large-sieve/moment interface. Its GRH-conditional central-density theorem is not invoked. Abelian Kummer identification uses the classical reciprocity theorem, with the project's pinned Milne *Class Field Theory*, version 4.03 (6 August 2020), Theorem 0.8 and Chapter I, Section 1, a reference: Milne's notes. The primitive degree-one Hecke continuation and completed functional equation are explicit classical external inputs; the project's pinned Kudla notes on Tate's thesis, Theorem 4.3 and Corollary 4.4, supply a reference. Their sketch and incomplete displayed epsilon formulas are not used as independently certified constants. Standard Stirling, Mellin inversion, Poisson representation and scalar convexity complete the external analytic dependencies. None is replaced by a finite diagnostic or a GRH-equivalent assumption.

Chapter 40

Weighted cutoffs and original-family moments

40.1 Recombining the actual weighted cutoff

Keep the finite-order Eisenstein family and original masks of Section 39.1. For $U \geq 1$ and a squarefree ideal m, put

$$A_U(m) = \sum_{d|m} \beta_U(d) = \sum_{\substack{ab|m \\ (a,b)=1,\ Na,Nb\leq U}} \mu(a)\mu(b).$$

Every summation variable here is an integral ideal. The last formula uses squarefreeness of m; an unconstrained square of a Möbius polynomial would also include forbidden overlapping supports.

Theorem 40.1 (Exact recombination and an absolute-half-plane rate)**.** *Write $T_0 = S \cup \mathrm{supp}(u)$ and $J_{u,U}(s) = \sum_{d \text{ squarefree},\ (d,S)=1} \beta_U(d)\nu(d)\chi_d(u)(Nd)^{-s}F_{u,d}(s)$. For $\mathrm{Re}\, s > 1$,*

$$J_{u,U}(s) = \sum_{m \text{ squarefree},\ (m,T_0)=1} A_U(m)\psi_u(m)(Nm)^{-s},$$

$$|A_U(m)| \leq 3^{\omega(m)}, \qquad A_U(m) = \mu(m) \quad (Nm \leq U).$$

For every $\kappa > 0$ and $0 < \epsilon < \kappa$, uniformly for $\mathrm{Re}\, s \geq 1 + \kappa$, all original rows and all $U \geq 1$,

$$\left| J_{u,U}(s) - \frac{1}{L^{T_0}(s,\psi_u)} \right| \leq U^{-\kappa+\epsilon}\{\zeta_K(1+\epsilon)^3 + \zeta_K(1+\epsilon)\}.$$

Here L^{T_0} removes every prime of T_0, including conductor-drop primes; the bound is in the absolute-convergence half-plane only.

Proof. On a surviving term $m = dc$, the two squarefree ideals c, d are coprime, and both avoid T_0. The original product $\nu(d)\chi_d(u)\psi_u(c)$ is then $\psi_u(m)$. Grouping by m gives A_U. Each prime of m has three possible positions in $(a, b, m/(ab))$, so the absolute sum is at most $3^{\omega(m)}$. When $Nm \leq U$ all divisors fit both cutoffs; the primewise sum is $1 - 1 - 1 = -1$, giving $\mu(m)$.

The same bound justifies absolute convergence and regrouping for $\mathrm{Re}\, s > 1$, because on squarefree ideals $3^{\omega(m)} = \tau_3(m)$ and $\sum_m \tau_3(m)(Nm)^{-v} = \zeta_K(v)^3$ for $v > 1$, where this latter sum runs over all nonzero integral ideals. Subtract the absolutely convergent Möbius series for $1/L^{T_0}$. Only $Nm > U$ remain. Rankin's inequality with exponent $\eta = \kappa - \epsilon$ bounds their absolute sum by

$$U^{-\eta} \sum_m \{\tau_3(m) + 1\}(Nm)^{-1-\epsilon},$$

which proves the stated constant independently of deleted primes, row multiplicities or character phases. □

For W supported in $[1,2]$, the same exact regrouping gives the original normalized type-I polynomial

$$I_u = D^{-1/2} \sum_{m \text{ squarefree},\ (m,S)=1} A_U(m)\nu(m)\chi_m(u)W(Nm/D).$$

This formula retains all original zero sentinels. It permits a direct family large sieve before any absolute d sum; its quantitative moment is developed separately below. The displayed absolute-half-plane rate alone is not that critical-strip moment.

40.2 Euler packaging, coprimality and the analytic boundary

For $p \notin T_0$, set $z_p = \psi_u(p)(Np)^{-s}$ and $t_p = z_p/(1+z_p)$. On $\operatorname{Re} s > 1$, deleting an additional surviving prime divides the squarefree Euler product by $1+z_p$. Consequently the exact retained expression is

$$J_{u,U}(s) = F_{u,1}(s)B_{u,U}(s), \qquad B_{u,U}(s) = \sum_{d \text{ squarefree},\ (d,T_0)=1} \beta_U(d) \prod_{p\mid d} t_p.$$

Original zeros enforce $(d,u)=1$ even when a sixth power drops from its primitive conductor. This factorization cannot restore a forbidden d row by replacing a zero sentinel with an unramified primitive value. The equality continues wherever both sides are holomorphic.

Without the cutoffs, $\beta_\infty(d) = \mu(d)2^{\omega(d)}$ on squarefree ideals. Absolute convergence justifies

$$B_{u,\infty} = \prod_{p\notin T_0}(1-2t_p) = \prod_{p\notin T_0}\frac{1-z_p}{1+z_p}, \qquad F_{u,1}B_{u,\infty} = \prod_{p\notin T_0}(1-z_p) = \frac{1}{L^{T_0}(s,\psi_u)}.$$

Theorem 40.1 gives a quantitative rate rather than an unsupported exchange of this limit with a critical-strip contour.

A local counterexample to the naive square. In a one-prime projection at a good Eisenstein prime of norm 7, take the principal local phase and $s=1$. Then $z=1/7$, $t=1/8$ and, for $U \geq 7$, the exact polynomial is $B_U = 1-2t = 3/4$. The unconstrained square $(1-t)^2 = 49/64$ differs by $1/64$: it admits the forbidden pair $a=b=p$. After multiplying by $F = 1+z = 8/7$ it gives $7/8$ instead of the correct $6/7$. This is an actual local Euler calculation, not an infinite-series or mean-square counterexample. It identifies the exact coprimality condition that a proposed mollifier-square simplification must preserve.

The exact intermediate coefficient band. For a squarefree m with $U < Nm \leq U^2$, one has $A_U(m) = -\mu(m)$. Indeed the unrestricted disjoint-assignment sum is $\mu(m)$. If $Na > U$, every $b \mid m/a$ automatically has $Nb \leq Nm/Na < U$, and $\sum_{b\mid m/a}\mu(b)$ vanishes unless $a=m$. Hence the excluded a assignments contribute exactly $\mu(m)$; the excluded b assignments contribute another $\mu(m)$. They cannot overlap because $NaNb > U^2 \geq Nm$ contradicts $ab \mid m$. Subtraction proves the claim. Together with the small-norm band, this gives $A_U = \mu$ for $Nm \leq U$ and $A_U = -\mu$ for $U < Nm \leq U^2$. The original smoothed columns have $Nm \geq D \geq U^2$, so the new band does not justify replacing their coefficients by $-\mu(m)$: generally they lie beyond it.

Theorem 40.2 (A stronger cutoff convergence would require zero-freeness)**.** *Fix a nonprincipal primitive ψ_u. If these actual $J_{u,U}$ converge locally uniformly on $\operatorname{Re} s > 1/2$ as $U \longrightarrow \infty$, then $L(s, \psi_u)$ has no zero there.*

Proof. Classical abelian Hecke continuation makes the numerator of $F_{u,1} = L^{T_0}(s, \psi_u)/L^{T_0}(2s, \psi_{u,2})$ holomorphic. Its denominator is nonzero on $\operatorname{Re} s > 1/2$ by the absolute Euler product at $2s$. Each $B_{u,U}$ is a finite sum with nonzero denominators $1 + z_p$ on $\operatorname{Re} s > 0$. Thus every $J_{u,U}$ is holomorphic on the asserted half-plane. A locally uniform limit G is holomorphic there. On $\operatorname{Re} s > 1$, the already proved convergence gives $L^{T_0}(s, \psi_u)G(s) = 1$. The identity theorem extends this equality to the connected half-plane, precluding a zero of L^{T_0}. The finitely deleted factors $1 - \psi_u(p)(Np)^{-s}$ do not vanish when $\operatorname{Re} s > 0$, so the same conclusion holds for the primitive L-function. □

This is an implication, not a proof that the stronger convergence holds, and it does not assert a converse. In particular, a family-averaged energy bound is not silently promoted to locally uniform convergence for each individual character. Principal rows have a pole at 1 and were excluded from this proposition. General Artin holomorphy is not an input.

Reproducible exact diagnostics. The new source `examples/arithmetic_cutoff/exact_recombination.py` uses actual split/inert prime ideals and raw sextic symbols in $\mathbb{Z}[\omega]$, with exact rational arithmetic. It checks the direct masked sum, coefficient regrouping, Euler packaging, both finite full-cutoff limits and original zeros, including third/sixth-power rows. Its overlapping- support negative controls are not tests of an infinite large sieve or of zero location. The analytic convergence argument above uses ordinary ideal Euler products and the explicitly stated Hecke continuation theorem; no new Lean declaration or complete GRH proof is claimed.

40.3 A cutoff-uniform envelope for the original masked remainder

Fix $K = \mathbb{Q}(\omega)$, $\mathcal{O} = \mathbb{Z}[\omega]$, a finite-order Hecke character ν, and a finite set S containing the primes above 6 and the conductor of ν. All unspecified ideal sums below are over nonzero integral ideals. Let $\chi_m(u) = (u/m)_6$ be the original symbol, zero when $(m, u) > 1$, and put

$$\beta_U(d) = \sum_{\substack{ab=d \\ Na, Nb \le U}} \mu(a)\mu(b), \qquad A_U(m) = \sum_{d \mid m} \beta_U(d).$$

The columns d, c, m are squarefree and prime to S where indicated. Retain the primitive characters $\psi_u = \operatorname{prim}(\nu\kappa_u)$, $\psi_{u,2} = \operatorname{prim}(\psi_u^2)$, and the full deleted set $T(u, d) = S \cup \operatorname{supp}(u) \cup \operatorname{supp}(d)$. For $H, D, U \ge 1$, $U^2 \le D$, and $W \in C_c^\infty((0, \infty))$ supported in $[1, 2]$, the original normalized type-I piece is

$$I_u = D^{-1/2} \sum_{\substack{m \text{ squarefree} \\ (m,S)=1}} A_U(m)\nu(m)\chi_m(u)W(Nm/D). \tag{40.1}$$

Its exact principal residue is

$$P_u = \mathbf{1}_{\psi_u=1}\sqrt{D}\,\widehat{W}(1) \sum_{\substack{d \text{ squarefree} \\ (d,S)=1}} \frac{\beta_U(d)\nu(d)\chi_d(u)}{Nd}\rho_{T(u,d)},$$

$$\rho_T = \frac{\operatorname{res}_{s=1}\zeta_K(s)}{\zeta_K(2)} \prod_{p \in T}(1 + (Np)^{-1})^{-1}. \tag{40.2}$$

Define $E_u = I_u - P_u$; this is the same residue-subtracted remainder as the fully masked Mellin contour, with no cutoff limit or profile supremum.

Theorem 40.3 (Uniformity in the actual truncated cutoff)**.** *For every $\varepsilon > 0$,*

$$\sum_{0<Nu\le H} |E_u|^2 \ll_{\nu,S,\varepsilon} \|W\|_\infty^2 (HD)^\varepsilon \{H + DH^{1/3} + (HD)^{2/3}\}. \tag{40.3}$$

The sum is over every actual nonzero Eisenstein element, including units, S-supported powers and sixth-power rows. The constant is independent of U under $U^2 \le D$. This is an application of the classical sextic large sieve with exact original coefficients, not a zero-location theorem.

Proof. On an absolutely convergent line, expand the restored squarefree series $F_{u,d}$. Its condition $(c, T(u,d)) = 1$ includes $(c,d) = 1$, and the original symbols multiply. Grouping $m = cd$ gives (40.1) by Mellin inversion. Each prime of m may belong to the first truncated Möbius divisor, to the second, or to neither. Consequently $|A_U(m)| \le 3^{\omega(m)} \ll_\eta (Nm)^\eta$, uniformly in U. The length-D coefficient sequence in (40.1) therefore has squared norm $\ll_\eta \|W\|_\infty^2 D^\eta$.

The all-ideal row norm in Section 3 of Blomer–Goldmakher–Louvel, arXiv:1112.1650v1 gives

$$B_2^1(X, D) \ll_\eta (XD)^\eta \{X + DX^{1/3} + (XD)^{2/3}\}.$$

For completeness, split $a = a_1 a_2^2 \cdots a_5^5 a_6^6$ dyadically; $a_1, \dots, a_5$ are squarefree and pairwise coprime. If their dyadic sizes are A_j, put $R = \prod_{j=1}^6 A_j$ and $M = \max(A_1, A_2)$. Pivot on the first or second variable, using the squarefree powered sieve proved simultaneously in that paper's Section 3.2. The other variables are bounded column multipliers. The block energy is at most

$$(XD)^\eta \{R + DR/M + D^{2/3} R/M^{1/3}\} \sum_m |\lambda_m|^2.$$

The inequalities $R \le X$, $R^3 \le XM^3$ and $R^3 \le X^2 M$ follow from $\prod_j A_j^j \le X$ and the pivot choice. Summing the logarithmically many blocks proves the displayed bound.

Finite S-unit and ray-class partitions convert the original literal symbol into the canonical column value $\vartheta_m(a)$ with fixed modulus-one coefficient multipliers. On noncoprime pairs both values are zero: squarefree m has outside-S conductor exactly m. This orientation preserves sixth-power zeros. At most six elements generate each outside-S ideal times an S-supported ideal; the S-supported sums converge at powers 1, 1/3 and 2/3. Thus (40.3) holds first with I_u in place of E_u.

A principal ψ_u requires every outside-S valuation of u to be divisible by 6. There are $O_{\nu,S}(H^{1/6})$ such literal rows. Equation (40.2), $|\rho_T| \ll_K 1$, and the actual coefficient sum

$$\sum_d \frac{|\beta_U(d)|}{Nd} \le \left(\sum_{Na \le U} \frac{1}{Na} \right)^2 \ll \log^2(2U)$$

give $\sum |P_u|^2 \ll DH^{1/6} \|W\|_\infty^2 \log^4(2U)$. This is absorbed by the right side of (40.3), using $U^2 \le D$ and a smaller internal exponent. Finally $|E_u|^2 \le 2|I_u|^2 + 2|P_u|^2$. The extended proof specifies the canonical-family transfer and the powered-sieve input precisely. □

Combining this with the previously proved fixed-twist AFM transfer yields

$$\sum_{0<Nu\le H} |E_u|^2 \ll_{\nu,S,\delta,\varepsilon} \mathcal{M}_4(W)^2 (HD)^\varepsilon \min\{D^{2\delta} U^{2-4\delta} H,\ H + DH^{1/3} + (HD)^{2/3}\}. \tag{40.4}$$

At $H = D^{3/4}$ and $U = D^a$, $0 \le a \le 1/2$, the excess over H is at most $\min\{2\delta + (2-4\delta)a, 1/2\}$, up to arbitrarily small losses. The new envelope improves the old one for $a > 1/4$ as $\delta \downarrow 0$, but still leaves an exponent loss of 1/2. It does not settle the original signed short-row bound, type-II covariance, positive arithmetic determinant comparison or GRH. The principal-residue bound used here is sufficient for this envelope, not the stronger target needed to reassemble the full signed argument.

40.4 All-ideal reciprocity and the surviving block obstruction

The proof uses no new zero-free input. Its external analytic ingredient is the pinned BGL large sieve and the powered estimates established in its proof; elementary ideal counting and the already restored Mellin identity supply the remaining interfaces. All constants may depend on fixed K, S, ν and declared small exponents, never on U.

40.4.1 Exact recombination retains the primitive corrections

On $\operatorname{Re} s > 1$, start from the full defining series, with its original zero masks:

$$F_{u,d}(s) = \sum_{\substack{c \text{ squarefree} \\ (c,T(u,d))=1}} \nu(c)\chi_c(u)(Nc)^{-s}.$$

Its primitive ratio involves $L(s,\psi_u)$, the independently primitive $L(2s,\psi_{u,2})$ and every deleted Euler factor. Expanding this *restored* series gives the exact equality

$$\begin{aligned}\sum_{\substack{d \text{ squarefree} \\ (d,S)=1}} &\beta_U(d)\nu(d)\chi_d(u)(Nd)^{-s}F_{u,d}(s) \\ &= \sum_{\substack{m \text{ squarefree} \\ (m,S)=1}} A_U(m)\nu(m)\chi_m(u)(Nm)^{-s}. \end{aligned} \tag{40.5}$$

Indeed $(c,d)=1$ makes $m=cd$ squarefree, with $d \mid m$. If m meets u, both original symbols retain their zero. Only on the absolutely convergent line is this infinite series used. Mellin inversion there gives the finite smoothed polynomial (40.1). Nothing evaluates (40.5) as a Dirichlet series on $\operatorname{Re} s = 1/2+\delta$ or interchanges a cutoff limit with continuation across unknown zeros.

For squarefree m, a factorization $ab = d \mid m$ assigns each prime to a, to b, or to neither. The actual inequalities $Na, Nb \le U$ select a subset of these assignments. Thus

$$|A_U(m)| \le 3^{\omega(m)} \ll_\eta (Nm)^\eta.$$

The last divisor bound follows by choosing a fixed threshold so $3 \le (Np)^\eta$ beyond it, then absorbing the finitely many smaller prime ideals in a constant. When $Nm \le U$ all assignments occur, so $A_U(m) = \prod_{p\mid m}(1-1-1) = \mu(m)$; no such simplification is made for the length-D columns in general. With $\lambda_m = D^{-1/2}A_U(m)\nu(m)W(Nm/D)$, ideal counting and a smaller internal η give

$$\sum_m |\lambda_m|^2 \ll_\eta \|W\|_\infty^2 D^\eta, \qquad \operatorname{supp}\lambda \subseteq \{D \le Nm \le 2D\}. \tag{40.6}$$

40.4.2 The powered squarefree input and all-ideal pivot

Let ϑ_a be BGL's canonical primitive sixth-order family. Their Section 3 defines B_1^j using squarefree row/column ideals and kernel $\vartheta_a(m)^j$, while B_2^j uses *all* ideal rows and kernel $\vartheta_m(a)^j$. Theorem 1.3 states the squarefree bound for $j=1$; its Section 3.2 proves the estimates simultaneously for $1 \le j \le 5$, because the recursion in Lemma 3.4 uses $j\ell$. In particular the two inputs needed here are

$$B_1^j(M,D) \ll_\eta (MD)^\eta\{M + D + (MD)^{2/3}\}, \qquad j = 1,2. \tag{40.7}$$

To see the final step in the published recursion explicitly, its $E_{4/3}$ estimate is $M^{4/3} + D + (MD)^{2/3}$. If $M \le D$, its first term is at most $(MD)^{2/3}$; if $M > D$, use reciprocity/duality (3.2) and the

estimate with M, D reversed. The finite set of powers is treated together; no inference from a fixed conductor count to an arbitrary primitive-character sieve occurs.

Write each ideal row uniquely as

$$a = a_1 a_2^2 a_3^3 a_4^4 a_5^5 a_6^6,$$

where $a_1, \dots, a_5$ are pairwise-coprime squarefree ideals and a_6 is arbitrary. For valuation $6q + r$, $0 \le r \le 5$, place the prime in a_r if $r > 0$ and its power q in a_6. Dyadically let $A_j \le Na_j < 2A_j$, with $A_j \ge 1$, and put $R = \prod_{j=1}^{6} A_j$. A nonempty block satisfies $\prod_j A_j^j \le X$ when $Na \le X$. Choose $\ell = 1$ if $A_1 \ge A_2$, and $\ell = 2$ otherwise; put $M = A_\ell$. Keep every other ideal fixed. Evaluation of the single *column* character gives

$$\vartheta_m(a) = \vartheta_m(a_\ell)^\ell \vartheta_m(a/a_\ell^\ell).$$

The second factor is a bounded column multiplier, including its original zero if m meets any fixed factor. It may depend on all the fixed ideals but not on the pivot row. Pairwise-coprimality and the exact row norm restriction merely select a subset of the positive pivot-row sum. Apply (40.7) to the first factor. There are $O_K(R/M)$ choices of the other ideals by ideal counting. The block energy is bounded by

$$(XD)^\eta \{R + DR/M + D^{2/3} R/M^{1/3}\} \sum_m |\lambda_m|^2. \tag{40.8}$$

All three monomial bounds used to sum these blocks are elementary. First $R \le \prod_j A_j^j \le X$. If $M = A_1$, then

$$(R/M)^3 = A_2^3 \cdots A_6^3 \le A_1 A_2^2 A_3^3 A_4^4 A_5^5 A_6^6 \le X,$$

since $A_2 \le A_1$ and $j \ge 3$ for the remaining factors. If $M = A_2$, use $A_1 \le A_2$ in the same comparison. Finally,

$$\frac{R^3}{M(\prod_j A_j^j)^2} = \frac{A_1}{M A_2 A_3^3 A_4^5 A_5^7 A_6^9} \le 1.$$

Thus $R/M \le X^{1/3}$ and $R/M^{1/3} \le X^{2/3}$. Insert these in (40.8) and sum the logarithmically many blocks. This proves the all-ideal estimate used in Theorem 40.3. It is precisely the mechanism of BGL Lemma 3.4 and (3.6)–(3.9), with the final powered bound inserted. The simpler fixed-squarefull-row argument would leave the weaker $D\sqrt{X}$ term.

40.4.3 Literal rows, reciprocal orientation and principal count

Let $a = (u)_S$ denote the outside-S ideal. The finite S-unit comparison gives $\kappa_u = \eta_u \vartheta_a$ as primitive characters, with η_u in a finite fixed set. For $(a, m) = 1$, BGL reciprocity therefore gives

$$\chi_m(u) = \eta_u(m) C([a], [m]) \vartheta_m(a). \tag{40.9}$$

The notation is deliberate: the left side is the project's original $(u/m)_6$, not BGL's canonical character indexed by m. When $(a, m) > 1$, the left side is zero. The right side is also zero, because squarefree m has outside-S primitive conductor exactly m. Equation (40.9) hence extends to every pair. Using $\vartheta_a(m)$ on noncoprime pairs instead would be false: primitive ϑ_{b^6} has restored primes of b, whereas the original symbol must still vanish there.

Partition rows by η_u and $[a]$, both finite. On each part the factor $\eta_u(m)C([a], [m])$ is a fixed modulus-one column multiplier. A positive row sum over that part is bounded by the full B_2^1 row sum. For each S-supported ideal b and outside-S ideal a, at most six actual elements generate ab.

Thus the required literal energy is bounded by the all-ideal norm summed over b, with $X = H/Nb$. The geometric products

$$\sum_{b \ S\text{-supported}} (Nb)^{-q} = \prod_{p \in S} (1 - (Np)^{-q})^{-1} < \infty, \qquad q = 1,\ 1/3,\ 2/3,$$

transfer the three terms without losing any unit or S-power row. Together with (40.6), this proves the claimed I energy.

If ψ_u is principal, ν is unramified outside S, and tame Kummer inertia at $v_p(u)$ has order $6/\gcd(6, v_p(u))$. It must be trivial, so each such valuation is divisible by 6. Writing $(u) = ba_6^6$ with b supported in S, ideal counting gives

$$\#\{0 < Nu \le H : \psi_u = 1\} \ll_K H^{1/6} \prod_{p \in S} (1 - (Np)^{-1/6})^{-1}.$$

This is only a necessary condition, sufficient for an upper count. The exact residue formula (40.2) and $|\widehat{W}(1)| \le \|W\|_\infty$ then give the principal energy bound used above. No sign or positivity of that residue is assumed.

40.4.4 What the envelope still fails to prove

The $DH^{1/3}$ term is still larger than $H(HD)^\varepsilon$ at $H = D^{3/4}$. The monomial comparison itself is saturated by $A_1 = A_2 = X^{1/3}$ and $A_3 = \cdots = A_6 = 1$. This proves sharpness of that *particular comparison*, not an energy lower bound for actual arithmetic coefficients. In particular, no conclusion that the signed A_U cannot cancel is justified. The next load-bearing input must exploit those actual truncated Möbius coefficients inside the mixed moment, or establish the required signed type-II minus type-I covariance. The smaller-scale short term, principal contribution, full arithmetic determinant identification and GRH remain separate obligations.

Exact finite checks use the split Eisenstein primes generated by $3 + \omega$, $4 + \omega$, $5 + 2\omega$, $6 + \omega$, of norms $7, 13, 19, 31$. Their actual residue symbols are computed in $\mathbb{Q}(\zeta_6)$, retaining sixth-power zeros. Coefficient recombination and dyadic inequalities pass; they check finite algebra and bookkeeping, not the external analytic sieve or the contour theorem. No new Lean declarations accompany this argument.

40.5 High cutoffs, actual bilinear factors and a signed covariance test

Retain the original Eisenstein family, fixed finite-order ν, fixed S, common $W \in C_c^\infty((0,\infty))$ supported in $[1,2]$, and every raw shared-prime zero. Put

$$C_U(m) = \sum_{\substack{abc=m \\ Na>U,\, Nb>U}} \mu(a)\mu(b), \qquad r_U(m) = \#\{(a,b) : ab = m,\ Na, Nb > U\}.$$

All factors are ideals, squarefree and pairwise coprime; on the active annulus $A_U = C_U - \mu$. A coefficient identity is different from a row-energy bound.

Proposition 40.4 (The high-cutoff window)**.** *If $D > 1$ and $2D/7 \le U^2 \le D$, then for every surviving squarefree column $D \le Nm \le 2D$,*

$$C_U(m) = \mu(m) r_U(m), \qquad A_U(m) = \mu(m)(r_U(m) - 1), \qquad |A_U(m)| \ge 1.$$

For each fixed nonzero W, the normalized squared coefficient norm satisfies

$$D^{-1} \sum_{\substack{m \text{ sf} \\ (m,S)=1}} |A_U(m)W(Nm/D)|^2 \gg_{W,S} 1 \tag{40.10}$$

for large D, uniformly in this window. This is not a lower bound for row energy.

Proof. The least norm of a nonunit ideal outside S is at least 7. A long-long term with $c \neq 1$ would have $Nm > 7U^2 \geq 2D$. Thus $ab = m$, including both endpoints. The fixed-point-free swap $(a, b) \mapsto (b, a)$ makes r_U even, so A_U is an odd nonzero integer. The last claim follows by counting squarefree ideals on a fixed interval where $|W|$ is bounded below; the constant and error are proved in the extended proof. □

The exact remaining polynomial is genuinely bilinear, with $(a, b) = 1$, $U < Na, Nb < 2D/U$, $D \leq Na\,Nb \leq 2D$, and $x_{ab}(u) = x_a(u)x_b(u)$, including zeros. Both factors see the same row $u = \varepsilon\alpha\beta^2$. Cauchy followed by the accepted powered BGL bound gives only

$$Q_{B_X}(C_U, C_U) \ll_{\nu,S,\epsilon} (DX)^{\epsilon}\|W\|_\infty^2\{\sqrt{D}\,X^2 + DX + D^{5/6}X^{5/3}\}. \tag{40.11}$$

At $X \asymp D^{1/4}$ the exponents are $1, 5/4, 5/4$; the earlier regrouped bound has $1/2, 5/4, 13/12$ and is stronger. No BT_σ saving is obtained. Multiplying two marginal operator norms does not supply a coupled fourth moment.

A finite test in the original family. There is no automatic nonnegative signed covariance, even when $C_U(m)\mu(m) \geq 0$. Take $\nu = 1$, S the primes above $2, 3$, $D = 400$, $U = 17$, and all 72 literal rows of B_7. Choose the common nonnegative smooth profile constructed in the extended proof, with values 10 at $439/400$, 1 at $475/400$, and zero at every other integer norm divided by 400. There are exactly four active squarefree ideal columns, of norms $439, 439, 475, 475$. In that order,

$$A = (1, 1, 1, 1), \quad C = (0, 0, 2, 2), \quad \mu = (-1, -1, 1, 1), \qquad \Re G_{B_7} = \begin{pmatrix} 72 & 0 & 0 & 18 \\ 0 & 72 & 18 & 0 \\ 0 & 18 & 72 & 0 \\ 18 & 0 & 0 & 72 \end{pmatrix}.$$

Exact raw-symbol enumeration, independently reproducible from the ideal and residue-field definitions, gives

$$Q(C, \mu) = -\frac{27}{25}, \qquad Q(C, C) = \frac{36}{25}, \quad Q(\mu, \mu) = \frac{864}{25}, \quad Q(A, A) = \frac{954}{25}. \tag{40.12}$$

The real Gram matrix is positive definite, with eigenvalues $54, 90$; its positivity does not force a cross covariance to be positive. This fixed finite example refutes that shortcut, not the asymptotic BT_σ target or the original signed mean-square estimate.

The two-cutoff contour remains coupled. For $T_0 = S \cup \operatorname{supp}(u)$, $\psi = \psi_u$ and independently primitive $\psi_2 = \operatorname{prim}(\psi^2)$, put $q_p = \psi(p)(Np)^{-s}$, $\alpha_p = (Np)^{-z}$, $\beta_p = (Np)^{-w}$ outside T_0. The actual three-placement Euler factor is $1 + q_p - q_p\alpha_p - q_p\beta_p$. Its exact factorization is

$$\mathcal{F}(s, z, w) = \frac{L^{T_0}(s, \psi)}{L^{T_0}(s + z, \psi)L^{T_0}(s + w, \psi)} \prod_{p \notin T_0} \left(1 - \frac{q_p^2(1 - \alpha_p)(1 - \beta_p)}{(1 - q_p\alpha_p)(1 - q_p\beta_p)}\right). \tag{40.13}$$

Exact double Perron inversion is valid on positive auxiliary lines $c, d > 1 - \Re s$ for $1/2 < \Re s < 1$, retaining the original principal pole exclusion. These safe lines reproduce the previous $U^{2-4\delta}$ energy loss at $\Re s = 1/2 + \delta$, with the same common-profile derivative and fixed-margin dependencies. The correction product alone does not justify moving those lines through reciprocal-L poles. In fact $\mathcal{F}(s, z, 0) = 1/L^{T_0}(s + z, \psi)$ as a meromorphic identity. No zero-free region, reciprocal moment, analytic saving, new Lean formalization or GRH proof is supplied by this construction.

40.6 Proof details for the high-window and two-cutoff tests

40.6.1 The coefficient lower bound and its precise limitation

The element lattice $\mathbb{Z}[\omega] \subset \mathbb{C}$ has covolume $\sqrt{3}/2$. Counting disks with boundary error $O(\sqrt{x})$ and dividing by the six units, using that this ring is a PID, gives

$$N_K(x) = \kappa x + O(\sqrt{x}), \qquad \kappa = \frac{\pi}{3\sqrt{3}}.$$

Finite inclusion-exclusion at S gives $N_{K,S}(y) = \kappa y \prod_{p \in S}(1 - (Np)^{-1}) + O_S(\sqrt{y})$. Insert $1_{\mathrm{sf}}(m) = \sum_{d^2 | m} \mu(d)$. Absolute convergence at 2, the tail $\sum_{Nd > \sqrt{x}} (Nd)^{-2} = O(x^{-1/2})$, and $\sum_{Nd \le \sqrt{x}} (Nd)^{-1} = O(\log(2x))$ yield

$$N_{\mathrm{sf},S}(x) = c_S x + O_S(\sqrt{x}\log(2x)), \qquad c_S = \frac{\kappa}{\zeta_K(2)} \prod_{p \in S} (1 + (Np)^{-1})^{-1} > 0.$$

These tail estimates follow by partial summation from the displayed lattice count. For a fixed nonzero W, choose $[a, b] \subset (1, 2)$ with $|W| \ge \eta > 0$. Proposition 40.4 gives, for large D,

$$D^{-1} \sum |A_U(m) W(Nm/D)|^2 \ge \tfrac{1}{2} \eta^2 c_S (b - a).$$

There is no uniform lower constant over all profiles with one specified supremum norm. Nor can a coefficient lower bound be combined with an operator upper bound to produce a row-energy lower bound: no lower singular value has been established on the actual vector.

40.6.2 What legal factor Cauchy actually proves

For dyadic $Na \asymp A, Nb \asymp B$, retain the exact $(a, b) = 1$ mask, hyperbolic support and $W(Na\, Nb/D)$ in

$$T_a(u) = \sum_b \mu(b) \nu(b) W(Na\, Nb/D) x_b(u).$$

Cauchy gives

$$|\sum_a \mu(a) \nu(a) x_a(u) T_a(u)|^2 \ll A \sum_a |T_a(u)|^2.$$

For fixed a, fixed second row factor and fixed unit/ray classes, the b coefficients are independent of the pivot row and have squared norm $\ll B\|W\|_\infty^2$. The prior classical power-one/two BGL input has $\Delta(X, B) = X + B + (XB)^{2/3}$. Summing the $O(A)$ fixed columns and $O(X)$ other row factors gives

$$\mathcal{E}_{A,B} \ll_{\nu,S,\epsilon} (DX)^\epsilon \|W\|_\infty^2 \frac{A^2 B}{D} X \Delta(X, B) \ll (DX)^\epsilon \|W\|_\infty^2 \{AX^2 + DX + D^{2/3} A^{1/3} X^{5/3}\}.$$

In the high window $A, B \asymp \sqrt{D}$, and only boundedly many dyadic pairs occur. This proves (40.11); exchanging factors or row pivots leaves its DX term. A product of marginal second-moment bounds supplies no estimate for the two transforms on the same (r, s). Any useful saving must control that coupled fourth moment or the signed actual-coefficient covariance, with all masks retained.

40.6.3 A smooth profile and the exact covariance computation

Let

$$\phi(t)=\begin{cases}\exp(1-1/(1-t^2)), & |t|<1,\\ 0, & |t|\ge 1,\end{cases}\qquad W_x(y)=x\phi(4(400y-439))+\phi(4(400y-475)).$$

For $x\ge 0$ this is nonnegative and smooth; its disjoint supports lie strictly inside $(1,2)$. For every integer n, $W_x(n/400)$ equals x at $n=439$, 1 at $n=475$ and zero otherwise. Thus the computation uses exact values of a genuine common C_c^∞ profile, rather than claiming a finite rational weight is smooth. At $x=10$, $\|W_x\|_\infty=10$.

The primary ideal generators, in the order used above, are

$$(-23,-18),\quad (-5,18),\quad (10,-15),\quad (25,15),$$

where (a,b) denotes $a+b\omega$. The first two have norm 439. The last two factor as $(-2,3)(-5,0)$ and $(-5,-3)(-5,0)$, with norms $19\cdot 25$. Since $19,25>17$, the long-factor count is 2 there and zero on the prime columns. All squarefree ideals at both selected norms are included. The complete B_7 uses the four good primes of norms $7,7,13,13$ for distinct ordered row factors and all six units. It has 72 distinct rows, maximum norm 2197; each is nonprincipal by its outside-S Kummer valuation 1 or 2 modulo 6, whose nontrivial tame character has conductor exponent 1.

For the raw Gram $G_{ij}=\sum_{u\in B_7} x_{m_i}(u)\overline{x_{m_j}(u)}$, exact finite-field exponentiation and lattice enumeration give the displayed real matrix. The weighted real vectors are $\ell=(0,0,2,2)$, $v=(-x,-x,1,1)$, and $a=(x,x,1,1)$. Therefore

$$Q(C_U,\mu)=D^{-1}\ell^t(\Re G)v=\frac{36-9x}{50}.$$

Its diagonal contribution is $36/50>0$ and its off-diagonal contribution is $-9x/50$. For $x=10$ this is $-27/25$ and gives (40.12). The identity $(\Re G-72I)^2=18^2I$ proves the real eigenvalues $54,90$; these are not being asserted as the eigenvalues of the full complex Gram. The exact source is `examples/arithmetic_cutoff/signed_covariance.py`. A second test retains raw zeros on the 246 rows $0<Nu\le 89$ whose outside-S part is nonunit. Its covariance at $x=10$ is $-69/50$. This subset is guaranteed nonprincipal; it is not called the entire nonprincipal family. Here $89=\lfloor 400^{3/4}\rfloor$. These are finite counterexamples to automatic covariance positivity, not asymptotic counterexamples to BT_σ or GRH.

40.6.4 Double Perron without a divergent critical-strip series

For $T_0=S\cup\operatorname{supp}(u)$ retain $F_0(s)=L^{T_0}(s,\psi)/L^{T_0}(2s,\psi_2)$, with the independently primitive square character. Set $t_p=q_p/(1+q_p)$ outside T_0. The finite actual cutoff is

$$J_U(s,u)=F_0(s)B_U(s),\qquad B_U(s)=\sum_{\substack{a,b\ \mathrm{sf},\ (a,b)=1\\ (ab,T_0)=1,\ Na,Nb\le U}}\mu(a)\mu(b)\prod_{p\mid ab}t_p.$$

For $\sigma=\Re s>1/2$, the series

$$\mathcal{G}(s,z,w)=\sum_{\substack{a,b\ \mathrm{sf},\ (a,b)=1\\ (ab,T_0)=1}}\mu(a)\mu(b)\prod_{p\mid ab}t_p\,(Na)^{-z}(Nb)^{-w}=\prod_{p\notin T_0}\left(1-t_p(Np)^{-z}-t_p(Np)^{-w}\right)$$

converges absolutely on $\sigma+\Re z>1$, $\sigma+\Re w>1$, uniformly in all vertical parts at fixed positive margins. This follows from $|t_p|\le (Np)^{-\sigma}/(1-(Np)^{-\sigma})$. There $\mathcal{F}=F_0\mathcal{G}$, without evaluating an infinite c series in the critical strip. Initial absolute convergence also proves (40.13) by the local identity

$$(1-q)(1+q-q\alpha-q\beta)=(1-q\alpha)(1-q\beta)-q^2(1-\alpha)(1-\beta).$$

The correction product is holomorphic on

$$\sigma+\Re z>0,\quad \sigma+\Re w>0,\quad 2\sigma+\min(\Re z,0)+\min(\Re w,0)>1.$$

On margins $\sigma+\Re z,\sigma+\Re w\ge\eta>0$ and last exponent $\ge 1+\epsilon$, its local deviation from 1 is at most $4(1-2^{-\eta})^{-2}(Np)^{-1-\epsilon}$. This proves normal convergence and a phase/deletion-uniform vertical upper bound. Nonvanishing of the correction is not asserted.

For $1/2<\sigma<1$, positive lines $c,d>1-\sigma$, and $V=\lfloor U\rfloor+1/2$, define

$$\mathcal{I}_{T_1,T_2}=\frac{1}{(2\pi i)^2}\int_{c-iT_1}^{c+iT_1}\int_{d-iT_2}^{d+iT_2}\mathcal{F}(s,z,w)\frac{V^{z+w}}{zw}\,dw\,dz.$$

The half-integer V includes the actual equality cutoff, since $Na\le U$ is exactly $Na<V$. Put $\Delta_V=\inf_{n\in\mathbb{Z}_{\ge1}}|\log(V/n)|\ge 1/(2V+1)$, and let $\mathcal{A}=\sum_{a,b}|\mu(a)\mu(b)\prod_{p\mid ab}t_p|(Na)^{-c}(Nb)^{-d}$ with the same disjoint support. For $c,T>0$ and $v>0$, $v\ne1$, define

$$K_{c,T}(v)=\frac{1}{2\pi i}\int_{c-iT}^{c+iT}\frac{v^z}{z}\,dz.$$

Finite-height termwise integration of the absolutely convergent $\mathcal{G}$ and the one-variable tail estimate $|K_{c,T}(v)-1_{v>1}|\le 2v^c/(\pi T|\log v|)$ give

$$|\mathcal{I}_{T_1,T_2}-J_U|\le|F_0|\mathcal{A}V^{c+d}\left\{\frac{2}{\pi T_1\Delta_V}+\frac{2}{\pi T_2\Delta_V}+\frac{4}{\pi^2T_1T_2\Delta_V^2}\right\}. \tag{40.14}$$

Thus $\mathcal{I}_{T_1,T_2}\to J_U$ as both heights tend independently to infinity, away from the original principal pole. This is an oscillatory limit, not an absolutely integrable infinite vertical integral.

Taking $T_1=T_2=V^2$ gives the safe upper bound $|J_U|\ll(Nu)^\eta|L(s,\psi)|V^{c+d}\log^2(2V)$, with constants retaining fixed margins, ν,S, and σ. Choosing c,d close to $1-\sigma$ reproduces $U^{2-2\sigma+\eta}$ in amplitude and $U^{2-4\delta+\eta}$ in energy on $\sigma=1/2+\delta$. Insertion into the original common-profile Mellin argument retains $M_4(W)^2$ and all previously required height/conductor uniformities. No derivative-free improvement follows from this Perron estimate.

The correction converges even on some negative auxiliary lines, but moving there can cross $z=\rho-s$ or $w=\rho-s$, from zeros of the primitive L-function. The exact meromorphic slice $\mathcal{F}(s,z,0)=1/L^{T_0}(s+z,\psi)$ forbids assuming universal cancellation of these poles. At a numerator zero the slice must be understood meromorphically, not by an unjustified pointwise substitution. Sequential shifts have single boundary integrals and crossed-zero residues as well as the kernel double residue; away from s zeros or poles that double residue is $1/L^{T_0}(s,\psi)$. A principal L pole supplies a reciprocal zero, not a reciprocal pole. Uniform control of actual reciprocal integrals/residues or the signed covariance remains a new input. Numerator AFM alone supplies neither.

40.7 A quantitative covariance budget without a new exponent

Retain the original Eisenstein sextic symbols, fixed finite-order ν, fixed S, one possibly complex common $W\in C_c^\infty$ supported in $[1,2]$, all squarefree columns prime to S, and every raw shared-prime

zero. In the accepted window $2D/7 \le U^2 \le D$, put $r_m = r_U(m)$, $\lambda_m = \mu(m)\nu(m)W(Nm/D)$ and $v_m = \overline{\lambda_m}$. Thus $C_U = \mu r$ and $A_U = \mu(r-1)$ on the active annulus. For a finite literal row block B, let

$$G_{mn} = \sum_{u\in B} x_m(u)\overline{x_n(u)}, \qquad R = \operatorname{diag}(r_m), \qquad M_j = \sum_m r_m^j |W(Nm/D)|^2 \quad (0 \le j \le 2).$$

The primitive $\psi_u, \psi_{u,2}$ and full deleted sets retain their previous meanings; no conductor-drop value replaces a raw zero.

Proposition 40.5 (An actual-vector lower budget)**.** *If $0 \le G \le \Lambda_B I$, then*

$$\Re Q_B(C_U, \mu) \ge -\frac{\Lambda_B}{2D}\{\sqrt{M_0 M_2} - M_1\}. \tag{40.15}$$

In this high window, uniformly in U,

$$\sum_{D\le Nm\le 2D} r_m \ll_K D, \qquad \sum_{D\le Nm\le 2D} r_m^2 \ll_K D\log(2D). \tag{40.16}$$

Consequently

$$\Re Q_B(C_U, \mu) \ge -C_K \|W\|_\infty^2 \Lambda_B \sqrt{\log(2D)}.$$

The vector inequality is sharp among positive contractions with the specified v, Rv; no such sharpness is asserted for the arithmetic Gram. The moment bound counts actual balanced ideal factorizations, rather than assuming independence of the two row factors.

On B_X, inserting the previously accepted powered-BGL norm gives only

$$\Re Q_{B_X}(C_U, \mu) \ge -C_{\nu,S,\epsilon}\|W\|_\infty^2 (DX)^\epsilon \{X^2 + DX + D^{2/3}X^{5/3}\}.$$

At $X \asymp D^{1/4}$ the exponents remain $1/2, 5/4, 13/12$. At $H = D^{3/4}$ this budget still has the old $D^{1/2}$ excess over H; it supplies no BT_σ saving. A negative-part budget is weaker than $2\Re Q(C_U, \mu) \ge Q(C_U, C_U) + Q(\mu, \mu) - R_\sigma$.

For $S_R = \sqrt{R}$, the exact identity

$$\tfrac{1}{2}(RG + GR) = S_R G S_R + \tfrac{1}{2}[S_R, [S_R, G]]$$

localizes the commutator to unequal factor-count levels, with entry $(\sqrt{r_m} - \sqrt{r_n})^2 G_{mn}$. If B retains all six literal units, the actual unit sum further gives $G_{mn} = 0$ unless $Nm \equiv Nn \pmod{36}$. These are exact deletions, not a power saving. Even zero different-level pairings leave the nonnegative within-level energies $\sum_k (k-1)^2 Q_B(\mu \mathbf{1}_{r=k}, \mu \mathbf{1}_{r=k})$. The unequal-product coupled fourth moment and its mixed Möbius term remain unestimated. No new analytic exponent, energy lower bound, Lean formalization or GRH conclusion follows.

40.8 Proof and arithmetic boundary of the covariance budget

40.8.1 The positive-contraction calculation

Since G is the exact raw Gram, it is positive semidefinite. If $\Lambda_B > 0$, put $T = 2G/\Lambda_B - I$, a self-adjoint contraction. Then

$$\Re(v^* R G v) = \frac{\Lambda_B}{2}\{M_1 + \Re(v^* R T v)\} \ge \frac{\Lambda_B}{2}\{M_1 - \|Rv\|_2 \|v\|_2\},$$

which is (40.15); $\Lambda_B = 0$ is immediate. The Hermitian rank-two matrix $\{(Rv)v^* + v(Rv)^*\}/2$ has possible nonzero eigenvalues $(M_1 \pm \sqrt{M_0 M_2})/2$. Its negative spectral projection realizes the lower bound among all $0 \le G \le \Lambda_B I$, a linear-algebra sharpness statement only. If $a \le r_m \le b$ on the weighted support, $a + b > 0$, the pointwise inequality $r_m^2 \le (a+b)r_m - ab$ also gives

$$\Re Q_B(C_U, \mu) \ge -\frac{\Lambda_B M_0 (b-a)^2}{8D(a+b)}.$$

For $a = b = 0$ the covariance is zero. The constant follows by maximizing $\sqrt{(a+b)t - ab} - t$ on $[a, b]$.

40.8.2 The balanced-divisor second moment

Set $T_0 = \sqrt{D}$. The high-window factor restrictions imply

$$\sqrt{2/7}\, T_0 < Na, Nb < \sqrt{14}\, T_0.$$

The elementary ideal count $\#\{a : Na \le Y\} \ll_K Y$ proves the first assertion of (40.16). For the second, two ordered factorizations $ab = cd = m$ have the unique form

$$a = gh, \quad c = gk, \quad b = k\ell, \quad d = h\ell, \qquad g = (a, c).$$

Squarefreeness makes g, h, k, ℓ pairwise coprime and squarefree. To upper-bound this positive count, enlarge to arbitrary ideals. For $M = \max(Nh, Nk)$ the individual bounds are

$$Ng \le \frac{\sqrt{14}\, T_0}{M}, \qquad N\ell \le \frac{\sqrt{14}\, T_0}{M}, \qquad 1 \le M \le \sqrt{14}\, T_0.$$

On $2^j \le M < 2^{j+1}$ there are $O_K(2^{2j})$ choices of (h, k) and $O_K((T_0/2^j)^2)$ choices of (g, ℓ), with bounded terminal ranges absorbed in the constant. Each dyadic range contributes $O_K(D)$; there are $O(\log(2D))$ ranges. This proves the second moment with no extra logarithm from counting only $NgN\ell$. Restricting to primes outside fixed S decreases the count. Hence

$$M_0, M_1 \ll_K \|W\|_\infty^2 D, \qquad M_2 \ll_K \|W\|_\infty^2 D \log(2D).$$

These constants are independent of the cutoff in the stated window. Only the common supremum norm is used, including for complex W.

40.8.3 What the commutator actually controls

Write

$$t_{mn} = D^{-1}\Re\{\lambda_m \overline{\lambda_n} G_{mn}\}, \qquad \delta_{mn} = (\sqrt{r_m} - \sqrt{r_n})^2.$$

The exact commutator identity proves

$$\Re Q_B(C_U, \mu) \ge Q_B(\sqrt{r}\,\mu, \sqrt{r}\,\mu) - \tfrac{1}{2}\sum_{m,n} \delta_{mn}|t_{mn}|.$$

The displayed loss retains the actual character and profile phases before taking absolute values; it is at most the phase-blind loss obtained from $|t_{mn}| \le D^{-1}|\lambda_m \lambda_n G_{mn}|$. On the accepted four-column smooth B_7 fixture at amplitude $x \ge 0$, the positive term is $18/25$, this coefficient-adapted loss is $9x/50$, and the lower bound is attained. Purely imaginary entries of the full complex Gram make the phase-blind loss larger. This calibrates the new budget and does not give an asymptotic obstruction.

For the unit deletion let $\zeta_6 = 1+\omega$. Every good prime norm q is $1 \pmod 6$, and direct residue-field exponentiation gives $x_p(\zeta_6) = \zeta_6^{(q-1)/6}$. Multiplying over $p \mid m$ and reducing $Nm = \prod_{p|m}(1+6e_p)$ modulo 36 gives

$$x_m(\zeta_6) = \zeta_6^{(Nm-1)/6 \bmod 6}.$$

Multiplication of all literal rows by ζ_6 preserves their raw zeros and proves the norm-congruence deletion in the core. The vector budget may be applied separately on these six classes. No D-dependent number of classes or conductor saving is produced.

The moment proof above counts the coefficient diagonal $ab = cd$. It has not estimated the unequal-product character quadruples in the coupled row fourth moment. Replacing the inherited DX norm by $D^{1-\sigma}X$ merely because equal-level and different-class entries vanish is the unsupported step. Small negative commutator loss alone also leaves the within-level energies in the core. Principal residues are unchanged; this covariance is used on the nonprincipal blocks where the original residue is zero, not as a new centering prescription.

40.8.4 The complete near-saturating face

For a six-factor row block let $R_0 = \prod_{j=1}^{6} A_j$, $M = \max(A_1, A_2)$ and $\prod_j A_j^j \le H$. The accepted exact-mask block norm is

$$\Lambda_A \ll_{\nu,S,\epsilon} (HD)^{\epsilon}\{R_0 + DR_0/M + D^{2/3}R_0/M^{1/3}\}.$$

The column moment and covariance proofs apply to every such block. Write $x_j = \log A_j$, $h = \log H$, $c_0 = \sum_j jx_j$ and $r_0 = \sum_j x_j$. Then, for $x_1 \ge x_2$,

$$h - 3(r_0 - \max(x_1, x_2)) = h - c_0 + (x_1 - x_2) + x_4 + 2x_5 + 3x_6;$$

for $x_2 \ge x_1$ replace $x_1 - x_2$ by $2(x_2 - x_1)$. All terms are nonnegative. Thus the middle monomial is saturated on

$$A_1 = A_2, \qquad A_1A_3 = H^{1/3}, \qquad A_4 = A_5 = A_6 = 1,$$

with full capacity. The balanced $A_3 = 1$ case is only an endpoint. The a_3 direction remains nonprincipal by its outside-S valuation $3 \pmod 6$. If $R_0/M \ge H^{1/3}D^{-\eta}$, the total displayed slack is at most $3\eta \log D$. Therefore a fixed power gain must be uniform on this full neighboring region. The proved budget still costs DR_0/M; it gives no global improvement over the accepted envelope.

The independent standard-library diagnostic checks nine ideal moment cases, eight raw Gram cases with 27 000 phase values and 5 184 raw zeros, exact radical commutator/vector budgets, and 227 exponent cases. Finite tables use common norm profiles realizable by smooth disjoint bumps; they are not tests of an infinite analytic estimate. Full derivation, source bindings and preserved checks are under `planning/covariance-budget-20261105/attempt/` and `outputs/checks/2026-11-05-covariance-budget/attempt/`.

40.9 The fourth-moment conductor and its full raw zero set

Retain the original Eisenstein sextic symbols $x_m(u) = (u/m)_6$, fixed finite-order ν, fixed S, and one possibly complex common smooth W supported in $[1,2]$. Put $\lambda_m = \mu(m)\nu(m)W(Nm/D)$ and $r_m = r_U(m)$. Columns remain squarefree and prime to S. In $2D/7 \le U^2 \le D$, the actual polynomial is

$$\mathcal{C}_U(u) = \sum_{\substack{(a,b)=1,\ Na,Nb>U \\ D \le Na\,Nb \le 2D}} \mu(a)\mu(b)\nu(ab)W(Nab/D)x_a(u)x_b(u).$$

Its squared row energy has four factor indices a, b, c, d, with $(a, b) = (c, d) = 1$. These internal masks are essential. At each prime,

$$e_p = \mathbf{1}_{p|a} + \mathbf{1}_{p|b} - \mathbf{1}_{p|c} - \mathbf{1}_{p|d} \quad \text{belongs to } \{0, \pm 1\}.$$

Thus, for the two squarefree products $m = ab, n = cd$, the primitive oscillatory conductor outside fixed S is $q = mn/(m, n)^2$. The full raw zero-preserving period is $L = mn/(m, n)$:

$$x_m(u)\overline{x_n(u)} = \mathbf{1}_{(u,(m,n))=1}\theta_{m/(m,n),\, n/(m,n)}(u).$$

No common-prime zero is restored by taking the primitive character.

A generic fourth moment $|\sum_m \lambda_m x_m(u)|^4$ has four individually squarefree columns $m_1, \ldots, m_4$ with no such internal coprimality. Its signed local exponent $e_p = \sum_{i=1}^{2} \mathbf{1}_{p|m_i} - \sum_{i=3}^{4} \mathbf{1}_{p|m_i}$ can also be ± 2, giving a nontrivial cubic component. For $L = \mathrm{rad}(m_1 m_2 m_3 m_4)$, the exact row-power interface is

$$Q_j = \prod_{\substack{p|L \\ je_p \not\equiv 0 \ (6)}} p, \qquad Z_j = L/Q_j, \qquad \prod_{i=1}^{2} x_{m_i}(v^j)\overline{\prod_{i=3}^{4} x_{m_i}(v^j)} = \theta_{j,e}(v)\mathbf{1}_{(v,Z_j)=1}.$$

Here $\theta_{j,e}$ is primitive on Q_j, with its own zero extension. At $j = 3$ an exponent ± 2 becomes primitive-principal but its raw zero remains. For the original two-squarefree-product expansion, $Q_j = q$ for all $1 \le j \le 5$, including the quadratic $j = 3$ direction. For the accepted row blocks $Nr_j \asymp A_j$, put $R_0 = \prod_j A_j$, $P = \max(A_1, \ldots, A_5)$ and retain $\prod_j A_j^j \le H$. The full A_3 saturation face and all row-factor masks remain.

The small-conductor pair count recovers an already controlled high-gcd sector; it is not a new analytic advance. On the remaining original sector $Nq > P^2$, favorable smooth completion costs $\min(A_j, \sqrt{Nq}) = A_j$ for $1 \le j \le 5$. The literal sharp cutoff is not replaced by this smooth trial. The signed large-conductor fourth-moment and mixed Möbius sums remain open; no improved full exponent, BT_σ, new Lean theorem, zero-location result or GRH conclusion follows.

40.10 Scope of the raw fourth-moment reduction

Write $c_{a,b} = \mu(a)\mu(b)\nu(ab)W(Nab/D)$ on the exact factor support in the core. Before absolute Cauchy, the normalized energy is

$$\frac{1}{D} \sum_{(a,b),(c,d) \text{ on that support}} c_{a,b}\overline{c_{c,d}} \sum_{u \in B} x_a(u)x_b(u)\overline{x_c(u)x_d(u)}.$$

Squarefreeness of ab and cd forces each positive and negative prime multiplicity to be at most one, proving $e_p \in \{0, \pm 1\}$. For the mixed term against the actual μ polynomial the exponent is $\mathbf{1}_{p|a} + \mathbf{1}_{p|b} - \mathbf{1}_{p|n}$, with the same conclusion and the same full union mask. The common possibly complex W, ν, hyperbolic support and all raw zeros stay in these identities.

In contrast, unrestricted four-column memberships $(1, 1, 0, 0)$ give $e_p = 2$, a cubic component; $(1, 1, 1, 0)$ give $e_p = 1$ although both product supports contain p. Neither the parity symmetric difference of four supports nor the symmetric difference of two nonsquarefree product supports gives the general conductor. For the interface in the core, its local character order is

j	$1, 5$	$2, 4$	3	6
$e_p = \pm 1$	6	3	2	1
$e_p = \pm 2$	3	3	1	1

Nontrivial entries have tame conductor exponent one; trivial entries remain deleted at $p \mid v$. Multiplying the interface over all six row factors, with the fixed unit/S phase, preserves every original zero, including those at sixth-power factors. All inter-factor, squarefree, ray and capacity restrictions remain external restrictions on the same row sum; this identity asserts no independence.

At a residue field of size Q, let χ have order six and ρ be nontrivial additive. The zero-extended complete sum $G_k(t) = \sum_{z \neq 0} \chi(z)^k \rho(tz)$ satisfies

	$t = 0$	$t \neq 0$
$k \not\equiv 0$ (6)	0	$\lvert G_k(t)\rvert = \sqrt{Q}$
$k \equiv 0$ (6)	$Q - 1$	-1.

For $t \neq 0$, substitution gives $G_k(t) = \overline{\chi(t)^k} G_k(1)$; for nontrivial k, expanding the norm square gives $(Q-1) - \sum_{a \neq 0,1} \chi(a)^k = Q$. The proof applies at split and inert primes. By CRT the full period-L transform vanishes if any local frequency on Q_j is zero; otherwise its magnitude is

$$(NQ_j)^{1/2} \prod_{p \mid Z_j} \left| -1 + Np\, \mathbf{1}_{\text{local frequency at } p \text{ is } 0} \right|.$$

Canceled common primes thus supply Ramanujan factors.

Exact deletion, with all remaining restrictions kept in F, gives

$$\sum_r \theta(r) F(r) \mathbf{1}_{(r,Z)=1} = \sum_{d \mid Z} \mu(d) \theta(d) \sum_z \theta(z) F(dz).$$

For a squarefree pivot let E be the radical of its fixed excluded primes, including Z and the relevant other row factors, with conductor primes omitted since θ already vanishes there. The additional squarefree identity is

$$\mu(r)^2 \mathbf{1}_{(r,E)=1} = \sum_{\substack{h^2 \mid r \\ (h,E)=1}} \mu(h) \sum_{\substack{d \mid E \\ d \mid r}} \mu(d).$$

Since $(d,h) = 1$, its lifted row sum has terms $\mu(d)\mu(h)\theta(d)\theta(h)^2 \sum_z \theta(z) F(dh^2 z)$. The scaled F retains the exact window, primary/ray restrictions and other masks. Divisor triangles cost at most $(HD)^\epsilon$; they do not restore a forbidden nonzero.

The previous fixed-radial-profile high-gcd proof (`research/short-row-high-gcd.md`, independently reviewed in `planning/reviews/book/short-row-formal.md`) already bounds its off-diagonal tail by $O_{\Phi,\epsilon}(D^{2+\epsilon}/G_0^2)$ for $Nh \geq G_0$. For annular $m = hr, n = ht$, $Nq \leq Y$ implies $Nh \geq D/\sqrt{Y}$, so the old smooth-scope bound is $O_{\Phi,\epsilon}(D^\epsilon Y)$. The present elementary count $O(D\sqrt{Y})$, factor multiplicities $r_U(m) r_U(n) \ll_\epsilon D^\epsilon$, and $\#B_A = O(R_0)$ give only $O(\|W\|_\infty^2 D^\epsilon R_0 \sqrt{Y})$ on a literal sharp block. This is a weaker conductor-form recovery in its own bookkeeping scope, not a new high-gcd theorem; the smooth estimate is not silently transferred to a selected sharp off-diagonal piece. The full A_3 face and neighborhood slack are also inherited.

Finally, primitive smooth Poisson completion has bound $O_V(\min(A_j, \sqrt{Nq}))$ on the original support. For $Nq > P^2$ and $1 \leq j \leq 5$, every scaled length $A_j/(Nd\,Nh^2)$ is below $\sqrt{Nq}$, so even this favorable trial takes its trivial length term. Its constant uses fixed smooth seminorms and need not stay bounded when a sharp boundary is approached. In the admissible subsector $(m,n) = 1$, $Nq = Nm\,Nn \asymp D^2$. A complete zero mean does not control the nonzero frequencies of the short original masked row window. The unresolved target is their joint signed sum with weights $r_U(m) r_U(n) \lambda_m \overline{\lambda_n}$ and $r_U(m) \lambda_m \overline{\lambda_n}$, before per-conductor absolute estimates. No new global analytic conclusion is claimed.

40.11 A quadratic pivot on the cube factor

Retain the original zero-extended sextic symbols $\chi_m(u) = (u/m)_6$ over $K = \mathbb{Q}(\omega)$, the fixed S containing all primes above 6 and comparison moduli, and the squarefree good columns $D \le Nm \le 2D$. Write an outside-S row ideal uniquely as $r_1 r_2^2 r_3^3 r_4^4 r_5^5 r_6^6$: only $r_1, \dots, r_5$ are pairwise-coprime squarefree ideals; r_6 is arbitrary and may overlap them. Use primary generators. Fix one literal unit and one S-supported row factor, retaining their original values. Let $A_j \le Nr_j < 2A_j$, $A_j \ge 1$, $R_0 = \prod_j A_j$ and $\prod_j A_j^j \le H$; the actual capacity restriction on rows is retained. Coefficients $b_m \in \mathbb{C}$ are arbitrary and fixed independently of every variable row.

Proposition 40.6 (The cube-factor block norm)**.** *For every $\varepsilon > 0$, the raw Gram on this actual block obeys*

$$\sum_{u \text{ in the block}} \left| \sum_m b_m \chi_m(u) \right|^2 \ll_{\nu,S,\varepsilon} (HD)^{\varepsilon} \left\{ R_0 + \frac{DR_0}{A_3} \right\} \sum_m |b_m|^2.$$

The constant is uniform in the fixed unit/S-factor, frozen good factors, H, D and the coefficient sequence. There is no rational-norm-squarefree restriction. Consequently, with $M = \max(A_1, A_2)$, the old powered-BGL bound and this bound give

$$\Lambda_A \ll_{\nu,S,\varepsilon} (HD)^{\varepsilon} \left\{ R_0 + \min\left(\frac{DR_0}{M} + \frac{D^{2/3} R_0}{M^{1/3}}, \frac{DR_0}{A_3} \right) \right\}. \tag{40.17}$$

The external analytic input is Goldmakher–Louvel, arXiv:1112.1642v2, Corollary 1.2 with $n = 6$, already an explicit classical cube-power sieve. The refinement is this application, not a new large-sieve theorem. For the original normalized coefficients $b_m = D^{-1/2} A_U(m) \nu(m) W(Nm/D)$, the accepted divisor bound gives $\sum_m |b_m|^2 \ll_\eta \|W\|_\infty^2 D^\eta$, uniformly in $U \ge 1$ with $U^2 \le D$ (and the common W may be complex). Choosing smaller internal exponents yields the corresponding uniform block energy envelope. General cutoff or factor-count weights remain inside the arbitrary coefficient norm; that norm is not silently replaced by one. Summing S-supported row factors uses the reduced capacity $H/N\mathfrak{b}$ and the established convergent geometric sums.

On the complete old saturated face $A_1 = A_2 = A$, $A_3 = B$, $A_4 = A_5 = A_6 = 1$, $AB = H^{1/3}$, the new bound is $A^2 B + DA^2$ in place of the old middle monomial DAB. For $H = D^{3/4}$ put $A = D^a$, $B = D^{1/4-a}$, $0 \le a \le 1/4$. When $a < 1/8$, its leading exponent is $1 + 2a < 5/4$; the gain requires B/A to grow by a power for a power improvement. For $a \ge 1/8$, the combined bound still has leading exponent $5/4$. Thus the A_3-dominant part improves, while no new global exponent, BT_σ estimate, signed covariance theorem, Lean theorem or GRH conclusion follows.

Inspecting the surviving sector. The quadratic-pivot inspector plots the complete face, the five monomial powers and the remaining target gap. These are analytic bound exponents, not measured operator norms or trained-network predictions. The refined norm can be inserted in the earlier covariance budget; it does not remove its within-level energies.

A necessary near-face condition. Put $\mathcal{M}_A = DR_0 / \max(M, A_3)$. The combined envelope is at most $(HD)^{\varepsilon}\{R_0 + \mathcal{M}_A + D^{2/3} R_0 / M^{1/3}\}$. If $\mathcal{M}_A \ge DH^{1/3} D^{-\eta}$, then the earlier near-face slack is at most $3\eta \log D$ and, additionally, $A_3 \le MD^\eta$. Thus a uniform remaining leading-term estimate may focus on this smaller neighborhood; it must still cover the entire $B \le A$ part of the face. This is a necessary condition on explicit upper-bound monomials, not a lower bound for actual arithmetic energy.

40.12 Proof and scope of the quadratic pivot

Freeze all factors except r_3, and write the actual literal row $u = Fr_3^3$. Multiplicativity of the original numerator gives the exact zero-preserving identity

$$\chi_m(u) = \chi_m(F)\chi_m(r_3)^3.$$

Put $c_m = b_m\chi_m(F)$, a coefficient sequence independent of r_3 with $\sum |c_m|^2 \le \sum |b_m|^2$. In particular the arbitrary sixth-power factor is the coefficient mask

$$\chi_m(r_6^6) = \mathbf{1}_{(m,r_6)=1},$$

not the constant one. No condition $(r_3, r_6) = 1$ is introduced. The actual capacity and coprimality of r_3 with r_1, r_2, r_4, r_5 only restrict this positive outer row sum; after freezing, it may be enlarged to all squarefree good pivot ideals in the dyad. The variable collision mask (m, r_3) remains in the original symbol.

Apply the previously proved literal comparison (40.9) to the primary generator of r_3 itself:

$$\chi_m(r_3)^3 = \eta_{r_3}(m)^3 C([r_3], [m])^3 \vartheta_m(r_3)^3.$$

The twist η_{r_3} ranges over a fixed finite set of S-unit Kummer characters, and $[r_3]$ over the fixed finite reciprocity group. Partition pivot rows by $(\eta_{r_3}, [r_3])$. On each part the first two factors are one fixed modulus-one column multiplier. Thus its coefficient sequence is independent of the pivot row and has squared norm at most $\sum |b_m|^2$. This finite partition, rather than an assertion that arbitrary row-dependent phases may be absorbed, resolves the fixed-S phase issue.

Goldmakher–Louvel Definition 1 and Remark 3 identify the cubic powers of a sixth-order Hecke family as a quadratic Hecke family; their Corollary 1.2 gives directly

$$\sum_{\substack{a \text{ sf,good} \\ Na \le 2A_3}} \left| \sum_{\substack{m \text{ sf,good} \\ Nm \le 2D}} z_m \vartheta_m(a)^3 \right|^2 \ll_{K,S,\eta} (A_3 D)^\eta (A_3 + D) \sum_m |z_m|^2.$$

This is the required column-indexed orientation and allows arbitrary complex coefficients and squarefree ideals of nonsquarefree rational norm. The canonical family has primitive trivial-infinity-type characters, a fixed finite reciprocity group, and the same-class primitive-product property required by Definition 1. At each $p \mid m$ outside S, the local tame sextic character has order six, so its cube has order two and conductor exponent one. Thus its outside-S primitive conductor is exactly m; the S-part has only finitely many fixed conductor types. Accordingly both sides of the comparison are zero at $(m, a) > 1$. No conductor-drop value replaces the raw zero, and no global formula for the full conductor is required. The fixed ν stays in coefficients.

Enlarge the positive row sum separately on each finite part and apply this sieve. Ideal counting gives $O_K(A_j)$ possibilities for each frozen r_j, including arbitrary r_6, hence $O_K(R_0/A_3)$ frozen tuples. Summing gives $(A_3D)^\eta(R_0 + DR_0/A_3)\sum |b_m|^2$. Since $A_3 \le H$, adjust η to obtain Proposition 40.6; literal unit multiplicity is at most six. Together with the prior block bound this proves (40.17). It does not change the actual coefficient normalization or principal residues.

On the face in the core, the old bound has exponents $a + 1/4$, $5/4$, $11/12 + 2a/3$, whereas the quadratic bound has $a + 1/4$ and $1 + 2a$. Its improvement for $a < 1/8$ leaves the balanced point and $a \ge 1/8$ with the old $5/4$ leading exponent. Even the improved endpoint $a = 0$ costs D, above the target $D^{3/4}$. The pinned GL PDF has SHA256 `5cc5f03388d3996b4333f07be51f989f`

`60779fe172f8bd24c7aa6ddad64dd304`. This proof invokes that classical result; finite exponent checks do not reprove it, and no new formalization is claimed.

For the last condition, use $R_0/M \le H^{1/3}$ from the exact capacity inequalities. The hypothesis implies $R_0/A_3 \ge H^{1/3}D^{-\eta}$, so $A_3/M = (R_0/M)/(R_0/A_3) \le D^{\eta}$. It also implies $R_0/M \ge H^{1/3}D^{-\eta}$, which is exactly the previous slack hypothesis. Finally $\min(a+b,c) \le \min(a,c)+b$ for nonnegative a,b,c proves the separated envelope, with no replacement of a signed moment by a positive lower bound.

40.13 Joint completion before conductor absolute values

In the original C–C expansion write $m = hr, n = ht$ with h,r,t pairwise coprime squarefree, $q = rt \ne 1$, $L = hq$, $Q = Nq$, $\ell = NL$. Set $\theta = x_r\overline{x_t}$ and $\xi_q = x_q^3$. The original internal masks give $\theta^3 = \xi_q$ and primitive θ^j on q for $1 \le j \le 5$, while $\mu(hr)\mu(ht) = \mu(q)$. Fix generators α of h, β of q, choosing $\alpha = 1$ for $h = 1$. With $\delta = 1 + 2\omega$, put $e_\beta(z) = \exp(2\pi i \operatorname{Tr}(z/(\delta\beta)))$, $\tau_\beta(\eta) = \sum_{z \bmod q} \eta(z)e_\beta(z)$, and $c_h(k) = \prod_{p\mid h}(Np\mathbf{1}_{k\in p} - 1)$, $c_1 = 1$. For $f_j(v) = \theta(v)^j\mathbf{1}_{(v,h)=1}$, $1 \le j \le 5$, $f_6(v) = \mathbf{1}_{(v,L)=1}$ and $G_j(k) = \sum_{v \bmod L} f_j(v)e_{\alpha\beta}(kv)$, joint completion gives

$$\prod_{j=1}^{6} G_j(k_j) = Q^2\xi_q(-\alpha)\tau_\beta(\xi_q)\theta\Big(\overline{\prod_{j=1}^{5} k_j^j}\Big)\prod_{j=1}^{5} c_h(k_j)c_L(k_6). \tag{40.18}$$

This holds when the first five frequencies are q-units; otherwise the left side is zero. The mixed Gauss phase is orientation-independent, with every common-prime zero retained. The exact row Fourier weight still contains all squarefree, ray, inter-factor, capacity and profile restrictions, including the full A_3 face. Its weighted joint conductor/frequency estimate remains open. This identity and its finite Parseval budget give no improved global exponent or GRH conclusion.

40.14 The surviving joint identity and its missing estimate

CRT gives $G_j(k) = \theta(\alpha)^j\tau_\beta(\theta^j)\overline{\theta(k)^j}c_h(k)$ for q-unit k, and $G_6 = c_L$. Pairing Gauss powers $1,5$ and $2,4$ yields $\prod_{j=1}^5 \tau_\beta(\theta^j) = Q^2\xi_q(-1)\tau_\beta(\xi_q)$; the CRT factors multiply to $\theta(\alpha)^{15} = \xi_q(\alpha)$. This proves (40.18), with all additive-generator phases explicit.

On a fixed literal class write $u = u_0\prod_{j=1}^6 v_j^j$ and let $F(v)$ be its exact finite row weight. Only $v_1,\dots,v_5$ are squarefree and pairwise coprime; v_6 is arbitrary with its permitted overlaps. Retain every original mask and the sharp capacity boundary in F. Define $\widehat{F}_L(k) = \sum_v F(v)e_{\alpha\beta}(-\sum_j k_jv_j)$ and, with $t = q/r$, put

$$\begin{aligned} a(r) &= r_U(hr)r_U(ht)\nu(r)\overline{\nu(t)} \\ &\qquad \times W(Nh\,Nr/D)\overline{W(Nh\,Nt/D)}\theta_{r,t}(u_0), \\ A(K) &= \sum_{r\mid q} a(r)\overline{\theta_{r,q/r}(K)}, \\ B(K) &= \sum_{\substack{k \bmod L,\ (k_1\cdots k_5,q)=1 \\ \prod_{j=1}^5 k_j^j = K \bmod q}} \widehat{F}_L(k)\prod_{j=1}^{5} c_h(k_j)c_L(k_6). \end{aligned}$$

Set $a(r) = 0$ at excluded orientations; the actual factor counts and common possibly complex W

remain. Fourier inversion gives exactly

$$E_{\mathcal{T}} = \frac{1}{D} \sum_{(h,q)\in\mathcal{T}} \mu(q) \frac{Q^2 \xi_q(-\alpha)\tau_\beta(\xi_q)}{\ell^6} \sum_{K\in(\mathcal{O}/q)^\times} B(K)A(K). \tag{40.19}$$

Sum the original u_0 classes and blocks. This retains low gcd, including $h = 1$, before conductor absolute values. For C–μ replace the second $r_U(ht)$ by 1. A column-orientation-dependent restriction cannot be hidden in a common F when applying the next identity.

Distinct orientations have nontrivial cubic quotient, so

$$\sum_K |A(K)|^2 = \varphi(q) \sum_{r|q} |a(r)|^2, \qquad |E_{h,q}| \le \frac{Q^{5/2}}{D\ell^6} \left(\varphi(q) \sum_{r|q} |a(r)|^2 \right)^{1/2} \|B\|_2.$$

The product-frequency fibers have size $\varphi(q)^4$ under uniform averaging. The actual B is not uniform: all orientations agree on the coherent set $x_p(K)^2 = 1$ for every $p \mid q$, of size $\varphi(q)/3^{\omega(q)}$. Centered representatives have $|k_j| \le \sqrt{\ell}$. Restricting to any frequency subset Ω has error bounded by the same displayed budget with $\|B - B_\Omega\|_2$; no small lower-height tail is proved.

The full face $A_1 = A_2 = A$, $AA_3 = H^{1/3}$, $A_4 = A_5 = A_6 = 1$ remains. At its pure A_3 endpoint, inversion in the fixed factors leaves $(\sum_r a(r)) \sum_v F_3(v)\xi_q(v)\mathbf{1}_{(v,h)=1}$: the actual row character there is orientation-independent. Literal length-one Fourier factors can undo complete phase balance. A quantitative signed estimate for the actual h, q, K sum is still required. Exact split/inert Gauss, full-mask CRT and orientation tests pass 991 assertions; receipt: `outputs/checks/2026-11-05-joint-dual/research/joint-gauss-check-v1.json`. These diagnostics do not prove an incomplete-moment saving or GRH.

40.15 A radical-conductor refinement of the raw envelope

Retain the original literal symbols $\chi_m(u) = (u/m)_6$, extended by zero, the fixed good set S, and the squarefree ideal columns $D \le Nm \le 2D$. On an actual dyadic row block write

$$u = u_0 r_1 r_2^2 r_3^3 r_4^4 r_5^5 r_6^6, \qquad A_j \le N r_j < 2A_j, \qquad \prod_{j=1}^{6} A_j^j \le H.$$

Only $r_1, \dots, r_5$ are pairwise-coprime squarefree ideals; r_6 is arbitrary and may overlap them. Fix primary generators, a literal unit and an S-supported factor in u_0. Put $R = \prod_j A_j$, $M = \max(A_1, A_2)$ and $Q = R/A_6$. For arbitrary complex coefficients b_m, independent of every variable row, define

$$\mathcal{E}_A(b) = \sum_{u \text{ in the actual block}} \left| \sum_m b_m \chi_m(u) \right|^2, \qquad \Lambda_A = \sup_{b\ne 0} \frac{\mathcal{E}_A(b)}{\sum_m |b_m|^2}.$$

Proposition 40.7 (An ordinary conductor comparison)**.** *For every $\varepsilon > 0$,*

$$\Lambda_A \ll_{S,\varepsilon} (HD)^\varepsilon A_6 \{D + Q^2\}. \tag{40.20}$$

Consequently the original residue-subtracted remainder satisfies, uniformly for $H, D, U \ge 1$ and $U^2 \le D$,

$$\sum_{0<Nu\le H} |E_u|^2 \ll_{\nu,S,\varepsilon} \|W\|_\infty^2 (HD)^\varepsilon \{H + DH^{1/6} + (DH)^{2/3}\}. \tag{40.21}$$

Here ν, S are fixed and $W \in C_c^\infty((0,\infty))$ is one common, possibly complex profile supported in $[1,2]$; there is no profile supremum.

The input to (40.20) is the classical ordinary sieve for *all* primitive characters of conductor norm at most Q, with constant $D+Q^2$, not a higher-order-family theorem for arbitrary conductor labels. The following section gives its standard Gauss-sum and two-dimensional lattice proof, including prime-power conductors at S. For fixed r_6, the first five factors have primitive outside-S conductor $q = r_1 \cdots r_5$. The literal primitive character agrees with the raw symbol even at collisions with q; the sixth-power factor instead remains the coefficient mask $\mathbf{1}_{(m,r_6)=1}$. At most $5^{\omega(q)} \ll_\eta (Nq)^\eta$ tuples give the same primitive character. Applying the ordinary sieve and then counting r_6 proves (40.20). No rational-norm-squarefree restriction is imposed.

To obtain (40.21), combine this with the accepted powered-BGL block bound from Section 40.3. With $S_A = R/M$ and $T_A = D^{2/3}R/M^{1/3}$, capacity gives $R \le H$, $A_6 \le H^{1/6}$, $RS_A \le H$ and $T_A \le (DH)^{2/3}$. Hence

$$\begin{aligned}\min(R + DS_A + T_A, DA_6 + R^2/A_6) &\le R + T_A + DA_6 + \min(DS_A, H^2/S_A^2)\\ &\le H + DH^{1/6} + 2(DH)^{2/3}.\end{aligned}$$

Dyadic and fixed-S summation, the uniform actual coefficient norm, and the principal-residue estimate give the assertion for $E_u = I_u - P_u$.

At $H = D^{3/4}$ the new envelope has exponent $7/6$, improving the old $5/4$ by $1/12$; its excess above the target H is still $D^{5/12}$. On the *entire* old face $A_1 = A_2 = A$, $A_3 = B$, $A_4 = A_5 = A_6 = 1$, $AB = H^{1/3}$, one has $Q = A^2B = AH^{1/3} \le H^{2/3}$, so (40.20) costs $D^{1+\varepsilon}$ there. This includes $B \le A$. The new combined upper bounds reach $7/6$ at $(\log_D A_1, \log_D A_2) = (5/12, 1/6)$ with other coordinates zero; the pure point $\log_D A_1 = 3/4$ also retains the old BGL cross term. These are upper-envelope witnesses, not arithmetic energy lower bounds or counterexamples to signed cancellation.

The simpler proposed replacement of the radicand ab^2 by its radical ab inside BGL remains unjustified: after the existing fixed reciprocity phases, the mixed reciprocity quotient is $\vartheta_b(a')/\vartheta_a(b')$, which varies outside S. The present application does not require that replacement. No target signed moment, type-II covariance estimate, positive arithmetic determinant comparison, zero-location result, new Lean theorem or GRH conclusion follows from (40.21).

40.16 Proof of the ordinary-conductor refinement

40.16.1 Primitive Gauss sums at every conductor

Let $\mathcal{O} = \mathbb{Z}[\omega]$, $\delta = 1 + 2\omega$, and choose one generator f of each nonzero ideal $\mathfrak{f}$. Write $e_f(x) = \exp(2\pi i \operatorname{Tr}(x/(\delta f)))$, $U(\mathfrak{f}) = (\mathcal{O}/\mathfrak{f})^\times$, and $\varphi(\mathfrak{f}) = |U(\mathfrak{f})|$. This additive character is primitive, since the different is (δ). For a primitive multiplicative character ρ modulo $\mathfrak{f}$, extended by zero at nonunits, set $\tau_f(\rho) = \sum_{x \bmod \mathfrak{f}} \rho(x) e_f(x)$. We verify the full-modulus identity

$$|\tau_f(\rho)|^2 = N\mathfrak{f}, \qquad \sum_{x \bmod \mathfrak{f}} \rho(x) e_f(zx) = \overline{\rho(z)}\tau_f(\rho) \quad (z \in \mathcal{O}). \tag{40.22}$$

No squarefree-conductor hypothesis is used, so this includes wild prime powers in the fixed S-part.

The Ramanujan sum is

$$c_{\mathfrak{f}}(y) = \sum_{x \in U(\mathfrak{f})} e_f(xy) = \sum_{\mathfrak{d} \mid (\mathfrak{f}, (y))} N\mathfrak{d}\, \mu(\mathfrak{f}/\mathfrak{d}).$$

Indeed insert $\mathbf{1}_{(x,\mathfrak{f})=1} = \sum_{\mathfrak{b}\mid(x,\mathfrak{f})} \mu(\mathfrak{b})$; the complete additive sum with $\mathfrak{b} \mid x$ is $N(\mathfrak{f}/\mathfrak{b})$ when $\mathfrak{f}/\mathfrak{b} \mid (y)$ and zero otherwise. Changing variables $x = ay$ in the Gauss square now gives

$$\begin{aligned}|\tau_f(\rho)|^2 &= \sum_{a\in U(\mathfrak{f})} \rho(a) c_{\mathfrak{f}}(a-1) \\ &= \sum_{\mathfrak{d}\mid\mathfrak{f}} N\mathfrak{d}\,\mu(\mathfrak{f}/\mathfrak{d}) \sum_{\substack{a\in U(\mathfrak{f}) \\ a\equiv 1 \pmod{\mathfrak{d}}}} \rho(a) = N\mathfrak{f}.\end{aligned}$$

For every proper $\mathfrak{d} \mid \mathfrak{f}$, the reduction $U(\mathfrak{f}) \to U(\mathfrak{d})$ is surjective by local lifting and CRT. Primitivity says ρ is nontrivial on its kernel, so that inner sum vanishes. For $\mathfrak{d} = \mathfrak{f}$ it equals one. For unit z, substitution proves the second identity in (40.22). For all frequencies together, finite additive Parseval gives

$$\sum_{z \bmod \mathfrak{f}} \left| \sum_x \rho(x) e_f(zx) \right|^2 = N\mathfrak{f}\,\varphi(\mathfrak{f}).$$

The unit frequencies already exhaust this quantity by the first identity; every nonunit-frequency sum is therefore zero. This proves the asserted zero extension. For $\mathfrak{f} = \mathcal{O}$ there is one residue class and one character; take $\tau_1 = 1$ and the single frequency zero.

40.16.2 The classical ordinary sieve in these lattice conventions

For $D, Q \geq 1$, coefficients z_α supported on any subset of $\{\alpha \in \mathcal{O} : |\alpha|^2 \leq C_0 D\}$ satisfy

$$\sum_{N\mathfrak{f}\leq Q} \sum_{\rho \text{ primitive mod } \mathfrak{f}} \left| \sum_\alpha z_\alpha \rho(\alpha) \right|^2 \ll_{\mathcal{O},C_0} (D + Q^2) \sum_\alpha |z_\alpha|^2. \tag{40.23}$$

Here the primitive characters may be restricted to the unit-trivial subfamily. We give the standard proof to make the conductor comparison explicit.

First the reduced fractions x/f, with $x \in U(\mathfrak{f})$ and $N\mathfrak{f} \leq Q$, are distinct modulo $\mathcal{O}$. Their denominator ideal is intrinsic: $\{a \in \mathcal{O} : a(x/f) \in \mathcal{O}\} = \mathfrak{f}$. Thus equality modulo $\mathcal{O}$ forces the same denominator ideal and residue numerator. For different fractions and every $k \in \mathcal{O}$,

$$\left| \frac{x}{f} - \frac{y}{g} - k \right| = \frac{|xg - yf - kfg|}{|fg|} \geq \frac{1}{Q},$$

because the numerator is a nonzero Eisenstein integer and $|fg| = (N\mathfrak{f}N\mathfrak{g})^{1/2} \leq Q$. The fixed codifferent factor $1/\delta$ changes only the lattice constants. The modulus-one frequency zero obeys the same separation from all others.

For completeness, a ρ_0-separated set t_r in a fixed two-dimensional torus obeys the additive bound

$$\sum_r \left| \sum_{|\alpha|\ll\sqrt{D}} z_\alpha \exp(2\pi i \operatorname{Tr}(\alpha t_r)) \right|^2 \ll (D + \rho_0^{-2}) \sum_\alpha |z_\alpha|^2. \tag{40.24}$$

Use fixed linear coordinates to write the lattice as $\mathbb{Z}^2$ and its additive pairing as $e(n \cdot t)$. The support lies in $|n_i| \leq T$ with $T \asymp \max(1, \sqrt{D})$. To prove the dual inequality, majorize this box indicator by $e^{2\pi} \exp(-\pi\|n\|^2/T^2)$, expand the square, and apply Gaussian Poisson summation. Up to fixed constants the resulting kernel is

$$T^2 \sum_{\ell\in\mathbb{Z}^2} \exp(-cT^2\|t_r - t_s + \ell\|^2).$$

Take ρ_0 at most a fixed torus constant. The lifted points are $c'\rho_0$-separated, so disjoint disks bound their count in a disk of radius L by $O(1+(L/\rho_0)^2)$. Gaussian annular summation bounds every absolute kernel row sum by $O(T^2+\rho_0^{-2})$. Schur's inequality and finite-dimensional duality prove (40.24), with constants independent of the number of frequencies.

Put $\mathcal{S}(x/f)=\sum_\alpha z_\alpha e_f(\alpha x)$. By (40.22),

$$\rho(\alpha)=\tau_f(\overline{\rho})^{-1}\sum_{x\in U(\mathfrak{f})}\overline{\rho(x)}e_f(\alpha x).$$

After taking squared absolute values, enlarging the primitive-character sum to all characters of $U(\mathfrak{f})$ and using orthogonality yields

$$\sum_{\rho\ \text{primitive mod }\mathfrak{f}}\left|\sum_\alpha z_\alpha\rho(\alpha)\right|^2\le\frac{\varphi(\mathfrak{f})}{N\mathfrak{f}}\sum_{x\in U(\mathfrak{f})}|\mathcal{S}(x/f)|^2\le\sum_{x\in U(\mathfrak{f})}|\mathcal{S}(x/f)|^2.$$

Apply (40.24) with $\rho_0\gg Q^{-1}$ to prove (40.23).

Finally $\mathcal{O}$ has class number one. Choose one generator α_m of each ideal column, with $|\alpha_m|^2=Nm$; these are an injective subset of the lattice disk. A primitive trivial-infinity-type Hecke character is a unit-trivial primitive residue character on $\mathcal{O}/\mathfrak{f}$, and its ideal value equals its value on α_m. Descent of the residue character to a proper divisor would preserve unit-triviality and contradict primitive Hecke conductor. Thus (40.23) applies to arbitrary ideal coefficients of norm at most $2D$, including squarefree ideals of nonsquarefree rational norm.

40.16.3 Raw zeros, tuple multiplicity and block transfer

Freeze r_6 and the literal unit/S-factor, putting

$$c_m=b_m\chi_m(u_0)\mathbf{1}_{(m,r_6)=1},\qquad\sum_m|c_m|^2\le\sum_m|b_m|^2.$$

This is independent of every first-five variable. In particular the arbitrary overlapping sixth-power factor is not replaced by one. Let $v=\prod_{j=1}^5 r_j^j$ denote the chosen literal product. Every outside-S valuation is between one and five. BGL, arXiv:1112.1650v1, Lemma 2.1, together with the established finite S-unit comparison in (40.9), gives its primitive literal Kummer character κ_v of trivial infinity type, with

$$q=r_1\cdots r_5\mid\operatorname{cond}(\kappa_v)\mid\mathfrak{c}_S q,\qquad\kappa_v(m)=\chi_m(v)\quad((m,S)=1).$$

The equality includes collisions with q: both sides are zero. The fixed $\mathfrak{c}_S$ includes all wild conductor types and literal comparison twists. No row-dependent phase enters the coefficients.

A fixed primitive character determines its outside-S conductor q. Each prime of q has at most five assignments to the pairwise-coprime $r_1,\dots,r_5$, so tuple multiplicity is at most $5^{\omega(q)}\ll_\eta(Nq)^\eta$. All conductors in the dyadic block have norm at most C_SQ. Enlarge the positive row sum, apply (40.23), and count $O(A_6)$ possibilities for the frozen arbitrary r_6. This proves (40.20); the actual capacity, squarefree, ray and inter-factor restrictions only shrink the positive sum. Equivalently $\mathcal{E}_A(b)\le\Lambda_A\sum_m|b_m|^2$; there is no coefficient norm factor in the definition of Λ_A.

40.16.4 Uniform coefficient and principal-residue assembly

The other block estimate is exactly the accepted powered-BGL input (40.8), whose squarefree powers are justified in BGL Section 3.2. The capacity comparisons and elementary minimum in Section 40.15 give

$$\Lambda_A \ll (HD)^{\varepsilon}\{H + DH^{1/6} + (DH)^{2/3}\}.$$

Sum logarithmically many blocks with smaller internal exponents. An S-supported literal factor $\mathfrak{b}$ reduces capacity to $H/N\mathfrak{b}$; the required sums over $\mathfrak{b}$ converge at powers 1, 1/6, 2/3. Literal units have multiplicity at most six. This proves the raw bound with arbitrary fixed b_m.

For the actual coefficients use (40.6): $|A_U(m)| \le 3^{\omega(m)} \ll_\eta (Nm)^\eta$ gives

$$b_m = D^{-1/2}A_U(m)\nu(m)W(Nm/D), \qquad \sum_m |b_m|^2 \ll_\eta \|W\|_\infty^2 D^\eta,$$

uniformly for $U \ge 1$, $U^2 \le D$. The common W is not optimized separately for different rows. If the primitive ψ_u is principal, ν is unramified outside S, so tame Kummer inertia forces every outside-S valuation of u to be divisible by six. Ideal counting and the convergent S-supported sum at power 1/6 give $O_{\nu,S}(H^{1/6})$ such literal rows. In the exact formula (40.2), $|\rho_T| \ll_K 1$, $|\widehat{W}(1)| \le \|W\|_\infty$, and

$$\sum_d \frac{|\beta_U(d)|}{Nd} \le \left(\sum_{Na\le U} \frac{1}{Na}\right)^2 \ll \log^2(2U).$$

Thus $|P_u| \ll \sqrt{D}\|W\|_\infty \log^2(2U)$ on principal rows, and

$$\sum_{0<Nu\le H} |P_u|^2 \ll DH^{1/6}\|W\|_\infty^2 \log^4(2U).$$

This fits the new envelope. The exact identity $E_u = I_u - P_u$ and $|E_u|^2 \le 2|I_u|^2 + 2|P_u|^2$, with smaller internal exponents, prove (40.21). No cutoff limit or profile supremum occurs.

The ordinary comparison is an application refinement. A direct BGL radical relabelling would additionally require reciprocity of its mixed family, not just its conductor count: for pairwise-coprime a, b, a', b', the quotient after the original fixed ray phases is $\vartheta_b(a')/\vartheta_a(b')$, which varies outside S. GL, arXiv:1112.1642v2, Definition 1(2), is therefore not supplied by that shortcut. This does not rule out a different mixed-family theorem; it is simply unneeded for the proved weaker ordinary comparison. The remaining exponent gap and every independent signed, spectral, formal and GRH obligation stated in Section 40.15 remain open.

40.17 Why the common profile must stay fixed

The unsigned envelope of Section 40.15 and the unresolved signed estimate have different profile quantifiers. We give an obstruction to an H-sized bound uniform through the sup norm alone. It uses the *actual* coefficients and nonprincipal rows, rather than replacing the columns by arbitrary weights. It does not contradict an estimate for one fixed smooth profile or one with adequate derivative dependence.

Fix $K = \mathbb{Q}(\omega)$, $\omega^2 + \omega + 1 = 0$, principal $\nu = 1$, and a finite good set S containing the primes above 2, 3. Write $\zeta = 1 + \omega$, $\delta = 1 + 2\omega$, so ζ has order six and $\delta^2 = -3$. Retain the literal raw symbols and normalization

$$I_u(W) = D^{-1/2} \sum_{m \text{ squarefree } (m,S)=1} A_U(m)\chi_m(u)W(Nm/D), \qquad E_u = I_u - P_u.$$

Here and below squarefree means *ideal* squarefree. For $U^2 = D$ the accepted high-window identity gives $A_U(m) = \mu(m)(r_U(m) - 1)$ on $D < Nm < 2D$, with $r_U(m)$ even and $|A_U(m)| \geq 1$. The multiset of prime-ideal norms of a squarefree ideal is determined by its rational norm. Thus $A_U(m) = A_N$ depends only on $N = Nm$, including divisor-norm multiplicities. Moreover

$$\eta(m) := \chi_m(\zeta) = \zeta^{(Nm-1)/6}, \qquad (m, S) = 1. \tag{40.25}$$

The primitive character η has conductor $(2)^2(\delta)^3$, of norm 432; its powers $1, 5$ have conductor norm 432, powers $2, 4$ norm 27, and power 3 norm 16. All five powers are nonprincipal. These row conductors do not remove the raw zero at any prime dividing a sixth factor.

Put $\phi(t) = \exp(1 - 1/(1 - t^2))$ for $|t| < 1$ and zero otherwise. For integer D set $w_N = \operatorname{sgn}(A_N)\overline{\zeta^{(N-1)/6}}$ when a good squarefree ideal of norm N exists and $D < N < 2D$, and zero otherwise. Define one common, complex profile

$$W_D(y) = \sum_{D<N<2D} w_N \phi(4(Dy - N)). \tag{40.26}$$

Its disjoint supports lie strictly inside $(1, 2)$, its sup norm is one for large D, and $\|W_D^{(j)}\|_\infty \ll_j D^j$. In particular the endpoints have value zero. This is a profile varying with scale, independent of the row, not a separate choice for each ideal or each row.

Proposition 40.8 (A moving-profile lower bound)**.** *For every fixed $0 < \theta < 1$, take $H = D^\theta$, $U = \sqrt{D}$, and $X = H^{1/6}$. As integer $D \to \infty$,*

$$\sum_{0<Nu\leq H} |E_u(W_D)|^2 \geq (c_S + o(1))DH^{1/6}, \qquad c_S > 0. \tag{40.27}$$

This lower bound already comes from literal rows $u_v = \zeta\beta_v^6$, where v is an arbitrary good ideal of norm at most X and β_v is a generator. These rows have nonprincipal primitive character η, so $P_{u_v} = 0$. Their exact values are

$$E_{u_v}(W_D) = D^{-1/2} \sum_{\substack{m \text{ squarefree, } (m,Sv)=1 \\ D<Nm<2D}} |A_U(m)|. \tag{40.28}$$

Every collision with v remains deleted, even when the primitive conductor drops to 432. No squarefree condition is imposed on v.

At $H = D^{3/4}$ the lower exponent is $9/8$, whereas the current upper exponent is $7/6$. Thus this does not establish sharpness of $7/6$ or a new upper saving. For $0 < \theta < 2/3$, the term $DH^{1/6}$ dominates the current unsigned envelope; it is necessary up to subpower losses in this *varying-profile* class, even on nonprincipal rows.

For $k \geq 0$ put $M_k(W) = \sum_{j=0}^k \|(y\partial_y)^j W\|_\infty$. If, for every $\varepsilon > 0$, a bound uniform over all common profiles with constants independent of W, D were to assert

$$\sum_{0<Nu\leq H} |E_u(W)|^2 \ll_\varepsilon M_k(W)^\alpha (HD)^\varepsilon H, \qquad \alpha \geq 0,$$

then necessarily $k\alpha \geq 1 - 5\theta/6$. At $\theta = 3/4$ this is $k\alpha \geq 3/8$. For a single fixed ε the necessary condition is only $k\alpha + (1 + \theta)\varepsilon \geq 1 - 5\theta/6$. These are necessary cost comparisons, not sufficient estimates. A fixed-W result, a class with bounded seminorms, or the existing $M_4(W)^2$ dependence is not refuted.

The same rows expose a concrete centering error in the joint completion: removing the orientation mean of the actual correlation can delete a nonzero signed contribution on *nonprincipal* rows. The extended proof retains the literal unit phase, gives an exact four-orientation example, and explains why orientation projection alone supplies no saving. The standalone profile and coherent-mean inspector shows the complete finite norm groups, arbitrary sixth-factor masks and exact residual quantities. Its finite tables are diagnostics of this construction, not asymptotic estimates, training or GRH evidence.

40.18 Proof and joint-mean boundary of the moving-profile construction

40.18.1 Norm groups and primitive conductors

For a split rational prime p, a squarefree ideal contains zero, one or both conjugate primes. Its rational norm exponent is respectively $0, 1, 2$; at exponent one there are two choices, and at exponent two its divisor norms include two copies of p. For an inert prime, the exponent is zero or two, and the nontrivial choice is the single prime ideal of norm p^2. Thus the rational norm determines μ, the divisor-norm multiset and r_U, even though it need not determine the ideal. For example norm 49 has squarefree ideal divisor norms $1, 7, 7, 49$, whereas the inert prime of norm 25 has divisor norms $1, 25$. Additional fixed S deletions remove some ideals without changing this constancy among those remaining. The high-window formula and its parity are the already proved facts of Section 40.5, not a new coefficient estimate.

At a good prime ideal $\mathfrak{p}$ of norm q, Euler's definition gives $\chi_{\mathfrak{p}}(\zeta) = \zeta^{(q-1)/6}$. All such norms are 1 modulo 6; for $a = 1+6r, b = 1+6s$ one has $(ab-1)/6 = r+s+6rs$. Multiplicativity proves (40.25). Write $\chi_4(N) = (-1)^{(N-1)/2}$ for odd N. On good ideals,

$$\eta = \chi_4(N)\omega^{(N-1)/3},$$
$$\eta^2 = \omega^{2(N-1)/3} = \omega^{-(N-1)/3}, \qquad \eta^3 = \chi_4(N).$$

The inverse orientation in the middle expression is essential.

For completeness the local conductors are exact, not merely upper bounds. The quadratic norm character factors modulo $(2)^2 = (4)$. Since $\mathrm{Tr}(\delta\gamma) \in 3\mathbb{Z}$ for every $\gamma \in \mathcal{O}$, expanding the norm gives $N(\alpha + \delta^3\beta) \equiv N\alpha \pmod 9$. The cubic norm character therefore factors modulo δ^3. The coprime local witnesses

$$\alpha_2 = 13 + 6\omega, \quad N\alpha_2 = 127, \quad \alpha_2 - 1 = 2\omega\delta^3,$$
$$\alpha_3 = -11, \quad N\alpha_3 = 121, \quad \alpha_3 - 1 = 4\delta^2.$$

show minimality. The first is 1 modulo 2, is $1 + 2\omega$ modulo 4, and is 1 modulo δ^3; its η value is -1. The second is 1 modulo 4 and $-2 = 1 + \delta^2$ modulo δ^3, but not 1 modulo δ^3; its η value is ω and its square is ω^2. Thus the quadratic local exponent is two and the cubic one is three. The two moduli are coprime, giving the stated norms $432, 27, 16$ for the nontrivial powers. Global units have norm one, so these residue characters are unit trivial and descend to ideal Hecke characters in this class-number-one field. A norm-seven prime has value ζ, proving order six. A larger finite S does not principalize the character: CRT gives representatives of the same nontrivial ray classes avoiding the extra excluded primes. Primitive conductor reduction never restores raw primes excluded by S or the sixth factor.

40.18.2 Exact alignment, with arbitrary overlapping sixth factors

The bumps in (40.26) have radius $1/(4D)$ and center N/D. Distinct supports are disjoint. At an active integer node their value is exactly w_N, and all endpoints are zero. Differentiation gives $\|W_D^{(j)}\|_\infty \le (4D)^j \|\phi^{(j)}\|_\infty$. Expanding $(y\partial_y)^j$ into ordinary derivatives and using $1 < y < 2$ gives $M_k(W_D) \ll_k D^k$.

Every nonzero ideal v has a generator β_v. The literal element $u_v = \zeta\beta_v^6$ is independent of that choice, since all units have sixth power one; distinct ideals yield distinct rows. Its norm is $(Nv)^6$. For squarefree good m, exact raw multiplicativity says

$$\chi_m(u_v) = \eta(m)\mathbf{1}_{(m,v)=1}.$$

Repeated primes of v are allowed and its collisions with m remain zero. The primitive row character is always η, so the actual principal indicator in (40.2) is zero when $\nu = 1$. Substituting the nodal profile proves (40.28) with no factor six, unit averaging or residue replacement.

40.18.3 The coprime-triple density and the selected $h = 1$ block

Put $\kappa = \pi/(3\sqrt{3})$. Lattice counting, with six unit generators per ideal, gives

$$A_K(Y) := \#\{a : Na \le Y\} = \kappa Y + O(\sqrt{Y} + 1), \qquad A_K(Y) \le CY \quad (Y \ge 1).$$

This is the existing elementary ideal count. Let $T(D, X)$ count ordered triples (m, n, v) with m, n squarefree good, $D < Nm, Nn < 2D$, $Nv \le X$, v good and arbitrary, and the three ideals pairwise coprime. For $D, X \to \infty$, $X \le D$, we claim

$$\begin{aligned} T(D, X) &= (\kappa^3 \mathcal{C}_S + o(1))D^2 X, \\ \mathcal{C}_S &= \prod_{\mathfrak{p}\in S}(1 - t_\mathfrak{p})^3 \prod_{\mathfrak{p}\notin S}(1 - 5t_\mathfrak{p}^2 + 6t_\mathfrak{p}^3 - 2t_\mathfrak{p}^4) > 0, \\ t_\mathfrak{p} &= (N\mathfrak{p})^{-1}. \end{aligned} \tag{40.29}$$

Here a product over S means its prime ideals. To prove this, first impose the local restrictions at a fixed finite set of primes containing S. They are finite Boolean combinations of divisibility by $\mathfrak{p}$ and $\mathfrak{p}^2$ in m, n, and by $\mathfrak{p}$ in v. Finite inclusion-exclusion and the count for fixed ideal multiples give the product of the local densities, with relative error tending to zero. At a good prime the allowed cases are no positive valuation, a single valuation one in m or n, or an arbitrary positive valuation in v. The factor is therefore

$$(1 - t)^3\left(1 + 2t + \frac{t}{1 - t}\right) = (1 - t)^2(1 + 2t - 2t^2) = 1 - 5t^2 + 6t^3 - 2t^4.$$

At S all three valuations must vanish, giving $(1 - t)^3$. The geometric series for v is essential; v is not squarefree.

An omitted failure belongs to one of five events: $\mathfrak{p}^2 \mid m$, $\mathfrak{p}^2 \mid n$, $\mathfrak{p} \mid (m, n)$, $\mathfrak{p} \mid (m, v)$ or $\mathfrak{p} \mid (n, v)$. Divisibility counts and $A_K(Y) \le CY$ bound each by $O(D^2X/(N\mathfrak{p})^2)$, uniformly; if a quotient scale is below one its count is zero. Thus the tail after norm P is

$$O\left(D^2X \sum_{N\mathfrak{p}>P} (N\mathfrak{p})^{-2}\right) = o_P(D^2X).$$

The series converges by the ideal count (or $\zeta_K(2) < \infty$). Take the large-scale limit first at fixed P, then $P \to \infty$. Each local factor is positive and differs from one by $O(t^2)$, proving (40.29). Strict

annulus endpoints have no effect on the main term by the same lattice count. The secondary range $X/2 \le Nv < X$ has half this limiting volume, though it may be empty at small X.

On the selected literal unit class every expanded pair term in (40.28) is nonnegative. Keeping only $(m,n)=1$ gives its exact $h=1$ A–A contribution

$$\mathcal{E}^{AA}_{\text{selected},h=1} = D^{-1} \sum_{v \text{ good}} \sum_{Nv\le X} \sum_{\substack{m,n \text{ squarefree,good} \\ (m,n)=(m,v)=(n,v)=1}} \sum_{D<Nm,Nn<2D} |A_U(m)A_U(n)| \ge D^{-1}T(D,X).$$

Consequently, with $X = H^{1/6}$,

$$\sum_{0<Nu\le H} |E_u|^2 \ge \sum_{Nv\le X,\ v \text{ good}} |E_{u_v}|^2 \ge \mathcal{E}^{AA}_{\text{selected},h=1} \ge (\kappa^3\mathcal{C}_S + o(1))DX.$$

The first inequality is positivity of the *outer squared row sum*. The selected $h=1$ block does not lower-bound the signed $h=1$ sum over other literal rows or a unit-complete family. No positive-semidefinite claim about a gcd-truncated Gram matrix is needed. This is A–A, not a positive-density assertion for C–C long-long weights, which may vanish. This proves Proposition 40.8 with $c_S = \kappa^3\mathcal{C}_S$. The derivative tradeoff follows by comparing powers in $DH^{1/6} \ll D^{k\alpha+(1+\theta)\varepsilon}H$ and then letting $\varepsilon \downarrow 0$ only when the proposed bound holds for every positive ε.

40.18.4 Projection preserves the coupled problem, not a saving

Use the exact joint notation of Section 40.14. For fixed h,q with $q \ne 1$ (including $h=1$), let $n=\varphi(q)$, $\ell = N(hq)$, $Q = Nq$, and

$$c = \frac{Q^2\xi_q(-\alpha)\tau_\beta(\xi_q)}{\ell^6},$$
$$\Gamma^F_r = c\sum_K B_F(K)\overline{\theta_r(K)}, \qquad A(K) = \sum_{r\in J} a_r\overline{\theta_r(K)}.$$

The active orientations J include all original restrictions, and the literal unit phase belongs to a_r. The distinct θ_r are orthonormal for $n^{-1}\sum_K$. If P projects onto their span, then

$$PB_F = (cn)^{-1}\sum_{r\in J}\Gamma^F_r\theta_r, \qquad \sum_K |PB_F(K)|^2 = (|c|^2n)^{-1}\sum_r |\Gamma^F_r|^2.$$

Replacing B_F by PB_F in the full bilinear pairing is exact. Cauchy–Schwarz is precisely $|c\sum_K B_F A| \le \|a\|_2\|\Gamma^F\|_2$. The conductor and group-size factors cancel. Projection rank alone gives no arithmetic saving for this particular coupled vector.

For $s=\omega(q)$ let $C = \{K : x_{\mathfrak{p}}(K)^2 = 1 \text{ for all } \mathfrak{p} \mid q\}$. All orientations agree on C. If M_C denotes multiplication by its indicator, the matrix in the orthonormal orientation basis is

$$PM_CP = 3^{-s}\mathbf{1}\mathbf{1}^*, \qquad \lambda = |J|/3^s, \qquad \|(1-P)M_CP\|^2 = \lambda(1-\lambda).$$

Thus coherent restriction does not commute with projection. For example

$$\left|\sum_C (B_F - PB_F)A\right| \le \sqrt{\lambda(1-\lambda)}\|(1-P)B_F\|_2\|A\|_2,$$

where all norms in this inequality are counting ℓ^2 norms. Normalized norms would require an additional factor n on the right. Counting a coherent subset alone is not a lower bound for its actual signed pairing.

40.18.5 A nonzero orientation mean on actual nonprincipal rows

For the selected rows let V be any finite set of good ideals, put the first five row factors equal to one, and retain the sixth-factor mask. For each h, q define $Z_{h,q} = \#\{v \in V : (v, hq) = 1\}$. After removing the separately displayed literal unit phase, the exact correlation is

$$\Gamma_r^F = Z_{h,q} = c \sum_K B_V(K)\overline{\theta_r(K)} \quad \text{for every active orientation } r.$$

To pass from the published C–C identity to A–A replace each r_U by $r_U - 1$. At $h = 1$, $m = r, n = q/r$, the coefficient is

$$a_r^{AA} = (r_U(m) - 1)(r_U(n) - 1)W_m\overline{W_n}\theta_{m,n}(\zeta), \qquad \mu(q)a_r^{AA} = |A_U(m)A_U(n)|.$$

This retains $\mu(q)$, the common complex profile and its conjugation, all deleted common primes, and the literal ζ phase. If $Z_{1,q} > 0$ and at least one active interior A–A coefficient is nonzero, the actual pairing is positive, whereas $\sum_r |\Gamma_r^F - \text{mean}\,\Gamma^F|^2 = 0$. An orientation-variance-only replacement with no mean term is therefore false. The mean is not a principal residue: these rows have character η, with nonprincipal powers. This does not refute a properly formulated fixed-profile signed estimate.

A fresh exact example uses $D = 4000$, $U = 63$ and chosen prime ideals of norms $7, 13, 79, 67, 97$. Their product has four active orientations: the pairs 6097/7663, 7189/6499 and both reversals. Here $r_U = 2$, and A_U is -1 on the three-prime columns and $+1$ on the two-prime columns. The four good ideals with $10 \le Nv \le 20$ have norms $13, 13, 19, 19$. Exactly one collides with the chosen 13-prime, so $Z = 3$ for all four orientations. The exact selected $h = 1$ contribution is $12/4000 = 3/1000$ despite zero orientation variance. Dropping the literal ζ phase incorrectly changes the coefficient sum from 4 to -1, giving $-3/4000$. The coherent fraction is $4/243$ and the squared leakage is $956/59049$. The residue group and infinite Fourier tail are not estimated by this finite check. The fixed row conductor 432 must be distinguished from the pair-column conductor $q = mn$, whose norm here and in the asymptotic annulus is comparable to D^2.

The exact implementation at `examples/profile_uniformity/` keeps complete norm groups and arbitrary sixth factors, including distinct ideals of norm 49 with different masks. The saved six-scale examples, exact joint fixture and their independent checks certify finite identities only. Full-union masks, coherent means, fixed-profile uniformity and the remaining mixed/pure upper-envelope neighborhoods still require a new signed estimate. No determinant comparison, zero location, analytic or categorical Lean theorem, quantum result or GRH proof is obtained.

40.19 A bound for the signed coprime slice and an exact character twist

The coprime-column contribution can be negative, so it needs its own bound. Fix the original ν, S, one common possibly complex smooth W supported in $[1, 2]$, $D > 1$, $U \ge 1$ and $U^2 \le D$. Consider an actual block

$$u = u_0 v_1 v_2^2, \quad A_j \le Nv_j < 2A_j \ (j = 1, 2), \quad Nu \le H, \qquad R = A_1 A_2, \quad M = \max(A_1, A_2).$$

The good ideals v_1, v_2 are squarefree and coprime, with their literal primary/ray representatives; all other good factors are the unit ideal. Let F be the actual indicator, including capacity and every row mask. In the remaining neighborhoods the first factor is nonunit, so the primitive row character

is nonprincipal and $E_u = I_u$ there. For $X, Y \in \{A_U, C_U, \mu\}$ define the actual signed slice

$$S_1^{XY} = \frac{1}{D}\sum_u F(u) \sum_{\substack{m,n \text{ squarefree,good} \\ (m,n)=1}} X(m)Y(n)\nu(m)\overline{\nu(n)}\chi_m(u)\overline{\chi_n(u)}W(Nm/D)\overline{W(Nn/D)}. \tag{40.30}$$

All columns in this formula are the original annular columns, including raw zero sentinels. No positive-semidefinite claim about the coprime truncation is made.

Proposition 40.9 (A bound for the actual signed $h = 1$ slice)**.** *Uniformly in the original cutoff and this actual block,*

$$|S_1^{XY}| \ll_{\nu,S,\epsilon} \|W\|_\infty^2 (HD)^\epsilon \min\left\{R + \frac{DR}{M} + \frac{D^{2/3}R}{M^{1/3}},\ D + R^2\right\}. \tag{40.31}$$

The exact identity underlying the estimate is

$$\begin{aligned} DS_1^{XY} &= \sum_{\substack{d \text{ squarefree} \\ (d,S)=1}} \mu(d) \sum_{\substack{u \text{ in the actual block} \\ (d,u)=1}} T_d^X(u)\overline{T_d^Y(u)}, \\ T_d^X(u) &= \sum_{\substack{a \text{ squarefree} \\ (a,dS)=1}} X(da)\nu(a)\chi_a(u)W(Nd\,Na/D). \end{aligned} \tag{40.32}$$

In particular $X(da)$ is not replaced by $X(d)X(a)$, and the mask $(d, u) = 1$ remains.

The proof applies the accepted block sieves inside each positive row norm in (40.32), then explicitly loses the d signs in an absolute triangle. At $H = D^{3/4}$ the two remaining power-scale neighborhoods $A_1 \asymp D^{5/12}, A_2 \asymp D^{1/6}$ and $A_1 \asymp D^{3/4}, A_2 \asymp 1$, with feasible capacity constants, both retain power 7/6. The desired 3/4 still needs a signed saving of 5/12. This proves a separate signed-slice bound; it does not improve the published global envelope or supply the missing cancellation.

There is also an exact arithmetic description of the two-pivot phase. Put $\delta = 1 + 2\omega$ and, at each good prime ideal p, set $j(p) = J_p(\chi_p, \chi_p^2)$. Extend j multiplicatively on squarefree columns. Let $\Psi(a)$ be the unique generator of an ideal prime to 2δ satisfying $\Psi(a) \equiv 1 \pmod{2\delta}$.

Proposition 40.10 (The actual Jacobi column twist)**.** *The map Ψ is an algebraic Hecke character with exact finite conductor (2δ), of norm 12, and principal convention $\Psi((\alpha)) = \alpha$ for $\alpha \equiv 1 \pmod{2\delta}$ (infinity type $(1, 0)$). For good squarefree columns,*

$$(j(p)) = p, \quad -j(p) = \Psi(p), \qquad \mu(m)j(m) = \Psi(m). \tag{40.33}$$

Define $\vartheta(m) = \Psi(m)/\sqrt{Nm}$ and $\rho(m) = j(m)/\sqrt{Nm} = \mu(m)\vartheta(m)$ on those columns. In the high window the actual gauged coefficients are $b_A = (r_U - 1)\vartheta\nu W$, $b_C = r_U\vartheta\nu W$ and $b_\mu = \vartheta\nu W$.

This does not replace the original row kernel. Its compensating inverse gauge remains, so all ordinary coefficient/operator norms are unchanged. The new character has nonzero infinity type and is not silently covered by a theorem stated only for finite-order twists. The identities in (40.33) involving μ must not be extended to arbitrary nonsquarefree sixth factors.

A fresh fixed-profile example takes $\nu = 1$, S the primes above $2, 3$, literal unit one and primary row generators 1 modulo 3. It lies in an actual $A_6 = 1$ block at $D = 60000$, $U = 244$, $H = 3833$, $A_1 = 37$, $A_2 = 7$. All 20 rows of the stated literal class are nonprincipal. A selected q has exactly two

legal column orientations, of norms 97051/96091 and its reversal. Their correlations in the ω basis are $(-4,-2)$ and $(-2,2)$, with mean -3. Their selected contribution is $S_{1,q}^{AA} = -1/10000$; deleting the mean gives zero. The centered squared norm is 6, not zero, and the proposed variance-only Cauchy bound would incorrectly require $36 \le 12$. This refutes that centering rule in a fixed-profile row block, not the asymptotic target. Other q contributions remain. The coprime-kernel inspector shows the actual rows, raw zeros, two-column Gram matrix and compensated gauge; no training or arithmetic spectrum is inferred from that finite view.

40.20 Proof of the signed-slice budget and its surviving analytic burden

40.20.1 Gcd inversion before an absolute bound

Insert $\mathbf{1}_{(m,n)=1} = \sum_{d\mid m,\ d\mid n} \mu(d)$ in (40.30), and write $m = da, n = db$. Squarefreeness forces $(a,d) = (b,d) = 1$. The common factors give $\nu(d)\overline{\nu(d)} = 1$ and $\chi_d(u)\overline{\chi_d(u)} = \mathbf{1}_{(d,u)=1}$. This proves (40.32), retaining the original coefficient $X(da)$ and the full row-zero mask. For $X = Y$ each inner squared row sum is nonnegative; its $\mu(d)$-weighted sum need not be.

Put $L = D/Nd$. Whenever a column survives, $L \ge 1/2$. The actual divisor-assignment bound and ideal counting give

$$\sum_{\substack{a \text{ squarefree}\\(a,dS)=1}} |X(da)\nu(a)W(Nd\,Na/D)|^2 \ll_\eta D^\eta \|W\|_\infty^2 L.$$

Indeed $N(da) \le 2D$, $|X(da)| \ll_\eta D^\eta$ uniformly in d, U, and there are $O(L)$ ideals of norm at most $2L$ for $L \ge 1/2$. This includes C_U by $C_U = A_U + \mu$ on the active annulus. There is no multiplicativity assertion for $X(da)$. For $L \ge 1$, the powered block bound and the ordinary-conductor comparison of Section 40.15, followed by Cauchy for the cross term, imply

$$|G_d^{XY}| \ll (HD)^\eta \|W\|_\infty^2 L \min\left\{R + \frac{LR}{M} + \frac{L^{2/3}R}{M^{1/3}},\ L + R^2\right\}, \tag{40.34}$$

where G_d^{XY} denotes the inner row sum in (40.32). The raw (d,u) restriction is only enlarged inside these positive norms; u_0 is a fixed column multiplier of modulus at most one. For $1/2 \le L < 1$, only the unit column can survive. The direct row count is $O(R)$, and the right side of (40.34) is at least a constant times R since $R \ge 1$ and $L \ge 1/2$. Thus this endpoint does not require a sieve with an unstated subunit length.

Now take the absolute triangle in d explicitly. The two estimates may be summed separately and their minimum taken. The elementary ideal sums

$$\sum_{Nd\le 2D} \frac{1}{Nd} \ll \log(2D), \qquad \sum_d (Nd)^{-2} \ll 1, \qquad \sum_d (Nd)^{-5/3} \ll 1$$

turn the first estimate into $R\log(2D) + DR/M + D^{2/3}R/M^{1/3}$ after division by D; the second gives $D + R^2\log(2D)$. Absorb the logarithms with smaller internal exponents to obtain (40.31). All raw zeros, literal/ray/squarefree/capacity restrictions were retained before the stated positive enlargements. No bound for an indefinite submatrix was inferred from positivity of a larger Gram matrix.

At the mixed power-scale point the powered exponents are $7/12, 7/6, 10/9$, and the ordinary exponents are $1, 7/6$. At the pure point they are $3/4, 1, 7/6$ versus $1, 3/2$. These are upper-bound

exponents with feasible dyadic constants, not actual energy lower bounds. A sufficient $h = 1$ target for the A–A combination is

$$\left|\sum_d \mu(d) G_d^{AA}\right| \ll_{\nu,S,W,\epsilon} DH(HD)^{\epsilon}. \tag{40.35}$$

At $H = D^{3/4}$ this asks for power 7/4 before division by D, while (40.31) gives 13/6, leaving 5/12. This is sufficient for this slice, not a necessary bound for every separate C–C/C–μ term if their signed assembly cancels further. The quantities G_d depend on prime supports, $X(da)$ and row deletions; they are not an independent smooth function of Nd to which a scalar Möbius partial-sum estimate can simply be applied.

40.20.2 The correctly oriented Jacobi generator

At a good prime ideal p, let $n = Np$ and $\chi = \chi_p$ be the literal positive sextic residue character. In $\mathcal{O}/p$, its value reduces to $x^{(n-1)/6}$. For $j(p) = J(\chi, \chi^2)$, the elementary Gauss–Jacobi identity and the three nontrivial Gauss norms give $|j(p)|^2 = n$. Reduction in that *same* residue field gives

$$j(p) \equiv \sum_x x^{(n-1)/6}(1-x)^{(n-1)/3} = 0 \pmod{p}.$$

Every exponent after expansion lies strictly between 0 and $n-1$, so the finite-field power sums vanish. Hence $(j(p)) = p$. This includes an inert prime of norm p_0^2, and inverting the literal character conjugates the ideal at a split prime.

This raw sum equals the old $J(\chi^2, \chi^3)$: the quotient of the two Gauss–Jacobi expressions is $G(\chi)G(\chi^5)/G(\chi^3)^2 = 1$. It differs from the theta-curve Frobenius normalization by its explicitly stated factor $-\chi^3(-1)$; that sign is not imported silently. No new Gauss or Jacobi norm theorem is claimed.

Let $f = (2\delta)$. The six units map bijectively onto $(\mathcal{O}/f)^\times$: the components at 2 and δ have orders three and two, with complementary kernels. Since $\mathcal{O}$ is a PID, every ideal prime to f has a unique generator $\Psi(a) \equiv 1 \pmod{f}$. Uniqueness gives multiplicativity. If $u_f(\alpha)$ is the unit having the residue of α modulo f, then

$$\Psi((\alpha)) = \alpha/u_f(\alpha), \qquad |\Psi(a)|^2 = Na.$$

This explicitly defines the finite part and the principal infinity-type convention. The finite conductor divides f. A proper divisor omits a component: the unit -1 is 1 modulo 2, and ω is 1 modulo δ. A smaller defining modulus would require the unit ideal to have value -1 or ω. Thus the finite conductor is exactly f.

To identify the actual $j(p)$, now reduce in the *character-value* ring, a different operation from reduction modulo p above. Modulo δ, a sixth root v satisfies $v = v^3$ and $v^2 = 1$. The zero branches at $x = 0, 1$ are kept, so $j(p) \equiv \sum_{x \neq 0,1} \chi^3(x) = -1 \pmod{\delta}$. Modulo 2, $v = v^4$, and $J(\chi, \chi^2) \equiv J(\chi^4, \chi^2) = -\chi^4(-1) = -1$. The inverse-character Jacobi identity here follows by the bijection $x/(1-x)$ onto the nonzero field elements other than -1. Consequently $-j(p) \equiv 1 \pmod{f}$, proving $-j(p) = \Psi(p)$. Multiplication proves (40.33) on squarefree columns. For nonsquarefree ideals μ vanishes, so that last identity must not be extended to arbitrary sixth factors. This construction establishes the fixed character directly; it assumes no elliptic modularity, spectral comparison, or distribution of prime arguments.

40.20.3 The actual two-factor completion, not a new row kernel

Freeze the literal u_0, v_3, v_4, v_5, v_6 and put $Z = u_0 v_3^3 v_4^4 v_5^5 v_6^6$. The last factor is arbitrary, with its allowed overlaps. For $h = 1$, write $q = mn \neq 1$, $Q = Nq$, $\theta = \chi_m \overline{\chi_n}$ and $\xi_q = \theta^3$. For $q = (\beta)$ use the original inverse-different pairing $e_\beta(z) = \exp(2\pi i \operatorname{Tr}(z/(\delta\beta)))$. Let $F(v_1, v_2)$ be the exact common finite weight, retaining the first-five coprimality, primary/ray and capacity restrictions. It must be independent of the column orientation. Define

$$\widehat{F}_q(k_1, k_2) = \sum_{v_1, v_2} F(v_1, v_2) e_\beta(-k_1 v_1 - k_2 v_2),$$
$$T_{q,F}(\theta) = \sum_{k_1, k_2 \in (\mathcal{O}/q)^\times} \widehat{F}_q(k_1, k_2) \overline{\theta(k_1 k_2^2)}.$$

Periodization sums every actual representative; no injectivity assumption is needed. The primitive powers θ, θ^2 have zero Gauss sums at nonunit frequencies, including at inert primes. Exact inversion gives

$$\sum F \theta(v_1) \theta(v_2)^2 = Q^{-2} \tau_\beta(\theta) \tau_\beta(\theta^2) T_{q,F}(\theta) = Q^{-2} J_q(\theta, \theta^2) \tau_\beta(\xi_q) T_{q,F}(\theta).$$

Jacobi sums CRT without additive-generator multipliers, so $J_q = j(m)\overline{j(n)} = \sqrt{Q}\, \rho(m)\overline{\rho(n)}$. The quadratic central phase is the already recorded period-four law

$$\gamma(\beta) = \tau_\beta(\xi_q)/\sqrt{Q} = \tfrac{1}{2}\{1 + i^{-b} + i^a + i^{b-a}\}, \qquad \beta = a + b\omega.$$

For composite squarefree q, identifying $\tau_\beta(\xi_q)$ with $\sum_x e_\beta(x^2)$ requires CRT expansion of the local root counts; $1+\xi_q$ is not the root-count function on a composite ring. The known quadratic Gaussian evaluation is reused, not retested as a new phase theorem. Its pairing is exactly the displayed e_β.

With $b_X = \rho X \nu W$, the actual two-pivot identity is

$$DS_1^{XY} = \sum_q \frac{\gamma(\beta_q)}{Q} \sum_{mn=q} b_X(m) \overline{b_Y(n)} \theta_{m,n}(Z) T_{q,F}(\theta_{m,n}). \tag{40.36}$$

The two Gauss magnitudes, equivalently the central Gauss and Jacobi magnitudes, give exactly $1/Q$. There is no extra $\xi_q(-1)$ in this two-factor identity; the full six-factor formula of Section 40.13 retains that sign. If β changes to $u\beta$, both γ and T acquire the same quadratic sign $\xi_q(u)$, which cancels in their product. If Z shares any prime with q, $\theta(Z) = 0$, including at a sixth-power collision. No dropped primitive-conductor prime is restored.

Multiplying columns by ρ changes the kernel by its compensating inverse unitary gauge. It preserves operator norms and eigenvalues even for an indefinite coprime-truncated matrix. A fixed-character coefficient estimate cannot replace a bound for the actual q-dependent $T_{q,F}$. At the pure endpoint $v_2 = c$ with $(c, q) = 1$, exact summation gives

$$T_{q,F}(\theta) = \theta(c)^2 \tau_\beta(\overline{\theta^2}) \sum_{k_1 \in (\mathcal{O}/q)^\times} \widehat{F}_1(k_1) \overline{\theta(k_1)}.$$

Since $\theta^2(-1) = 1$, the extra Gauss pair multiplies to Q, returning the original one-pivot scalar $\tau_\beta(\theta)/Q$. A nonunit c gives the original zero. Thus a putative central-phase gain cannot be retained after discarding a literal length-one Fourier factor.

40.20.4 A central reciprocal remains after the gauge

On squarefree columns put $B_U = \mu A_U$ and $\vartheta = \Psi/\sqrt{N}$. The original ternary assignment gives exactly

$$B_U(m) = \sum_{\substack{abc=m \\ Na,Nb\le U}} \mu(c), \qquad \rho(m)A_U(m) = \vartheta(m)B_U(m).$$

All factors are squarefree and pairwise coprime. Fix a nonzero numerator z and keep the full deleted set $T = S \cup \operatorname{supp}(z)$. Write Ξ for the unitary primitive character of $\vartheta\nu\kappa_z$, with these raw deletions retained. Its nonzero infinity type prevents a silent reuse of a finite-order-only moment theorem. For $\Re s > 1$,

$$J_U^{\sharp,T}(s) = \sum_{m \text{ squarefree},\ (m,T)=1} B_U(m)\Xi(m)(Nm)^{-s} = N_U^T(s)/L^T(s,\Xi),$$

$$N_U^T(s) = \sum_{\substack{a,b \text{ squarefree} \\ (a,b)=1,\ (ab,T)=1 \\ Na,Nb\le U}} \frac{\Xi(ab)}{(Nab)^s} \prod_{p\mid ab}(1-\Xi(p)(Np)^{-s})^{-1}.$$

Fixing a, b leaves the Möbius Euler product in c; this proves the identity by absolute convergence. The numerator is finite and analytic for $\Re s > 0$. At $U = 1$ it is one, so the series is exactly $1/L^T(s,\Xi)$. That boundary identity is not a high-window counterexample. It shows why cancellation of central reciprocal poles cannot simply be inferred from the column-character identification.

For $x_p = \Xi(p)(Np)^{-s}$, $\alpha_p = (Np)^{-v}$ and $\beta_p = (Np)^{-w}$, the gauged three-placement Euler factor is $1 + x_p(\alpha_p + \beta_p - 1)$, with the opposite signs from the ungauged factor in Section 40.5. In the initial absolute domain it gives

$$\prod_{p\notin T}\{1 + x_p(\alpha_p + \beta_p - 1)\} = \frac{L^T(s+v,\Xi)L^T(s+w,\Xi)}{L^T(s,\Xi)} \prod_{p\notin T} H_p,$$

where

$$H_p = \frac{\{1 + x_p(\alpha_p + \beta_p - 1)\}(1 - x_p\alpha_p)(1 - x_p\beta_p)}{1 - x_p}.$$

Expansion gives

$$H_p - 1 = \frac{x_p^2(\alpha_p + \beta_p - \alpha_p^2 - \beta_p^2 - \alpha_p\beta_p)}{1 - x_p} + \frac{x_p^3\alpha_p\beta_p(\alpha_p + \beta_p - 1)}{1 - x_p}.$$

Thus the correction converges normally in the open region $\Re s > 0$ where the real parts of all of

$$2s + v,\ 2s + w,\ 2s + 2v,\ 2s + 2w,\ 2s + v + w,$$
$$3s + 2v + w,\ 3s + v + 2w,\ 3s + v + w$$

exceed one. In particular, for $\Re s \ge 1/2 + \eta$ and $\Re v, \Re w \ge 0$, its terms differ from one by $O_\eta((Np)^{-1-2\eta})$. Deleted primes only remove factors. Finite correction factors may vanish; no zero-free product is asserted. The displayed factorization is first an absolute-domain identity and is used meromorphically only where the functions have been continued. At $v = w = 0$ it simplifies to $L^T(s,\Xi)/L^T(2s,\Xi^2)$, a special slice cancellation which does not remove the general central reciprocal. No finite-height inversion is declared exact without truncation errors; no new contour, reciprocal family moment or analytic saving is proved. Most importantly, this fixed-z coefficient series is not the actual q-dependent joint weight in (40.36).

40.20.5 The fixed-profile remaining-sector diagnostic

Use the fixed smoothstep $s(t) = e^{-1/t}/(e^{-1/t} + e^{-1/(1-t)})$ for $0 < t < 1$, extended by zero and one at the two sides, and set $W(y) = s(8(y-1))s(8(2-y))$. It is smooth, supported in $[1,2]$, and identically one on $[9/8, 15/8]$, independently of D. Take $\nu = 1$ and S the primes above $2, 3$. At $D = 60000, U = 244, H = 3833$, select the actual block $A_1 = 37, A_2 = 7$, literal unit one and primary row generators 1 modulo 3. Complete enumeration gives 44 candidate pairs, with two coprimality and 22 capacity rejections, leaving 20 distinct nonprincipal rows. The first outside-S valuation is one in each row.

Choose $\mathfrak{p}_p = (p, \omega - \lambda_p)$ for

$$(p, \lambda_p) \in \{(37, 10), (43, 6), (61, 13), (307, 17), (313, 98)\}.$$

Their product q has exactly two legal annular column orientations: 97051/96091 and its reversal. Direct small- and long-divisor assignments give $r_U = (0, 2)$, $\mu = (-1, 1)$, $C_U = (0, 2)$ and $A_U = (1, 1)$. Both profile values are exactly one. Twelve orientation/row evaluations are raw zeros. Exact residue-field exponentiation yields

$$\Gamma_1 = -4 - 2\omega, \qquad \Gamma_2 = -2 + 2\omega, \qquad \Gamma_{\mathrm{av}} = -3.$$

Here Γ_{av} is the orientation average. With $a^{AA} = (-1, -1)$ and $\mu(q) = -1$,

$$S_{1,q}^{AA} = -6/60000 = -1/10000, \qquad \sum_r a_r(\Gamma_r - \Gamma_{\mathrm{av}}) = 0.$$

The centered norm is $\sum_r |\Gamma_r - \Gamma_{\mathrm{av}}|^2 = 6$ and $\sum_r |a_r|^2 = 2$, whereas $|\sum_r a_r \Gamma_r|^2 = 36 > 12$. A variance-only Cauchy bound therefore fails even with nonzero variance. It is not a negative full row energy or an asymptotic counterexample.

The corresponding *selected two-column* Gram matrix has diagonal $14, 20$ and the displayed conjugate off-diagonal entries. Its eigenvalues are $17 \pm \sqrt{21}$ and its A quadratic form is 28 before division by D. Removing the diagonal for coprimality gives eigenvalues $\pm 2\sqrt{3}$ and the A form -6. Other original columns and q values have not been suppressed in a full-family claim: this display is a selected-q contribution with its complete stated row block. All finite data and scalar identities have independent exact checks; no finite spectrum or learned label implies a determinant or GRH theorem. The next estimate must retain the signed mean, reciprocal burden and actual coupled q weights, closing the still-open 5/12 gap.

40.21 The signed divisor mean and a complete-column laboratory

The preceding signed-slice estimate loses the sign of the common ideal divisor. We now retain that variable in an exact analytic reduction and in a complete finite computation. Neither supplies the missing 5/12 saving at $H = D^{3/4}$. The computations below use a new fixed profile; they do not fill in the uncomputed columns of the earlier broad-plateau profile.

Let $\mathcal{C}$ be original squarefree good ideal columns in $[D, 2D]$, and let $\mathcal{R}$ be an actual finite literal row block, with nonnegative multiplicities w_u. All shared-prime zeros of the original $\chi_m(u)$ remain. For arbitrary complex coefficient vectors define the linear-first form

$$DQ_1(x, y) = \sum_{u \in \mathcal{R}} w_u \sum_{\substack{m,n \in \mathcal{C} \\ (m,n)=1}} x_m \overline{y_n} \chi_m(u) \overline{\chi_n(u)}. \tag{40.37}$$

The original component is obtained with $x_m = X_U(m)\nu(m)W(Nm/D)$ and the corresponding y_m. On the nonprincipal row blocks used below the original residue term vanishes. Equation (40.37) is a raw coprime form on a generic block; principal rows would still require their separate residue assembly.

For every ideal divisor of an active column put

$$F_d(x;u) = \sum_{m\in\mathcal{C},\ d|m} x_m\chi_m(u), \qquad Z_d(x,y) = \sum_u w_u F_d(x;u)\overline{F_d(y;u)}.$$

The exact identity is

$$DQ_1(x,y) = \sum_d \mu(d) Z_d(x,y). \tag{40.38}$$

There is no extra $\mu(q)$: the vectors already contain the original coefficients. Full divisors $d = m$ are essential to cancel self-pairs. Divisors and squarefreeness refer to ideals, including distinct ideals with the same rational norm.

Proposition 40.11 (A weighted divisor-incidence lift)**.** *Suppose $\lambda_d \geq 0$ is an arbitrary-coefficient bound*

$$\sum_u w_u|F_d(x;u)|^2 \leq \lambda_d \sum_{m\in\mathcal{C},\ d|m} |x_m|^2.$$

With $B(m) = \sum_{d|m}\lambda_d$ and $\|x\|_B^2 = \sum_m B(m)|x_m|^2$, one has

$$|DQ_1(x,y)| \leq \|x\|_B\|y\|_B. \tag{40.39}$$

For a finite literal phase table one may take the exactly computed

$$\lambda_d = E_d := \sum_u w_u \#\{m\in\mathcal{C} : d \mid m,\ \chi_m(u)\neq 0\}.$$

This last choice is a Frobenius certificate, not a new analytic estimate. For $x = t + e$ it gives the finite perturbation bound

$$|Q_1(x,x) - Q_1(t,t)| \leq D^{-1}(2\|t\|_B\|e\|_B + \|e\|_B^2). \tag{40.40}$$

Proof. Insert ideal-divisor inversion in (40.37). Apply row Cauchy to each Z_d and weighted Cauchy to the resulting sum over d. Then $\sum_d \lambda_d\|x_d\|_2^2 = \|x\|_B^2$. The squared Frobenius norm of the actual F_d matrix is exactly E_d. Expand $Q_1(t+e,t+e) - Q_1(t,t)$ to obtain the last assertion. Positivity of the coprime-truncated matrix was never assumed. □

Using an accepted positive-row sieve bound for λ_d only recovers the old exponent up to ideal-divisor factors. It does not estimate the signed sum before the triangle in (40.38).

There is also a genuinely signed scalar expansion. Fix squarefree residual ideals a, b, which may overlap, and an actual row u. Keep the full deleted set $\mathcal{T} = S \cup \mathrm{supp}(abu)$ and set

$$\mathcal{Z}_{U;a,b,\mathcal{T}}(s) = \sum_{\substack{d \text{ squarefree}\\ (d,\mathcal{T})=1}} \frac{\mu(d)A_U(da)A_U(db)}{(Nd)^s}, \qquad \Re s > 1.$$

For four positive cutoff variables put $P_p = 1-(Np)^{-v_1}-(Np)^{-v_2}$ and $Q_p = 1-(Np)^{-w_1}-(Np)^{-w_2}$. The common-divisor Euler factor is $1-(Np)^{-s}P_pQ_p$. Its first-order factorization has four numerator and five denominator zeta factors:

$$\prod_{p\notin\mathcal{T}}(1-(Np)^{-s}P_pQ_p) = \frac{\prod_{i=1}^2\zeta_K^{\mathcal{T}}(s+v_i)\zeta_K^{\mathcal{T}}(s+w_i)}{\zeta_K^{\mathcal{T}}(s)\prod_{i,j=1}^2\zeta_K^{\mathcal{T}}(s+v_i+w_j)}\,\mathcal{H}_{\mathcal{T}}(s;v,w). \tag{40.41}$$

The correction is normally convergent at $\Re s \geq \frac{1}{2} + \eta$, $\Re v_i, \Re w_j \geq 0$, for each fixed $\eta > 0$. This says nothing about zeros or residues of the zeta ratio. Finite-height Perron kernels, with their explicit endpoint/error costs, recover the cutoffs by successive limits.

A direct finite cutoff expansion gives more explicit information:

$$\mathcal{Z}_{U;a,b,\mathcal{T}}(s) = \frac{\mathcal{N}_{U;a,b,\mathcal{T}}(s)}{\zeta_K^{\mathcal{T}}(s)}. \tag{40.42}$$

The numerator is a finite sum over eight nonzero joint short-divisor states, holomorphic on $\Re s > 0$. Uniformly for $\sigma \geq \sigma_0 > 0$,

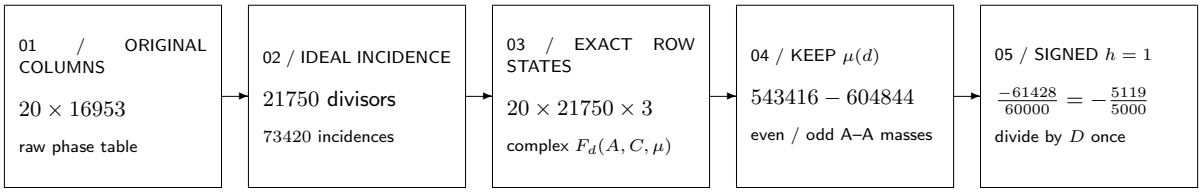
$$|\mathcal{N}_{U;a,b,\mathcal{T}}(\sigma + i\tau)| \ll_{K,\sigma_0,\epsilon} (Na\, Nb)^{\epsilon} U^{4\max(1-\sigma,0)+\epsilon}.$$

The costs near $\sigma = 1/2$ persist. The remaining long state has the Möbius sign, but the eight finite short states cannot be omitted. A fixed-residual reciprocal zeta factor also does not prove an uncancelled pole in the complete coherent sum.

Exact complete-column reference. Choose once $\delta = 1/240000$ and $W_\delta(y) = s((y-1)/\delta)s((2-y)/\delta)$, where s is the smooth step from zero to one. For the finite grid $D \leq 60000$ every strict integer norm node has $W_\delta = 1$; endpoints vanish. Its derivatives cost $O_k(\delta^{-k})$. The three cases have different declared row blocks, not a common asymptotic scaling experiment. They use principal ν, S above $2, 3$, literal class one and nonprincipal actual rows.

D	columns	divisors	rows	S_1^{AA}
144	41	53	5	$-19/36$
576	164	212	11	$-221/288$
60000	16953	21750	20	$-5119/5000$

In the last case the exact even/odd Möbius masses are 543416 and 604844, giving numerator -61428 before division by D. All 339060 raw column–row values, including 47908 zeros, and all nine cross components are retained. In particular 1361 columns have nonsquarefree rational norm while remaining squarefree as ideals. The signed-divisor inspector exposes the actual states and dimensions. These finite negative slices are neither whole-family asymptotic counterexamples nor a positive arithmetic determinant or GRH result.



$D = 60000$, $U = 244$, $H = 3833$, $A_1 = 37$, $A_2 = 7$; literal unit 1, principal ν, S above $2, 3$.
New fixed W_δ, $\delta = 1/240000$; every annular squarefree ideal retained. Finite row block; no asymptotic saving.

Figure 40.1: Exact divisor workflow for the complete D=60000 reference: 16953 columns, 21750 divisor buckets and twenty rows. The fixed study profile and literal class are specified in the text; no asymptotic saving is asserted.

40.22 Proofs and limits of the signed-divisor development

40.22.1 Actual divisor incidence and a finite error certificate

The identity $\mathbf{1}_{(m,n)=1} = \sum_{d|m,\ d|n} \mu(d)$ is an identity of ideal divisors. Expanding the finite sums proves (40.38). When $m = da$ is squarefree, $(d, a) = 1$. If $(d, u) = 1$, multiplication by $\chi_d(u)$ is a rowwise unit phase; if $(d, u) > 1$ it is the original zero. For original $x_m = X_U(m)\nu(m)W(Nm/D)$, precisely $F_d(x; u) = \nu(d)\chi_d(u)T_d^X(u)$ on $(d, u) = 1$, and it is zero otherwise. Thus their row norms agree on the actual restricted support. For general vectors the coefficient x_{da} remains unfactored. No identity $X_U(da) = X_U(d)X_U(a)$ is used. Residual a, b may overlap.

Write $\|x_d\|_2^2 = \sum_{d|m} |x_m|^2$. The hypotheses of Proposition 40.11 give

$$\begin{aligned} |DQ_1(x, y)| &\le \sum_d |Z_d(x, y)| \le \sum_d \lambda_d \|x_d\|_2 \|y_d\|_2 \\ &\le \left(\sum_d \lambda_d \|x_d\|_2^2\right)^{1/2} \left(\sum_d \lambda_d \|y_d\|_2^2\right)^{1/2} = \|x\|_B \|y\|_B. \end{aligned}$$

This is a divisor-incidence lift of positive-row bounds to an indefinite coprime form. It is not an inference from positivity of a larger Gram matrix. In particular $B(m) \le \lambda_{\max} \tau_{\text{ideal}}(m)$, with $\tau_{\text{ideal}}(m) = 2^{\omega(m)}$ on squarefree ideals. The subpolynomial divisor bound recovers the existing exponent; this triangle does not supply the desired signed cancellation.

For the original unweighted two-pivot block ($w_u = 1$), the accepted arbitrary-coefficient inputs at $L = D/Nd \ge 1$ allow

$$\lambda_d \ll_\epsilon (HD)^\epsilon \min\left\{R + \frac{LR}{M} + \frac{L^{2/3}R}{M^{1/3}},\ L + R^2\right\}, \qquad R = A_1A_2, \quad M = \max(A_1, A_2).$$

Their constants are classical-input constants, not computed numbers. Any removal of a d-row mask occurs only inside the positive norm. For $1/2 \le L < 1$, $Na \in [L, 2L]$ permits at most the unit ideal; its operator norm is bounded directly by the actual row measure. For an empty subsequence take $\lambda_d = 0$.

For the fully computable choice $\lambda_d = E_d$, the matrix entries are $\sqrt{w_u}\chi_m(u)$ on d-divisible columns. The squared Frobenius norm is precisely the stated raw nonzero-entry count. It is valid for arbitrary coefficient vectors, not just the saved trajectory. No unknown sieve constant enters that finite certificate. For approximations t_x, t_y with errors $e_x = x - t_x, e_y = y - t_y$,

$$|Q_1(x, y) - Q_1(t_x, t_y)| \le D^{-1}(\|e_x\|_B \|y\|_B + \|t_x\|_B \|e_y\|_B).$$

The AA specialization follows by expanding three terms. To verify it without floating square roots, put $T = \|t\|_B^2, E = \|e\|_B^2$ and $L = D|Q_1(x, x) - Q_1(t, t)| - E$. If $L > 0$, the certificate is the equivalent real inequality $L^2 \le 4TE$; if $L \le 0$ it is immediate. In the saved exact $\mathbf{Z}[\omega]$ computations with rational weights, these are integer/rational checks rather than floating-root tests. These are finite coefficient-error statements. They do not prove a varying-family remainder estimate, spectral positivity or a determinant comparison.

40.22.2 A signed common-divisor Euler product

From here restore ALL original annular squarefree good columns, not an arbitrary subset from the vector lemma, and use the actual unweighted raw row block of Section 40.19. On the stated

nonprincipal blocks it is the corresponding component of the residue-subtracted moment. On a block containing principal rows the raw identity remains valid, but the original principal correction is additional and is not discarded. Expand the exact d identity while keeping its sign. For fixed a, b, u the inner sum is

$$\sum_{\substack{d \text{ squarefree} \\ (d,Sabu)=1}} \mu(d) A_U(da) A_U(db) W(Nd\,Na/D)\overline{W(Nd\,Nb/D)}. \tag{40.43}$$

The exact outer coefficient is $\nu(a)\overline{\nu(b)}\chi_a(u)\overline{\chi_b(u)}$. The residual a, b are individually squarefree but need not be coprime. If their quotient character loses a common prime, that prime remains in $\mathcal{T} = S \cup \operatorname{supp}(abu)$ and in every original zero. The common d character cancels only to $\mathbf{1}_{(d,u)=1}$.

For $\Re s > 1$ the series $\mathcal{Z}$ is absolutely convergent, with coefficient majorant $3^{\omega(a)+\omega(b)}9^{\omega(d)}$, uniformly in U. Use four positive Perron variables. Write $\mathcal{E}_{\mathcal{T}}(s; v, w) = \prod_{p \notin \mathcal{T}}(1-(Np)^{-s}P_pQ_p)$. The fixed residual prefactor is $P_a(v)Q_b(w) = \prod_{p|a} P_p(v) \prod_{p|b} Q_p(w)$; a common prime of a, b contributes both factors. The common d prime has nine joint cutoff positions and the sign $\mu(p) = -1$, giving local factor $1 - zPQ$ with $z = (Np)^{-s}$, $\alpha_i = (Np)^{-v_i}$ and $\beta_j = (Np)^{-w_j}$. Thus the exact correction in (40.41) is

$$H_p = \frac{(1 - zPQ)\prod_{i=1}^{2}(1 - z\alpha_i)\prod_{j=1}^{2}(1 - z\beta_j)}{(1 - z)\prod_{i,j=1}^{2}(1 - z\alpha_i\beta_j)}. \tag{40.44}$$

The linear coefficient of numerator and denominator is $-1 - \sum_{i,j} \alpha_i\beta_j$, fixing all nine zeta signs. At all four auxiliary variables zero the product is $1/\zeta_K^{\mathcal{T}}(s)$ and $H_p = 1$. At $v_2 = w_2 = 0$ it is $1/\zeta_K^{\mathcal{T}}(s + v_1 + w_1)$, again with $H_p = 1$. These are generating-function checks, not finite-cutoff identifications.

For $\Re s \geq 1/2 + \eta$, $\Re v_i, \Re w_j \geq 0$, the degree-five numerator and denominator of (40.44) have equal constant and linear coefficients. The sums of absolute coefficient majorants in degrees two through five are at most 146 and 26. Since $|PQ| \leq 9$ and $|\alpha_i|, |\beta_j| \leq 1$,

$$|H_p - 1| \leq C_\eta (Np)^{-1-2\eta}, \qquad C_\eta = \frac{172}{(1 - 7^{-1/2-\eta})^5}. \tag{40.45}$$

Indeed the five denominator factors have modulus at least $1 - |z|$; good prime ideal norms are at least seven. Ideal counting proves normal convergence, uniform in deleted primes and vertical phases, and

$$|\mathcal{H}_{\mathcal{T}}| \leq \exp\left(C_\eta \sum_p (Np)^{-1-2\eta}\right).$$

Local correction factors can vanish; no inverse-correction bound is asserted. Normal convergence controls neither the four numerator nor five reciprocal zeta factors in the critical region. Their poles, zeros and crossed residues cannot be suppressed.

40.22.3 Finite Perron heights and the exact eight-state numerator

Set $V = \lfloor U \rfloor + 1/2$ and $\Delta_V = \min_{n \geq 1} |\log(V/n)| \geq 1/(2V+1)$. For four finite vertical heights T_j on positive real lines c_j, let $I_T(s)$ be the fourfold integral of $P_aQ_b\mathcal{E}_{\mathcal{T}}(s; v, w)$ against $\prod_j V^{z_j}\, dz_j/(2\pi i z_j)$. In the initial half-plane $\sigma = \Re s > 1$, finite-height Fubini is justified by the absolute placement majorant. Put

$$\begin{aligned} A_{\mathrm{abs}}(\sigma, c) = {} & \prod_{p|a}(1 + q^{-c_1} + q^{-c_2}) \prod_{p|b}(1 + q^{-c_3} + q^{-c_4}) \\ & \cdot \prod_{p \notin \mathcal{T}} \{1 + q^{-\sigma}(1 + q^{-c_1} + q^{-c_2})(1 + q^{-c_3} + q^{-c_4})\}, \quad q = Np. \end{aligned}$$

Then

$$|I_T(s) - \mathcal{Z}_{U;a,b,\mathcal{T}}(s)| \le V^{\sum c_j} A_{\mathrm{abs}}(\sigma, c) \left\{ \prod_{j=1}^{4} \left(1 + \frac{2}{\pi T_j \Delta_V} \right) - 1 \right\}, \tag{40.46}$$

and $A_{\mathrm{abs}} \le 3^{\omega(a)+\omega(b)} \zeta_K(\sigma)^9$. For one short integer norm n, the indicator is at most $(V/n)^c$, and the truncated Perron error is at most $2(V/n)^c/(\pi T \Delta_V)$. Expand the difference of four products and sum every nonempty error subset to prove (40.46). Consequently successive Perron limits recover the exact cutoffs. The half-integer gap also gives a height-uniform $C_U(V/n)^c$ bound, allowing dominated convergence in the initial absolutely convergent series. Four infinite Perron integrals are not declared absolutely convergent or interchanged silently with Mellin inversion.

There is an entirely finite alternative. Partition $a = a_0 a_1 a_2$ and $b = b_0 b_1 b_2$, internally coprime in each column. Cross-column overlaps remain allowed. A common d prime occupies one state $(i, j) \in \{0, 1, 2\}^2$. Separate its $(0, 0)$ part e from eight pairwise coprime squarefree atomic ideals h_{ij} avoiding $\mathcal{T}$, and let h be their product. Define

$$h_i^L = \prod_{j=0}^{2} h_{ij} \ (i = 1, 2), \qquad h_j^R = \prod_{i=0}^{2} h_{ij} \ (j = 1, 2).$$

An atomic h_{ij} with both indices nonzero belongs to one short factor in each column. These four short factors must not be forced globally disjoint. Let $\mathcal{A}_U$ comprise precisely these tuples satisfying $N(a_i h_i^L) \le U$ and $N(b_j h_j^R) \le U$ for $i, j = 1, 2$. The numerator in (40.42) is exactly

$$\mathcal{N}_{U;a,b,\mathcal{T}}(s) = \sum_{\mathcal{A}_U} \frac{\mu(a_1 a_2)\mu(b_1 b_2)\mu(h_{11}h_{12}h_{21}h_{22})}{(Nh)^s} \prod_{p \mid h} (1 - (Np)^{-s})^{-1}. \tag{40.47}$$

At a common prime the sign is $(-1)^{1+\mathbf{1}_{i>0}+\mathbf{1}_{j>0}}$. It is negative for $(0, 0)$, positive for the four single-short states, and negative for the four double-short states. Summing the remaining squarefree e, coprime to $\mathcal{T}h$, gives $1/\zeta_K^{\mathcal{T}}(s)$ times the local product in (40.47). This proves the exact identity, including its sign.

Multiplying the four cutoff inequalities yields $Nh \le U^4$; double states are counted twice in that product. Hence the numerator is finite and holomorphic on $\Re s > 0$. At $U = 1$ it equals one: this boundary is not a high-window counterexample or a global pole obstruction. For $\sigma \ge \sigma_0 > 0$ and every $\epsilon > 0$,

$$|\mathcal{N}_{U;a,b,\mathcal{T}}(\sigma + i\tau)| \ll_{K,\sigma_0,\epsilon} (Na\, Nb)^{\epsilon} U^{4\max(1-\sigma,0)+\epsilon}. \tag{40.48}$$

There are at most $3^{\omega(a)+\omega(b)}$ residual partitions and $8^{\omega(h)}$ atomic placements at fixed h. The finite local product is $\ll_{\sigma_0,\epsilon} (Nh)^{\epsilon}$. Apply the ideal-divisor bound and ideal counting up to U^4, using smaller internal exponents; a logarithm at the transition is absorbed in U^{ϵ}. Uniformity as $\sigma_0 \to 0$ is not claimed. For $\sigma = 1/2 + \eta$ with $0 < \eta < 1/2$, the old-type cutoff cost is $U^{2-4\eta+\epsilon}$, not a new saving.

40.22.4 A uniform common-profile Mellin embedding of the actual mean

For residual a, b put $M = \max(Na, Nb)$ and $\varrho = \min(Na, Nb)/M$. At $\varrho \le 1/2$ the product of the two profile values vanishes, including equality because of endpoint vanishing. Otherwise put

$$\Phi_{\varrho}(t) = W(t)\overline{W(\varrho t)}$$

when $Na \ge Nb$, and use its conjugate for the reversed orientation. It is supported in $[1/\varrho, 2] \subset [1, 2]$. With $M_k(W) = \max_{j \le k} \|(t\, d/dt)^j W\|_\infty$,

$$|\widehat{\Phi}_\varrho(\sigma + i\tau)| \le C_{I,k} M_k(W)^2 (1 + |\tau|)^{-k} \tag{40.49}$$

uniformly for σ in any fixed compact strip I and all $\varrho \in [1/2, 1]$. Leibniz and log-coordinate integration by parts prove this bound; no ratio-dependent change of W is made. The transform is entire. For $c > 1$, ordinary Mellin inversion after the finite numerator identity gives the exact scalar (40.43) as

$$\frac{1}{2\pi i} \int_{\Re s = c} \widehat{\Phi}_\varrho(s) (D/M)^s \frac{\mathcal{N}_{U;a,b,\mathcal{T}}(s)}{\zeta_K^{\mathcal{T}}(s)}\, ds. \tag{40.50}$$

This integral is vertically absolutely convergent in its initial half-plane. The original profile forces $M \le 2D$, so the residual a, b and actual row sums are finite.

Keep the full local deletion factor

$$\frac{1}{\zeta_K^{\mathcal{T}}(s)} = \frac{1}{\zeta_K(s)} \prod_{p \in \mathcal{T}} (1 - (Np)^{-s})^{-1}.$$

At fixed $\sigma_0 > 0$ it costs $\ll_{S,\sigma_0,\epsilon} (N \operatorname{rad}(abu))^\epsilon$, hence at most $(HD^2)^\epsilon$ on actual support. This estimates the finite mask dependence, not the central reciprocal. Multiplying (40.50) by every original outer coefficient and summing the actual rows and residuals gives

$$DS_1^{AA} = \frac{1}{2\pi i} \int_{\Re s = c} \frac{D^s \mathcal{A}_{D,H,U,W}(s)}{\zeta_K(s)}\, ds. \tag{40.51}$$

Explicitly, with each profile orientation retained,

$$\mathcal{A}_{D,H,U,W}(s) = \sum_{u \in \mathcal{R}} \sum_{\substack{a,b \text{ squarefree,good} \\ Na, Nb \le 2D,\ \varrho > 1/2}} \nu(a)\overline{\nu(b)} \chi_a(u) \overline{\chi_b(u)}\, M^{-s}\, \widehat{\Phi}_\varrho(s) \cdot \mathcal{N}_{U;a,b,\mathcal{T}}(s) \prod_{p \in \mathcal{T}} (1 - (Np)^{-s})^{-1}.$$

This is a *finite coherent sum*, not an independent marginal moment or a positive sum. All raw zeros remain in its outer coefficients. For fixed finite D, H, U it is holomorphic on $\Re s > 0$ and rapidly decreasing on fixed vertical strips there, with constants depending on those finite parameters. No uniform target estimate for it is supplied. This is an exact signed embedding, not a zero-location theorem.

40.22.5 A nonzero short-state correction and the unproved step

An actual annular control uses good prime ideals of norms $7, 13, 19, 31, 43$ with primary generators $(1, 3), (4, 3), (-2, 3), (1, 6), (7, 6)$ in the $1, \omega$ basis. Take $D = 1500, U = 25$, $d = p_7$, $a = p_{13}p_{19}$, $b = p_{13}p_{31}$ and the nonprincipal row $u = p_{43}$ in the pure block $A_1 = 37, A_2 = 1, H = 241$, literal class one. The full raw supports are disjoint from u, and $N(da) = 1729, N(db) = 2821$ lie in the annulus. A single fixed smooth profile with plateau $[1.1, 1.9]$ equals one at both nodes. Direct assignments give $A_U(a) = A_U(b) = -1$, $A_U(da) = 1$, $A_U(db) = -1$. The actual signed d coefficient is $+1$. The $(0, 0)$ state alone would give -1; states $(1, 0)$ and $(2, 0)$ each contribute $+1$. Dropping all short states therefore misses a nonzero $e = 1$ correction. This illustrates the new eight-state identity, not a new discovery of coefficient nonmultiplicativity.

The original pair has gcd p_7p_{13}. Its contributions across $d = 1, p_7, p_{13}, p_7p_{13}$ cancel exactly. Thus a fixed-residual reciprocal does not prove an uncancelled pole or an obstruction in the complete coherent mean. The missing step is to estimate that full mean by $DH(HD)^{\epsilon}$, retaining fixed-profile/seminorm dependence, raw masks and conductor/ray/capacity restrictions. Scalar Mertens cancellation in the long state, a normal correction product, or an absolute cutoff numerator bound does not prove it. Principal and short assembly, independent positive determinant/zero-location bridges and separate Dirichlet, Hecke, Dedekind, elliptic and Artin obligations remain open. No holomorphy or desired zero location is assumed to close them.

40.22.6 Exact arithmetic and source-bound computational scope

The evaluator streams each actual row and accumulates original $x_m\chi_m(u)$ into every ideal-divisor bucket $d \mid m$. It then forms all nine cross products for A_U, C_U, μ and sums with $\mu(d)$. Write $n_{\mathrm{col}} = |\mathcal{C}|$, $I = \sum_m \tau_{\mathrm{ideal}}(m)$, K for the distinct divisors and r for the listed rows. This bucket stage costs $O(r(I + K))$ arithmetic operations with a fixed three channels. Its streaming storage is $O(K)$ plus incidences and either a streamed row or separately retained phase table. Character construction, factorization and integer bit lengths are additional costs, not declared free. For coefficients bounded by C, bucket coordinates are $O(n_{\mathrm{col}}C)$, products $O(n_{\mathrm{col}}^2C^2)$ and accumulated values $O(rn_{\mathrm{col}}^2C^2)$ for unit row weights. For compressed integer multiplicities replace r in this bit-size bound by $\sum_u w_u$ and account for weight multiplication.

For $D = 60000$, the actual phase table has shape 20×16953; the incidence has 73420 nonzeros over 21750 divisor buckets, and F_d has $20 \times 21750 \times 3$ complex states. There are 271688516 ordered coprime column pairs. The naive all-pair row loop would visit 5748084180 pairs and was *not executed* at this size. This is an operation count, not an unexecuted timing benchmark. Independent direct pair evaluation covers the two complete small families; the large family is checked linearly from literal field arithmetic and divisor-poset inversion.

The exact large results also include

$$S_1^{CC} = \frac{661}{7500}, \qquad S_1^{C\mu} = \frac{13931}{30000}, \qquad S_1^{\mu\mu} = -\frac{229}{1250}.$$

For the ordered vectors (A_U, C_U, μ) the full pairing table is

$$\frac{1}{30000}\begin{pmatrix} -30714 & -11287 & 19427 \\ -11287 & 2644 & 13931 \\ 19427 & 13931 & -5496 \end{pmatrix}.$$

This is the table of three original coefficient vectors, not a spectral carrier for GRH. The conjugate μC entry and the AA identity retain their actual linear-first convention. All three saved computations use source v1. A separate v2 helper fixes its unused $N = U = 1$ high-window assertion; every one of the 17158 executed columns has $N > U$, so no accepted row/table or source snapshot was silently replaced. The fixed-profile flat-node implementation refuses requests above its stated $D \le 60000$ certificate. Neither these three different finite blocks nor their measured runtimes imply an asymptotic saving.

40.23 A target-sized budget for rough-prime masks

The actual signed divisor mean admits a useful quantitative simplification: the rough-prime coprimality mask can be restored with an explicit correction bound. The remaining main term still retains the Möbius sign and the coherent row mean; it is not estimated by this result.

Work over $\mathbb{Z}[\omega]$. Fix a finite S containing the primes above $2, 3$, a unitary multiplicative ν on good ideals, and one common complex profile W supported on $[1, 2]$, smooth and zero at both endpoints. Put $B = \|W\|_\infty$ and assume

$$1 \le U, \qquad U^2 \le D, \qquad 2D \le 7U^2, \qquad H \ge 1. \tag{40.52}$$

Let $\mathcal{R}$ be the actual finite family of nonzero literal rows, with original weights $w_u \ge 0$, $1 \le Nu \le H$, and $R_w = \sum_u w_u$. All original internal squarefree/coprime conditions, unit and S-ray classes, capacity and sixth-factor masks remain in this family. Write S_1^{AA} for the raw form (40.37) with $x_m = A_U(m)\nu(m)W(Nm/D)$, where

$$A_U(g) = \sum_{\substack{xy|g,\ (x,y)=1\\ Nx\le U,\ Ny\le U}} \mu(x)\mu(y). \tag{40.53}$$

Here the columns in (40.37) are the COMPLETE original good squarefree annulus $[D, 2D]$, with the common W as its norm cutoff and the original full-good-ideal/ν, S formulation. No selected-column indicator or additional column-ray filter is allowed in this reduction; all actual row unit/ray/capacity filters remain. Principal-row residues, if present, require their separate assembly. For the intended $A_1 > 1$ blocks the defining conductor of ν is supported in S, and the rows are nonprincipal.

Let f range over good squarefree U-smooth ideals, put $F = Nf$, and set

$$T_f(t; u) = \sum_{\substack{a \text{ good squarefree}\\ (a,f)=1}} A_U(fa)\nu(a)\chi_a(u)W(FtNa/D). \tag{40.54}$$

Here $\chi_a(u) = 0$ on $(a, u) > 1$. For a prime ideal p, let $T_f^{(p)}(t; u)$ impose the additional condition $(a, p) = 1$. The smooth factor f is distinct from the original column-pair gcd sector $h = 1$. Define the following *unnormalized* expressions:

$$K_0 = \sum_u w_u \sum_{\substack{f \text{ good SF, } U\text{-smooth}\\ (f,u)=1}} \mu(f)|T_f(1; u)|^2, \tag{40.55}$$

$$K_T = \sum_u w_u \sum_{\substack{f \text{ good SF, } U\text{-smooth}\\ (f,u)=1}} \mu(f) \sum_{\substack{p\notin S,\ Np>U\\ p\nmid u}} |T_f^{(p)}(Np; u)|^2, \tag{40.56}$$

$$K_S = \sum_u w_u \sum_{\substack{f \text{ good SF, } U\text{-smooth}\\ (f,u)=1}} \mu(f) \sum_{p\notin S,\ Np>U} |T_f(Np; u)|^2. \tag{40.57}$$

Throughout, p denotes a prime ideal. None of these expressions is declared positive, since the $\mu(f)$ signs remain.

The exact decomposition of the common ideal divisor $d = fe$ has at most one rough prime when the residual pair is nonunit. The unit residual pair also permits two distinct rough primes, necessarily with $f = 1$. Its exact correction is

$$C_2 = \sum_{\substack{\{p,q\} \text{ unordered, } p\ne q\\ p,q\notin S,\ Np,Nq>U}} |W(NpNq/D)|^2 \sum_{\substack{u\in\mathcal{R}\\ (u,pq)=1}} w_u. \tag{40.58}$$

Conjugate primes of equal rational norm are included. One has

$$DS_1^{AA} = K_0 - K_T + C_2. \tag{40.59}$$

In K_S, terms with $p \mid a$ or $p \mid u$ are explicitly auxiliary: fpa can fail to be squarefree. They use $A_U(fa)$ as written, not a new original column or a substitution for $A_U(fpa)$.

Theorem 40.12 (Explicit rough-prime mask budget)**.** *Put* $\kappa_U(u) = \#\{p \notin S : p \mid u,\ Np > U\}$ *and* $\Delta = (K_S - K_T)/D$*. Under* (40.52)*,*

$$|\Delta| \le B^2 \left(229376 \sum_u w_u \kappa_U(u) + 2048 R_w \right), \tag{40.60}$$

$$0 \le C_2/D \le 1792 B^2 R_w. \tag{40.61}$$

Consequently

$$S_1^{AA} = \frac{K_0 - K_S}{D} + E, \tag{40.62}$$

$$|E| \le B^2 \left(229376 \sum_u w_u \kappa_U(u) + 3840 R_w \right). \tag{40.63}$$

If $H \le D^{3/4}$*, then every row has* $\kappa_U(u) \le 1$*, and in particular*

$$|E| \le 233216 B^2 R_w \le 2^{18} B^2 R_w. \tag{40.64}$$

Only the rough-prime deletion has been restored; the smooth-divisor mask, literal row family and original coefficients remain. The explicit bound uses the exact restricted identity

$$A_U(g) = \mu(g)(2\mathbf{1}_{Ng \le U} - 1) \quad (Ng \le 7U,\ g \text{ good squarefree}).$$

Every active term of $T_f(Np; u)$ has $N(fa) < 7U$, hence $|A_U(fa)| = 1$ there. This is not a shrinkage or proxy for the whole original coefficient family. Only absolute correction bounds use it; the signed coefficients in the clean main remain unchanged.

For general H, one has $\kappa_U(u) \le 2\log(2H)/\log(2U)$, also at $U = 1$. For an actual two-pivot block with $R_w \ll A_1 A_2 \le H$ and $H \le D^{3/4}$, (40.64) gives an $O(B^2 H)$ error with no divisor-power or profile-derivative loss. The remaining target problem for this raw A–A slice is the clean signed main $(K_0 - K_S)/D$. It has not been bounded here; the 7/6 envelope and missing 5/12 improvement for the complete original remainder are unchanged. The argument neither deletes a coherent mean nor treats the coprime-truncated form as positive.

Three exact finite controls. These use principal ν, S above $2, 3$, literal unit class one and complete original good squarefree annuli. The first two row variables are squarefree, good and coprime and may include the unit ideal; all other factors equal one.

D	U	H	A_1	A_2	columns	rows
200	10	53	13	1	52	5
512	16	107	19	1	139	7
900	30	384	7	7	250	2

Put $\eta_0(t) = \exp(-1/t)$ for $t > 0$ and $\eta_0(t) = 0$ for $t \le 0$, and define

$$s(t) = \frac{\eta_0(t)}{\eta_0(t) + \eta_0(1 - t)}.$$

Choose once $\delta = 1/4096$ and $W_\delta(t) = s((t-1)/\delta)s((2-t)/\delta)$. For integer $D \le 1024$, strict integer norm nodes have weight one and endpoints have weight zero; its derivatives cost $O_k(4096^k)$. The following numbers are RAW, before division by D:

D	K_0	K_S	K_T	E_{row}	E_{res}	C_2	DS_1^{AA}
200	339	235	209	20	6	21	151
512	366	781	711	48	22	89	−256
900	436	410	366	0	44	28	98

In every case $K_S - K_T = E_{\mathrm{row}} + E_{\mathrm{res}}$ and $DS_1^{AA} = K_0 - K_T + C_2$. The displayed nonnegative values of $E_{\mathrm{row}}, E_{\mathrm{res}}$ are finite observations; no general nonnegativity is assumed for either signed correction. Only C_2 is nonnegative by definition. The first two capacities are $\lfloor D^{3/4} \rfloor$. The third $H = 384$ is a declared noncritical fixture capacity, not $\lfloor 900^{3/4} \rfloor$; both of its rows have $\kappa_U = 0$. All ideal and raw-zero masks, unit residual states and explicitly auxiliary non-squarefree p^2 terms are retained. The exact control summary records the scopes and exact fractions after one division by D. These are finite identities, not a proof or numerical fit of the analytic bounds, and do not estimate the signed clean main.

40.24 Proof of the rough-prime mask budget

40.24.1 The common ideal divisor and the exact rough part

Here (40.37) uses the complete original good squarefree annulus and common W, without an additional selected-column or column-ray indicator. The actual row filters are unchanged. The identity $\mathbf{1}_{(m,n)=1} = \sum_{d \mid m,\ d \mid n} \mu(d)$ in (40.37) is an identity of ideal divisors. Write $m = da, n = db$. The residual ideals a, b are squarefree but may overlap; squarefreeness of the original columns requires $(d, ab) = 1$. On $(d, u) = 1$ the original common phases satisfy

$$|\nu(d)|^2 \chi_d(u) \overline{\chi_d(u)} = 1.$$

On $(d, u) > 1$ the product is the original raw zero. Hence the full deleted set is $\mathcal{T} = S \cup \mathrm{supp}(abu)$, including residual primes where $\chi_a \overline{\chi_b}$ might become imprimitive. With

$$F_{a,b}(x) = W(xNa/D)\overline{W(xNb/D)}, \qquad M = \max(Na, Nb), \quad \alpha = \min(Na, Nb),$$

the inner signed sum is

$$\sum_{\substack{d \ \mathrm{SF} \\ (d,\mathcal{T})=1}} \mu(d) A_U(da) A_U(db) F_{a,b}(Nd). \tag{40.65}$$

If its profile is nonzero, then

$$D/\alpha < Nd < 2D/M. \tag{40.66}$$

All endpoints have zero profile value. In particular the profile is identically zero if $\alpha \le M/2$. No independent marginal row family or changed profile has been substituted.

Factor $d = fe$ uniquely, with f squarefree U-smooth and e squarefree with every prime norm greater than U. Whenever ez is squarefree,

$$A_U(ez) = A_U(z). \tag{40.67}$$

Indeed neither short divisor in (40.53) can contain a prime of e; deleting e preserves the two cutoffs and both Möbius signs in a bijection of the original assignments. There is no factor $\mu(e)$ in (40.67). This invariance is specific to A_U; it does not hold unchanged for the other coefficient channels. The values $A_U(fa), A_U(fb)$ are not factorized.

If $M > 1$, goodness gives $M \geq 7$. From (40.52) and (40.66), $Nd \leq 2D/M \leq U^2$. Thus e is either 1 or one prime ideal, and (40.65) is exactly

$$\sum_{\substack{f \text{ good SF, } U\text{-smooth} \\ (f,\mathcal{T})=1}} \mu(f) A_U(fa) A_U(fb) \left(F_{a,b}(Nf) - \sum_{\substack{p \notin \mathcal{T} \\ Np > U}} F_{a,b}(NfNp) \right). \tag{40.68}$$

The rough part here belongs to the *common divisor* d; the full columns can have additional rough primes in a or b.

If $M = 1$, then $a = b = 1$. Three rough prime ideals would have norm product strictly greater than $7U^2 \geq 2D$: two contribute more than U^2, and the third good prime has norm at least 7. Two rough primes are possible, but then a nonunit f would similarly give $Nf\,Ne > 7U^2 \geq 2D$. Hence that case has $f = 1$ only. Its sign is $\mu(pq) = 1$ and its coefficient is $A_U(pq) = A_U(1) = 1$. Summing this case over the unchanged literal rows gives (40.58); summing all other cases of (40.68) over a, b gives the completed squares in (40.55)–(40.56). This proves (40.59). The unit ideal among residuals and conjugate split primes must both be retained. The condition $f = 1$ is not a termwise assertion that the original pair has gcd 1: the Möbius expansion cancels noncoprime original pairs across its divisor sectors.

40.24.2 An exact disjoint error identity

We restore only $(p, abuS) = 1$ to $p \notin S$. In particular the conditions $(f, abuS) = 1$ and every raw $\chi_a(u)$ remain in the two residual sums. The full deleted union has the disjoint partition

$$\mathbf{1}_{p|abu} = \mathbf{1}_{p|u} + \mathbf{1}_{p\nmid u}\mathbf{1}_{p|a \text{ or } p|b}. \tag{40.69}$$

Therefore $K_S - K_T = E_{\text{row}} + E_{\text{res}}$, where the errors are *unnormalized*:

$$E_{\text{row}} = \sum_u w_u \sum_{\substack{f \text{ good SF, } U\text{-smooth} \\ (f,u)=1}} \mu(f) \sum_{\substack{p \notin S,\ Np > U \\ p|u}} |T_f(Np; u)|^2, \tag{40.70}$$

$$E_{\text{res}} = \sum_u w_u \sum_{\substack{f \text{ good SF, } U\text{-smooth} \\ (f,u)=1}} \mu(f) \sum_{\substack{p \notin S,\ Np > U \\ p\nmid u}} \left(|T_f(Np; u)|^2 - |T_f^{(p)}(Np; u)|^2 \right). \tag{40.71}$$

The two errors are signed; their bounds below use absolute values, and neither is assumed nonnegative. At $p \mid u$, all residuals divisible by p already have raw character zero. This is consistent with the full square in (40.70); it does not make that square zero. These formulas keep the complete row/residual union without double counting.

Suppose a nonzero omitted residual has $p \mid a$, and write $a = pc$. Its profile requires $Nf\,(Np)^2 Nc < 2D$. If fc is nonunit, then

$$Nf\,(Np)^2 Nc > 7U^2 \geq 2D,$$

a contradiction. Thus necessarily $f = c = 1$ and $a = p$. This is a support statement about the explicitly auxiliary extension; the formal column $fpa = p^2$ is not an original squarefree column. With $P = Np$, set

$$z_p(u) = \nu(p)\chi_p(u) W(P^2/D), \qquad T_p(u) = T_1(P; u). \tag{40.72}$$

Here $A_U(p) = 1$, since $P > U$. The difference $T_f - T_f^{(p)}$ vanishes unless $f = 1$, when it equals z_p. Consequently

$$E_{\text{res}} = \sum_u w_u \sum_{\substack{p \notin S,\ Np > U \\ p\nmid u}} \left(2\,\mathrm{Re}(T_p(u)\overline{z_p(u)}) - |z_p(u)|^2 \right). \tag{40.73}$$

The subtraction $-|z_p|^2$ is the exact intersection $p \mid a$ and $p \mid b$; omitting it would count that intersection twice. Complex profiles and all remaining literal phases are allowed. If $z_p \neq 0$, then

$$\sqrt{D} < P < \sqrt{2D}. \tag{40.74}$$

The condition $P > U$ is automatic here from $U^2 \leq D$.

40.24.3 Elementary ideal and coefficient estimates

We give all counting inputs; no prime distribution theorem or Mertens estimate is needed. The Eisenstein norm is Euclidean. After rounding both real coordinates of a complex quotient in the basis $1, \omega$, the error $s + t\omega$ has $|s|, |t| \leq 1/2$ and norm at most $3/4 < 1$. A least-norm nonzero element of any ideal therefore generates it by Euclidean division. Multiplication by $a + b\omega$ has determinant $a^2 - ab + b^2$, giving the principal ideal norm. Since $a^2 - ab + b^2 \geq (a^2 + b^2)/2$, counting all possible generators, with harmless overcounting by units, proves for $X \geq 1$ that

$$\#\{a : Na \leq X\} \leq (2\sqrt{2X} + 1)^2 < 16X. \tag{40.75}$$

An annulus $L < Na < 2L$ therefore contains at most $32L$ ideals when $2L > 1$. If $2L \leq 1$ its profile contribution is zero, including the unit endpoint when $2L = 1$. This proves the needed uniform bound even when $1/2 < L < 1$; the unit ideal must not be dropped in that range.

There is an exact coefficient identity on the restricted support:

$$A_U(g) = \mu(g)(2\mathbf{1}_{Ng \leq U} - 1) \quad (g \text{ good squarefree, } Ng \leq 7U). \tag{40.76}$$

Every proper divisor of a nonunit good g has norm at most $Ng/7 \leq U$. If $Ng \leq U$, all ternary assignments are allowed and their sum is $\prod_{p|g}(1 - 1 - 1) = \mu(g)$. If $Ng > U$, only the assignments $(x, y) = (g, 1), (1, g)$ are omitted; each has sign $\mu(g)$, leaving $-\mu(g)$. The unit ideal gives $A_U(1) = 1$ and is included. No approximation or multiplicativity of the cutoff coefficient is used.

In an active term of (40.54), $P = Np > U$ gives

$$N(fa) < 2D/P < 2D/U \leq 7U.$$

Therefore $|A_U(fa)| = 1$ exactly there. This statement concerns only the rough-prime support, not the entire original coefficient family. With $L = D/(FP)$, the ideal count and $|\chi_a(u)| \leq 1$ now give

$$|T_f(P; u)| \leq 32B\,\frac{D}{FP}. \tag{40.77}$$

The same statement holds if the sum is empty, and covers $L < 1$ by the preceding endpoint discussion. A dyadic use of (40.75) gives

$$\sum_f \frac{1}{(Nf)^2} \leq \sum_{j \geq 0} 16\, 2^{j+1} 2^{-2j} = 64, \tag{40.78}$$

where the left side may even include all ideals. The smooth squarefree restriction only decreases this bound.

40.24.4 The normalized row-mask budget

Apply triangle only to (40.70), use (40.77), and then (40.78). The raw square contributes D^2/P^2; dividing by D once gives

$$\frac{|E_{\mathrm{row}}|}{D} \le 65536B^2 \sum_u w_u \sum_{\substack{p\mid u,\ p\notin S\\ Np>U}} \frac{D}{(Np)^2}. \tag{40.79}$$

By (40.52), $D/(Np)^2 \le D/U^2 \le 7/2$. Let $\kappa_U(u)$ count the distinct good rough prime ideals dividing u. Each $P = Np$ is at least 7 and greater than U, so $P^2 > 7U \ge 2U$. The complete ideal norm of the literal row therefore gives

$$\kappa_U(u) \le \frac{2\log(Nu)}{\log(2U)} \le \frac{2\log(2H)}{\log(2U)}. \tag{40.80}$$

The denominator is positive also at $U = 1$; unit rows have $\kappa_U = 0$. All sixth-factor divisors remain in this bound, and no rational-norm gcd is substituted for an ideal mask. Using $D/(Np)^2 \le 7/2$ in (40.79) gives the sharper form

$$\frac{|E_{\mathrm{row}}|}{D} \le 229376B^2 \sum_u w_u \kappa_U(u). \tag{40.81}$$

The logarithmic bound (40.80) is available for arbitrary H.

40.24.5 The residual intersection budget

Use (40.73), $|z_p| \le B$, and (40.77) at $f = 1$. After the single division by D,

$$\frac{|E_{\mathrm{res}}|}{D} \le B^2 R_w \sum_{\sqrt{D}<Np<\sqrt{2D}} \left(\frac{64}{Np} + \frac{1}{D}\right). \tag{40.82}$$

Here absolute values bound only the correction; the exact identity (40.73) retains its original phases. Since $D \ge 1$ and $Np \le \sqrt{2D} \le 2D$, one has $1/D \le 2/(Np)$. Also

$$\sum_{\sqrt{D}<Np<\sqrt{2D}} \frac{1}{Np} \le 16\sqrt{2} \tag{40.83}$$

by (40.75). Thus

$$|E_{\mathrm{res}}|/D \le 1056\sqrt{2}\, B^2 R_w \le 2048B^2 R_w.$$

Together with (40.81), this proves (40.60).

40.24.6 The exact unit-residual correction and the clean main

In (40.58), each contributing pair has $P, Q > U$ and $PQ \le 2D$. Hence both prime norms are less than $2D/U$. There are at most $32D/U$ such prime ideals by (40.75), so the number of unordered distinct pairs is at most $512D^2/U^2$. Only inside this *nonnegative* expression enlarge the masked row count to R_w and the profile to B^2. Thus

$$0 \le \frac{C_2}{D} \le 512\frac{D}{U^2} B^2 R_w \le 1792B^2 R_w,$$

proving (40.61). Conjugate primes of equal rational norm remain included; no rational-squarefree restriction or new diagonal exclusion is imposed. This is a bookkeeping bound for the exact correction, not an oscillatory saving or a lower bound for the full signed slice. Other residual sectors can cancel it.

Now (40.59) gives (40.62) with $E = \Delta + C_2/D$, and the explicit bounds give (40.63). Suppose $H \le D^{3/4}$. If two distinct good rough primes divided a row, then $H \ge Nu \ge (Np)(Nq) \ge 49$, but also

$$H \ge Nu \ge (Np)(Nq) > U^2 \ge 2D/7.$$

Combining with $H \le D^{3/4}$ gives $D^{1/4} < 7/2$ and hence $H < (7/2)^3 = 343/8 < 49$, a contradiction. Thus $\kappa_U(u) \le 1$ at every scale in this capacity range. Substitution in (40.63) gives $|E| \le 233216B^2R_w \le 2^{18}B^2R_w$, proving (40.64). This is an exact endpoint argument, not an asymptotic approximation.

For a two-pivot block, counting each of its two dyadic ideal variables by (40.75) gives $R_w \ll A_1A_2$ when the original fixed unit classes and multiplicities are bounded. Internal coprimality and capacity reduce that count; grouping literal fibers preserves total multiplicity. Under $A_1A_2 \le H \le D^{3/4}$ the correction is therefore $O(B^2H)$. The exact local coefficient identity and these correction bounds do not estimate the remaining signed main $(K_0 - K_S)/D$. Its original $A_U(fa)$, coherent rows, common fixed profile and Möbius mean remain the analytic obligation; no new global exponent follows.

40.24.7 Finite control scope

The tables in the shared core retain complete original squarefree ideal columns and raw character zeros. Their residual-prime extension is a separate auxiliary sum, including the non-squarefree p^2 terms needed for (40.73); those are not original columns. The exact intersection subtraction and unit residual states with $1/2 < L < 1$ are checked separately. The common profile has fixed $\delta = 1/4096$ and large fixed derivative constants. The capacities and row blocks differ between cases, and the $H = 384$ case is outside the critical capacity range. These finite equalities neither determine the analytic constants nor imply an asymptotic saving.

40.24.8 A coherent prime-substitution budget, and its remaining cost

This subsection requires $U \ge 7$. It does not extend the prime-density argument to $U = 1$, although the coefficient and mask lemmas above hold for all $U \ge 1$. For real $t \ge U$, put

$$G_f(t) = \sum_{\substack{u\in\mathcal{R}\\(f,u)=1}} w_u|T_f(t;u)|^2, \qquad M_1(W) = \max\{B, \|xW'(x)\|_\infty\}.$$

The active residuals satisfy $Na \le 2D/(FU)$, so their union is finite; G_f is smooth and vanishes for $t \ge 2D/F$. Since the rough prime in K_S is unmasked, it enters only this radial common profile. Let

$$E_S(t) = \pi_K^S(t) - \mathrm{Li}(t), \qquad \delta_S(U) = \sup_{t\ge U}\frac{|E_S(t)|}{t}, \qquad \mathcal{J} = \sum_f \mu(f)\int_U^\infty \frac{G_f(t)}{\log t}\,dt,$$

where π_K^S counts prime *ideals* outside the fixed finite S with multiplicity, including inert prime norms and distinct conjugate ideals. Stieltjes partial summation gives the exact coherent identity

$$\begin{aligned} K_S &= \mathcal{J} + \mathcal{E}_{\mathrm{PIT}},\\ \mathcal{E}_{\mathrm{PIT}} &= \sum_f \mu(f)\left(-G_f(U)E_S(U) - \int_U^\infty E_S(t)G_f'(t)\,dt\right). \end{aligned} \tag{40.84}$$

The lower term uses $\pi_K^S(U)$, so the condition $Np > U$ is exact even when a prime norm equals U. A conjugate pair contributes a jump of two. This equality precedes any absolute sum over f.

Let $\lambda(L)$ be a TRUE arbitrary-coefficient squared norm bound for the specified positive row operator on good squarefree ideals of norm in $[L, 2L]$, including the actual weights. For $1/2 \le L < 1$, set $\lambda_*(L) = R_w$ by the direct unit-column bound; for $L \ge 1$, use $\lambda_*(L) = \lambda(L)$. No columns are active for $L < 1/2$. With $L = D/(Ft)$, differentiate only the common W: multiplication by $t\,d/dt$ replaces $W(x)$ by $xW'(x)$. The exact restricted identity (40.76), ideal counting and weighted row Cauchy give

$$G_f(t) + |tG_f'(t)| \ll M_1(W)^2 \lambda_*(L) L.$$

Any enlargement of a common f-row mask here occurs only inside these positive norm estimates. Substitution in (40.84), with $L_f = D/(FU)$, proves

$$\frac{|\mathcal{E}_{\mathrm{PIT}}|}{D} \ll M_1(W)^2 \delta_S(U) \sum_{\substack{f \text{ good SF, } U\text{-smooth} \\ F<2D/U}} \frac{1}{F} \left(\lambda_*(L_f) + \int_{1/2}^{L_f} \lambda_*(L)\, \frac{dL}{L} \right). \tag{40.85}$$

The original Möbius sign remains in K_S and $\mathcal{J}$ themselves; the absolute f sum appears only in this error majorant.

Specialize now ONLY to the established positive input for the actual $A_6 = 1$ unweighted two-pivot block, or bounded natural literal weights for which the same input has been established. Put

$$R = A_1 A_2, \qquad M_{\mathrm{row}} = \max(A_1, A_2), \qquad A_1 A_2^2 \le H.$$

At $L \ge 1$ that input is

$$\lambda(L) \ll_\epsilon (HD)^\epsilon \min \left\{ R + \frac{LR}{M_{\mathrm{row}}} + \frac{L^{2/3} R}{M_{\mathrm{row}}^{1/3}},\ L + R^2 \right\}. \tag{40.86}$$

It is not asserted for arbitrary nonnegative weights, enlarged primitive conductor families or arbitrary sixth-factor enlargements. Using its first branch in (40.85) gives

$$\frac{|\mathcal{E}_{\mathrm{PIT}}|}{D} \ll_\epsilon (HD)^\epsilon M_1(W)^2 \delta_S(U) \mathcal{B}_{\mathrm{op}}, \tag{40.87}$$

$$\mathcal{B}_{\mathrm{op}} = R \log^2(2D) + \frac{D}{U} \frac{R}{M_{\mathrm{row}}} + \left(\frac{D}{U} \right)^{2/3} \frac{R}{M_{\mathrm{row}}^{1/3}}. \tag{40.88}$$

The logarithmic term uses $\sum_{Nf \le X} (Nf)^{-1} \ll \log(2X)$; the other terms use convergent ideal sums of powers 2 and 5/3. The same positive bounds give $|\mathcal{J}|/D \ll_\epsilon (HD)^\epsilon B^2 \mathcal{B}_{\mathrm{op}} / \log U$. These are inherited majorants, not a new signed gain or an estimate of $K_0 - \mathcal{J}$.

Capacity implies

$$\mathcal{B}_{\mathrm{op}} \ll H \log^2(2D) + (D/U) H^{1/3} + (D/U)^{2/3} H^{2/3}.$$

At $H = D^{3/4}$ and $U \asymp \sqrt{D}$, these terms have powers $3/4, 3/4, 5/6$. The last power occurs in this majorant already on pure scales $A_1 \asymp H, A_2 = 1$ with fixed capacity slack. It is not an actual-error lower bound.

For the fixed field, Thorner–Zaman, *Algebra & Number Theory* 13 (2019), 1039–1068, Theorem 1.1, applied to the trivial extension K/K with absolute degree $[K : \mathbb{Q}] = 2$ and absolute discriminant 3, supplies for sufficiently large U a bound

$$\delta_S(U) \ll_{K,S} \exp(-c_K \sqrt{\log U}).$$

The possible exceptional real zero is fixed: retain its secondary $\mathrm{Li}(x^\beta)$ term, or absorb it only into fixed-field constants and the threshold. Finite S deletions are included. No prime theorem uniform in the growing deleted set or row conductor is used. The DOI, publisher URL and pinned reading-cache hashes are in the public citation record.

A fixed-field subpower prime error does not make the available $D^{5/6+\epsilon}\delta_S(U)$ majorant certify the target $D^{3/4+\epsilon}$ for every $\epsilon > 0$. Actual signed errors might cancel. Even an exact prime density would leave the coherent signed $K_0 - \mathcal{J}$ unestimated. The elementary correction theorem uses only B, whereas the prime-substitution error requires $M_1(W)^2$. The complete original remainder's $7/6$ envelope remains unchanged.

40.25 The coherent signed main and its remaining inputs

The physical sixth-power-free comparison in Section 40.27 provides a new positive upper bound. We now collect the exact coherent reductions that it can enter. They preserve the original mean and all raw masks; none proves the target by a scalar cancellation assertion.

Use the complete original good squarefree annulus and common complex profile of Section 40.23. Write $\mathcal{U}$ for the actual nonzero literal rows, $w_u \ge 0$, $R_w = \sum_u w_u$ and $B = \|W\|_\infty$. Retain fixed S, ν, all internal row masks and (40.52). Every identity below is a raw A–A identity; principal residues still require their separate assembly. Classical operator specializations are only for the original unweighted $A_6 = 1$ rows, or their already justified bounded natural multiplicities.

First there is a useful distinction between two auxiliary kernels. Let K_{all} be K_S of (40.57) with the U-smooth restriction on its squarefree f removed, retaining $(f,u) = 1$ and exactly $A_U(fa)$ in every T_f. Set

$$\begin{aligned} P_2 &= \sum_u w_u \sum_{\substack{p\notin S\\ Np>U}} \sum_{\substack{q\notin S,\ Nq>U\\ q\nmid u}} |W(NpNq/D)|^2, \\ K_S &= K_{\mathrm{all}} + P_2, \qquad 0 \le P_2/D \le 3584 B^2 R_w. \end{aligned} \tag{40.89}$$

Here (p,q) is ordered, $p = q$ is allowed, and only q has the stated row mask. This is distinct from the original unordered, distinct-prime C_2 in (40.58). In particular

$$S_1^{AA} = \frac{K_0 - K_{\mathrm{all}}}{D} + \Delta + \frac{C_2 - P_2}{D}. \tag{40.90}$$

At $H \le D^{3/4}$ the error in this *new* auxiliary main is at most $236800 B^2 R_w$. The old $233216 B^2 R_w$ bound for $(K_0 - K_S)/D$ is unchanged. The physical comparison in (40.112) estimates the new combined main, in its stated $A_6 = 1$ scope, without estimating its two summands separately.

The prime-discrepancy clauses below additionally require $U \ge 7$. Define

$$E_S(t) = \pi_K^S(t) - \mathrm{Li}_2(t), \qquad \mathrm{Li}_2(t) = \int_2^t \frac{dv}{\log v}, \qquad M_1(W) = \max\{B, \|xW'(x)\|_\infty\}.$$

The count is of prime ideals outside fixed S, including distinct conjugate ideals and inert prime norms. Put

$$Q(t) = \sum_{\substack{f \text{ good SF}\\ f\ U\text{-smooth}}} \mu(f) \sum_{\substack{u\in\mathcal{U}\\ (f,u)=1}} w_u |T_f(t;u)|^2, \qquad \mathcal{J} = \int_U^\infty \frac{Q(t)}{\log t}\, dt.$$

Proposition 40.13 (A joint form retaining its mean)**.** *On the finite space of good squarefree g with $Ng \le 2D/U$, let*

$$b_g(t) = A_U(g)\nu(g)W(Ng\,t/D), \quad (\mathsf{R}c)(u) = \sqrt{w_u}\sum_g c_g\chi_g(u), \quad (\mathsf{P}_f c)_g = \mathbf{1}_{f|g}c_g.$$

With ordinary counting ℓ^2 norms,

$$Q(t) = b(t)^*\mathcal{M}_U b(t), \qquad \mathcal{M}_U = \sum_{f\ U\text{-smooth}} \mu(f)\mathsf{P}_f\mathsf{R}^*\mathsf{R}\mathsf{P}_f, \quad t \ge U. \tag{40.91}$$

The matrix is self-adjoint, with no positivity assertion. The exact prime substitution is

$$K_S = \mathcal{J} + \mathcal{E}_{\mathrm{PIT}}, \qquad \mathcal{E}_{\mathrm{PIT}} = -E_S(U)Q(U) - \int_U^\infty E_S(t)Q'(t)\,dt. \tag{40.92}$$

The endpoint excludes $Np = U$ exactly. It must remain.

For any true arbitrary-coefficient row norm $\lambda_*(L)$, use the direct unit-column value R_w on $1/2 \le L < 1$. On the active range $1 \le L \le D/U$, the current original two-pivot bound is the minimum in Proposition 40.19; it is not a theorem for arbitrary row weights. Let $\lambda^{\#}(D/T)$ dominate this norm on the two adjacent active length dyads. Then

$$\frac{|\mathcal{E}_{\mathrm{PIT}}|}{D} \ll_\epsilon (HD)^\epsilon M_1(W)^2\left\{\frac{|E_S(U)|}{U}\lambda_*(D/U) + \sum_T \mathfrak{d}_2(T)\lambda^{\#}(D/T)\right\}, \tag{40.93}$$

where $T = 2^jU < 2D$ and $\mathfrak{d}_2(T)^2 = \int_T^{2T}|E_S(t)|^2t^{-3}\,dt$. This is a sufficient-input budget, not an asserted power estimate for $\mathfrak{d}_2$ or for the endpoint. The pointwise version retains $\lambda_*(D/U) + \int_{1/2}^{D/U}\lambda_*(L)\,dL/L$, with the current minimum inside that integral.

On good rough-prime columns the exact quadratic-form compression is $\Pi_{\mathcal{P}}\mathcal{M}_U\Pi_{\mathcal{P}} = \Pi_{\mathcal{P}}\mathsf{R}^*\mathsf{R}\Pi_{\mathcal{P}}$. This is not an invariant-subspace assertion: off-block couplings remain and can cancel its contribution. Radial Mellin Parseval likewise retains equal-norm ideal correlations, including their derivatives; it neither orthogonalizes orientations nor permits deleting their mean. Even exact prime density leaves $K_0 - \mathcal{J}$ to estimate.

Proposition 40.14 (A sufficient smooth-divisor tail cutoff)**.** *For the original unweighted $A_6 = 1$ two-pivot rows put $R = A_1A_2$, $M_{\mathrm{row}} = \max(A_1, A_2)$. Restrict the smooth f sums in K_0, K_S to $Nf > Y \ge 1$. The inherited positive input gives*

$$\begin{aligned}\frac{|K_0^{>Y}|}{D} &\ll_\epsilon (HD)^\epsilon B^2\left\{R + \frac{DR}{M_{\mathrm{row}}Y} + \frac{D^{2/3}R}{M_{\mathrm{row}}^{1/3}Y^{2/3}}\right\},\\ K_S^{>Y} &= 0 \qquad (Y \ge 2D/U).\end{aligned} \tag{40.94}$$

If $R \ll H$, a sufficient target-size tail cutoff is

$$Y \ge \max\left\{1, \frac{2D}{U}, \frac{DR}{M_{\mathrm{row}}H}, \frac{DR^{3/2}}{M_{\mathrm{row}}^{1/2}H^{3/2}}\right\}.$$

This is a coarse inherited sufficient bound, not signed cancellation or an optimal localization. The smooth incidence divisor f is not the original column-pair gcd h.

Theorem 40.15 (A conditional input diagnostic)**.** *Fix S and $0 < \alpha < 1/2$. If for every $\epsilon > 0$,*

$$\mathfrak{d}_2(T) \ll_{\epsilon,K,S} T^{-\alpha+\epsilon}$$

holds for all sufficiently large real T, then

$$\zeta_K(s) \neq 0 \qquad (\operatorname{Re} s > \max\{1-\alpha, 1/2\},\ s \neq 1).$$

This is a strict-region implication from an explicitly hypothetical input, not a new zero-free theorem or a necessary condition for the actual signed target.

With the current physical input the pure witness has the sufficient PIT majorant 19/24, and the mixed witness retains the smaller 7/9 from the minimum. Independent scalar powers $U^{-1/12}$ and $U^{-1/18}$ would suffice for those majorants, with compatible endpoint control; their all-scale mean-square versions would entail the strict strips 11/12 and 17/18 above. None is asserted available. The old pure 5/6 budget and $U^{-1/6}$ input, with conditional strip 5/6, are historical values for the former operator bound. Proposition 40.17 gives the current global 9/8 comparison, and Proposition 40.18 the scoped $A_6 = 1$ comparison 13/12. The target, principal/short assembly beyond the stated scopes, independent determinant/zero-location bridges and full analytic/category Lean formalization remain open.

40.26 Proofs for the coherent main reductions

Throughout, squarefree and prime mean ideal squarefree and prime. The original symbol is extended by zero, the complete good annulus is unchanged, and the same complex W is used for every row. The common smooth divisor f is an incidence variable after ideal Möbius inversion; it is not the original column-pair gcd sector $h = 1$.

40.26.1 Removing only the auxiliary smooth restriction

The high-window support of a rough-prime term satisfies

$$N(fa), N(fb) < 2D/U \leq 7U.$$

The accepted exact coefficient identity (40.76) therefore applies to these squarefree products, including the unit:

$$A_U(g) = \mu(g)(2\mathbf{1}_{Ng\leq U} - 1), \qquad Ng \leq 7U. \tag{40.95}$$

For completeness, every proper divisor of a nonunit good g has norm at most $Ng/7 \leq U$. The unrestricted ordered disjoint-divisor sum is $\prod_{p|g}(1-1-1) = \mu(g)$. If $Ng > U$, precisely the two assignments $(g,1),(1,g)$ are omitted, each with weight $\mu(g)$. If $Ng \leq U$ none is omitted; $g = 1$ is direct. This does not simplify the general annular K_0 coefficients, whose norms can reach $2D$.

For a nonunit residual pair put $M = \max(Na, Nb) \geq 7$. On active rough-prime support, with $F = Nf$ and $P = Np > U$, $FMP < 2D \leq 7U^2$, hence $F < U$. Such f is automatically U-smooth. Thus dropping its smoothness changes only $a = b = 1$. There $F < 2D/P < 7U$. If a squarefree good f contains a prime q with $Nq > U$, any additional nonunit factor would give $F > 7U$. The omitted nonsmooth f is consequently exactly q, with $\mu(q) = -1$ and $|A_U(q)| = 1$. This proves the sign and all masks in (40.89). The outer p was already deliberately unmasked in K_S; only $q \nmid u$ comes from the original f-row mask. In particular $p = q$ gives a permitted auxiliary p^2 term, not an original squarefree column.

A nonzero pair has both prime norms below $2D/U$. Using (40.75), the number of ordered pairs is at most $(32D/U)^2$. Therefore

$$P_2/D \le 1024B^2R_wD/U^2 \le 3584B^2R_w.$$

Substitute $K_S = K_{\mathrm{all}} + P_2$ into (40.62). The old critical error $233216B^2R_w$ and the new charged $3584B^2R_w$ give $236800B^2R_w$ in (40.90). The original C_2 remains unordered and distinct, with both row masks; it is not this ordered correction. No lower bound for the full indefinite raw slice is inferred from either nonnegative correction.

40.26.2 An exact two-jump masked Mertens functional

Expand the nonunit residual part of K_S before any absolute sum in f, a conductor or a row. Retain

$$\mathcal{T} = S \cup \mathrm{supp}(abu), \qquad \eta_{a,b}(u) = \nu(a)\overline{\nu(b)}\chi_a(u)\overline{\chi_b(u)}.$$

The ideals a, b are individually squarefree but may overlap. Every common support prime remains in $\mathcal{T}$, even if their quotient character loses that prime. The rough p in K_S may belong to $\mathcal{T}$; this is its defined auxiliary enlargement. Only the common f phases cancel, leaving the full $(f, \mathcal{T}) = 1$ mask. By (40.95), the remaining coefficient is

$$\mu(f)A_U(fa)A_U(fb) = \mu(f)\mu(a)\mu(b)(2\mathbf{1}_{FNa\le U} - 1)(2\mathbf{1}_{FNb\le U} - 1).$$

Put $\alpha = \min(Na, Nb)$, $M = \max(Na, Nb)$ and

$$X = \frac{D}{PM}, \quad r = \frac{\alpha}{M}, \quad c_0 = \frac{U}{M}, \quad d_0 = \frac{U}{\alpha}.$$

At $r \le 1/2$ the profile product vanishes, including equality. Otherwise let $\Phi_r(v) = W(v)\overline{W(rv)}$ when $Na = M$, and use its conjugate in the reversed orientation. Set $h(t) = \Phi_r(t/X)$, supported on $[X/r, 2X]$ with zero endpoints. The exact cutoff product is

$$(2\mathbf{1}_{FNa\le U} - 1)(2\mathbf{1}_{FNb\le U} - 1) = 1 - 2\mathbf{1}_{c_0<F\le d_0}.$$

No half-weight occurs at a norm cutoff. With the closed-prefix sum

$$M_{\mathcal{T}}(y) = \sum_{\substack{Nf\le y\\(f,\mathcal{T})=1}} \mu(f), \qquad M_{\mathcal{T}}(y) = 0 \quad (y < 1),$$

the scalar factor, multiplied outside by $\mu(a)\mu(b)\eta_{a,b}(u)$, is

$$\mathcal{I}_{a,b,u}(P) = \sum_{(f,\mathcal{T})=1} \mu(f)h(Nf)(1 - 2\mathbf{1}_{c_0<Nf\le d_0}). \tag{40.96}$$

Ordinary finite Abel summation gives, for every real y,

$$\sum_{\substack{Nf\le y\\(f,\mathcal{T})=1}} \mu(f)h(Nf) = h(y)M_{\mathcal{T}}(y) - \int_0^y M_{\mathcal{T}}(t)h'(t)\,dt.$$

Subtracting the two closed prefixes proves the endpoint-sensitive identity

$$\begin{aligned}\mathcal{I}_{a,b,u}(P) = &-\int_0^\infty M_{\mathcal{T}}(t)h'(t)\,dt + 2\int_{c_0}^{d_0} M_{\mathcal{T}}(t)h'(t)\,dt\\ &+ 2h(c_0)M_{\mathcal{T}}(c_0) - 2h(d_0)M_{\mathcal{T}}(d_0).\end{aligned} \tag{40.97}$$

When $c_0 = d_0$ all extra terms cancel. A boundary outside the profile has $h = 0$. Combining the two integrals gives a multiplier of absolute value one almost everywhere, rather than three separate derivative costs. Log-coordinate differentiation yields

$$\int |h'(t)|\,dt \le 2\log 2\, M_1(W)^2, \qquad 2|h(c_0)| + 2|h(d_0)| \le 4B^2.$$

Consequently

$$|\mathcal{I}_{a,b,u}(P)| \le 6M_1(W)^2 \sup_{X\le t\le 2X} |M_{\mathcal{T}}(t)|. \tag{40.98}$$

The full outer residual and row sum is still coherent.

A useful explicit uniformity quantity is

$$m_Q(Z) = \sup_{\substack{E \text{ finite good prime ideals} \\ N\prod_{p\in E} p\le Q}} \sup_{t\ge Z} \frac{|M_{S\cup E}(t)|}{t}.$$

It always satisfies $m_Q(Z) \le 16$ by (40.75). For the original residuals,

$$N\,\mathrm{rad}(abu)_{S^c} \le Na\,Nb\,Nu \le (2D/P)^2 H \le 14DH.$$

Restrict the expanded nonunit K_S to $X \ge Z \ge 1/2$. This cuts the residual f-length X, not $F = Nf$ in the tail below. Equation (40.98) bounds each scalar by $12M_1(W)^2 X m_{14DH}(Z)$. For fixed P put $V = D/P$. Ideal counting gives

$$\#\{(a,b) : \max(Na, Nb) \le t\} \le 256t^2, \qquad \sum_{\max(Na,Nb)\le T} \frac{1}{\max(Na,Nb)} \le 512T.$$

The second inequality follows by partial summation and is vacuous for $T < 1$. Since $M \le V/Z$, the absolute residual cost is at most $6144M_1(W)^2 m_{14DH}(Z)V^2/Z$. Also $\sum_{Np>U}(Np)^{-2} \le 32/U$, again by ideal counting. Only now taking the residual, prime and row triangle proves

$$\frac{|K_S[\text{nonunit}; X \ge Z]|}{D} \le 196608M_1(W)^2 R_w \frac{D}{UZ}\, m_{14DH}(Z). \tag{40.99}$$

No arbitrary-weight sieve is hidden here: the only row input is $|\eta_{a,b}(u)| \le 1$ and R_w. A *hypothetical* uniform estimate $|M_{S\cup E}(t)| \ll_{\theta,\epsilon,S} (N\prod_{p\in E} p)^{\epsilon} t^{\theta}$, $0 < \theta \le 1$, would give, for $Z \ge 1$, the restricted bound

$$\frac{|K_S[\text{nonunit}; X \ge Z]|}{D} \ll M_1(W)^2 (DH)^{\epsilon} R_w (D/U) Z^{\theta-2}.$$

No $\theta < 1$ hypothesis is assumed. On the region $2X \le 7$, every nonunit good f has zero profile (the possible norm-7 endpoint is zero). Hence only $f = 1$ survives, and (40.96) is exactly $h(1)(1 - \mathbf{21}_{c_0<1\le d_0})$. For instance $a = b$ gives $|W(1/X)|^2$. Thus even a strong long-sum Mertens estimate cannot supply cancellation in this one-term region after the outer residual triangle. This is a limitation of that scalar route, not a lower bound for the complete signed sum; other residual and row sectors may cancel it.

40.26.3 Deleted-prime transfer and its fixed-field subpower input

The deletion has an exact fixed-zeta interpretation. Put $M_K(x) = \sum_{Na\le x} \mu(a)$, and let $\mathcal{D}_{\mathcal{T}}$ be *all* ideals supported on $\mathcal{T}$, including prime powers. For $\sigma > 0$ set

$$E_{\mathcal{T}}(\sigma) = \prod_{p\in\mathcal{T}} (1 - (Np)^{-\sigma})^{-1}.$$

Absolute Euler multiplication initially on $\operatorname{Re} s > 1$ gives the coefficient identity and hence the finite convolution

$$M_{\mathcal{T}}(x) = \sum_{\substack{d \in \mathcal{D}_{\mathcal{T}} \\ Nd \le x}} M_K(x/Nd). \tag{40.100}$$

Restricting d to squarefree ideals would be false. This is an artificial finite Euler deletion, not a new primitive Hecke conductor. Its finite factors have possible poles only on $\operatorname{Re} s = 0$.

Choose C_K with $A_K(x) \le C_K x$, and define $\rho_K(y) = \sup_{v \ge y} |M_K(v)|/(C_K v) \le 1$. For $x \ge 1$ and $0 < \delta < 1$, split (40.100) at $Nd = \sqrt{x}$. On the first part use $\rho_K(\sqrt{x})$ and $\sum (Nd)^{-1} \le E_{\mathcal{T}}(1-\delta)$. Rankin's inequality bounds the second positive sum by $x^{-\delta/2} E_{\mathcal{T}}(1-\delta)$. Thus

$$|M_{\mathcal{T}}(x)| \le C_K x E_{\mathcal{T}}(1-\delta)\{\rho_K(\sqrt{x}) + x^{-\delta/2}\}. \tag{40.101}$$

Its minimum with the trivial $C_K x$ bound is always valid.

For clarity, the fixed-field analytic input used to estimate ρ_K is separate from this elementary transfer. The already pinned Thorner–Zaman, Theorem 3.1 gives the classical Dedekind zero-free region, with a possible single fixed exceptional real zero. Specialize only to the trivial extension K/K, of absolute degree 2 and discriminant 3. Shrink the fixed constant so any fixed exceptional zero is outside the chosen region, retaining its dependence in the fixed threshold. For $|t| \ge 2$, the Euler bound just right of 1, fixed-degree functional equation/convexity in a strip of width $O(1/\log(|t|+3))$, and Borel–Carathéodory for an analytic logarithm on smaller zero-free disks give

$$|1/\zeta_K(\sigma + it)| \ll_K \log^A(|t|+3), \qquad \sigma \ge 1 - c_K/\log(|t|+3).$$

Indeed the upper bound for $\operatorname{Re} \log \zeta_K$ and its value at a center to the right of 1 are $O(\log\log(|t|+3))$; a smaller disk has the same bound for its absolute logarithm. Bounded t is handled in a fixed zero-free neighborhood of 1, where the reciprocal is holomorphic also at the pole of ζ_K. No logarithm is continued through that pole.

Here is the Perron error needed for the deduction. The planar fundamental-cell count in this class-number-one field gives $A_K(x+h) - A_K(x) \ll_K h + \sqrt{x} + 1$ for $h \ge 0$. Apply truncated Perron to $1/\zeta_K$ at $x' = \lfloor x \rfloor + 1/2$, whose summatory value equals $M_K(x)$. The coefficients are bounded in absolute value by the ideal counts. Dyadic annuli around x' control the near-integer terms by $x \log^A(2x)/T + \sqrt{x}\log^A(2x)$; the remote terms have the first cost. Shift to $1 - c_K/\log(T+3)$, which lies inside the shrunken zero-free region for every $|t| \le T$. There is no residue at 1, since the reciprocal has a zero there. The vertical and horizontal bounds give

$$|M_K(x)| \ll_K x \log^A(2x) \left\{ \exp\left(-\frac{c_K \log x}{\log(T+3)} \right) + T^{-1} \right\} + \sqrt{x}\log^A(2x).$$

Choosing $T = \exp(c'_K \sqrt{\log(2x)})$ and absorbing logarithms proves

$$|M_K(x)| \ll_K x \exp(-c''_K \sqrt{\log(2x)}). \tag{40.102}$$

Small x is absorbed in the fixed constant. This is fixed-field subpower cancellation; it asserts no fixed power or uniformity over varying primitive conductors or fields.

The remaining deletion factor can be quantified elementarily. Put $R_{\mathcal{T}} = N \prod_{p \in \mathcal{T} \setminus S} p$ and $Z_0 = \log(e^3 R_{\mathcal{T}}) \ge 3$. For $0 < \delta \le 1/2$, split the prime sum for $\log E_{\mathcal{T}}(1-\delta)$ at Z_0^2. Ideal counting bounds the small part by $O_K(Z_0^{2\delta} \log Z_0)$. For the large part use $\sum_{p \in \mathcal{T} \setminus S} \log Np \le \log R_{\mathcal{T}}$ and the monotonicity of $v^{1-\delta}\log v$; its bound is $O(\log R_{\mathcal{T}}/(Z_0^{2-2\delta}\log Z_0)) = O(1)$. Fixed S factors cost a fixed constant. Hence

$$\log E_{\mathcal{T}}(1-\delta) \le C_{K,S}\{1 + Z_0^{2\delta}\log Z_0\}.$$

If $\delta \log Z_0 \le 1$, this is $E_{\mathcal{T}}(1-\delta) \ll Z_0^A$. Taking $\delta = \min\{c/\sqrt{\log(2x)}, 1/\log Z_0, 1/2\}$ in (40.101) proves, for $x \ge 3$,

$$|M_{\mathcal{T}}(x)| \ll_{K,S} x Z_0^A \exp\left(-c \min\left\{\sqrt{\log(2x)}, \frac{\log(2x)}{\log Z_0}\right\}\right). \tag{40.103}$$

For $R_{\mathcal{T}} \le D^C$ and $x \ge D^v$, fixed $C, v > 0$, this gives a uniform $x \log^A(2D) \exp(-c\sqrt{\log(2x)})$ bound. It is useful on long scalar ranges, but gives no power saving and no cancellation in the unit-f range above. The exact product bound (40.101) retains every raw deletion before any convenient larger estimate.

40.26.4 The joint matrix, raw zeros and its compression

All spaces here carry ordinary counting ℓ^2 norms. On the fixed finite short-column space of Proposition 40.13, $g = fa$ is squarefree precisely when $(f, a) = 1$. For $(f, u) = 1$, multiplicativity gives

$$(\mathsf{RP}_f b)(u) = \sqrt{w_u}\nu(f)\chi_f(u)T_f(t;u).$$

If $(f, u) > 1$, every g in that projected column support has the original zero $\chi_g(u) = 0$. Thus its row is exactly zero, rather than being restored through a primitive character. Squaring proves $G_f(t) = \|\mathsf{RP}_f b(t)\|^2$ and (40.91). The Gram entries remain

$$(\mathsf{R}^*\mathsf{R})_{g,h} = \sum_u w_u \overline{\chi_g(u)}\chi_h(u).$$

No coherent orientation mean is removed.

The divisor sum in each matrix entry is the exact Schur factor

$$C_U(g,h) = \sum_{\substack{f \mid (g,h) \\ f \ U\text{-smooth}}} \mu(f) = \mathbf{1}_{(g,h) \text{ has no prime norm } \le U}.$$

On active $t \ge U$ support, $Ng, Nh < 7U$. Any such g containing a rough prime must be that prime alone. It follows that

$$C_U(g,h) = \mathbf{1}_{(g,h)=1} + \mathbf{1}_{g=h=p,\ p\notin S,\ Np>U}. \tag{40.104}$$

For the projection $\Pi_{\mathcal{P}}$ onto rough-prime columns, $\mathsf{P}_f\Pi_{\mathcal{P}} = 0$ for every nonunit smooth f and $\mathsf{P}_1\Pi_{\mathcal{P}} = \Pi_{\mathcal{P}}$. Therefore

$$\Pi_{\mathcal{P}}\mathcal{M}_U\Pi_{\mathcal{P}} = \Pi_{\mathcal{P}}\mathsf{R}^*\mathsf{R}\Pi_{\mathcal{P}}. \tag{40.105}$$

This is a quadratic-form *compression*, not an invariant restriction: in general $\mathcal{M}_U\Pi_{\mathcal{P}}$ and $\Pi_{\mathcal{P}}\mathcal{M}_U$ differ. Off-block couplings and other columns can cancel its contribution. It is no lower bound for full Q, the prime error or the original raw slice.

On any common active length dyad $[L, 2L]$, a true squared row norm $\lambda_*(L)$ gives, for arbitrary coefficients c there,

$$|c^*\mathcal{M}_U c| \le \sum_f \|\mathsf{RP}_f c\|^2 \le \lambda_*(L)\sum_g d_U(g)|c_g|^2, \qquad d_U(g) = \#\{f \mid g : f \ U\text{-smooth}\}.$$

This is a positive incidence-frame majorant, not Möbius cancellation. Since g is squarefree, $d_U(g) \le 2^{\omega(g)} \ll_\eta (Ng)^\eta$. Self-adjointness bounds the compressed operator norm by the same $\lambda_*(L)\max d_U$ and permits polarization for cross terms. For $L = D/t$, the exact short coefficient and ideal counting give

$$\|b(t)\|^2 \ll B^2 L, \qquad \|tb'(t)\|^2 \ll M_1(W)^2 L.$$

The direct unit endpoint covers $1/2 \le L < 1$; no column survives below $1/2$. Differentiating the fixed matrix, not a moving support matrix, gives $Q'(t) = 2\,\mathrm{Re}(b'(t)^* \mathcal{M}_U b(t))$ and

$$|Q(t)| + |tQ'(t)| \ll_\eta (HD)^\eta M_1(W)^2 \lambda_*(D/t) D/t. \tag{40.106}$$

Only here may the classical specialization be inserted, in exactly its original natural-row scope. For arbitrary weights a true weighted norm is needed; the elementary Frobenius alternative is $\lambda_*(L) \ll R_w L$.

40.26.5 Exact Stieltjes boundary and squarefunction criterion

The finite Q vanishes for $t \ge 2D$, including its endpoint. Stieltjes integration over (U, ∞) counts precisely $Np > U$; comparing its prime measure with $dt/\log t$ proves (40.92). Changing the normalization of Li by a constant changes the two boundary/integral terms by opposite amounts and changes no identity. We fix Li_2 here. The original raw slice is consequently

$$S_1^{AA} = \frac{K_0 - \mathcal{J}}{D} + \Delta + \frac{C_2}{D} - \frac{\mathcal{E}_{\mathrm{PIT}}}{D}.$$

It keeps the original masks and the full mean. The prime measure contains only fixed S, never a growing deleted set $S \cup \mathrm{supp}(abu)$.

Let $\delta_S(U) = \sup_{t \ge U} |E_S(t)|/t$. Use (40.106) and substitute $L = D/t$ to obtain

$$\frac{|\mathcal{E}_{\mathrm{PIT}}|}{D} \ll_\epsilon (HD)^\epsilon M_1(W)^2 \delta_S(U) \left\{ \lambda_*(D/U) + \int_{1/2}^{D/U} \lambda_*(L)\, \frac{dL}{L} \right\}. \tag{40.107}$$

One may keep $\max d_U$ explicitly instead of absorbing it into a subpower; no uniform logarithmic improvement is thereby claimed. With the current physical input of Proposition 40.19, the minimum of its three branches remains inside this integral. All constants and internal small exponents are chosen uniformly on the neighboring capacity-feasible blocks.

For $I_T = [T, 2T] \cap [U, 2D]$, let $\lambda^\#(D/T)$ dominate $\lambda_*(L)$ on $L \in [D/(2T), D/T]$, using the direct endpoint when necessary. Equation (40.106) implies

$$\|Q'\|_{L^2(I_T)} \ll (HD)^\eta M_1(W)^2 \lambda^\#(D/T) D/T^{3/2}.$$

Our weighted squarefunction convention gives $\|E_S\|_{L^2(I_T)} \le (2T)^{3/2} \mathfrak{d}_2(T)$. Cauchy on each dyad and the retained endpoint prove (40.93). The weighted definition is comparable by absolute constants to $T^{-3/2} \|E_S\|_{L^2([T,2T])}$. Global Cauchy across unrelated dyads need not improve this bound. The sufficient target condition is that its braces be $\ll H(HD)^\epsilon$, including the pointwise term. It is an explicit input to investigate, not an established estimate or an independence assumption between E_S and the signed derivative.

40.26.6 Mellin Parseval retains equal-norm coherence

Extend only the same finite short-column vector to $t > 0$ for this identity; below U it need not equal the unrestricted original T_f with additional longer columns. No signed equality for K_S is enlarged below U. For fixed f, u let $c_g = A_U(g)\nu(g)\chi_g(u)\mathbf{1}_{f|g}$, and use

$$\widehat{W}(i\tau) = \int_0^\infty W(x) x^{i\tau} \frac{dx}{x}.$$

Ordinary Mellin Plancherel for the finite amplitude gives exactly

$$\begin{aligned}&\int_0^\infty \left|\sum_g c_g W(Ng\,t/D)\right|^2 \frac{dt}{t}\\ &= \frac{1}{2\pi}\int_{\mathbb{R}} |\widehat{W}(i\tau)|^2 \left|\sum_g c_g (D/Ng)^{i\tau}\right|^2 d\tau.\end{aligned} \tag{40.108}$$

For the derivative of this *amplitude*, replace $|\widehat{W}|^2$ by $\tau^2|\widehat{W}|^2$. This does not assert a diagonal Mellin formula for the square of the quadratic derivative Q'. Finite signed summation in f and the actual rows preserves the matrix form at the norm-twisted coefficient vector. No absolute-value or centering operation is inserted into that equality.

If distinct ideals g, h have $Ng = Nh$, their radial profiles and all their t derivatives are identical. Their radial cross correlation is the same nonzero profile norm as the diagonal when $W \neq 0$. The Mellin phases $(Ng)^{-i\tau}$ also coincide; distinct conjugate split ideals provide actual such orientations. Thus neither radial Parseval nor the derivative removes their coherent mean. The safe decomposition is

$$\sum_r a_r \Gamma_r = \Gamma_{\mathrm{av}} \sum_r a_r + \sum_r a_r(\Gamma_r - \Gamma_{\mathrm{av}}).$$

Both terms remain. The already recorded fixed-profile example in Section 40.19 has centered variance sum 6, coefficient norm squared 2, but full scalar squared $36 > 12$; it is not rerun or identified with this prime error. It illustrates why a variance-only replacement is invalid. Applying an existing arbitrary-coefficient norm at every τ in (40.108) leaves its operator power unchanged; the twist has modulus one.

40.26.7 Proof of the inherited smooth-divisor localization

Now specialize only to the original unweighted $A_6 = 1$ two-pivot rows. The exact K_0 positive summand is

$$G_f(1) = \sum_{\substack{u \in \mathcal{U}\\ (f,u)=1}} |T_f(1;u)|^2.$$

Here $A_U(fa)$ is in the general annular domain and stays unfactored. The divisor-assignment bound and ideal counting give its coefficient squared norm $\ll_\eta B^2 D^\eta L$, $L = D/F$. The accepted powered subsequence norm (40.34) gives

$$G_f(1) \ll (HD)^\eta B^2 \left\{ LR + \frac{L^2 R}{M_{\mathrm{row}}} + \frac{L^{5/3} R}{M_{\mathrm{row}}^{1/3}} \right\}.$$

For $1/2 < L < 1$ count the unit residual directly. Its $O(RD^\eta B^2)$ cost is covered by the same expression up to a constant; for $L = 1/2$ the endpoint is zero. No subunit sieve is used. Now take the triangle only in the tail $F > Y$, and enlarge the nonnegative squarefree smooth-ideal upper sums to all ideals. Partial summation from ideal counting yields

$$\sum_{Y<F<2D} F^{-1} \ll \log(2D), \quad \sum_{F>Y} F^{-2} \ll Y^{-1}, \quad \sum_{F>Y} F^{-5/3} \ll Y^{-2/3}.$$

Division by D and absorption of logarithms and internal assignment powers prove (40.94). Every rough-prime K_S term has $FPNa > FU$, so $F > Y \geq 2D/U$ forces zero profile even in its auxiliary nonsquarefree cases. The C_2 and P_2 unit corrections are not silently removed by this tail split.

When $R \ll H$, solving the last two monomial inequalities for a sufficient Y gives the displayed cutoff in Proposition 40.14. At the mixed witness it is enough to take $Y = D^{13/24}$ with fixed capacity slack, giving tail exponents $7/12, 5/8, 3/4$. At the pure witness $Y = D^{5/8}$ gives $3/4, 3/8, 3/4$. Both exceed the rough support exponent $1/2$ for large D. These are inherited sufficient upper cutoffs, not energy lower bounds or assertions of current optimality after the new physical input. All small smooth divisors, including $f = 1$, remain; no signed main estimate follows from the positive tail. The current whole-form comparison in Proposition 40.18 is a different consequence of the new external norm input.

40.26.8 Proof of the conditional zero-free input diagnostic

Assume exactly the all-scale, all-ϵ hypothesis of Theorem 40.15. For $\operatorname{Re} s > 1$ put

$$F_S(s) = \int_2^\infty E_S(t) t^{-s-1}\, dt.$$

On a dyad, Cauchy gives

$$\int_T^{2T} |E_S(t)| t^{-\sigma-1}\, dt \le \mathfrak{d}_2(T) \left(\int_T^{2T} t^{1-2\sigma}\, dt \right)^{1/2} \le C_\sigma \mathfrak{d}_2(T) T^{1-\sigma}.$$

At $\sigma = 1$ use the logarithmic limit of the finite integral. On a compact subset of $\sigma > 1 - \alpha$, choose ϵ smaller than its distance to that boundary. The dyadic majorant is a summable geometric series, also after any fixed power of $\log t$. The same integral therefore converges normally, with all holomorphic derivatives, on $\sigma > 1 - \alpha$. Its bounded initial interval is entire. No contour has crossed an unknown zero.

For $\sigma > 1$, the prime-ideal series satisfies

$$P_S(s) = \sum_{p \notin S} (Np)^{-s} = L_0(s) + sF_S(s), \qquad L_0(s) = \int_2^\infty \frac{t^{-s}}{\log t}\, dt.$$

In this field $\pi_K^S(2) = 0$ and $\operatorname{Li}_2(2) = 0$, so no lower boundary atom is missing. Direct differentiation gives $L_0'(s) = -2^{1-s}/(s-1)$. Only this meromorphic derivative is continued; no single-valued logarithmic primitive is asserted through $s = 1$. Consequently

$$-P_S'(s) = \frac{2^{1-s}}{s-1} - (sF_S(s))'.$$

For $\zeta_K^S(s) = \zeta_K(s) \prod_{p \in S} (1 - (Np)^{-s})$, its initial logarithmic derivative is

$$-\frac{(\zeta_K^S)'(s)}{\zeta_K^S(s)} = -P_S'(s) + H_S(s), \quad H_S(s) = \sum_{p \notin S} \sum_{k \ge 2} \log(Np)(Np)^{-ks}.$$

The higher-prime-power series is normally holomorphic for $\sigma > 1/2$: its geometric tail is bounded on compact subsets by $C \sum_p \log(Np)(Np)^{-2\sigma}$, an absolutely convergent ideal series. Inert prime ideals are included, not mistaken for absent rational primes. The right side has no possible pole in $\sigma > \max\{1 - \alpha, 1/2\}$ except $s = 1$. Standard continuation of the fixed Dedekind zeta, or $\zeta_K(s) = \zeta(s) L(s, \chi_{-3})$, identifies it with the actual logarithmic derivative. A zero elsewhere would give a pole with nonzero integer residue, impossible there. Finite deleted Euler factors vanish only on $\sigma = 0$, so they change no zero in this region. This proves Theorem 40.15. A fixed exceptional

real zero, if inside the strict region, would be excluded by the hypothetical input itself; it is not assumed absent.

For orientation, the old and current sufficient scalar power accounting is recorded below. Every input and ensuing strip in the table is conditional, and endpoint control is additional to a mean-square norm. Here $\sigma = \operatorname{Re} s$ and the input column means $U^{-\alpha}$.

certificate	budget	input α	strict strip
old pure (historical)	5/6	1/6	$\sigma > 5/6$
current pure	19/24	1/12	$\sigma > 11/12$
current mixed	7/9	1/18	$\sigma > 17/18$

The current values use Proposition 40.19, not the historical pure 5/6 operator budget. Since $U \asymp D^{1/2}$, subtracting the target 3/4 from the respective PIT powers and doubling gives 1/12 and 1/18. A pointwise all-scale power for δ_S would imply the corresponding squarefunction power; the converse and its pointwise endpoint are not supplied. The accepted fixed-field subpower PIT is not one of these independent powers.

The new physical input does prove its stated global 9/8 and $A_6 = 1$ signed/combined 13/12 comparisons. The coherent reductions above do not improve them to the target, nor establish desired positivity, general Artin holomorphy, determinant/zero-location bridges, a varying-profile fixed-seminorm theorem or new Lean results. Finite formal controls and source-bound reviews check bookkeeping; they do not replace any infinite analytic hypothesis. Full primary reading caches remain local: only public citation/version/hash metadata accompanies these proofs.

40.27 A sieve comparison indexed by the physical radicand

This section applies a new external preprint input to the original rows. It is an application of that theorem, not a new proof of a large sieve, a signed target estimate, or an analytic Lean result. Throughout, $K = \mathbb{Q}(\omega)$, S is fixed and contains the primes above $2, 3$ and the original conductor exclusions, and ν is the original fixed finite-order Hecke column character. Let $D, H \geq 1$, $U \geq 1$, $U^2 \leq D$, and let W be one common possibly complex smooth profile supported on $[1, 2]$, zero at its endpoints. Write $B_W = \|W\|_\infty$. The estimates below concern the original unweighted literal rows, or already justified bounded natural multiplicities. They do not insert arbitrary positive row weights into an unweighted theorem.

Pinned external input. De Faveri's arXiv:2610.04045v1, Theorem 1.1, bounds the squared row norm $\Theta_n(A, B)$ for the Section 2.3 family of order-dividing-n Hecke characters, with both indices nth-power-free ideals prime to fixed S:

$$\Theta_n(A, B) \ll_\epsilon (AB)^\epsilon (A + B + A^{1-1/n} B^{2/n} + A^{2/n} B^{1-1/n}). \tag{40.109}$$

Here $n \geq 3$, K contains μ_n, and the chosen fixed S-integer ring has class number one. The constants may depend on the fixed family construction. We use $n = 6$, not a conjectural $A + B$ bound; the additional μ_{2n} condition of that paper's Theorem 1.4 is not a hypothesis of Theorem 1.1. Set

$$\Phi_6(A, B) = A + B + A^{5/6} B^{1/3} + A^{1/3} B^{5/6},$$
$$\Phi_{\mathrm{all}}(H, D) = H + DH^{1/6} + H^{5/6} D^{1/3} + H^{1/3} D^{5/6}.$$

Proposition 40.16 (Exact raw-family identification)**.** *There is an allowed fixed choice of the data in* (40.109) *for which, for every good ideal* $\mathfrak{a}$*, with unique generator* $\alpha_{\mathfrak{a}} \equiv 1 \pmod 3$*,*

$$\chi_{\mathfrak{a}}(\mathfrak{m}) = \left(\frac{\alpha_{\mathfrak{a}}}{\mathfrak{m}}\right)_6$$

including the original zero at each common prime. In particular, the row index is the physical sixth-power-free ideal, including valuations $2, 3, 4, 5$*, rather than its radical conductor.*

The extended proof specifies the data and removes the possible unit ambiguity. No extra column-ray selection is made. For the unique outside-S decomposition of an actual literal row,

$$\begin{aligned} u &= u_0 \alpha_{\mathfrak{a}} \alpha_{\mathfrak{r}_6}^6, & \mathfrak{a} &= \mathfrak{r}_1 \mathfrak{r}_2^2 \mathfrak{r}_3^3 \mathfrak{r}_4^4 \mathfrak{r}_5^5, \\ \chi_{\mathfrak{m}}(u) &= \chi_{\mathfrak{m}}(u_0) \chi_{\mathfrak{a}}(\mathfrak{m}) \mathbf{1}_{(\mathfrak{m},\mathfrak{r}_6)=1}, & Nu &= Nu_0 \, N\mathfrak{a} \, (N\mathfrak{r}_6)^6. \end{aligned} \tag{40.110}$$

The first five factors are squarefree and pairwise coprime; $\mathfrak{r}_6$ is arbitrary and may overlap them. All original union, common-prime, literal, ray and capacity restrictions remain.

Proposition 40.17 (Physical-row comparison)**.** *For the original raw sums* I_u *of* (40.1)*, and for the original residue-subtracted* $E_u = I_u - P_u$ *with fixed* ν, S*,*

$$\sum_{0<Nu\le H} |I_u|^2 + \sum_{0<Nu\le H} |E_u|^2 \ll_{\nu,S,\epsilon} B_W^2 (HD)^{\epsilon} \Phi_{\mathrm{all}}(H, D).$$

For $1 \le H \le D$ *one has*

$$\Phi_{\mathrm{all}}(H, D) \le 4DH^{1/6}. \tag{40.111}$$

Thus the critical positive envelope at $H = D^{3/4}$ *is* $D^{9/8+\epsilon}$*, improving the previous* $7/6$ *comparison by* $1/24$ *while still exceeding the* $3/4$ *target by* $3/8$*.*

The agreement with the varying-profile obstruction of Section 40.17 concerns only a supremum-norm-controlled class allowing W_D to vary. It is not a lower bound or a sharpness assertion for one fixed W, nor a GRH counterexample.

Proposition 40.18 (The actual $A_6 = 1$ signed slice)**.** *For an original unweighted two-pivot block, retaining all its actual filters and the complete annular columns, the raw form* S_1^{AA} *of* (40.30) *satisfies*

$$|S_1^{AA}| \ll_{\nu,S,\epsilon} B_W^2 (HD)^{\epsilon} \Phi_6(H, D).$$

The same bound holds after summing the fixed-S parts of such rows: the D term costs a fixed polylogarithmic count, absorbed in $(HD)^{\epsilon}$*, not a convergent exponent-zero Euler sum. At* $H = D^{3/4}$ *the available power is* $13/12$*, an improvement of* $1/12$ *from the old* $7/6$ *majorant, but still* $1/3$ *above the target.*

The proof inserts (40.109) into the exact original common-divisor identity (40.32); $A_U(dn)$ is not factored and is not put into the rough short-coefficient domain. Under the additional high-window and capacity hypotheses of Section 40.25, its exact ordered rough correction gives

$$\left|\frac{K_0 - K_{\mathrm{all}}}{D}\right| \le |S_1^{AA}| + 236800 B_W^2 R_w. \tag{40.112}$$

This estimates the actual combined form through its exact identity; it does not take separate main-term triangles in K_0, K_{all}, and does not prove signed cancellation at the target scale.

Proposition 40.19 (Updated short positive certificate)**.** *On an original unweighted block, put* $R = A_1A_2$*,* $M = \max(A_1, A_2)$ *and* $H_b = \min\{H/Nu_0, 8A_1A_2^2\}$ *for fixed literal/S factor* u_0*. Empty blocks contribute zero; a nonempty block has* $H_b \geq 1$*. For* $1 \leq L \leq D$ *the actual squared row-operator norm has the bound*

$$\lambda_{\mathrm{now}}(L) \ll (HD)^{\epsilon} \min \begin{Bmatrix} R + \dfrac{LR}{M} + \dfrac{L^{2/3}R}{M^{1/3}}, & L + R^2, \\ \Phi_6(H_b, L) \end{Bmatrix}.$$

For $1/2 \leq L < 1$ *use the direct unit-column norm* R_w*. This new norm may be substituted into the mean-retaining joint Abel criterion of Proposition 40.13, with its lower endpoint intact. At* $H = D^{3/4}$*,* $U \asymp D^{1/2}$*, its pure witness costs* $19/24$*; at the displayed mixed witness the minimum retains the old* $7/9$ *bound, which beats the generic* $19/24$*.*

In this positive certificate sufficient independent scalar discrepancy powers are respectively

$$U^{-1/12+\epsilon} \quad \text{and} \quad U^{-1/18+\epsilon}. \tag{40.113}$$

If imposed as all-scale mean-square inputs, these would entail the conditional zero-free strips $\Re s > 11/12$ and $\Re s > 17/18$ of Theorem 40.15. Neither input nor strip is proved here; they are not necessary conditions for the actual signed target. The endpoint and coherent $K_0 - J$ remain. Smooth-tail localization (Proposition 40.14) does not remove $f = 1$ or supply this estimate.

40.28 Proof of the physical-row sieve application

40.28.1 The precise literature input and the primary generator

The external input is de Faveri, *Optimal large sieve for fixed order characters*, arXiv:2610.04045v1, 2 October 2026, Theorem 1.1, printed page 2. Input (40.109) is invoked with the family in its Sections 2.2–2.5; its deep proof is not reproduced or claimed as a new sieve or Lean theorem here. The primary PDF SHA-256 is the concatenation of these two lines:

`97720b3cacccbedb9c2014520ad4d128`
`ae23afd0a781bdeff27dab4e86b7c726`

The public citation receipt records the version and text hash. Full PDF/text reading snapshots are local cache and excluded from public closure.

The ring $\mathcal{O} = \mathbb{Z}[\omega]$ is a PID. Its six units map bijectively onto $(\mathcal{O}/(3))^{\times}$, which has six elements. Consequently every fractional ideal prime to 3 has a unique generator $\alpha_{\mathfrak{a}} \equiv 1 \pmod 3$, interpreted locally at 3. This choice is multiplicative, since a product of two such generators is again 1 modulo 3 and generates the product ideal.

Choose the source's fixed modulus $\mathfrak{c}_0$ sufficiently divisible at S that its stipulated local sixth-power condition holds, and choose it divisible by (3). In the source's Section 2.3 choose ordinary ideal representatives E_0 prime to S, and set $m_{E_0} = \alpha_{E_0}$. Global principality makes these allowed generators after S-localization too. The prescribed products then give $m_E = \alpha_E$ for each representative E. For coprime good ideals $\mathfrak{a}, \mathfrak{m}$, the construction gives

$$\mathfrak{a} = (x)E\mathfrak{g}^6, \qquad x \equiv 1 \pmod{\mathfrak{c}_0}, \qquad (\mathfrak{g}, \mathfrak{m}) = 1, \qquad \chi_{\mathfrak{a}}(\mathfrak{m}) = \left(\frac{xm_E}{\mathfrak{m}}\right)_6.$$

Choose an ordinary fractional generator $\gamma_{\mathfrak{g}}$ of $\mathfrak{g}$. Ordinary ideal equality implies

$$\alpha_{\mathfrak{a}} = \eta x m_E \gamma_{\mathfrak{g}}^6, \qquad \eta \in \mu_6. \tag{40.114}$$

All factors are units at 3, and $\gamma_{\mathfrak{g}}^6 \equiv 1 \pmod 3$ because the residue unit group has order six. The other three displayed generators are 1 modulo 3. Hence $\eta \equiv 1 \pmod 3$ and injectivity on μ_6 forces $\eta = 1$. Taking the sixth-power residue symbol proves the exact identification in Proposition 40.16. For a common prime the source's induced character and the original raw symbol are both zero. Thus no primitive-conductor transfer can silently restore a nonunit value.

The field contains μ_6; it need not contain μ_{12} for the Theorem 1.1 input. Its characters have order dividing six and trivial infinite type, so physical valuations $2, 3, 4, 5$ are included. They are not replaced by a squarefree radical or indexed by its norm. The fixed choice of $S, \mathfrak{c}_0, E, m_E$ is independent of D, H, U and of all coefficient masks below. We fix the complex embedding to agree with the original sextic symbol. This is a deliberate allowed construction, not an assertion that every noncanonical choice in the source is identical.

40.28.2 The complete raw row family and the sixth factor

At each prime outside S, divide its valuation in (u) by six. The remainder defines the sixth-power-free ideal $\mathfrak{a}$, and the quotient defines $\mathfrak{r}_6$. The quotient may exceed one and may be positive at a prime of $\mathfrak{a}$. Thus $\mathfrak{r}_6$ is neither assumed squarefree nor made coprime to the first five factors. With the multiplicative primary generators, the quotient $u_0 = u/(\alpha_{\mathfrak{a}}\alpha_{\mathfrak{r}_6}^6)$ is an integral S-supported element, including its literal unit. This decomposition is unique and has the norm relation in (40.110).

For a squarefree good column $\mathfrak{m}$, the sixth-power factor has symbol one when $(\mathfrak{m}, \mathfrak{r}_6) = 1$ and zero otherwise. The exact family identification gives (40.110), even when $\mathfrak{a}, \mathfrak{r}_6$ overlap. In particular a prime common to both factors is still an original raw zero, not two independent masks. For fixed $u_0, \mathfrak{r}_6$ set

$$c_{\mathfrak{m}} = A_U(\mathfrak{m})\nu(\mathfrak{m})\chi_{\mathfrak{m}}(u_0)W(N\mathfrak{m}/D)\mathbf{1}_{(\mathfrak{m},\mathfrak{r}_6)=1}.$$

These coefficients are independent of the remaining row $\mathfrak{a}$. They vanish outside the COMPLETE original good squarefree annulus; putting zero on the extra sixth-power-free indices is permitted. The actual row restrictions can only decrease this positive norm, and

$$\sum_{\mathfrak{m}} |c_{\mathfrak{m}}|^2 \ll_\epsilon B_W^2 D^{1+\epsilon}. \tag{40.115}$$

Indeed $|A_U(\mathfrak{m})| \le 3^{\omega(\mathfrak{m})}$ uniformly in U, and there are $O_K(D)$ ideal columns. This is the original assignment bound; it does not assert $A_U(dn) = A_U(d)A_U(n)$ or use the rough short-coefficient formula on K_0.

The fixed ν and literal/S phase have modulus one on good columns. A row-independent unitary Jacobi factor of nonzero infinity type could also be included in these arbitrary coefficients. This does not turn it into an order-six row character, supply a theorem for varying infinite types, or improve the operator norm by a gauge. Arbitrary positive row weights are not part of this application; they require a true weighted operator bound in the exact identities of Proposition 40.13.

40.28.3 The raw global sum and the principal assembly

For fixed $u_0, \mathfrak{r}_6$, use (40.109) with

$$A = \frac{H}{Nu_0(N\mathfrak{r}_6)^6}, \qquad B = 2D.$$

If $A < 1$ there is no remaining ideal row. If $A = 1$ the unit row remains; it is not dropped as a subunit endpoint. Equations (40.110) and (40.115), and the factor D^{-1} in $|I_u|^2$, give a bound

by $B_W^2(HD)^\epsilon\Phi_6(A,D)$. Now sum all $\mathfrak{r}_6$ of norm at most $(H/Nu_0)^{1/6}$. The $A, A^{5/6}D^{1/3}, A^{1/3}D^{5/6}$ terms use respectively

$$\sum_{\mathfrak{r}_6}(N\mathfrak{r}_6)^{-6}, \qquad \sum_{\mathfrak{r}_6}(N\mathfrak{r}_6)^{-5}, \qquad \sum_{\mathfrak{r}_6}(N\mathfrak{r}_6)^{-2},$$

which converge. The D term instead uses the ideal count $O_K((H/Nu_0)^{1/6})$. Thus the four resulting terms are

$$\begin{aligned} &H(Nu_0)^{-1}, \qquad DH^{1/6}(Nu_0)^{-1/6}, \\ &H^{5/6}D^{1/3}(Nu_0)^{-5/6}, \qquad H^{1/3}D^{5/6}(Nu_0)^{-1/3}. \end{aligned} \tag{40.116}$$

Every exponent on the fixed finite S-supported semigroup is positive, so these sums converge geometrically, with the six literal units included. This proves the raw part of Proposition 40.17, with every arbitrary sixth-factor overlap still represented by its coefficient mask.

For the residue-subtracted family, use the original formula (40.2). Its deleted Euler residue is bounded by a fixed constant and

$$\sum_d \frac{|\beta_U(d)|}{Nd} \le \left(\sum_{Na\le U}\frac{1}{Na}\right)^2 \ll_K \log^2(2U).$$

Therefore $|P_u| \ll_{\nu,S} B_W\sqrt{D}\log^2(2U)$ on a principal row. Outside S, such a row has all valuations divisible by six, since the original ν has its defining conductor in S. The already established count is $O_{\nu,S,\epsilon}(H^{1/6}(HD)^\epsilon)$. Consequently

$$\sum_u |P_u|^2 \ll_{\nu,S,\epsilon} B_W^2(HD)^\epsilon DH^{1/6}. \tag{40.117}$$

Using $|I-P|^2 \le 2|I|^2+2|P|^2$ proves the stated E_u bound. No Artin holomorphy, spectral positivity or zero-location assertion is used. For $1\le H\le D$, each of the four terms in Φ_{all} is at most $DH^{1/6}$, proving (40.111). The varying-W_D construction of Section 40.17 gives a compatible supremum-norm-class obstruction; it does not make a fixed-W lower bound.

40.28.4 The signed $A_6 = 1$ common-divisor form

For a fixed u_0 the first-five physical ideal is sixth-power-free. For the two-pivot block it is exactly $v_1v_2^2$, of norm at most H/Nu_0, not Nv_1Nv_2. Apply the positive norm (40.109) inside the exact common-divisor identity (40.32). For each squarefree good d, put $L = D/Nd$ and keep the original coefficient $A_U(dn)$, the column mask $(n, dS) = 1$, and the raw row mask $(d,u) = 1$. The row mask may be enlarged only inside the positive bound. The assignment bound and ideal count give coefficient squared norm $\ll_\epsilon B_W^2D^\epsilon L$ for $L\ge 1$. For $1/2\le L<1$ the only possible good residual is the unit; its direct row count is bounded by the same polynomial up to an absolute factor. There are no active columns for $L<1/2$. Thus, only now taking the triangle over d,

$$|S_1^{AA}| \ll B_W^2(HD)^\epsilon \sum_{Nd\le 2D}\frac{1}{Nd}\Phi_6(H/Nu_0, D/Nd).$$

The four ideal sums have exponents $1, 2, 4/3, 11/6$. The first is logarithmic, and the others converge, which proves the fixed-u_0 assertion of Proposition 40.18. If all S-supported u_0 are included, the terms with positive Nu_0 exponent sum geometrically. The D term has exponent zero and costs

only the finite count $O_S((\log(2H))^{|S|})$, absorbed into $(HD)^{\epsilon}$. It is not summed as a convergent exponent-zero Euler product.

The accepted identity of Section 40.25 gives

$$S_1^{AA} = \frac{K_0 - K_{\mathrm{all}}}{D} + \mathcal{E}_{\mathrm{corr}}, \qquad |\mathcal{E}_{\mathrm{corr}}| \le 236800 B_W^2 R_w$$

in its stated high window and at $H \le D^{3/4}$. This retains its ordered (p, q) correction, including $p = q$ and the asymmetric restored prime mask; it is distinct from the unordered unit correction C_2. Taking this already bounded correction gives (40.112). Neither K_0 nor K_{all} is separately bounded by a substituted marginal mean. The resulting 13/12 bound is an improved positive comparison, not the target signed estimate.

40.28.5 The updated short certificate and its unresolved input

For a nonempty block $H_b \ge 1$. At $1 \le L \le D$, the two already established block bounds and the new physical-row bound are all valid positive estimates of the SAME actual unweighted operator. Their minimum is Proposition 40.19. The factor 8 in H_b is the literal dyadic bound $Nv_1(Nv_2)^2 < 8A_1A_2^2$, with the original capacity retained. No radical conductor is substituted for that physical norm. At $1/2 \le L < 1$ retain the actual unit-column norm. For the exact mean-retaining Abel identity of Proposition 40.13, write $X_0 = D/U$ and $M_1(W) = \max(\|W\|_\infty, \|xW'\|_\infty)$. Its sufficient positive discrepancy certificate is

$$\frac{|\mathcal{E}_{\mathrm{PIT}}|}{D} \ll (HD)^{\epsilon} M_1(W)^2 \delta_S(U) \left\{ \lambda_{\mathrm{now},*}(X_0) + \int_{1/2}^{X_0} \lambda_{\mathrm{now},*}(L) \frac{dL}{L} \right\}.$$

Here $U \ge 7$ is retained for the Li/Stieltjes definition, and the lower endpoint $E_S(U)Q(U)$ is still part of the exact identity. The minimum must stay inside the integral for general neighboring capacity-feasible blocks. It is not a variance-only substitution. At the critical line, the four new short monomial powers are $3/4, 1/2, 19/24, 2/3$. The pure minimum is 19/24; in the mixed $A_1 \asymp D^{5/12}, A_2 \asymp D^{1/6}$ neighborhood the old 7/9 entry remains smaller. Equating those majorant powers with the 3/4 target gives the sufficient scalar exponents in (40.113). These are not actual-error lower bounds. The conditional strip implication in Theorem 40.15 therefore has boundaries 11/12 and 17/18 for these proposed inputs; no such input or strip has been established here. In particular, pointwise endpoint control and the coherent signed $K_0 - J$ are not supplied by an independent mean-square assumption alone.

The new primary input improves a positive norm certificate. Equal-norm ideal orientations, coherent means, original common profiles, full-union raw zeros and all fixed-conductor qualifications remain. The actual signed target, independent determinant bridge and analytic/category Lean work remain open.

40.29 Coherent dual bands, actual cutoffs and arithmetic localization

The physical-row comparison in Section 40.27 leaves a signed problem. We now retain its exact primitive roots and sharp row capacity, prove quantitative finite-prefix and divisor-band comparisons, and localize a coherent sector that can already be controlled. The remaining unequal-norm signed moment is stated explicitly. These results do not improve the whole signed power 13/12 or the global unsigned power 9/8. The deep sieve input remains the pinned external theorem (40.109); its cubic specialization is used below.

40.29.1 The original form and the scope of the dual representation

Let $K=\mathbb{Q}(\omega)$, $\mathcal{O}=\mathbb{Z}[\omega]$ and $\delta=1+2\omega=i\sqrt{3}$. The fixed set S contains the primes above $2,3$ and the original exclusions. All columns are the complete good squarefree *ideal* annulus $D\le N\mathfrak{m}\le 2D$, $D>1$. Distinct ideals of the same norm remain distinct. Put

$$\begin{aligned} A_U(\mathfrak{m}) &= \sum_{\substack{\mathfrak{r}\mathfrak{s}\mid\mathfrak{m}\\(\mathfrak{r},\mathfrak{s})=1\\ N\mathfrak{r},N\mathfrak{s}\le U}} \mu(\mathfrak{r})\mu(\mathfrak{s}),\\ c_{\mathfrak{m}} &= A_U(\mathfrak{m})\nu(\mathfrak{m})R_{\mathfrak{m}}(u_0)W(N\mathfrak{m}/D). \end{aligned} \tag{40.118}$$

Here $1\le U\le\sqrt{D}$, ν is the original fixed unitary finite-order column character, and W is one common possibly complex smooth profile supported on $[1,2]$, zero at its endpoints. Write $B_W=\|W\|_\infty$. For a good ideal $\mathfrak{v}$, let $\alpha_{\mathfrak{v}}\equiv 1 \pmod 3$ be its unique primary generator and set $R_{\mathfrak{m}}(\mathfrak{v})=(\alpha_{\mathfrak{v}}/\mathfrak{m})_6$. The literal symbol is zero at a common prime. A primitive extension at an S-argument below is a different object, not restoration of a deleted raw row value.

Let $A_1,A_2\ge 1$. Only the original unweighted two-pivot rows are used:

$$u=u_0\alpha_{\mathfrak{v}_1}\alpha_{\mathfrak{v}_2}^2,\qquad A_i\le N\mathfrak{v}_i<2A_i,\qquad Nu_0N\mathfrak{v}_1(N\mathfrak{v}_2)^2\le H.$$

The ideals $\mathfrak{v}_1,\mathfrak{v}_2$ are good, squarefree and coprime; all actual literal and ray restrictions remain. The other four factors are the unit ideal. The fixed u_0 is literal unit/S-supported, without good-prime support. Extra good frozen factors, a sum over varying u_0, and arbitrary row weights are not included. Write $R=A_1A_2$ and let R_w be the actual number of rows. The normalization is

$$\begin{aligned} \mathcal{P}_D &= DS_1^{AA}\\ &= \sum_{(\mathfrak{v}_1,\mathfrak{v}_2)\ \text{actual}}\ \sum_{(\mathfrak{m},\mathfrak{n})=1} c_{\mathfrak{m}}\overline{c_{\mathfrak{n}}}R_{\mathfrak{m}}(\mathfrak{v}_1\mathfrak{v}_2^2)\overline{R_{\mathfrak{n}}(\mathfrak{v}_1\mathfrak{v}_2^2)}. \end{aligned} \tag{40.119}$$

The original Möbius signs are already in the two A_U coefficients; no additional $\mu(\mathfrak{m}\mathfrak{n})$ is inserted. This raw coprime form is not a positive energy or principal-term assembly.

40.29.2 Primitive normalization and an exact finite-cutoff kernel

For each source class A, use the fixed decomposition $\widetilde{\chi}_{\mathfrak{m}}=\xi_{\mathfrak{m}}\psi_A$, $\mathrm{cond}(\xi_{\mathfrak{m}})=\mathfrak{m}$, and $\beta_{\mathfrak{m}}=\epsilon(\xi_{\mathfrak{m}})\psi_A(\mathfrak{m})$. Individual ξ and ψ may have nonzero fixed angular and radial unitary types; they are not declared sixth-order. The finite source reciprocity factors and the *whole* original row-ray projector are expanded in their complete finite character basis, with coefficients $h_{AB\rho}(\mathfrak{v}_2)$. On coprime class-$A,B$ columns the resulting primitive character is

$$\begin{aligned} &\sigma=\mathrm{prim}(\rho\psi_A\overline{\psi_B}),\quad \mathfrak{f}_S=\mathrm{cond}(\sigma),\\ &\eta=\xi_{\mathfrak{m}}\overline{\xi_{\mathfrak{n}}}\sigma,\qquad\qquad F=N\mathfrak{f}_S\,N\mathfrak{m}\,N\mathfrak{n}. \end{aligned} \tag{40.120}$$

Its total infinity type is zero. The actual S conductor, including any drop, is retained.

Proposition 40.20 (Primitive roots with their types retained)**.** *For a primitive unitary Hecke character $\chi((\alpha))=\theta(\alpha)\,\mathrm{phase}(\alpha)^kN(\alpha)^{it}$, with conductor (γ), let*

$$\tau_\gamma(\theta)=\sum_{x \bmod \gamma}\theta(x)\exp\bigl(2\pi i\,\mathrm{Tr}(x/(\delta\gamma))\bigr).$$

Then

$$\epsilon(\chi) = (3N\mathfrak{f})^{it} i^{-|k|} \operatorname{phase}(\delta\gamma)^k \frac{\tau_\gamma(\theta)}{\sqrt{N\mathfrak{f}}}. \tag{40.121}$$

The unit-conductor/principal formula has its usual meromorphic terms. For pairwise coprime primitive conductors,

$$\epsilon\Big(\prod_j \chi_j\Big) = i^{\sum_j |k_j| - |\sum_j k_j|} \prod_j \epsilon(\chi_j) \prod_{i\neq j} \chi_i(\mathfrak{f}_j). \tag{40.122}$$

Consequently the actual character in (40.120) *satisfies*

$$\begin{aligned} \epsilon(\eta) &= \kappa_{AB\rho} u_{\mathfrak{m}} \overline{v_{\mathfrak{n}}}, \\ u_{\mathfrak{m}} &= \beta_{\mathfrak{m}} \xi_{\mathfrak{m}}(\mathfrak{f}_S) \rho(\mathfrak{m}), \\ v_{\mathfrak{n}} &= \beta_{\mathfrak{n}} \xi_{\mathfrak{n}}(\mathfrak{f}_S) \overline{\rho(\mathfrak{n})}. \end{aligned} \tag{40.123}$$

The scalar $\kappa_{AB\rho}$ is fixed. These are two distinct unitary column gauges. The primitive values $\sigma(\mathfrak{e})$ and $\sigma(\mathfrak{h})$ at S, including zero, remain separately in the kernel; they cannot be replaced by ρ there.

This closes the normalization hypothesis for these stated conventions. A bounded, invertible change of phases gives no power saving by itself.

For a fixed actual $\mathfrak{v}_2$, define the exact integer endpoints

$$a = \lceil A_1 \rceil, \qquad b = \min\{\lceil 2A_1 \rceil - 1, \lfloor H/(Nu_0(N\mathfrak{v}_2)^2) \rfloor\}.$$

An empty interval contributes zero. Choose one fixed nondecreasing smooth step s_0, equal to zero on $(-\infty, 0]$ and one on $[1, \infty)$, and put

$$G_{\mathfrak{v}_2}(x) = s_0(4(A_1 x - a + 1/2)) s_0(4(b + 1/2 - A_1 x)). \tag{40.124}$$

It is the exact row indicator at every ideal norm node, has amplitude at most one, support in $[1/2, 5/2]$ and total variation at most two. Its derivatives cost powers of A_1; it is not the fixed column W. Set $C_0 = 3/(4\pi^2)$ and

$$\dot{G}(X) = C_0^{-1/2} \int_0^\infty G(t) J_0(2\sqrt{Xt/C_0})\, dt. \tag{40.125}$$

Proposition 40.21 (The actual signed kernel before absolute norms)**.** *For every nonzero class/ray component, the good conductor of η is $\mathfrak{mn}$, so η is nonprincipal. Put $P_S = \prod_{p\in S} p$ and*

$$L_{\mathfrak{e}} = \frac{A_1}{(N\mathfrak{k})^2 N\mathfrak{l} N\mathfrak{e}}, \qquad K_{\mathfrak{l}} = \sqrt{b/N\mathfrak{l}}.$$

Squarefree-row inversion, finite S deletion and primitive Poisson give (40.119) *by summing the following kernel:*

$$\begin{aligned} &c_{\mathfrak{m}} \overline{c_{\mathfrak{n}}} R_{\mathfrak{m}}(\mathfrak{v}_2^2) \overline{R_{\mathfrak{n}}(\mathfrak{v}_2^2)} h_{AB\rho}(\mathfrak{v}_2) \\ &\quad \cdot \mu(\mathfrak{k})\mu(\mathfrak{l})\mu(\mathfrak{e}) \eta(\mathfrak{k}^2\mathfrak{l}\mathfrak{e}) \epsilon(\eta) \frac{L_{\mathfrak{e}}}{\sqrt{F}} \sum_{\mathfrak{y}} \dot{G}_{\mathfrak{v}_2}(L_{\mathfrak{e}} N\mathfrak{y}/F) \overline{\eta(\mathfrak{y})}. \end{aligned} \tag{40.126}$$

The outer sums are over every actual $\mathfrak{v}_2$, every class/ray component and original coprime column pair, all $\mathfrak{l} \mid \mathfrak{v}_2$ with $N\mathfrak{l} \le b$, all good squarefree $\mathfrak{k}$ with $(\mathfrak{k}, \mathfrak{v}_2) = 1$ and $N\mathfrak{k} \le K_{\mathfrak{l}}$, and every $\mathfrak{e} \mid P_S$. The dual sum is over all *nonzero integral ideals, including S-supported ones. It converges at each fixed parameter set with the actual derivative constants of G. The original pre-S cutoff is never extended in this identity.*

All signs, means, product norms and raw zeros occur before a triangle. A higher induced modulus does not have a unit Gauss root automatically: its nonprimitive additive frequencies may vanish.

40.29.3 What finite prefixes and actual divisor bands now satisfy

Write

$$\begin{aligned}\Phi(Z,L) &= Z + LZ^{1/6} + Z^{5/6}L^{1/3} + Z^{1/3}L^{5/6},\\ I(t) &= \sum_{j\ge 0} \frac{t^j}{(j!)^2}.\end{aligned} \tag{40.127}$$

Let $\mathcal{P}_{\le X}$ retain all terms of (40.126) with $N\mathfrak{y} \le X$, including every source/ray/S component.

Proposition 40.22 (All-component exact finite prefixes)**.** *For every finite $X \ge 1$,*

$$\frac{|\mathcal{P}_{\le X}|}{D} \ll B_W^2 (DXA_2)^{\epsilon} \frac{A_1A_2}{D} \Phi(X,D). \tag{40.128}$$

A separate exact all-orders estimate is

$$|\mathcal{P}_{\le X}| \ll B_W^2 (DXA_2)^{\epsilon} A_1A_2 \Phi(X,D) I\left(\frac{(5/2)A_1X}{C_0D^2}\right). \tag{40.129}$$

No completed Euler model, low-frequency approximation or $X \le \sqrt{H}$ hypothesis is used in (40.128)*. On a fixed same-source-class/$\rho = 1$ component, the additional critical-half band estimate is*

$$\frac{|\mathcal{P}_{C,1}(Y,2Y]|}{D} \ll B_W^2 (DYA_2)^{\epsilon} A_2 \sqrt{A_1/Y}\, \Phi(Y,D)(1+\log(2A_1))^2. \tag{40.130}$$

Constants depend on the fixed S, ray/source data, ν, step and ϵ, not on any hidden uniform smoothness of the sharp G.

At $H \asymp D^{3/4}$, the mixed witness $(A_1,A_2) \asymp (D^{5/12}, D^{1/6})$ has a target-sized full finite prefix $X \asymp D$. The pure prefix at $X = D$ has upper power $11/12$. At $X = D^{3/8}$ the pure/mixed powers are $13/16$ and $31/48$. These growing bounds cannot be sent to $X = \infty$.

Proposition 40.23 (Finite transfer of the actual cutoff and profile)**.** *Let $X \ge 2$, $1 \le U \le X$, and let $K = (K_{\mathfrak{d}\mathfrak{a}})$ be a finite matrix indexed by good squarefree ideals of norms at most X, zero unless $(\mathfrak{d},\mathfrak{a}) = 1$ and $N\mathfrak{d}N\mathfrak{a} \le X$. All additional masks may remain in K. Set*

$$\begin{aligned}G_{\mathcal{I}\mathcal{J}} &= \max_{\mathfrak{d}\in\mathcal{I}} 3^{\omega(\mathfrak{d})} \max_{\mathfrak{a}\in\mathcal{J}} 3^{\omega(\mathfrak{a})},\\ c_P &= 1/\log(4X), \qquad L_T = \operatorname{asinh}(T/c_P)/\pi.\end{aligned}$$

Empty matrices are zero. For every finite $T \ge 8X$,

$$\|[A_U(\mathfrak{d}\mathfrak{a})K_{\mathfrak{d}\mathfrak{a}}]\|_{\mathrm{op}} \le G_{\mathcal{I}\mathcal{J}} \left(e^2L_T^2 + \frac{32X^{3/2}}{T}\right) \|K\|_{\mathrm{op}}. \tag{40.131}$$

For $T = (4X)^4$ this is $O_\epsilon(X^\epsilon \log^2(4X))\|K\|$. The common complex multiplier $W(N\mathfrak{d}N\mathfrak{a}/D)$ costs

$$\begin{aligned}M(W) &= \frac{1}{2\pi}\int_{\mathbb{R}} |\widehat{W}(it)|\,dt, \qquad \widehat{W}(s) = \int_0^\infty W(x)x^s\,\frac{dx}{x},\\ M(W) &\le \frac{\log 2}{\pi}(B_W + \|xW'(x) + x^2W''(x)\|_\infty).\end{aligned} \tag{40.132}$$

Two occurrences in a bilinear/Gram estimate cost the square of the transfer norm. This is not $A_U(\mathfrak{d}\mathfrak{a}) = A_U(\mathfrak{d})A_U(\mathfrak{a})$ or coefficient shrinkage.

Proposition 40.24 (A cubic comparison for an actual auxiliary band)**.** *Fix one same-source-class/$\rho = 1$ component of the auxiliary individual-column extension of* (40.126)*. Insert the exact coprime identity $\sum_{\mathfrak{d}|(\mathfrak{m},\mathfrak{n})} \mu(\mathfrak{d})$, and retain the* identity-source-class *divisors $E < N\mathfrak{d} \le 2E$, $1 \le E \le D/2$. Denote the resulting exact signed dual band by $\mathcal{P}^{\mathrm{id}}_{E,C}(Y, 2Y]$. Put $L = D/E$ and $\Theta_3(E, L) = E + L + (EL)^{2/3}$. For fixed $0 < \lambda < 1/2$,*

$$\begin{aligned}\frac{|\mathcal{P}^{\mathrm{id}}_{E,C}(Y, 2Y]|}{D} &\ll M(W)^2 (DYA_2)^{\epsilon} A_2 A_1^{1-\lambda} D^{2\lambda-1} Y^{-\lambda} \\ &\quad \cdot \min\{\Phi(Y, L),\ (Y/E)\Theta_3(E, L)\}.\end{aligned} \tag{40.133}$$

The arithmetic identity behind the new branch is

$$\beta_{\mathfrak{d}\mathfrak{a}} = \epsilon(\widetilde{\chi}_{\mathfrak{d}})\beta_{\mathfrak{a}}\alpha(1, C)\widetilde{\chi}_{\mathfrak{a}}(\mathfrak{d})^2, \qquad [\mathfrak{d}] = 1, \quad [\mathfrak{a}] = C. \tag{40.134}$$

It exposes the physical cubic residue matrix in $\mathfrak{d}, \mathfrak{a}$. The external input is de Faveri, Theorem 1.1 and Example 2.2, now at $n = 3$, not a conductor-parametric sieve.

This improves a *scoped norm comparator*: at $E \asymp D^{2/3}$ the second branch is $O(Y)$. It still uses $|\mu(\mathfrak{d})| \le 1$ at its final Cauchy step. Such $\mathfrak{d}$ are auxiliary divisors, not the original column-pair gcd h. All divisor classes, small $\mathfrak{d}$ and the full high-dual sum are not bounded here.

40.29.4 Coherent means that can be localized, and those that remain

Proposition 40.25 (The full equal-norm sector)**.** *Original coprime squarefree columns with $N\mathfrak{m} = N\mathfrak{n} = N > 1$ satisfy $\mathfrak{n} = \overline{\mathfrak{m}}$, with rational-squarefree N supported on split rational primes. The original good masks require* both *primes above each such rational prime to avoid S; S need not be enlarged or conjugation-stable. There are $O(D)$ ordered annular pairs. Define S_{eq} as the normalized contribution to S_1^{AA}, namely D^{-1} times their full primal contribution to $\mathcal{P}_D$ in* (40.119)*. Then*

$$|S_{\mathrm{eq}}| \ll B_W^2 R_w D^{\epsilon} \ll B_W^2 R (DH)^{\epsilon}. \tag{40.135}$$

Before the factor D^{-1}, their ordered orientation sum at norm N is

$$\begin{aligned}a_U(N)^2 |W(N/D)|^2 \prod_{p|N} \{a_p \chi_p(t) + \overline{a_p \chi_p(t)}\}, \\ t = N u_0 N \mathfrak{v}_1 (N\mathfrak{v}_2)^2,\end{aligned} \tag{40.136}$$

where $a_p = \nu(\pi_p)\overline{\nu(\bar{\pi}_p)}$, $\chi_p(t) = (t/\pi_p)_6$, and $a_U(N) = \sum_{rs|N,(r,s)=1,r,s\le U} \mu_{\mathbb{Z}}(r)\mu_{\mathbb{Z}}(s)$. This includes all ordered orientations and every raw collision zero. For the all-component primitive-ideal prefix/band,

$$\frac{|\mathcal{P}_{\mathrm{eq}}(\le Y)| + |\mathcal{P}_{\mathrm{eq}}(Y, 2Y]|}{D} \ll B_W^2 (DYA_2)^{\epsilon} RY/D. \tag{40.137}$$

The signed complement is bounded by the whole primal term minus that prefix, not by an absolute high-mode summation.

Since $R \ll H$ on nonempty blocks, the desired full fixed-W target is equivalent, up to (40.135), to that for unequal norms. Its desired constants may depend on fixed W or appropriate specified seminorms. Formula (40.136) is neither identically zero nor positive in general.

Proposition 40.26 (Literal-ray recombination in the pure sector)**.** *In the pure case $\mathfrak{v}_2 = \mathcal{O}$, choose an S-supported ray modulus $\mathfrak{c} = (\gamma_c)$ divisible by (6). For an original coprime pair put $\mathfrak{q} = \mathfrak{m}\mathfrak{n}$, $Q = N\mathfrak{q}$, $\gamma_q = \alpha_{\mathfrak{m}}\alpha_{\mathfrak{n}}$, and let $\vartheta_{\mathfrak{q}}(x) = (x/\mathfrak{m})_6\overline{(x/\mathfrak{n})_6}$ be the primitive finite character modulo $\mathfrak{q}$. Let $P_{\mathfrak{k}^2}$ be the full literal primary/good-S/ray indicator on $\mathcal{O}/\mathfrak{c}$ after $v_1 = k^2 z$, with finite additive transform $\widehat{P}$. The exact common-modulus Fourier coefficient is*

$$\widehat{F}_{\mathfrak{k}^2}(\beta) = \tau_{\mathfrak{q}}\vartheta_{\mathfrak{q}}(\gamma_c)\overline{\vartheta_{\mathfrak{q}}(\beta)}\widehat{P}_{\mathfrak{k}^2}(\beta\gamma_q^{-1} \bmod \mathfrak{c}). \tag{40.138}$$

Its literal-lattice radial Poisson prefactor is $L_{\mathfrak{k}}/(N\mathfrak{c}Q)$, $L_{\mathfrak{k}} = A_1/(N\mathfrak{k})^2$. The S-local Fourier-mean sublattice $\beta = \gamma_c\zeta$ has coefficient $r_{\mathfrak{k}^2}\tau_{\mathfrak{q}}\overline{\vartheta_{\mathfrak{q}}(\zeta)}$, where $r = \sum P$. The six-unit projection annihilates every nontrivial unit restriction and retains the unit-trivial branch, whose condition is

$$N\mathfrak{m} \equiv N\mathfrak{n} \pmod{36}. \tag{40.139}$$

For the basic S above $2, 3$ with no extra ray condition, $\mathfrak{c} = (6)$ has $r = 3$ and ideal coefficient $6r/N\mathfrak{c} = 1/2$. This is not the global $\beta = 0$ mode, which vanishes. All S-supported dual ideals remain, with values defined by any generator once the character is unit-trivial.

Literal additive bands and the earlier primitive-ideal bands have different fixed-S frequency support/rescalings; no unmatched windows are identified. Unequal norms congruent modulo 36 and all other literal residue channels remain. Finite ray recombination supplies no automatic zero mean or signed target estimate.

Remaining arithmetic obligation. A finite-prefix comparison, the sparse equal-norm sector and the cubic auxiliary-band comparison do not bound the complete signed unequal-norm kernel. The required additional estimate must retain all small divisors/source classes and the literal S mean together with complementary residues before the final conductor/divisor/dual triangle. No desired positivity, energy lower bound, new zero-free strip, determinant comparison, analytic Lean or GRH claim follows.

40.30 Proofs for the coherent-band comparisons

These proofs use de Faveri's pinned arXiv:2610.04045v1, Theorem 1.1 and its stated character family as external input. The primitive Poisson convention agrees with its Lemma 3.1; the formulas below also derive the normalization. This is not a proof of that deep large-sieve theorem. The source version and independent proof reviews are bound by the accompanying source map; full third-party reading caches are not public source dependencies.

40.30.1 Finite Fourier transforms and the primitive Gaussian

For $\mathfrak{f} = (\gamma)$ use the primitive additive pairing

$$e_\gamma(x) = \exp\bigl(2\pi i \operatorname{Tr}(x/(\delta\gamma))\bigr), \qquad \delta = 1 + 2\omega.$$

Let θ be primitive modulo $\mathfrak{f}$, extended by zero at nonunits of this *actual* conductor. For every $\beta \in \mathcal{O}$,

$$\sum_{x \bmod \gamma} \theta(x)e_\gamma(\beta x) = \overline{\theta(\beta)}\tau_\gamma(\theta). \tag{40.140}$$

At a unit this is change of variable. At a nonunit frequency the additive character factors through a proper conductor quotient. Primitivity supplies a unit in the kernel of unit reduction on which

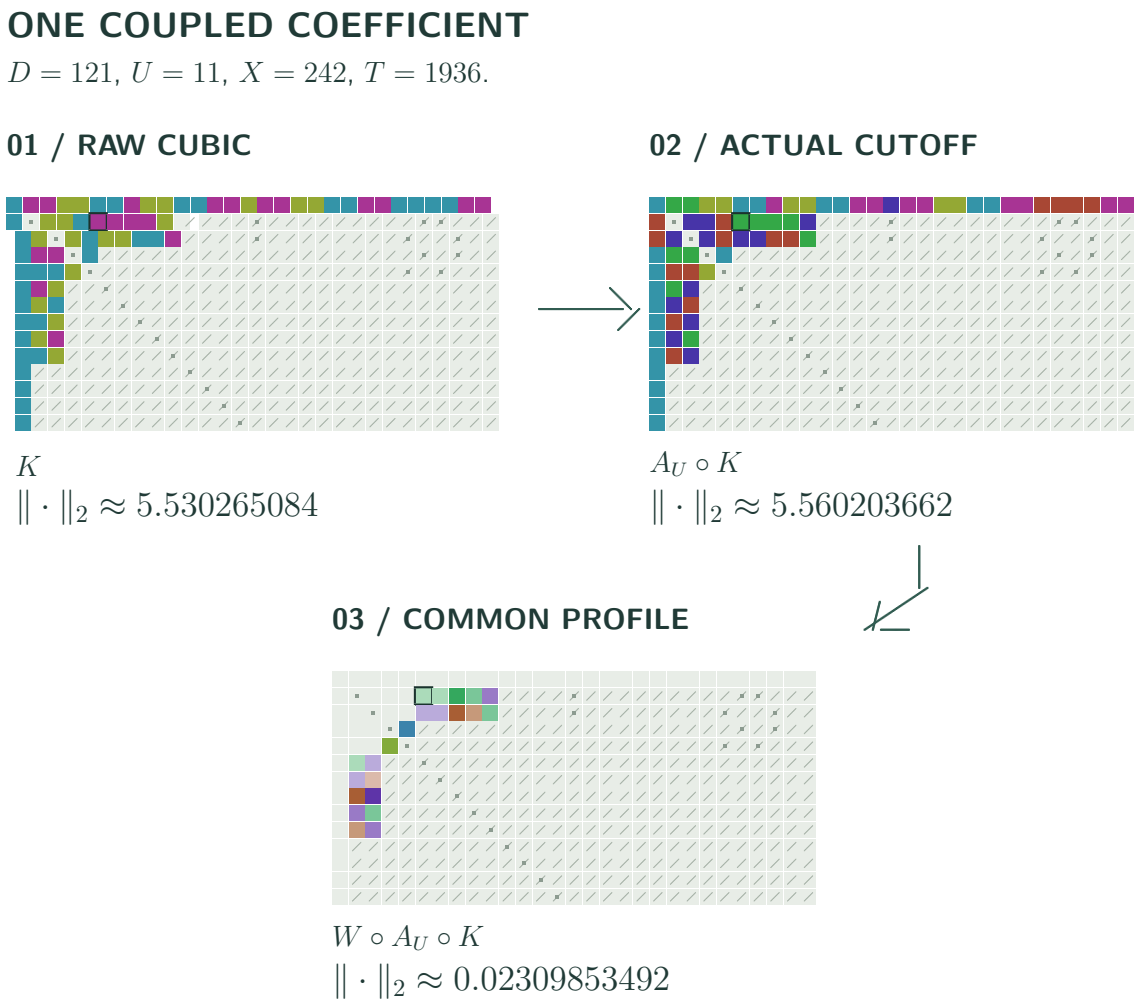


Figure 40.2: A source-bound finite Schur replay. All three cases retain the full 14×29 matrix and every support zero; the workflow distinguishes saved numerical consistency values from analytic uniform bounds. The full signed unequal-norm kernel remains open.

θ is nontrivial. Multiplication by that unit leaves the additive factor unchanged and forces the sum to vanish. Unit reduction is surjective prime by prime and hence by CRT. Parseval for this nondegenerate finite additive pairing gives

$$\sum_{\beta \bmod \mathfrak{f}} \left| \sum_{x} \theta(x) e_\gamma(\beta x) \right|^2 = N\mathfrak{f}\, \varphi(\mathfrak{f}), \qquad |\tau_\gamma(\theta)|^2 = N\mathfrak{f}.$$

For the unit conductor use its one-element convention $\tau = 1$. For coprime γ_1, γ_2, the two CRT frequencies are γ_2^{-1} and γ_1^{-1}, so

$$\tau_{\gamma_1\gamma_2}(\theta_1\theta_2) = \theta_1(\gamma_2)\theta_2(\gamma_1)\tau_{\gamma_1}(\theta_1)\tau_{\gamma_2}(\theta_2). \tag{40.141}$$

The product is primitive because each ramified local conductor occurs in only one factor.

Here are the archimedean factors that a raw Gauss sum alone would miss. Put $d = |k|$ and

$$P_k(z) = \begin{cases} z^k, & k \geq 0, \\ \bar{z}^{-k}, & k < 0. \end{cases}$$

With Euclidean Fourier transform $\widehat{g}(w) = \int_{\mathbb{C}} g(z) e^{-2\pi i \operatorname{Re}(z\bar{w})}\, dz$, differentiating the two-dimensional Gaussian gives

$$\widehat{P_k(z)e^{-\pi b|z|^2}}(w) = (-i)^d b^{-d-1} P_k(w) e^{-\pi|w|^2/b}, \qquad b > 0. \tag{40.142}$$

Holomorphic or antiholomorphic harmonicity removes the lower contraction terms. The sign is $(-i)^{|k|}$ for either sign of k. Let $\chi_0 = \chi N^{-it}$ and $a_\gamma = 2/(\sqrt{3}|\gamma|)$. Its theta series is

$$\Theta_{\chi_0}(t) = \sum_{\alpha \in \mathcal{O}} \theta(\alpha) P_k(\alpha) e^{-\pi a_\gamma t |\alpha|^2}.$$

The lattice $\gamma\mathcal{O}$ has covolume $(\sqrt{3}/2)|\gamma|^2$ and dual lattice $2/(\bar{\gamma}\bar{\delta})\mathcal{O}$. Write a dual point as $w = 2\bar{\beta}/(\bar{\gamma}\bar{\delta}) = c\bar{\beta}$. Then $|c| = a_\gamma$ and $\operatorname{phase}(c) = \operatorname{phase}(\delta\gamma)$. Equations (40.140) and (40.142), applied in each residue class, yield

$$\Theta_{\chi_0}(t) = i^{-d} \operatorname{phase}(\delta\gamma)^k \frac{\tau_\gamma(\theta)}{\sqrt{N\mathfrak{f}}} t^{-d-1} \Theta_{\bar{\chi}_0}(1/t). \tag{40.143}$$

The inverse different and the conductor generator have not been replaced by a raw character value at δ.

Use $\Gamma_{\mathbb{C}}(s) = 2(2\pi)^{-s}\Gamma(s)$ and

$$\Lambda(s, \chi) = (3N\mathfrak{f})^{s/2} \Gamma_{\mathbb{C}}(s - it + d/2) L(s, \chi).$$

Every nonzero ideal has six generators; their contributions agree because $\theta(u)u^k = 1$. The Mellin transform of the theta series, with exponent $s + d/2$, is therefore exactly $3(3N\mathfrak{f})^{d/4}\Lambda(s, \chi_0)$. The same constant occurs on the conjugate side. Mellin integration of (40.143) proves the root formula for $t = 0$. At nonunit conductor the zero frequency vanishes by primitivity. At unit conductor and $k \neq 0$, $P_k(0) = 0$. At unit conductor and $k = 0$, retain the Gaussian zero term when splitting its Mellin integral at one; this gives the usual meromorphic polar terms and root one. They are not dropped from the functional equation.

Changing γ to $u\gamma$ multiplies its Gauss sum by $\theta(u)$ and its angular factor by u^k, whose product is one. Thus the formula is independent of the conductor generator. Complex conjugation gives

$\tau_\gamma(\bar\theta)=\theta(-1)\overline{\tau_\gamma(\theta)}$, where $\theta(-1)=(-1)^k$; together with the angular factor this proves $\epsilon(\bar\chi)=\overline{\epsilon(\chi)}$. Finally

$$\Lambda(s,\chi_0N^{it})=(3N\mathfrak{f})^{it/2}\Lambda(s-it,\chi_0),\qquad \epsilon(\chi_0N^{it})=(3N\mathfrak{f})^{it}\epsilon(\chi_0).$$

This proves (40.121) also for radial unitary twists.

In (40.141), the angular cross factors $\mathrm{phase}(\gamma_2)^{k_1}\,\mathrm{phase}(\gamma_1)^{k_2}$ convert the finite residue values into ideal values $\chi_1(\mathfrak{f}_2)\chi_2(\mathfrak{f}_1)$. The remaining i factor is $i^{|k_1|+|k_2|-|k_1+k_2|}$. Radial cross factors satisfy

$$\prod_j(3N\mathfrak{f}_j)^{it_j}\prod_{i\neq j}(N\mathfrak{f}_j)^{it_i}=\left(3N\prod_j\mathfrak{f}_j\right)^{i\sum_j t_j}.$$

Iteration proves (40.122). Coprimality is a hypothesis on the *actual primitive ideal conductors*, not on rational norms or higher induced moduli.

40.30.2 Transport to every original class and ray component

Let the types of $\xi_{\mathfrak{m}},\xi_{\mathfrak{n}}$ be $(k_A,t_A),(k_B,t_B)$. The character σ in (40.120) has types (k_B-k_A,t_B-t_A). The three primitive conductors $\mathfrak{m},\mathfrak{n},\mathfrak{f}_S$ are pairwise coprime; no good local ramification can cancel against the other two. Applying (40.122) gives

$$\begin{aligned}\epsilon(\eta)&=\gamma_{AB\rho}\epsilon(\xi_{\mathfrak{m}})\overline{\epsilon(\xi_{\mathfrak{n}})}\xi_{\mathfrak{m}}(\mathfrak{n}\mathfrak{f}_S)\overline{\xi_{\mathfrak{n}}(\mathfrak{m}\mathfrak{f}_S)}\sigma(\mathfrak{m}\mathfrak{n}),\\ \gamma_{AB\rho}&=i^{|k_A|+|k_B|+|k_B-k_A|}\epsilon(\sigma).\end{aligned}\tag{40.144}$$

Source reciprocity is $\widetilde{\chi}_{\mathfrak{m}}(\mathfrak{n})\overline{\widetilde{\chi}_{\mathfrak{n}}(\mathfrak{m})}=\alpha(A,B)$. Substituting $\widetilde{\chi}=\xi\psi$ in (40.144) cancels all crossed ψ values and proves (40.123), with $\kappa_{AB\rho}=\alpha(A,B)\gamma_{AB\rho}$. In particular the remaining factor is $\rho(\mathfrak{m})\rho(\mathfrak{n})$, not an assumed class constant; ρ need not factor through the source class group.

For good dual $\mathfrak{z}$, write $\widetilde{\chi}_{\mathfrak{m}}(\mathfrak{z})=\gamma_A(\mathfrak{z})R_{\mathfrak{m}}(\mathfrak{z})$, with the fixed finite reciprocity phase in that class. Then

$$\begin{aligned}\overline{\sigma(\mathfrak{z})\xi_{\mathfrak{m}}(\mathfrak{z})}\xi_{\mathfrak{n}}(\mathfrak{z})&=\Omega_{AB\rho}(\mathfrak{z})\overline{R_{\mathfrak{m}}(\mathfrak{z})}R_{\mathfrak{n}}(\mathfrak{z}),\\ \Omega_{AB\rho}&=\bar\sigma\,\psi_A\bar\psi_B\,\bar\gamma_A\gamma_B,\qquad |\Omega_{AB\rho}(\mathfrak{z})|=1.\end{aligned}\tag{40.145}$$

The equality includes raw collision zeros. This is a fixed unitary *row* phase for each component, not equality of the two column classes. At S the separate scalar $\sigma(\mathfrak{k}^2\mathfrak{l}_{\mathfrak{e}})\overline{\sigma(\mathfrak{h})}$ is kept, including zero. There is no division by such a scalar, and no substitution of $\rho(\mathfrak{e}/\mathfrak{h})$ at a conductor drop. Off the original coprime column support, products of individual column gauges below are only an auxiliary extension. They are not roots or primitive conductors of overlapping pairs.

40.30.3 The sharp capacity, square-divisor signs and exact Poisson

The endpoints in (40.124) are integers. The two smooth transitions lie between ideal norm nodes, so its value at $x=N\mathfrak{v}_1/A_1$ is exactly one or zero according to the original interval and capacity. For nonempty fibres these transitions are disjoint. Their monotonicity gives total variation two; their jth derivatives cost powers of A_1. The elementary identity

$$\sum_{\mathfrak{v}\ \text{good}}\mu(\mathfrak{v})^2\mathbf{1}_{(\mathfrak{v},\mathfrak{v}_2)=1}B(\mathfrak{v})=\sum_{\substack{\mathfrak{k}\ \text{good,SF}\\(\mathfrak{k},\mathfrak{v}_2)=1}}\mu(\mathfrak{k})\sum_{\mathfrak{l}\mid\mathfrak{v}_2}\mu(\mathfrak{l})\sum_{\mathfrak{z}\ \text{good}}B(\mathfrak{k}^2\mathfrak{l}\mathfrak{z})\tag{40.146}$$

follows by expanding the squarefree indicator and then the remaining coprimality indicator. Auxiliary $\mathfrak{z}$ need not be squarefree, and may overlap $\mathfrak{k}$ or $\mathfrak{l}$. The original norm support fixes $N\mathfrak{l}\le b$ and

$N\mathfrak{k} \le \sqrt{b/N\mathfrak{l}}$ *before* Poisson. Including more $\mathfrak{k}$ would add zero primal terms whose individual dual windows need not be zero.

On good $\mathfrak{v}_1$, expand exactly

$$\mathbf{1}_{\mathrm{ray}} R_{\mathfrak{m}}(\mathfrak{v}_1)\overline{R_{\mathfrak{n}}(\mathfrak{v}_1)} = \sum_{\rho} h_{AB\rho}(\mathfrak{v}_2)\eta_{\mathfrak{m},\mathfrak{n},\rho}(\mathfrak{v}_1).$$

This includes every reciprocity/ray component, not a selected same class term. With $L = A_1/((N\mathfrak{k})^2 N\mathfrak{l})$, good-$S$ deletion is the *finite* identity

$$\sum_{\mathfrak{z}\ \text{good}} G(N\mathfrak{z}/L)\eta(\mathfrak{z}) = \sum_{\mathfrak{e}\mid P_S} \mu(\mathfrak{e})\eta(\mathfrak{e}) \sum_{\mathfrak{y}} G(N\mathfrak{y}/(L/N\mathfrak{e}))\eta(\mathfrak{y}). \tag{40.147}$$

Primitive zeros at S suppress the corresponding terms automatically. They do not assign forbidden raw values to an original row.

For a nonprincipal primitive type-zero η of conductor norm F, its normalized functional equation and ordinary Mellin inversion give

$$\sum_{\mathfrak{y}} G(N\mathfrak{y}/L)\eta(\mathfrak{y}) = \epsilon(\eta)\frac{L}{\sqrt{F}} \sum_{\mathfrak{y}} \dot{G}(LN\mathfrak{y}/F)\overline{\eta(\mathfrak{y})}. \tag{40.148}$$

To see the field constant explicitly, put

$$\gamma_K(s) = C_0^{s-1/2}\frac{\Gamma(s)}{\Gamma(1-s)}, \qquad \widehat{G}(s) = \int_0^\infty G(t)t^s\,\frac{dt}{t}.$$

The Mellin transform of (40.125) is $\gamma_K(s)\widehat{G}(1-s)$. The Bessel identity may first be justified absolutely in $0 < \operatorname{Re} s < 1/4$; smooth compact support and repeated Hankel integration by parts continue it to $\operatorname{Re} s > 0$ at each fixed G. Mellin inversion of the primal ideal sum, its primitive functional equation, and the change $s \mapsto 1-s$ now give (40.148) with exactly $L/\sqrt{F}$. There is no principal residue since η has nonempty good ramification. The intermediate contour moves involve the entire nonprincipal completed function and the fixed smooth transform, not an inverse L function or an assumed zero-free strip. This also recovers the pinned source Lemma 3.1 convention.

At a good prime ideal of norm P, a nontrivial primitive character modulo p lifted to p^j, $j \ge 2$, has raw Gauss sum zero for a primitive additive frequency. More generally it vanishes unless the frequency has valuation $j-1$, when its value is $P^{j-1}\bar{\chi}(\beta/\pi^{j-1})\tau_p(\chi)$ with compatible additive normalizations. This follows by summing the lifts first. Thus neither lower character order nor a higher physical modulus licenses a unit root. Applying (40.148) only at the actual F in (40.120), and inserting (40.147) into (40.146), proves the exact signed kernel. Splitting every dual ideal uniquely as $\mathfrak{y} = \mathfrak{h}\mathfrak{z}$, with $\mathfrak{h}$ supported on S and $\mathfrak{z}$ good, retains all modes.

40.30.4 The joint bilinear estimate behind finite prefixes

The external sixth-order norm gives the following arbitrary-column- coefficient comparison, for every $Z, L \ge 1$:

$$\sum_{\substack{\mathfrak{z}\ \text{good}\\ N\mathfrak{z}\le Z}} \left| \sum_{\substack{\mathfrak{a}\ \mathrm{SF,good}\\ N\mathfrak{a}\asymp L}} b_{\mathfrak{a}} R_{\mathfrak{a}}(\mathfrak{z}) \right|^2 \ll (ZL)^{\epsilon}\Phi(Z,L)\sum_{\mathfrak{a}} |b_{\mathfrak{a}}|^2. \tag{40.149}$$

For completeness, extract $\mathfrak{z} = \mathfrak{r}\mathfrak{s}^6$ with sixth-power-free $\mathfrak{r}$. Freeze $\mathfrak{s}$ as the original column collision mask $(\mathfrak{a},\mathfrak{s}) = 1$ and apply (40.109) to $\mathfrak{r}$. The four sums have factors $\sum (N\mathfrak{s})^{-6}$, the count $N\mathfrak{s} \le Z^{1/6}$,

$\sum(N\mathfrak{s})^{-5}$ and $\sum(N\mathfrak{s})^{-2}$, respectively. Ideal counting proves (40.149). This is not an arbitrary *row*-weight theorem or an extension of a residue-subtracted energy estimate. For $1/2 \le L < 1$ use the direct unit residual column; below $1/2$ there is no annular residual column. Primitive ξ is not treated as sixth-order: convert to raw R inside each fixed residual-class positive norm, where its common ψ row phase cancels.

At $s = \lambda + i\tau$, use (40.123) to form the two *distinct* vectors

$$\begin{aligned} b_{\mathfrak{m}}(s) &= c_{\mathfrak{m}} u_{\mathfrak{m}} R_{\mathfrak{m}}(\mathfrak{v}_2^2)\xi_{\mathfrak{m}}(\mathfrak{k}^2\mathfrak{l}_{\mathfrak{e}})\overline{\xi_{\mathfrak{m}}(\mathfrak{h})}(N\mathfrak{m})^{s-1/2}, \\ d_{\mathfrak{n}}(s) &= c_{\mathfrak{n}} v_{\mathfrak{n}} R_{\mathfrak{n}}(\mathfrak{v}_2^2)\xi_{\mathfrak{n}}(\mathfrak{k}^2\mathfrak{l}_{\mathfrak{e}})\overline{\xi_{\mathfrak{n}}(\mathfrak{h})}(N\mathfrak{n})^{s-1/2}. \end{aligned} \tag{40.150}$$

The pairing is $b_{\mathfrak{m}}(s)\overline{d_{\mathfrak{n}}(\bar{s})}$, not a PSD form at s. The exact remaining primitive-conductor factor is

$$(N\mathfrak{f}_S)^{s-1/2}\left(\frac{A_1}{N\mathfrak{l}N_{\mathfrak{e}}}\right)^{1-s}, \tag{40.151}$$

with scalar $\sigma(\mathfrak{k}^2\mathfrak{l}_{\mathfrak{e}})\bar{\sigma}(\mathfrak{h})$ and finite $\mathfrak{k}$ weight $(N\mathfrak{k})^{-2+2s}$. Its S exponent is $s - 1/2$, not its inverse. On $0 < \lambda < 1/2$ its modulus is at most one.

Insert exact gcd inversion before comparison and put $\mathfrak{m} = \mathfrak{d}\mathfrak{a}$, $\mathfrak{n} = \mathfrak{d}\mathfrak{b}$. Residual $\mathfrak{a}, \mathfrak{b}$ may overlap each other but are individually coprime to $\mathfrak{d}$. Raw multiplicativity gives

$$\overline{R_{\mathfrak{d}\mathfrak{a}}(\mathfrak{z})}R_{\mathfrak{d}\mathfrak{b}}(\mathfrak{z}) = \mathbf{1}_{(\mathfrak{d},\mathfrak{z})=1}\overline{R_{\mathfrak{a}}(\mathfrak{z})}R_{\mathfrak{b}}(\mathfrak{z}).$$

Their source classes are $A[\mathfrak{d}]^{-1}$ and $B[\mathfrak{d}]^{-1}$, generally different. Bilinear Cauchy in the row variable, including (40.145), gives two separate positive norms. Only *inside* them may the raw $(\mathfrak{d}, \mathfrak{z})$ mask be dropped. Uniformly in the fixed column phases and τ,

$$\sum_{\mathfrak{a}} |b_{\mathfrak{d}\mathfrak{a}}(s)|^2, \quad \sum_{\mathfrak{b}} |d_{\mathfrak{d}\mathfrak{b}}(\bar{s})|^2 \ll B_W^2 D^{2\lambda+\epsilon}/N\mathfrak{d}. \tag{40.152}$$

Indeed $|A_U(\mathfrak{m})| \le 3^{\omega(\mathfrak{m})}$ and an annular subsequence has $O(D/N\mathfrak{d})$ columns. Neither $A_U(\mathfrak{d}\mathfrak{a})$ nor $\beta_{\mathfrak{d}\mathfrak{a}}$ is factored. For the small residual interval the direct unit count has the same bound.

Apply (40.149) to the two separate vectors. The divisor sums have exponents $1, 2, 4/3, 11/6$:

$$\sum_{N\mathfrak{d}\le 2D} \frac{1}{N\mathfrak{d}}\Phi(Z, D/N\mathfrak{d}) \ll \log(2D)\Phi(Z, D), \tag{40.153}$$

with the direct endpoint understood. For $Y < N\mathfrak{h}N\mathfrak{z} \le 2Y$, the weight modulus is at most $Y^{-\lambda}$ and the legal positive row prefix is $N\mathfrak{z} \le 2Y/N\mathfrak{h} \ge 1$. The four positive row exponents in Φ give

$$\sum_{\mathfrak{h}\ S\text{-supported},\, N\mathfrak{h}\le 2Y} \Phi(2Y/N\mathfrak{h}, D) \ll_S \Phi(Y, D).$$

This is a summation over *all* S-supported modes, not an exponent-zero convergent sum or a missing raw S value.

The sharp G requires an honest transform bound. Integration by parts against its finite variation gives

$$\widehat{G}(1-s) = -\frac{1}{1-s}\int t^{1-s}\, dG(t).$$

For fixed $0 < \lambda < 1/2$, Stirling's ratio estimate is $|\gamma_K(\lambda + i\tau)| \ll_\lambda (1 + |\tau|)^{2\lambda-1}$. Thus

$$\int_{\mathbb{R}} |\widehat{G}(1-\lambda-i\tau)\gamma_K(\lambda+i\tau)|\, d\tau \ll_\lambda 1, \tag{40.154}$$

using the integrable tail $(1+|\tau|)^{2\lambda-2}$ and $\mathrm{TV}(G)\le 2$. No derivative seminorm growing with A_1 is hidden here. Only after the joint estimate may the original finite $\mathfrak{k}$ sum be bounded by $\zeta_K^S(2-2\lambda)$; the identity has not been Euler-completed. Finite $\mathfrak{e}$, the original $\mathfrak{l}\mid\mathfrak{v}_2$ divisor sum, and unweighted actual $\mathfrak{v}_2$ counting cost a fixed constant and $A_2(DA_2)^{\epsilon}$. Equations (40.152)– (40.154) give

$$\frac{|\mathcal{P}_D(Y,2Y]|}{D}\ll_\lambda B_W^2(DYA_2)^{\epsilon}A_2A_1^{1-\lambda}D^{2\lambda-1}Y^{-\lambda}\Phi(Y,D). \tag{40.155}$$

Every finite source/ray component is reconstructed using the distinct gauges and bilinear argument, rather than a same-class inference.

For $0<\lambda<1/6$, each of the four powers of Y after multiplication by $Y^{-\lambda}$ is positive. Finite dyadic summation, a last partial band and the dual unit separately therefore give the same bound with $Y=X$ for every finite prefix $X\ge 1$. For a requested final loss $\epsilon_0>0$, fix $\lambda=\min\{1/12,\epsilon_0/4\}$, independently of all scales, and use the positive-norm loss $\epsilon_0/2$. Since $A_1,X\ge 1$,

$$D^{2\lambda}(A_1X)^{-\lambda}\le D^{\epsilon_0/2},\qquad (DXA_2)^{\epsilon_0/2}D^{\epsilon_0/2}\le (DXA_2)^{\epsilon_0}.$$

This proves (40.128); neither endpoint $\lambda=0$ nor $\lambda=1/2$ is invoked.

For the independent all-orders bound, expand J_0 exactly at every finite dual prefix. The jth moment satisfies $|M_j|=|\int t^jG(t)dt|\le 2(5/2)^j$. The resulting original-column factors $(D/N\mathfrak{m})^j$ and $(D/N\mathfrak{n})^j$ are contractions, including on $\mathfrak{m}=\mathfrak{d}\mathfrak{a}$; they are not replaced by $(D/N\mathfrak{a})^j$. The exact S factor is $(N\mathfrak{f}_S)^{-j-1/2}$, and the finite $\mathfrak{k}$ norm exponent is $2+2j$ with the *same* character phase $\eta(\mathfrak{k})^2$ as before. After gcd inversion, weighted bilinear Cauchy may bound $(N\mathfrak{h}N_{\mathfrak{z}})^j\le X^j$ inside each positive norm; the product of the square roots costs X^j, not X^{2j}. All remaining divisor/S/subsequence constants are uniform in j. The jth joint bound is the prefactor of (40.129) times $((5/2)A_1X/(C_0D^2))^j/(j!)^2$. Summing this absolutely convergent series proves (40.129) without an infinite-dual interchange.

For completeness, the scoped critical-half estimate uses $H(v)=e^{v/2}G(e^v)$. Its Fourier transform is $\widehat{G}(1/2-i\tau)$. The fixed smooth step and its two transitions give $\|H\|_1+\|H'\|_1\ll 1$ and $\|H''\|_1\ll 1+A_1$. The minimum of the three Fourier bounds $O(1)$, $O(1/|\tau|)$ and $O(A_1/\tau^2)$ has integral $O(1+\log(2A_1))$. On the half line $|\gamma_K(1/2+i\tau)|=1$ exactly. The original finite square-divisor sum is harmonic, $\sum_{N\mathfrak{k}\le K_{\mathfrak{l}}}(N\mathfrak{k})^{-1}\ll 1+\log(2A_1)$; it is not an infinite $\zeta_K(1)$. The same joint argument in the stated same-class/ $\rho=1$ component proves (40.130). This estimate is not summed over all dual bands to infer a whole target.

40.30.5 Finite-height Schur transfer, including the operator error

For $x\ne 1$ define

$$I_T(x)=\frac{1}{2\pi}\int_{-T}^{T}\frac{x^{c_P+it}}{c_P+it}\,dt.$$

Fourier inversion of $e^{-c_Pv}\mathbf{1}_{v\ge 0}$ gives its full vertical limit $\mathbf{1}_{x>1}$. Integration by parts in each oscillatory tail gives

$$|I_T(x)-\mathbf{1}_{x>1}|\le\frac{2x^{c_P}}{\pi T|\log x|}. \tag{40.156}$$

There is no pole-free inverse-L contour assertion. Set $U^{\#}=\lfloor U\rfloor+1/2$. Every divisor norm $n\le X$ is a positive integer, so

$$|\log(U^{\#}/n)|\ge\frac{1}{2X+1}\ge\frac{1}{3X},\qquad (U^{\#}/n)^{c_P}\le e.$$

The indicator is exactly $n \le U$, even when U is an integer. Since $6e/\pi < 6$, (40.156) is at most $e_T = 6X/T \le 3/4$. A product of the two indicators therefore has error at most $2e_T + e_T^2 \le 18X/T$.

For squarefree $\mathfrak{m}$ put

$$H_{\mathfrak{m}}(v,w) = \prod_{p\mid\mathfrak{m}} (1 - (Np)^{-v} - (Np)^{-w}).$$

There are exactly $3^{\omega(\mathfrak{m})}$ ordered disjoint divisor assignments. On the supported coprime products only, $H_{\mathfrak{d}\mathfrak{a}} = H_{\mathfrak{d}} H_{\mathfrak{a}}$, so

$$\begin{aligned} A_U(\mathfrak{d}\mathfrak{a}) &= \frac{1}{(2\pi i)^2} \int_{c_P - iT}^{c_P + iT} \int_{c_P - iT}^{c_P + iT} \frac{(U^{\#})^{v+w}}{vw} H_{\mathfrak{d}}(v,w) H_{\mathfrak{a}}(v,w)\, dv\, dw + R_T(\mathfrak{d},\mathfrak{a}), \\ |R_T(\mathfrak{d},\mathfrak{a})| &\le (18X/T) 3^{\omega(\mathfrak{d})} 3^{\omega(\mathfrak{a})}. \end{aligned} \tag{40.157}$$

Forbidden entries of K remain zero. The integral is the actual operator $\operatorname{diag}(H_{\mathfrak{d}}) K \operatorname{diag}(H_{\mathfrak{a}})$, with an ordinary right diagonal, not a Hermitian assumption. The two diagonal norms cost $G_{\mathcal{I}\mathcal{J}}$, $(U^{\#})^{2c_P} \le e^2$, and each normalized absolute vertical integral is L_T.

A uniform entry error alone does not multiply operator norms. Instead, with counting ℓ^2 norms,

$$\|R_T \circ K\|_{\mathrm{op}} \le \|R_T \circ K\|_F \le \max|R_T|\, \|K\|_F \le \max|R_T| \sqrt{\min(\#\mathcal{I}, \#\mathcal{J})}\, \|K\|_{\mathrm{op}}.$$

The accepted fixed-field ideal bound $\#\{N\mathfrak{a} \le X\} \le 2X$ gives an error at most $18\sqrt{2} X^{3/2} G_{\mathcal{I}\mathcal{J}}/T$, less than the displayed 32 constant. This proves (40.131). Splitting the finite set of prime ideals $Np < 3^{1/\eta}$ from the rest proves $3^{\omega(\mathfrak{m})} \ll_\eta (N\mathfrak{m})^\eta$. Use $\eta = \epsilon/2$ and $T = (4X)^4$ to obtain the subpower/log bound. This is a mathematical finite-matrix transfer, not a claim of fast numerical Perron evaluation at that height.

Let $F_0(v) = W(e^v)$. Two integrations by parts give $|\widehat{F_0}(t)| \le \min\{\|F_0\|_1, \|F_0''\|_1/t^2\}$. Split at $|t| = 1$ to get

$$M(W) \le (\|F_0\|_1 + \|F_0''\|_1)/\pi.$$

Here $F_0''(v) = xW'(x) + x^2 W''(x)$ and its support has length $\log 2$, proving (40.132). Absolute Fourier inversion expresses $W(N\mathfrak{d}N\mathfrak{a}/D)$ as an integral of two unitary norm diagonals and a scalar. Its Schur multiplier norm is at most $M(W)$. Compose with (40.157); two coefficient occurrences cost the square. All original zeros remain throughout, and no factorization of a primitive $\beta_{\mathfrak{d}\mathfrak{a}}$ is supplied by this lemma.

40.30.6 The cubic transposition in an identity divisor class

Fix the scope of Proposition 40.24. On good arguments the primary-generator source construction is index-multiplicative. For $[\mathfrak{d}] = 1$, comparison with the unit source class removes the S conductor of $\widetilde{\chi}_{\mathfrak{d}}$; its type is zero. For $[\mathfrak{a}] = C$ and $(\mathfrak{d},\mathfrak{a}) = 1$,

$$\xi_{\mathfrak{d}\mathfrak{a}} = \widetilde{\chi}_{\mathfrak{d}} \xi_{\mathfrak{a}}.$$

The primitive conductors are coprime and their angular correction in (40.122) is one. Multiplication by the actual $\psi_C(\mathfrak{d}\mathfrak{a})$ yields

$$\beta_{\mathfrak{d}\mathfrak{a}} = \epsilon(\widetilde{\chi}_{\mathfrak{d}}) \beta_{\mathfrak{a}} \widetilde{\chi}_{\mathfrak{d}}(\mathfrak{a}) \widetilde{\chi}_{\mathfrak{a}}(\mathfrak{d}).$$

Source reciprocity is $\widetilde{\chi}_{\mathfrak{d}}(\mathfrak{a}) \overline{\widetilde{\chi}_{\mathfrak{a}}(\mathfrak{d})} = \alpha(1, C)$, proving (40.134). In the product for residuals $\mathfrak{a}, \mathfrak{b}$, their common ϵ and α cancel:

$$\beta_{\mathfrak{d}\mathfrak{a}} \overline{\beta_{\mathfrak{d}\mathfrak{b}}} = \beta_{\mathfrak{a}} \overline{\beta_{\mathfrak{b}}} (\widetilde{\chi}_{\mathfrak{a}} \overline{\widetilde{\chi}_{\mathfrak{b}}})^2(\mathfrak{d}). \tag{40.158}$$

If $\mathfrak{g} = (\mathfrak{a}, \mathfrak{b})$, the primitive cubic conductor is $(\mathfrak{a}/\mathfrak{g})(\mathfrak{b}/\mathfrak{g})$, nonprincipal when $\mathfrak{a} \neq \mathfrak{b}$. The same source class cancels its S component. Common good primes have dropped only from that primitive conductor; the full $\mathfrak{ab}$ union still remains excluded from $\mathfrak{d}$.

The other common $\mathfrak{d}$ phases from ν, u_0 and the $\mathfrak{k}, \mathfrak{l}, \mathfrak{v}_2, \mathfrak{e}, \mathfrak{h}$ modulations cancel in the pair. Their raw zeros, together with the $\mathfrak{z}$ factor, retain

$$(\mathfrak{d}, S\mathfrak{a}\mathfrak{b}\mathfrak{k}\mathfrak{v}_2\mathfrak{z}) = 1.$$

This notation means coprimality with the union of the displayed prime supports. Primitive values at $\mathfrak{e}, \mathfrak{h}$ are legitimate unitary phases of a good-conductor character. The radial factor $(N\mathfrak{d})^{2s-1}$ is kept, not called a cancelled phase.

At fixed $\mathfrak{z}, s$ the core matrix is

$$K^{(\mathfrak{z})}_{\mathfrak{d}\mathfrak{a}} = \mathbf{1}_{[\mathfrak{d}]=1,[\mathfrak{a}]=C,(\mathfrak{d},\mathfrak{k}\mathfrak{v}_2\mathfrak{z})=1}\widetilde{\chi}_{\mathfrak{a}}(\mathfrak{d})^2\overline{R_{\mathfrak{a}}(\mathfrak{z})}. \tag{40.159}$$

Its cubic character already has the $(\mathfrak{d}, \mathfrak{a})$ zero. All additional fixed residual phases are column contractions. On good arguments the squared sextic symbol is the actual primary cubic symbol $(\alpha_{\mathfrak{a}}/\mathfrak{d})_3$. The pinned external Example 2.2 constructs precisely this family with primary generators congruent to one modulo 3. Both variables are squarefree and hence cube-free; source-sixth-class selectors and deleting the prime above 2 only restrict the positive matrix. Theorem 1.1 at $n = 3$, or its transpose, therefore gives

$$\|K^{(\mathfrak{z})}\|^2_{\mathrm{op}} \ll_\eta (EL)^\eta \Theta_3(E, L). \tag{40.160}$$

The lengths are physical ideal norms E, L, not varying conductor labels.

The original annular condition implies $L/2 \leq N\mathfrak{a} \leq 2L$, a bounded number of dyads with lower endpoint at least one. On the encompassing rectangle $N\mathfrak{d}N\mathfrak{a} \leq 4D$, apply Proposition 40.23 with $X = 4D$. This is the necessary repair: $A_U(\mathfrak{d}\mathfrak{a})$ depends on *both* matrix indices and cannot be put into a fixed coefficient vector by fiat. Composing the common W costs $M(W)$. With $0 < \lambda < 1/2$, the squared row radial factor is $O(E^{2\lambda-1})$, and the column squared norm is

$$\sum_{L/2\leq N\mathfrak{a}\leq 2L} (N\mathfrak{a})^{2\lambda-1} \ll_\lambda L^{2\lambda}.$$

The product is $D^{2\lambda}/E$. Thus the two Mellin vectors have squared norms at most

$$M(W)^2 D^{2\lambda+\eta}\Theta_3(E, L)/E.$$

Cauchy in $\mathfrak{d}$ now uses $|\mu(\mathfrak{d})| \leq 1$, explicitly losing rather than exploiting its sign. A final triangle over $N\mathfrak{z} \leq Z$ gives the new inner branch

$$|T_E(Z; s)| \ll M(W)^2 D^{2\lambda+\eta}(Z/E)\Theta_3(E, L). \tag{40.161}$$

The accepted separate positive-divisor argument gives $|T_E(Z; s)| \ll M(W)^2 D^{2\lambda+\eta}\Phi(Z, L)$: there are $O(E)$ divisors and each actual subsequence norm is $O(M(W)^2 D^{2\lambda+\eta}/E)$. Both estimates apply to the same quantity, so their minimum is legal.

For $Y < N\mathfrak{h}N\mathfrak{z} \leq 2Y$, put $Z_{\mathfrak{h}} = 2Y/N\mathfrak{h} \geq 1$. The new branch uses the convergent positive exponent-one sum $\sum_{\mathfrak{h}} Z_{\mathfrak{h}} \ll_S Y$; the old branch uses its four positive Φ exponents. Sum each branch to obtain the minimum after summation. The same finite $\mathfrak{k}$ majorant, $\mathfrak{e}/\mathfrak{l}$ bounds, actual A_2 count and fixed-line BV integral as above now prove (40.133), including the once-only $1/D$ normalization. No all-divisor or whole-dual conclusion follows.

On rough prime divisors $\mathfrak{d} = p$, $Np > U$, no short divisor can contain p, so $A_U(p\mathfrak{a}) = A_U(\mathfrak{a})$ exactly. The remaining fixed-residual arithmetic sum has the shape

$$-A_U(\mathfrak{a})A_U(\mathfrak{b}) \sum_{\substack{E<Np\le 2E,\ Np>U,\ [p]=1\\ p\notin S\cup\mathrm{supp}(\mathfrak{a}\mathfrak{b}\mathfrak{k}\mathfrak{v}_2\mathfrak{z})}} \lambda_{\mathfrak{a}\mathfrak{b}}(p)(Np)^{2s-1} \cdot W(NpN\mathfrak{a}/D)\overline{W(NpN\mathfrak{b}/D)}, \tag{40.162}$$

up to the already fixed residual phases, with $\lambda_{\mathfrak{a}\mathfrak{b}} = (\widetilde{\chi}_{\mathfrak{a}}\overline{\widetilde{\chi}_{\mathfrak{b}}})^2$. Here $\mu(p) = -1$ is constant. A fixed-field scalar Mertens estimate is not a uniform bound for these varying cubic prime twists. The auxiliary principal case $\mathfrak{a} = \mathfrak{b}$ may cancel against other divisor sectors; it is no physical lower obstruction.

40.30.7 Classification and proof of the full equal-norm sector

Factor the common rational norm prime by prime. At an inert prime there is only one ideal of norm p^2; equal norms force the same squarefree valuation in both columns and coprimality forces it to zero. The same argument excludes a ramified prime. At a split prime write the two pairs of valuations as $(x, y), (z, w) \in \{0, 1\}^2$. Then $x + y = z + w$ and $xz = yw = 0$. Sum two is forbidden; sum one forces opposite choices. Hence $\mathfrak{n} = \bar{\mathfrak{m}}$ and the common norm is rational-squarefree supported on split primes. Both primes above each such prime must already be good. This does not assume that the original S is conjugation-stable or enlarge it. Each eligible $\mathfrak{m}$ has exactly one partner, so the ordered pair count is at most $\#\{N\mathfrak{m} \le 2D\} \le 4D$. All other rational-nonsquarefree norms remain in the *full* annulus; only this sector has been classified.

The ternary bound is uniform in the original cutoff: $|A_U(\mathfrak{m})| \le 3^{\omega(\mathfrak{m})} \ll_\eta D^\eta$. For each actual row the absolute triangle in this sparse sector costs $O(B_W^2 D^{1+\epsilon})$ before normalization. Divide once by D and sum the actual rows to obtain (40.135). Original row masks give $R_w \ll R$, and a nonempty capacity block has $Nu_0A_1A_2^2 \le H$, hence $R \le H/(Nu_0A_2) \le H$. For each fixed W, $S_1^{AA} = S_{\mathrm{eq}} + S_{\mathrm{neq}}$ proves the target equivalence stated in the core, with constants allowed to depend on that fixed profile.

Conjugating the residue-field definition gives, including zeros,

$$R_{\bar{\mathfrak{m}}}(x) = \overline{R_{\mathfrak{m}}(\bar{x})}, \qquad R_{\mathfrak{m}}(x)\overline{R_{\bar{\mathfrak{m}}}(x)} = R_{\mathfrak{m}}(Nx). \tag{40.163}$$

For a split rational p, $p \mid Nx$ exactly when x meets at least one of its two conjugate primes, so the right side retains the original *union* zero. For an orientation of rational- squarefree norm N, restriction to rational integers gives a primitive Dirichlet character $\psi_{\mathfrak{m}} \pmod N$: $\mathbb{Z}/N\mathbb{Z} \longrightarrow \mathcal{O}/\mathfrak{m}$ is an isomorphism, and each local character has exact order six. Its ideal norm pullback has conductor $(N) = \mathfrak{m}\bar{\mathfrak{m}}$ and infinity type zero. There is no smaller radical or common truncated-frequency assertion.

Choose one prime π_p above each admissible split rational p. Every divisor of an orientation $\mathfrak{m}$ has a unique rational divisor norm and the same Möbius parity. Thus $A_U(\mathfrak{m}) = a_U(N)$ with the *two original* cutoffs, and the partner has the same coefficient. At $t = Nu_0N\mathfrak{v}_1(N\mathfrak{v}_2)^2$, (40.163) makes the local orientation factors $a_p\chi_p(t)$ and its conjugate. Expanding their product gives all $2^{\omega(N)}$ ordered orientations exactly, proving (40.136). Both reversals are included, not divided by two. The common complex profile gives $|W(N/D)|^2$. For $\nu = 1$ and no raw collision the character factors are $2\,\mathrm{Re}\,\mu_6 \in \{2, 1, -1, -2\}$, so they need not vanish or be positive; a_U or W can still vanish. This is not a row-energy lower bound.

For (40.137), use the exact primitive representation *restricted first* to these $O(D)$ pairs. Its conductor norm is $N\mathfrak{f}_S N^2 \ge D^2$, and $|\dot{G}| \le 2C_0^{-1/2}$ by $|J_0(t)| \le 1$ on real t. The Poisson amplitude

is at most $A_1/((N\mathfrak{k})^2 N\mathfrak{l} N\mathfrak{c}D)$. There are $O(Y)$ integral dual ideals in a prefix or band, counting every S-supported ideal once. The finite square-divisor sum is bounded by its convergent positive Nk^{-2} majorant; finite S/ray and $\mathfrak{l}$ divisor costs give $A_2(DA_2)^{\epsilon}$. With the sparse pair count and coefficient product $B_W^2 D^{\epsilon}$, the numerator is $O(B_W^2(DYA_2)^{\epsilon}RY)$. Division by D proves the bound. This uses no general row-weight norm and no root cancellation.

At fixed parameters, exact Poisson gives $DS_{\mathrm{eq}} = \mathcal{P}_{\mathrm{eq}}(\le Y) + \mathcal{P}_{\mathrm{eq}}(> Y)$, with its actual smooth derivative constants. Therefore

$$\frac{|\mathcal{P}_{\mathrm{eq}}(> Y)|}{D} \ll B_W^2\{D^{\epsilon}R_w + (DYA_2)^{\epsilon}RY/D\}. \tag{40.164}$$

This is a *signed* whole-minus-prefix identity and triangle, not absolute summation of high modes. The condition $RY/D \le H$ gives pure $Y \asymp D$ and mixed $Y \asymp D^{7/6}$ target-sized prefix/complement sectors. Unequal norms and arbitrary larger individual windows remain unestimated.

40.30.8 A common literal modulus and the surviving ray mean

This last construction concerns the pure block only. The primary section on good ideals is multiplicative because $\mu_6 \to (\mathcal{O}/3)^{\times}$ is bijective. Let $\mathfrak{c} = (\gamma_c)$ be fixed, S-supported and divisible by (6), large enough for all actual row-ray congruences. For $\mathfrak{q} = \mathfrak{m}\mathfrak{n}$ coprime to it, put

$$\vartheta_{\mathfrak{q}}(x) = (x/\mathfrak{m})_6\overline{(x/\mathfrak{n})_6}, \qquad \tau_{\mathfrak{q}} = \sum_{x \bmod \mathfrak{q}} \vartheta_{\mathfrak{q}}(x)e_{\gamma_q}(x).$$

Every good local factor is nontrivial sextic, so its finite conductor is exactly $\mathfrak{q}$, including nonunit frequency zeros. It need not yet be unit-trivial or an ideal character. The finite indicator $P_{\mathfrak{k}^2}$ imposes residual generator $x \equiv 1 \pmod 3$, original S-goodness and the actual ray condition on $\alpha_{\mathfrak{k}}^2 x$. It is independent of $\mathfrak{m}, \mathfrak{n}$. Literal square-divisor inversion is

$$\mathcal{P}_D = \sum_{(\mathfrak{m},\mathfrak{n})=1} c_{\mathfrak{m}}\bar{c}_{\mathfrak{n}} \sum_{\substack{\mathfrak{k}\ \text{good,SF} \\ N\mathfrak{k} \le \sqrt{b}}} \mu(\mathfrak{k})\vartheta_{\mathfrak{q}}(\alpha_{\mathfrak{k}}^2) \sum_{x \in \mathcal{O}} P_{\mathfrak{k}^2}(x \bmod \mathfrak{c})\vartheta_{\mathfrak{q}}(x)G(Nx/L_{\mathfrak{k}}). \tag{40.165}$$

The original $(\mathfrak{k}, \mathfrak{q})$ zero is kept. Auxiliary lattice x need not generate a squarefree ideal.

Use the same positive additive-pairing sign as above. CRT separates the common-modulus Fourier transform into the $\mathfrak{q}$ sum at frequency $\beta\gamma_c^{-1}$ and the $\mathfrak{c}$ sum at $\beta\gamma_q^{-1}$. Primitive finite Gauss Fourier proves (40.138) for *every* β, including its zero at $(\beta, \mathfrak{q}) > 1$. This is the finite recombination of all ray components; it is not a unit root at the larger induced modulus $\mathfrak{c}\mathfrak{q}$. For $g_L(x) = G(|x|^2/L)$ the Euclidean radial transform is

$$\widehat{g}_L(w) = \pi L \int_0^{\infty} G(t)J_0(2\pi\sqrt{Lt}|w|)\,dt.$$

At the common dual vector $w = 2\bar{\beta}/(\bar{\delta}\bar{\gamma}_c\bar{\gamma}_q)$ this equals $(\sqrt{3}/2)L\dot{G}(LN\beta/(N\mathfrak{c}Q))$. The lattice covolume is $(\sqrt{3}/2)N\mathfrak{c}Q$. Consequently, writing $F_{\mathfrak{k}^2} = P_{\mathfrak{k}^2}\vartheta_{\mathfrak{q}}$,

$$\sum_{x \in \mathcal{O}} F_{\mathfrak{k}^2}(x)G(Nx/L) = \frac{L}{N\mathfrak{c}Q} \sum_{\beta \in \mathcal{O}} \widehat{F}_{\mathfrak{k}^2}(\beta)\dot{G}(LN\beta/(N\mathfrak{c}Q)). \tag{40.166}$$

No class/root phase is discarded: the original finite function itself has been transformed. Primitive-conductor descriptions induced to the common modulus must reproduce precisely this frequency support, rather than a falsely flat lifted Gauss sum.

Combining the formulas gives the explicit signed literal additive band

$$\begin{aligned}\mathcal{B}_Y = \sum_{(\mathfrak{m},\mathfrak{n})=1} c_{\mathfrak{m}}\bar{c}_{\mathfrak{n}} \sum_{\substack{\mathfrak{k}\ \text{good,SF}\\ N\mathfrak{k}\le\sqrt{b}}} \frac{\mu(\mathfrak{k})L_{\mathfrak{k}}\tau_{\mathfrak{q}}\vartheta_{\mathfrak{q}}(\gamma_c)}{N\mathfrak{c}Q}\vartheta_{\mathfrak{q}}(\alpha_{\mathfrak{k}}^2)\\ \cdot \sum_{Y<N\beta\le 2Y} \overline{\vartheta_{\mathfrak{q}}(\beta)}\widehat{P}_{\mathfrak{k}^2}(\beta\gamma_q^{-1})\dot{G}(L_{\mathfrak{k}}N\beta/(N\mathfrak{c}Q)).\end{aligned} \tag{40.167}$$

All finite $\mu(\mathfrak{k})$, the original unfactored coefficients and the full pair/ray/raw masks precede any absolute norm. There is no gcd triangle or positive completion in this identity. The frequency band is literal and unit-invariant; it is not simply the old primitive-ideal band under a new name.

On $\beta = \gamma_c\zeta$, the fixed-residue Fourier frequency is zero. The factor $\vartheta_{\mathfrak{q}}(\gamma_c)$ cancels and

$$\widehat{F}_{\mathfrak{k}^2}(\gamma_c\zeta) = r_{\mathfrak{k}^2}\tau_{\mathfrak{q}}\overline{\vartheta_{\mathfrak{q}}(\zeta)}.$$

This S-local mean is not the global $\beta = 0$, which is zero by primitive nontriviality. A six-unit orbit sum in this radial band vanishes if $\vartheta_{\mathfrak{q}}|_{\mu_6}$ is nontrivial. Otherwise it is six times the sum over *all* integral ideals; values there are defined with any generator, not a nonexistent primary generator for an S-supported ideal. At $\varepsilon = 1+\omega$, local residue powers give

$$\vartheta_{\mathfrak{q}}(\varepsilon) = \varepsilon^{(N\mathfrak{m}-N\mathfrak{n})/6}.$$

Every good prime-ideal norm is one modulo six, and $(\prod Np-1)/6 \equiv \sum(Np-1)/6 \pmod 6$, proving (40.139). In the surviving case $\vartheta_{\mathfrak{q}}$ is a primitive type-zero ideal character and $\epsilon_{\mathfrak{q}} = \tau_{\mathfrak{q}}/\sqrt{Q}$. The exact retained mean channel is

$$\begin{aligned}\mathcal{B}_Y^{S\text{-mean}} = \sum_{\substack{(\mathfrak{m},\mathfrak{n})=1\\ N\mathfrak{m}\equiv N\mathfrak{n}\ (36)}} c_{\mathfrak{m}}\bar{c}_{\mathfrak{n}} \sum_{\substack{\mathfrak{k}\ \text{good,SF}\\ N\mathfrak{k}\le\sqrt{b}}} \mu(\mathfrak{k})\vartheta_{\mathfrak{q}}(\alpha_{\mathfrak{k}}^2)\frac{6r_{\mathfrak{k}^2}}{N\mathfrak{c}}\frac{L_{\mathfrak{k}}}{\sqrt{Q}}\epsilon_{\mathfrak{q}}\\ \cdot \sum_{Y/N\mathfrak{c}<N\mathfrak{z}\le 2Y/N\mathfrak{c}} \overline{\vartheta_{\mathfrak{q}}(\mathfrak{z})}\dot{G}(L_{\mathfrak{k}}N\mathfrak{z}/Q).\end{aligned} \tag{40.168}$$

This includes nonunit and S-supported dual modes. The $\mathfrak{k}$ phase is cubic, $\vartheta_{\mathfrak{q}}(\mathfrak{k})^2$, not one, and its original cutoff has not been Euler-completed.

For the basic S above $2,3$ and no additional ray condition, modulo (6) the allowed coordinates $a+b\omega$ are $(1,0),(1,3),(4,3)$. The fourth primary residue $(4,0)$ is excluded by the original 2-adic coprimality condition. Thus $r=3$, $N\mathfrak{c}=36$, and $6r/N\mathfrak{c} = 1/2$ exactly. Dropping that condition would give the incorrect $2/3$. The new exact local Fourier check has $\sum|\widehat{P}|^2 = 36\cdot 3 = 108$; it is a finite S-ring consistency check, not an arithmetic-family or asymptotic band test.

Proposition 40.25 controls the whole primal equal-norm sector. That alone does not control this sector in an individual literal band or S-mean channel. To formulate a literal unequal-norm problem, impose $N\mathfrak{m} \neq N\mathfrak{n}$ on the original pair sum before applying (40.165) and (40.166). The projected formula retains unequal norms congruent modulo 36 as well as all complementary literal residues. Neither the full $\mathcal{B}_Y$ nor its separately projected unequal-norm version is proved small here. At a pure critical block a sufficient band estimate would be

$$|\mathcal{B}_Y| \ll_{S,\nu,W,\epsilon} B_W^2 DA_1(DA_1Y)^{\epsilon},$$

with the fixed-profile dependence retained. This is not necessary for the whole kernel, where bands may cancel. Finite ray/root recombination alone does not provide it; nor does a nonzero local mean give a lower bound for the whole band. This identifies the remaining coherent unequal-norm arithmetic problem without deleting its means or changing any original conductor, capacity or profile.

40.31 An arithmetic Gauss tail with the original finite cutoff

The coherent kernel of Section 40.29 contains a difficult root-weighted mean. A large part of its *short-divisor expansion* can now be bounded by retaining a cubic interaction before taking a triangle. This gives a signed cutoff comparison, not a smaller norm for the original coefficients. A direct exact-discrete-frequency version is included as well. The remaining small-short-divisor moment and the separate discrete-frequency error are stated below. The whole signed power 13/12 and global unsigned power 9/8 do not change.

40.31.1 Original objects and a fixed common profile

Keep $K = \mathbb{Q}(\omega)$, $\mathcal{O} = \mathbb{Z}[\omega]$, $\delta = 1 + 2\omega$, and the fixed exclusions S of Section 40.29.1. A good ideal is prime to S. All columns are the complete good squarefree ideal annulus $D \le N\mathfrak{m} \le 2D$, $D > 1$. Equal norms do not identify ideals. For a real cutoff $1 \le T \le \sqrt{D}$ put

$$\begin{aligned} A_T(\mathfrak{m}) &= \sum_{\substack{\mathfrak{a}\mathfrak{b}\mid\mathfrak{m}\\(\mathfrak{a},\mathfrak{b})=1\\ N\mathfrak{a},N\mathfrak{b}\le T}} \mu(\mathfrak{a})\mu(\mathfrak{b}),\\ c_f(\mathfrak{m}) &= f(\mathfrak{m})\nu(\mathfrak{m})R_{\mathfrak{m}}(u_0)W(N\mathfrak{m}/D). \end{aligned} \tag{40.169}$$

Here ν is the original fixed unitary finite-order character; u_0 is the fixed literal unit/S-supported factor with no good support. The actual coefficient is c_{A_U}, $1 \le U \le \sqrt{D}$. The function W is one fixed, possibly complex, smooth common profile supported on $[1, 2]$, zero at the endpoints. Define

$$\begin{aligned} B_W &= \|W\|_\infty, \qquad \widehat{W}(t) = \int_0^\infty W(x)x^{-it}\,\frac{dx}{x},\\ \mathcal{M}(W) &= \frac{1}{2\pi}\int_{\mathbb{R}} |\widehat{W}(t)|\,dt. \end{aligned} \tag{40.170}$$

This explicit seminorm is finite and controls B_W. It is a seminorm of the column profile, not of the sharp nodal row function.

Only the original unweighted *pure* two-pivot block is used: $A_2 = 1$, $\mathfrak{v}_2 = \mathcal{O}$, and the other four factors are units. The first row is good and squarefree, with the original literal/ray conditions and capacity. Its integer endpoints are

$$a = \lceil A_1 \rceil, \qquad b = \min\{\lceil 2A_1 \rceil - 1, \lfloor H/Nu_0 \rfloor\}, \qquad K = \sqrt{b}. \tag{40.171}$$

An empty interval contributes zero throughout. Otherwise $b \ge a \ge 1$. Use the exact G of (40.124), its transform $\dot{G}$ in (40.125), and $C_0 = 3/(4\pi^2)$. In particular $0 \le G \le 1$, $\operatorname{supp} G \subset [1/2, 5/2]$, and $\int G \le 2$. The original *pre-S* cutoff K is never recomputed after another deletion.

Let $\mathcal{I}$ be the original ordered coprime column pairs. One may also impose the *original* unequal-norm projection; the same choice is then used in every expression below. For each source pair A, B and original ray character ρ use the primitive η, $\mathfrak{f}_S$ and F of (40.120). Thus $F = N\mathfrak{f}_S N\mathfrak{m}N\mathfrak{n}$, and η has total infinity type zero. Put

$$\begin{aligned} T_q &= S \cup \operatorname{supp}(\mathfrak{m}\mathfrak{n}),\\ Q_s^{T_q}(K;\eta^2) &= \sum_{\substack{\mathfrak{k}\ \text{good,SF}\\ N\mathfrak{k}\le K,\ (\mathfrak{k},T_q)=1}} \frac{\mu(\mathfrak{k})\eta(\mathfrak{k})^2}{(N\mathfrak{k})^s},\\ P_S(\eta) &= \sum_{\mathfrak{e}\mid P_S} \frac{\mu(\mathfrak{e})\eta(\mathfrak{e})}{N\mathfrak{e}}, \qquad P_S = \prod_{p\in S} p. \end{aligned} \tag{40.172}$$

The symbol $(\mathfrak{k}, T_q) = 1$ means avoidance of every prime in that set. Squaring η never restores a deleted prime. Values at $\mathfrak{e}$ and at any later S-supported frequency are separate primitive values, including zero.

40.31.2 The actual retained mean and its finite leading model

In the exact primitive kernel (40.126), write each dual ideal uniquely as $\mathfrak{y} = \mathfrak{h}\mathfrak{r}\mathfrak{s}^6$: $\mathfrak{h}$ is S-supported, $\mathfrak{r}$ is good and sixth-free, and $\mathfrak{s}$ is good. Overlap of $\mathfrak{r}, \mathfrak{s}$ is allowed. For $X \geq 64$ set

$$V = X^{1/6}/2, \qquad b_{\mathfrak{w}} = (X/N\mathfrak{w})^{1/6}, \qquad t_{\mathfrak{w}} = \big((N\mathfrak{w})^{-1/6} - 1/2\big)_+. \tag{40.173}$$

The top band is $V < N\mathfrak{s} \leq 2V$, $N\mathfrak{y} \leq X$. Replacing its $\mathfrak{s}$ count by its principal fixed-ray density defines the retained mean M_{top}. This operation keeps, rather than deletes, its coherent main term. The selected branches are $\rho^6 = 1$. At this top window $N\mathfrak{h}N\mathfrak{r} < 64 < 7^6$, so $\mathfrak{w} = \mathfrak{h}\mathfrak{r}$ runs over *all* integral ideals of norm below 64, including S-supported ideals.

Set

$$\kappa_S = \frac{\pi}{3\sqrt{3}} \prod_{p \in S} (1 - (Np)^{-1}), \qquad g(\mathfrak{m}) = \prod_{p \mid \mathfrak{m}} (1 - (Np)^{-1}). \tag{40.174}$$

On original coprime support the density is $\kappa_S g(\mathfrak{m}) g(\mathfrak{n})$. For $\theta = (A, B, \rho, \mathfrak{m}, \mathfrak{n}, \mathfrak{e}, \mathfrak{w})$ in the preceding sets, with $\rho^6 = 1$, define

$$\begin{aligned} d_\theta[f_1, f_2] = \frac{\kappa_S A_1}{D} h_{AB\rho}(\mathcal{O}) c_{f_1}(\mathfrak{m}) \overline{c_{f_2}(\mathfrak{n})} \frac{g(\mathfrak{m}) g(\mathfrak{n}) \epsilon(\eta)}{\sqrt{F}} \\ \cdot \frac{\mu(\mathfrak{e}) \eta(\mathfrak{e})}{N\mathfrak{e}} \overline{\eta(\mathfrak{w})}, \qquad \lambda_\theta = \frac{A_1 N\mathfrak{w}}{N\mathfrak{e} F}. \end{aligned} \tag{40.175}$$

The exact definition of the normalized retained mean is

$$\begin{aligned} \mathcal{M}_{\mathrm{top}} := \frac{M_{\mathrm{top}}}{D} = \sum_\theta d_\theta[A_U, A_U] \sum_{\substack{\mathfrak{k} \text{ good,SF} \\ N\mathfrak{k} \leq K,\ (\mathfrak{k}, T_q) = 1}} \frac{\mu(\mathfrak{k}) \eta(\mathfrak{k})^2}{(N\mathfrak{k})^2} \\ \cdot \int_V^{b_{\mathfrak{w}}} \dot{G}\left(\frac{\lambda_\theta t^6}{(N\mathfrak{k})^2} \right) dt. \end{aligned} \tag{40.176}$$

All sums here are finite. In particular there is no $\mathfrak{k} \mid \mathfrak{w}$ or $(\mathfrak{k}, \mathfrak{w}) = 1$ condition. The finite original source/ray coefficients $h_{AB\rho}(\mathcal{O})$ have not been centered. An argument at $\mathfrak{e}$ is not divided by a value at $\mathfrak{w}$.

Put $g_0 = C_0^{-1/2} \int G$ and define

$$\mathcal{L}_0[f_1, f_2] = g_0 X^{1/6} \sum_\theta d_\theta[f_1, f_2]\, t_{\mathfrak{w}} Q_2^{T_q}(K; \eta^2). \tag{40.177}$$

Replacing both column functions here is an explicitly defined auxiliary model, not a change to the original primal data.

Proposition 40.27 (Matched leading model with its original cutoff)**.** *For the actual coefficients and every finite $X \geq 64$,*

$$|\mathcal{M}_{\mathrm{top}} - \mathcal{L}_0[A_U, A_U]| \ll B_W^2 (DX)^\epsilon \frac{A_1^2 X^{7/6}}{D^2}. \tag{40.178}$$

The constant uses no derivative bound for the sharp G. Both interval endpoints and the original finite K occur in $\mathcal{L}_0$. This estimates the model error, not the leading signed model.

40.31.3 The root is an incomplete cubic Gauss weight

For each good ideal use its primary generator $\alpha_{\mathfrak{a}} \equiv 1 \pmod 3$ and write $\chi_{j,\mathfrak{a}}$ for its positive residue character of order $j = 3, 6$. For good squarefree $\mathfrak{m}$ put

$$\begin{aligned} G_{\mathfrak{m}} &= \frac{1}{\sqrt{N\mathfrak{m}}} \sum_{x \bmod \alpha_{\mathfrak{m}}} \chi_{3,\mathfrak{m}}(x) \exp\Big(2\pi i \operatorname{Tr} \frac{x}{\delta\alpha_{\mathfrak{m}}}\Big), \\ g_{\mathfrak{m}}(z) &= \overline{\chi_{3,\mathfrak{m}}(z)} G_{\mathfrak{m}}. \end{aligned} \tag{40.179}$$

The second expression is the normalized finite Gauss sum at frequency z, including zero when $(\mathfrak{m}, z) > 1$. For $\mathfrak{q} = \mathfrak{m}\mathfrak{n}$ put $\theta_q = \chi_{6,\mathfrak{m}}\overline{\chi_{6,\mathfrak{n}}}$. Let θ_S be the *actual finite S part* of the total type-zero η, at its own primitive conductor $\mathfrak{f}_S = (\gamma_S)$. Then

$$\mathcal{S}_{\mathfrak{m},\mathfrak{n},\rho} = \theta_S(\alpha_{\mathfrak{m}}\alpha_{\mathfrak{n}})\theta_q(\gamma_S)\frac{\tau_{\gamma_S}(\theta_S)}{\sqrt{N\mathfrak{f}_S}}. \tag{40.180}$$

The unit-conductor convention is one. This scalar has modulus one; it is not obtained by discarding the infinity type of a constituent. The accepted Jacobi character in (40.33) gives $\vartheta = \Psi/\sqrt{N}$, with conductor (2δ) of norm 12 and nonzero infinity type. The exact root formula is

$$\begin{aligned} \epsilon(\eta) &= \mathcal{S}_{\mathfrak{m},\mathfrak{n},\rho}\Gamma(\alpha_{\mathfrak{m}}\alpha_{\mathfrak{n}})\mu(\mathfrak{m})\mu(\mathfrak{n})\vartheta(\mathfrak{m})\overline{\vartheta(\mathfrak{n})}\,\overline{G_{\mathfrak{m}}}G_{\mathfrak{n}}, \\ \Gamma(a+b\omega) &= \tfrac{1}{2}\{1 + i^{-b} + i^{a} + i^{b-a}\}. \end{aligned} \tag{40.181}$$

No extra quadratic sign is inserted. In the original kernel, $\eta(\mathfrak{k}^2)$ and the second-row phase, when present, produce the raw cubic frequency $\overline{g_{\mathfrak{m}}(\alpha_{\mathfrak{k}}\alpha_{\mathfrak{v}_2})}g_{\mathfrak{n}}(\alpha_{\mathfrak{k}}\alpha_{\mathfrak{v}_2})$; here $\mathfrak{v}_2 = \mathcal{O}$. This incomplete weighted frequency set is not a complete residue average.

40.31.4 A signed short-divisor tail from a physical cubic matrix

For squarefree $\mathfrak{m}$ there is an exact sign-preserving assignment identity:

$$\mu(\mathfrak{m})A_T(\mathfrak{m}) = \sum_{\substack{\mathfrak{a}\mathfrak{b}\mathfrak{c}=\mathfrak{m} \\ N\mathfrak{a}, N\mathfrak{b} \le T}} \mu(\mathfrak{c}). \tag{40.182}$$

The factors are pairwise coprime and squarefree. For $Y \le U$ the difference of cutoff boxes has two disjoint pieces. After interchanging $\mathfrak{a}, \mathfrak{b}$ in the second and setting $\mathfrak{z} = \mathfrak{b}\mathfrak{c}$, the exact coefficient is

$$T_U(\mathfrak{z}) + T_Y(\mathfrak{z}), \qquad T_L(\mathfrak{z}) = \sum_{\substack{\mathfrak{b} \mid \mathfrak{z} \\ N\mathfrak{b} \le L}} \mu(\mathfrak{z}/\mathfrak{b}). \tag{40.183}$$

It is independent of $\mathfrak{a}$. The conjugate Gauss CRT identity retains the cross interaction

$$\overline{G_{\mathfrak{a}\mathfrak{z}}} = \overline{G_{\mathfrak{a}}G_{\mathfrak{z}}}\chi_{3,\mathfrak{a}}(\alpha_{\mathfrak{z}}), \qquad (\mathfrak{a}, \mathfrak{z}) = 1. \tag{40.184}$$

The raw cubic entry is zero at a common prime.

The deep input is explicitly external: de Faveri, arXiv:2610.04045v1, Theorem 1.1 and Example 2.2, at $n = 3$. For the physical primary cubic matrix on good squarefree ideals of norms comparable to A, Z it gives

$$\big\|[\chi_{3,\mathfrak{a}}(\alpha_{\mathfrak{z}})]\big\|_{\mathrm{op}}^2 \ll_{\epsilon} (AZ)^{\epsilon}\{A + Z + (AZ)^{2/3}\}. \tag{40.185}$$

Both indices are actual ideals and hence cube-free, not arbitrary primitive-conductor labels. This is the same pinned input as the cubic comparison in Proposition 40.24.

Theorem 40.28 (Actual Gauss-weighted cutoff tail)**.** *For any bounded multiplicative ideal function λ on good ideals, with $|\lambda| \le 1$, and $1 \le Y \le U \le \sqrt{D}$,*

$$\begin{aligned}\left|\sum_{\mathfrak{m}\ \mathrm{good,SF}} \frac{\mu(\mathfrak{m})(A_U - A_Y)(\mathfrak{m})\overline{G_{\mathfrak{m}}}\lambda(\mathfrak{m})}{\sqrt{N\mathfrak{m}}} W(N\mathfrak{m}/D)\right| \\ \ll_\epsilon \mathcal{M}(W) D^\epsilon \{D^{1/3} + \sqrt{D/Y}\}.\end{aligned} \tag{40.186}$$

The constant is uniform in the conductor or raw deletion set in λ. For the actual pure leading model, with every original finite K, class/ray/root/S component and coprime pair retained,

$$|\mathcal{L}_0[A_U, A_U] - \mathcal{L}_0[A_Y, A_Y]| \ll B_W \mathcal{M}(W) D^\epsilon A_1 X^{1/6}\{Y^{-1/2} + D^{-1/6}\}. \tag{40.187}$$

The original unequal-norm projection is also allowed.

This uses the cubic interaction before the short-divisor triangle. It does not assert pointwise or coefficient-norm shrinkage of A_U, nor a separate cancellation theorem for $\mu(\mathfrak{c})$.

40.31.5 What has been reduced, and what remains

Combining Proposition 40.27 and Theorem 40.28 gives

$$\begin{aligned}|\mathcal{M}_{\mathrm{top}} - \mathcal{L}_0[A_Y, A_Y]| \ll (DX)^\epsilon \Big\{ B_W^2 \frac{A_1^2 X^{7/6}}{D^2} \\ + B_W \mathcal{M}(W) A_1 X^{1/6}(Y^{-1/2} + D^{-1/6})\Big\}.\end{aligned} \tag{40.188}$$

At $A_1 \asymp H = D^{3/4}$, $X = D^{3/8}$ and $Y = \min\{U, D^{1/8}\}$, the errors are target-sized. If $Y = U$ the coefficient tail is exactly zero; otherwise the three displayed powers are $-1/16$, $3/4$ and $31/48$. The remaining exact coefficients satisfy

$$\mu(\mathfrak{m})A_Y(\mathfrak{m}) = \sum_{\substack{\mathfrak{abc}=\mathfrak{m}\\ N\mathfrak{a}, N\mathfrak{b} \le Y}} \mu(\mathfrak{c}), \qquad N\mathfrak{c} \ge D/Y^2 \ge D^{3/4}. \tag{40.189}$$

The small-short-divisor, long residual-Möbius cubic Gauss bilinear moment $\mathcal{L}_0[A_Y, A_Y]$ is still unestimated at the target.

40.31.6 The exact discrete top prefix, with every ray retained

There is also a direct reduction that does not introduce the principal-density split. Its exact support is

$$\mathcal{T}_X = \{(\mathfrak{w}, \mathfrak{s}) : N\mathfrak{w} < 64,\ \mathfrak{s} \text{ good},\ V < N\mathfrak{s} \le 2V,\ N\mathfrak{w}(N\mathfrak{s})^6 \le X\}. \tag{40.190}$$

There is no squarefree restriction on $\mathfrak{s}$. Overlap of $\mathfrak{w}, \mathfrak{s}$ and of $\mathfrak{k}, \mathfrak{s}$ remains allowed. Let $\widetilde{\Theta}$ be the same outer set as θ above, but with *every* original ρ, and put

$$\begin{aligned}\widetilde{d}_\theta[f_1, f_2] = \frac{A_1}{D} h_{AB\rho}(\mathcal{O}) c_{f_1}(\mathfrak{m})\overline{c_{f_2}(\mathfrak{n})}\frac{\epsilon(\eta)}{\sqrt{F}} \\ \cdot \frac{\mu(\mathfrak{e})\eta(\mathfrak{e})}{N\mathfrak{e}}\overline{\eta(\mathfrak{w})}.\end{aligned} \tag{40.191}$$

This is an explicit definition, not division by a density or a primitive value. With the original $\mathfrak{k}$ support as in (40.172), define the normalized exact piece

$$\begin{aligned}\mathcal{P}_X[f_1,f_2]=\sum_{\theta\in\widetilde{\Theta}}\widetilde{d}_\theta[f_1,f_2]\sum_{\mathfrak{k}}\frac{\mu(\mathfrak{k})\eta(\mathfrak{k})^2}{(N\mathfrak{k})^2}\\ \cdot\sum_{\mathfrak{s}:\ (\mathfrak{w},\mathfrak{s})\in\mathcal{T}_X}\bar{\rho}(\mathfrak{s})^6\mathbf{1}_{(\mathfrak{s},\mathfrak{mn})=1}\dot{G}\left(\frac{\lambda_\theta(N\mathfrak{s})^6}{(N\mathfrak{k})^2}\right).\end{aligned}\tag{40.192}$$

Then $\mathcal{P}_X[A_U,A_U]$ is the actual original top primitive-prefix contribution divided by D. It is a signed representation-fixed piece, not a positive energy or the whole infinite dual sum.

Let $\mathcal{L}_X^K[f_1,f_2]$ be exactly (40.192) with $\dot{G}$ replaced by g_0. Only in that leading model can the finite $\mathfrak{k}$ sum be factored as $Q_2^{T_q}(K;\eta^2)$. The discrete $\mathfrak{s}$ sum and its endpoints remain. Unlike $\mathcal{L}_0$, this model has no $\kappa_S g(\mathfrak{m})g(\mathfrak{n})$ density, no $\rho^6=1$ projection and no integral replacing the $\mathfrak{s}$ family.

Proposition 40.29 (Direct original-prefix cutoff reduction)**.** *Put $\Lambda=A_1X/D^2$. With precisely the original support,*

$$|\mathcal{P}_X[A_U,A_U]-\mathcal{L}_X^K[A_U,A_U]|\ll B_W^2(DX)^\epsilon A_1V\Lambda,\tag{40.193}$$

and

$$\begin{aligned}|\mathcal{L}_X^K[A_U,A_U]-\mathcal{L}_X^K[A_Y,A_Y]|\ll B_W\mathcal{M}(W)(DX)^\epsilon A_1V\\ \cdot\{Y^{-1/2}+D^{-1/6}\}.\end{aligned}\tag{40.194}$$

In particular the actual original piece satisfies

$$\begin{aligned}|\mathcal{P}_X[A_U,A_U]-\mathcal{L}_X^K[A_Y,A_Y]|\ll(DX)^\epsilon A_1V\{B_W^2\Lambda\\ +B_W\mathcal{M}(W)(Y^{-1/2}+D^{-1/6})\}.\end{aligned}\tag{40.195}$$

The original unequal-norm projection is allowed.

At the critical pure parameters used above the three powers are again $-1/16$, $3/4$ and $31/48$, with exact zero coefficient tail when $Y=U$. This is a reduction of the *actual discrete* piece to a different, still unestimated, small-short-divisor model. That model retains every ρ, every nonunit S mode, the exact $\mathfrak{w},\mathfrak{s}$ support, root/conductor data, original finite K and both long residual-Möbius column coefficients.

Separate open errors and scope. The accepted fixed-ray disk count gives the distinct top-band certificate

$$\frac{|\mathcal{P}_{\mathrm{top}}-M_{\mathrm{top}}|}{D}\ll B_W^2(DX)^\epsilon A_1X^{1/18}\{1+\sqrt{A_1X/D^2}\}.\tag{40.196}$$

Its pure critical power is $37/48>3/4$; this is an upper certificate, not a lower bound for the actual error. The direct reduction in Proposition 40.29 does not introduce that split: its discrete model retains those effects. No improved bound for the separate discrepancy, for the remaining small-cutoff models, or for the other original sectors is proved here. The result is an application of a named external cubic sieve to an actual arithmetic tail, not a new sieve, a complete analytic Lean formalization, a determinant/zero-location bridge or a proof of GRH. Fixed-profile constants and the explicit $\mathcal{M}(W)$ cannot be replaced by a uniform supnorm-only claim for varying profiles.

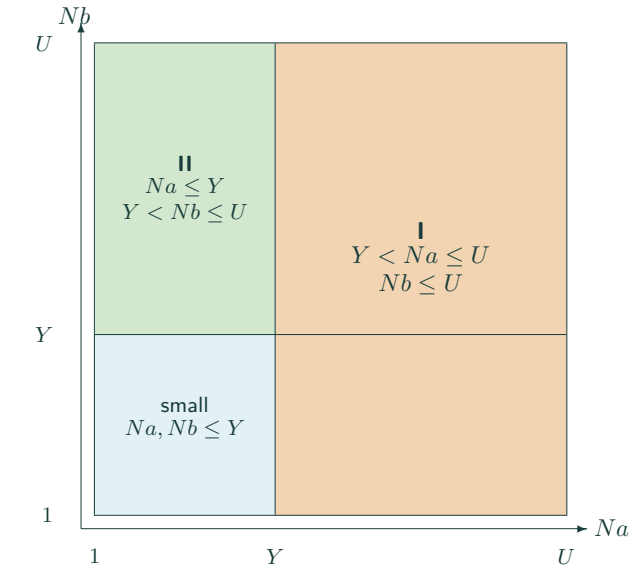


Figure 40.3: The two disjoint cutoff regions fold into the exact coefficient $T_U + T_Y$, followed by the physical cubic matrix on coprime good squarefree ideal factors. Norm axes are schematic, not ideal counts; a common prime gives a raw zero. The displayed tail is the normalized Gauss moment, not an energy or the raw numerator. The bound uses the explicitly cited external cubic sieve. At $U \geq D^{1/8}$ the choice $Y = D^{1/8}$ fits the stated pure critical error budget; if $Y = U$ the coefficient tail is zero. The small-cutoff moment and the full kernel remain open.

40.32 Proofs for the finite-cutoff Gauss tail

The arithmetic norm input is the explicitly pinned de Faveri, arXiv:2610.04045v1, Theorem 1.1 and Example 2.2, at order three. It is used on its actual primary cube-free ideal family. We do not reprove that deep theorem. The primitive root conventions are those already established in Proposition 40.20, and the Jacobi orientation is that of (40.33). The accompanying source map binds the accepted research proofs and their independent reviews. Full third-party reading caches are not public proof inputs.

40.32.1 The coherent main retains all sixth-part and ray data

For a good ideal $\mathfrak{s}$, the original fixed-source transport in (40.120) gives

$$\overline{\eta(\mathfrak{s}^6)} = \overline{\rho(\mathfrak{s})}^6 \mathbf{1}_{(\mathfrak{s},\mathfrak{mn})=1}. \tag{40.197}$$

This is an assertion about the total character on good arguments, not about the order of the individual possibly angular/radial $\xi_{\mathfrak{m}}$. Write $\psi = \bar{\rho}^6$, and let δ_ψ be one if it is principal on good ideals and zero otherwise. The conductor of ψ belongs to fixed S data.

Here is the fixed-ray counting input, with its full deletion. For $t \geq 0$, the classical disk estimate gives

$$\begin{aligned} N_{\psi,q}(t) &:= \sum_{\substack{\mathfrak{s} \text{ good} \\ N\mathfrak{s}\leq t,\ (\mathfrak{s},\mathfrak{q})=1}} \psi(\mathfrak{s}) \\ &= \delta_\psi \kappa_S g(\mathfrak{q}) t + E_{\psi,q}(t), \\ |E_{\psi,q}(t)| &\ll_{S,\psi} t^{1/3} \sum_{\mathfrak{d}|\mathfrak{q}} (N\mathfrak{d})^{-1/3} \ll_\epsilon D^\epsilon t^{1/3}, \qquad N\mathfrak{q} \leq 4D^2. \end{aligned} \tag{40.198}$$

We recall a proof to specify the uniformity being used. For a fixed ideal modulus, count elements in each translated lattice coset inside a disk of radius R. Convolve the disk indicator with a fixed compact smooth nonnegative mollifier of radius Δ. The smoothed disks of radii $R - \Delta$ and $R + \Delta$ sandwich the original disk. Their zero modes differ from its area by $O(R\Delta + \Delta^2)$.

For a nonzero dual vector ξ, polar integration gives

$$\widehat{\mathbf{1}_{|z|\leq R}}(\xi) = \frac{R J_1(2\pi R|\xi|)}{|\xi|}, \qquad |J_1(u)| \ll \min\{1, u^{-1/2}\}. \tag{40.199}$$

The decay follows directly from the angular integral for J_1: for $u \geq 1$, remove arcs of length $u^{-1/2}$ around the two stationary points. Their total contribution is $O(u^{-1/2})$. On the complement integrate once by parts in the phase; the boundary terms and the integral of the derivative of the reciprocal phase derivative are also $O(u^{-1/2})$. For $u \leq 1$ the angular formula gives the bounded estimate. Thus no unproved cancellation of lattice points is inserted. The mollifier supplies arbitrarily rapid decay beyond $|\xi| \asymp \Delta^{-1}$. Counting points of the fixed dual lattice in unit-width radial shells yields

$$\sum_{\xi \neq 0} |\widehat{\mathbf{1}_{|z|\leq R}}(\xi) \widehat{\varphi}(\Delta\xi)| \ll R^{1/2} \Delta^{-1/2}. \tag{40.200}$$

The translation only changes unit phases. Choose Δ comparable to $R^{-1/3}$ for large R. The boundary and dual errors are both $O(R^{2/3})$. Bounded R is absorbed into the fixed constant.

A type-zero finite ray character is a fixed periodic generator function, trivial on the six units. Apply the preceding count to its finitely many residue cosets, and only then form the possibly

complex weighted sum. Division by six and the covolume $\sqrt{3}/2$ of $\mathcal{O}$ give the coefficient $\pi/(3\sqrt{3})$. The principal coset average is the good-S density; a nonprincipal character has mean zero. For $t \ge 1$ this proves the undeleted error $O(t^{1/3})$. For $0 < t < 1$ the ideal count is zero and $t \le t^{1/3}$, so the same ideal estimate remains valid; $t = 0$ is exact.

Now use the *entire* finite inclusion–exclusion:

$$N_{\psi,q}(t) = \sum_{\mathfrak{d}\mid\mathfrak{q}} \mu(\mathfrak{d})\psi(\mathfrak{d})N_{\psi,1}(t/N\mathfrak{d}). \tag{40.201}$$

Divisors with $N\mathfrak{d} > t$ are still present, with their subunit arguments. For principal ψ the main sum is $\kappa_S t \prod_{p\mid q}(1-(Np)^{-1})$; otherwise it is zero. The error in (40.198) follows. Its final divisor product is $O_\epsilon(D^\epsilon)$ by separating finitely many small primes and using $1 + P^{-1/3} \le P^\eta$ at all sufficiently large P. This is ideal-squarefreeness, not rational-squarefreeness.

For fixed $\mathfrak{h}, \mathfrak{r}$, the original sum over $V < N\mathfrak{s} \le b_{\mathfrak{h}\mathfrak{r}}$ has weight $\dot{G}(c\,t^6)$. In the pure block the scale is

$$c = \frac{A_1 N\mathfrak{h} N\mathfrak{r}}{(N\mathfrak{k})^2 N\mathfrak{e} F}. \tag{40.202}$$

Closed prefixes at both endpoints give the exact error formula

$$w(b)E_{\psi,q}(b) - w(V)E_{\psi,q}(V) - \int_V^b E_{\psi,q}(t)w'(t)\,dt, \qquad w(t) = \dot{G}(ct^6). \tag{40.203}$$

There are no half-weights at ideal norm ties. The angular representations of J_0, J_1 imply, with $\Lambda = A_1 X/D^2$,

$$\|\dot{G}\|_\infty \ll 1, \qquad |x\dot{G}'(x)| \ll \sqrt{x}, \qquad \int_V^b |w'(t)|\,dt \ll \sqrt{\Lambda}. \tag{40.204}$$

Indeed $ct^6 \le \Lambda$ and $b/V \le 2$; differentiating the Bessel factor, not G, proves the last assertion. Consequently the error at each fixed outer set is $O(D^\epsilon V^{1/3}(1+\sqrt{\Lambda}))$.

At the top window $N\mathfrak{h}N\mathfrak{r} < 64$. Every good ideal of norm below 64 is sixth-free, because a nontrivial good prime has norm at least seven. Therefore the unique decomposition into its S part and good part runs exactly over all $\mathfrak{w}$ in (40.176). The principal condition is precisely $\rho^6 = 1$. On the original coprime support $g(\mathfrak{m}\mathfrak{n}) = g(\mathfrak{m})g(\mathfrak{n})$. This proves the stated finite formula for M_{top}/D.

For the separate error, $|A_U| \le 3^{\omega(\mathfrak{m})} \ll_\epsilon D^\epsilon$, and there are $O(D)$ original annular ideals. After normalizing once by D, $A_1/(D\sqrt{F}) \le A_1/D^2$ cancels the two column counts. The S/ray/$\mathfrak{e}$ sets are fixed, the top $\mathfrak{w}$ set is finite, and the *original* finite $\mathfrak{k}$ sum is majorized by $\sum (N\mathfrak{k})^{-2}$. Since $V^{1/3} \asymp X^{1/18}$, this proves (40.196). Only its error uses these triangles; the mean in (40.176) stays signed.

40.32.2 Exact good-modulus Gauss factors and separate primitive S values

The finite cubic sum at frequency z is

$$\frac{1}{\sqrt{N\mathfrak{m}}} \sum_{x \bmod \alpha_{\mathfrak{m}}} \chi_{3,\mathfrak{m}}(x) \exp\!\left(2\pi i \operatorname{Tr} \frac{zx}{\delta\alpha_{\mathfrak{m}}}\right) = \overline{\chi_{3,\mathfrak{m}}(z)} G_{\mathfrak{m}}. \tag{40.205}$$

For a unit frequency this is change of variable. At a collision, one local additive frequency is zero and its nonprincipal local cubic character has zero sum. CRT proves the assertion for every good squarefree ideal, including inert primes and nonsquarefree rational norms. The normalized sum has modulus one at unit frequencies.

The total η has type zero, so the previously proved root formula is its finite Gauss sum divided by $\sqrt{F}$. CRT at the coprime primitive conductors $\mathfrak{f}_S, \mathfrak{q}$ gives exactly (40.180) times $\tau_q(\theta_q)/\sqrt{Nq}$. Although their product is unit-trivial, the finite S and good-q characters need not be unit-trivial separately. No extra unit average is taken. The actual finite S character, including its conductor drop, is used at its own primitive modulus. At unit conductor its Gauss sum is one.

On good squarefree q, all local powers $\theta_q, \theta_q^2, \theta_q^3$ are nonprincipal and primitive. The Gauss–Jacobi identity therefore gives

$$\tau_q(\theta_q)\tau_q(\theta_q^2) = J_q(\theta_q, \theta_q^2)\tau_q(\theta_q^3). \tag{40.206}$$

Over a residue field this follows by setting $x + y = t$ in the product of Gauss sums; the zero-t term vanishes because the product character is nonprincipal. Multiplication by CRT proves the composite identity: its additive cross multipliers on the left combine to those of θ_q^3 on the right. The Jacobi sum itself has no additive-generator multiplier.

The correctly oriented result already proved in Section 40.19 is

$$\begin{aligned} J_q(\theta_q, \theta_q^2) &= j(\mathfrak{m})\overline{j(\mathfrak{n})}, \\ j(\mathfrak{m})/\sqrt{N\mathfrak{m}} &= \mu(\mathfrak{m})\vartheta(\mathfrak{m}), \qquad \vartheta = \Psi/\sqrt{N}, \quad \operatorname{cond}\Psi = (2\delta). \end{aligned} \tag{40.207}$$

Its sign is fixed by $-j(p) \equiv 1 \pmod{2\delta}$ and $(j(p)) = p$ for the positive sextic character. The reduction argument includes inert primes. Unique generators congruent to one modulo 2δ then identify $-j(p)$ with $\Psi(p)$. Multiplication yields the displayed identity only on squarefree columns. In particular Ψ has its actual infinity type $(1, 0)$; it is not a finite-order gauge.

Cubic reciprocity for the same primary section and the fact that $\chi_3(-1) = 1$ yield

$$\begin{aligned} \chi_{3,\mathfrak{m}}(\alpha_\mathfrak{n}) &= \chi_{3,\mathfrak{n}}(\alpha_\mathfrak{m}), \\ \tau_q(\theta_q^2)/\sqrt{Nq} &= G_\mathfrak{m}\overline{G_\mathfrak{n}}. \end{aligned} \tag{40.208}$$

The cubic cross factors cancel, while $\tau(\bar{\chi}_3) = \overline{\tau(\chi_3)}$. The quadratic Gaussian evaluation in the same two-factor completion is $\tau_q(\theta_q^3)/\sqrt{Nq} = \Gamma(\alpha_\mathfrak{m}\alpha_\mathfrak{n})$, with the period-four formula in (40.181). For composite q, this uses that Gauss evaluation with its exact pairing; $1 + \theta_q^3$ is not the root-count function of a composite residue ring. Combining these facts with (40.206) proves (40.181). There is no additional $\theta_q^3(-1)$ factor.

For the original good $\mathfrak{k}$,

$$\begin{aligned} \eta(\mathfrak{k}^2) &= \theta_S(\alpha_\mathfrak{k})^2\chi_{3,\mathfrak{m}}(\alpha_\mathfrak{k})\overline{\chi_{3,\mathfrak{n}}(\alpha_\mathfrak{k})}, \\ \overline{G_\mathfrak{m}}G_\mathfrak{n}\chi_{3,\mathfrak{m}}(z)\overline{\chi_{3,\mathfrak{n}}(z)} &= \overline{g_\mathfrak{m}(z)}g_\mathfrak{n}(z). \end{aligned} \tag{40.209}$$

Before the pure specialization the row factor $R_\mathfrak{m}(\mathfrak{v}_2^2)\overline{R_\mathfrak{n}(\mathfrak{v}_2^2)}$ makes $z = \alpha_\mathfrak{k}\alpha_{\mathfrak{v}_2}$. All raw collisions are zeros. The separate original $(\mathfrak{k}, \mathfrak{v}_2) = 1$ condition is not replaced by a frequency assertion. The primitive factors at $\mathfrak{e}$ and $\mathfrak{w}$ are $\eta(\mathfrak{e})$ and $\overline{\eta(\mathfrak{w})}$. When expressed with generators, their S parts are the separate factors $\theta_S(\gamma_\mathfrak{e})$ and $\overline{\theta_S(\gamma_\mathfrak{w})}$. If either is zero the component vanishes. No quotient of these arguments, division by a primitive zero, or primary section for an S-supported ideal is used. Changes of these generators cancel in the total unit-trivial character.

40.32.3 Matched finite endpoint models and a real-axis remainder

For $z \geq 0$ and an integer $J \geq 0$, the angular cosine formula and its real Taylor remainder give

$$\left| J_0(2\sqrt{z}) - \sum_{j=0}^{J} \frac{(-z)^j}{(j!)^2} \right| \leq \frac{z^{J+1}}{((J+1)!)^2}. \tag{40.210}$$

Indeed use the cosine Taylor polynomial through degree $2J+1$ inside its angular integral. The remainder is at most $|2\sqrt{z}\cos\theta|^{2J+2}/(2J+2)!$, and the normalized angular moment of $\cos^{2j}\theta$ is $(2j)!/(4^j(j!)^2)$. This proves both the coefficients and the bound for every nonnegative z, without an exponential majorant or a sign assertion about the error.

Set

$$m_j=\int_0^\infty v^jG(v)\,dv,\qquad I_j(\mathfrak{w})=\frac{b_{\mathfrak{w}}^{6j+1}-V^{6j+1}}{6j+1}=\int_V^{b_{\mathfrak{w}}}t^{6j}\,dt. \tag{40.211}$$

The exact order-J signed model of (40.176) is

$$\mathcal{L}_J[f_1,f_2]=C_0^{-1/2}\sum_\theta d_\theta[f_1,f_2]\sum_{j=0}^{J}\frac{(-1)^jm_j\lambda_\theta^jI_j(\mathfrak{w})}{C_0^j(j!)^2}\,Q_{2+2j}^{T_q}(K;\eta^2). \tag{40.212}$$

The character in every Q_s is still η^2. Both finite endpoints, every primitive root and every original finite $\mathfrak{k}$ cutoff remain. In particular $I_0=X^{1/6}t_{\mathfrak{w}}$ and (40.212) at $J=0$ is exactly (40.177).

Applying (40.210) before the original $\mathfrak{k}$ sum and the t integral gives a per-θ bound

$$\frac{C_0^{-1/2}m_{J+1}(\lambda_\theta/C_0)^{J+1}I_{J+1}(\mathfrak{w})}{((J+1)!)^2}\sum_{\mathfrak{k}\text{ original}}(N\mathfrak{k})^{-4-2J}. \tag{40.213}$$

Only this certified remainder takes absolute values. On the full support $\lambda_\theta b_{\mathfrak{w}}^6=A_1X/(N\mathfrak{e}F)\le\Lambda$. Since $m_{J+1}\le 2(5/2)^{J+1}$ and $\sum(N\mathfrak{k})^{-4-2J}$ is bounded by one constant independent of J and all deletions, put $\Omega=(5/2)\Lambda/C_0$. Counting the two actual annular column sets only in the error yields

$$|\mathcal{M}_{\mathrm{top}}-\mathcal{L}_J[A_U,A_U]|\ll B_W^2(DX)^{\epsilon}A_1X^{1/6}\frac{\Omega^{J+1}}{((J+1)!)^2}. \tag{40.214}$$

Here the two $O(D)$ column counts cancel $1/(D\sqrt{F})\le D^{-2}$, the S/source/ray sets are fixed, the $\mathfrak{w}$ set has bounded size, and each interval has length at most V. The constant in this inequality is independent of J and of derivatives of G. At $J=0$ it proves (40.178). The infinite Bessel hierarchy was already available; the statement used here is the finite real-axis certificate. It bounds the remainder, not the signed polynomial.

40.32.4 All source and ray phases give bounded multiplicative columns

Freeze $\mathfrak{n},\mathfrak{e},\mathfrak{w},\mathfrak{k}$ and one source/ray component in the pure model. After (40.181), every $\mathfrak{m}$ dependence apart from $\mu(\mathfrak{m})f(\mathfrak{m})\overline{G_{\mathfrak{m}}}W(N\mathfrak{m}/D)/\sqrt{N\mathfrak{m}}$ is a product of bounded multiplicative functions, except for two fixed finite selectors. The multiplicative factors include ϑ,ν,g, fixed-numerator residue symbols at $u_0,\gamma_S,\mathfrak{k},\mathfrak{e},\mathfrak{w}$, the value $\theta_S(\alpha_{\mathfrak{m}})$, and the original $(\mathfrak{m},\mathfrak{n})=1$ deletion. They include zeros: a numerator valuation divisible by six does not restore a collision. Primary generators multiply on the required coprime products.

Let $\mathcal{C}$ be the fixed source group and $\mathcal{H}=(\mathcal{O}/(4))^\times$, of order 12. Finite character expansions give

$$\begin{aligned}\mathbf{1}_{[\mathfrak{m}]=A}&=\frac{1}{|\mathcal{C}|}\sum_{\chi\in\widehat{\mathcal{C}}}\overline{\chi(A)}\chi([\mathfrak{m}]),\\ \Gamma(x\alpha_{\mathfrak{n}})&=\sum_{\chi\in\widehat{\mathcal{H}}}a_{\chi,\mathfrak{n}}\chi(x),\qquad\sum_\chi|a_{\chi,\mathfrak{n}}|\le\sqrt{12}.\end{aligned} \tag{40.215}$$

The first coefficient mass is one. The second follows by normalized Parseval and Cauchy since the function has modulus one on $\mathcal{H}$. These bounds are independent of $\mathfrak{n},\mathfrak{k},D$. Extending a fixed formula

off its source class only extends a coefficient function; the finite selector sum restores the original class. No primitive root of a wrong-class or overlapping-conductor pair is asserted.

Consequently every actual fixed-other-column expression is a finite linear combination, of fixed total coefficient mass, of the linear forms in (40.186). The associated λ may have growing conductor and other-column deletion, but $|\lambda| \le 1$ and multiplicativity on coprime products suffice. This does not flatten the original roots or make the coprime matrix positive. It is not a silent extension of a same-class, $\rho = 1$ formula.

40.32.5 Two exact cutoff boxes expose a physical cubic matrix

To prove (40.182), in each term of (40.169) set $\mathfrak{c} = \mathfrak{m}/(\mathfrak{a}\mathfrak{b})$. Squarefreeness makes the factors pairwise coprime and $\mu(\mathfrak{m})\mu(\mathfrak{a})\mu(\mathfrak{b}) = \mu(\mathfrak{c})$. The cutoff difference is the exact disjoint assignment

$$\begin{aligned}&\mathbf{1}_{N\mathfrak{a},N\mathfrak{b}\le U} - \mathbf{1}_{N\mathfrak{a},N\mathfrak{b}\le Y}\\ &\quad = \mathbf{1}_{Y<N\mathfrak{a}\le U,\, N\mathfrak{b}\le U} + \mathbf{1}_{N\mathfrak{a}\le Y,\, Y<N\mathfrak{b}\le U}.\end{aligned} \tag{40.216}$$

Swap $\mathfrak{a}, \mathfrak{b}$ in the second piece and put $\mathfrak{z} = \mathfrak{b}\mathfrak{c}$ in both. On coprime primary $\mathfrak{a}, \mathfrak{z}$, Gauss CRT has the cross $\chi_{3,\mathfrak{a}}(\alpha_{\mathfrak{z}})^2$. Conjugation and cubic reciprocity give exactly (40.184). Thus the left side of (40.186), before taking its absolute value, is

$$\begin{aligned}\sum_{\substack{\mathfrak{a},\mathfrak{z}\ \text{good,SF}\\ Y<N\mathfrak{a}\le U}} &\frac{\overline{G_{\mathfrak{a}}}\lambda(\mathfrak{a})}{\sqrt{N\mathfrak{a}}}\,\frac{\overline{G_{\mathfrak{z}}}\lambda(\mathfrak{z})[T_U(\mathfrak{z}) + T_Y(\mathfrak{z})]}{\sqrt{N\mathfrak{z}}}\\ &\cdot \chi_{3,\mathfrak{a}}(\alpha_{\mathfrak{z}})W(N\mathfrak{a}N\mathfrak{z}/D).\end{aligned} \tag{40.217}$$

At a common prime the cubic entry is zero. Hence this encompassing SF rectangle encodes the original squarefreeness of $\mathfrak{m} = \mathfrak{a}\mathfrak{z}$, without inventing a primitive overlapping root. Also $\mathbf{1}_{(\mathfrak{a}\mathfrak{z},\mathfrak{n})=1} = \mathbf{1}_{(\mathfrak{a},\mathfrak{n})=1}\mathbf{1}_{(\mathfrak{z},\mathfrak{n})=1}$, and the other fixed-numerator collision masks split in the same way. In particular the full other-column mask survives. There is no assumption that A_U or T_L is multiplicative. The elementary estimate $|T_U(\mathfrak{z}) + T_Y(\mathfrak{z})| \le 2\tau(\mathfrak{z})$ is uniform in both cutoffs.

40.32.6 Cubic Cauchy before the distinguished-divisor triangle

Use dyads $N\mathfrak{a} \asymp A$ in $(Y, U]$. Only $N\mathfrak{z} \asymp Z$, $Z \asymp D/A$, can meet the original profile. Both indices in (40.217) are good squarefree ideals, hence cube-free. Primary cubic reciprocity identifies the entry with the physical family of (40.185), or its transpose. Additional row/column masks are coefficient contractions inside that arbitrary-coefficient norm. No character indexed only by a growing conductor is substituted.

Ideal counting and the divisor estimate show, with arbitrarily small exponent losses,

$$\begin{aligned}\sum_{N\mathfrak{a}\asymp A}\left|\frac{\overline{G_{\mathfrak{a}}}\lambda(\mathfrak{a})}{\sqrt{N\mathfrak{a}}}\right|^2 &\ll 1,\\ \sum_{N\mathfrak{z}\asymp Z}\left|\frac{\overline{G_{\mathfrak{z}}}\lambda(\mathfrak{z})[T_U(\mathfrak{z}) + T_Y(\mathfrak{z})]}{\sqrt{N\mathfrak{z}}}\right|^2 &\ll_\epsilon D^\epsilon.\end{aligned} \tag{40.218}$$

These are coefficient bounds after the exact signed grouping, not a new bound for the norm of A_U.

The exact Mellin separation of the one common occurrence of W is

$$W(N\mathfrak{a}N\mathfrak{z}/D) = \frac{1}{2\pi}\int_{\mathbb{R}} \widehat{W}(t)D^{-it}(N\mathfrak{a})^{it}(N\mathfrak{z})^{it}\,dt. \tag{40.219}$$

Its powers are unitary on this line, so it costs $\mathcal{M}(W)$ once. The arbitrary-coefficient cubic operator norm and (40.218) therefore give

$$|\text{one dyadic form}| \ll_\epsilon \mathcal{M}(W)D^\epsilon\sqrt{A + D/A + D^{2/3}}. \tag{40.220}$$

This is a bilinear matrix inequality, not positivity of the original coprime form. Summing the finite dyads with $A \geq Y/2$ and $A \leq U \leq \sqrt{D}$ gives

$$\mathcal{M}(W)D^\epsilon\{\sqrt{U} + \sqrt{D/Y} + D^{1/3}\} \ll \mathcal{M}(W)D^\epsilon\{\sqrt{D/Y} + D^{1/3}\}. \tag{40.221}$$

Dyadic logarithms and divisor losses are absorbed by distributing a prescribed ϵ among the preceding bounds. Partial dyads and real cutoff ties are literal coefficient indicators. Empty tails, including $Y = U$, are exactly zero. This proves (40.186).

40.32.7 Full pair support and the original finite k reassembly

Fix the other column $\mathfrak{n}$. Its raw coprimality and numerator deletions are already in λ by Section 40.32.4. An optional condition $N\mathfrak{m} \neq N\mathfrak{n}$ is not multiplicative. The number of ideals of a fixed rational norm N is at most the integer divisor function: at a split prime an exponent e gives at most $e + 1$ choices, at an inert prime at most one, and at a ramified prime one. Consequently there are $O_\epsilon(D^\epsilon)$ ideals in the forbidden norm fibre, with all orientations separate. Since $|A_U| + |A_Y| \ll_\epsilon D^\epsilon$, subtracting it costs

$$O_\epsilon(B_W D^{-1/2+\epsilon}) \quad \text{in the fixed-other-column sum.} \tag{40.222}$$

This is below (40.186); $\mathcal{M}(W) \geq B_W$ by Fourier inversion. No whole equal-norm energy is subtracted from a different frequency sector.

The untouched original column has the elementary bound

$$\sum_{\mathfrak{n}\ \text{original}} \frac{|A_T(\mathfrak{n})W(N\mathfrak{n}/D)|}{\sqrt{N\mathfrak{n}}} \ll_\epsilon B_W D^{1/2+\epsilon}, \qquad T \in \{U, Y\}. \tag{40.223}$$

Take this triangle only after (40.186). In the leading model all S, source/ray and $N\mathfrak{w} < 64$ coefficient masses are fixed; g_0 is bounded independently of capacity derivatives, and $F^{-1/2}$ supplies the two square-root norm weights already used. The normalization is once by $1/D$. For each actual fixed $\mathfrak{k}$, the column estimate is uniform in its bounded multiplicative numerator phase. Thus its *original finite* sum is bounded by $\sum(N\mathfrak{k})^{-2} < \infty$, with no $(N\mathfrak{k})^\epsilon$ or altered conductor cost. One does not need to complete that sum.

Equivalently, define $\mathcal{G}_D^K$ by $\mathcal{L}_0[f_1, f_2] = A_1 X^{1/6}\mathcal{G}_D^K[f_1, f_2]$. The preceding estimates give

$$|\mathcal{G}_D^K[A_U - A_Y, A_T]| \ll B_W\mathcal{M}(W)D^\epsilon\{D^{-1/6} + Y^{-1/2}\}. \tag{40.224}$$

For a tail on the second column, conjugate the scalar expression and reverse the roles. This sends $G_\mathfrak{n}$ to $\overline{G_\mathfrak{n}}$, W to $\bar{W}$ and the finite coefficients to their conjugates. The conjugate cubic matrix has the same norm, and $\mathcal{M}(\bar{W}) = \mathcal{M}(W)$. No Hermitian assertion about an individual source block is required. Finally use the exact bilinear identity

$$\begin{aligned}\mathcal{G}_D^K[A_U, A_U] - \mathcal{G}_D^K[A_Y, A_Y] = \mathcal{G}_D^K[A_U - A_Y, A_U] \\ + \mathcal{G}_D^K[A_Y, A_U - A_Y].\end{aligned} \tag{40.225}$$

This proves (40.187) with all original finite cutoffs, primitive S zeros and pair masks.

40.32.8 The critical reduction is not a bound for its residual mean

Equations (40.178) and (40.187) prove (40.188). When $U \geq D^{1/8}$, substituting $A_1 \asymp D^{3/4}$, $X = D^{3/8}$, $Y = D^{1/8}$ gives the exact exponent calculations

$$\begin{aligned} 2(3/4) + (7/6)(3/8) - 2 &= -1/16, \\ 3/4 + (1/6)(3/8) - (1/2)(1/8) &= 3/4, \\ 3/4 + (1/6)(3/8) - 1/6 &= 31/48. \end{aligned} \tag{40.226}$$

If $U < D^{1/8}$ choose $Y = U$; the coefficient difference then vanishes identically, rather than replacing $Y^{-1/2}$ by a smaller number. The small-cutoff moment remains exactly the auxiliary expression with that Y. Since both short divisors have norms at most Y, their residual in (40.189) has norm at least D/Y^2. All other-column and finite-frequency couplings remain in its two-column sum.

The current separate discrepancy has critical power

$$3/4 + (1/18)(3/8) = 37/48 > 3/4. \tag{40.227}$$

This upper certificate is not a noncancellation theorem. A bound for the small-cutoff leading model alone does not cancel or improve it. Both it and the remaining original sectors require additional signed arithmetic.

40.32.9 Direct discrete frequencies require no principal-density approximation

For each original dual ideal, its good valuations determine uniquely $\mathfrak{y} = \mathfrak{w}\mathfrak{s}^6$ with good $\mathfrak{s}$ and good part of $\mathfrak{w}$ sixth-free. At $V = X^{1/6}/2$, the lower-open condition $N\mathfrak{s} > V$ implies $N\mathfrak{w} < 64$. Conversely every ideal of norm below 64 has sixth-free good part, since the least good prime norm is seven. This proves the exact support (40.190) with all its nonunit S modes and possible overlaps. No squarefreeness of $\mathfrak{s}$ or new coprimality with $\mathfrak{k}$ is introduced.

Equation (40.197) holds for *every* original ρ. Retaining that factor and the actual discrete $\mathfrak{s}$ family in (40.126) gives (40.192). The prefactor is exactly $A_1/(D\sqrt{F})$, including the once-only normalization. All primitive factors at $\mathfrak{e}, \mathfrak{w}$ are still separate, and a good collision remains zero even when its exponent is a sixth power.

The pointwise real-axis remainder (40.210) at $J = 0$ implies

$$|\dot{G}(x) - g_0| \leq C_0^{-3/2} x \int_0^\infty vG(v)\, dv \leq 3C_0^{-3/2} x, \qquad x \geq 0. \tag{40.228}$$

Every argument in (40.192) is at most $\Lambda = A_1 X/D^2$. Count only in this error: there are $O(D^2)$ annular column pairs, $A_1/(D\sqrt{F}) \leq A_1/D^2$, the original coefficient products are $O(B_W^2 D^{\epsilon})$, and the original finite $\mathfrak{k}$ absolute budget is bounded by $\sum(N\mathfrak{k})^{-2}$. The $\mathfrak{e}$/source/ray and $\mathfrak{w}$ sets have fixed finite mass. Since $V \geq 1$, the exact good $\mathfrak{s}$ annulus contains $O(V)$ ideals. This proves (40.193), without a ray count, interpolated endpoint, density or arbitrary row-weight norm.

It remains to justify applying the column-tail theorem to every original ray. The good-q powers in the proof of (40.181) are local powers $1, 2, 3$ of θ_q; that proof never uses $\rho^6 = 1$. For every original component the total η is type zero and its finite θ_S is fixed at its actual primitive S conductor. Hence the finite selector expansion in (40.215) and its coefficient mass are valid on all these components. No new assertion of sixth order for an individual ξ or replacement of a primitive S Gauss sum is made.

Now freeze $\mathfrak{s}$ as well as $\mathfrak{n}, \mathfrak{k}, \mathfrak{e}, \mathfrak{w}$. Relative to Section 40.32.4, the only new $\mathfrak{m}$ factor is $\mathbf{1}_{(\mathfrak{m},\mathfrak{s})=1}$. It is a bounded multiplicative ideal function and splits exactly in the grouped column as

$$\mathbf{1}_{(\mathfrak{a}\mathfrak{z},\mathfrak{s})=1} = \mathbf{1}_{(\mathfrak{a},\mathfrak{s})=1} \mathbf{1}_{(\mathfrak{z},\mathfrak{s})=1}. \tag{40.229}$$

The $\mathfrak{n}/\mathfrak{s}$ mask is a scalar which may be zero. The fixed $\bar{\rho}(\mathfrak{s})^6$ phase is another bounded scalar. All earlier full-union raw deletions and separate primitive S values remain. Thus (40.186) is uniform in $\mathfrak{s}$ as well as in $\mathfrak{n}, \mathfrak{k}$, with no $(N\mathfrak{s})^\epsilon$ or $(N\mathfrak{k})^\epsilon$ cost. Their growing deleted primes are coefficient diagonals in the same physical cubic matrix.

There is no density in the new exact discrete model. Use the underlying arbitrary-λ theorem with the factor $g(\mathfrak{m})$ omitted, rather than dividing the earlier density-weighted moment by $g(q)$. If a $\mathfrak{k}$ domain has been written with q deletion, first express it on the common original good-SF set $N\mathfrak{k} \le K$ with its exact raw $\eta(\mathfrak{k})^2$ zero. This permits a fixed $\mathfrak{k}$ column argument, restores no prime and adds no $(\mathfrak{k}, \mathfrak{s})$ condition.

Apply the signed column estimate before the other column triangle. The latter is (40.223); after once-only $1/D$ it yields $B_W \mathcal{M}(W) D^\epsilon (Y^{-1/2} + D^{-1/6})$ for each fixed $\mathfrak{s}, \mathfrak{w}, \mathfrak{k}, \mathfrak{e}$ and finite component, with the original $A_1 g_0$ factor. Sum the original finite $\mathfrak{k}$ norm weights and the fixed $\mathfrak{e}, \mathfrak{w}$ components. Only now use the $O(V)$ count of the exact $\mathfrak{s}$ family. Reversed tails use conjugation, as in Section 40.32.7, and the original unequal-norm selector uses the same separate fixed-norm fibre bound (40.222). The exact identity

$$\begin{aligned} \mathcal{L}_X^K[A_U, A_U] - \mathcal{L}_X^K[A_Y, A_Y] = \mathcal{L}_X^K[A_U - A_Y, A_U] \\ + \mathcal{L}_X^K[A_Y, A_U - A_Y] \end{aligned} \tag{40.230}$$

then proves (40.194). Combining it with the one Bessel error proves (40.195).

This direct proof does not assert a smaller value for the separate 37/48 certificate in the continuous mean route; it never introduces that split. All of its nonprincipal-ray and exact-discrete effects remain in $\mathcal{L}_X^K[A_Y, A_Y]$. At $Y \le D^{1/8}$ the residual column norms are at least $D/Y^2 \ge D^{3/4}$, just as in (40.189). The new model is still unbounded at target size. It is different from the principal-density $\mathcal{L}_0[A_Y, A_Y]$.

A capacity-empty integer interval, or empty exact $\mathcal{T}_X$, gives zero by definition. Absence of actual good squarefree rows in a *nonempty* integer interval alone does not imply that each dual prefix piece is zero; cancellation with other frequencies can be required. No full dual complement, other block, whole signed assembly or determinant/zero-location obligation is resolved by this direct small-cutoff reduction.

Why the completed shortcuts do not supply that arithmetic. The inverse-different cubic Gauss frequency is incomplete: expanding it leaves the actual weighted primary $\mathfrak{k}$ set, not a complete residue system modulo $\mathfrak{m}\mathfrak{n}$. The bounded number of $\mathfrak{w}$ modes supplies no such completion. Likewise, expanding both short divisors and taking their absolute triangles before the cubic cross does not give the proved estimate. Even an explicitly hypothetical uniform inner exponent $\alpha < 1$ would produce the diagnostic

$$D^{\alpha - 1/2} \left(\sum_{N\mathfrak{a} \le U} (N\mathfrak{a})^{-\alpha} \right)^2 \ll_\alpha D^{\alpha - 1/2} U^{2(1-\alpha)}. \tag{40.231}$$

At $U \asymp \sqrt{D}$ this is $D^{1/2}$. It is a conditional failure of that method, not an available smooth-coefficient Gauss theorem or an impossibility result. The actual proof above retains the physical cubic cross until its joint matrix norm. It bounds one specified signed tail and leaves the long residual-Möbius, finite-$\mathfrak{k}$ small-short moment as the next arithmetic problem. No whole signed, global unsigned, determinant, zero-location, analytic Lean or GRH conclusion is implied.

40.33 Ramified theta transforms and the original pure dual prefix

The exact discrete prefix introduced in Section 40.31 can be estimated with its original coefficient A_U. The argument constructs the previously missing finite-character transform at the ramified prime and groups all original short and Heath–Brown factors before taking a short-factor triangle. The resulting power is 101/144 for this specified pure finite dual prefix. The whole signed comparison 13/12, the global unsigned comparison 9/8, and the remaining infinite-frequency assembly retain their earlier status.

The retained principal-density mean in the earlier discussion is a different expression with its own comparison problem. The result here uses every original ray component and the actual discrete sixth-part set. It supplies a new proof for the actual finite discrete prefix rather than modifying the historical cutoff stages.

40.33.1 The normalized object and its original support

Put $\omega = e^{2\pi i/3}$, $K = \mathbb{Q}(\omega)$, $\mathcal{O} = \mathbb{Z}[\omega]$ and $\lambda = 1 + 2\omega = i\sqrt{3}$. A good ideal avoids the original fixed set S, containing the primes above $2, 3$. All ideal columns are good and squarefree; different ideals of equal norm remain different columns. Use the unique multiplicative primary generator $\alpha_{\mathfrak{a}} \equiv 1 \pmod 3$. The original character ν has fixed finite order, with its conductor exclusions in S; no order-dividing-six hypothesis is imposed on ν.

Assume

$$D \ge 2^{64}, \quad 1 \le U \le \sqrt{D}, \quad A_1 \asymp H = D^{3/4}, \quad X = D^{3/8}, \quad V = X^{1/6}/2. \tag{40.232}$$

Only the original unweighted pure two-pivot block is asserted: $A_2 = 1$, its second good factor and the other four good factors are units, and u_0 is the fixed literal unit/S-supported factor with no good prime support. Keep its original capacity endpoints, nodal function G, and pre-S cutoff $K_{\mathrm{cut}} = \sqrt{b}$. An empty capacity interval gives zero. None of these data is recomputed during a coefficient decomposition.

Let W be one fixed possibly complex smooth function supported on $[1, 2]$, with $W(1) = W(2) = 0$, and write

$$\begin{aligned} B_W &= \|W\|_\infty, \qquad \widehat{W}(t) = \int_0^\infty W(x) x^{-it}\,\frac{dx}{x}, \\ \mathcal{M}(W) &= \frac{1}{2\pi}\int_{\mathbb{R}} |\widehat{W}(t)|\,dt, \qquad\qquad V_1(W) = B_W + \int_1^2 |W'(x)|\,dx. \end{aligned} \tag{40.233}$$

These are seminorms of the common column profile. No uniform derivative hypothesis on the sharp capacity interpolant is added. The exact frequency set is

$$\mathcal{T}_X = \left\{ (\mathfrak{w}, \mathfrak{s}) : \begin{array}{l} \mathfrak{w} \text{ integral, } N\mathfrak{w} < 64, \quad \mathfrak{s} \text{ good integral,} \\ V < N\mathfrak{s} \le 2V, \quad N\mathfrak{w}(N\mathfrak{s})^6 \le X \end{array} \right\}. \tag{40.234}$$

There is no squarefreeness requirement on $\mathfrak{s}$. The permitted overlaps among $\mathfrak{k}, \mathfrak{s}, \mathfrak{w}$ remain permitted, including nonunit S-supported $\mathfrak{w}$.

Here is a full definition of the piece being bounded. Let $\Omega = (A, B, \rho, \mathfrak{m}, \mathfrak{n})$ range over the original finite source/ray components and their ordered coprime good squarefree columns in $[D, 2D]$, with the original source classes. An original unequal-norm projection may be imposed consistently. Use the actual primitive character η_Ω of (40.120), its actual S-conductor $\mathfrak{f}_S$, and

$$F_\Omega = N\mathfrak{f}_S\, N\mathfrak{m}\, N\mathfrak{n}, \qquad \mathfrak{q} = \mathfrak{m}\mathfrak{n}, \qquad c_U(\mathfrak{m}) = A_U(\mathfrak{m})\nu(\mathfrak{m})R_{\mathfrak{m}}(u_0)W(N\mathfrak{m}/D).$$

The numerator value $R_{\mathfrak{m}}(u_0)$ includes its original raw zeros. Put $P_S = \prod_{\mathfrak{p}\in S}\mathfrak{p}$. With $C_0 = 3/(4\pi^2)$, the normalized prefix is

$$\begin{aligned}\mathcal{P}_X[A_U, A_U] = \frac{A_1}{D}\sum_{\Omega} h_{AB\rho}(\mathcal{O})c_U(\mathfrak{m})\overline{c_U(\mathfrak{n})}\frac{\varepsilon(\eta_\Omega)}{\sqrt{F_\Omega}} \\ \cdot \sum_{\mathfrak{e}\mid P_S}\frac{\mu(\mathfrak{e})\eta_\Omega(\mathfrak{e})}{N\mathfrak{e}}\sum_{\substack{\mathfrak{k}\ \text{good,SF}\\ N\mathfrak{k}\le K_{\mathrm{cut}}}}\frac{\mu(\mathfrak{k})\eta_\Omega(\mathfrak{k})^2}{(N\mathfrak{k})^2} \\ \cdot \sum_{(\mathfrak{w},\mathfrak{s})\in\mathcal{T}_X}\overline{\eta_\Omega(\mathfrak{w})}\,\overline{\rho(\mathfrak{s})}^{\,6}\mathbf{1}_{(\mathfrak{s},\mathfrak{q})=1}\dot{G}\left(\frac{A_1 N\mathfrak{w}(N\mathfrak{s})^6}{(N\mathfrak{k})^2 N\mathfrak{e}F_\Omega}\right).\end{aligned} \tag{40.235}$$

All sums are finite. The ray label ρ here is distinguished from the Jacobi column weight below. Values at $\mathfrak{e}$ and $\mathfrak{w}$ are separate primitive values, including zero; a conductor drop does not restore a deleted prime. The original $1/D$ occurs once. The raw numerator is $D\mathcal{P}_X$.

Define $\mathcal{L}_X^{K_{\mathrm{cut}}}$ by replacing $\dot{G}$ in (40.235) by $g_0 = C_0^{-1/2}\int_0^\infty G(v)\,dv$, with every other datum fixed. For the original coefficients the established real-axis estimate is

$$|\mathcal{P}_X - \mathcal{L}_X^{K_{\mathrm{cut}}}| \ll B_W^2(DX)^{\epsilon}A_1V\Lambda, \qquad \Lambda = A_1X/D^2. \tag{40.236}$$

It uses $0 \le G \le 1$, its fixed compact support and a pointwise Bessel remainder. The value g_0 may vanish and is never divided out.

40.33.2 Actual finite characters and a sharp ramified row

The actual root calculation leaves one angular Jacobi gauge and a cubic Gauss root in each varying column. On good squarefree ideals the Jacobi function is $\rho_J = \mu\vartheta$, where $\vartheta = \Psi/\sqrt{N}$ has infinity type $(1,0)$; here $\Psi(\mathfrak{a})$ is the chosen generator 1 mod 2λ. The arithmetic μ belongs in the coefficient opening. There is exactly one varying ϑ, or its conjugate; an additional finite-order assertion about ρ_J would be false.

Write $\chi_{3,\mathfrak{a}}$ for the positive cubic residue character, with its zero at every shared prime. The source Gauss root is

$$G_{\mathfrak{a}}^{\mathrm{src}} = \frac{1}{\sqrt{N\mathfrak{a}}}\sum_{x \bmod \alpha_{\mathfrak{a}}}\chi_{3,\mathfrak{a}}(x)e^{2\pi i\,\mathrm{Tr}(x/\alpha_{\mathfrak{a}})}. \tag{40.237}$$

The actual root uses $\lambda\alpha_{\mathfrak{a}}$ in this additive denominator. The normalization of the angular factor is explicit:

$$\begin{aligned}\Theta_\ell(\mathfrak{a}) &= (\alpha_{\mathfrak{a}}/|\alpha_{\mathfrak{a}}|)^\ell, \\ \vartheta(\mathfrak{a}) &= \Theta_1(\mathfrak{a})\overline{\chi_{3,\mathfrak{a}}(2)}, \\ G_{\mathfrak{a}}^{\mathrm{act}} &= \chi_{3,\mathfrak{a}}(\lambda)G_{\mathfrak{a}}^{\mathrm{src}}.\end{aligned} \tag{40.238}$$

Thus the two fixed corrections may be written as source frequency $12t$. The factor 12 belongs to the fixed finite character data; $12t$ is not declared a good squarefree moving level.

After exact product-character expansion of the joint finite S/source/Γ selectors, every remaining own-variable phase has the form $\Theta_{\pm1}\kappa$, where κ belongs to a fixed finite residue family, with its original modulus-zero extension. It includes higher 3-primary conductors of ν. The finite source quotient is a fixed ray quotient; fixed numerator symbols are finite Kummer characters. The full Fourier sums retain their actual coefficient masses and reconstruct the primitive $\mathfrak{e}/\mathfrak{w}$ zeros. Growing other-column deletions remain literal masks.

For a physical good squarefree frequency $\mathfrak{t}$, an exact interval $I \subset [T, 2T]$, and a finite good deletion ideal Q, write the actual row in either required conjugate orientation as

$$\mathcal{F}_\psi(T; \mathfrak{t}; Q, I) = \sum_{\substack{\mathfrak{a} \text{ good,SF} \\ N\mathfrak{a} \in I,\ (\mathfrak{a}, Q)=1}} \psi(\mathfrak{a}) \overline{G_{\mathfrak{a}}^{\mathrm{act}}} \chi_{3,\mathfrak{a}}(\alpha_{\mathfrak{t}}) \frac{W(N\mathfrak{a}/T)}{\sqrt{N\mathfrak{a}}}. \tag{40.239}$$

Here ψ is from this actual fixed family, including its angular factor. It is not an arbitrary bounded multiplicative function.

Theorem 40.30 (The actual fixed-family sharp row)**.** *For every such member, both conjugate orientations and every physical good squarefree* $\mathfrak{t}$*, including the unit,*

$$|\mathcal{F}_\psi(T; \mathfrak{t}; 1, I)| \ll_{\mathrm{fixed},\epsilon} V_1(W)(2 + TN\mathfrak{t})^\epsilon \min\{\sqrt{T},\ T^{1/4}(N\mathfrak{t})^{3/8}\}, \qquad T \geq 1. \tag{40.240}$$

The constant may depend on the fixed conductor/character family. A literal unit calculation extends the estimate to $1/2 \leq T < 1$*; for* $T \leq 1/2$ *the row is zero with the stated endpoint convention.*

Proof. Use the unconditional theta modularity and known 27 integral cusps in Dunn–Radziwiłł, arXiv:2109.07463v3, Section 5 and Appendix A. Its weight-zero cubic theta θ is automorphic with Kubota multiplier χ on $\Gamma_2 = \mathrm{SL}_2(\mathbb{Z})\Gamma_1(3)$, where $\Gamma_1(3)$ is the principal congruence subgroup of $\mathrm{SL}_2(\mathcal{O})$. Fix its known representatives γ_j and $F_j = \theta \circ \gamma_j$. The correct ramified coefficient projector acts on $\lambda^3\mu$. Its primary selector is $\mathbf{1}_{\lambda^3\mu \equiv 1 \bmod 3}$. A finite Fourier expansion writes it, and the away-3 periodic twist, as actual rational translates of theta.

For $a = A/C$ reduced, choose $\gamma = \left(\begin{smallmatrix} A & B \\ C & D_0 \end{smallmatrix}\right)$ of determinant one, and choose j so that $\delta = \gamma\gamma_j^{-1} \in \Gamma_2$. Use $U(x) = \left(\begin{smallmatrix} 1 & x \\ 0 & 1 \end{smallmatrix}\right)$ and $W_C = \left(\begin{smallmatrix} 0 & -1/C \\ C & 0 \end{smallmatrix}\right)$. Then

$$\gamma^{-1}U(a) = U(-D_0/C)W_{-C}, \qquad \theta(U(a)w) = \chi(\delta)F_j(U(-D_0/C)W_{-C}w).$$

The multiplier is its literal Kubota value. Pure nonzero angular derivatives kill the pulled-back radial constants. Their Mellin identity has factor $(NC)^{1-2s}$, including the Jacobian. The explicit cusp coefficients have absolute Dirichlet norm at most

$$3^8 \zeta_K^{(\lambda)}(\sigma)\zeta_K^{(\lambda)}(3\sigma - \tfrac{1}{2}), \qquad 1 < \sigma < 13/12.$$

Normalized finite Fourier mass is $O_{\mathrm{fixed}}(\sqrt{N\mathfrak{t}})$ and each reduced denominator has norm $O_{\mathrm{fixed}}(N\mathfrak{t})$. This gives the conservative dual cost $(N\mathfrak{t})^{3/2+\epsilon}$.

Coefficientwise cube completion retains the raw $L(3s - \frac{1}{2}, \kappa^3\Theta_{3\ell})$, with every stipulated Euler omission. Apply convexity to this entire completed numerator first. Its reciprocal is used only where $\Re(3s - \frac{1}{2}) > 1$, by absolutely convergent Euler products. Exact half-integer Perron thresholds and partial summation give (40.240). The optimized height is $(T/(N\mathfrak{t})^{3/2})^{1/4}$ when this is at least one; the elementary count gives the other branch. The extended edition retains the constants and the zeroth-angular residues explicitly. □

40.33.3 The full original coefficient and its finite prefix

On the actual contributing annulus $N\mathfrak{m} > U$, put

$$B_U(\mathfrak{m}) := \mu(\mathfrak{m})A_U(\mathfrak{m}) = \sum_{\substack{\mathfrak{abc}=\mathfrak{m} \\ N\mathfrak{a}, N\mathfrak{b} \leq U}} \mu(\mathfrak{c}). \tag{40.241}$$

This B_U is not the project's original C_U. Equation (40.241) is not asserted for arbitrary small columns or the unit. Unit factors inside an annular factorization remain present.

Theorem 40.31 (Original pure finite dual-prefix bound)**.** *Under* (40.232)*, with the complete original support and fixed data of* (40.235)*,*

$$|\mathcal{P}_X[A_U, A_U]| \ll_{\mathrm{fixed},\epsilon} (DXA_1)^{\epsilon} A_1 V\{B_W[\mathcal{M}(W) + V_1(W)]D^{-1/9} + B_W^2[\Lambda + D^{-1}]\}. \tag{40.242}$$

In particular its normalized leading power is

$$13/16 - 1/9 = 101/144 < 3/4, \qquad 3/4 - 101/144 = 7/144. \tag{40.243}$$

The raw numerator has one additional factor D.

Proof. Open (40.241) and the exact $J = 5$ finite Heath–Brown identity at $z_0 = (2D)^{1/5}$. There are at most eleven factors, including the original $\mathfrak{a}, \mathfrak{b}$. Choose their grouping from fixed independent dyadic scales. A balanced whole-factor partition has a physical cubic matrix bound $\mathcal{M}(W)D^{1/3+\epsilon}$, using the pinned de Faveri, arXiv:2610.04045v1, Theorem 1.1 and Example 2.2, at order three.

An unbalanced box has one long unrestricted coefficient-one factor $\mathfrak{v}$. At $D \geq 2^{64}$ neither an original short factor nor a short Möbius factor can occupy that scale. The product $\mathfrak{p}$ of all other factors has norm $O(D^{1/3})$ and its intrinsic signed assignment coefficient is divisor-bounded. This retains the $j = 1$ boxes, which are all balanced.

For $N\mathfrak{p} > Z$ the cubic matrix gives $\mathcal{M}(W)D^{\epsilon}[D^{1/3} + \sqrt{D/Z}]$. For $N\mathfrak{p} \leq Z$, freeze the original opposite column $\mathfrak{n}$ first. Keep $\mathbf{1}_{(\mathfrak{p},\mathfrak{n})=1}$ and all prefix $\mathfrak{k}/\mathfrak{s}/\mathfrak{w}$ zeros in its actual coefficient. The remaining long-variable deletion is $Q = \mathrm{rad}_{\mathrm{good}}(\mathfrak{p}\mathfrak{n}\mathfrak{k}\mathfrak{s}\mathfrak{w})$. Its exact divisor $\mathfrak{h}$ changes frequency to $\mathfrak{p}\mathfrak{k}\mathfrak{h}$ and length to $D/(N\mathfrak{p}N\mathfrak{h})$. Including the original prefix weight, Theorem 40.30 gives

$$\frac{1}{\sqrt{N\mathfrak{p}N\mathfrak{h}}}\left(\frac{D}{N\mathfrak{p}N\mathfrak{h}}\right)^{1/4}(N(\mathfrak{p}\mathfrak{k}\mathfrak{h}))^{3/8} = D^{1/4}(N\mathfrak{k})^{3/8}(N\mathfrak{p})^{-3/8}(N\mathfrak{h})^{-3/8}. \tag{40.244}$$

Thus the small-prefix column costs $V_1(W)D^{\epsilon}D^{1/4}(N\mathfrak{k})^{3/8+\epsilon}Z^{5/8}$. Choose $Z = D^{2/9}$; both column costs have power $7/18$.

Only after that bound take the opposite-column elementary $B_W D^{1/2+\epsilon}$ count. Use the original A_1/D once, sum the original finite $\mathfrak{k}$ with the convergent positive majorant $\sum(N\mathfrak{k})^{-13/8+\epsilon}$, and count the exact $\mathfrak{s}$ family by $O(V)$. Optional unequal norms cost the same fixed-norm fibre bound $O(B_W^2 A_1 V D^{-1+\epsilon})$. Finally (40.236) applies directly to A_U, A_U. No A_U-to-A_Y replacement or common-long-divisor opening is used. □

The estimate has fixed-conductor and explicit profile-seminorm dependence. It does not supply a supremum-norm estimate for varying W_D, an arbitrary weighted-row operator, the infinite dual complement, mixed or neighboring blocks, short/principal assembly, an independent positive determinant, or a zero-location theorem. The Dirichlet, Hecke, Dedekind, elliptic and general Artin obligations remain separate. No analytic/category Lean formalization or GRH proof is claimed.

40.34 Proofs of the ramified transform and full-coefficient prefix bound

The external theta input is the unconditional Section 5 and Appendix A of Dunn–Radziwiłł, *Bias in cubic Gauss sums: Patterson's conjecture*, arXiv:2109.07463v3, 14 May 2024. Its GRH-conditional prime theorems are not used. The matrix input is the already admitted physical ideal family in de Faveri, *Optimal large sieve for fixed order characters*, arXiv:2610.04045v1, Theorem 1.1 and Example 2.2, at order three. The theta modularity and deep cubic norm remain external theorems. The constructions and estimates below specify how they apply to the actual finite-character family.

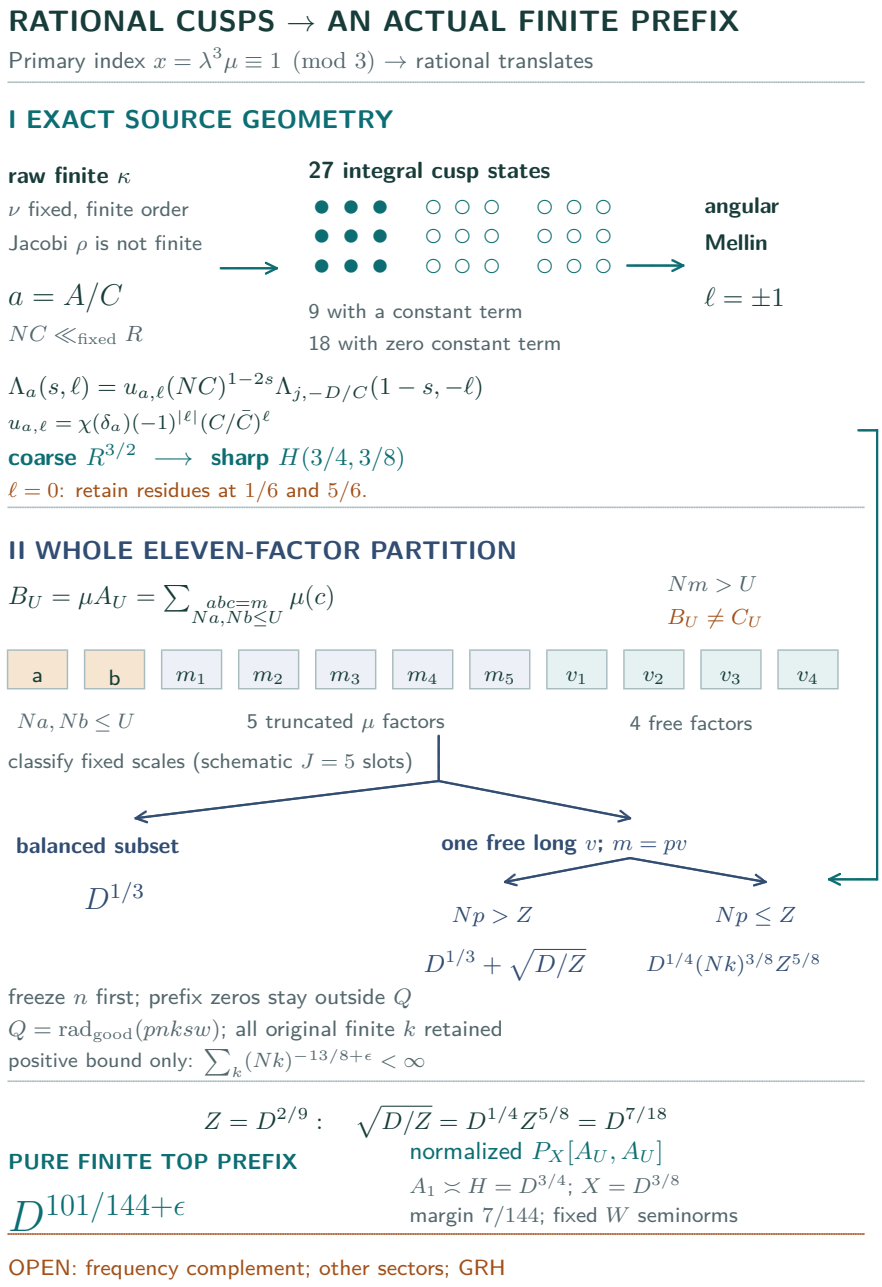


Figure 40.4: The rational-cusp construction feeds a whole-factor partition of the original coefficient. Here $R = N\mathfrak{t}$, the angular orders are $\ell = \pm 1$, and the pure finite-prefix budget uses $D \ge 2^{64}$, fixed character data and the displayed profile seminorms. The positive $\mathfrak{t}$ majorant requires sufficiently small $\epsilon < 5/8$; the actual cutoff remains finite. The diagram shows a proof construction, not measured energy. The full signed kernel and GRH remain open.

40.34.1 Fixed residue data, angular order and raw evaluations

The full varying-column phase list, after the arithmetic μA_U opening, consists of one ϑ or its conjugate, the cubic Gauss root, the original finite-order ν, finite source/ray factors, the mod-4 Fourier factors of Γ, the actual primitive S-type factors, and residue symbols at the fixed numerators $u_0, \gamma_S, \mathfrak{e}, \mathfrak{w}$. The set $N\mathfrak{w} < 64$, the S-types and the $\mathfrak{e}$ set are fixed finite sets. The growing $\mathfrak{k}$ numerator belongs to the cubic frequency instead of this list.

There is a common fixed residue modulus for this list. A finite-order Hecke character has infinity type zero and factors through its actual conductor. The source group is explicitly a ray quotient: Section 2.3.2 of de Faveri defines $\mathcal{C} = H_{\mathfrak{c}} \otimes \mathbb{Z}/6\mathbb{Z}$ for one sufficiently deep S-supported ray modulus $\mathfrak{c}$. The chosen primary generators realize these ray characters as finite residue characters. The Γ factors are characters of $(\mathcal{O}/(4))^{\times}$.

The local sixth-power tests also have a fixed finite modulus. For a prime $\mathfrak{p}$, Hensel's criterion at 1 gives $1 + \mathfrak{p}^e \subset (K_{\mathfrak{p}}^{\times})^6$ when $e > 2v_{\mathfrak{p}}(6)$. One may use $e_{(2)} = 3$ and $e_{(\lambda)} = 5$. These are moduli for testing local classes, not replacements for primitive character evaluation moduli. For a fixed nonzero integral numerator ζ, its n-th residue function, $n \mid 6$, is a finite Kummer character for $K(\zeta^{1/n})/K$. A safe sextic conductor bound is supplied by the polynomial discriminant ideal $(6)^6(\zeta)^5$. A field/order discriminant divides this separable polynomial discriminant, including when a proper factor supplies the field. A fractional numerator can be cleared by a fixed sixth power, retaining its original numerator and denominator exclusions. This uses finite one-dimensional Kummer characters, without a general Artin-holomorphy hypothesis.

A joint finite S-type or primitive-value selector is not assumed multiplicative. If $\mathcal{H}$ is its fixed finite residue group, write its actual function as

$$\begin{aligned} f(x,y) &= \sum_{\chi,\psi \in \widehat{\mathcal{H}}} b_{\chi,\psi}\chi(x)\psi(y), \\ b_{\chi,\psi} &= |\mathcal{H}|^{-2} \sum_{x,y \in \mathcal{H}} f(x,y)\overline{\chi(x)\psi(y)}, \\ \sum_{\chi,\psi} |b_{\chi,\psi}| &\le |\mathcal{H}|\,\|f\|_{\infty}. \end{aligned} \tag{40.245}$$

Normalized Parseval and Cauchy prove the last line. This expansion precedes freezing a primitive type or separating column factors. Forbidden primitive $\mathfrak{e}/\mathfrak{w}$ values are zero in f; individual Fourier terms can be nonzero there, and only their full sum reconstructs the zero. No term is individually renamed an original nonzero row.

Thus one may use a common fixed raw modulus F_{raw} and functions

$$\kappa_{\mathrm{raw}}(\mathfrak{a}) = \kappa_{\mathrm{prim}}(\alpha_{\mathfrak{a}})\mathbf{1}_{(\mathfrak{a},F_{\mathrm{raw}})=1}. \tag{40.246}$$

They are imprimitive residue characters on that modulus. All stipulated prime zeros survive a primitive conductor drop.

The Jacobi function $\rho_J = \mu\vartheta$ is not one of these finite characters. Its μ has already entered the arithmetic coefficient B_U, and its unique remaining angular factor is ϑ, with order $+1$ or -1 in the two conjugate orientations. Common or prefix Jacobi factors stay in their actual outer coefficients when those variables are frozen. An arbitrary bounded multiplicative function, a growing opposite column, a Möbius coefficient or the nonperiodic density $\prod_{\mathfrak{p}\mid\mathfrak{a}}(1-(N\mathfrak{p})^{-1})$ is not made into a member of this fixed family. That density does not occur in $\mathcal{P}_X$.

40.34.2 Known integral cusps and an explicit absolute coefficient norm

Let $\Gamma = \mathrm{SL}_2(\mathcal{O})$, $\Gamma_1(3) = \ker(\Gamma \to \mathrm{SL}_2(\mathcal{O}/(3)))$ and $\Gamma_2 = \mathrm{SL}_2(\mathbb{Z})\Gamma_1(3)$. The source theta function is a weight-zero function on hyperbolic three-space with $\theta(\delta w) = \chi(\delta)\theta(w)$ for $\delta \in \Gamma_2$. The multiplier χ is the source Kubota character. The quotient $\Gamma_2\backslash\Gamma$ has 27 cosets. One can see the finite count from $\mathcal{O}/(3) \simeq \mathbb{F}_3[\varepsilon]/(\varepsilon^2)$: the reduction kernel in SL_2 has 3^3 elements, and $\mathrm{SL}_2(\mathbb{F}_3)$ has 24.

Fix the published integral representatives γ_j and put $F_j(w) = \theta(\gamma_j w)$. For the exact chosen function define its actual Fourier coefficient $a_j(\mu)$ by

$$F_j(z,v) = \sigma_j v^{2/3} + \sum_{\mu\neq 0} a_j(\mu) v K_{1/3}(4\pi|\mu|v) e(\mathrm{Tr}(\mu z)), \qquad e(x) = e^{2\pi i x}. \tag{40.247}$$

For those representatives $\sigma_j = 3^{5/2}/2$ for $j \le 9$ and zero for $j \ge 10$. The support lies in $\lambda^{-4}\mathcal{O}$. The symbol a_j always means this actual coefficient; a source table using $d_j(\mu)$, $d_j(-\mu)$ or a conjugated function is converted before using an exact phase formula.

The source formulas (5.7), (5.13), (5.14) and Appendix A express these coefficients through τ, τ_1, τ_2, unit rotations, fixed unit factors and additive phases. The first nine families have the τ absolute norm and the other eighteen have the τ_1, τ_2 norms. Rotations, conjugation and index reversal preserve absolute norm.

Proposition 40.32 (Known-cusp absolute norm)**.** *For $1 < \sigma < 13/12$, every one of these actual cusp families satisfies*

$$\mathcal{A}_j(\sigma) := \sum_{\mu\neq 0} \frac{|a_j(\mu)|}{(N\mu)^\sigma} \le 3^8 \zeta_K^{(\lambda)}(\sigma)\zeta_K^{(\lambda)}(3\sigma - \tfrac{1}{2}). \tag{40.248}$$

The right side is independent of a moving good level or a translation. Here $\zeta_K^{(\lambda)}$ omits the prime above 3.

Proof. In the τ formula write $c, d \equiv 1 \pmod 3$, with c squarefree and d arbitrary, possibly sharing primes with c. For the first family $\mu = \pm\epsilon\lambda^{3n-4}cd^3$, $n \ge 1$, there are at most six sign/unit branches and

$$|\tau(\mu)| \le 3^{n/2+2}\sqrt{Nd}.$$

For the second family $\mu = \pm\lambda^{3n-3}cd^3$, $n \ge 0$, there are at most two branches and $|\tau(\mu)| \le 3^{n/2+5/2}\sqrt{Nd}$. These follow from the literal unnormalized primitive Gauss magnitude $|g(a,c)| = \sqrt{Nc}$ and the source factor $|d/c|$; the fixed Gauss numerators are units modulo good c. Retain the separate c and cube variables. A generic $(N\mu)^{1/6}$ coefficient bound would lose convergence near 1.

Put $z = 3^{1/2-3\sigma}$ and $Z_{\mathrm{SF}}(\sigma) = \sum_{c\ \mathrm{primary,SF}} (Nc)^{-\sigma}$, with the prime λ excluded. Then

$$\mathcal{A}_\tau(\sigma) \le \left\{ \frac{6\,3^{2+4\sigma}z + 2\,3^{5/2+3\sigma}}{1-z} \right\} Z_{\mathrm{SF}}(\sigma)\zeta_K^{(\lambda)}(3\sigma - \tfrac{1}{2}). \tag{40.249}$$

The τ_1, τ_2 families each have three unit branches at $\lambda^{-4}cd^3$, with magnitude at most $9\sqrt{Nd}$; their possible opposite signs do not change the norm. Consequently

$$\mathcal{A}_{\tau_i}(\sigma) \le 27\,3^{4\sigma} Z_{\mathrm{SF}}(\sigma)\zeta_K^{(\lambda)}(3\sigma - \tfrac{1}{2}), \qquad i = 1, 2. \tag{40.250}$$

In the stated range $z \le 1/9$, $3^{2+4\sigma} \le 3^7$, $3^{5/2+3\sigma} \le 3^6$, and $27\,3^{4\sigma} \le 3^8$. The brace in (40.249) is at most $3^8/2$. Finally $Z_{\mathrm{SF}}(\sigma) \le \zeta_K^{(\lambda)}(\sigma)$. The actual coefficient convention and all unit phases therefore give (40.248). □

For later comparison, an affine state $F_j(Az+B,|A|v)$, $A\neq 0$, has index and coefficient

$$\nu = A\mu, \qquad a_{j,A,B}(\nu) = |A|\, a_j(\mu) e(\operatorname{Tr}(\mu B)). \tag{40.251}$$

Its absolute Dirichlet norm is exactly $|A|^{1-2\sigma}\mathcal{A}_j(\sigma)$. For the ramified diagonal $A=\lambda^{-2B_0}$, this factor is $3^{B_0(2\sigma-1)}$. Commuting a moving translation past that diagonal changes $U(-\lambda^4 c/r)$ to $U(-\lambda^{4+2B_0}c/r)$. Together with $\nu=\lambda^{-2B_0}\mu$ its phase is still $e(-\operatorname{Tr}(\lambda^4\mu c/r))$. This explains why an omitted ramified scale changes actual phases, even though the eventual absolute bound is fixed-data controlled.

40.34.3 Exact rational reduction and the actual Kubota multiplier

For $a=A/C\in K$ reduced, choose $B_0,D_0\in\mathcal{O}$ with $AD_0-B_0C=1$ and put $\gamma_a=\left(\begin{smallmatrix}A & B_0\\ C & D_0\end{smallmatrix}\right)$. The Euclidean property of $\mathcal{O}$ supplies this choice. Let

$$U(x)=\begin{pmatrix}1 & x\\ 0 & 1\end{pmatrix}, \qquad W_C=\begin{pmatrix}0 & -1/C\\ C & 0\end{pmatrix}.$$

Integral a is included by $C=1$. Direct multiplication proves

$$\gamma_a^{-1}U(a)=\begin{pmatrix}D_0 & 1/C\\ -C & 0\end{pmatrix}=U(-D_0/C)W_{-C}. \tag{40.252}$$

Choose j with $\delta_a=\gamma_a\gamma_j^{-1}\in\Gamma_2$. Then the exact function identity is

$$\theta(U(a)w)=\chi(\delta_a)F_j(U(-D_0/C)W_{-C}w). \tag{40.253}$$

It uses known integral cusp functions rather than an unconstructed new cusp coefficient family.

The phase is computable, not an unspecified unit set to one. Find a rational integral $\sigma\in\mathrm{SL}_2(\mathbb{Z})$ with the same reduction modulo 3 as δ_a. Then $\delta'=\sigma^{-1}\delta_a\in\Gamma_1(3)$. If $\delta'=\left(\begin{smallmatrix}a' & b'\\ c' & d'\end{smallmatrix}\right)$, the source rule is

$$\chi(\delta_a)=\chi(\delta')=\begin{cases}(c'/a')_3, & c'\neq 0,\\ 1, & c'=0.\end{cases} \tag{40.254}$$

Here $a'\equiv 1 \pmod 3$ is nonzero and coprime to c'. The index j can be found by reducing modulo 3 and testing the 24-element rational subgroup against the 27 fixed cosets. Equivalently, a finite traversal of elementary generators constructs representatives. A representative differing from the published one changes its function by the fixed multiplier just computed. Its Fourier coefficients and constants carry that multiplier too.

One can also display the fixed ramified states explicitly. If a moving good level r survives the fixed denominator reduction, write $C=c_0r$, with c_0 in a fixed finite set and $(c_0,r)=1$. The matrix identity

$$U(A/C)W_r=\gamma_a U(-D_0/C)\operatorname{diag}(r/C,C/r)$$

and $D_0=br+9c_0d$ give the fixed state $F_j|U(-b/c_0)\operatorname{diag}(c_0^{-1},c_0)$ followed by the moving translation $U(-9c_0^2d/r)$. The general formula (40.253) also handles cancelled or nonunit fixed Fourier residues directly; this special display does not impose a primitive Fourier-support condition on them.

40.34.4 Radial cusp constants, angular derivatives and the Mellin Jacobian

Write $w = (z, v)$. The action in (40.253) is

$$z' = -D_0/C - \frac{\bar{z}}{C^2(|z|^2 + v^2)}, \qquad v' = \frac{v}{NC(|z|^2 + v^2)}. \tag{40.255}$$

The pulled-back constant of F_j is therefore

$$\chi(\delta_a)\sigma_j(NC)^{-2/3}v^{2/3}(|z|^2 + v^2)^{-2/3}. \tag{40.256}$$

It is radial in z. Every nonzero pure Wirtinger derivative ∂_z^m or $\partial_{\bar{z}}^m$ at $z = 0$ kills it. At large v the original translated theta constant is also independent of z. The known nonconstant lattice support gives exponential decay after angular differentiation at both ends, with the reciprocal-end rate depending on NC.

For completeness, the zeroth-angular constants have not disappeared. For a finite combination $\sum_a c(a)\theta(z + a, v)$ put

$$C_\infty = \frac{3^{5/2}}{2}\sum_a c(a), \qquad C_0^* = \sum_a c(a)\chi(\delta_a)\sigma_{j(a)}(NC_a)^{-2/3}. \tag{40.257}$$

Its regularized Mellin transform with weight v^{2s-2} has residues

$$\operatorname*{Res}_{s=1/6}\Lambda(s, 0) = -C_\infty/2, \qquad \operatorname*{Res}_{s=5/6}\Lambda(s, 0) = C_0^*/2. \tag{40.258}$$

These signs follow by integrating the powers at infinity and zero. A projector with zero sum kills C_∞, but need not kill C_0^*. No finite noncubic label implies such a cancellation.

For $\ell > 0$ set $\mathcal{D}_\ell = (2\pi i)^{-\ell}\partial_z^\ell$; for $\ell < 0$ use $\mathcal{D}_\ell = (2\pi i)^{-|\ell|}\partial_{\bar{z}}^{|\ell|}$. The angular Mellin transform is

$$\Lambda_a(s, \ell) = \int_0^\infty \mathcal{D}_\ell[\theta(z + a, v)]_{z=0}v^{2s+|\ell|-2}\,dv. \tag{40.259}$$

For $\ell \neq 0$ it is entire by the endpoint bounds just proved.

Proposition 40.33 (Exact angular rational-cusp identity)**.** *For every reduced rational translate and $\ell \neq 0$,*

$$\Lambda_a(s, \ell) = \chi(\delta_a)(-1)^{|\ell|}(C/\bar{C})^\ell(NC)^{1-2s}\Lambda_{j,-D_0/C}(1 - s, -\ell). \tag{40.260}$$

The right Mellin transform uses the actual known function $F_j(z - D_0/C, v)$.

Proof. For $\ell > 0$, set $\bar{z} = 0$ in the full-coordinate chain rule. Then z' and v' in (40.255) are constant as functions of z, while $\bar{z}'$ is affine with derivative $-1/(\bar{C}^2v^2)$. Thus the pure derivative has exactly the factor $\chi(\delta_a)(-1)^\ell\bar{C}^{-2\ell}v^{-2\ell}$ and the opposite angular derivative of F_j at $(-D_0/C, 1/(NCv))$. There are no lower angular or radial terms. The negative sign case is the conjugate-coordinate calculation.

In the integral substitute $y = 1/(NCv)$. Its Jacobian and power weight give $(NC)^{-2s+\ell+1}y^{\ell-2s}\,dy$. Combining the factor $\bar{C}^{-2\ell}$ produces precisely $(C/\bar{C})^\ell(NC)^{1-2s}$. The exponent $1 - 2s$, rather than $-2s$, is essential. This proves (40.260) for both signs. □

If the real part of the dual Dirichlet variable exceeds one, its series is

$$\sum_{\mu\neq 0} a_j(\mu)e(-\operatorname{Tr}(\mu D_0/C))(\mu/|\mu|)^{-\ell}(N\mu)^{-(1-s)}. \tag{40.261}$$

The additive and angular phases remain literal; their absolute values are one only after this exact expression has been established. Proposition 40.32 controls the series.

40.34.5 The integral-index primary projector and raw cube completion

Let κ be any one fixed residue member on the primary section. Use a fixed modulus containing its actual conductor and all original fixed exclusions. Separate its λ-part κ_λ and away-λ part κ_0. Choose $f \geq 2$ containing the λ-conductor, and put

$$\Phi(x) = \kappa_\lambda(x)\mathbf{1}_{x\equiv 1 \bmod \lambda^2} \quad (x \bmod \lambda^f), \qquad \Phi(x) = 0 \text{ on nonunits.} \tag{40.262}$$

The entire theta support has $\lambda^3\mu \in \mathcal{O}$. The correct argument is this integral index, not $\lambda^4\mu$ for a ramified character.

From the two τ families above, $\Phi(\lambda^3\mu)$ selects exactly

$$\mathcal{S} = \{\lambda^{-3}cd^3 : c, d \equiv 1 \pmod 3,\ c \text{ squarefree}\}. \tag{40.263}$$

Indeed the first family has positive λ-valuation after multiplication by λ^3, as do the second-family terms with $n \geq 1$. They are killed as nonunits. At $n = 0$ the negative branch is -1 modulo 3, and only the positive branch is 1. This proves the unit-state selection as well as its valuation condition.

For a moving good squarefree level $\mathfrak{t}$, let $\psi_\mathfrak{t}$ be either cubic orientation on its literal residue modulus. Let F_0 be the fixed away-λ raw modulus. The product $\psi_M(x) = \kappa_0(x)\psi_\mathfrak{t}(x)$ is a bounded periodic function on the valid period $M = F_0\mathfrak{t}$. This period is not asserted to be its primitive conductor. It is allowed to be imprimitive and to have overlapping $F_0, \mathfrak{t}$. No value $\kappa(\mathfrak{t})$ is divided out.

Define the coefficient-projected theta function using $\Phi(\lambda^3\mu)\psi_M(\lambda^3\mu)$. Its infinite constant is zero. On $\mathcal{S}$, $\tau(\mu) = 3^{5/2}\widetilde{g}(c)\sqrt{Nd}$. Multiplicativity on the primary section gives the exact cube identity

$$\Phi(\lambda^3\mu)\psi_M(\lambda^3\mu) = \kappa(c)\kappa(d)^3\psi_\mathfrak{t}(c)\mathbf{1}_{(d,\mathfrak{t})=1}. \tag{40.264}$$

Write

$$\mathcal{R}_{\kappa,\mathfrak{t},\ell}(s) = \sum_{c \text{ primary,SF}} \frac{\widetilde{g}(c)\kappa(c)\psi_\mathfrak{t}(c)\Theta_\ell(c)}{(Nc)^s}, \tag{40.265}$$

with every fixed raw zero in κ. Then initially $\Re s > 1$,

$$D_{\Phi,\psi}(s,\ell) = 3^{5/2+3s}i^\ell L^{\mathrm{raw}}(3s - \tfrac{1}{2}, \kappa^3\Theta_{3\ell})\mathcal{R}_{\kappa,\mathfrak{t},\ell}(s). \tag{40.266}$$

The factor i^ℓ is the actual angle of λ^{-3}. The cube series has denominator $(Nd)^{3s-1/2}$, and L^{raw} retains all original exclusions above $\lambda F_0\mathfrak{t}$, even after primitive conductor drop. There is no $\kappa(\lambda)$ factor or untwisted-zeta substitution. Conjugating the whole construction gives the actual conjugate Gauss root and opposite angular/cubic orientations.

The full ramified projector has an exact finite translation formula. The trace dual of $\mathcal{O}$ is $\lambda^{-1}\mathcal{O}$, so

$$\begin{aligned} b_h &= 3^{-f}\sum_{x \bmod \lambda^f} \Phi(x)e(-\operatorname{Tr}(xh/\lambda^{f+1})), \\ \Phi(x) &= \sum_{h \bmod \lambda^f} b_h e(\operatorname{Tr}(xh/\lambda^{f+1})), \qquad \sum_h |b_h| \leq 3^{f/2}. \end{aligned} \tag{40.267}$$

For the away period use normalized Fourier coefficients q_u with positive inversion sign and pairing $e(\operatorname{Tr}(xu/\alpha_M))$. Since M avoids λ, that pairing is perfect, and

$$\psi_M(x) = \sum_{u \bmod M} q_u e(\operatorname{Tr}(xu/\alpha_M)), \qquad \sum_u |q_u| \leq \sqrt{NM}. \tag{40.268}$$

Both mass bounds are Parseval followed by Cauchy. They hold for arbitrary bounded periodic functions; no primitive Fourier-support condition is inserted.

Consequently the exact projected function is a finite sum of $\theta(z + a_{h,u}, v)$ with

$$a_{h,u} = h\lambda^{2-f} + \lambda^3 u/\alpha_M, \qquad \sum_{h,u} |b_h q_u| \le 3^{f/2}\sqrt{NM}. \tag{40.269}$$

The inverse different explains the exponent $2 - f$. Every raw zero is reconstructed by this full sum. Each reduced denominator $C_{h,u}$ divides a fixed λ-power times M; hence $1 \le NC_{h,u} \ll_{\text{fixed}} N\mathfrak{t}$. Nonunit Fourier residues may lower that denominator. They remain terms of the exact transform, rather than being discarded.

40.34.6 The coarse dual bound, safe convexity and literal Perron endpoints

Let $R = N\mathfrak{t}$, and set

$$E(s) = L^{\text{raw}}(3s - \tfrac{1}{2}, \kappa^3\Theta_{3\ell})\mathcal{R}_{\kappa,\mathfrak{t},\ell}(s).$$

For $\ell \neq 0$ the finite sum of entire angular Mellins is entire. The source Fourier–Mellin calculation has factor

$$\gamma_\ell(s) = \frac{1}{4}(2\pi)^{-2s-|\ell|}\Gamma(s + \tfrac{|\ell|}{2} - \tfrac{1}{6})\Gamma(s + \tfrac{|\ell|}{2} + \tfrac{1}{6}). \tag{40.270}$$

Thus division by γ_ℓ, whose reciprocal is entire, and the nonzero elementary factor in (40.266) makes E entire as well.

On $s = -\eta + i\tau$, $0 < \eta < 1/12$, (40.260), (40.248) and (40.269) give

$$\begin{aligned} \sum_{h,u} |b_h q_u|(NC_{h,u})^{1+2\eta}\mathcal{A}_{j(h,u)}(1+\eta) &\ll_{\text{fixed},\eta} R^{3/2+2\eta}, \\ |E(-\eta + i\tau)| &\ll_{\text{fixed},\ell,\eta} R^{3/2+O(\eta)}(1+|\tau|)^{2+O(\eta)}. \end{aligned} \tag{40.271}$$

The height exponent follows from the quotient of the two Gamma products. The exact multiplier $\chi(\delta_{h,u})(-1)^{|\ell|}(C_{h,u}/\bar{C}_{h,u})^\ell$ has been written before bounding its modulus. This is a conservative $R^{3/2+\epsilon}$ cost. No refined $R^{1/2+\epsilon}$ Ramanujan estimate is used.

The line $\Re s = 1 + \eta$ is absolutely bounded uniformly in R, by the original Gauss and cube coefficients. For a requested final $\epsilon > 0$, choose $\eta > 0$ sufficiently small in terms of ϵ; the constants may depend on that choice. The finite-order continuation from the theta Mellin representation permits the damped strip maximum principle. Applying it to the entire numerator, then allocating small exponents, gives

$$|E(\sigma + i\tau)| \ll_{\text{fixed},\ell,\epsilon} (R(2+|\tau|))^\epsilon R^{\frac{3}{2}(1-\sigma)}(1+|\tau|)^{2(1-\sigma)} \tag{40.272}$$

on the safe half-strip $1/2 + \eta \le \sigma \le 1 + \eta$. Only there divide by L^{raw}: the real part of $3s - \frac{1}{2}$ exceeds one, so its inverse is bounded by absolutely convergent Euler products, uniformly in all raw omissions. No inverse-L continuation through unknown zeros or zero-free strip is asserted. Equation (40.272) therefore bounds $\mathcal{R}$ on that half-strip.

Here are the endpoint details needed for Theorem 40.30. Replace each real endpoint by the half-integer threshold selecting exactly the same integer norms. All ideals in a repeated norm fibre are counted. Such a fibre has divisor-bounded multiplicity in this quadratic field. For an unnormalized sharp prefix at length T, truncated Perron at height $\mathcal{H} \ge 1$ has error

$$O_\epsilon\big(T^\epsilon[1 + (T/\mathcal{H})\log(2T)]\big). \tag{40.273}$$

This follows by summing $\min(1, T/(\mathcal{H}|n-y|))$ over integer distances from the half-integer endpoint y. No norm tie receives a half-weight.

At $\sigma = 1/2 + \eta$ the vertical contribution is bounded by

$$(RT)^{\epsilon} T^{1/2} R^{3/4} \mathcal{H}.$$

If $T \geq R^{3/2}$, choose $\mathcal{H} = (T/R^{3/2})^{1/4}$. On horizontal sides the bound is at most $T/\mathcal{H}$, up to allocated subpowers, since $R^{3/2}\mathcal{H}^2 \leq T$. The vertical integral, truncation and horizontal contributions are then $O((RT)^{\epsilon} T^{3/4} R^{3/8})$. An interval is a difference of two prefixes. If $T < R^{3/2}$, the elementary $O(T)$ count is the better branch.

Finally apply partial summation to the same $T^{-1/2} W(x) x^{-1/2}$, $x = N\mathfrak{a}/T$. Its supremum and total variation are bounded by $O(T^{-1/2} V_1(W))$. This proves (40.240) with the exact profile. For $1/2 \leq T < 1$ only the unit can occur; its coefficient and profile are literal and satisfy the same bound with a fixed endpoint constant. For $T \leq 1/2$ there is no contribution. This extension uses no analytic theorem at a fictitious length.

40.34.7 The actual annular coefficient and exact eleven-factor expansion

The opened coefficient $B_U = \mu A_U$ in (40.241) is asserted on the actual annulus $N\mathfrak{m} > U$. It is distinct from original C_U. No identity for $B_U(\mathcal{O})$ is needed or asserted. Unit factors within the factorization of an annular column are essential and stay in every convolution below.

Let $\mathbf{1}$ be the constant-one function on good ideals, $\delta_{\mathcal{O}}$ the ideal-convolution identity, and $M_z(\mathfrak{a}) = \mu(\mathfrak{a}) \mathbf{1}_{N\mathfrak{a} \leq z_0}$, $z_0 = (2D)^{1/5}$. The exact good-ideal convolution identity is

$$\mu = \sum_{j=1}^{5} (-1)^{j-1} \binom{5}{j} \mathbf{1}^{*(j-1)} * M_z^{*j} + \mathbf{1}^{*4} * (\mu - M_z)^{*5}. \tag{40.274}$$

Indeed $\mathbf{1} * \mu = \delta_{\mathcal{O}}$, so expand $\mu * [\delta_{\mathcal{O}} - (\delta_{\mathcal{O}} - \mathbf{1} * M_z)^{*5}]$; also $\delta_{\mathcal{O}} - \mathbf{1} * M_z = \mathbf{1} * (\mu - M_z)$. Each factor of $\mu - M_z$ has norm strictly above z_0. The last term in (40.274) is supported strictly above $z_0^5 = 2D$ and vanishes at every residual $\mathfrak{c}$ under consideration.

The j-th term has j truncated Möbius factors and $j-1$ unrestricted coefficient-one factors. Together with the two original short factors it has $2j+1 \leq 11$ labels. The $j = 1$ term and unit labels remain. Restricting the total column to squarefree support forces all factors to be squarefree and pairwise coprime.

Use independent dyads $[M_i, 2M_i)$, $M_i \geq 1$, with the original own-factor cutoffs at U, z_0. If the box meets the annulus,

$$D/2^{11} \leq P_{\mathrm{box}} := \prod_i M_i \leq 2D. \tag{40.275}$$

Choose the partition from these scales only. If some $M_i \in [P_{\mathrm{box}}^{1/3}, P_{\mathrm{box}}^{2/3}]$, it is a balanced subset. If all $M_i < P_{\mathrm{box}}^{1/3}$, multiply successive scales until first reaching $P_{\mathrm{box}}^{1/3}$; the result is below $P_{\mathrm{box}}^{2/3}$. If no balanced subset exists, a unique scale exceeds $P_{\mathrm{box}}^{2/3}$; two such scales would have product above P_{box}. The product of all remaining scales is below $P_{\mathrm{box}}^{1/3}$.

At $D \geq 2^{64}$,

$$P_{\mathrm{box}}^{2/3} \geq D^{2/3}/2^{22/3} > \sqrt{D} \geq U, \qquad P_{\mathrm{box}}^{2/3} > (2D)^{1/5}.$$

Therefore an unbalanced unique long factor is genuinely one of the unrestricted coefficient-one factors. It cannot be an original short factor or a truncated Möbius factor. The actual whole prefix

$\mathfrak{p}$, the product of all remaining factors, satisfies $N\mathfrak{p} \le 2^{10} P_{\mathrm{box}}^{1/3} \ll D^{1/3}$. The $j = 1$ term has no unrestricted factor and is automatically balanced; its unit assignments have not been discarded.

For a fixed box define each macro coefficient by summing all its signed assignments within its assigned factor group. On a squarefree ideal the number of at most eleven labelled factorizations is at most $11^{\omega(\mathfrak{a})}$. Fixed binomial factors and dyadic logarithms thus give a uniform D^{ϵ} pointwise bound, with every own cutoff retained. There is no separate count over $N\mathfrak{a}, N\mathfrak{b} \le U$.

40.34.8 Whole-factor cubic matrices and the large-prefix part

A balanced partition gives two physical squarefree macro ideals $\mathfrak{u}, \mathfrak{v}$, each with scale in fixed multiples of $[D^{1/3}, D^{2/3}]$ and product comparable to D. Their own coefficients contain the original cutoffs and signs. Cubic Gauss CRT gives on coprime products

$$\overline{G_{\mathfrak{u}\mathfrak{v}}^{\mathrm{act}}} = \overline{G_{\mathfrak{u}}^{\mathrm{act}}}\,\overline{G_{\mathfrak{v}}^{\mathrm{act}}}\,\chi_{3,\mathfrak{u}}(\alpha_{\mathfrak{v}}). \tag{40.276}$$

The raw matrix entry is zero at a collision, so summing all squarefree macro pairs implements the original squarefree product. No primitive root at an overlapping product is invented.

The external physical cubic norm is

$$\big\|[\chi_{3,\mathfrak{u}}(\alpha_{\mathfrak{v}})]_{N\mathfrak{u}\asymp P,\, N\mathfrak{v}\asymp L}\big\|_{\mathrm{op}} \ll_{\epsilon} (PL)^{\epsilon}\sqrt{P + L + (PL)^{2/3}}. \tag{40.277}$$

The rows and columns are actual good squarefree ideals. All raw fixed/growing multiplicative masks are coefficient diagonals in this norm, after finite-selector expansion. Ideal counting gives squared coefficient norms D^{ϵ} when each coefficient is weighted by the inverse square root norm. Separate the one occurrence of the common W by

$$W(N\mathfrak{u}N\mathfrak{v}/D) = \frac{1}{2\pi}\int_{\mathbb{R}} \widehat{W}(t) D^{-it} (N\mathfrak{u})^{it} (N\mathfrak{v})^{it}\, dt.$$

The powers are unitary diagonals, costing $\mathcal{M}(W)$ once. Balanced boxes therefore cost $\mathcal{M}(W) D^{1/3+\epsilon}$.

For a Type-I box write $\mathfrak{m} = \mathfrak{p}\mathfrak{v}$, where $\mathfrak{v}$ has coefficient one and the intrinsic $H_{\mathfrak{p}}$ contains all remaining assignments. Then $N\mathfrak{p} \ll D^{1/3}$. The portion $N\mathfrak{p} > Z$, with its literal own-variable indicator, has dyadic bound

$$\mathcal{M}(W) D^{\epsilon}\sqrt{P + D/P + D^{2/3}},$$

and hence total bound

$$\mathcal{M}(W) D^{\epsilon}[D^{1/3} + \sqrt{D/Z}]. \tag{40.278}$$

Macro own-factor constraints remain coefficients. A chosen equivalent row-dependent norm interval costs the reviewed logarithmic interval-Schur factor, preserving complete norm fibres. It is not assigned operator norm one.

40.34.9 The full original opposite-column mask in the small-prefix row

Freeze the original $\mathfrak{n}$, the exact $\mathfrak{k}, \mathfrak{s}, \mathfrak{w}, \mathfrak{e}$, and a finite source component before estimating a Type-I row. The original pair mask is exactly

$$\mathbf{1}_{(\mathfrak{p}\mathfrak{v},\mathfrak{n})=1} = \mathbf{1}_{(\mathfrak{p},\mathfrak{n})=1}\mathbf{1}_{(\mathfrak{v},\mathfrak{n})=1}. \tag{40.279}$$

The first factor stays in the actual prefix coefficient, along with all original prefix/$\mathfrak{k}, \mathfrak{s}, \mathfrak{w}$ collisions, fixed numerator zeros and prefix phases. The intrinsic arithmetic $H_{\mathfrak{p}}$ still depends only on its own

factor assignments. Multiplication by these outer factors preserves its divisor bound. A forbidden prefix is zero before a row bound is applied.

The remaining long-variable deletion is

$$Q = \mathrm{rad}_{\mathrm{good}}(\mathfrak{p}\mathfrak{n}\mathfrak{k}\mathfrak{s}\mathfrak{w}).$$

It is not a substitute for the first factor in (40.279), and the growing $\mathfrak{n}$ is not part of a fixed character conductor. On the nonzero support $\mathfrak{p}, \mathfrak{k}$ are squarefree and coprime, by the original $\eta(\mathfrak{k})^2$ zero. The physical cubic frequency is $\mathfrak{t} = \mathfrak{p}\mathfrak{k}$.

The exact deletion formula is

$$\mathcal{F}_\psi(T; \mathfrak{t}; Q, I) = \sum_{\substack{\mathfrak{h} \mid Q \\ (\mathfrak{h}, \mathfrak{t}) = 1}} \frac{\mu(\mathfrak{h})\psi(\mathfrak{h})\overline{G_{\mathfrak{h}}^{\mathrm{act}}}\chi_{3,\mathfrak{h}}(\alpha_{\mathfrak{t}})}{\sqrt{N\mathfrak{h}}} \cdot \mathcal{F}_\psi(T/N\mathfrak{h}; \mathfrak{h}\mathfrak{t}; 1, I/N\mathfrak{h}). \tag{40.280}$$

Insert $\sum_{\mathfrak{h} \mid (Q, \mathfrak{v})} \mu(\mathfrak{h})$ and set $\mathfrak{v} = \mathfrak{h}\mathfrak{a}$. Gauss CRT and reciprocity combine the actual crosses into $\chi_{3,\mathfrak{a}}(\alpha_{\mathfrak{h}\mathfrak{t}})$. This raw entry is zero at $(\mathfrak{a}, \mathfrak{h}) > 1$ and encodes the squarefree-product condition. The outer raw entry kills $(\mathfrak{h}, \mathfrak{t}) > 1$. No zero is inverted, including if a numerator exponent becomes divisible by three. Original interval endpoints divide literally by $N\mathfrak{h}$.

Here $T = D/N\mathfrak{p}$, and the exact product is

$$(T/N\mathfrak{h})N(\mathfrak{h}\mathfrak{t}) = DN\mathfrak{k}. \tag{40.281}$$

There is no common-long-divisor decomposition between the two columns in this proof. The other original column remains fixed.

Using the sharp bound and the original prefix factor gives (40.244). For $T/N\mathfrak{h} \in [1/2, 1)$ use the actual unit contribution; smaller arguments contribute zero, with the profile endpoint rule. Large frequencies are allowed by the proven all-level sharp bound, with its trivial fallback. Thus

$$\sum_{\mathfrak{h} \mid Q} (N\mathfrak{h})^{-3/8} \le \tau(Q) \ll_\epsilon (NQ)^\epsilon.$$

On the exact support, $N\mathfrak{n} \le 2D$, $N\mathfrak{s} \le 2V$, $N\mathfrak{w} < 64$, so $NQ \ll DZVN\mathfrak{k}$. Summing $(N\mathfrak{p})^{-3/8}$ over $N\mathfrak{p} \le Z$ by ideal counting proves the small-prefix column bound

$$V_1(W)(DXA_1)^\epsilon D^{1/4}(N\mathfrak{k})^{3/8+\epsilon} Z^{5/8}. \tag{40.282}$$

Every prefix zero was retained until that positive estimate. No coherence or orientation mean has been removed.

40.34.10 The exact discrete prefix and the final normalization

Combine the balanced, large-prefix and small-prefix bounds, and put

$$Z = D^{2/9}, \qquad \sqrt{D/Z} = D^{1/4} Z^{5/8} = D^{7/18}. \tag{40.283}$$

The untouched original A_U column has the elementary bound $B_W D^{1/2+\epsilon}$. Apply it after the left estimate and use the original A_1/D once. All finite source/ray/primitive $\mathfrak{e}/\mathfrak{w}$ coefficient masses stay fixed, and the actual $\mathfrak{s}$ family is counted by $O(V)$ only at the end. The scalar g_0 is bounded and is never divided out.

The original finite $\mathfrak{k}$ sum is unchanged in the identity. Its small-prefix positive majorant is

$$\sum_{\substack{\mathfrak{k}\ \text{good,SF}\\ N\mathfrak{k}\le K_{\mathrm{cut}}}} (N\mathfrak{k})^{-13/8+\epsilon} \le \zeta_K(13/8-\epsilon), \qquad \epsilon < 5/8. \tag{40.284}$$

Product and divisor losses can be allocated smaller exponents first; their $N\mathfrak{k}$ factors are absorbed by this convergent series. Balanced and large-prefix pieces use the easier exponent 2. This is a bound on a finite sum, not an Euler replacement of the model.

For the optional original unequal-norm projection, a fixed rational norm has $O_\epsilon(D^\epsilon)$ ideal coordinates. The actual A_U and every fixed HB component are divisor-bounded. Removing that same fixed-$\mathfrak{n}$ fibre costs $O(B_W D^{-1/2+\epsilon})$ in the left column, and therefore $O(B_W^2 A_1 V D^{-1+\epsilon})$ in the normalized form. Conjugate ideals remain different, and a norm inequality has not been made multiplicative.

This proves the leading-model part of (40.242). For the original exact prefix, all its Bessel arguments are at most $\Lambda = A_1 X/D^2$, and

$$|\dot G(x) - g_0| \le 3C_0^{-3/2} x.$$

There are $O(D^2)$ annular column pairs and $A_1/(D\sqrt{F_\Omega}) \le A_1/D^2$. The coefficient product is $O(B_W^2 D^\epsilon)$, the original finite $\mathfrak{k}$ absolute budget is bounded by $\sum (N\mathfrak{k})^{-2}$, and the actual sixth-part band has $O(V)$ ideals. Only in this remainder are these absolute counts taken. They give (40.236) directly for A_U, A_U. No A_U-to-A_Y error, principal density or scalar ray-count split is introduced.

Finally the exact powers are

$$\begin{aligned} 3/4+1/16-1/9 &= 101/144, & 3/4-101/144 &= 7/144,\\ 3/4+1/16-1/6 &= 31/48, & 13/16+(3/4+3/8-2) &= -1/16. \end{aligned} \tag{40.285}$$

The same norm-fibre correction has power $-3/16$. This completes the pure finite-prefix theorem with its once-only normalization and all original finite cutoffs.

40.34.11 Verification scope and the remaining arithmetic comparison

The accepted evidence includes exact rational cusp matrices and finite quotient/coset calculations, angular-coordinate and Mellin checks, literal primary-support cases, affine coefficient transport, and synthetic scale-composition/exponent checks. The typed exponent grid is a formal subfamily; it is not exhaustive physical dyad coverage after the constants in (40.275). The proof uses the separate exact $D \ge 2^{64}$ inequalities for those constants. None of these checks is actual-family energy data, training, asymptotics or a kernel-checked Lean proof.

All original sources, primary versions, raw outputs and failed preliminary harnesses remain preserved. The new theorem is a prose proof with the identified external theta and cubic-norm inputs. Its domain is the representation-fixed pure $\mathcal{T}_X$ prefix in (40.235). The infinite dual complement, other pure sectors, mixed and neighboring blocks, short/principal assembly, independent positive arithmetic determinant and zero-location comparisons remain open. The Dirichlet, Hecke, Dedekind, elliptic and general Artin scopes retain their separate hypotheses; no Artin holomorphy, desired positivity, zero location or GRH premise has been inserted. The whole signed and global unsigned comparisons have not changed.

40.35 Paired cutoffs, exact divisor signs and proved regimes

The comparison in this section concerns a specified part of the signed coprime-column form for the original unweighted, nonprincipal, two-pivot Eisenstein rows. We use the physical ideal norms and the original ordered cutoff. Let D, U, H be the column, cutoff and capacity parameters, with $U^2 \le D \le 7U^2/2$ and $A_1A_2^2 \ll H \le D$. The first two row ideals have dyadic norms A_1, A_2, $R = A_1A_2$, and the actual primitive conductor of row u has norm $Q_u \asymp R$. The finite bad-prime set S, row type, and twist are fixed. The same smooth complex profile W supported on $[1, 2]$ is used on both sides. Ideal labels, including conjugate primes of the same norm, are retained individually.

40.35.1 The selected pairing

For each good squarefree intermediate Möbius divisor d, put $E = Nd$. Let V_d be its original row amplitude and $\mathcal{E}_d$ the equal-norm part of the original middle Poisson window. We study selections of

$$\frac{2}{D}\operatorname{Re}\sum_d \mu(d)\langle \mathcal{E}_d, V_d - \mathcal{E}_d\rangle. \tag{40.286}$$

Here the counting inner product is linear in the first argument. This is one term in the expansion of the original signed norm. In particular the intermediate d is different from the gcd of the final column pair.

On an original allocation let $z = e_0z_0$ with $J \le Nz < 2J$, let $e_1 \mid \operatorname{rad}(Sd)$ be the other deletion label, and put $h = re_0$, with r the original squarefree short divisor. Set

$$X = \frac{D}{E(Nr)^2}, \qquad X' = \frac{X}{(Ne_0)^2}, \qquad M = \frac{R\,Ne_0\,Ne_1\,J}{X}.$$

The original middle window has $X' > B_*$ and $K_0 < Nk \le MD^\eta$, for its specified B_*, K_0, η. The primal test discards the guaranteed zero cells $X/((Ne_0)(Ne_1)J) \le 1/2$, and the original weights retain any further zeros. An allocation with $X' \le B_*$ belongs to the direct component. Its re-expressed Poisson sum stays in the complement in (40.286).

On the equality side write $z_{0,0} = g\ell$ and $k_0 = g\bar{\ell}$, so $Nz_{0,0} = Nk_0$. On the partner side the selected changes in the good exponents consist of erasing the squarefree cutoff part x, erasing a part of the good conjugate overlap, and inserting allowed positive increments at other good primes outside d. A conjugate erasure removes the full original exponent, which can be two. At an insertion prime the old residue plus the increment is at most five. Changes at the good primes of d keep their exact new residues. For fixed other labels write $z_{0,1} = z_*x$ and $k = Ik_*$. The physical insertion ideal I keeps each exponent $1, \dots, 5$ and is disjoint from the selected erasure supports and d. Thus $Nx \asymp B$ and $NI \asymp K$ are physical lengths. The two varying raw phases are $\psi_u(x)\overline{\psi_u(I)}$, or their conjugates if the pairing is conjugated. The fixed row factors retain the union of deleted primes, the literal section, the twist and the primitive S-values.

The subtraction on the partner imposes $Nz_*Nx = Nk_*NI$ only in its original middle window. At fixed x this fixes at most one integer norm for I, and the reverse count fixes at most one norm for x. An integer norm supports at most divisor-many ideals on the polynomial clip. With the physical inverse $1/Nx$, the paired count therefore costs $\min(1, K/B)$ up to subpowers. The two half radial powers leave

$$(B/K)^{1/2}\min(1, K/B) = \sqrt{\min(B/K, K/B)}.$$

The remaining harmonic weights give $O(R/E)$ for this subtraction at each d, with the inherited profile and subpower costs. Both original endpoints remain in the count. Equal norms in the direct and other components remain in the pairing.

40.35.2 Target bounds on the selected cross

The bounds have the common cost $O_{\epsilon,S,\nu,u_0}((DH)^{\epsilon}\mathcal{M}_{24}(W)^2)$, where $\mathcal{M}_{24}$ controls the indicated smooth profile derivatives. The live partner primal test supplies $E \ll D/B$ and partner radial scale $y_1' \gg Nk/R \gg K/R$. The proof first sums each actual column array. It then uses the row comparisons and the original label sums.

At the mixed scales $A_1 \asymp D^{5/12}$, $A_2 \asymp D^{1/6}$, the selected normalized cross has upper power $57/80$ over all physical ratios and all d. If $H \ll D^{3/4}$, a perturbed primitive sharp moment gives the target power $3/4$ for the same selected cross on

$$\frac{7}{24} \le \log_D A_1 \le \frac{439}{912}, \qquad A_1 A_2^2 \ll H.$$

The second pivot need only satisfy the stated original admissibility and capacity. The conductor comparison uses the actual R.

At the pure critical scales $A_1 \asymp R \asymp D^{3/4}$, $A_2 \asymp 1$, the target power $3/4$ holds over all d in each of the following physical sectors:

- $K \gtrsim D^{1089/1420}$, with any erasure length B.
- $B \gtrsim D^{1355/1482}$, with any insertion length K.
- $B \gtrsim R$ and $K \lesssim D^{921/1652}$.

The flexible central windows give further short and long threshold curves. There are also separate comparisons for a small fixed residual label product and for a small d-prefix. The comparable pure all-divisor comparison has power $55/68$, and the target holds on $Nd \le D^{9/68}$ in that sector. Each assertion concerns the selected changes described above. The remaining pure rectangles and the coherently averaged signed divisor sum are open.

40.35.3 Ordered assignment signs

Fix an ordered factorization $\zeta = \zeta_1\zeta_2$ of the actual squarefree cutoff label $\zeta = e_0 z_0$ on either side, with $(d,\zeta) = 1$ and $N\zeta_i \le U$. Write $T_i = U/N\zeta_i$. The assignment sum multiplying $\mu(\zeta)$ is

$$F_d = \sum_{\substack{a,b \mid d,\ (a,b)=1 \\ Na \le T_1,\ Nb \le T_2}} \mu(a)\mu(b).$$

Complete the b-sum and then subtract its excluded terms. With $m = d/b$ in the subtraction, squarefreeness gives the exact identity

$$\frac{F_d}{\mu(d)} = \mathbf{1}_{E \le T_1} + \mathbf{1}_{E \le T_2} - 1 - \sum_{\substack{m \mid d \\ T_1 < Nm < E/T_2}} \sum_{\substack{a \mid m \\ Na \le T_1}} \mu(m/a). \tag{40.287}$$

The complete b-sum forces $a = d$. The unit $m = 1$ gives the indicator at T_2, while the nonunit terms with $Nm \le T_1$ vanish by the full inner Möbius sum. Both inequalities of the remaining band are strict. Below the product cap the band is empty. The three possible assignment values are $\mu(d), 0, -\mu(d)$ according as both, just one, or neither individual capacity reaches E.

Fix the row, both ordered factorizations and the primal and dual labels. Select both e_1 labels to be fixed S-supported ideals, take the good changed-residue ideal on d to be the unit, and require d to avoid the full fixed prime union of the row and the primal and dual labels. When $EN\zeta \le U^2$ on both

sides, their capacity step functions multiply the original outer Möbius sign. The fixed-field deleted Möbius estimate supplies subpower cancellation for the resulting fixed-label scalar on $Nd \asymp Y$ with $Y \geq D^{\kappa}$ for a fixed $\kappa > 0$. In the pure comparable block, a physical Nx-interval of width $O(BD^{-1/8})$ gives the target after the full divisor sum by a separate sparse erased-column estimate. This includes the narrow interval immediately above the product cap on the actual partner allocation. The wide correction and the remaining coherent signed estimate require additional arguments. The whole signed and unsigned powers 13/12 and 9/8, the independent determinant comparison, and the scope-specific zero-location obligations remain as in the preceding sections.

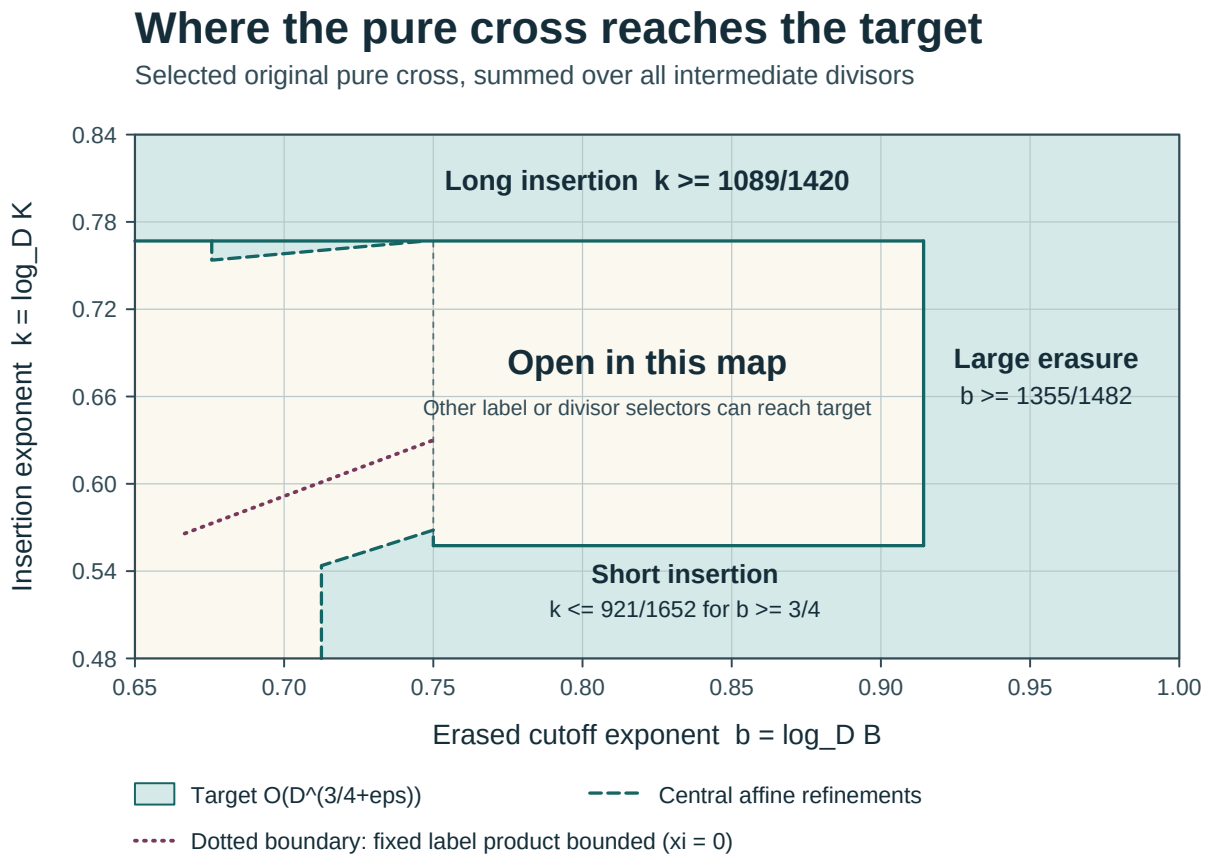


Figure 40.5: Physical norm exponents for the selected pure equality–complement cross. The filled regions reach power 3/4 over all intermediate divisors under the hypotheses of Section 40.35. Dashed boundaries show central refinements. The dotted curve uses a fixed residual label selection. Unfilled parts of the displayed range remain outside the proved regions shown here.

40.36 Sharp insertion and ordered cutoff estimates

Throughout this section, x denotes the erased squarefree cutoff factor, I the positive insertion ideal, and B, K their respective physical dyadic lengths. The exact partner norms are $Nz = Nz_{*}Nx$ and $N\mathfrak{k} = Nk_{*}NI$. Here $\mathfrak{k}$ is the original dual ideal, and k_{*} is its fixed residual factor in a given cell.

Write

$$E = Nd, \qquad A = A_1, \qquad R = A_1A_2, \qquad a = \log_D A, \quad r = \log_D R, \quad b = \log_D B, \quad k = \log_D K.$$

At the critical pure scales $a = r = 3/4$ at the level of powers, and at the critical mixed scales $a = 5/12,\ r = 7/12$. Fixed comparison constants in the scales are allowed throughout. A bound in this section includes the common factor $(DH)^{\epsilon}\mathcal{M}_{24}(W)^2$ for the paired cross, with the original fixed-data constants. In row moments the appropriate one-profile factor is understood separately.

The estimates concern the selected pairing with both original erasures, all positive off-d increases whose sum with the old residue is at most five, and the exact new residues on d. The old cutoff and conjugate erasures, including old exponent two in the conjugate erasure, remain in the phase. The cutoff is $Z = U^2$, with $U^2 \le D \le 7U^2/2$. The rows are the original unweighted literal nonprincipal rows. We keep the common W, fixed S, ν, u_0, literal ray, capacity and squarefree selectors, and the actual primitive $Q_u \asymp R$, Gauss root and raw zeros. The physical sieve is the order-six application in Section 40.28. Its exponent at column length D^t, relative to A, is

$$\Delta_a(t) = \max(0, t - a, t/3 - a/6, 5t/6 - 2a/3). \tag{40.288}$$

Its growth slope is at most one. A live subunit dyad is treated at constant scale.

40.36.1 The middle subtraction and scalar comparisons

First remove the negligible inherited tail $N\mathfrak{k} > D^5$. Its absolute estimate applies to each selection below. Fix the original allocation and dyad on the partner side. The compact logarithmic separation of the partner profile uses $\log(NI/K) - \log(Nx/B) - \log(Q_u/R)$. Its weighted Fourier absolute integral, with the extra factor $1 + |\xi|$ in log frequency ξ, is bounded by a constant times $\mathcal{M}_{24}(W)(1 + y_1')^{-4}$ at the actual dyadic profile scale y_1'. This follows by extending the profile on a fixed-width log interval and integrating by parts. The phase factors then separate on the erased array, insertion array and row. There is no condition on B/K in this separation. Sharp subinterval partial summation removes the insertion norm twist with the erased array and every other row multiplier fixed.

For the original middle equality, the equation $Nz_*Nx = Nk_*NI$ fixes at most one integer norm on either side given the other ideal. There are divisor-many ideals of each integer norm on the clipped support. This counts the entire insertion ideal, including its powerful part. The physical $1/Nx$ yields weighted mass $O((DH)^{\epsilon}\min(1, K/B))$. The two half radial powers supply $(B/K)^{1/2}$, giving the factor $\sqrt{\min(B/K, K/B)} \le 1$. The remaining label sums give $O(R/E)$. Apply this subtraction only in the original middle window with its exact two endpoints. Equal norms in the re-expressed direct, low and far pieces remain there.

The original live primal test gives

$$E \ll D/B, \qquad D/(EE_1(Nh_1)^2) > Nz/4, \qquad y_1' \gg N\mathfrak{k}/R \gg K/R. \tag{40.289}$$

For each side $i = 0, 1$ write $h_i = r_i e_{0,i}$ for the original grouped square-divisor label and $E_i = Ne_{1,i}$ for its deletion norm. The good part of $e_{1,i}$ is a divisor of d, and its other part is supported on S. Write $h_0 = fa_{\mathrm{id}},\ h_1 = fb_{\mathrm{id}}$ with $f = (h_0, h_1)$. The three ideals $f, a_{\mathrm{id}}, b_{\mathrm{id}}$ are pairwise coprime and squarefree. The ideal b_{id} is distinguished from the length exponent b. On the equality side $z_{0,0} = g\ell,\ \mathfrak{k}_0 = g\bar{\ell}$. For the good part $\bar{\ell}_{\mathrm{g}}$ of the conjugate define

$$j = (\bar{\ell}_{\mathrm{g}}, d), \quad c = (z_*, a_{\mathrm{id}}, \bar{\ell}_{\mathrm{g}}), \quad a_0 = a_{\mathrm{id}}/c, \quad \ell_0 = \ell/(\ell, z_* b_{\mathrm{id}}).$$

The good conjugate erasure support $\mathfrak{q}_\ell$ is a squarefree divisor of $\bar{\ell}_{\mathrm{g}}$ avoiding $a_{\mathrm{id}}, b_{\mathrm{id}}, d$. Its full erased factor is $\mathfrak{e}_\ell = \prod_{p\mid \mathfrak{q}_\ell} p^{1+\mathbf{1}_{p\mid z_*}}$. Let $\widetilde{q}_d$ be the actual sixth-free new representative at the good primes of d. With k_S the original S-part and v_6 the full sixth-power repetition, the exact partner residual is

$$\begin{aligned} k_* = k_S v_6^6 \frac{z_* a_{\mathrm{id}}^4 b_{\mathrm{id}}^2 \ell_0^6}{\ell\, c^6} \\ \times \frac{(\bar{\ell}_{\mathrm{g}}/j)\widetilde{q}_d}{\mathfrak{e}_\ell}. \end{aligned} \tag{40.290}$$

The quotient follows from the good exponent difference of the two primitive phases. Away from d, before changing any residue, that difference has representative exponent

$$v_p(z_{0,1}) + 4v_p(a_{\mathrm{id}}) + 2v_p(b_{\mathrm{id}}) - v_p(\ell) + v_p(\bar{\ell}_{\mathrm{g}}) \pmod 6.$$

At ℓ_0 one adds six to the negative exponent, and at c one subtracts the overflow six. The selected cutoff erasure removes x from this product. The selected conjugate erasure divides by $\mathfrak{e}_\ell$, and the d-part uses $\widetilde{q}_d$ in place of the matched residue. The positive increases multiply this exact residual by I. The norm and raw value of v_6^6 are retained, including any overlap with the other factors. On the original admissible pairs these operations give the literal product $\psi_u(x)\overline{\psi_u(I)}$ times the fixed row phases, with the original raw zeros.

Let D^ρ be the product of the two row norms relative to $R\sqrt{K/B}$, after the projectors and powerful sums. The full cutoff inverse norm is included in these norms. For the exact paired scalar, start with

$$\frac{D}{E^2E_0E_1\, Ng\, N\ell\, Nz_*(Nf)^4(Nc)^2(Na_0)^2(Nb_{\mathrm{id}})^2}.$$

Up to the fixed dyadic constants its profile scales are

$$\begin{aligned} y_0 &= \frac{D}{EE_0R(Nf\, Nc\, Na_0)^2}, \\ y_1' &\asymp \frac{D}{EE_1R}\frac{(Na_0)^4}{(Nf\, Nc)^2}(N\ell_0 Nv_6)^6\frac{N\widetilde{q}_d}{Nj}\frac{Nk_SK}{B\, N\mathfrak{e}_\ell}. \end{aligned}$$

The actual profile uses Q_u, the physical ideal norms and the original fixed S-factors. Multiplying by $y_0^{-\alpha}(y_1')^{-\theta}$ gives the following weights before the relative row moment:

$$\begin{aligned} &D^{1-\alpha-\theta}R^{\alpha+\theta}E^{\alpha+\theta-2}E_0^{\alpha-1}E_1^{\theta-1}(B/K)^\theta \\ &\quad\times \frac{(Nf)^{2\alpha+2\theta-4}(Nc)^{2\alpha+2\theta-2}(Na_0)^{2\alpha-4\theta-2}}{Ng\, N\ell\, Nz_*(Nb_{\mathrm{id}})^2(N\ell_0Nv_6)^{6\theta}(Nk_S)^\theta}(N\mathfrak{e}_\ell)^\theta(Nj/N\widetilde{q}_d)^\theta. \end{aligned} \tag{40.291}$$

The scalar is accompanied by the retained decay $(1+K/R)^{-(4-\theta)}$ from (40.289). Every absolute comparison follows the exact pairing with those labels.

In the harmonic ℓ-count the fixed $\bar{j} \mid \ell$ pays Nj to power one. A conjugate erasure prime p uses a distinct $\bar{p} \mid \ell$. Its conjugate lies in exactly one of $\ell_0, z_*, b_{\mathrm{id}}$, paying a second inverse norm. In the old exponent-two case, the original $p \mid z_*$ pays a third inverse norm. Thus the resulting local exponents are at most $-2+\theta$ and $-3+2\theta$, respectively. When Nc or its half power is needed, charge $c \mid z_*$. This charge is disjoint from both conjugate charges since $\mathfrak{q}_\ell \perp a_{\mathrm{id}}$, its conjugates lie in ℓ, and $c \mid a_{\mathrm{id}}, \bar{\ell}_{\mathrm{g}}$. The other sums below are harmonic on polynomial support, convergent inverse-power sums, or fixed-divisor choices.

For $1/6 \le \theta \le 1$, take $\alpha = 1-\theta$. The harmonic comparison at each d is

$$\frac{R}{E}D^\rho(B/K)^{\theta-1/2}(1+K/R)^{-(4-\theta)}. \tag{40.292}$$

The two three-half choices give the comparisons

$$\begin{aligned}&\frac{R^{3/2}D^{\rho}}{\sqrt{D}\sqrt{E}}, && (\alpha,\theta)=(1,1/2),\\ &\frac{R^{3/2}D^{\rho}(K/B)^{1/6}}{\sqrt{D}E^{1/3}}, && (\alpha,\theta)=(7/6,1/3),\end{aligned}$$

with the corresponding retained decays. In the second choice $E_0^{1/6}\ll_S E^{1/6}$. With $(\alpha,\theta)=(1,1/4)$, the E_0 cancels, the weights in f,a_0,ℓ_0v_6 have exponents $-3/2,-1,-3/2$, and the disjoint charge on c pays its half power. The resulting comparison is

$$\frac{R^{5/4}D^{\rho}}{D^{1/4}E^{3/4}}(K/B)^{1/4}(1+K/R)^{-15/4}. \tag{40.293}$$

By the first inequality in (40.289), summing the $E^{-3/4}$ costs $O((D/B)^{1/4})$ on its live range. The two three-half choices on $E\le D^{e}$ cost $D^{e/2}$ and $D^{2e/3}$, respectively.

The higher choice $(\alpha,\theta)=(5/2,1)$ leaves $(Nf)^3(Nc)^5$ in (40.291). The exact primal restriction gives

$$(Nf)^2(Nb_{\mathrm{id}})^2Nz_*Nx\ll D/(EE_1),\qquad (Nf\,Nc)^4\ll (D/(EE_1B))^4.$$

Write the remaining numerator as $(Nf)^{-1}Nc\,(Nf\,Nc)^4$ and pay the first two factors by the preceding harmonic counts. The additional E^{-4} and $E_0\ll_S E$ give the harmonic comparison

$$\frac{R^{7/2}D^{3/2+\rho}}{B^4E}(B/K)^{1/2}(1+K/R)^{-3}. \tag{40.294}$$

There is also a fixed-label selection for $(\alpha,\theta)=(1,0)$. For $p\mid a_0$, the original eligibility excludes $b_{\mathrm{id}},\ell,d,x,\mathfrak{q}_\ell$, and at most one of $z_*,\bar{\ell}_{\mathrm{g}}$ contains p. The exact residual has valuation four or five at this prime before adding the full sixth repetition. Thus $a_0^4v_6^6\mid k_*$. On $(Na_0)^4(Nv_6)^6\ll D^{\xi}$, the joint count of a_0,v_6 is $O(D^{\xi/4})$, by summing $(Nv_6)^{-3/2}$. Formula (40.291) then gives $RD^{\rho+\xi/4}(K/B)^{1/2}/E$. This selection is sufficient when $Nk_*\ll D^{\xi}$. The comparison uses the full residual ideal, with its S-part and repetitions.

40.36.2 The sharp moment and the grouped sparse tail

Write $I=I_1P$ uniquely, where I_1 is squarefree and the nonzero valuations of P are $2,3,4,5$. We have $I_1\perp P$. Fix P at first. The common-prime projector for x,I_1 uses $s_1\mid(x,I_1)$, with $\mu(s_1)$ and the two raw values on s_1. Require s_1 itself to satisfy the original fixed prime eligibility of I_1, including $s_1\perp P$, before stripping it. The residual I_1' avoids s_1 by its squarefreeness, along with the original forbidden union. Keep the original fixed P-deletion on the erased array. After stripping s_1, the squared erased mass is $O((DH)^{\epsilon}/(BNs_1))$, including its actual $1/Nx$. The insertion length is $K/(NP\,Ns_1)$. A dyad $NP\asymp M$ has $O(\sqrt{M})$ powerful ideals, by the unique representation $P=a_{\mathrm{p}}^2b_{\mathrm{p}}^3$ with b_{p} squarefree and the convergent $\sum_{b_{\mathrm{p}}}(Nb_{\mathrm{p}})^{-3/2}$. Overlap is allowed at exponent five. This pays the $M^{-1/2}$ shortening in the product of the two moments.

For the sharp insertion bound at length L, expand the fixed deletion and squarefree selectors in the order $I_1'=e(r')^2m$, where $e=e_fe_P$ divides the full forbidden union and r' avoids that union. All Möbius signs and fixed raw factors are retained. At fixed P,e,r' the remaining sharp interval is an unweighted m-interval after the exact partial summation. Its endpoints can be treated as sharp disk endpoints. Smooth a disk of norm length L at radial width proportional to $\delta\sqrt{L}$. The normalized shell row norm is bounded by a subpower times

$$D^{\Delta_a(l)/2}\big(\sqrt{\delta L}+L^{1/6}\big),\qquad l=\log_D L.$$

To see the additive term, split each ideal uniquely as $\mathfrak{s}\, b_0 v^6$ with $\mathfrak{s}$ supported on S and b_0 good sixth-free. At fixed $\mathfrak{s}, v$, the shell contains divisor-many ideals per integer norm and has norm width $O(\delta L/(N\mathfrak{s}(Nv)^6))$. Apply the physical sieve to b_0. The square roots of the width weights sum absolutely. The constant atoms sum over $N\mathfrak{s}(Nv)^6 \ll L$, giving $L^{1/6}$ up to subpowers. This also accounts for open or closed endpoints.

The smoothed primitive Poisson transform has the original $Q_u^{-1/2}$ and primitive Gauss root. On a dual dyad T put $Y = \sqrt{LT/R}$. The disk transform is L times the Fourier transform of the unit disk's chord length $2\sqrt{1-v^2}$ at frequency comparable to Y. Integrating once by parts, separating the two endpoint intervals of width $1/Y$, and integrating by parts again on the interior gives $O(L(1+Y)^{-3/2})$. The endpoint derivative integral is $O(Y^{-1/2})$; the interior boundary and second derivative terms are $O(Y^{1/2})$ before the second division by Y. The same argument with the chord length multiplied by v bounds the frequency derivative, so its logarithmic derivative costs one power of $1+Y$. The convolution bump and its log derivative provide $(1+\delta Y)^{-M_0}$ for arbitrarily large fixed M_0. Consequently the cutoff log function m and m' have L^2 bounds $O(L(1+Y)^{-3/2}(1+\delta Y)^{-M_0})$ and $O(L(1+Y)^{-1/2}(1+\delta Y)^{-M_0})$, respectively. Splitting the Fourier integral at $1 + \|m'\|_2/\|m\|_2$ and applying Cauchy and Plancherel gives absolute log Fourier mass $O(L(1+Y)^{-1}(1+\delta Y)^{-M_0})$. Multiplying by $\sqrt{T}/\sqrt{Q_u}$ yields

$$O_{M_0}\left(\sqrt{L}(1+\delta\sqrt{LT/R})^{-M_0}\right).$$

The zero frequency is absent by nonprincipality. With $\delta \asymp D^{\lambda-\Delta_a(l)}$ when $\Delta_a(l) > \lambda$, the effective dual exponent is

$$t = \max(0, r - l + 2(\Delta_a(l) - \lambda)). \tag{40.295}$$

The main shell term has row RMS $O(\sqrt{L}D^{\lambda/2})$. The additive term has the same bound whenever $\Delta_a(l) \le 2l/3$. The smoothed term has that bound if $\Delta_a(t) \le \lambda$. Above the cutoff the arbitrary smoothing decay pays the degree-one growth of the sieve and the divisor subpowers. The ordinary estimate applies directly if $\Delta_a(l) \le \lambda$.

In pure use $\lambda = 0$ for $l \le 4/5$. For $l \ge 3/8$ the convex function in (40.295) before truncation is at most $3/8$ by the endpoints. In mixed use $\lambda = 1/20$ for $l \le 5/8$. The smoothing branch requires $l > 43/120$, and the same convex comparison gives $t \le 43/120$. The additive term meets the stated criterion in both cases. The exact deletion e-sum has divisor cost at fixed P, the r'-sum is harmonic, and the P-count pays the shortening above. The resulting sharp rectangle loss is $(\Delta_a(b) + \lambda)/2$. It uses the physical ratio $\sqrt{K/B}$ even when B and K are unequal. The ordinary two-moment alternative has loss $(\Delta_a(b) + \Delta_a(k))/2$.

The coupled comparison keeps a sharper tail for $Nr' \ge D^q$ at $NP \asymp M$. Freeze e_f, expand the remaining $(x, P) = 1$ by $s_2 \mid (x, P)$, with $s_2 \perp s_1$, and fix the powered portion P_s on s_2. Set $P = P_s P'$ and group the insertion coefficients by the actual $P' e_P(r')^2 m$, of length $K' = K/(Ns_1\, Ne_f\, NP_s)$. The coefficients are divisor bounded and signed. They include the original full P-dyad, threshold, old residue test and clipped physical interval. For the sixth-free reduction of this grouped ideal, write it as $\mathfrak{s}\, b_0 v^6$, and split $P' = P_0 P_1,\ r' = r_0 r_1$ by the support of v. The original $r' \perp P$ gives $P_1 r_1^2 \mid b_0$. The two inverse-norm sums in the support count are bounded by

$$\min(1, (NP_s NP_0/M)^{1/2}), \qquad \min(1, Nr_0 D^{-q}).$$

The first is the powerful reciprocal dyad count and the second the inverse-square ideal tail. The resulting squared mass at fixed $\mathfrak{s}, v, P_0, r_0$ is at most their product times $K'/(N\mathfrak{s}(Nv)^6)$, up to subpowers. After square roots the v-sum converges, since $(NP_0)^{1/4}(Nr_0)^{1/2}(Nv)^{-3} \le (Nv)^{-5/4}$.

The S-part sum also converges. Finally $NP_s \geq (Ns_2)^2$ makes the product of the insertion shortening and the erased s_2-shortening harmonic. Thus the relative norm saving in this branch is $M^{-1/4}D^{-q/2}$. It holds at the actual physical lengths for both ratio orientations.

40.36.3 Coupling the dual to the shorter ordered factor

Open x into its actual two ordered cutoff factors. Fix the assignments of the cutoff base and of s_1, and retain the individual cutoff bounds. Before expanding their remaining coprimality, both factors are individually squarefree and keep all their fixed deletions. Use the common squarefree w projector, with pre-stripping eligibility in both arrays and with both residual factors avoiding w after shortening. The fixed phase is $\mu(w)\psi_u(w)^2$. Sharp norm product tests separate with polylogarithmic Fourier mass on the clipped polynomial ranges, keeping their endpoints. The auxiliary primitive insertion dual has the same raw orientation as x. Multiply it by the shorter cutoff factor as an actual ideal before forming row norms. The grouped coefficients have divisor bound and no added coprimality with the auxiliary frequency. With shortened lengths X_s, X_l the physical product is $X_sX_l \asymp B/(Ns_1(Nw)^2)$. The actual cutoff inverse norm and the smoothed transform mass $\sqrt{L}$ therefore give the factor

$$\frac{\sqrt{K/B}}{Ns_1Nw\,Nr'\sqrt{Ne}\sqrt{M}}.$$

The P-count pays the $M^{-1/2}$, and the s_1, w, r' sums remain harmonic.

For reference, set $n = \log_D Ns_1,\ j = \log_D Ne,\ p = \log_D Nr',\ v = \log_D M$, and write $\ell = k - v - n - j - 2p$ for the ordinary insertion log length. In each coupled application choose the relative target loss ρ, then use the sharp branch for large n and the extra deletion shortening $D^{-j/2}$ for large j. Put

$$\sigma = \Delta_a(b) + \Delta_a(k) - 2\rho, \qquad q = \max(0, \sigma - v/2).$$

The grouped branch $p \geq q$ pays the ordinary excess down to ρ. In the remaining branch take $\delta \asymp D^{-\beta}$. With $\beta = \max(0, \Delta_a(b-n) + \Delta_a(\ell) - j - 2\rho)$ the main shell meets the chosen loss directly. The additive term has exponent $(\Delta_a(b-n) + \Delta_a(\ell))/2 - \ell/3 - j/2$. The smoothed dual exponent is

$$t = \max(0, r - k + v + n + j + 2p + 2\beta).$$

Its two sieve losses are evaluated at $u_s + t, u_l$, where $u_i = \log_D X_i$, $u_s \leq u_l \leq 1/2$, and $u_s + u_l \leq b - n$. The degree bound pays all larger dual dyads using the same smoothing decay. The following computations specify the small-p shell and cutoff choices in the regions of interest.

40.36.4 Pure central and comparable regions

Set $a = r = 3/4$. On $2/3 \leq b \leq a,\ 1/2 \leq k \leq 31/40$ the coupled loss is the smaller of $\Delta_a(b)/2$ and

$$\rho_c = \begin{cases} (25b - 2k)/204 - 7/272, & k \leq a, \\ (25b + 22k)/204 - 31/272, & k \geq a. \end{cases}$$

To verify the second choice when it is smaller, put $j_0 = \Delta_a(b) - 2\rho_c,\ n_0 = 3j_0$. Use the sharp branches at $n \geq n_0$ or $j \geq j_0$, as described above. In the remaining small-p range choose

$$\beta = \sigma - v/3 - 2n/3 - 4j/3 - 2p/3, \qquad 6\rho_c = (a+b)/2 - k + 8\sigma/3.$$

Since $v + 2p \le 2\sigma$, the lower bounds for ℓ, β on the two k-pieces are, respectively,

	ℓ	β
$k \le a$	$47/68 - 9b/17 + 11k/51$	$73/408 - 9b/34 + 8k/153$
$k \ge a$	$13/34 - 9b/17 + 32k/51$	$-97/204 - 9b/34 + 283k/306.$

Their minima are $41/102, 1/153$ and $31/68, 1/51$. Thus $\ell > 3/8$ and $\beta > 0$. The lower slope $1/3$ gives $\Delta_a(\ell) \le \Delta_a(k) - (k - \ell)/3$; the main shell costs at most ρ_c. For $k \le a$ the additive excess is at most $-\ell/6 - n/6 - j/2$. For $k \ge a$ it is at most $13/96 - 31/204 < 0$.

The dual satisfies $t \le a - k + 8\sigma/3$. In the two k-pieces, $b/2 - k + 8\sigma/3$ is $(25b - 2k - 18)/34$ and $(25b + 22k - 36)/34$, respectively, both negative on the stated rectangle. Thus $u_s + t < a$. The geometric mean excess is bounded by

$$\tfrac{1}{6} \max(1/8, (a + b)/2 - k + 8\sigma/3) = \rho_c.$$

Indeed both sieve arguments use the lower slope, with $u_s \le b/2 - n/2,\ u_s + u_l \le b - n$ and $u_l \le 1/2$.

Write ρ for the smaller loss. Substituting it into the harmonic comparison at $\theta = 1/6$ gives the short target for $57/80 \le b \le a,\ k \le (172b + 21)/264$. The ordinary sharp loss already covers $k \le b/2 + 3/16$. At $\theta = 1$ and $k \ge a$, the retained decay gives the long target for $273/404 \le b \le a,\ k \ge (508b + 1743)/2768$. The sharp comparison covers $k \ge 5/8 + 4b/21$ through $4/5$, and the ordinary long insertion comparison decreases above $4/5$. The fixed product selection of Section 40.36.1 instead gives $k \le (308b + 21 - 204\xi)/400$ on the lower k-piece. The two divisor-prefix choices with partner exponents $1/2, 1/4$, retaining the actual partner decay, give target through

$$e \le \max\left\{\tfrac{1}{4} - 2\rho + 7(k - a)_+,\ \tfrac{1}{4} - 4\rho + b - k + 15(k - a)_+\right\}, \qquad Nd \le D^e.$$

For $B \asymp K$ and $b \le a$, the central formula gives $\rho \le 1/17$, with the sharp branch sufficient below its central rectangle. For comparable $b \ge a$, the shifted comparison below has loss at most $1/17 + (1/51 + 5/12)(b - a)$ until the long target applies. The partner decay in the half split pays this additional loss. The two half powers and the one-plus-half powers then give $D^{55/68+\epsilon}$ over all d and the target on $Nd \le D^{9/68}$, respectively. The latter follows from $5/8 + 1/17 + 9/136 = 3/4$.

40.36.5 Pure long insertion for every erasure length

Take $k = a + y,\ 0 \le y \le 1/56$. Work first at the reference erased exponent a, and put

$$\rho_0 = 1/17 + y/51, \quad n_0 = 6(1/16 - \rho_0), \quad j_0 = n_0/3, \quad \sigma = 9/68 + 27y/34.$$

The sharp and sparse branches use these reference thresholds, with the actual insertion length. Their erased ordinary excess increases by at most $5(b - a)_+/6$, before its square root. In the remaining branch use $\beta = \Delta_a(a - n) + \Delta_a(\ell) - j - 2\rho_0$. Here $\ell \ge 31/68 - 22y/51 > 3/8$ and $\beta \ge 1/51 - 16y/153 > 0$. The main shell has reference loss ρ_0; the additive term has excess at most $1/8 + 5y/12 - (31/68 - 22y/51)/3 < 0$.

If $\ell \le a$, then $\beta = \sigma - y/2 - v/3 - 2n/3 - 4j/3 - 2p/3$. If $\ell \ge a$, then $\beta = \sigma - 5v/6 - 7n/6 - 11j/6 - 5p/3$. The first gives $t \le 8\sigma/3 - 2y$, and the second $t \le 2\sigma - y \le 8\sigma/3 - 2y = 6\rho_0$. At $b > a$, reduce u_s to at most $(a - n)/2$ and then u_l only enough to make the sum at most $a - n$. The reference pair remains ordered and nonnegative. The total reduction is at most $b - a$, either by the shorter-factor cap alone or by the original bound on the sum. The reference grouped length is below a, since $3/8 + 6\rho_0 < a$. Restoring the removed lengths adds at most $5(b - a)/12$ in the

geometric mean, by the 5/6 Lipschitz bound through actual exponent one. Thus the relative loss is $\rho_0 + 5(b-a)_+/12$.

For $b \le a$ use (40.292) at $\theta = 1$; for $b \ge a$ use (40.293) with the live divisor cap. The respective exponents after summation are at most

$$a + \rho_0 + (b-a)/2 - 7y/2, \qquad a + \rho_0 - (b-a)/12 - 7y/2.$$

Both meet target at $y \ge 6/355$. For $k \ge a + 1/56$ the sharp loss $\Delta_a(b)/2$ already suffices through 4/5, by the same two radial comparisons. Above 4/5 the ordinary insertion adds $\Delta_a(k)/2$; at the endpoint $1/16 + 1/12 - 7/40 < 0$, and the bound decreases thereafter. This gives $K \gtrsim D^{1089/1420}$ over all B and d.

40.36.6 Pure long erasure and the intermediate gap

For $a \le b \le 1,\ k \le 4/5$, the sharp loss is $\rho_{\mathrm{sh}} = 5b/12 - 1/4$. The three-half choice with partner exponent 1/3, summed over $E \ll D/B$, has exponent $a + 5(1-b)/12 - (a-k)_+/6 - 7(k-a)_+/2$. The high radial comparison (40.294) has exponent $31/8 - 37b/12 - k/2 - 3(k-a)_+$. For $k \le a$ the two reach target when

$$k \le L_b = -7/4 + 5b/2 \quad \text{or} \quad k \ge H_b = 25/4 - 37b/6.$$

They overlap for $b \ge 12/13$. For $k \ge 4/5$ the ordinary insertion in the high comparison adds $\Delta_a(k)/2$. Its endpoint exponent $409/120 - 37b/12$ is below target for $b \ge 9/10$, and decreases with k. For the small residual product selection, the low endpoint is instead $1/2 + b/6 - \xi/2$; it overlaps the high endpoint at $b \ge 69/76 + 3\xi/38$.

For $1355/1482 \le b \le 12/13$, work in the gap $L_b \le k \le H_b$. Define

$$g = \min((k - L_b)/6, (H_b - k)/2), \qquad \rho = \rho_{\mathrm{sh}} - g, \qquad C_b = 17/4 - 4b.$$

The two losses agree at C_b, where $\rho_C = 3b/2 - 5/4$ is the minimum of ρ. It suffices to achieve the chosen ρ, by using the smaller radial comparison. Use $j_0 = \Delta_a(b) - 2\rho,\ n_0 = 6j_0/5,\ \sigma = j_0 + \Delta_a(k)$, and the exact nonnegative width exponent from Section 40.36.3. The two sharp branches and the grouped tail apply with these choices. The minimum of $k - 2\sigma - n_0 - j_0$ occurs at C_b and equals $(233b - 202)/30 > 1/3$; this bounds ℓ from below. The shell additive excess is at most $1/5 - 1/9 < \rho_C$.

When $\ell \ge 3/8$ and $\beta > 0$, the slopes on $b - n$ and on $[\ell, k]$ bound t by $t_1 = a - k + 8\sigma/3$. When $\beta = 0$, the bound is $t_2 = a - k + 2\sigma + n_0 + j_0$. For $\ell < 3/8,\ \beta > 0$ use $\beta = j_0 - 5n/6 - j$, which again gives $t \le t_2$. Both upper expressions peak at C_b, as is seen from the slopes $1/3, -1$ of j_0. At C_b their difference is $(438b - 397)/180 \ge 0$, so $t \le t_* = (95 - 96b)/18$.

For $u_s + u_l \le b$, convexity and monotonicity of the sieve losses reduce the geometric mean maximum to $(u_s, u_l) = (b - 1/2, 1/2)$ and $(b/2, b/2)$. Indeed the maximizing u_l at fixed u_s is $\min(1/2, b - u_s)$. Before the breakpoint use monotonicity and after it use convexity. At the two endpoints the shifted length is between a and one. The second endpoint is larger by $(1-b)/8$, with value

$$7b/24 + 5t_*/12 - 5/16 = 815/432 - 139b/72 \le \rho_C.$$

The last inequality is exactly $b \ge 1355/1482$. This closes the gap for every K after the two radial comparisons and the independent middle subtraction.

40.36.7 Pure short insertion over large erasures

For $b \ge a$ and $k < a$, the harmonic choice $\theta = 1/6$ and the quarter choice with the primal divisor cap meet target if the rectangle loss is at most

$$\rho = \max\{(b-k)/3,\ b/2 - k/4 - 3/16\}.$$

With the sharp loss this covers $b \le 3 - 4k$ or $b \ge 3k - 3/4$, which is exhaustive for $k \le 15/28$. For $15/28 \le k \le 921/1652$, work inside the remaining triangle and split it at $b = 9/8 - k/2$. Use the same j_0, n_0, σ and exact width as in the intermediate gap. Here

$$j_0 \le 3/236, \quad b - n_0 \ge 3117/4130 > a, \quad \ell \ge 3159/8260 > 3/8, \quad \rho \ge 1/16.$$

These bounds follow by the affine formulas on the two triangles. The main shell meets ρ, and its additive term is at most $(7/26 + 1/16)/2 - 1/8 < 1/16$. The same t_1, t_2 estimates apply, with $t_1 - t_2 \ge 67/4130$. Thus it is enough to evaluate $(\Delta_a(u_s + t_1) + \Delta_a(u_l))/2 - \rho$ at the two cutoff endpoints of the previous proof. On each triangle these expressions are convex. Their vertex values in the two endpoint orders are

k	b	$(b - 1/2, 1/2)$	$(b/2, b/2)$
15/28	6/7	−5/168	−1/48
921/1652	318/413	−83/9912	−83/9912
921/1652	699/826	−51/3304	0
921/1652	381/413	−787/19824	−85/2832.

The sharp branches, sparse tail and smoothed dual therefore meet ρ throughout. This proves the target for $K \lesssim D^{921/1652}$ and $B \gtrsim R$ over all d.

40.36.8 Mixed ratios and the critical-capacity strip

At $a_* = 5/12,\ r_* = 7/12$ use the mixed sharp insertion loss $\lambda/2 = 1/40$ through $k_0 = 5/8$. Denote Δ_{a_*} by Δ. For $k \ge b,\ k \le k_0$, the harmonic $\theta = 1$ comparison is at most $r_* + \Delta(k)/2 + 1/40 - 3(k - r_*)_+$, maximal at $k = r_*$. For $k \le b \le r_*$ use $\theta = 1/6$ and the sharp moment, with the same bound 57/80. For $k \le b,\ b \ge r_*$ and $k \le k_0$ the quarter comparison and live divisor cap give exponent

$$23/48 + \Delta(b)/2 + 1/40 + (k-b)/4 + (1-b)/4 - 15(k - r_*)_+/4.$$

At fixed b this is maximal at $k = r_*$. It equals 57/80 at $b = r_*$, decreases with slope $-1/12$ through 5/6, and is constant thereafter. For $k > k_0,\ k \ge b$ the ordinary $\theta = 1$ exponent is at most $r_* + \Delta(k) - 3(k - r_*)$, maximal at k_0 with value 101/144. For $k > k_0,\ k \le b$ use $\theta = 1/6$. The exponent decreases in k; at $k = k_0$ it is convex in b on $[k_0, 1]$, with endpoint values $2/3, 205/288$. Both are below 57/80. Adding the separate harmonic equality count gives 57/80 over all physical ratios and divisors.

Under $A_1 A_2^2 \ll H \ll D^{3/4}$, the capacity bounds $r \le (3/4 + a)/2$ at the level of exponents. The actual Q_u is still used in each moment. On the left, put $a = a_* - z,\ 0 \le z \le 1/8$. Use $\lambda = 1/20 + 3z/5$ through $k_0 = 5/8$. At $l = 43/120$ the three nonconstant monomials of $\Delta_a(l)$ are $-7/120 + z,\ 1/20 + z/6,\ 1/48 + 2z/3$, each at most λ. The smoothing branch is therefore longer than this l. The reference convex dual expression has endpoint maximum 31/90, and the capacity and $\Delta_a(l) \le \Delta_{a_*}(l) + z$ give $t \le 31/90 + 3z/10$. The three nonconstant monomials at that upper bound are

$$-13/180 + 13z/10, \quad 49/1080 + 4z/15, \quad 1/108 + 11z/12,$$

each at most λ by the endpoints in z. The additive term is controlled since $3a \ge 7/8$. The erased and sharp insertion half-losses together increase by at most $4z/5$. In the harmonic branches the capacity prefactor saves $z/2$, while in the quarter branch it saves $5z/8$. In both ordinary branches $k > 5/8 > r_*$, so the active partner decay and capacity prefactor pay the increase of the two sieve factors. This gives $57/80 + 3z/10 \le 3/4$.

On the right take $a = a_* + x$, $0 \le x \le 59/912$, and use $\lambda = 1/20 + x/4$ through $k_0 = 31/48$. On the smoothing branch $l > 43/120$. In (40.295) the possible r-increase of $x/2$ is paid by $2(\lambda - 1/20)$. The reference convex function on $[43/120, 31/48]$ has endpoint values $9/40, 43/120$. Thus $\Delta_a(t) \le 1/20$; the additive term is controlled by $k_0 < 3a$. In the ratio comparisons take the capacity upper bound $r_b = r_* + x/2$. The scalar estimates increase with r, while the sharp proof has already retained the actual conductor. In the sharp ranges the maximum is $r_b + (\Delta_a(r_b) + \lambda)/2 = 57/80 + x/2$. For the quarter range, after setting $k = r_b$, the b-dependent term $(\Delta_a(b) - b)/2$ is nonincreasing, giving the same maximum. In the ordinary ranges the $\theta = 1$ endpoint is $21/32 + 4x/3$. The $\theta = 1/6$ bound at $k = k_0$ has b-endpoint values $29/48 + 7x/4$ and $373/576 + 19x/12$; convexity bounds its interior. All are at most $3/4$, with the last endpoint attaining that value at $x = 59/912$. The union is the first-pivot strip $7/24 \le a \le 439/912$, subject to the original capacity and with no independent closeness requirement on A_2.

All comparisons here preserve the original $\mu(d)$ in the identity and use an absolute divisor bound at the end. The remaining pure rectangles, the coherent divisor sum, other signed components and the determinant and zero-location comparisons remain open.

40.37 Wide cutoff corrections and full-frequency compensation

Keep the pairing (40.286), the exact ordered cutoff identity (40.287), and all the original allocation, primitive-conductor and raw-zero conditions. At one live allocation put $h = re_0$, $E_1 = Ne_1$, and write the actual cutoff ideal as $\zeta = e_0 z_0 = \zeta_1 \zeta_2$. Thus $T_i = U/N\zeta_i \ge 1$, $E = Nd$, and

$$\Omega = \frac{E}{T_1 T_2} = \frac{EN\zeta}{U^2} < \frac{14}{E_1 N h}.$$

Let $\mathcal{P}$ consist of the good prime ideals of norms seven or thirteen, with the original S-deletion. These are at most four separate ideal labels. Put $s(E) = \mathbf{1}_{E \le T_1} + \mathbf{1}_{E \le T_2} - 1$. The exact wide correction is

$$\begin{aligned} F_d(T_1, T_2) &= \mu(d)\big(s(E) + C_d(T_1, T_2)\big), \\ C_d(T_1, T_2) &= \sum_{\substack{mn = d \\ Nm > T_1,\ Nn > T_2}} \left(1 - \sum_{\substack{p \in \mathcal{P} \\ p \mid m}} \mathbf{1}_{Nm > T_1 Np} \right). \end{aligned} \tag{40.296}$$

The two factors are coprime because d is squarefree. The strict tests retain the original cutoff endpoints. For $E_1 N h \ge 2$ only the unweighted factorization count remains. For $E_1 N h \ge 14$ the correction vanishes.

At fixed row and fixed primal and dual labels, prescribe the exact intersection δ of d with the full forbidden prime union, including $\mathcal{P}$. In a divisor dyad $Y \le Nd < 2Y$ put $Y' = Y/N\delta$. For fixed $\kappa > 0$ and $Y' \ge D^\kappa$, the fixed-label scalar after taking out its fixed coefficient and row phase has bound

$$\ll_\kappa \mathcal{M}_{24}(W)^2 \frac{4^{\omega(\delta)} \log^C(2D)}{Y N \delta} \exp\!\big(-c_\kappa \sqrt{\log(2Y')}\big). \tag{40.297}$$

The estimate includes both wide corrections, with the original full prime deletions. It gives subpower cancellation before a coherent average over the rows and other labels.

For each $p \in \mathcal{P}$, replacing the partner coefficient by its signed p-subtraction in (40.296) gives a zero primal amplitude $V_d^{[p]}$. The exact full-frequency complement is $V_d^{[p]} - \mathcal{E}_d^{[p]} = -\mathcal{E}_d^{[p]}$, where $\mathcal{E}_d^{[p]}$ is its middle equality projection. The original elementary equality norm gives a contribution of order at most $R(DH)^{\epsilon}\mathcal{M}_{24}(W)^2$ after the full divisor sum. This comparison requires all partner modes, including the re-expressed direct component.

In the pure comparable sector $A_1 \asymp R \asymp D^{3/4}$, $A_2 \asymp 1$, $B, K \asymp R$, the equality-side wide correction reaches $D^{3/4+\epsilon}$ on $Nd \le D^{13/56}$ with the inherited profile cost. Its partner can carry the original coefficient, the step part, or the correction part. Thus this prefix includes their double correction. The remaining coherent wide sum and the other signed components remain open.

40.38 Derivations for the wide cutoff correction

40.38.1 The strict band and its prime terms

Use the original r, e_0, e_1, J, z_0 on each side. The primal-zero removal at the dyad $J \le N\zeta < 2J$ implies $D/(EE_1(Nh)^2) > Nz_0/4$. Hence

$$\frac{EN\zeta}{U^2} < \frac{4D}{U^2}\frac{Ne_0}{E_1(Nh)^2} \le \frac{14}{E_1 Nh},$$

using $e_0 \mid h$ and $2D \le 7U^2$. For a band label $T_1 < Nm < E/T_2$ in (40.287), $m \ne 1$, so the full inner Möbius sum vanishes. In its omitted part use $c = m/a$. The inner sum in (40.287) becomes

$$-\sum_{\substack{c \mid m \\ Nc < Nm/T_1}} \mu(c).$$

Here $1 < Nm/T_1 < \Omega < 14$. In the Eisenstein field the primes above two and three lie in S. The remaining inert primes have norm at least 25, and the only possible good prime norms below 14 are $7, 13$. Two good prime factors already have norm at least 49. Consequently this sum includes the unit and precisely the primes specified in (40.296). Substituting $n = d/m$ turns $Nm < E/T_2$ into $Nn > T_2$. The upper bound on Ω also proves the two stated conditions for vanishing of the prime term and the band.

If a p-subtraction is present, $Nm > T_1 Np$ and $Nn > T_2$ give $EN\zeta > NpU^2 \ge 2D$. The original primal profile for that individual cutoff is

$$W\left(\frac{EE_1(Nh)^2 Nz_0\, Nb}{D}\right), \qquad Nb \ge 1.$$

Its argument exceeds two, since $E_1(Nh)^2 \ge Ne_0$. The individual cutoff has zero primal contribution even if its dyad survived the original primal-zero removal. Its Poisson components are still present in the exact paired selection.

40.38.2 The fixed-intersection scalar estimate

Fix the actual row, primal and dual labels, ordered factorizations, original dyads, and both deletion allocations. Let $\mathcal{L}$ be the union of the primes of S, of the row, of all these labels, and of $\mathcal{P}$. Its radical has polynomial norm after the inherited $N\mathfrak{k} \le D^5$ clip and the original support bounds.

Choose the exact intersection of d with $\mathcal{L}$ as a squarefree ideal δ, subject to all required memberships and deletions. The good e_1 factors, conjugate d-overlaps, and actual new d-residue supports are fixed by these choices. Thus the original row phase is fixed on the free part of d, and an original zero stays zero. The free part avoids the full union $\mathcal{L}$.

In the product of the two copies of (40.296), their real factors $\mu(d)$ leave the original outer $\mu(d)$. The step-step term needs one ideal variable and a step-correction term uses $d = mn$. For two corrections, use the four cells of primes in d specified by their membership in the two factors m_0, m_1. Both m_i's and their complements are products of the appropriate cells. This is an exact squarefree factorization with pairwise coprime cells, including units. Expand the finite small-prime choices and assign the fixed primes of δ among the cells, with at most $4^{\omega(\delta)}$ assignments. The tests $p \mid m_i$ are thereby fixed. The cell ideals have form $\delta_j q_j$, and the sign is $\mu(\delta)\prod_j \mu(q_j)$.

Select the largest free cell by its norm, with deterministic index order on ties, and fix the other free cells. If its norm is t, then $t \ge (Y')^{1/4}$. Its interval lies on the scale $L = Y'/\prod_{\text{other}} Nq_j$, with $L \gg (Y')^{1/4}$ for every nonempty selection. Its deleted set $\mathcal{T}$ consists of $\mathcal{L}$ and the primes in the other free cells, and still has polynomial radical norm. Every factorization inequality is an interval test in t, since each m_i, n_i either includes the selected cell or is fixed. The tie order changes only an endpoint. The original primal and direct tests and the middle cutoffs also give finitely many interval tests. At fixed labels X' is proportional to $1/E$, the middle parameter M is proportional to E, and the integer norm equality is fixed. The original strict and nonstrict endpoints remain in the scalar sum.

For the fixed field $\mathbb{Q}(\omega)$, write $M_{\mathcal{T}}(x) = \sum_{Nc\le x,\,(c,\mathcal{T})=1} \mu(c)$. The fixed-field deleted Möbius input used here is

$$|M_{\mathcal{T}}(x)| \ll_\kappa x \log^C(2D) \exp(-c_\kappa \sqrt{\log(2x)})$$

for $x \ge D^\kappa$ and polynomial radical norm. The underlying fixed-field zero-free input is Thorner–Zaman, *Algebra & Number Theory* 13 (2019), 1039–1068, Theorem 3.1, specialized to the trivial extension of this one fixed field. The classical truncated Perron shift for the reciprocal zeta function gives $M_\varnothing(x) \ll x\exp(-c\sqrt{\log(2x)})$. A possible fixed exceptional zero affects the fixed starting threshold. Artificial deletions are transferred exactly by

$$M_{\mathcal{T}}(x) = \sum_{\substack{Na\le x\\ \operatorname{supp} a\subseteq\mathcal{T}}} M_\varnothing(x/Na).$$

All powers of the deleted primes occur in this convolution. Split at $Na = \sqrt{x}$. In the first range use the fixed-field bound. In the second use the elementary ideal count and $1/Na \le x^{-\eta/2}(Na)^{-1+\eta}$, with $\eta \asymp 1/\sqrt{\log(2x)}$. The finite reciprocal Euler product at $1-\eta$ costs a power of $\log(2D)$. Indeed, if the deleted radical has norm $\ll D^{C_0}$, split its primes at $\log^2(2D)$. Below that threshold the ideal count bounds the reciprocal-power sum by $O((\log(2D))^{2\eta}\log\log(3D))$. Above it use the bound $O(\log(2D))$ for the sum of their log norms. For $x \ge D^\kappa$, these estimates give the claimed uniform logarithmic Euler factor and subpower decay. The underlying analytic zeta function stays fixed.

After factoring out the fixed scalar and phase, the weight is $E^{-2}G_W(c_0/E)\overline{G_W(c_1/E)}$ for fixed positive c_i. Its supremum plus integrated absolute derivative is $O(\mathcal{M}_{24}(W)^2Y^{-2})$ on each remaining interval. This follows from boundedness of the radial transform and its first log derivative, and the fixed dyadic range of E. Partial summation gives

$$\ll_\kappa \mathcal{M}_{24}(W)^2Y^{-2}L\log^C(2D)\exp(-c_\kappa\sqrt{\log(2Y')}).$$

Here $L \gg (Y')^{1/4}$ permits the deleted bound with a fixed smaller exponent in its polynomial lower cutoff. The remaining free cells sum harmonically by the factors $1/Nq_j$ in L. Together with the

fixed-prime assignments this proves (40.297). It applies to a scalar with the row and all other ideal labels fixed.

40.38.3 The complete partner sum and the equality prefix

For each $p \in \mathcal{P}$, use the coefficient

$$-\mu(\zeta)\mu(d) \sum_{\substack{mn=d,\ p\mid m \\ Nm>T_1Np,\ Nn>T_2}} 1$$

on the partner and sum its original ordered factorizations. This coefficient is independent of the partner frequency and divisor bounded. The individual primal zero above proves $V_d^{[p]} = 0$. The exact original Poisson identity therefore gives the full complement $-\mathcal{E}_d^{[p]}$, with the same middle projection. Recombining all modes includes the re-expressed direct part and preserves every original raw value.

For the elementary equality bound, at fixed r, e_0, e_1, J put $L_0 = D/(EE_1(Nh)^2)$ and $J' = J/Ne_0$. The equal-norm ideals have $z_0 = g\ell$, $\mathfrak{k} = g\bar{\ell}$. There are $O(J'\log(2+2J'))$ choices on the dyad, up to the original constant-scale convention. Their norm Nz_0 appears inversely in the Poisson scalar, and the equal-norm profile scale is comparable to L_0/R. Thus the pointwise row bound is at most a subpower times $\mathcal{M}_{24}(W)L_0R^{-1/2}(1+L_0/R)^{-4}$. The $O(R)$ original rows give squared counting norm $O((DH)^{\epsilon}\mathcal{M}_{24}(W)^2RL_0)$. Summing the square roots over the original r, e_0, e_1, J uses the harmonic factors $1/(Nr\,Ne_0)$ and fixed divisor costs. After division by D, the squared norm is $O((DH)^{\epsilon}\mathcal{M}_{24}(W)^2R/E)$. The same proof handles the modified coefficient because it is divisor bounded and row independent at each allocation. Apply Cauchy to the original and modified middle projections and sum harmonically in d. This proves the target-size full-frequency compensation of Section 40.37.

For the pure comparable prefix, keep the correction on the equality side. Its coefficient is divisor bounded on its fixed labels. A partner correction, when included, is a coefficient on x alone after fixing the other labels. The insertion interval remains complete inside the original eligibility. The sharp insertion proof with powerful freezing and exact common-factor eligibility applies. Its relative loss is $D^{1/16}$ from the erased sieve factor $\Phi(A_1, B/Ns_1)/A_1 \ll D^{1/8}$. A nonzero equality correction implies $E_0Nh_0 < 14$, hence $E_0(Nh_0)^2 < 196$. Therefore the equality radial scale is $y_0 = D/(EE_0(Nh_0)^2R) \gg D/(ER)$. Use both half radial powers and keep the remaining equality-side $7/2$ decay. The fixed-d rectangle is bounded by a constant times

$$(DH)^{\epsilon}\mathcal{M}_{24}(W)^2\frac{R}{E}\,D^{1/16}\left(1+\frac{D}{ER}\right)^{-7/2}.$$

Count the exact original middle subtraction independently at the same inherited R/E cost with the common factors. For $E \le D^{13/56}$, $D/(ER) \gg D^{1/56}$ at the pure scales. The remaining decay pays $D^{1/16}$ because $(7/2)(1/56) = 1/16$. Harmonic summation gives the stated prefix. The partner-only argument retains its own ratio $N\mathfrak{k}/Nz$, so the same automatic lower bound on its radial scale is unavailable. The coherent masked wide divisor sum remains open.

40.39 Joint moments for the wide cutoff pairing

We work at the pure scales $A = A_1 \asymp R \asymp D^{3/4}$, $A_2 \asymp 1$, with $U^2 \le D \le 7U^2/2$. The rows are the original unweighted nonprincipal rows, with fixed S, ν, u_0, their literal ray and capacity

restrictions, and their primitive conductors $Q_u \asymp R$. Use one smooth complex W supported on $[1,2]$, the full ordered cutoff, and the original raw zeros. A target bound means $O((DH)^{\epsilon}\mathcal{M}_{24}(W)^2 D^{3/4})$ for the specified contribution to the normalized pairing (40.286). Constants may depend on the fixed arithmetic data, scale constants and $\epsilon > 0$. Put $E = Nd$ and $e = \log_D E$. Here d is the intermediate divisor from the exact Möbius identity. All estimates include the original middle equality subtraction.

Theorem 40.34 (Full-frequency partner unit part)**.** *Take the unit part of C_d on the partner side of* (40.296)*, with all partner frequencies including the re-expressed direct term. A selection of the actual ordered pairs $mn = d$ may depend on d, m, n. Write $L_1 = U/Nm$, $L_2 = U/Nn$ and $l_s = \log_D \max(1, \min(L_1, L_2))$. The target holds over all $E \lesssim D^{1/6}$, and more generally on the dyads with $e \le 1/4$ and $l_s \ge 1/4 + e/2$ at the level of powers. The remaining upper cost at a single dyad with $e \le 1/4$, relative to R/E, has exponent $(1/4 + e/2 - l_s)_+/6$, where $x_+ = \max(0, x)$. The all-divisor bound for this component has power* $37/48$*.*

The low-divisor estimate uses the whole wide product support, even for balanced pairs with bounded nonunit d. Its gain comes from the forced radical of the actual product ideal in the joint positive norm. For instance, at $e = 1/4$ with the longer length of order $D^{1/2}$, the upper comparison still costs $D^{1/48}$ above R/E. This excess describes the estimate.

Theorem 40.35 (Selected partner frequencies)**.** *Let $T \le N\mathfrak{k} < 2T$ be an actual partner frequency dyad and write $t = \log_D T$. A selector of modulus at most one may depend on $\mathfrak{k}$, the actual equality allocation and the fixed partner labels. It is independent of the row and the two varying partner cutoff ideals. In the actual Poisson representation of the unit part, including the direct term and the corresponding selected middle subtraction, the target holds in the following regions:*

$$\begin{array}{c|l} 0 \le e \le 1/8 & t \le 15/32 + 3e/8 \\ 1/8 \le e \le 1/4 & t \le 33/64 \\ 1/4 \le e \le 5/16 & t \le 17/64 + e \\ 5/16 \le e < 27/56 & t \le 11/32 + 3e/4 \\ e \ge 27/56 & \textit{all frequency lengths.} \end{array} \tag{40.298}$$

Thus $T \lesssim D^{15/32}$ is sufficient over all intermediate divisors. Constant factors at the endpoints are allowed.

For selectors independent of the varying equality labels, further regions follow by grouping frequencies with prescribed ideal parts. If the rational content of $\mathfrak{k}$ is at least D^b, with $0 \le b \le 9/28$, then $T \lesssim D^{9/20+3b/5}$ suffices across all d. Here the content is the largest positive integer prime to the rational primes under S whose principal ideal divides $\mathfrak{k}$. At $E \gtrsim D^{1/4}$, content of order at least $D^{41/144}$ permits $T \lesssim D^{2/3}$. A good sixth-power base of norm at least of order $D^{1/16}$, or an S-part of norm at least of order $D^{3/10}$, suffices at every frequency length. These are conditions on the actual frequency, with all ideal labels and raw zeros retained.

Theorem 40.36 (Equality-wide correction)**.** *In the equality-side wide correction, write the equal-norm pair as $z_0 = g\ell,\ k = g\bar{\ell}$. Let ℓ_{g} retain the prime ideals of ℓ whose conjugates also avoid S. Against the full original partner complement, or its full-frequency step or wide part with its own subtraction, the target holds on $N\ell_{\mathrm{g}} \gtrsim D^{\theta(e)}$, where*

$$\theta(e) = \begin{cases} -17/12 + 37e/6, & 17/74 \le e \le 1/4, \\ 11/24 - 4e/3, & 1/4 \le e \le 11/32, \\ 0, & \textit{otherwise.} \end{cases}$$

In the distinct pure comparable selected rectangles $B, K \asymp R$ of the preceding wide analysis, the equality-side prefix extends to $Nd \lesssim D^{111/476}$, with the original allocation tests and the same choices of partner coefficient.

The small-conjugate-support band, unbalanced middle divisors and small-part main frequency range leave contributions to the coherent signed problem. The full signed assembly and the independent determinant and zero-location arguments remain open.

40.40 Proofs of the joint cutoff estimates

Write $[F]_p = R^{-1/p}\|F\|_{\ell^p}$ for counting norms on the actual rows and $[F]_\infty = \|F\|_\infty$. Use the same convention after fixing the second pivot, since $A \asymp R$ and there are only boundedly many second pivots. The physical sieve factors are

$$\begin{aligned}\Phi_6(A,B) &= A + B + A^{5/6}B^{1/3} + A^{1/3}B^{5/6},\\ \Phi_3(A,B) &= A + B + 2(AB)^{2/3},\\ \Delta_6(x) &= \max(0, x - 3/4, x/3 - 1/8, 5x/6 - 1/2),\\ \Delta_3(x) &= \max(0, x - 3/4, 2x/3 - 1/4).\end{aligned}$$

The last two functions record the power of the corresponding sieve divided by A at $B = D^x$. We display bounds up to $(DH)^\epsilon$ and the appropriate W seminorms. The dyads, divisor multiplicities and harmonic norm sums have subpower cost. Shortened lengths are replaced by one only in the sieve factor, with a bounded nonempty subunit counted directly.

40.40.1 Exact cutoff arrays and the equality moment

For Theorem 40.34, fix the ordered $d = mn$. On the support $N\zeta_i > L_i$, the primal unused good squarefree ideal c has $Nc < 2D/(EN\zeta) < 7$. Thus the partner primal unit part is the sum with $c = 1$. Its coefficient is $\mu(d)\mathbf{1}_{(d,u)=1}$ times the product of the two Möbius and raw factors at ζ_1, ζ_2, with the common weight $W(EN\zeta_1 N\zeta_2/D)$. It keeps $(d, \zeta) = 1$, both original upper bounds $N\zeta_i \le U$, and $(\zeta_1, \zeta_2) = 1$. Each nonzero summand has $N\zeta_i < 7L_i$. Expand the common-prime test using $\sum_{w|(\zeta_1,\zeta_2)} \mu(w)$, with w good squarefree and coprime to d, and set $\zeta_i = wb_i$. The residual b_i avoid w, d. Keep $\mu(w)\psi_u(w)^2$ and the row deletion. Logarithmic Fourier separation of W gives two arrays B_s, B_l with lengths $M_i = L_i/Nw$, where s, l are the shorter and longer cutoffs. Their coefficients retain the exact endpoints. In particular their true masses multiply to $U/(\sqrt{E}Nw)$.

For the equality vector, at fixed e_1, g, ℓ and a dyad $P \le Nh < 2P$, group the actual $h = re_0$ coefficients over the permissible e_0-allocations. The row factor of the resulting sum F_P is $\psi_u(h)^2$. The coefficient is divisor bounded with the original middle and cutoff predicates. The external inverse norm is $D/(EE_1NgN\ell\sqrt{R})$, where $E_1 = Ne_1$ and the actual primitive factor $Q_u^{-1/2}$ is bounded using $Q_u \asymp R$. The Gauss root and fixed raw factors are retained. Put $T_0 = \sqrt{D/(ER)}$, $T_1 = T_0/\sqrt{E_1}$. On a dyad $P \le Nh < 2P$, the normalized weight from the inverse square and the radial log separation is

$$P^{-2}\bigl(1 + (T_1/P)^2\bigr)^{-4}\mathcal{M}_{12}(W).$$

This keeps Q_u in the separated phase.

For a fixed integer $j \ge 2$, take the j-th power of the formed h-array and group by the product of its j ideals. The fixed factors on the second pivot and on S stay in the coefficients. In the variable first pivot the h-character is cubic. Write the grouped column as b_0q^3, with b_0 cubefree,

and freeze q with its raw multiplier $\psi_u(q)^6$. The squared mass on a fibre is bounded by $P^j/(Nq)^3$ up to divisor factors. The sum of the square roots converges in q, and the cubic comparison gives $[F_P]_{2j} \ll \sqrt{P}\,(\Phi_3(A,P^j)/A)^{1/(2j)}$. When $T_1 \geq 1$ the radial dyad sum is bounded at $P \asymp T_1$: below it use the eighth power in the weight, and above it the sieve factor grows at most as $P^{1/2}$ against $P^{-3/2}$. When $T_1 < 1$ use unit scale. For $e \leq 1/4$, take $\tau = (1/4 - e)/2$; the replacement of T_1 by T_0 in the sieve costs only the monotone enlargement, and $E_1^{-1}T_1^{-3/2} = E_1^{-1/4}T_0^{-3/2}$. In the subunit case $E_1^{-1} \leq T_0^{-2}$ when $T_0 \geq 1$. The equality bound after the g, ℓ harmonic sums is

$$[\mathcal{E}_d]_{2j} \ll \sqrt{D/E}\, D^{-\tau/2+\Delta_3(j\tau)/(2j)}(DH)^{\epsilon}\mathcal{M}_{12}(W). \tag{40.299}$$

The same dyad calculation with the elementary ideal count gives the pointwise factor

$$\sqrt{D/E}\min(1, \sqrt{D/(ER)}).$$

Set $l_i = \log_D \max(1, L_i)$. The cutoff second moment has excess $\Delta_6(l_i)/2$ over its square-root mass. For the fourth moment, square the actual cutoff sum. The grouped product is sixth-free, with exponent two allowed at a common prime, and has divisor-bounded multiplicity. Its fourth-root cost is $D^{\Delta_6(2l_i)/4}$. For $e \leq 1/8$, pair the equality sixth moment with the shorter third and longer second moments. Interpolating the shorter between second and fourth with weight $2/3$ on the fourth yields

$$\frac{\Delta_6(l_l)}{2} + \frac{\Delta_6(l_s)}{6} + \frac{\Delta_6(2l_s)}{6} - \frac{\tau}{2} + \frac{\Delta_3(3\tau)}{6} = \frac{1}{48} - \frac{l_l - l_s}{12}.$$

Here $3/8 \leq l_s \leq l_l \leq 1/2$, $l_s + l_l = 1 - e$ at the level of powers, and $\Delta_3(3\tau) = 0$. For $e \geq 1/8$ the pointwise equality bound and the two second moments have excess at most $1/48$, because $(l_s/3 - 1/8)_+ + (l_l/3 - 1/8)_+ \leq 1/24$. The normalized masses and w-sum give R/E. The original $\mathcal{E}_d^{\mathrm{unit}}$ compensation has normalized energy of order at most R/E by the grouped elementary equality bound, and so does $\mathcal{E}_d$. Their inner product has the same upper bound. Summing over d harmonically proves the $37/48$ comparison.

40.40.2 A forced radical in the physical sieve

For an actual good sixth-free ideal $\mathfrak{b}$ of norm of order B, put $\mathfrak{b}^\sharp = \mathfrak{b}/\operatorname{rad}\mathfrak{b}$. If every column satisfies $N\operatorname{rad}(\mathfrak{b}^\sharp) \gtrsim P$, the physical positive comparison can use

$$\begin{aligned}\widetilde{\Psi}(A,B,P) = A + B + A^{5/6}B^{1/3}P^{-1/3} \\ + A^{1/6}BP^{-1/2} + A^{2/3}B^{1/2}P^{-1/2}.\end{aligned} \tag{40.300}$$

The factor multiplies the original squared coefficient mass, up to subpowers. Here is the support restriction inside the pinned de Faveri argument. In its Lemma 4.4 remove the outer common ideal of norm F. The remaining scales obey $B' \asymp B/F$ and $A/(CF) \leq A' \leq CA$ for a fixed constant C, and the radical threshold can drop at most by F. A prime lost from that radical divides the removed ideal. The sharp part has norm at least the norm of its radical.

In the two positive norms of the proof of Lemma 5.1, fix the sharp label s_i and the internal Möbius divisor r, with squarefree part ru_i. The original coefficient already requires $\operatorname{rad}(s_i) \mid ru_i$. Set $q_i = \operatorname{rad}(s_i)/(\operatorname{rad}(s_i), r)$, so $u_i = q_i v_i$. The v_i are squarefree and avoid r, q_i. The new label is in bijection with the original label at these fixed indices. Keep the original denominator at rq_iv_i, the ray predicates, and the raw factor χ_{q_i} at the grouped row variable. Multiplicativity gives the same zeros, including when a row prime divides q_i. This factor is a contraction in the formed norm. The original squared coefficient sum is unchanged by the reindexing.

If P_i and C_i are the norm scales of s_i and its radical, the row cap is still $K_i \lesssim (B')^2/(A'P_i)$. The column cap is now $B'/(P_iC_i)$, since $N(rq_i) \geq N\,\mathrm{rad}(s_i)$. Both P_i, C_i are at least of order $\max(1, P/F)$. Insert the four terms of the sixth-power comparison from de Faveri's Theorem 1.1 and Lemma 6.1, $K + K^{1/6}L + K^{5/6}L^{1/3} + K^{1/3}L^{5/6}$. The two factors in its positive Cauchy estimate carry the prefactor $A'\sqrt{P_1P_2}/B'$. Consequently the four monomials before taking their geometric mean are bounded by

$$\begin{aligned} B', \quad & (A')^{5/6}(B')^{1/3}P_i^{-1/6}C_i^{-1}, \\ & (A')^{1/6}B'P_i^{-1/6}C_i^{-1/3}, \\ & (A')^{2/3}(B')^{1/2}P_i^{-1/6}C_i^{-5/6}. \end{aligned}$$

Put $G = \max(1, P/F)$. The resulting factors satisfy

$$\begin{aligned} F^{-1/3}G^{-7/6} &\leq P^{-1/3}, \\ F^{-1}G^{-1/2} &\leq P^{-1/2}, \\ F^{-1/2}G^{-1} &\leq P^{-1/2}. \end{aligned}$$

These follow by considering $F \leq P$ and $F \geq P$. The source diagonal term gives A. This proves (40.300) with its full masks.

For the pure joint norm apply Cauchy with the longer cutoff as one factor. The other norm, of $F_P\overline{B_s}$, equals that of F_PB_s by pointwise modulus. The exact signed pairing keeps its original conjugation. The latter positive norm groups actual h^2b_s injectively: exponents $0, 1, 2, 3$ determine membership of h, b_s at each prime. The radical of its sharp part is h. The length is of order $P^2\max(1, M_s)$ and the squared mass is bounded by PM_s up to subpowers. The square root of (40.300) grows at most linearly in P at fixed M_s; the inverse square and square-root mass supply $P^{-3/2}$. Thus the same radial maximum at T_0, with the E_1-factor as above, applies. For $e \leq 1/4$ the joint excess over the square-root mass is $\frac{1}{2}(l_s/3 + \tau/3 - 1/8)_+$; the B term is below A in power, and the other two terms in (40.300) have no larger exponent. With the longer second moment the total relative power is

$$\tfrac{1}{2}(l_s/3 + \tau/3 - 1/8)_+ + \tfrac{1}{2}(l_l/3 - 1/8)_+ - \tau/2 = \tfrac{1}{6}(1/4 + e/2 - l_s)_+.$$

The equality follows from $l_l \geq 3/8$ and $l_s + l_l = 1 - e$. If $e \leq 1/6$, then $l_s \geq 1/2 - e \geq 1/4 + e/2$. The middle compensation still costs R/E, proving the low-divisor and length claims of Theorem 40.34.

40.40.3 The selected Poisson product

For Theorem 40.35, keep the actual selected partner frequencies in the Poisson expression. The live dyad gives $N\zeta_i < 14L_i$, and $E_1Nh < 14$ on the partner wide support. Keep the ordered e_0-assignment, the common-prime projector and all shortened residual deletions. The actual partner frequency weight separates in logarithmic variables on a frequency dyad, with absolute Fourier mass bounded by $\mathcal{M}_{12}(W)(1 + T/R)^{-4}$. The primitive factor remains $Q_u^{-1/2}$ and the factor from the re-expressed direct term remains in the array.

At fixed equality g, ℓ, e_1 and $P \leq Nh_0 < 2P$, the raw equality phase times the conjugated partner dual phase is $\psi_u(h_0^2\mathfrak{k})$. The row-independent selector is included in the coefficient at fixed $h_0, \mathfrak{k}$ by summing the exact equality allocations. It can give a nonseparable coefficient, with divisor-bounded multiplicity and all the original signs. Write the grouped product uniquely as $\mathfrak{s}b_0v^6$, with $\mathfrak{s}$ supported on S, v good and b_0 good sixth-free. Factor $h_0 = h_{\mathrm{in}}h_{\mathrm{out}}$ by support in v. Then $h_{\mathrm{in}} \mid v$ and $h_{\mathrm{out}}^2 \mid b_0$,

even when the actual frequency meets h_0. At fixed $\mathfrak{s}, v, h_{\mathrm{in}}$, count h_{out} at length P/Nh_{in} and divide the physical residual length by $(Nh_{\mathrm{out}})^2$. The squared coefficient mass is bounded by

$$(DH)^{\epsilon}\,\frac{PT\,Nh_{\mathrm{in}}}{N\mathfrak{s}\,(Nv)^6}.$$

The exact multipliers at $\mathfrak{s}, v$ remain in the positive comparison. The sums of the square-root weights converge, since the sum over $h_{\mathrm{in}} \mid v$ costs at most $(Nv)^{1/2+\epsilon}$. Also $N\,\mathrm{rad}(b_0^{\sharp}) \geq P/Nv$. Apply (40.300) with this threshold, truncated below by one, and with the true length at most of order $P^2T/(N\mathfrak{s}(Nv)^6)$. Each inverse threshold exponent β is at most six times its length exponent α. Thus the sieve may use the nominal arguments P^2T, P after this shortening. The radial sum at fixed T still has its maximum at the equality scale, as the sieve square root grows at most linearly in P.

Put $\Gamma_4 = (\Delta_6(2l_s) + \Delta_6(2l_l))/4$. The two fourth moments of the cutoffs give this excess, with their true shortened masses. Before the sieve factors, the normalized mass at fixed labels and radial dyad, omitting the harmless fixed shortening and the harmonic common-prime factor, is

$$\frac{\sqrt{L_1L_2}\sqrt{T}\,P^{-3/2}}{EE_1NgN\ell}.$$

The factor $P^{-3/2}$ includes the equality inverse square and its square-root mass. The outer normalization by D cancels the equality prefactor D; conversion of the counting norm back to the row sum supplies R against the two factors of size $Q_u^{-1/2}$. For $e \leq 1/4$ and the indicated frequency ranges above $t = 3/8$, the relative joint sieve excess is $(t/3 + \tau/3 - 1/8)/2$. Adding the physical frequency factor, the cutoff moments and the equality radial gain gives $2t/3 - 7/16 + \Gamma_4 - \tau/3$. For $e \leq 1/8$, $\Gamma_4 = 1/6 - 5e/12$. For $1/8 \leq e \leq 1/4$, convexity and the individual length caps give $\Gamma_4 \leq 13/96 - e/6$. These are the first two branches of (40.298); smaller t follows by monotonicity of the upper comparison.

For $e \geq 1/4$, use the unit-scale equality dyad and the unshortened frequency sieve at T. The total power above R/E is

$$t/2 - 1/4 - e/2 + \Gamma + \Delta_6(t)/2.$$

For the third and fourth branches one may take $\Gamma = \Gamma_4$, bounded by $13/96 - e/6$ through $e = 5/16$ and by $1/12$ thereafter. For $e \geq 27/56$ use the lesser of Γ_4 and $\Gamma_2 = l_s/2 + \Delta_6(l_l)/2$; the latter uses the shorter pointwise bound and longer second moment. Under $l_s + l_l \leq 29/56$ and $l_l \leq 1/2$, the maximum of this minimum is $3/56$. Indeed l_l may be increased to its permitted endpoint; the two affine bounds cross at $l_s = 5/56,\ l_l = 3/7$. For $l_s \leq 1/56$ the pointwise option is smaller than $3/56$, and for $l_s \geq 1/7$ convexity bounds the fourth-moment option by its values at $1/7, 29/112$. At $t = 3/4$ the resulting power is at most $3/16 - e/2 + 3/56 \leq 0$. Above R, the remaining growth has slope at most one and the factor $(1 + T/R)^{-4}$ gives a summable tail. For equality-dependent selectors, sum the actual equality label vectors only after using each label's own selected middle equality subtraction. Each of these subtractions has the elementary normalized energy R/E. The sum of the equality-label pointwise majorants is $O((DH)^{\epsilon}\mathcal{M}_{12}(W)\sqrt{D/E})$, by the original harmonic g, ℓ sums and the inverse-square radial bound. Cauchy at each label gives the required total compensation of order R/E. The divisor sum is harmonic.

40.40.4 Sparse frequency and equality support

For a frequency-only selector, rational content at least D^b leaves $O(TD^{-b})$ ideals on a dyad. Divide each frequency by its rational principal factor and sum the inverse squares of the possible contents.

For $j = 1, 2$, power the formed frequency array j times before taking its second moment. Grouping by product gives squared mass at most $(DH)^{\epsilon}(TD^{-b})^{j}$ by the divisor bound. At fixed S-part $\mathfrak{s}$, a dyad Q of the sixth-power base q has two bounds for the sum of square-root masses. They are $T^{j/2}Q^{1/2}D^{-jb/2}$ by Cauchy over disjoint fibres, and $T^{j/2}Q^{-2}$ by the individual shortened length and ideal count. The sieve length is at most of order $\max(1, T^{j}/Q^{6})$. On writing $x = \log_{D} Q/j$, the bound is convex up to $b/5$ and nonincreasing afterwards. Its maximum is bounded by the larger value at $0, b/5$. Thus the $2j$-norm of the frequency array has excess

$$\lambda_{j} = \max\left\{\frac{\Delta_{6}(jt)}{2j} - \frac{b}{2},\ \frac{\Delta_{6}(j(t - 6b/5)_{+})}{2j} - \frac{2b}{5}\right\}.$$

The two cutoff moments and (40.299) give the following upper powers above R/E:

$$\begin{cases} t/2 - 13/48 + \lambda_{1}/3 + 2\lambda_{2}/3, & e \le 1/8, \\ t/2 - 9/32 + 5\lambda_{1}/6 + \lambda_{2}/6, & 1/8 \le e \le 1/4, \\ t/2 - 11/32 + \lambda_{2}, & e \ge 1/4. \end{cases}$$

In the first two lines use the equality sixth and twenty-fourth moments respectively and interpolate the frequency second and fourth moments. The last line uses the equality supremum, the longer second and shorter fourth moments. At $t = 9/20 + 3b/5$, the first branch of λ_{j} dominates for both j, since the lost sieve growth across the length shortening is at least $b/10$. The first excess is zero, and the other two are nonpositive. The last branch at $t = 2/3,\ b = 41/144$ is zero. The fixed S-part and sixth-power multipliers retain their exact raw values on each fibre.

If the frequency sixth-power base is at least D^{a}, the product of j such bases divides the grouped base, and summing its inverse-cube weights gives D^{-2ja}. The replacement λ_{j} is $-2a + \Delta_{6}(j(t - 6a)_{+})/(2j)$. If the S-part has norm at least D^{σ}, its product has norm at least $D^{j\sigma}$. Summing the inverse square roots over this fixed prime support costs $D^{-j\sigma/2+\epsilon}$; use the Euler product with any fixed positive exponent below $1/2$. Now $\lambda_{j} = -\sigma/2 + \Delta_{6}(j(t - \sigma)_{+})/(2j)$. At $t = 3/4$ these comparisons meet the target with $a = 1/16$ and $\sigma = 3/10$. Monotonicity gives smaller t and the original radial decay sums the upper tail. All comparisons keep the corresponding middle subtraction.

For the equality-wide sector, fix $g, h, e_{0}, e_{1}, \ell/\ell_{\mathrm{g}}$. The last factor lies on finitely many conjugates of primes in S, and its phase is retained. The live dyad gives $E_{1}Nh < 14$. On the remaining conjugate-good part the actual phase is $\nu(\ell_{\mathrm{g}})\overline{\nu(\bar{\ell}_{\mathrm{g}})}(Nu/\ell_{\mathrm{g}})_{6}$, including zeros at either orientation. On $T \le N\ell_{\mathrm{g}} < 2T$ the rational conductor is $N\ell_{\mathrm{g}}$ and the squared coefficient mass is of order at most $1/T$ up to subpowers. Fixing the second pivot, the oriented rational Gram bound has sieve factor $A + T^{5/3}$ in the integer variable Nv_{1}; equal-norm row multiplicity has divisor cost. The sum over g is harmonic. Including the alternative direct count gives normalized equality energy at most

$$\frac{D}{E^{2}}\left(1 + \frac{D}{ER}\right)^{-8} \min\left(1, \frac{A + T^{5/3}}{AT}\right)(DH)^{\epsilon}\mathcal{M}_{24}(W)^{2}.$$

For the full partner complement the four upper powers of normalized energy are $3/4 - e,\ 1 - 2e,\ 23/24 - 4e/3,\ 13/12 - 11e/6$. For its wide coefficient the same bound follows by the primal unit reduction, the exact small-prime compensation and the physical sieve at D/E; for the step use the difference of the full and wide coefficients. Cauchy requires the extra equality gain $\max(0, P(e) - 1/2 - 8(1/4 - e)_{+})$, where $P(e)$ is the maximum of the four displayed powers. This gives $\theta(e)$ in Theorem 40.36. The actual support $ET \ll D$ ensures that the $T^{2/3}/A$ term does not obstruct this threshold. The harmonic divisor sum finishes the full-complement bound.

For the distinct comparable selected rectangles, retain the extra equality factor $(1+D/(ER))^{-7/2}$ after the original two half radial powers. The coupled cutoff estimate on the same insertion rectangles costs $D^{1/17}$ relative to R/E. This estimate accepts the original coefficient or its step and wide parts. At fixed ordered m, n and, for a subtraction, fixed p, the additional wide tests are single-factor lower endpoints on the two ordered arrays. The step tests are single-factor upper endpoints. The exact common-prime projectors and actual insertion dual retain these endpoints. Since $(7/2)(1/4 - 111/476) = 1/17$, the equality radial factor pays that cost on the stated prefix. The selected middle subtraction has its separate R/E bound. This proves the second assertion of Theorem 40.36.

Bibliography

[1] A. Schreiber, *Surface Algebras I: Dessins D'enfants, Surface Algebras, and Dessin Orders*, arXiv:1810.06750v5 (2023).

[2] A. Schreiber, *Surface Algebras and Surface Orders II: Affine Bundles on Curves*, arXiv:1812.00621v1; record 2018, downloaded PDF internally dated November 27, 2024.

[3] A. Schreiber, *Multiparameter Persistent Homology—Generic Structures and Quantum Computing*, arXiv:2210.11433v1 (2022).

[4] C. Bessenrodt and T. Holm, *Weighted locally gentle quivers and Cartan matrices*, arXiv:math/0511610v1 (2005).

[5] S. Ford, A. Oswald and J.J. Zhang, *Homological conditions on locally gentle algebras*, arXiv:2409.08333v3 (5 September 2026).

[6] S. Opper, P.-G. Plamondon and S. Schroll, *A geometric model for the derived category of gentle algebras*, arXiv:1801.09659v7 (10 July 2025).

[7] W. Chang, *Geometric models for the algebraic hearts in the derived category of a gentle algebra*, arXiv:2305.03998v2 (4 September 2024).

[8] Y.-Z. Liu, C. Zhang and H. Zhang, *Constructing projective resolution and taking cohomology for gentle algebras in the geometric model*, arXiv:2308.07220v1 (2023).

[9] Z. Li, Y. Qiu and Y. Zhou, *A geometric realization of Koszul duality for graded gentle algebras*, arXiv:2403.15190v1 (2024).

[10] W. Chang, H. Jin and S. Schroll, *Recollements of partially wrapped Fukaya categories and surface cuts*, arXiv:2206.11196v2 (2023).

[11] B. Dequêne and M. Schoonheere, *Resolving subcategories for gentle algebras I: Monogeneous resolving subcategories for gentle trees*, arXiv:2502.20994v3 (2026).

[12] D.A. Buchsbaum and D. Eisenbud, *What makes a complex exact?*, J. Algebra 25 (1973), 259–268, primary paper.

[13] W. Bruns, *The existence of generic free resolutions and related objects*, Math. Scand. 55 (1984), 33–46.

[14] D. Eisenbud, *Homological algebra on a complete intersection, with an application to group representations*, Trans. AMS 260 (1980), 35–64.

[15] A. Beauville and Y. Laszlo, *Un lemme de descente*, C. R. Acad. Sci. Paris 320 (1995), 335–340, author text.

[16] P. Magyar, *Affine Schubert varieties and circular complexes*, arXiv:math/0210151v1 (2002).

[17] F.F. Knudsen and D. Mumford, *The projectivity of the moduli space of stable curves I: Preliminaries on 'det' and 'Div'*, Math. Scand. 39 (1976), 19–55, doi:10.7146/math.scand.a-11642.

[18] M. Breuning, *Determinant functors on triangulated categories*, arXiv:math/0610435v1 (2006).

[19] D. Eriksson and G. Freixas i Montplet, *Deligne–Riemann–Roch and intersection bundles*, J. Éc. polytech. Math. 11 (2024), 247–361, doi:10.5802/jep.254.

[20] P. Deligne, *La conjecture de Weil I*, Publ. Math. IHÉS 43 (1974), 273–307, primary text.

[21] P. Deligne, *La conjecture de Weil II*, Publ. Math. IHÉS 52 (1980), 137–252, primary text.

[22] P. Deligne, *Cohomologie étale (SGA* $4\frac{1}{2}$*)*, Lecture Notes in Mathematics 569, Springer-Verlag, 1977, doi:10.1007/BFb0091516.

[23] G. Tabuada, *Noncommutative Weil conjecture*, arXiv:1808.00950v7 (6 December 2019).

[24] C. Deninger, *Arithmetic geometry and analysis on foliated spaces*, arXiv:math/0505354v1 (2005).

[25] D.B. Ray and I.M. Singer, *R-Torsion and the Laplacian on Riemannian manifolds*, Advances in Math. 7 (1971), 145–210, doi:10.1016/0001-8708(71)90045-4.

[26] F. Bornemann, *On the numerical evaluation of Fredholm determinants*, arXiv:0804.2543v1; Math. Comp. 79 (2010), 871–915.

[27] B. Dequêne and M. Schoonheere, *Resolving subcategories for gentle algebras II: Resolving subcategories for gentle trees*, arXiv:2509.10120v2 (3 October 2025).

[28] C. Procesi, *The invariant theory of* $n \times n$ *matrices*, Advances in Math. 19 (1976), 306–381, doi:10.1016/0001-8708(76)90027-X.

[29] L. Le Bruyn and C. Procesi, *Semisimple representations of quivers*, Trans. Amer. Math. Soc. 317 (1990), 585–598, doi:10.1090/S0002-9947-1990-0958897-0.

[30] A. Craw and R. Yamagishi, *The Le Bruyn–Procesi theorem following Lusztig*, arXiv:2312.08527v4 (14 November 2025).

[31] P. Etingof, O. Golberg, S. Hensel, T. Liu, A. Schwendner, D. Vaintrob and E. Yudovina, *Introduction to Representation Theory*, with historical interludes by S. Gerovitch, Student Mathematical Library 59, American Mathematical Society, 2011, doi:10.1090/stml/059; author-hosted text.

[32] K. Akin, D.A. Buchsbaum and J. Weyman, *Schur functors and Schur complexes*, Advances in Math. 44 (1982), 207–278, doi:10.1016/0001-8708(82)90039-1.

[33] Q. Jiang, *Derived Grassmannians and derived Schur functors*, arXiv:2212.10488v3 (6 July 2023).

[34] A. Price, A. Stelzer and A. Yong, *Representations from matrix varieties, and filtered RSK*, arXiv:2403.09938v2 (6 October 2025).

[35] H. Derksen and J. Weyman, *Semi-invariants of quivers and saturation for Littlewood–Richardson coefficients*, J. Amer. Math. Soc. 13 (2000), 467–479, primary author text.

[36] A. Schofield and M. Van den Bergh, *Semi-invariants of quivers for arbitrary dimension vectors*, arXiv:math/9907174v1 (27 July 1999); Indag. Math. 12 (2001), 125–138.

[37] J.S. Milne, *Reductive Groups*, author's course notes, version 2.00 (10 March 2018), §5.18.

[38] W. Crawley-Boevey, *Classification of modules for infinite-dimensional string algebras*, Trans. Amer. Math. Soc. 370 (2018), 3289–3313, doi:10.1090/tran/7032; arXiv:1308.6410v2 (4 March 2016).

[39] M. Auslander and I. Reiten, *Almost split sequences for Cohen–Macaulay-modules*, Math. Ann. 277 (1987), 345–349, doi:10.1007/BF01457367.

[40] R. Bautista, S. Liu and C. Paquette, *Representation Theory of an Infinite Quiver*, arXiv:1109.3176v1 (14 September 2011); published as *Representation theory of strongly locally finite quivers*, Proc. London Math. Soc. 106 (2013), 97–162.

[41] C. Paquette, *Irreducible morphisms and locally finite dimensional representations*, arXiv:1508.04353v3 (4 January 2016).

[42] S. Liu, P. Ng and C. Paquette, *Almost split sequences and approximations*, arXiv:1203.5009v1 (19 March 2012).

[43] C.M. Ringel, *The Minimal Representation-Infinite Algebras which are Special Biserial*, author-hosted ICRA Tokyo 2010 proceedings text, 57 pages, retrieved 3 November 2026.

[44] G. Puninski and M. Prest, *Ringel's conjecture for domestic string algebras*, arXiv:1407.7470v2 (13 September 2015).

[45] R. Laking, M. Prest and G. Puninski, *Krull–Gabriel dimension of domestic string algebras*, arXiv:1506.07703v2 (29 June 2015).

[46] H.-L. Huang, Z. Lin and X. Su, *The Auslander–Reiten quivers of string algebras of affine type $\widetilde{C}$ and a conjecture by Geiss–Leclerc–Schröer*, arXiv:2110.02777v2 (16 November 2021).

[47] G. Abrams and G. Aranda Pino, *The Leavitt path algebra of a graph*, arXiv:math/0509494v1 (21 September 2005).

[48] T. Bates, D. Pask, I. Raeburn and W. Szymański, *The C^*-algebras of row-finite graphs*, New York J. Math. 6 (2000), 307–324, primary journal text.

[49] N.J. Fowler and I. Raeburn, *The Toeplitz algebra of a Hilbert bimodule*, arXiv:math/9806093v3 (23 June 1998).

[50] N. Brownlowe, M. Laca, D. Robertson and A. Sims, *Reconstructing directed graphs from generalised gauge actions on their Toeplitz algebras*, arXiv:1812.08903v1 (21 December 2018).

[51] E.T.A. Kakariadis and O.M. Shalit, *On operator algebras associated with monomial ideals in noncommuting variables*, arXiv:1501.06495v3 (21 November 2018).

[52] O.M. Shalit and B. Solel, *Subproduct systems*, arXiv:0901.1422v3 (26 May 2009).

[53] A. Connes and C. Consani, *Knots, primes and class field theory*, arXiv:2501.06560v1 (11 January 2025).

[54] A. Connes, C. Consani and H. Moscovici, *Zeta zeros and prolate wave operators*, arXiv:2310.18423v2 (4 May 2024).

[55] A. Connes, C. Consani and H. Moscovici, *On q-series and the moment problem associated to local factors*, arXiv:2403.01247v1 (2 March 2024).

[56] A. Connes, C. Consani and H. Moscovici, *Zeta Spectral Triples*, arXiv:2511.22755v1 (27 November 2025).

[57] A. Connes and W.D. van Suijlekom, *Quadratic Forms, Real Zeros and Echoes of the Spectral Action*, arXiv:2511.23257v1 (28 November 2025).

[58] A. Connes, *The Riemann Hypothesis: Past, Present and a Letter Through Time*, arXiv:2602.04022v1 (3 February 2026).

[59] A. Connes and C. Consani, *On the Jacobian of* $\overline{\mathrm{Spec}\,\mathbb{Z}}$, arXiv:2602.15941v1 (17 February 2026).

[60] C. Deninger, *Dynamical systems for arithmetic schemes*, arXiv:1807.06400v4 (7 February 2024); Indag. Math. 37 (2026), 25–136, doi:10.1016/j.indag.2024.05.007.

[61] C. Deninger, *Primes, knots and periodic orbits*, arXiv:2301.11643v1 (27 January 2023).

[62] C. Deninger, *There is no "Weil-"cohomology theory with real coefficients for arithmetic curves*, arXiv:2204.02714v2 (27 January 2023).

[63] R. Ponge and Y. Tian, *Nonclassical Weyl laws and Connes' Integration for weak Lorentz ideals, I*, arXiv:2605.25591v2 (28 September 2026).

[64] F.W.J. Olver et al. (eds.), *NIST Digital Library of Mathematical Functions*, finite summation by parts, Eq. 2.10.9 and Dirichlet L-functions, §25.15, consulted 3 November 2026.

[65] A. Chirvasitu, P.M. Hajac and M. Tobolski, *Non-surjective pullbacks of graph C*-algebras from non-injective pushouts of graphs*, arXiv:1907.10260v3 (31 December 2019), Theorems3.4 and4.3; doi:10.1112/blms.12389.

[66] Y. Lekili and A. Polishchuk, *Derived equivalences of gentle algebras via Fukaya categories*, arXiv:1801.06370v5 (27 August 2019), Definition3.1.1, Lemma3.1.3 and Theorem3.2.2.

[67] M. Tomforde, *Uniqueness theorems and ideal structure for Leavitt path algebras*, arXiv:math/0612628v6 (27 February 2007), Theorem7.3, pp.29–30.

[68] A. Weil, *Numbers of solutions of equations in finite fields*, Bull. Amer. Math. Soc.55 (1949),497–508, especially pp.499–502 and Eq.(4), doi:10.1090/S0002-9904-1949-09219-4; primary-paper scan.

[69] The Stacks Project, Tag0FJ9 and Tag0GSX (retrieved 3 November 2026).

[70] J. Alper, *Good moduli spaces for Artin stacks*, Ann. Inst. Fourier63 (2013),2349–2402, Theorem10.3, pp.2386–2387, doi:10.5802/aif.2833.

[71] The Stacks Project, Tag04V8: Taking roots of line bundles (retrieved 3 November 2026).

[72] G. Zwara, *Smooth morphisms of module schemes*, Proc. London Math. Soc. (3) 84 (2002), 539–558, primary publication.

[73] C. Riedtmann and G. Zwara, *Orbit closures and rank schemes*, Comment. Math. Helv. 88 (2013), 55–84, primary publication, Section6.

[74] Y. Liu, N. Li, B. Xing and P. Chen, *A lecture note on covering theory in representation theory of algebras*, arXiv:2508.01563v5, 28 May 2026.

[75] Q. Dong, Z. Lin, M. Lu and S. Ruan, *Representation-tame Geiß–Leclerc–Schröer algebras and a revised GLS conjecture on root systems*, arXiv:2609.26503v1, 22 September 2026.

[76] S. Schroll, *On geometric models in representation theory*, Proceedings of ICM 2026, vol.3, pp.250–271, doi:10.1137/25M1810647; author preprint arXiv:2601.14396v1.

[77] B. Keller, *Introduction to A_∞ algebras and modules*, arXiv:math/9910179v2 (2001), especially §§3.1,3.3,6.2.

[78] The Stacks Project Authors, *The Koszul complex*, Tag 0621, especially Definitions15.29.1–2 and Lemma15.29.5; snapshot November3,2026, hash recorded in the repository.

[79] The Stacks Project Authors, *Regular sequences are Koszul regular*, Tag 062F, Lemma15.31.2; snapshot November3,2026, hash recorded in the repository.

[80] S. Datta, S. Howard and D. Cochran, *Geometry of the Welch Bounds*, arXiv:0909.0206v2 (2012), Section2.1, Theorem2.2.

[81] K.G. Wilson and J. Kogut, *The renormalization group and the epsilon expansion*, Physics Reports12(1974),75–199, DOI10.1016/0370-1573(74)90023-4; pinned institutional scan and review scope in `planning/ACTUAL_RG_SOURCES.json`.

[82] M. Levin and C.P. Nave, *Tensor renormalization group approach to2Dclassical lattice models*, arXiv:cond-mat/0611687v2 (2008); Phys. Rev. Lett.99(2007),120601.

[83] J. Kim et al., *Pure Transformers are Powerful Graph Learners*, arXiv:2207.02505v2 (2022). Our finite measured-feature prototype does not reproduce its full benchmarks.

[84] S. Liu et al., *Unsupervised Discovery of Steerable Factors When Graph Deep Generative Models Are Entangled*, arXiv:2401.17123v1 (2024); scoped primary reading in the computational source manifest.

[85] S. Lahlou et al., *A theory of continuous generative flow networks*, arXiv:2301.12594v2 (2023); state measures and trajectory balance.

[86] M. Gross and B. Siebert, *Mirror Symmetry via Logarithmic Degeneration Data II*, arXiv:0709.2290v2; used as a geometric research context, not an implemented mirror comparison.

[87] B. Green and T. Tao, *Quadratic uniformity of the Möbius function*, arXiv:math/0606087v2, Section4, Lemma4.1, printed pages12–13. Focused identity reading only; no nilsequence estimate is asserted for the moving sextic family here.

[88] S.S. Kudla, *Tate's thesis*, expanded Jerusalem lecture notes (2001), Theorem4.3 and Corollary4.4, pinned primary notes.

[89] J.S. Milne, *Class Field Theory*, version4.03 (6August2020), Theorem0.8 and ChapterI,§1, author notes.

[90] A. Jacot, F. Gabriel and C. Hongler, *Neural Tangent Kernel: Convergence and Generalization in Neural Networks*, arXiv:1806.07572v4; specified classical scaling hypotheses.

[91] J. Liu et al., *Representation Learning via Quantum Neural Tangent Kernels*, arXiv:2111.04225v3; focused version/abstract review.

[92] M. Kontsevich and Y. Soibelman, *Affine structures and non-archimedean analytic spaces*, arXiv:math/0406564v1; valued and integral-affine data.

[93] Y. Lekili and A. Polishchuk, *Derived equivalences of gentle algebras via Fukaya categories*, arXiv:1801.06370v5; category and smoothness hypotheses retained.

[94] Z. Cui, P. Zhang and Y. Tang, *Quantum Flow Matching*, arXiv:2508.12413v1; abstract-level comparison, not an upstream reproduction.

[95] L. Abrams, *Two-dimensional topological quantum field theories and Frobenius algebras*, J. Knot Theory Ramifications 5 (1996), 569–587, author-hosted paper.

[96] G. Segal, *The definition of conformal field theory*, in *Topology, Geometry and Quantum Field Theory* (2004); primary publisher metadata and sewing-scope comparison.

[97] S. Ryu and T. Takayanagi, *Holographic Derivation of Entanglement Entropy from AdS/CFT*, arXiv:hep-th/0603001v2; external setting only.

[98] S. Mochizuki, *The Absolute Anabelian Geometry of Hyperbolic Curves*, author-hosted paper, introduction and Theorem 1.3.4; arithmetic extension hypotheses retained.

[99] Z. Ji, A. Natarajan, T. Vidick, J. Wright and H. Yuen, *MIP*=RE*, arXiv:2001.04383v4 (16 October 2026); external theorem and version record, not rerun locally.

[100] T. Fukui, Y. Hatsugai and H. Suzuki, *Chern Numbers in Discretized Brillouin Zone*, arXiv:cond-mat/0503172v2, 2005.

[101] RDKit contributors, *MMFF94 force fields and ETKDG conformer APIs*, `https://www.rdkit.org/docs/`; executed version2026.03.1.

[102] Worldwide Protein Data Bank, *Usage Policies*, CC0-1.0 coordinate archive, `https://www.wwpdb.org/about/usage-policies`.

[103] F. Evers et al., *Theory of Chirality Induced Spin Selectivity: Progress and Challenges*, arXiv:2108.09998v1, 2021.

[104] A. Privitera et al., *Direct detection of spin polarization in photoinduced charge transfer through a chiral bridge*, arXiv:2205.05353v1, 2022.

[105] wwPDB, Atomic Coordinate Entry Format3.3, secondary structure and coordinate sections, accessed2026-11-04. `https://www.wwpdb.org/documentation/file-format-content/format33/sect5.html`.

[106] Y. Song et al., Score-Based Generative Modeling through Stochastic Differential Equations, arXiv:2011.13456v1 (2020).

[107] Y. Lipman et al., Flow Matching for Generative Modeling, arXiv:2210.02747v1 (2022).

[108] R. T. Q. Chen and Y. Lipman, Flow Matching on General Geometries, arXiv:2302.03660v1 (2023).

[109] The Univalent Foundations Program, *Homotopy Type Theory: Univalent Foundations of Mathematics*, first-edition-257-g5561b73 (2013), Sections 6.6–6.8, especially Remarks 6.7.1–6.7.2, pinned official edition.

[110] A. Jacot, F. Gabriel and C. Hongler, *Neural Tangent Kernel: Convergence and Generalization in Neural Networks*, arXiv:1806.07572v4 (2020). This is background; our diagonal holomorphic readout limit is derived separately.

[111] NIST Digital Library of Mathematical Functions, *Dirichlet L-functions*, Section 25.15, equations 25.15.1–25.15.5, primary reference, accessed 4 November 2026.

[112] F. Bornemann, *On the Numerical Evaluation of Fredholm Determinants*, arXiv:0804.2543v2 (2008), Section 4, equation (4.1); Math. Comp. 79 (2010), 871–915.

[113] C. Bamps and S. Pironio, *Sum-of-squares decompositions for a family of CHSH-like inequalities and their application to self-testing*, arXiv:1504.06960v1 (2015).

[114] M. Navascués, S. Pironio and A. Acín, *A convergent hierarchy of semidefinite programs characterizing the set of quantum correlations*, arXiv:0803.4290v1 (2008).

[115] Z. Ji, A. Natarajan, T. Vidick, J. Wright and H. Yuen, *MIP*=RE*, arXiv:2001.04383v4 (16 October 2026). External theorem, not re-proved or newly formalized here.

[116] H.-L. Huang, Z. Lin and X. Su, *The Auslander–Reiten quivers of string algebras of affine type $\widetilde{C}$ and a conjecture by Geiss–Leclerc–Schröer*, arXiv:2110.02777v2, 16 November 2021, especially Propositions 2.9 and 3.12, Lemma 3.10 and Theorem 3.14.

[117] C. M. Ringel, *The Minimal Representation-Infinite Algebras which are Special Biserial*, author-hosted ICRA Tokyo 2010 proceedings text, 57 pages, retrieved 3 November 2026; especially Sections 12.5 and 13.1–13.7. The unversioned retrieval does not determine an additional revision date.

[118] G. Zwara, *Smooth morphisms of module schemes*, Proc. London Math. Soc. (3) **84** (2002), 539–558, doi:10.1112/S0024611502013382.

[119] C. Riedtmann and G. Zwara, *Orbit closures and rank schemes*, Comment. Math. Helv. **88** (2013), 55–84, doi:10.4171/CMH/278, Section 6, especially the definition on p.71 and Theorems 6.1–6.2.

[120] S. Opper, P.-G. Plamondon and S. Schroll, *A geometric model for the derived category of gentle algebras*, arXiv:1801.09659v7, 10 July 2025, especially the category conventions and Section 5.1.

[121] A. Schofield and M. Van den Bergh, *Semi-invariants of quivers for arbitrary dimension vectors*, arXiv:math/9907174v1 (1999), Trans. Amer. Math. Soc. **353** (2001), 1631–1650.

[122] W. Crawley-Boevey, *Classification of modules for infinite-dimensional string algebras*, arXiv:1308.6410v2, 4 March 2016, Trans. Amer. Math. Soc. **370** (2018), 3289–3313.

[123] S. Fomin and A. Zelevinsky, *Total positivity: tests and parametrizations*, Math. Intelligencer **22** (2000), 23–33; arXiv:math/9912128.

[124] K. Osterwalder and R. Schrader, *Axioms for Euclidean Green's functions*, Commun. Math. Phys. **31** (1973), 83–112; doi:10.1007/BF01645738.

[125] G. A. Elliott and D. E. Evans, *The structure of the irrational rotation C^*-algebra*, Ann. Math. **138** (1993), 477–501; doi:10.2307/2946556.

[126] T. Jacobson, *Entanglement equilibrium and the Einstein equation*, Phys. Rev. Lett. **116** (2016), 201101; arXiv:1505.04753.

[127] W. F. Stinespring, *Positive functions on C^*-algebras*, Proc. Amer. Math. Soc. **6** (1955), 211–216.

[128] I. Cong, S. Choi and M. D. Lukin, *Quantum convolutional neural networks*, Nature Physics **15** (2019), 1273–1278; arXiv:1810.03787.

[129] J. Zheng, Q. Gao and Y. Lv, *Quantum graph convolutional neural networks*, arXiv:2107.03257 (2021).

[130] A. Ning, T. Y. Li and N. Y. Chen, *Quantum graph attention network: A novel quantum multi-head attention mechanism for graph learning*, arXiv:2508.17630 (2025).

[131] H. Ramsauer et al., *Hopfield networks is all you need*, ICLR 2021; arXiv:2008.02217.

[132] F. Pastawski, B. Yoshida, D. Harlow and J. Preskill, *Holographic quantum error-correcting codes: toy models for the bulk/boundary correspondence*, JHEP **2015** (6), 149; arXiv:1503.06237.

[133] H.-Y. Huang, R. Kueng and J. Preskill, *Predicting many properties of a quantum system from very few measurements*, Nature Physics **16** (2020), 1050–1057; arXiv:2002.08953.

[134] L. E. Rosaleny et al., *Peptides as versatile scaffolds for quantum computing*, arXiv:1708.09440 (2017), including supplementary information S2. Coherence observations cited here refer to the frozen-solution EPR measurements, not a calibrated QPU.

[135] M. Nitz, M. Sherawat, K. J. Franz, E. Peisach, K. N. Allen and B. Imperiali, *Structural origin of the high affinity of a chemically evolved lanthanide-binding peptide*, Angew. Chem. Int. Ed. **43** (2004), 3682–3685; doi:10.1002/anie.200460028. Structure: PDB 1TJB.

[136] J. Butcher et al., *De novo design of all-atom biomolecular interactions with RFdiffusion3*, bioRxiv 2025.09.18.676967 (2025); primary preprint. Implementation documentation: Rosetta-Commons Foundry RFD3.

[137] A. Schreiber, *ThermoGFN-IF for catalysis: a protein sequence design model tuned with GFlowNets for stable protein design and kinetic-aware enzyme engineering*, author project description (10 March 2026), project description; implementation scaffold. Cited as a proposed methodology, not completed molecular or qubit validation.

[138] *Generalizable and scalable protein stability prediction with rewired protein generative models*, Nature Communications (2026), primary article, doi:10.1038/s41467-025-67609-4; correction doi:10.1038/s41467-026-70929-8.

[139] S. Lewis et al., *Scalable emulation of protein equilibrium ensembles with generative deep learning*, Science (2025), eadv9817; doi:10.1126/science.adv9817. Scope of the cited v1 model: official BioEmu model card.

[140] B. M. Wood et al., *UMA: A family of universal models for atoms*, arXiv:2506.23971 (2025).

[141] N. P. Breuckmann and B. M. Terhal, *Constructions and noise threshold of hyperbolic surface codes*, IEEE Trans. Inform. Theory **62** (2016), 3731–3744; arXiv:1506.04029v2.

[142] N. Delfosse, *Tradeoffs for reliable quantum information storage in surface codes and color codes*, IEEE ISIT (2013), 917–921; arXiv:1301.6588.

[143] A. Schreiber, *ToricGT*, repository revision a5199bc, inspected 3 November 2026; README, graph-token schemas, toric-algebra and finite-certificate modules.

[144] A. Schreiber, *ToricGT Research Program*, repository revision f91ba18, inspected 3 November 2026, README and five-paper program outline.

[145] M. Kontsevich and Y. Soibelman, *Homological mirror symmetry and torus fibrations*, arXiv:math/0011041v2 (4 June 2001), Sections 6–8, especially Theorem 4.

[146] M. Abouzaid, *Morse Homology, Tropical Geometry, and Homological Mirror Symmetry for Toric Varieties*, arXiv:math/0610004v4 (21 April 2009), Theorem 1.2 and Corollary 1.4.

[147] A. Schreiber, *Surface Algebras I: Dessins D'enfants, Surface Algebras, and Dessin Orders*, arXiv:1810.06750v5 (24 February 2023), especially the surface-algebra/order constructions and Section 10 on projective resolutions.

[148] A. Schreiber, *Surface Algebras and Surface Orders II: Affine Bundles on Curves*, arXiv:1812.00621v1, record dated 3 December 2018; cached PDF internally dated 27 November 2024, especially Sections 5–7 and 9–11. The retrieval pin is recorded in the research notes.

[149] A. Schreiber, *Multiparameter Persistent Homology—Generic Structures and Quantum Computing*, arXiv:2210.11433v1 (20 October 2022), especially Sections 3–7 and 10. The chapter uses corrected discrete grading, exactness and specialization hypotheses rather than every literal survey assertion.

[150] D. A. Buchsbaum and D. Eisenbud, *What makes a complex exact?*, J. Algebra **25** (1973), 259–268, primary paper, Theorem and Corollaries 1–2, pp.260–261.

[151] W. Bruns, *The existence of generic free resolutions and related objects*, Math. Scand. **55** (1984), 33–46, author-hosted primary paper, Theorem 1 and direct-limit construction, pp.35–36.